Comprehensive Cellular-Resolution Atlas of the Adult Human Brain

Song-Lin Ding,[1]* Joshua J. Royall,[1] Susan M. Sunkin,[1] Lydia Ng,[1] Benjamin A.C. Facer,[1] Phil Lesnar,[1] Angie Guillozet-Bongaarts,[1] Bergen McMurray,[1] Aaron Szafer,[1] Tim A. Dolbeare,[1] Allison Stevens,[2] Lee Tirrell,[2] Thomas Benner,[2] Shiella Caldejon,[1] Rachel A. Dalley,[1] Nick Dee,[1] Christopher Lau,[1] Julie Nyhus,[1] Melissa Reding,[1] Zackery L. Riley,[1] David Sandman,[1] Elaine Shen,[1] Andre van der Kouwe,[2] Ani Varjabedian,[2] Michelle Write,[2] Lilla Zollei,[2] Chinh Dang,[1] James A. Knowles,[3] Christof Koch,[1] John W. Phillips,[1] Nenad Sestan,[4] Paul Wohnoutka,[1] H. Ronald Zielke,[5] John G. Hohmann,[1] Allan R. Jones,[1] Amy Bernard,[1] Michael J. Hawrylycz,[1] Patrick R. Hof,[6] Bruce Fischl,[2] and Ed S. Lein[1]*

[1]Allen Institute for Brain Science, Seattle, Washington 98109
[2]Department of Radiology, Harvard Medical School, Athinoula A. Martinos Center for Biomedical Imaging, Massachusetts General Hospital, Charlestown, Massachusetts 02129
[3]Zilkha Neurogenetic Institute, and Department of Psychiatry, University of Southern California, Los Angeles, California 90033
[4]Department of Neurobiology and Kavli Institute for Neuroscience, Yale University School of Medicine, New Haven, Connecticut 06510
[5]Department of Pediatrics, University of Maryland School of Medicine, Baltimore, Maryland 21201
[6]Fishberg Department of Neuroscience and Friedman Brain Institute, Icahn School of Medicine at Mount Sinai, New York, New York 11029

ABSTRACT

Detailed anatomical understanding of the human brain is essential for unraveling its functional architecture, yet current reference atlases have major limitations such as lack of whole-brain coverage, relatively low image resolution, and sparse structural annotation. We present the first digital human brain atlas to incorporate neuroimaging, high-resolution histology, and chemoarchitecture across a complete adult female brain, consisting of magnetic resonance imaging (MRI), diffusion-weighted imaging (DWI), and 1,356 large-format cellular resolution (1 μm/pixel) Nissl and immunohistochemistry anatomical plates. The atlas is comprehensively annotated for 862 structures, including 117 white matter tracts and several novel cyto- and chemoarchitecturally defined structures, and these annotations were transferred onto the matching MRI dataset. Neocortical delineations were done for sulci, gyri, and modified Brodmann areas to link macroscopic anatomical and microscopic cytoarchitectural parcellations. Correlated neuroimaging and histological structural delineation allowed fine feature identification in MRI data and subsequent structural identification in MRI data from other brains. This interactive online digital atlas is integrated with existing Allen Institute for Brain Science gene expression atlases and is publicly accessible as a resource for the neuroscience community. J. Comp. Neurol. 524:3127–3481, 2016.

© 2016 The Authors The Journal of Comparative Neurology Published by Wiley Periodicals, Inc.

INDEXING TERMS: brain atlas; cerebral cortex; hippocampal formation; thalamus; hypothalamus; amygdala; cerebellum; brainstem; MRI; DWI; cytoarchitecture; parvalbumin; neurofilament protein; RRIDs: AB_10000343; AB_2314904; SCR_014329

Grant sponsor: National Institutes of Health (NIH); Grant number: RC2 MH089921 (to E.S.L. and M.J.H.); Grant sponsor: Allen Institute for Brain Science; Grant sponsor: National Institute for Biomedical Imaging and Bioengineering; Grant numbers: P41 EB015896, R01 EB006758, R21 EB018907, and R01 EB019956; Grant sponsor: National Institute on Aging; Grant numbers: 5R01 AG008122 and R01 AG016495; Grant sponsor: National Institute for Neurological Disorders and Stroke; Grant numbers: R01 NS0525851, R21 NS072652, R01 NS070963, R01 NS083534, and 5U01 NS086625; Grant sponsor: Shared Instrumentation Grants; Grant numbers: 1S10 RR023401, 1S10 RR019307, and 1S10 RR023043; Grant sponsor: National Institutes of Health Blueprint for Neuroscience Research (part of the multi-institutional Human Connectome Project); Grant number: 5U01 MH093765.
© 2016 The Authors The Journal of Comparative Neurology Published by Wiley Periodicals, Inc.

This is an open access article under the terms of the Creative Commons Attribution-NonCommercial-NoDerivs License, which permits use and distribution in any medium, provided the original work is properly cited, the use is non-commercial and no modifications or adaptations are made.
*CORRESPONDENCE TO: Ed S. Lein or Song-Lin Ding, Allen Institute for Brain Science, Seattle, WA 98109. E-mail: EdL@alleninstitute.org, or songd@alleninstitute.org

Received May 20, 2016; Revised July 11, 2016;
Accepted July 13, 2016.
DOI 10.1002/cne.24080
Published online in Wiley Online Library (wileyonlinelibrary.com)

The advent and improvement of noninvasive techniques such as magnetic resonance imaging (MRI), functional (f)MRI, and diffusion-weighted imaging (DWI) have vastly enriched our understanding of the structure, connectivity, and localized function of the human brain in health and disease (Glover and Bowtell, 2009; Evans et al., 2012; Amunts et al., 2014). Interpretation of these data relies heavily on anatomical reference atlases for localization of underlying anatomical partitions, which also provides a common framework for communicating within and across allied disciplines (Mazziotta et al., 2001; Toga et al., 2006; Bonnici et al., 2012; Evans et al., 2012; Caspers et al., 2013a; Annese et al., 2014). While neuroimaging data are typically registered to probabilistic reference frameworks (Das et al., 2016) to deal with interindividual variation, they lack the cytoarchitectural resolution of single-brain histological reference atlases (Evans et al., 2012; Caspers et al., 2013a), which is essential for more detailed studies of structural and cellular organization of the brain. There is therefore a strong need to bridge these levels of resolution to understand structure–function relationships in the human brain (Caspers et al., 2013a; Pascual et al., 2015).

A tremendous amount of effort has been dedicated to histology-based parcellation of discrete regions of the human brain, including the frontal, parietal, temporal, occipital, cingulate, and perirhinal cortices (Hof et al., 1995a; Van Essen et al., 2001; Vogt et al., 2001; Öngür et al., 2003; Scheperjans et al., 2008; Zilles and Amunts, 2009; Ding et al., 2009; Ding and Van Hoesen, 2010; Goebel et al., 2012; Petrides and Pandya, 2012; Caspers et al., 2013b), and other regions such as the thalamus, amygdala, hippocampus, and brainstem (e.g., De Olmos, 2004; García-Cabezas et al., 2007; Jones, 2007; Morel, 2007; Mai et al., 2008; Ding et al., 2010; Paxinos et al., 2012; Ding and Van Hoesen, 2015). Currently available large-scale histological reference atlases of the human brain vary substantially in their degree of brain coverage, information content, and structural annotation (Table 1), and much of the more recent work is absent in these atlases. The most commonly used cytoarchitecture-based human brain atlas is Brodmann's cortical map (Brodmann, 1909; Talairach and Tournoux, 1988; Simić and Hof, 2015), particularly for its use in annotating fMRI data, although von Economo's (von Economo and Koskinas, 1925) and Sarkisov's (Sarkisov et al., 1955) cortical maps are also still referenced. More recently developed large-scale atlases possess greater anatomical coverage and multimodal information content, but are generally limited by their degree of structural delineation, particularly for neocortical areas that are often referenced only by gyral patterning (Duvernoy, 1999; Fischl et al., 2004; Damasio, 2005; Mai et al., 2008; Naidich et al., 2008; Destrieux et al., 2010; Nowinski and Chua, 2013). To overcome these limitations, a 3-dimensional (3D) model of an adult human brain based on whole-brain serial sectioning, silver staining, and MRI (Amunts et al., 2013) was recently created, and a probabilistic cytoarchitectural atlas (JuBrain; see Caspers et al., 2013a) is also being generated. However, the staining of these specimens is limited, the imaging of the histology data currently lacks cellular resolution, and detailed annotation or parcellation of all brain regions based on cytoarchitecture remains to be performed. Additional efforts have used ultra-high-resolution MRI of ex vivo brains to build intrinsically 3D models of cytoarchitectural boundaries, and quantify the predictive power of macroscopic features for localizing microscopically defined boundaries (Augustinack et al., 2005, 2010, 2012, 2013, 2014; Fischl et al., 2008, 2009; Iglesias et al., 2015). While these latter atlases represent major advances, currently available resources still lack many features of modern atlases available in rodents and non-human primates such as multimodality, dynamic user interfaces with scalable resolution and topographic interactivity, and brain-wide anatomic delineation with ordered hierarchical structural ontologies.

We aimed to develop an adult human brain atlas with many of the features of modern digital atlases in model organisms (Lein et al., 2007; Saleem and Logothetis, 2012; Papp et al., 2014). First, the atlas requires whole-brain coverage with neuroimaging (MRI, DWI) and histology using multiple stains in the same brain, allowing brain parcellation based on convergent evidence from cyto- and chemoarchitecture, to reflect functional properties of corresponding brain regions more accurately (Ding et al., 2009; Amunts et al., 2010; Caspers et al., 2013a,b; Pascual et al., 2015). Second, we aimed for true cellular resolution (1 μm/pixel) on histological images to link microscopic features with the macroscopic scales more common in neuroimaging studies. Most critically, we performed comprehensive structural annotation at a very detailed level, based on a hierarchical structural ontology and using multiple forms of neocortical annotations to link gross anatomical (gyral, sulcal) and histology-based parcellation schemes modified from Brodmann. Finally, these data are combined in an interactive, publicly accessible online application with direct linkage to other large-scale human brain gene expression databases (http://human.brain-map.org; Hawrylycz et al., 2012).

MATERIALS AND METHODS

Specimen

The brain used for this reference atlas was from a 34-year-old female donor with no history of neurological

TABLE 1.

Comparison of Main Large-Scale Anatomical Reference Atlases for Adult Human Brains[1]

	This atlas	Brodmann (1909)	von Economo and Koskinas (1925)	Talairach and Tournoux (1988)	Duvernoy (1999)	Mai et al. (2008)	Caspers et al. (JuBrain, 2013a)[3]
Coverage	Whole brain	Cerebral cortex	Cerebral cortex	Cerebrum	Cerebrum	Cerebrum	10 brains (mainly cerebral cortex)
Datasets	Nissl, SMI-32, PV, MRI, and DWI (from the same brain)	Nissl	Nissl	Based on Brodmann's map	Brain slices and MRI (not from the same brain)	Nissl, myelin, and MRI (MRI not from the same brain)	Nissl and receptors
Format and resolution	Digital (up to 1 μm/pixel)	Static	Static	Static	Static	Static (+electronic version)	Digital
Density of annotated plates	106 coronal plates	Very limited photographs	Limited photographs	38 coronal plates	86 coronal plates	69 coronal plates	Not known
Cortical parcellation	Modified Brodmann's areas and subareas as well as cortical sulci and gyri	Brodmann's areas	Von Economo's areas	Brodmann's areas	Cortical sulci & gyri only	Cortical sulci & gyri only	Cytoarchitectural areas
Labeled fiber tracts	Large and small tracts (~117)	No	No	Large fiber tracts (~15)	Large fiber tracts (~10)	Major fiber tracts (~40)	Large fiber tracts (~11)
Brainstem annotation	Nuclei, subdivisions, and fiber tracts	Not available	Not available	Not annotated	Basically not available[2]	Bascically not available[2]	Not available
Cerebellum annotation	Lobules, zones, deep nuclei, and fiber tracts	Not available	Not available	Not annotated	Not available	Not available	Not available
Total annotated structures	~862 (including nearly all gyri and sulci)	~50	~107	~65	Nearly all gyri and sulci	Nearly all gyri and sulci	~60 structures available so far
Dimension	2D	2D	2D	2D	2D	2D	3D
Interactivity	Highly interactive	No	No	No	No	Somewhat interactive (electronic form)	Interactive
Accessibility	Free to public (no registration needed)	Book	Book	Book	Book	Book	Free

[1]Many human brain MRI atlases generated on base of gross anatomy were not included.

[2]Only a small portion of the superior colliculus regions was available.

[3]BigBrain (Amunts et al., 2013) from this group is a whole brain 3D model based on silver stain with a resolution at 20 μm/pixel but little anatomical annotation was applied to it so far.

diseases or remarkable brain abnormality obtained from the University of Maryland Brain and Tissue Bank, a brain and tissue repository of the NIH NeuroBioBank. All work was performed according to guidelines for the research use of human brain tissue and with approval by the Human Investigation Committees and Institutional Ethics Committees of the University of Maryland, the institution from which the sample was obtained.

General tissue processing

A general workflow for generating this atlas is shown in Figure 1. After the brain was removed from the skull, 4% periodate-lysine-paraformaldehyde (PLP) was injected into the internal carotid and vertebral arteries following a phosphate-buffered saline (PBS) flush. The brain was then suspended and immersed in 4% PLP at 4°C. This preparation appeared to result in a slight elongation of the brain. Following complete fixation (48 hours), the brain was subjected to MRI and DWI (see details below) and stored in PLP at 4°C until further processing. The fixed brain was bisected through the midline. Following agarose embedding, each hemisphere was cut with a flexi-slicer in the anterior to posterior direction, resulting in eight 2-cm-thick slabs. The slabs were cryoprotected in PBS containing 10%, 20%, and 30% sucrose, respectively and then frozen in a dry ice/isopentane bath (between −50°C and −60°C). Finally, the frozen slabs were placed in plastic bags that were vacuumed sealed, labeled, and stored at −80°C until histological sectioning.

Sectioning was performed by Neuroscience Associates (Knoxville, TN). The slabs were individually thawed rapidly in PBS, treated overnight with 20% glycerol and 2% dimethylsulfoxide to prevent freezing artifacts, and embedded in a gelatin matrix using MultiBrain® Technology (NeuroScience Associates) to avoid loss of unconnected tissue. After curing in a 2% formaldehyde solution, the blocks were rapidly frozen by immersion in isopentane (chilled by crushed dry ice) and mounted on the frozen stage of a hydraulically driven sliding microtome (Lipshaw model 90A, Pittsburgh, PA). Each block was sectioned coronally in 50-μm-thick sections. All sections were collected sequentially (none were discarded) into a 4 × 6 array of containers filled with an antigen preserving solution (50% PBS, pH 7.0, 50% ethylene glycol, 1% polyvinyl pyrrolidone). During sectioning, block-face images were taken at intervals of 10–12 sections. Due to the challenges of sectioning and mounting thin sections from complete hemispheres, certain artifacts in the tissue sections are present. These artifacts include large cracks through most of the section in some cases as well as smaller tears in white and gray matter structures. In general these artifacts are easily identifiable but should not be confused with structural features of the underlying tissues.

Histology and immunohistochemistry

Out of 2,716 total sections, 679 (200-μm sampling interval) were mounted on gelatin-coated 3- × 5-inch glass slides, air-dried, and stained for Nissl substance using 0.05% thionine in acetate buffer (pH 4.5). For immunohistochemistry, 339 sections (400-μm sampling interval) were immunostained free-floating for the calcium-binding protein parvalbumin (PV) and 338 sections (400-μm sampling interval) for nonphosphorylated neurofilament proteins (NFPs). All incubation solutions, from blocking serum onward, used Tris-buffered saline (TBS) with Triton X-100 as the vehicle; all washes were done in TBS after antibody and avidin–biotin–horseradish peroxidase (HRP) incubation. Following treatment with hydrogen peroxide and a blocking serum, tissue sections were immunostained with antibody SMI-32 (1:3,000, BioLegend, San Diego, CA) and a monoclonal anti-PV antibody (1:10,000, Swant, Marly, Switzerland) overnight (~16 hours) at room temperature, with vehicle solutions containing Triton X-100 for permeabilization. A biotinylated secondary antibody (1:150, Vecta Elite horse anti-mouse, preabsorbed against rat IgG, Vector Burlingame, CA) and ABC solution (1:200, Vectastain Elite ABC kit, Vector) were then applied for 90 and 45 minutes, respectively. To complete this process, sections were treated with nickel-diaminobenzidine tetrahydrochloride (DAB) and hydrogen peroxide.

Antibody characterization

The antibody against NFP (BioLegend, Cat.# SMI-32, RRID: AB_2314904) is a mouse monoclonal IgG1 recognizing a double band at MW 200,000 and 180,000, which merge into a single neurofilament H line on 2D blots (Sternberger and Sternberger, 1983) (Table 2). The immunostaining of sections through human temporal cortex produced a pattern of NFP labeling that was identical to previous descriptions (Ding et al., 2009). In human and monkey cerebral cortex, the antibody stains a subpopulation of large pyramidal neurons with the labeling largely restricted to dendritic processes and soma (Campbell and Morrison, 1989; Hof et al., 1995a,b; Nimchinsky et al., 1997; Ding et al., 2003, 2009).

The anti-PV antibody is a mouse monoclonal IgG1 (Swant, Cat.# 235, RRID: AB_10000343). This antibody was produced by immunizing mice with PV from carp muscle and hybridizing mouse spleen cells with myeloma cell lines. This antibody specifically stained the 1999Ca-binding "spot" of PV (MW 12,000) from rat cerebellum on 2D immunoblot assays (Celio et al., 1988)

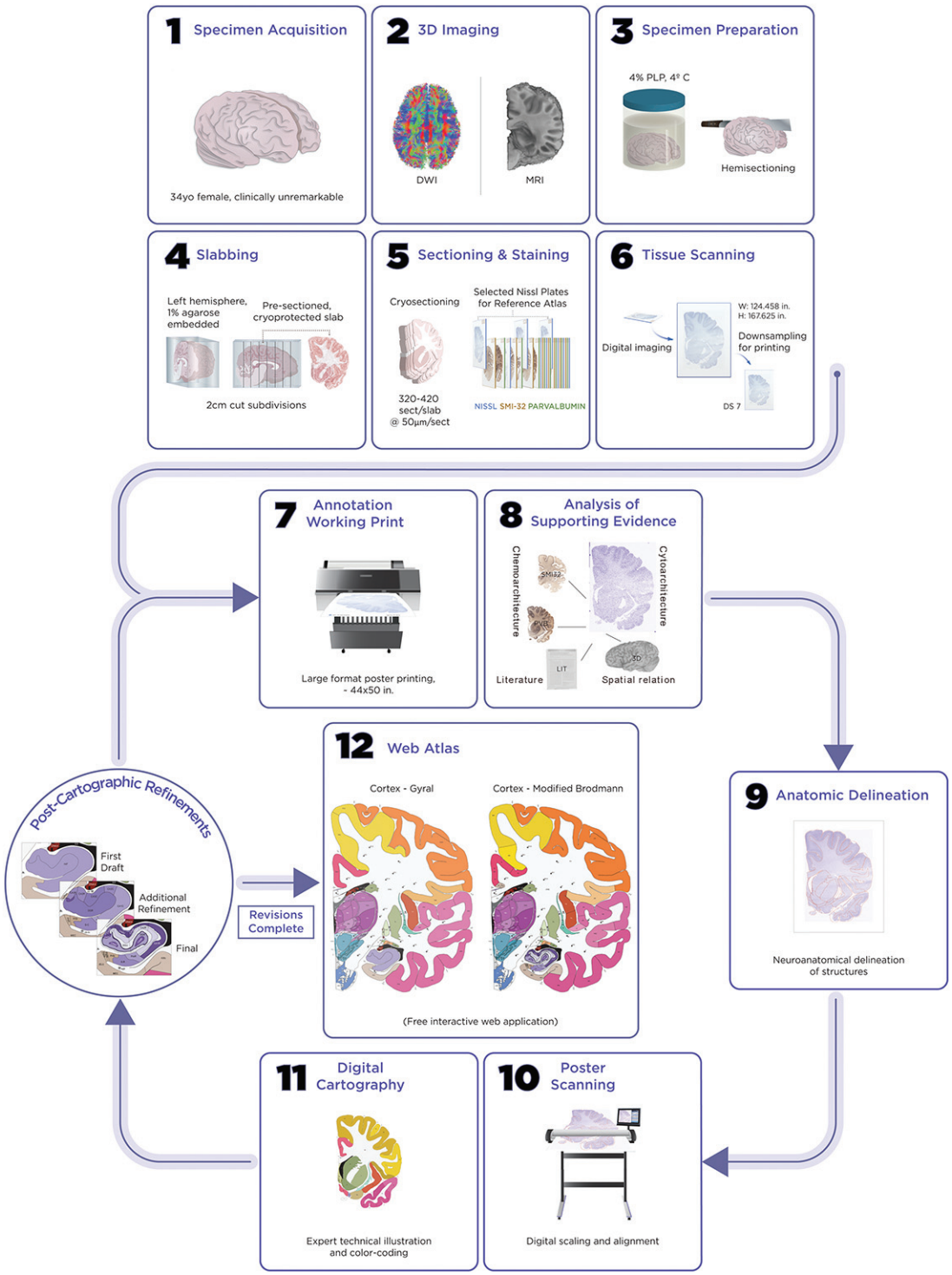

Figure 1. General workflow of atlas generation.

(Table 2). No staining was observed when the antibody was used to stain cortical tissues from PV knockout mice. This antibody labels subsets of nonpyramidal neurons in cerebral cortex of many species including human (Hof et al., 1999; Nimchinsky et al., 1997; Ding and Van Hoesen, 2010, 2015).

Digitization of all stained sections

A custom-designed large-format microscopy system was created to allow digital imaging and processing of all histologically stained sections (Nikon, Melville, NY). The system operates by collecting hundreds of images in lengthwise strips, which are montaged to create a

TABLE 2.
Primary Antibodies Used in This Study

Antibody	Immunogen	Source, cat. #, and RRID	Host species and type	Concentration
Anti-NFP	Nonphosphorylated epitopes on the medium and heavy subunits of the neurofilament triplet proteins	BioLegend, Cat.# SMI-32, RRID: AB_2314904	Mouse monoclonal IgG1	1:5,000
Anti-parvalbumin	Parvalbumin purified from carp muscles	Swant, Cat.# 235, RRID: AB_10000343	Mouse monoclonal IgG1	1:10,000

single hemispheric image at 1 μm/pixel resolution. A total of 1,356 sections on 3- × 5-inch slides were digitized for this resource, of which a single section (representative dimension: ~3.2 × 4.3 m) typically took 6–8 hours to complete. Exposure time, white balance, and flat-field correction were set independently for each slide. The Nikon NIS-Elements Advanced Research (AR) microscope imaging software suite (RRID: SCR_014329) was used for acquisition of ND2 format image files that were subsequently converted to TIFF format.

Digital atlas design and annotation

For detailed anatomical delineation, 106 Nissl-stained sections were selected out of 679. Sampling intervals varied from 0.4 to 3.4 mm across the full anterior–posterior (A-P) extent of the entire left hemisphere. Sparser sampling (3.4 mm) was selectively applied to the most anterior (prefrontal) and posterior (occipital) cortical levels that primarily contain cortex and a few large subcortical structures. Where smaller subcortical structures are more abundant, a much denser sampling was used (0.4–1.0-mm interval). In total, 862 brain structures were digitally annotated on the 106 whole-hemisphere images using 11,398 polygons.

Anatomical delineations were performed on poster-sized printouts of Nissl-stained sections and then digitally scanned and registered to the original Nissl images. Structure outlines were converted to digital polygons using Adobe (San Jose, CA) Creative Suite 5, and converted to Scalable Vector Graphics (SVG) format for web utilization. Polygons were linked to the hierarchical structural ontology and color-coded according to the ontology color scheme such that related structures fall into similar color groups. Furthermore, hues were assigned according to the relative cellular density of the structure: the higher the density, the deeper the shade (i.e., addition of black to hue); the lower the density, the deeper the tint (i.e., addition of white to hue).

Magnetic resonance and diffusion-weighted imaging

High-resolution structural imaging was performed using special coils designed to optimize signal-to-noise and contrast-to-noise ratios (SNR and CNR, respectively) in fixed specimens by reducing large spacing between the coil elements and the sample. DWI was performed using standard Siemens head coils. Sample packing was performed by vacuum-sealing the brain specimen in a polyethylene storage bag surrounded by PLP to avoid any artifacts caused by the interface between air and tissue. Diffusion-weighted images were collected on a 3 T TIM Trio whole-body scanner (Siemens Medical Solutions, Erlanger, Germany) with a Siemens 32 channel head coil. High-resolution structural images were acquired using a 7 T scanner (Siemens Medical Solutions) with a custom 30-channel receive-array coil designed to image the entire adult brain, utilizing a 36-cm head gradient coil.

For the 7 T scans, custom pulse sequence software was used to measure k-space in "chunks" small enough to be held in the scanner hard disk buffer, and a system was developed to stream each "chunk" of data from the buffer to a multiterabyte RAID array in parallel with it being measured by the scanner. Systems integration and custom software were developed for fast, reliable network and RAID connections and data stream management. Images from each coil channel were reconstructed and combined into a single image using a noise-weighted combination to optimize SNR.

The noise covariance matrix for a coil array is estimated from a noise-only measurement collected in the absence of any RF excitation. This acquisition lasts about 20 seconds and provides enough thermal noise samples to accurately estimate the noise covariance matrix for the 30-channel coil and describes the thermal noise coupling between the individual coil channel images for unaccelerated acquisitions. The final combined image is then computed as a noise-weighted sum of the complex-valued individual coil channel images and is given by

$$I = \sqrt{s^{H}\Psi^{-1}s}$$

where I represents the combined image intensity at a given pixel, Ψ represents the $N \times N$ noise covariance matrix, and s represents the $N \times 1$ vector of complex-valued image intensities at a given pixel across the N

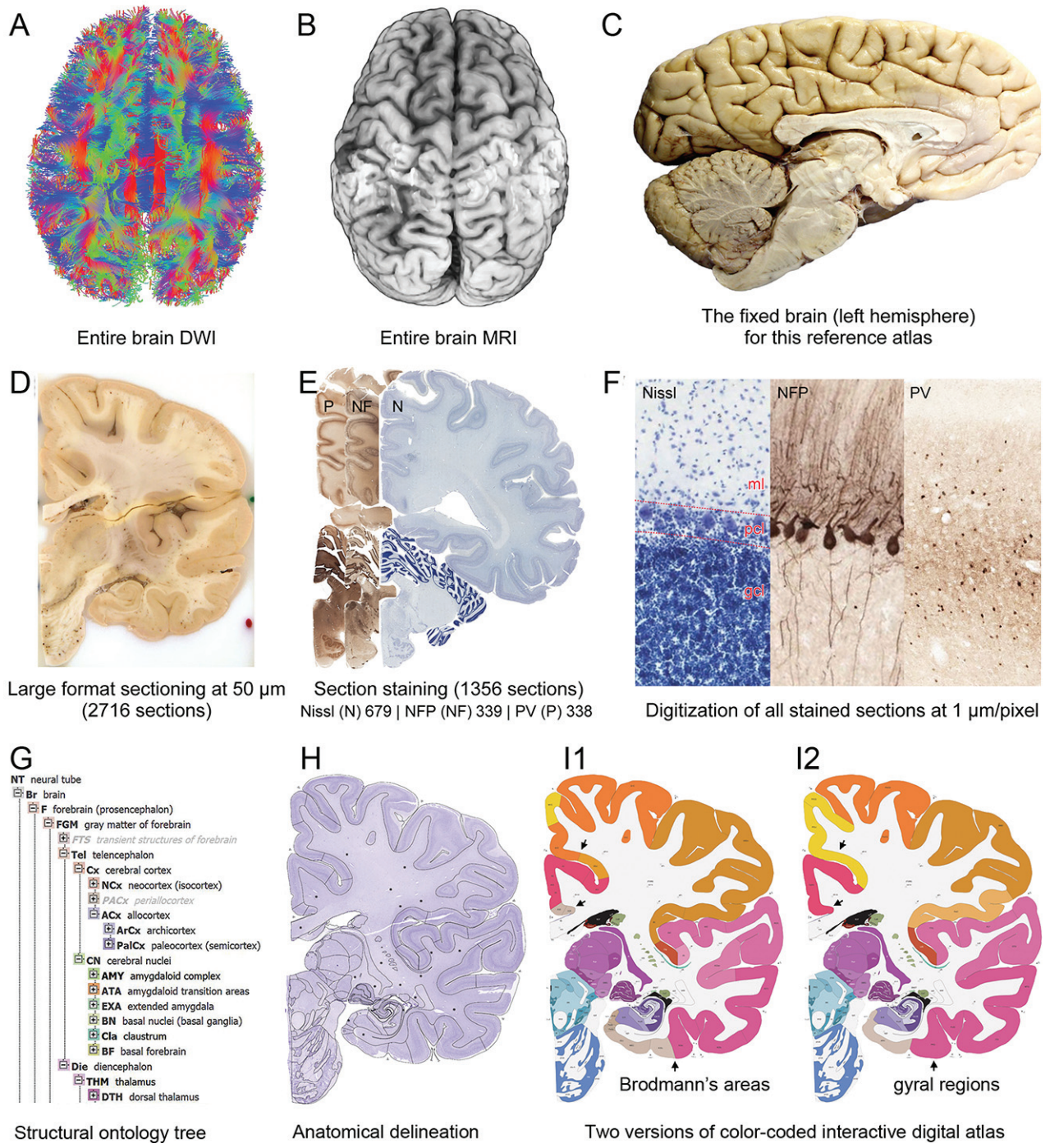

Figure 2. Whole-brain reference atlas components. **A,B**: DWI tractography and structural MRI. **C**: Midline-sagittal photograph of left hemisphere. **D**: Block-face image of a coronal slab. **E**: Digital images of adjacent sections stained for PV, NFP, and Nissl. **F**: Cellular-resolution detail in cerebellar (Nissl and NFP) and cingulate cortex (PV). **G**: Brain ontology with color codes, acronyms, full names, and hierarchical parent–daughter relationships. **H**: Anatomical delineation of a Nissl plate from a combined analysis of all three stains. **I**: Interactive color-coded digital atlas with both modified Brodmann (**I1**) and traditional gyral (**I2**) cortical maps. Black arrows point to some of the differences between these maps.

coils of the array (Roemer et al., 1990; Wright and Wald, 1997).

For 7 T images, gray and white matter CNR was optimized, to best distinguish these tissue classes as well as discern laminar intracortical architecture. Structural data were acquired using a multiecho flash sequence (TR = 50 ms, $\alpha = 20°$, 40°, 60°, 80°, 6 echoes, TE = 5.49 ms, 12.84 ms, 20.19 ms, 27.60

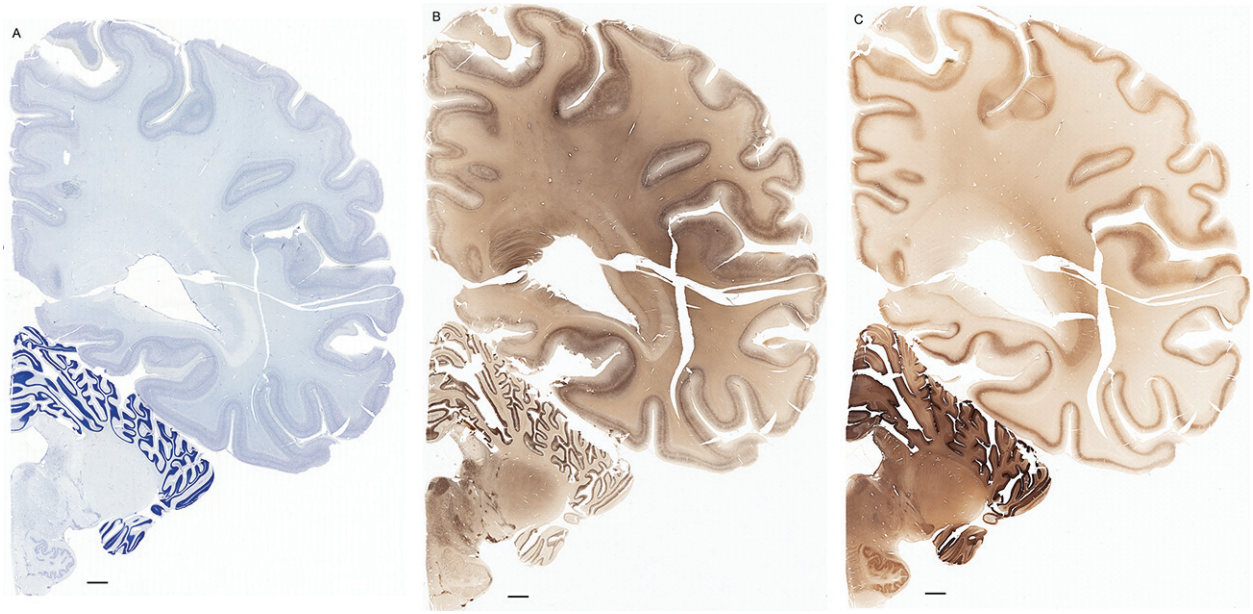

Figure 3. Examples of closely adjacent whole-hemisphere sections for the histological stains used in the atlas. A combined analysis of Nissl-stained (**A**), and NFP- (**B**) and PV- (**C**) immunostained sections greatly facilitated delineation of both cortical and subcortical regions of the human brain (see examples in Figs. 5–7). The size of a typical plate at native resolution (1 μm/pixel) is ~3.0 m wide and 4.3 m high. Scale bar = 3,108 μm in A–C.

ms, 35.20 ms, 42.80 ms, at 200-μm isotropic resolution).

Diffusion-weighted data were acquired over two averages using a 3D steady-state free precession (SSFP) sequence (TR = 29.9 ms, $\alpha = 60^{\circ}$, TE = 24.96 ms, 900-μm isotropic resolution). Diffusion weighting was applied along 44 directions distributed over the unit sphere (effective b-value = 3,686s/mm^2) (Miller et al., 2012) with eight b = 0 images. The two acquisitions were coregistered using FSL's FLIRT to correct for *B*0 drift and eddy-current distortions (Jenkinson and Smith, 2001) and then averaged before further processing. DWI analysis was done using Diffusion Toolkit (dtk), and Trackvis was used for visualization of tracts (http://trackvis.org/) (Wang et al., 2007). The fiber tracking algorithm is based on the fiber assignment by continuous tracking (FACT) algorithm (Mori et al., 1999). Diffusion-weighted images were rotated to the same orientation as the MRI volume to allow generation of plane-matched MRI and DWI images for the atlas, and the corresponding transformation was applied to the gradient table used to acquire the images. Tracts were created using a 60° angular threshold, masked so tracts are only contained within the approximate brain volume. The primary eigenvectors of the diffusion tensor were overlaid on the fractional anisotropy (FA) map in Freeview (part of the FreeSurfer software package, http://freesurfer.net) to create color FA images. Tractography images were generated in TrackVis with a tract threshold of 20 mm and 90% skip applied, using a Y filter to select all tracts that pass through each coronal plane.

RESULTS

Whole-brain multimodal data generation

To obtain multimodal datasets from the same specimen, ex vivo MRI and DWI scans (at 7 T and 3 T, respectively) of both hemispheres were collected (Fig. 2A,B) prior to histological processing. For anatomic atlasing, the left hemisphere including the connected brainstem and cerebellum (Fig. 2C) was coronally divided into 2-cm slabs, and each slab was serially sectioned at 50 μm (Fig. 2D). Every fourth section (200-μm sampling interval) was stained for Nissl substance (Fig. 2E), and every eighth section was immunostained for NFP (400-μm interval) or PV (400-μm interval) to facilitate accurate delineation of the Nissl-stained sections (Fig. 3A–C). Histological sections were imaged at cellular resolution allowing neuronal soma, dendrites, and axons to be clearly identified (Fig. 2F). A subset of Nissl-stained sections was selected for detailed anatomical delineation with sampling density higher in regions with greater structural complexity. This strategy enabled adequate sampling of small but functionally critical structures such as the suprachiasmatic nucleus

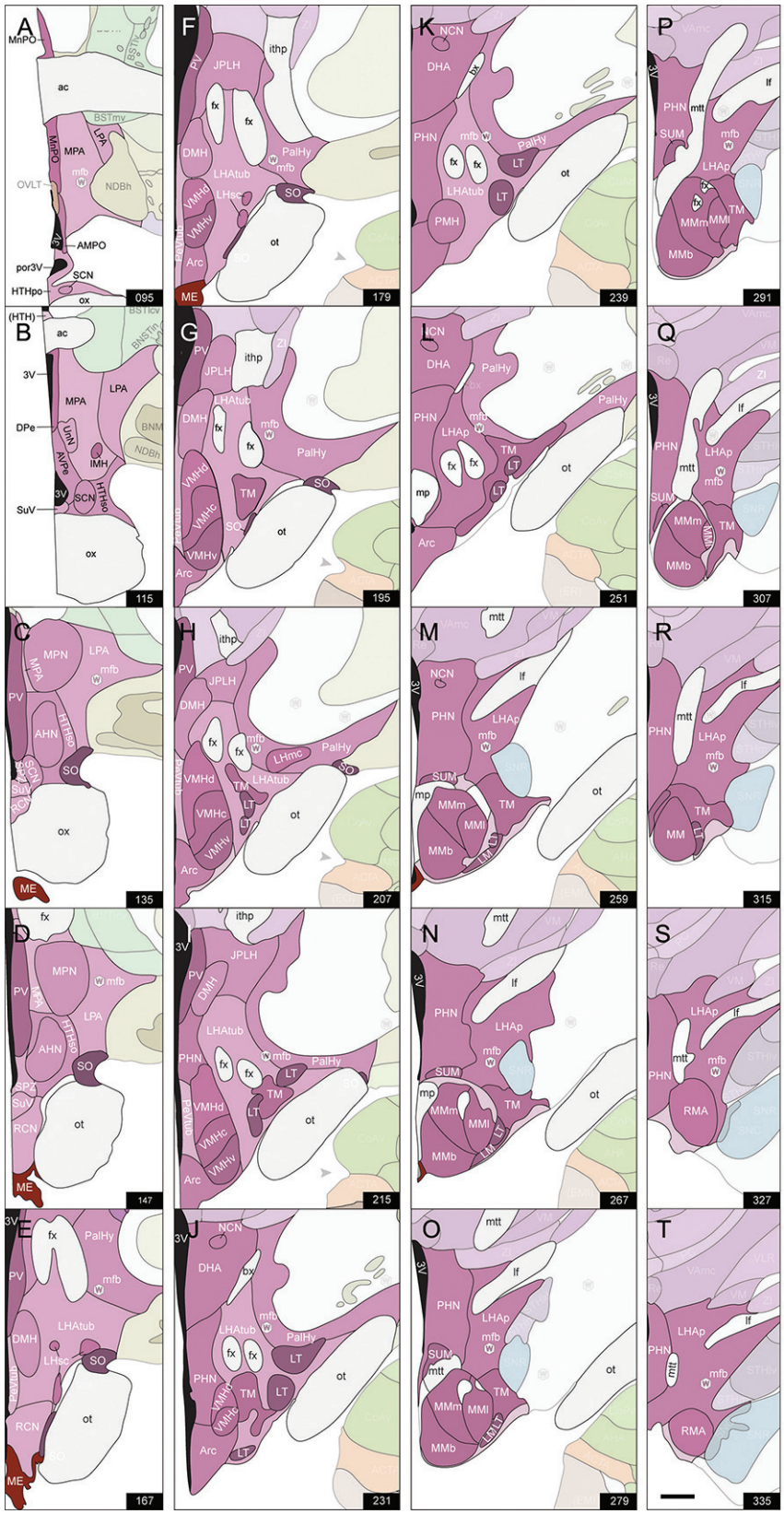

Figure 4. Detailed delineation of the human hypothalamus. A high sampling density (about 40 plates total, with 20 shown here) covering the entire anterior–posterior (**A**–**T**) extent of the hypothalamus was employed to ensure sampling and annotation of even the smallest structures such as the suprachiasmatic nucleus (SCN in **A**–**C**). For abbreviations see the hypothalamic part of the ontology in Table 3. Scale bar = 1,940 μm in T (applies to A–T).

in the hypothalamus (Fig. 4) and the area postrema in the medulla.

Creation of a unified structural brain ontology

An essential component of modern interactive digital atlases is a unifying hierarchical structural ontology that provides unique IDs (and colors for representation) for each structure in a parent–child architecture. We created a whole-brain ontology spanning all adult structures (Table 3) and including a developmental axis for transient structures observed during the specification and cytoarchitectural maturation (Miller et al. 2014). The ontology is fundamentally divided into the basic subdivisions of forebrain, midbrain, and hindbrain, further divided into four major branches comprising gray matter, white matter, ventricles, and surface features. For example, daughter structures of "gray matter of forebrain" (Fig. 2G) include the telencephalon, diencephalon, and transient structures of forebrain (e.g., subplate and ventricular zone of the neocortex), while "white matter of forebrain" includes nearly all commissural and long ipsilateral fiber tracts. "Ventricles of forebrain" includes the lateral and third ventricles and related structures, while "surface structures of forebrain" includes important gross landmark features such as cortical gyri and sulci.

For cortical structures, we aimed to accommodate both gyral and sulcal parcellation common to neuroimaging studies as well as cytoarchitectural parcellation based on histology, for which two basic terminologies based on Brodmann (Brodmann, 1909) and von Economo (von Economo and Koskinas, 1925; von Economo, 1927) are in usage. We used Brodmann's nomenclature as the primary reference because it is more commonly used, with modifications based on modern literature (see below) and the combined whole-brain large-scale cyto- and chemoarchitectural analysis here. Specifically, the following sources were used to modify the Brodmann scheme: for the frontal and cingulate cortex: Hof et al. (1995a), Vogt et al. (1995), Vogt et al. (2001), Öngür et al. (2003), Petrides and Pandya (2012), and Vogt and Palomero-Gallagher (2012); for parietal, temporal, and occipital cortices (mostly changed to Brodmann's terminology where other nomenclature was used): Caspers et al. (2013b), Ding et al. (2009), Ding and Van Hoesen (2010), Scheperjans et al. (2008), Van Essen et al. (2001), Zilles and Amunts (2009), and Goebel et al. (2012). The terminology for the hippocampal formation is derived from Ding and Van Hoesen (2015) and Ding (2013, 2015). For a few cortical areas that Brodmann (1909) did not parcellate in detail (Simić and Hof, 2015), such as posterior parahippocampal areas (areas TH, TL, and TF), we adopted a modified nomenclature from von Economo and Koskinas (1925; see Ding and Van Hoesen, 2010). Another example of modification of Brodmann's areas is the orbitofrontal cortex, where Brodmann's large area 11 was replaced with smaller areas 14, 11, and 13 according to a few modern anatomical studies in human (Hof et al., 1995a; Öngür et al., 2003) and our own investigation of Nissl preparations and PV- and NFP-immunostained sections. In addition, some of Brodmann's areas were further subdivided according to recent literature and the analysis here. For instance, Brodmann's areas 22 and 21 (roughly corresponding to von Economo's areas TA and TEd) were subdivided into rostral, intermediate, and caudal parts based on different staining intensity in PV-stained sections (Ding et al., 2009). Finally, for the insular cortex that was not numbered by Brodmann in human (1909; see Simić and Hof, 2015), three major subdivisions were delineated and these included agranular, dysgranular, and granular insula (e.g., Bauernfeind et al., 2013; Morel et al., 2013), with the latter two further divided into rostral and caudal parts.

Structures from the ontology were delineated as polygons on each Nissl digital image (Fig. 2H), and these structures include both gyral (Fig. 2I1) and modified Brodmann areas (Fig. 2I2) of the neocortex. Together, this comprehensive ontology covers all brain regions and can be used interactively to browse and search delineated structure polygons. It also provides enhanced interlinking capabilities among a broad range of datasets including adult (Hawrylycz et al., 2012) and developing (Miller et al., 2014) human brain transcriptional atlases included in the Allen Brain Atlas (www.brain-map.org).

Delineation of cortical and subcortical gray matter

Anatomical delineation for the 106 selected plates (Fig. 2H) was based on a combined analysis of cyto- (Nissl stain) and chemoarchitecture (NFP and PV immunohistochemistry). For example, the boundaries between areas 29 and the neighboring suprasplenial subiculum (SuS) and caudal presubiculum (PrSc; also known as the postsubiculum [PoS]) were confidently identified based on staining features revealed in Nissl- (Fig. 5A), and adjacent PV- and NFP- (Fig. 5B and inset) immunostained sections. Dark NFP and PV immunoreactivity highlights SuS and PrSc, respectively, and these complementary and corroborating data allowed a consensus digital annotation of these regions (Fig. 5C). Similarly, in the ventral temporal neocortex, the border between areas 36 and 20 can be more accurately defined with PV immunostaining than Nissl alone, as area 20 (20i) displays significantly stronger PV immunoreactivity than area 36 (Fig. 5D,E).

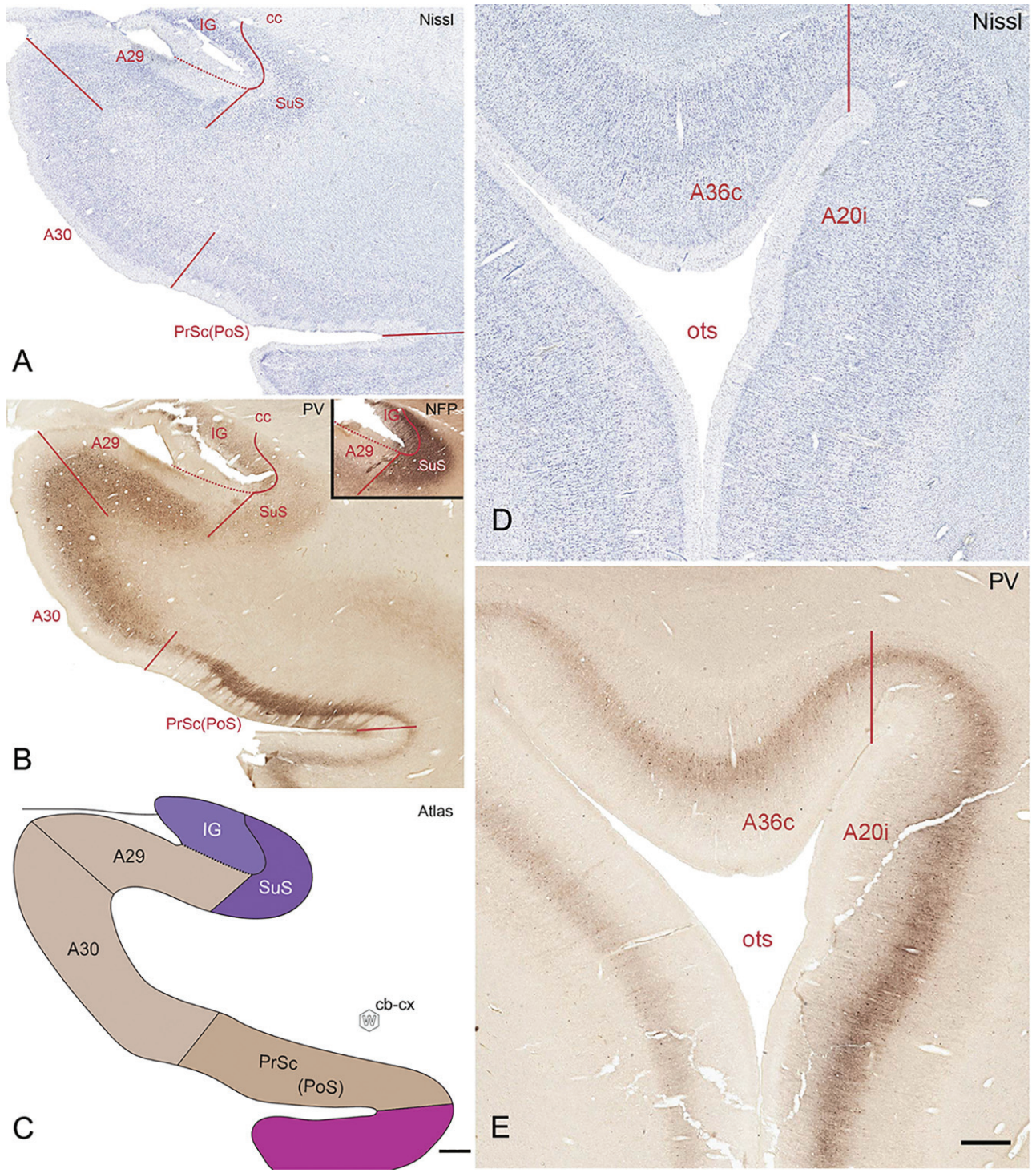

Figure 5. Defining cortical boundaries with a combined analysis of Nissl-, NFP-, and PV-stained sections. **A,B, and inset** in **B**: Boundary determining of the indusium griseum (IG), supracallosal subiculum (SuS), retrosplenial areas 29 (A29) and 30 (A30), and caudal presubiculum (PrSc; or postsubiculum [PoS]). **C**: Color-coded map of the region shown in A and B. cc, corpus callosum. PV and NFP immunostaining patterns help delineate neocortical borders and white matter tracts. **D,E**: Differences in PV immunolabeling intensity helps define the boundaries between area 36 and area 20 (20i). Scale bar = 1,106 μm in C (applies to A–C) and E (applies to D,E).

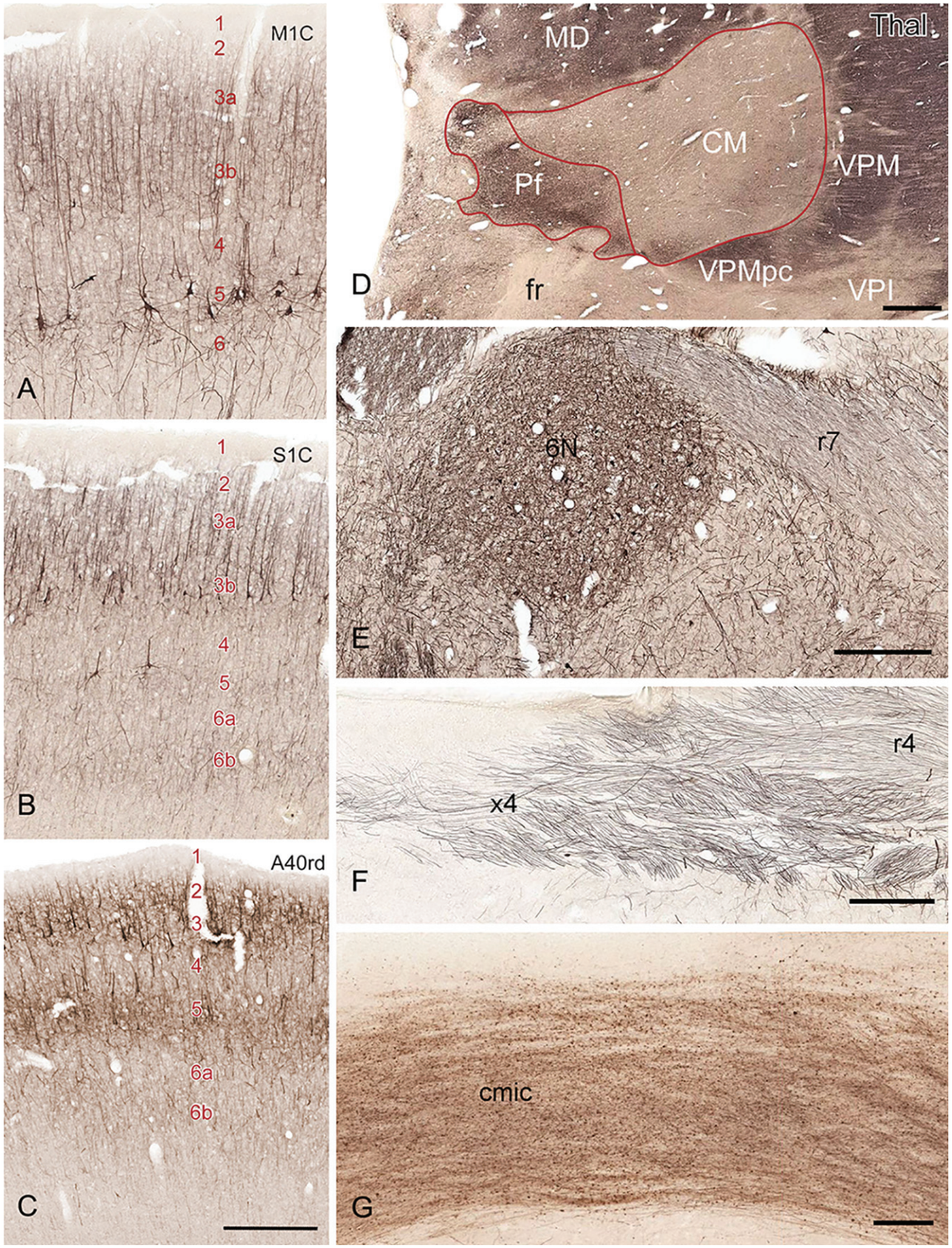

Figure 6. Defining boundaries of cortical and subcortical structures with NFP- (**A**–**F**) and PV- (**G**) stained sections. **A–C**: NFP staining patterns in primary motor cortex (M1C), primary somatosensory cortex (S1C), and the rostrodorsal portion of area 40 (A40rd). The locations of these three cortical areas were marked with *, **, and *** respectively in Figure 8A. Arabic numbers specify cortical layers. **D**: NFP staining pattern in the thalamus (Thal) defines Pf, CM, and adjoining structures. CM, centromedian nucleus; MD, mediodorsal nucleus; Pf, parafascicular nucleus. VPl, ventral posterior inferior nucleus; VPM, ventral posterior medial nucleus; VPMpc, parvocellular part of VPM. **E,F**: NFP is observed in select white matter tracts in the brainstem including the facial (r7 in **E**) and trochlear (r4 in **F**) nerve roots. 6N, abducens nucleus; r7, facial nerve root; x4, decussation of trochlear nerve roots (r4 in **F**). **G**: PV is selectively expressed in the commissure of the inferior colliculus (cmic). Scale bar = 777 μm in C (applies to A–C), D, and E; 277 μm in F; 88 μm in G.

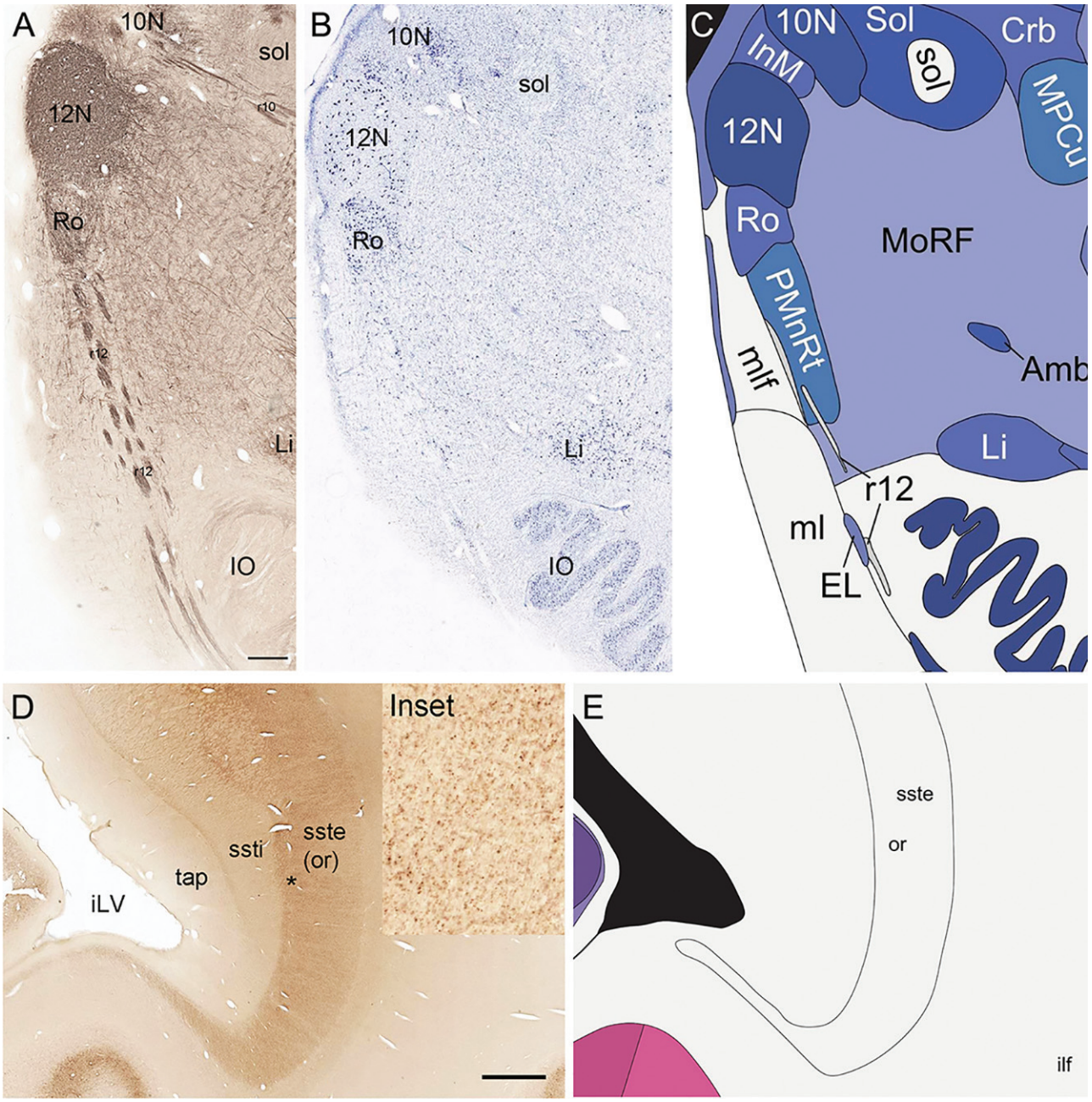

Figure 7. Defining white matter fiber tracts and subcortical structures with combined analysis of NFP and PV stains. **A**–**C**: Combined analysis of NFP immunoreactivity (**A**) and Nissl staining (**B**) in the medulla leading to anatomical parcellation (C). NFP clearly delineates specific cranial nuclei (e.g., 10N, 12N) and fiber tracts (e.g., r12). **D,E**: PV-immunoreactive axons in the external part of sagittal stratum/optic radiation ("or" in **D** and **inset**) compared with the internal part of the sagittal stratum (ssti) and tapetum of the corpus callosum (tap) that do not show PV immunoreactivity. **Inset**: High-magnification view of PV-immunoreactive axons in the optic radiation (*). 10N, dorsal motor nucleus of vagus nerve; 12N, hypoglossal nucleus; iLV, inferior horn of the lateral ventricle; IO, inferior olive; r12 and r10, hypoglossal and vagus nerve roots; Scale bar = 777 μm in A (applies to A,B); 1,554 μm in D.

NFP immunoreactivity was in many cases more informative than Nissl stain for delineation of cortical regions based on the selective labeling of pyramidal neuron populations in different layers. For example, many large pyramidal neurons in layer 5 of the primary motor cortex (M1C; Fig. 6A) are NFP-immunoreactive, while only a small number of medium-sized neurons are observed in that layer of the primary somatosensory cortex (S1C; Fig. 6B). In contrast, the inferior parietal area (rostrodorsal area 40 [area 40rd], located posterior

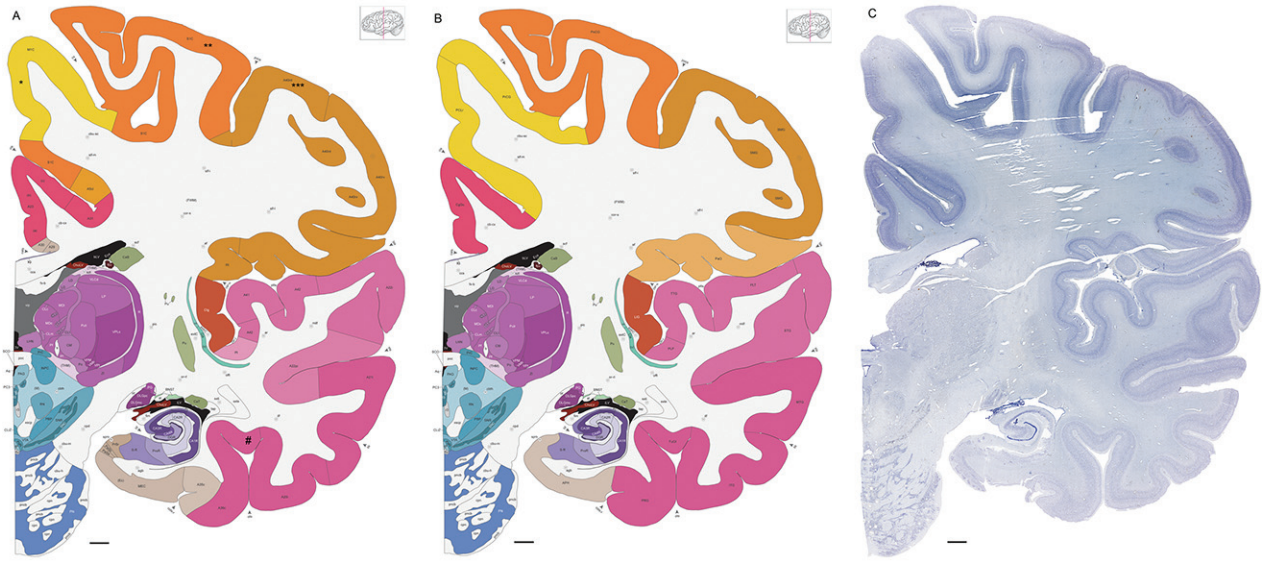

Figure 8. Alternate schemes for cortical parcellation. Modified Brodmann's areas (**A**) or sulci and gyri (**B**) were annotated on the same Nissl-stained plate (**C**) to show micro- and macrostructural relationships. Examples of how cortical areas were delineated are given in Figures 5 and 6. The markers (*, **, ***) and (#) in **A** indicate the locations of pictures in Figure 6A–C and Figure 5D,E, respectively. For abbreviations see the ontology in Table 3. Inset is a schematic representation of the whole hemisphere based on MRI, with the red vertical lines in A and B indicating the location of the section plate. Both modified Brodmann's areas and gyral/sulcal mapping of the cerebral cortex are available online at www.branspan.org. Scale bar = 3,108 μm in A–C.

to S1C; Fig. 6C), has a narrower band of superficial layer labeling and a stronger bilaminar pattern. The combined analysis of Nissl staining and NFP or PV immunolabeling was also useful in defining many subcortical regions and subdivisions such as ventroposterior inferior (VPI), parafascicular (Pf), and centromedian (CM) nuclei in the thalamus (Thal; Fig. 6D) and cranial motor nuclei of the brainstem (Figs. 6E, 7A–C).

Localization and delineation of white matter tracts

We also aimed for a comprehensive delineation of white matter tracts and cranial nerves (117 total), aided by NFP and PV fiber immunostaining. Motor roots of the cranial nuclei in the brainstem are clearly delineated by NFP staining (Figs. 6E, G, 7A). PV immunoreactivity shows similar discernment of a variety of fiber tracts and trajectories, such as the commissure of the inferior colliculus (Fig. 6F) and the optic radiation (Fig. 7D,E). A representative fully annotated atlas plate is shown in Figure 8A, with complete cyto- and chemoarchitecture-based parcellation and colorization superimposed on the original Nissl image (Fig. 8C). To relate macroscopic (landmarks) and microscopic (histology) cortical anatomy, parallel plates were created with parcellation by gyri and sulci (Fig. 8B) or modified Brodmann areas (Fig. 8A). The denser sampling of subcortical regions allowed comprehensive detailed annotation of fine nuclear architecture for all major regions, as illustrated for the hypothalamus (Fig. 4) and the amygdala (Fig. 9).

Identification of novel brain subregions

In addition to confirming previously identified structures, the combination of high image resolution and dense (200-μm-interval) Nissl sampling made it possible to reveal or clarify a number of complex or smaller brain structures, while the linkage to the Allen Human Brain Atlas (Hawrylycz et al., 2012) allowed corroboration of these structures with other gene expression data. One example is in the mediodorsal nucleus (MD) of the thalamus, where we observed a group of densely packed larger cells between the paraventricular nucleus (PaV) and the main portion of the MD, which we named the anteromedial subdivision of the MD (MDam in Fig. 10A). In situ hybridization data of both acetylcholinesterase (*ACHE*) and neurotensin (*NTS*) supports this partition, as they are selectively enriched in this region compared with the main part of the MD (Fig. 10B and inset). Similarly, we identified a novel subdivision of the basomedial nucleus (BM) of the amygdala. This

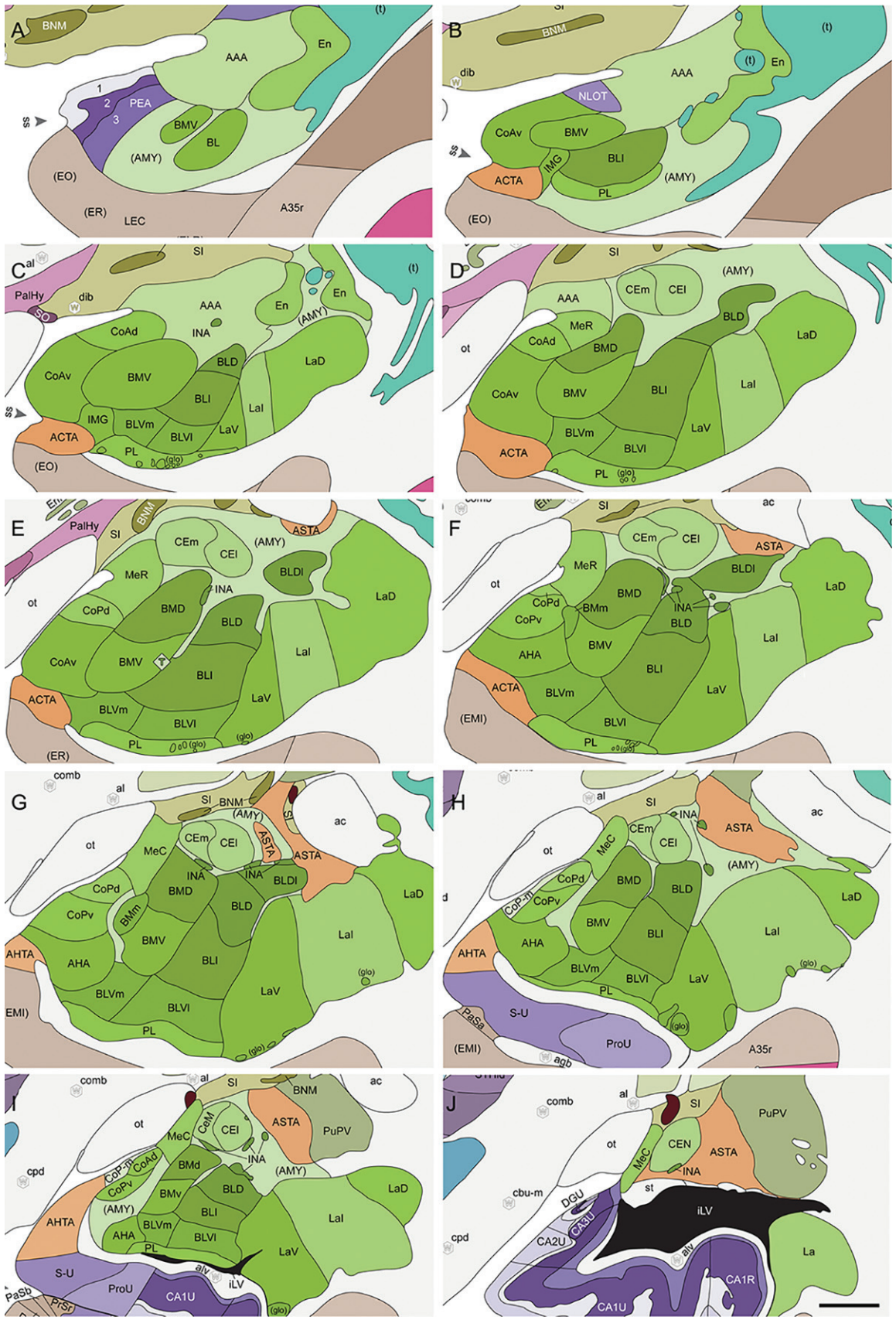

Figure 9. Detailed parcellation of the human amygdalar complex. Shown are ten of the 18 annotated plates covering the A-P extent (**A–J**) of the amygdala. For abbreviations see the amygdalar portion of the ontology in Table 3 Scale bar = 3,102 μm in J (applies to A–J).

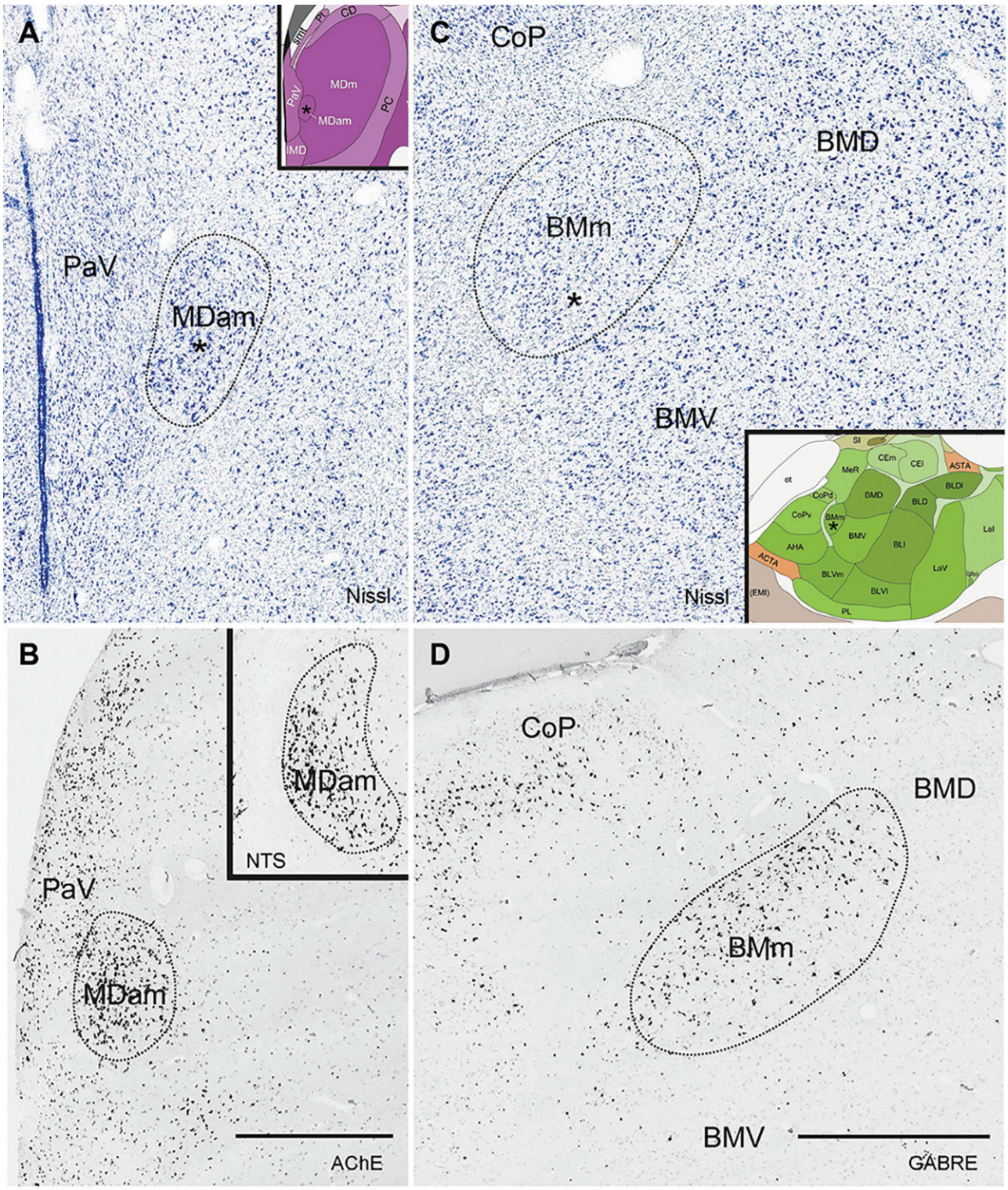

Figure 10. Novel subdivisions of the mediodorsal nucleus (MD) of the thalamus and basomedial nucleus (BM) of the amygdala. **A**: Nissl staining reveals a group of larger cells (termed MDam, labeled with * in high magnification image and overview atlas plate (inset)) located between the paraventricular nucleus (PaV) and anterior mediodorsal nucleus MDm) of the thalamus distinct from neighboring regions. **B**: Distinct molecular specificity of MDam is demonstrated by ISH for *ACHE* and *NTS* (**inset** in **B**). **C,D**: Novel subdivision of amygdalar basomedial nucleus differentiated by smaller and relatively lightly Nissl-stained cells (termed BMm, labeled with * in high magnification image and overview atlas plate (inset) in **C**) and selective enrichment for the *GABA receptor subunit E* (*GABRE*, in **D**) compared with neighboring dorsal and ventral regions (BMD and BMV) and posterior cortical nucleus (CoP). Scale bar = 1,109 μm in B (applies to A,B); 1,550 μm in D (applies to C,D).

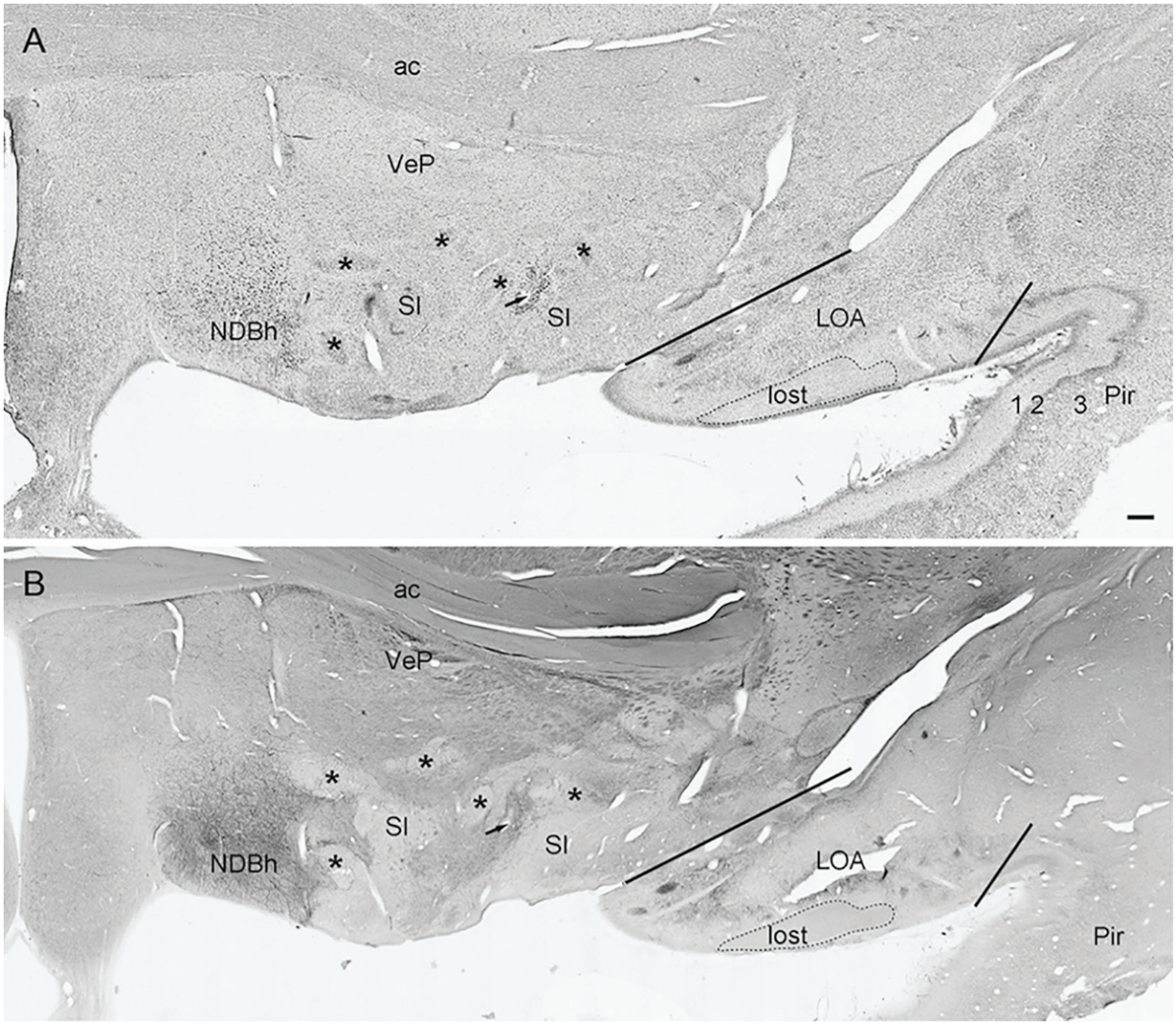

Figure 11. Identification of the lateral olfactory area (LOA) in the adult human brain. **A,B**: Adjacent sections stained for Nissl (**A**) and NFP (**B**) showing the architectural features of LOA that differ from neighboring substantia nominata (SI) and piriform cortex (Pir). In Nissl-stained sections, SI contains different types of cell patches (asterisks and arrowhead) while Pir is characterized by a darkly stained and densely packed layer 2 (**A**). LOA does not have these characteristic features, but shows cell patches that are different from those in SI (**A**). In NFP-immunostained sections, Pir is very light throughout while LOA shows strong labeling in the superficial layer (**B**). Only the large-celled patch (arrow) and scattered large cells of SI are strongly stained while other patches are negative (**B**). ac, anterior commissure; NDBh, horizontal part of nucleus of diagonal band; VeP, ventral pallidus; lost, lateral olfactory stria. Scale bar = 430 μm in A (applies to A,B).

subdivision is located medial to the dorsal and ventral subdivisions of the BM (BMD and BMV) and was termed BMm (medial subdivision of BM; Fig. 10C and inset). The BMm displays enriched cellular expression of the γ-aminobutyric acid (GABA) receptor subunit E (*GABRE*) compared with the neighboring BMD and BMV (Fig. 10D). The homologs of MDam and BMm in other species have not been reported.

Another new area was identified running along the side of lateral olfactory stria, situated medially to the piriform cortex (Pir) and laterally to the substantia innominata (SI). This was termed the lateral olfactory area (LOA) and was found to have distinct histological features from the neighboring Pir and SI (Fig. 11). Compared with the Pir, the LOA does not have a dark, densely packed layer 2 on Nissl stain and has much stronger NFP immunoreactivity. In Nissl-stained materials, the SI contains many cellular patches of differing sizes, packing densities, and staining intensities, with cells of contrasting shapes and sizes, compared with

Figure 12. Location and topographic relationship of area prostriata (APro). APro (labeled as Pro) is adjoined by the retrosplenial cortex (areas 29 and 30, not shown), postsubiculum (PoS in **A**), posterior cingulate cortex (area 23 in **B**–**D**) anterodorsally, and dorsal secondary visual cortex (V2d in **D**-**G**) posterodorsally. Anteroventrally, APro is adjoined by the ventral secondary visual cortex (V2 in **A**–**D**). Posteroventrally and posteriorly, APro is adjoined by the anteroventral part of the primary visual cortex (V1v in **E**–**H**). Scale bar = 4,420 μm in H (applies to A–H).

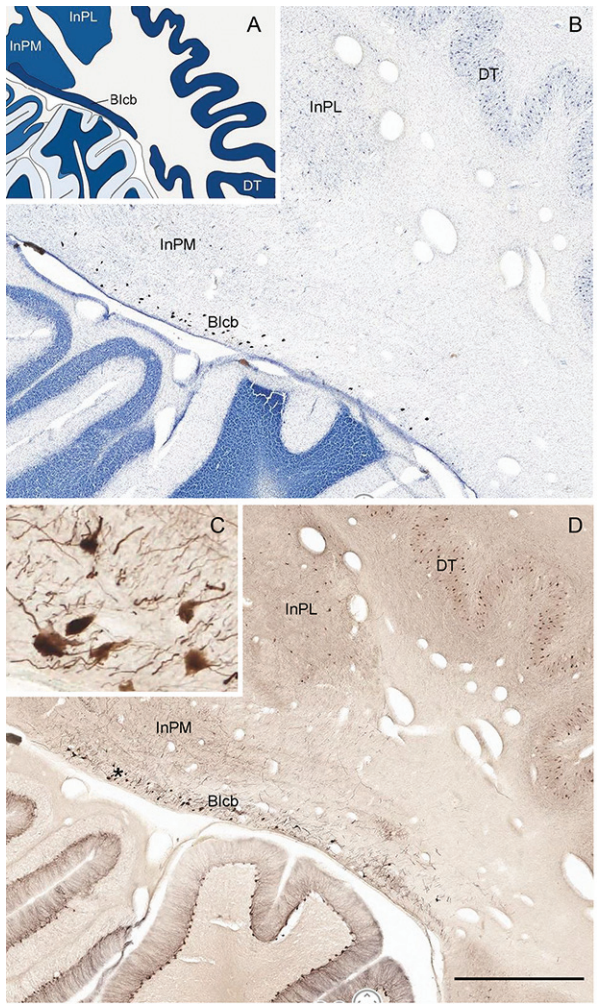

Figure 13. A novel subregion of the deep nuclei of the cerebellum. This has been named the basal interstitial nucleus of cerebellum (Blcb) and is embedded deep in the white matter medial to the dentate nucleus (DT) and lateral and inferior to the globose nucleus (i.e., the medial interpositus nucleus [InPM in **A**]). In Nissl stain, the cells in the Blcb are large and darkly stained (**B**). In NFP stain, these large cells are positively stained (**C,D**; **C** is the higher power view of the "*" region in **D**). Scale bar = 1,554 μm in D (applies to B,D).

the LOA (Fig. 11A). In sections immunostained for NFP, only the largest neurons are labeled (Fig. 11B). The SI does not display laminar organization, while the LOA has a clear but discontinuous layer 2 and one deep layer. In contrast, the Pir has a dark and continuous layer 2 and a less darkly stained layer 3.

Two other structures described previously only in non-human primates were identified as well, such as area prostriata (APro) and the basal interstitial nucleus of the cerebellum (Blcb). APro is a region located at the junction of the retrosplenial, post- and parasubiculum, posterior cingulate, and anterior–dorsal primary visual cortices. It has been described in detail in macaque monkey (Morecraft et al., 2000; Ding et al., 2003) and is important for fast procession of peripheral vision (Yu et al., 2012). Although its existence in the human brain was briefly described, its exact location and extent has not been reported in detail so far. Our mapping indicates that APro is much larger in human (Fig. 12) than in macaque monkey (Ding et al., 2003). The Blcb in the human brain is located deep to the medial interpositus nucleus (InPM; globose nucleus) of the cerebellum and consists of scattered large NFP-immunoractive neurons (Fig. 13).

Identifying anatomical landmarks in MRI data

Transposing the Nissl-based anatomical delineations into full 3D annotations registered to the accompanying MRI volume is challenging due to the incomplete and nonuniform sampling of those annotations. However, individual Nissl plates can be matched to corresponding planes of the MRI data to allow the identification of features of specific structures that can then be mapped onto MRI data from other brains without accompanying architecture-based delineations. The utility of this approach can be demonstrated in the case of the medial geniculate nucleus (MG) and the dorsal lateral geniculate nucleus (DLG). A comparison of the architecture-based atlas (Fig. 14A) and the corresponding MRI plate (Fig. 14B) from the same brain shows that the MG has high and the DLG low signal intensity. Combining these features with basic spatial topography, the MG and DLG in the MRI scans from other brains from the Allen Human Brain Atlas (Hawrylycz et al., 2012) are clearly discerned (Fig. 14C,D). The MG is so similar in signal intensity to the adjoining white matter (consistently high signal intensity in T1-weighted images) that it would probably be misidentified as white matter if the extracted feature (i.e., high signal intensity) was not used. With the topography of the histology-based parcellation as a guide, many fine structures can be similarly identified in MRI data that would otherwise be difficult to identify and discriminate, thus extending the value of this single brain atlas to the interpretation of neuroimaging data (Fig. 15).

Whole-brain histology-based atlas with corresponding MRI and DWI

The complete set of histology-based atlas plates is presented in Figures 16 and 17. These include a plate locator (Fig. 16) marking the A-P sampling locations of all 106 annotated atlas plates and selected corresponding Nissl-

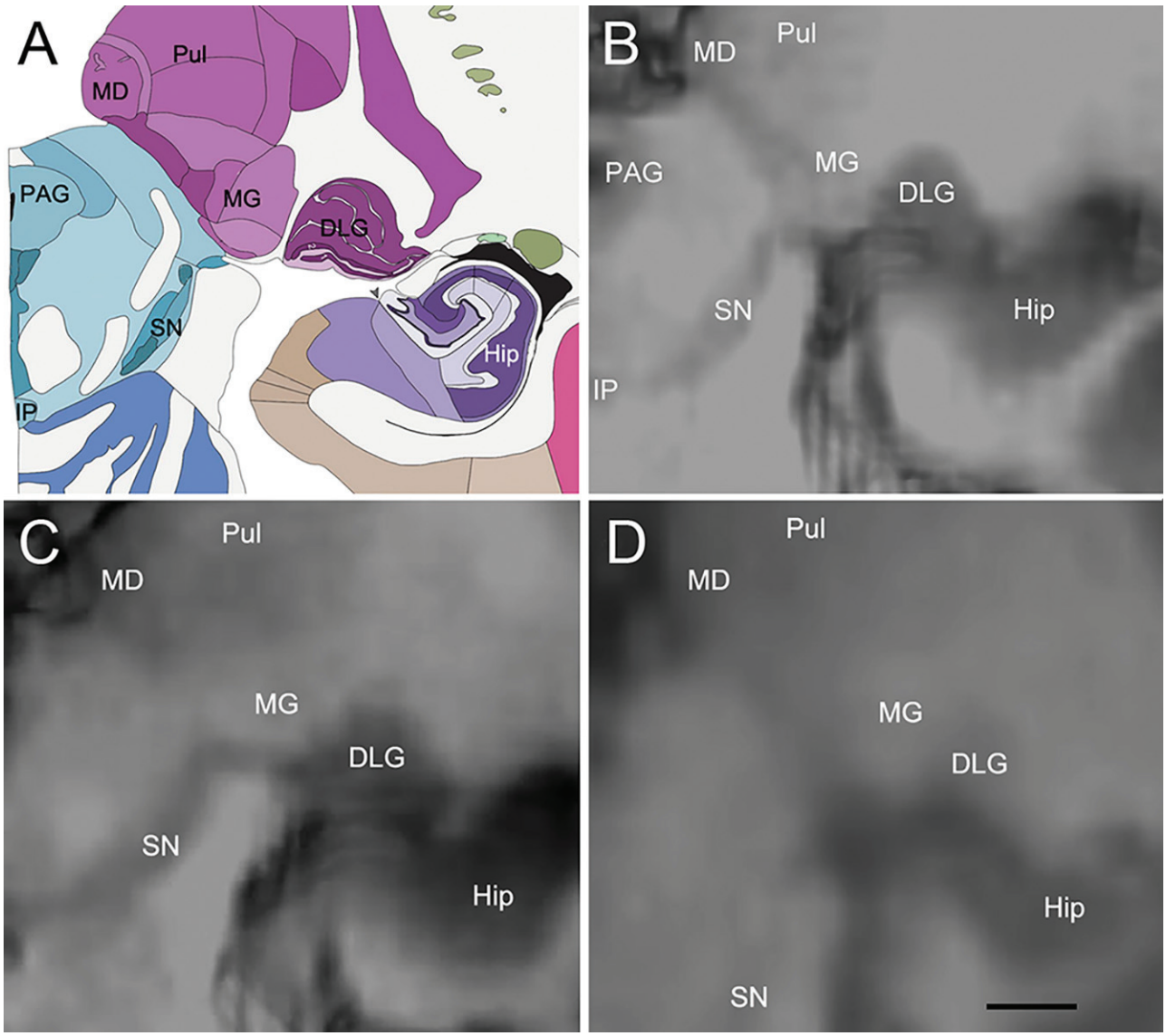

Figure 14. Identification of fine anatomical features in same-brain MRI and transfer to other brain MRI data. **A**: Reference atlas plate showing subdivisions of the medial geniculate nucleus (MG), dorsal lateral geniculate nucleus (DLG), and adjoining regions. **B**: Identification of the MG and DLG on the ex vivo MRI scan from the same brain by comparison with the corresponding reference plate based on subtle differences between MRI signal intensity of the MG and DLG and neighboring white and gray matter. The majority of the image contrast comes from T2* weighting and the contrast has been inverted. **C,D**: Identification of the MG and DLG on the MRI scans (T1 images) from other brains in the Allen Human Brain Atlas without histological stains using the extracted features of MG (bright) and DLG (dark) signal intensity at the same sectioning plane as the atlas. Hip, hippocampus; IP, interpeduncular nucleus; MD, mediodorsal thalamic nucleus; PAG, periaqueductal gray; Pul, pulvinar; SN, substantia nigra. Scale bar = 5,160 μm in D (applies to B–D).

stained and adjacent NFP and PV immunohistological plates (Fig. 17). To translate the atlas structural delineations onto the MRI dataset, a set of 76 coronal MRI slices at 2-mm intervals (Fig. 18) from the same hemisphere was selected and annotated (Fig. 19, left column). Macroscopic landmarks such as cortical sulci and gyri were used as guides to match histological and MRI planes of section, and local topography was used (e.g. see Figs. 14, 15) to label identifiable structures including all neocortical areas and major subcortical regions.

Some well-known white matter tracts such as the optic radiation ("or" in Fig. 19, levels 42–69) and auditory radiation ("ar") are clearly visible in the 7 T MRI images and can be clearly followed for a long distance due to their darker appearance than the surrounding white matter. Interestingly, a corresponding part of the somatosensory radiation (named here the "sr") is also clearly visible (Fig. 19, levels 38–46). The "sr" is normally treated as part of the superior radiation in the literature and mainly originates from the ventroposterior lateral nucleus of the

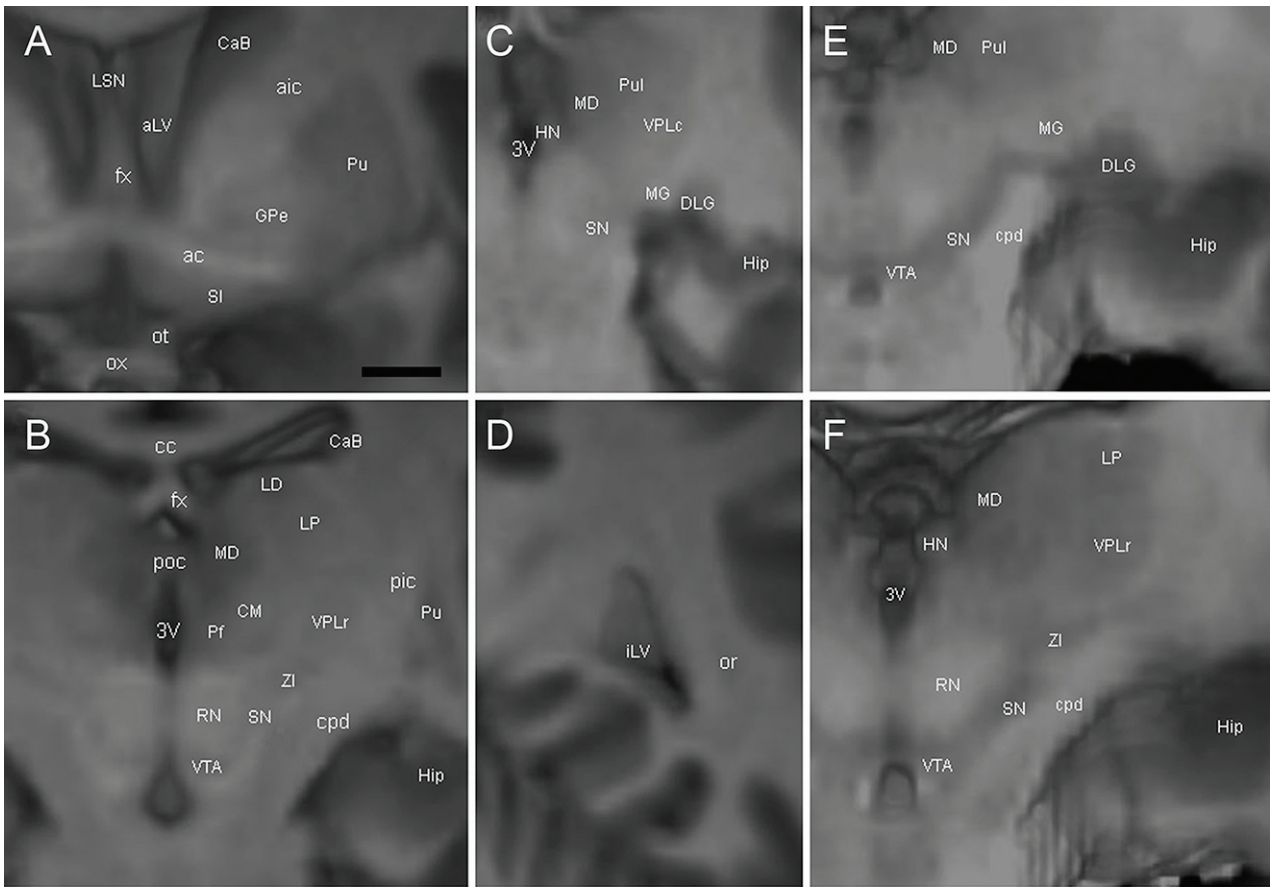

Figure 15. Structure identification on MRI of other brains. **A–D**: Identification of structures on T1-weighted MRI scans from case H0351.2002 of the Allen Human Brain Atlas (http://human.brain-map.org). By virtue of anatomical features extracted from this reference atlas (see Fig. 14), structures such as Pu, GPe (**A**), MD, RN, SN, ZI (**B**), Pul, MG, DLG (**C**), and "or" (optic radiation, **D**) are consistently identified. **E,F**: Pul, MG, DLG, SN, RN, ZI, and other structures were also confirmed in a T1-weighted MRI dataset from another case (H0351.2001). For abbreviations see the ontology in Table 3. Scale bar = 5,160 μm in A (applies to A–F).

thalamus and targets the primary somatosensory cortex. In this 7 T MRI dataset, like the "or" and "ar," the "sr" is observed to stand out from surrounding white matter and thus deserves an independent term (i.e., somatosensory radiation) as do optic and auditory radiations.

Finally, color-coded orientation maps and tractography maps of both hemispheres from the same brain are also available and are presented in Figure 19 (right column). By comparison with the accompanying MRI plates, some white matter fiber tracts can be identified. For example, at level 40 of Figure 19, the callosal and cingulate bundles, superior longitudinal fasciculus (slf-m, slf-l, and slf-l), and somatosensory radiation can be easily localized with the guide of the annotated MRI atlas.

For convenience Figures 16-19 are presented, together with Table 3, after the literature list at the end of the paper.

DISCUSSION

Brain reference atlases are essential resources for neuroscience research, serving to identify and annotate the complex anatomical architecture of the brain and allow communication across laboratories and various research disciplines attempting to link structure to function (Fischl et al., 1999; Toga et al., 2006; Amunts et al., 2007; Evans et al., 2012). Ideally, modern digital atlases should comprise 3D reference frameworks with comprehensive anatomical coverage and cellular resolution cyto- and chemoarchitectural histology-based structural annotation using hierarchical ontologies, and correlated histological and neuroimaging data (Toga et al., 2006; Destrieux et al., 2010; Evans et al., 2012; Caspers et al., 2013a). All currently available human brain reference atlases lack some of these features

(see Table 1), mainly due to the large size and structural complexity of the human brain and the resource-intensive and technology-limiting nature of the endeavor (Amunts et al., 2013). We sought to fill this gap by generating a fully annotated, high-resolution anatomical reference atlas for a complete adult female human brain as an open access community resource. The atlas consists of brain-wide neuroimaging (MRI, DWI) and histological data (Nissl, NFP, PV) based on whole-hemisphere serial sectioning, staining, and true cellular resolution imaging. Most importantly, the atlas is comprehensively annotated using a unified hierarchical structural ontology based on combined cyto- and chemoarchitectural parcellation of 862 gray matter and white matter structures. A freely accessible online atlas browser was created to allow easy visualization and navigation, and the resource is integrated with other human brain cellular resolution gene expression and transcriptomic atlases (Hawrylycz et al., 2012; Miller et al., 2014).

Parcellation of the human neocortex presents a particular challenge, as several different schemes based on cortical gyri and sulci or histological delineation are in common usage (Brodmann, 1909; Talairach and Tournoux, 1988; Fischl et al., 2004; Duvernoy, 1999; Damasio, 2005; Mai et al., 2008; Destrieux et al., 2010; Petrides, 2012), and the relationship between cortical geometry and architectonic identity is variable across the cortex (Fischl et al., 2008). To serve both communities, we chose to perform multiple annotations of the same dataset. The first is based on macroscopic annotation of gyri and sulci, while the second is based on microscopic analysis of combined cyto- and chemoarchitectural data to create a modified Brodmann parcellation. This unique human dataset of interleaved Nissl staining, and NFP and PV immunolabeling in a whole hemisphere, allowed a complete parcellation based on variations in overall cell density, NFP immunolabeling of subsets of long-range excitatory projection neurons, and PV-expressing neurons and neuropil. In many cases this parcellation agrees with those generated using other techniques such as receptor autoradiography and Nissl-based gray-level indices (Zilles and Amunts, 2009; Amunts et al., 2010; Vogt et al., 2013). For example, the inferior parietal lobule has been consistently divided into three basic regions based on cellular and receptor architecture (Caspers et al., 2013b), and our analysis of cyto- and chemoarchitecture corroborates this tripartite delineation (albeit with a different nomenclature). In many other cases these data allowed a detailed parcellation of regions that had not yet been examined in detail by others, such as the area prostriata and other structures described above. In principle, this dataset could be reannotated by other researchers to provide alternate interpretations. Finally, this dataset could be aligned to new functional parcellations based on neuroimaging data, such as a recent analyses from the Human Brainnetome Atlas (Fan et al., 2016) and the Human Connectome Project (www.humanconnectome.org; Glasser et al., 2016), opening up new possibilities for linking cytoarchitecture and function at microscopic and macroscopic scales.

There is a fundamental schism between probabilistic reference atlases used in neuroimaging (Hammers et al., 2003; Ahsan et al., 2007; Scheperjans et al., 2008; Shattuck et al., 2008; Diedrichsen et al., 2009; Kuklisova-Murgasova et al., 2011), based on thousands of individuals, and detailed histological reference atlases based on exhaustive analysis and annotation of single representative brain specimens (Brodmann, 1909; von Economo and Koskinas, 1925; Sarkisov et al., 1955). It is not currently possible to analyze large numbers of whole brains histologically and thus build a probabilistic histological atlas, although strong efforts are under way to move in the direction of generating probabilistic histological reference atlases using standard histological (JuBrain; Caspers et al., 2013a) as well as novel imaging techniques (Magnain et al., 2014, 2015; Wang et al., 2014; Zilles et al., 2016). Furthermore, human brains exhibit a remarkable amount of interindividual variability, particularly in the gyri and sulci of the cerebral cortex (Mazziotta et al., 2001; Uylings et al., 2005; Toga et al., 2006; Amunts et al., 2007; Ding and Van Hoesen, 2010; Zilles and Amunts, 2010, 2013). For instance, one brain may have area 35 located in the medial bank of a deep collateral sulcus (CoS), while another may have its area 35 in the lateral bank of a shallow CoS, or even the crown of the anterior fusiform gyrus (Ding and Van Hoesen, 2010). Thus it is not realistically meaningful to map histological annotations from a single specimen directly into a probabilistic reference space, even with advances in techniques for deformable registration. On the other hand, the current generation of both MRI and DWI data in the same specimen as the histological data allows the direct correlation of cytoarchitectural features with MRI features or landmarks. As we demonstrate, this dataset may thus allow feature extraction that can be applied to other brains to identify fine anatomical structures not otherwise identifiable, especially when higher resolution imaging techniques such as 9.4-Tesla MRI, optical coherence tomography, and polarized light microscopy become available (Fatterpekar et al., 2002; Magnain et al., 2015; Zilles et al., 2016).

In summary, we have created a cellular resolution, comprehensively annotated atlas for an entire adult human brain hemisphere (Fig. 17) based on a combined

analysis of cyto- and chemoarchitectures and modern literature. This combination of anatomic completeness, multimodal histological cellular-resolution imaging, modified Brodmann's areas delineations in neocortex, neuroimaging (Fig. 19), and intuitive digital interactivity provides an advance over other current large-scale human brain atlases. This versatile and publicly accessible resource gives a range of users a means to learn, teach, and investigate human brain structure and function, including the diagnosis and treatment of brain disease.

ACKNOWLEDGMENTS

We thank the Allen Institute founders, P.G. Allen and J. Allen, for their vision, encouragement, and support. We acknowledge NeuroScience Associates (Knoxville, TN) for sectioning and staining the human tissues. We are also grateful for the technical support of the staff members in the Allen Institute who are not part of the authorship of this paper. We thank Ling Li, M.D. (Office of the Chief Medical Examiner, Baltimore, Maryland) for assistance with obtaining the brain specimen used for the atlas. We acknowledge Gulgun Sengul for her comments on the brainstem part of the ontology, and Dan Fong and Gary Davis (Nikon USA) for their assistance with microscope customization. This work's contents are solely the responsibility of the authors and do not necessarily represent the official views of the National Institutes of Health and the National Institute of Mental Health.

CONFLICT OF INTEREST

B.F. has a financial interest in CorticoMetrics, a company whose medical pursuits focus on brain imaging and measurement technologies. B.F.'s interests were reviewed and are managed by Massachusetts General Hospital and Partners HealthCare in accordance with their conflict of interest policies. The authors declare no competing financial interests.

ROLE OF AUTHORS

All authors had full access to all the data in the study and take full responsibility for the integrity of the data and the accuracy of the data analysis. ESL, S-LD, JRR, and BACF contributed significantly to the atlas design; S-LD generated the anatomic ontology, analyzed the cyto- and chemoarchitectural and MRI data, and delineated anatomical boundaries; JRR, BACF, PL, and BM performed the cartography and quality control; SMS managed the project, and tissue sectioning and staining via NeuroScience Associates; S-LD, SMS, and JRR quality-controlled the stained sections; AB and ND contributed to methods development; TB, AS, LT, AVDK, AV, MW, LZ, and BF contributed to MR and DWI imaging; AG-B and RAD linked this atlas to human brain gene expression datasets; RAD, ES, ZLR, and HRZ contributed to the processing of the human specimen; SC, JN, DS, and MR provided technical support; LN, TAD, and CD managed the creation of the data pipeline, visualization, and mining tools; LN, AS, and CD conducted informatics data processing and online database development; JGH managed the annotation team; ESL, MJH, JGH, AB, CD, PW, JAK, NS, JWP, PRH, CK, and ARJ contributed to the overall project design; ESL and MJH conceived the project, and the manuscript was written by S-LD and ESL with input from BF, PRH, JGH, MJH, and JRR.

LITERATURE CITED

Ahsan RL, Allom R, Gousias IS, Habib H, Turkheimer FE, Free S, Lemieux L, Myers R, Duncan JS, Brooks DJ, Koepp MJ, Hammers A. 2007. Volumes, spatial extents and a probabilistic atlas of the human basal ganglia and thalamus. NeuroImage 38:261-270.

Amunts K, Schleicher A, Zilles K. 2007. Cytoarchitecture of the cerebral cortex–more than localization. NeuroImage 37:1061–1065; discussion 1066–1068.

Amunts K, Lenzen M, Friederici AD, Schleicher A, Morosan P, Palomero-Gallagher N, Zilles K. 2010. Broca's region: novel organizational principles and multiple receptor mapping. PLoS Biol 8:9.

Amunts K, Lepage C, Borgeat L, Mohlberg H, Dickscheid T, Rousseau ME, Bludau S, Bazin PL, Lewis LB, Oros-Peusquens AM, Shah NJ, Lippert T, Zilles K, Evans AC. 2013. BigBrain: an ultrahigh-resolution 3D human brain model. Science 340:1472–1475.

Amunts K, Hawrylycz MJ, Van Essen DC, Van Horn JD, Harel N, Poline JB, De Martino F, Bjaalie JG, Dehaene-Lambertz G, Dehaene S, Valdes-Sosa P, Thirion B, Zilles K, Hill SL, Abrams MB, Tass PA, Vanduffel W, Evans AC, Eickhoff SB. 2014. Interoperable atlases of the human brain. NeuroImage 99:525–532.

Annese J, Schenker-Ahmed NM, Bartsch H, Maechler P, Sheh C, Thomas N, Kayano J, Ghatan A, Bresler N, Frosch MP, Klaming R, Corkin S. 2014. Postmortem examination of patient H.M.'s brain based on histological sectioning and digital 3D reconstruction. Nat Commun 5:3122.

Augustinack JC, van der Kouwe AJ, Blackwell ML, Salat DH, Wiggins CJ, Frosch MP, Wiggins GC, Potthast A, Wald LL, Fischl BR. 2005. Detection of entorhinal layer II using 7 Tesla magnetic resonance imaging. Ann Neurol 57:489–494.

Augustinack JC, Helmer K, Huber KE, Kakunoori S, Zollei L, Fischl B. 2010. Direct visualization of the perforant pathway in the human brain with ex vivo diffusion tensor imaging. Front Hum Neurosci 4:42.

Augustinack JC, Huber KE, Postelnicu GM, Kakunoori S, Wang R, van der Kouwe AJ, Wald LL, Stein TD, Frosch MP, Fischl B. 2012. Entorhinal verrucae geometry is coincident and correlates with Alzheimer's lesions: a combined neuropathology and high-resolution ex vivo MRI analysis. Acta Neuropathol 123:85–96.

Augustinack JC, Huber KE, Stevens AA, Roy M, Frosch MP, van der Kouwe AJ, Wald LL, Van Leemput K, McKee AC, Fischl B. 2013. Predicting the location of human perirhinal cortex, Brodmann's area 35, from MRI. NeuroImage 64:32–42.

Augustinack JC, Magnain C, Reuter M, van der Kouwe AJ, Boas D, Fischl B. 2014. MRI parcellation of ex vivo medial temporal lobe. NeuroImage 93:252–259.

Bauernfeind AL, de Sousa AA, Avasthi T, Dobson SD, Raghanti MA, Lewandowski AH, Zilles K, Semendeferi K, Allman JM, Craig AD, Hof PR, Sherwood CC. 2013. A volumetric comparison of the insular cortex and its subregions in primates. J Hum Evol 64:263–279.

Bonnici HM, Chadwick MJ, Kumaran D, Hassabis D, Weiskopf N, Maguire EA. 2012. Multi-voxel pattern analysis in human hippocampal subfields. Front Hum Neurosci 6:290.

Brodmann K. 1909. Localisation in the cerebral cortex (Translated and edited by L. J. Garey, 1994). London: Smith-Gordon.

Campbell MJ, Morrison JH. 1989. Monoclonal antibody to neurofilament protein (SMI-32) labels a subpopulation of pyramidal neurons in the human and monkey neocortex. J Comp Neurol 282:191–205.

Caspers S, Eickhoff SB, Zilles K, Amunts K. 2013a. Microstructural grey matter parcellation and its relevance for connectome analyses. NeuroImage 80:18–26.

Caspers S, Schleicher A, Bacha-Trams M, Palomero-Gallagher N, Amunts K, Zilles K. 2013b. Organization of the human inferior parietal lobule based on receptor architectonics. Cereb Cortex 23:615–628.

Celio MR, Baier W, Schärer L, de Viragh PA, Gerday C. 1988. Monoclonal antibodies directed against the calcium binding protein parvalbumin. Cell Calcium 9:81–86.

Damasio H. 2005. Human Brain Anatomy in Computerized Images (2nd Edition). New York: Oxford University Press.

Das S, Glatard T, MacIntyre LC, Madjar C, Rogers C, Rousseau ME, Rioux P, MacFarlane D, Mohades Z, Gnanasekaran R, Makowski C, Kostopoulos P, Adalat R, Khalili-Mahani N, Niso G, Moreau JT, Evans AC. 2016. The MNI data-sharing and processing ecosystem. NeuroImage 124:1188–1195.

De Olmos JS. 2004. Amygdala. In: Paxinos G, Mai JK, editors. The human nervous system (second edition). San Diego: Academic Press, pp. 739–868.

Destrieux C, Fischl B, Dale A, Halgren E. 2010. Automatic parcellation of human cortical gyri and sulci using standard anatomical nomenclature. NeuroImage 53:1–15.

Diedrichsen J, Balsters JH, Flavell J, Cussans E, Ramnani N. 2009. A probabilistic MR atlas of the human cerebellum. NeuroImage 46:39–46.

Ding SL. 2013. Comparative anatomy of the prosubiculum, subiculum, presubiculum, postsubiculum, and parasubiculum in human, monkey, and rodent. J Comp Neurol 521:4145–4162.

Ding SL. 2015. Detailed segmentation of human hippocampal and subicular subfields using a combined approach. Neurosci Commun 1:e948.

Ding SL, Van Hoesen GW. 2010. Borders, extent, and topography of human perirhinal cortex as revealed using multiple modern neuroanatomical and pathological markers. Hum Brain Mapp 31:1359–1379.

Ding SL, Van Hoesen GW. 2015. Organization and detailed parcellation of human hippocampal head and body regions based on a combined analysis of cyto- and chemoarchitecture. J Comp Neurol 523:2233–2253.

Ding SL, Morecraft RJ, Van Hoesen GW. 2003. Topography, cytoarchitecture, and cellular phenotypes of cortical areas that form the cingulo-parahippocampal isthmus and adjoining retrocalcarine areas in the monkey. J Comp Neurol 456:184–201.

Ding SL, Van Hoesen GW, Cassell MD, Poremba A. 2009. Parcellation of human temporal polar cortex: a combined analysis of multiple cytoarchitectonic, chemoarchitectonic, and pathological markers. J Comp Neurol 514:595–623.

Ding SL, Haber SN, Van Hoesen GW. 2010. Stratum radiatum of CA2 is an additional target of the perforant path in humans and monkeys. Neuroreport 21:245–249.

Duvernoy HM. 1999. The human brain: surface, blood supply, and three-dimensional anatomy, 2nd ed. New York: Springer.

Evans AC, Janke AL, Collins DL, Baillet S. 2012. Brain templates and atlases. NeuroImage 62:911–922.

Fan L, Li H, Zhuo J, Zhang Y, Wang J, Chen L, Yang Z, Chu C, Xie S, Laird AR, Fox PT, Eickhoff SB, Yu C, Jiang T. 2016. The Human Brainnetome Atlas: A new brain atlas based on connectional architecture. Cereb Cortex 26:3508–3526.

Fatterpekar GM, Naidich TP, Delman BN, Aguinaldo JG, Gultekin SH, Sherwood CC, Hof PR, Drayer BP, Fayad ZA. 2002. Cytoarchitecture of the human cerebral cortex: MR microscopy of excised specimens at 9.4 Tesla. AJNR Am J neuroradiol 23:1313–1321.

Fischl B, Sereno MI, Tootell RB, Dale AM. 1999. High-resolution intersubject averaging and a coordinate system for the cortical surface. Hum Brain Mapp 8: 272–284.

Fischl B, van der Kouwe A, Destrieux C, Halgren E, Segonne F, Salat DH, Busa E, Seidman LJ, Goldstein J, Kennedy D, Caviness V, Makris N, Rosen B, Dale AM. 2004. Automatically parcellating the human cerebral cortex. Cereb Cortex 14:11–22.

Fischl B, Rajendran N, Busa E, Augustinack J, Hinds O, Yeo BT, Mohlberg H, Amunts K, Zilles K. 2008. Cortical folding patterns and predicting cytoarchitecture. Cereb Cortex 18:1973–1980.

Fischl B, Stevens AA, Rajendran N, Yeo BT, Greve DN, Van Leemput K, Polimeni JR, Kakunoori S, Buckner RL, Pacheco J, Salat DH, Melcher J, Frosch MP, Hyman BT, Grant PE, Rosen BR, van der Kouwe AJ, Wiggins GC, Wald LL, Augustinack JC. 2009. Predicting the location of entorhinal cortex from MRI. NeuroImage 47:8–17.

García-Cabezas MA, Rico B, Sánchez-González MA, Cavada C. 2007. Distribution of the dopamine innervation in the macaque and human thalamus. Neuroimage 34:965–984.

Glasser MF, Coalson TS, Robinson EC, Hacker CD, Harwell J, Yacoub E, Ugurbil K, Andersson J, Beckmann CF, Jenkinson M, Smith SM, Van Essen DC. 2016. A multimodal parcellation of the human cerebral cortex. Nature 536:171–178.

Glover P, Bowtell R. 2009. Medical imaging: MRI rides the wave. Nature 457:971–972.

Goebel R, Muckli L, Kim D-S. 2012. Visual system.In: Mai JK, Paxinos G, editors. The human nervous system, 3rd ed. New York: Elsevier. p 1301–1327.

Hammers A, Allom R, Koepp MJ, Free SL, Myers R, Lemieux L, Mitchell TN, Brooks DJ, Duncan JS. 2003. Three-dimensional maximum probability atlas of the human brain, with particular reference to the temporal lobe. Hum Brain Mapp 19:224–247.

Hawrylycz MJ, Lein ES, Guillozet-Bongaarts AL, Shen EH, Ng L, Miller JA, van de Lagemaat LN, Smith KA, Ebbert A, Riley ZL, Abajian C, Beckmann CF, Bernard A, Bertagnolli D, Boe AF, Cartagena PM, Chakravarty MM, Chapin M, Chong J, Dalley RA, Daly BD, Dang C, Datta S, Dee N, Dolbeare TA, Faber V, Feng D, Fowler DR, Goldy J, Gregor BW, Haradon Z, Haynor DR, Hohmann JG, Horvath S, Howard RE, Jeromin A, Jochim JM, Kinnunen M, Lau C, Lazarz ET, Lee C, Lemon TA, Li L, Li Y, Morris JA, Overly CC, Parker PD, Parry SE, Reding M, Royall JJ, Schulkin J, Sequeira PA, Slaughterbeck CR, Smith SC,

Sodt AJ, Sunkin SM, Swanson BE, Vawter MP, Williams D, Wohnoutka P, Zielke HR, Geschwind DH, Hof PR, Smith SM, Koch C, Grant SG, Jones AR. 2012. An anatomically comprehensive atlas of the adult human brain transcriptome. Nature 489:391–399.

Hof PR, Mufson EJ, Morrison JH. 1995a. Human orbitofrontal cortex: cytoarchitecture and quantitative immunohistochemical parcellation. J Comp Neurol 359:48–68.

Hof PR, Nimchinsky EA, Morrison JH. 1995b. Neurochemical phenotype of corticocortical connections in the macaque monkey: quantitative analysis of a subset of neurofilament protein-immunoreactive projection neurons in frontal, parietal, temporal, and cingulate cortices. J Comp Neurol 362:109–133.

Hof PR, Glezer II, Condé F, Flagg RA, Rubin MB, Nimchinsky EA, Vogt Weisenhorn DM. 1999. Cellular distribution of the calcium-binding proteins parvalbumin, calbindin, and calretinin in the neocortex of mammals: phylogenetic and developmental patterns. J Chem Neuroanat 16:77–116.

Iglesias JE, Augustinack JC, Nguyen K, Player CM, Player A, Wright M, Roy N, Frosch MP, McKee AC, Wald LL, Fischl B, Van Leemput K. 2015. A computational atlas of the hippocampal formation using ex vivo, ultra-high resolution MRI: application to adaptive segmentation of in vivo MRI. NeuroImage 115:117–137.

Jenkinson M, Smith S. 2001. A global optimisation method for robust affine registration of brain images. Med Image Anal 5:143–156.

Jones EG. 2007. The thalamus. Cambridge: Cambridge University Press.

Kuklisova-Murgasova M, Aljabar P, Srinivasan L, Counsell SJ, Doria V, Serag A, Gousias IS, Boardman JP, Rutherford MA, Edwards AD, Hajnal JV, Rueckert D. 2011. A dynamic 4D probabilistic atlas of the developing brain. NeuroImage 54:2750–2763.

Lein ES, Hawrylycz MJ, Ao N, Ayres M, Bensinger A, Bernard A, Boe AF, Boguski MS, Brockway KS, Byrnes EJ, Chen L, Chen L, Chen TM, Chin MC, Chong J, Crook BE, Czaplinska A, Dang CN, Datta S, Dee NR, Desaki AL, Desta T, Diep E, Dolbeare TA, Donelan MJ, Dong HW, Dougherty JG, Duncan BJ, Ebbert AJ, Eichele G, Estin LK, Faber C, Facer BA, Fields R, Fischer SR, Fliss TP, Frensley C, Gates SN, Glattfelder KJ, Halverson KR, Hart MR, Hohmann JG, Howell MP, Jeung DP, Johnson RA, Karr PT, Kawal R, Kidney JM, Knapik RH, Kuan CL, Lake JH, Laramee AR, Larsen KD, Lau C, Lemon TA, Liang AJ, Liu Y, Luong LT, Michaels J, Morgan JJ, Morgan RJ, Mortrud MT, Mosqueda NF, Ng LL, Ng R, Orta GJ, Overly CC, Pak TH, Parry SE, Pathak SD, Pearson OC, Puchalski RB, Riley ZL, Rockett HR, Rowland SA, Royall JJ, Ruiz MJ, Sarno NR, Schaffnit K, Shapovalova NV, Sivisay T, Slaughterbeck CR, Smith SC, Smith KA, Smith BI, Sodt AJ, Stewart NN, Stumpf KR, Sunkin SM, Sutram M, Tam A, Teemer CD, Thaller C, Thompson CL, Varnam LR, Visel A, Whitlock RM, Wohnoutka PE, Wolkey CK, Wong VY, Wood M, Yaylaoglu MB, Young RC, Youngstrom BL, Yuan XF, Zhang B, Zwingman TA, Jones AR. 2007. Genome-wide atlas of gene expression in the adult mouse brain. Nature 445:168–176.

Magnain C, Augustinack JC, Reuter M, Wachinger C, Frosch MP, Ragan T, Akkin T, Wedeen VJ, Boas DA, Fischl B. 2014. Blockface histology with optical coherence tomography: a comparison with Nissl staining. NeuroImage 84: 524–533.

Magnain C, Augustinack JC, Konukoglu E, Frosch MP, Sakadzic S, Varjabedian A, Garcia N, Wedeen VJ, Boas DA, Fischl B. 2015. Optical coherence tomography visualizes neurons in human entorhinal cortex. Neurophotonics 2:015004.

Mai JK, Paxinos G, Voss T. 2008. Atlas of the human brain, 3rd ed. New York: Elsevier Science.

Mazziotta J, Toga A, Evans A, Fox P, Lancaster J, Zilles K, Woods R, Paus T, Simpson G, Pike B, Holmes C, Collins L, Thompson P, MacDonald D, Iacoboni M, Schormann T, Amunts K, Palomero-Gallagher N, Geyer S, Parsons L, Narr K, Kabani N, Le Goualher G, Boomsma D, Cannon T, Kawashima R, Mazoyer B. 2001. A probabilistic atlas and reference system for the human brain: International Consortium for Brain Mapping (ICBM). Phil Trans R Soc Lond Ser B Biol Sci 356:1293–1322.

Miller JA, Ding SL, Sunkin SM, Smith KA, Ng L, Szafer A, Ebbert A, Riley ZL, Royall JJ, Aiona K, Arnold JM, Bennet C, Bertagnolli D, Brouner K, Butler S, Caldejon S, Carey A, Cuhaciyan C, Dalley RA, Dee N, Dolbeare TA, Facer BA, Feng D, Fliss TP, Gee G, Goldy J, Gourley L, Gregor BW, Gu G, Howard RE, Jochim JM, Kuan CL, Lau C, Lee CK, Lee F, Lemon TA, Lesnar P, McMurray B, Mastan N, Mosqueda N, Naluai-Cecchini T, Ngo NK, Nyhus J, Oldre A, Olson E, Parente J, Parker PD, Parry SE, Stevens A, Pletikos M, Reding M, Roll K, Sandman D, Sarreal M, Shapouri S, Shapovalova NV, Shen EH, Sjoquist N, Slaughterbeck CR, Smith M, Sodt AJ, Williams D, Zollei L, Fischl B, Gerstein MB, Geschwind DH, Glass IA, Hawrylycz MJ, Hevner RF, Huang H, Jones AR, Knowles JA, Levitt P, Phillips JW, Sestan N, Wohnoutka P, Dang C, Bernard A, Hohmann JG, Lein ES. 2014. Transcriptional landscape of the prenatal human brain. Nature 508:199–206.

Miller KL, McNab JA, Jbabdi S, Douaud G. 2012. Diffusion tractography of post-mortem human brains: optimization and comparison of spin echo and steady-state free precession techniques. Neuroimage 59:2284–2297.

Morecraft RJ, Rockland KS, Van Hoesen GW. 2000. Localization of area prostriata and its projection to the cingulate motor cortex in the rhesus monkey. Cereb Cortex 10: 192–203.

Morel A. 2007. Stereotactic atlas of the human thalamus and basal ganglia. New York: Informa Healthcare USA.

Morel A, Gallay MN, Baechler A, Wyss M, Gallay DS. 2013. The human insula: architectonic organization and postmortem MRI registration. Neuroscience 236:117–135.

Mori S, Crain BJ, Chacko VP, van Zijl PC. 1999. Three-dimensional tracking of axonal projections in the brain by magnetic resonance imaging. Ann Neurol 45:265–269.

Naidich TP, Duvernoy HM, Delman BN, Sorensen AG, Kollias SS, Haacke EM. 2008. Duvernoy's atlas of the human brain stem and cerebellum: high-field MRI, surface anatomy, internal structure, vascularization and 3D sectional anatomy. Vienna: Springer.

Nimchinsky EA, Vogt BA, Morrison JH, Hof PR. 1997. Neurofilament and calcium-binding proteins in the human cingulate cortex. J Comp Neurol 384:597–620.

Nowinski WL, Chua BC. 2013. Bridging neuroanatomy, neuroradiology and neurology: three-dimensional interactive atlas of neurological disorders. Neurorad J 26:252–262.

Öngür D, Ferry AT, Price JL. 2003. Architectonic subdivision of the human orbital and medial prefrontal cortex. J Comp Neurol 460:425–449.

Papp EA, Leergaard TB, Calabrese E, Johnson GA, Bjaalie JG. 2014. Waxholm space atlas of the Sprague Dawley rat brain. NeuroImage 97:374–386.

Pascual B, Masdeu JC, Hollenbeck M, Makris N, Insausti R, Ding SL, Dickerson BC. 2015. Large-scale brain networks of the human left temporal pole: a functional connectivity MRI study. Cereb Cortex 25:680–702.

Paxinos G, Huang XF, Sengul G, Watson C. 2012. Organization of human brainstem nuclei. In: Mai JK, Paxinos G, editors. The human nervous system, 3rd ed, New York: Elsevier. p 260–327.

Petrides M. 2012. The human cerebral cortex: an MRI atlas of the sulci and gyri in MNI stereotaxic space. New York: Elsevier.

Petrides M, Pandya DN. 2012. The frontal cortex.In: Mai JK, Paxinos G, editors. The human nervous system, 3rd ed. New York: Elsevier. p 988–1111.

Roemer PB, Edelstein WA, Hayes CE, Souza SP, Mueller OM. 1990. The NMR phased array. Magn Reson Med 16: 192–225.

Saleem KS, Logothetis NK. 2012. A combined MRI and histology atlas of the rhesus monkey brain in stereotaxic coordinates, 2nd ed. San Diego: Academic Press.

Sarkisov SA, Filimonoff IN, Kononowa EP, Preobraschenskaja IS, Kukuew LA. 1955. Atlas of the cytoarchitectonics of the human cerebral cortex. Moscow: Medgiz.

Scheperjans F, Eickhoff SB, Homke L, Mohlberg H, Hermann K, Amunts K, Zilles K. 2008. Probabilistic maps, morphometry, and variability of cytoarchitectonic areas in the human superior parietal cortex. Cereb Cortex 18: 2141–2157.

Shattuck DW, Mirza M, Adisetiyo V, Hojatkashani C, Salamon G, Narr KL, Poldrack RA, Bilder RM, Toga AW. 2008. Construction of a 3D probabilistic atlas of human cortical structures. NeuroImage 39:1064–1080.

Simić G, Hof PR. 2015. In search of the definitive Brodmann's map of cortical areas in human. J Comp Neurol 523:5–14.

Sternberger LA, Sternberger NH. 1983. Monoclonal antibodies distinguish phosphorylated and non-phosphorylated forms of neurofilaments in situ. Proc Natl Acad Sci U S A 80:6126–6130.

Talairach J, Tournoux P. 1988. Co-planar stereotaxic atlas of the human brain. New York: Thieme Medical Publishers.

Toga AW, Thompson PM, Mori S, Amunts K, Zilles K. 2006. Towards multimodal atlases of the human brain. Nat Rev Neurosci 7:952–966.

Uylings HB, Rajkowska G, Sanz-Arigita E, Amunts K, Zilles K. 2005. Consequences of large interindividual variability for human brain atlases: converging macroscopical imaging and microscopical neuroanatomy. Anat Embryol 210: 423–431.

Van Essen DC, Lewis JW, Drury HA, Hadjikhani N, Tootell RB, Bakircioglu M, Miller MI. 2001. Mapping visual cortex in monkeys and humans using surface-based atlases. Vision Res 41:1359–1378.

Vogt BA, Palomero-Gallagher N. 2012. Cingulate cortex.In: Mai JK, Paxinos G, editors. The human nervous system, 3rd ed. New York: Elsevier. p 943–987.

Vogt BA, Nimchinsky EA, Vogt LJ, Hof PR. 1995. Human cingulate cortex: surface features, flat maps, and cytoarchitecture. J Comp Neurol 359:490–506.

Vogt BA, Vogt LJ, Perl DP, Hof PR. 2001. Cytology of human caudomedial cingulate, retrosplenial, and caudal parahippocampal cortices. J Comp Neurol 438:353–376.

Vogt BA, Hof PR, Zilles K, Vogt LJ, Herold C, Palomero-Gallagher N. 2013. Cingulate area 32 homologies in mouse, rat, macaque and human: cytoarchitecture and receptor architecture. J Comp Neurol 521:4189–4204.

von Economo C. 1927. L'architecture cellulaire normale de l'écorce cérébrale. Paris, Masson.

von Economo C, Koskinas GN. 1925. Die Cytoarchitektonik der Hirnrinde des erwachsenen Menschen. Berlin: Springer.

Wang H, Zhu J, Reuter M, Vinke LN, Yendiki A, Boas DA, Fischl B, Akkin T. 2014. Cross-validation of serial optical coherence scanning and diffusion tensor imaging: a study on neural fiber maps in human medulla oblongata. NeuroImage 100:395–404.

Wang R, Benner T, Soresen AG, Wedeen VJ. 2007. Diffusion Toolkit: a software package for diffusion imaging data processing and tractograpy. Proceedings of 15th Annual Meeting of International Society for Magnetic Resonance in Medicine, p 3720.

Wright SM, Wald LL. 1997. Theory and application of array coils in MR spectroscopy. NMR Biomed 10:394–410.

Yu HH, Chaplin TA, Davies AJ, Verma R, Rosa MG. 2012. A specialized area in limbic cortex for fast analysis of peripheral vision. Curr Biol 22:1351–1357.

Zilles K, Amunts K. 2009. Receptor mapping: architecture of the human cerebral cortex. Curr Opin Neurol 22:331–339.

Zilles K, Amunts K. 2010. Centenary of Brodmann's map—conception and fate. Nat Rev Neurosci 11:139–145.

Zilles K, Amunts K. 2013. Individual variability is not noise. Trends Cogn Sci 17:153–155.

Zilles K, Palomero-Gallagher N, Gräßel D, Schlömer P, Cremer M, Woods R, Amunts K, Axer M. 2016. High-resolution fiber and fiber tract imaging using polarized light microscopy in the human, monkey, rat, and mouse brain.In: Rockland KS, editor. Axons and brain architecture. San Diego, CA: Elsevier. p 369–389.

TABLE 3.

Whole Brain Structure Ontology and Abbreviations

Acronym	col	Brain structures and their parent-daughter relationship
NT		neural tube
Br		brain
F		forebrain (prosencephalon)
FGM		gray matter of forebrain
Tel		telencephalon
Cx		cerebral cortex
NCx		neocortex (isocortex)
FCx		frontal neocortex
PFC		prefrontal cortex
A10		frontal polar cortex (area 10)
A10m		medial subdivision of area 10
A10l		lateral subdivision of area 10
A10o		orbital subdivision of area 10
DFC		dorsolateral prefrontal cortex
A8		caudal portion of DFC (area 8, area FC)
A8ld		laterodorsal subdivision of area 8
A8lv		lateroventral subdivision of area 8
A8m		medial subdivision of area 8
A9		rostrodorsal portion of DFC (area 9)
A9l		lateral subdivision of area 9
A9m		medial subdivision of area 9
A9/46		intermediate portion of DFC (area 9/46)
A9/46d		dorsal subdivision of A9/46
A9/46v		ventral subdivision of A9/46
A46		rostroventral portion of DFC (area 46)
A46d		dorsal subdivision of area 46
A46v		ventral subdivision of area 46
VFC		ventrolateral prefrontal cortex (Broca's area)
A44		caudal portion of VFC (area 44)
A44d		dorsal subdivision of area 44
A44v		ventral subdivision of area 44
A44op		opercular subdivision of area 44
A45		rostral portion of VFC (area 45)
A45r		rostral subdivision of A45
A45c		caudal subdivision of A45
A45op		opercular subdivision of A45
OFC		orbital frontal cortex
OFCm		medial orbital frontal cortex (area 14)
A14r		rostral subdivision of area 14
A14c		caudal subdivision of area 14
OFCi		intermediate orbital frontal cortex
A11		rostral division of OFCi (area 11)

TABLE 3. *Continued*

A11m		medial subdivision of area 11
A11l		lateral subdivision of area 11
A13		caudal division of OFCi (area 13)
A13m		medial subdivision of area 13
A13l		lateral subdivision of area 13
OFCl		lateral orbital frontal cortex (area 12/47)
A12/47m		medial subdivision of area 12/47
A12/47l		lateral subdivision of area 12/47
PoFC		posterior frontal cortex (motor cortex)
M1C (A4)		primary motor cortex (area M1, area 4, area FA)
PMC		premotor cortex (area 6, area FB)
A6ld		laterodorsal subdivision of area 6
A6lv		lateroventral subdivision of area 6
A6m		medial subdivision of area 6 (area MII)
A6/32		area 6/32
PCx		parietal neocortex
S1C (A3,1,2)		primary somatosensory cortex (area S1, areas 3,1,2)
ScC (A43)		subcentral cortex (gustatory cortex, area 43)
PoPC		posterior parietal cortex
SPC		posterodorsal (superior) parietal cortex
A5		rostral division of SPC (area 5)
A5ci		cingulate subdivision of area 5
A5l		lateral subdivision of area 5
A5m		medial subdivision of area 5
A7		caudal division of SPC (area 7, area PE)
A7r		rostral subdivision of area 7
A7m		medial subdivision of area 7
A7c		caudal subdivision of area 7
A7pc		postcentral subdivision of area 7
A7ip		intraparietal subdivision of area 7 (A7ip)
A7ipr		area 7ip, rostral part (A7ipr)
A7ipc		area 7ip, caudal part (A7ipc)
IPC		posteroventral (inferior) parietal cortex
A40		rostral division of IPC (area 40, area PF)
A40rd		rostrodorsal subdivision of area 40
A40rv		rostroventral subdivision of area 40
A40in		inferior subdivision of area 40
A40/39		intermediate division of IPC (area 40/39, area PFG)
A40/39r		rostral subdivision of area 40/39
A40/39c		caudal subdivision of area 40/39
A39		caudal division of IPC (area 39, area PG)
A39r		rostral subdivision of area 39
A39c		caudal subdivision of area 39
RI		retroinsular cortex
TCx		temporal neocortex
DLTC		dorsolateral temporal neocortex
A1C		primary auditory cortex (core)

TABLE 3. *Continued*

A41	main portion of A1C (area TC, area 41)
A1Cr	rostral portion of A1C
A42	secondary auditory cortex (belt, area 42, area TB)
SLTC	superolateral temporal cortex
ASTC (A22r)	anterior (rostral) superior temporal cortex (area 22r)
ISTC (A22i)	intermediate superior temporal cortex (area 22i)
STC (A22c)	posterior (caudal) superior temporal cortex (area 22c)
PSTC (A22p)	polysensory temporal cortex (area 22p)
A22pr	rostral division of 22p (area 22pr)
A22pi	intermediate division of 22p (area 22pi)
A22pc	caudal division of 22p (area 22pc)
PI	parainsular cortex (area 52)
VLTC	ventrolateral temporal neocortex
MTC (A21)	midlateral temporal cortex (area TEd, area 21)
A21r	rostral subdivision of area 21
A21i	intermediate subdivision of area 21
A21c	caudal subdivision of area 21
ITC (A20)	inferolateral temporal cortex (area TEv, area 20)
A20r	rostral subdivision of area 20
A20i	intermediate subdivision of area 20
A20c	caudal subdivision of area 20
MITC	midinferior (fusiform) temporal cortex
A36	rostral division of MITC (area 36)
A36r	rostral subdivision of area 36
A36c	caudal subdivision of area 36
TF	caudal division of MITC (area TF)
PPHC	posterior parahippocampal cortex
TH	medial division of PPHC (area TH)
TL	lateral division of PPHC (area TL)
TFO	medial temporal-occipital cortex (area TFO)
TFO-m	area TFO, medial part
TFO-l	area TFO, lateral part (fusiform face area)
A37	lateral temporal-occipital cortex (area 37)
A38	temporal polar cortex (area TG, area 38)
V5/MT	area V5 (mid temporal area)
Ocx	occipital neocortex
Pro	area prostriata
V1C	primary visual cortex (striate cortex, area V1/17, area OC)
ESOC	extrastriate occipital cortex
Vx	area x of visual cortex
V2 (A18)	parastriate cortex (area V2, area 18, area OB)
PSC (A19)	peristriate cortex (area 19, area OA)
V3	area V3 of peristriate cortex
VP	area VP (V3V) of peristriate cortex
V3A	area V3A of peristriate cortex
V4D	area V4D of peristriate cortex
V4	area V4 of peristriate cortex

TABLE 3. *Continued*

V3B		area V3B of peristriate cortex
V6		area V6 of peristriate cortex
V6A/PO		area V6 of peristriate cortex (parieto-occipital area)
V7		area V7 of peristriate cortex
LO		lateral occipital area
ICx		insular neocortex
Idg		dysgranular insular cortex
RIdg		rostral dysgranular insular cortex
CIdg		caudal dysgranular insular cortex
Ig		granular insular cortex
RIg		rostral granular insular cortex
CIg		caudal granular insular cortex
CCx		cingulate neocortex
MFC (ACC)		anterior (rostral) cingulate cortex (ventromedial prefrontal cortex)
A24		ventral division of MFC (area 24, area LA)
A32		dorsorostral division of MFC (area 32)
A25		subgenual (subcallosal) division of MFC (area 25, area FL)
MCC		midcingulate cortex
A24mc		ventral division of MCC (area 24mc)
A32mc		dorsal division of MCC (area 32mc)
PCC		posterior (caudal) cingulate cortex
A23		ventral division of PCC (area 23, area LC2)
A31		dorsal division of PCC (area 31, area LC1)
PACx		periallocortex
PArCx		periarchicortex
A35		perirhinal cortex (area 35)
A35r		rostral subdivision of area 35
A35c		caudal subdivision of area 35
EC		entorhinal cortex
LEC		lateral (anterior) entorhinal cortex
EO		olfactory part of entorhinal cortex
ER		rostral part of entorhinal cortex
ELR		laterorostral part of entorhinal cortex
EMI		medial intermediate part of entorhinal cortex
MEC		medial (posterior) entorhinal cortex
ELI		lateral intermediate part of entorhinal cortex
Ec		caudal part of entorhinal cortex
ECL		caudal limiting part of entorhinal cortex
ELC		laterocaudal part of entorhinal cortex
PaS		parasubicular cortex (parasubiculum)
PaSb		proximal parasubiculum
PaSa		distal parasubiculum
PrS		presubicular cortex (presubiculum)
PrSr		rostral presubiculum
PrSc		caudal presubiculum (postsubiculum)
RSC		retrosplenial cortex
A29		area 29 of retrosplenial cortex

TABLE 3. *Continued*

A30		area 30 of retrosplenial cortex
PPCx		peripaleocortex
Iag		agranular insular cortex (area Iag)
FI		frontal agranular insular cortex (area FI)
TI		temporal agranular insular cortex (area TI)
ACx		allocortex
ArCx		archicortex
HIP		hippocampus (hippocampal formation)
DG		dentate area (dentate gyrus)
DGU		uncal dentate gyrus
DGUmo		molecular layer of uncal dentate gyrus
DGUgr		granular layer of uncal dentate gyrus
DGUsg		subgranular zone of uncal dentate gyrus
DGUpf		polymorphic layer of uncal dentate gyrus
DGR		rostral dentate gyrus
DGRmo		molecular layer of rostral dentate gyrus
DGRgr		granular layer of rostral dentate gyrus
DGRsg		subgranular zone of rostral dentate gyrus
DGRpf		polymorphic layer of rostral dentate gyrus
DGC		caudal dentate gyrus
DGCmo		molecular layer of caudal dentate gyrus
DGCgr		granular layer of caudal dentate gyrus
DGCsg		subgranular zone of caudal dentate gyrus
DGCpf		polymorphic layer of caudal dentate gyrus
Hipp		hippocampal proper
CA1		CA1 region of hippocampus
CA1U		uncal CA1
CA1Uslm		stratum lacunosum-moleculare of uncal CA1
CA1Usmo		stratum moleculare of uncal CA1
CA1Usla		stratum lacunosum of uncal CA1
CA1Usr		stratum radiatum of uncal CA1
CA1Usp		stratum pyramidale of uncal CA1
CA1Uso		stratum oriens of uncal CA1
CA1R		rostral CA1
CA1Rslm		stratum lacunosum-moleculare of rostral CA1
CA1Rsmo		stratum moleculare of rostral CA1
CA1Rsla		stratum lacunosum of rostral CA1
CA1Rsr		stratum radiatum of rostral CA1
CA1Rsp		stratum pyramidale of rostral CA1
CA1Rso		stratum oriens of rostral CA1
CA1C		caudal CA1
CA1Cslm		stratum lacunosum-moleculare of caudal CA1
CA1Csmo		stratum moleculare of caudal CA1
CA1Csla		stratum lacunosum of caudal CA1
CA1Csr		stratum radiatum of caudal CA1
CA1Csp		stratum pyramidale of caudal CA1
CA1Cso		stratum oriens of caudal CA1

TABLE 3. *Continued*

CA2		CA2 region of hippocampus
CA2U		uncal CA2
CA2Uslm		stratum lacunosum-moleculare of uncal CA2
CA2Usmo		stratum moleculare of uncal CA2
CA2Usla		stratum lacunosum of uncal CA2
CA2Usr		stratum radiatum of uncal CA2
CA2Usp		stratum pyramidale of uncal CA2
CA2Uso		stratum oriens of uncal CA2
CA2R		rostral CA2
CA2Rslm		stratum lacunosum-moleculare of rostral CA2
CA2Rsmo		stratum moleculare of rostral CA2
CA2Rsla		stratum lacunosum of rostral CA2
CA2Rsr		stratum radiatum of rostral CA2
CA2Rsp		stratum pyramidale of rostral CA2
CA2Rso		stratum oriens of rostral CA2
CA2C		caudal CA2
CA2Cslm		stratum lacunosum-moleculare of caudal CA2
CA2Csmo		stratum moleculare of caudal CA2
CA2Csla		stratum lacunosum of caudal CA2
CA2Csr		stratum radiatum of caudal CA2
CA2Csp		stratum pyramidale of caudal CA2
CA2Cso		stratum oriens of caudal CA2
CA3		CA3 region of hippocampus
CA3U		uncal CA3
CA3Uslm		stratum lacunosum-moleculare of uncal CA3
CA3Usmo		stratum moleculare of uncal CA3
CA3Usla		stratum lacunosum of uncal CA3
CA3Usr		stratum radiatum of uncal CA3
CA3Usl		stratum lucidum of uncal CA3
CA3Usp		stratum pyramidale of uncal CA3
CA3Uso		stratum oriens of uncal CA3
CA3R		rostral CA3
CA3Rslm		stratum lacunosum-moleculare of rostral CA3
CA3Rsmo		stratum moleculare of rostral CA3
CA3Rsla		stratum lacunosum of rostral CA3
CA3Rsr		stratum radiatum of rostral CA3
CA3Rsl		stratum lucidum of rostral CA3
CA3Rsp		stratum pyramidale of rostral CA3
CA3Rso		stratum oriens of rostral CA3
CA3C		caudal CA3
CA3Cslm		stratum lacunosum-moleculare of caudal CA3
CA3Csmo		stratum moleculare of caudal CA3
CA3Csla		stratum lacunosum of caudal CA3
CA3Csr		stratum radiatum of caudal CA3
CA3Csl		stratum lucidum of caudal CA3
CA3Csp		stratum pyramidale of caudal CA3
CA3Cso		stratum oriens of caudal CA3

TABLE 3. *Continued*

CA4	CA4 region of hippocampus
CA4Upy	pyramidal cells of uncal CA4
CA4Rpy	pyramidal cells of rostral CA4
CA4Cpy	pyramidal cells of caudal CA4
Sub	subicular cortex
S	subiculum
S-U	uncal subiculum
S-R	rostral subiculum
S-C	caudal subiculum
ProS	prosubiculum
ProU	uncal prosubiculum
ProR	rostral prosubiculum
ProC	caudal prosubiculum
SuS	supracallosal subiculum
IG	indusium griseum
TT	taenia tecta
PalCx	paleocortex (semicortex)
OB	olfactory bulb
AON	anterior olfactory nucleus
NLOT	nucleus of lateral olfactory tract
OT	olfactory tubercle
LOA	lateral olfactory area
LOAlc	lightly-stained cell islands of lateral olfactory area
LOAdc	darkly-stained cell islands of lateral olfactory area
Pir	piriform cortex
Pir1	layer I of piriform cortex
Pir2	layer II of piriform cortex
Pir3	layer III of piriform cortex
PEA	piriform-entorhinal-amygdaloid area
PEA1	layer I of piriform-entorhinal-amygdaloid area
PEA2	layer II of piriform-entorhinal-amygdaloid area
PEA3	layer III of piriform-entorhinal-amygdaloid area
CN	cerebral nuclei
AMY	amygdaloid complex
AAA	anterior amygdaloid area
AAAd	dorsal part of AAA
AAAv	ventral part of AAA
CEN	central nuclear group
CEm	medial subdivision of central nucleus
CEmd	dorsal part of CEm
CEmv	ventral part of CEm
CEl	lateral subdivision of central nucleus
CElap	apical part of CEl
CElca	capsular part of CEl
CElpc	paracapsular part of CEl
CElcn	central part of CEl
CMN	corticomedial nuclear group

TABLE 3. *Continued*

Co		cortical amygdaloid nuclei
CoA		anterior cortical nucleus
CoAd		dorsal subdivision of CoA
CoAv		ventral subdivision of CoA
CoA-m		marginal layer of anterior cortical nucleus
CoP		posterior cortical nucleus
CoPd		dorsal subdivision of CoP
CoPv		venrtral subdivision of CoP
CoP-m		marginal layer of posterior cortical nucleus
Me		medial nucleus
MeR		rostral subdivision of medial nucleus
MeC		caudal subdivision of medial nucleus
MeCd		dorsal part of caudal medial nucleus
MeCv		ventral part of caudal medial nucleus
Me-m		marginal layer of medial amygdaloid nucleus
AHA		amygdalohippocampal area
AHAmc		magnocellular part of amygdalohippocampal area
AHApc		parvocellular part of amygdalohippocampal area
AHA-m		marginal layer of amygdalohippocampal area
BLN		basolateral nuclear group
La		lateral nucleus
LaD		dorsal division of lateral nucleus
LaDr		dorsal rostral subdivision of lateral nucleus
LaDl		dorsal lateral subdivision of lateral nucleus
LaCom		comb-like part of LaDl
LaDm		dorsal medial subdivision of lateral nucleus
LaI		intermediate division of lateral nucleus
LaV		ventral division of lateral nucleus
LaVl		ventral lateral subdivision of lateral nucleus
LaVm		ventral medial subdivision of lateral nucleus
LaVglo		glomerular subdivision of lateral nucleus
BL		basolateral nucleus (basal nucleus)
BLD		dorsal (magnocellular) division of basolateral nucleus
BLDl		dorsal lateral subdivision of basolateral nucleus
BLI		intermediate division of basolateral nucleus
BLV		ventral (parvicellular) division of basolateral nucleus
BLVl		ventral lateral subdivision of basolateral nucleus
BLVm		ventral medial subdivision of basolateral nucleus
BM		basomedial nucleus (accessory basal nucleus)
BMD		dorsal division of basomedial nucleus
BMDl		dorsolateral subdivision of basomedial nucleus
BMDm		dorsomedial (magnocellular) subdivsion of basomedial nucleus
BMV		ventral division of basomedial nucleus
BMVl		ventrolateral (parvocellular) subdivsion of basomedial nucleus
BMVm		ventromedial subdivsion of basomedial nucleus
BMm		medial division of basomedial nucleus
BV		basoventral nucleus

TABLE 3. *Continued*

PL	paralaminar nucleus
PLglo	glomerular part of paralaminar nucleus
En	endopiriform nucleus
INA	Intercalated nucleus of amygdala
IMG	intramedullary gray of the amygdala
ATA	amygdaloid transition areas
AHTA	amygdalohippocampal transition area
ASTA	amygdalostriatal transition area
ACTA	amygdalocortical (corticoamygdaloid) transition area
SA	supra-amygdaloid area
EXA	extended amygdala
BNST	bed nucleus of stria terminalis
BNSTm	medial subdivision of BNST
BSTmr	rostral subdivision of BNSTm
BSTmc	caudal subdivision of BNSTm
BSTmcl	lateral subdivision of BNSTmc
BSTmm	medial subdivision of BNSTmc
BSTmv	ventral subdivision of BNSTm
BNSTl	lateral subdivision of BNST
BSTlj	juxtacapsular subdivision of BNSTl
BSTld	dorsal subdivision of BNSTl
BSTlv	ventral subdivision of BNSTl
BSTlcn	central subdivision of BNSTl
BSTlcn-s	shell of central subdivision of BNSTl
BSTlc	caudal subdivision of BNSTl
BSTlcm	medial subdivision of BNSTlc
BSTlcd	dorsal subdivision of BNSTlc
BSTlcv	ventral subdivision of BNSTlc
BNSTsc	supracapsular division of BNST
BSTscl	lateral column of BNSTsc
BSTscm	medial column of BNSTsc
BNSTin	intercalated nuclei of BNST
SLEA	sublenticular extended amygdala
SLEAm	medial division of sublenticular extended amygdala
SLEAc	central division of sublenticular extended amygdala
IPAC	interstitial nucleus of posterior limb of anterior commissure
BN	basal nuclei (basal ganglia)
STR	striatum
Ca	caudate nucleus
CaH	head of caudate
CaB	body of caudate
CaT	tail of caudate
Eca	peri-caudate ependymal and subependymal zone
CaPu	caudate-putamen cell bridges
Pu	putamen
PuR	rostral putamen
PuRv	ventral part of rostral putamen

TABLE 3. *Continued*

PuC		caudal putamen
Pld		laterodorsal part of putamen
Pint		intermediate part of putamen
Pmv		medioventral part of putamen
PuPV		posteroventral putamen
PuMG		marginal subdivision (cell groups) of putamen
NAC		nucleus accumbens
NACc		core of nucleus accumbens
NACcl		lateral portion of the core
NACcm		medial portion of the core
NACs		shell of nucleus accumbens
NACsl		lateral portion of the shell
NACsi		intermediate portion of the shell
NACsm		medial portion of the shell
GP		globus pallidus
GPe		external segment of globus pallidus
GPi		internal segment of globus pallidus
GPic		central portion of GPi
GPip		peripheral portion of GPi
EnPN		entopeduncular nucleus
VeP		Ventral pallidus
Cla		claustrum
CLd		Dorsal claustrum
CLv		ventral claustrum
CLt		temporal claustrum
BF		basal forebrain
SEP		septal nuclei
MSN		medial septal nucleus
LSN		lateral septal nucleus
LSNd		dorsal division of lateral septal nucleus
LSNi		intermediate division of lateral septal nucleus
LSNv		ventral division of lateral septal nucleus
CSN		caudal septal nucleus
SFi		septofimbrial nucleus
TSN		triangular septal nucleus
SHi		septohipocampal nucleus
Ld		lambdoid septal zone
PLd		paralambdoid septal nucleus
SHy		septohypothalamic nucleus
BNM		basal nucleus of Meynert
BNMl		lateral cell groups of basal nucleus
BNMm		medial cell groups of basal nucleus
NDB		nucleus of diagonal band
NDBv		vertical subdivision of nucleus of diagonal band
NDBh		horizontal subdivision of nucleus of diagonal band
NSP		nucleus subputaminalis
IsCj		islands of Calleja

TABLE 3. *Continued*

IsCjm	major island of Calleja
IsCjs	scattered islands of Calleja
SI	substantia innominata
SI-pc	lightly-stained parvocellular islands of SI
SI-nc	darkly-stained nanocellular islands of SI
Die	diencephalon
THM	thalamus
DTH	dorsal thalamus
ANC	anterior nuclear complex of thalamus
AD	anterodorsal nucleus of thalamus
AM	anteromedial nucleus of thalamus
AV	anteroventral nucleus of thalamus
LD	lateral dorsal nucleus of thalamus
MNC	medial nuclear complex of thalamus
MD	mediodorsal nucleus of thalamus
MDd	densocelllular (paralamellar) division of MD
MDm	magnocellular (medial) division of MD
MDam	anteromedial large-celled island of MD
MDl	multiform (lateral) division of MD
MDc	parvocellular (central) division of MD
MDv	ventral division of MD
Re	reuniens nucleus (medioventral nucleus) of thalamus
Pt	parataenial nucleus of thalamus
LNC	lateral nuclear complex of thalamus
DLN	dorsal group of lateral nucleus
LP	lateral posterior nucleus of thalamus
Pul	pulvinar of thalamus
Pulr	anterior nucleus of pulvinar
Pulm	medial nucleus of pulvinar
Pull	lateral nucleus of pulvinar
Puli	inferior nucleus of pulvinar
Pulil	lateral subdivision of Puli
Pulim	medial subdivision of Puli
VLN	ventral group of lateral nucleus
VA	ventral anterior nucleus of thalamus
VApr	parvocellular division of VA
VAmc	magnocellular division of VA
VL	ventral lateral nucleus of thalamus
VLR	rostral division of VL
VLC	caudal division of VL
VLCd	dorsal subdivision of VLC
VLCv	ventral subdivision of VLC
VLCx	medial subdivision of VLC (thalamic nucleus X)
VPT	ventral posterior nucleus of thalamus
VPL	ventral posterior lateral nucleus
VPLr	rostral division of ventral posterior lateral nucleus
VPLc	caudal division of ventral posterior lateral nucleus

TABLE 3. *Continued*

VPM		ventral posterior medial nucleus
VPMpc		parvocellular division of VPM
VPI		ventral posterior inferior nucleus
VMb		basal ventral medial nucleus
VM		ventral medial nucleus of thalamus
PoN		posterior nuclear complex of thalamus
LG		lateral geniculate nucleus
DLG		dorsal lateral geniculate nucleus
DLGmc		magnocellular layer of DLG
DLG1		layer 1 of DLG
DLG2		layer 2 of DLG
DLGpc		parvicellular layer of DLG
DLG3		layer 3 of DLG
DLG4		layer 4 of DLG
DLG5		layer 5 of DLG
DLG6		layer 6 of DLG
DLGs		S layer of DLG
DLGk		koniocellular layer of DLG
PG		pregeniculate nucleus
MG		medial geniculate nuclei
DMG		dorsal medial geniculate nucleus
DMGad		anterodorsal subdivision of DMG
DMGpd		posterodorsal subdivision of DMG
VMG		ventral medial geniculate nucleus
MMG		magnocellular (medial) nucleus
LiMG		limitans part of medial geniculate nucleus
Po		posterior nucleus of thalamus
LSG		limitans/suprageniculate nucleus
Lim		limitans nucleus
SGN		suprageniculate nucleus of thalamus
ILN		intralaminar nuclear complex
AILN		anterior group of intralaminar nuclei
CL		central lateral nucleus of the thalamus
CLm		medial division of central lateral nucleus
CLl		lateral division of central lateral nucleus
CLs		dorsal division of central lateral nucleus
CLc		caudal division of central lateral nucleus
CeM		central medial nucleus of thalamus
PC		paracentral nucleus of thalamus
CD		central dorsal nucleus of thalamus
PILN		posterior group of intralaminar nuclei
CM		centromedian nucleus of thalamus
CMl		lateral division of centromedian nucleus of thalamus
CMm		medial division of centromedian nucleus of thalamus
Pf		parafascicular nucleus of thalamus
Pfl		lateral division of parafascicular nucleus of thalamus
Pfm		medial division of parafascicular nucleus of thalamus

TABLE 3. *Continued*

SPf	subparafascicular nucleus of thalamus
RPf	retroparafascicular area of thalamus
Fa	fasciculosus nucleus of thalamus
MiN	midline nuclear complex
Rh	rhomboid (central) nucleus of thalamus
PeVA	periventricular area of thalamus
IAM	interanteromedial nucleus of thalamus
IMD	intermediodorsal nucleus of thalamus
ETH	epithalamus
HN	habenular nuclei
LHN	lateral habenular nucleus
LHNmc	magnocellular division of lateral habenular nucleus
LHNpc	parvicellular division of lateral habenular nucleus
MHN	medial habenular nucleus
PaV	paraventricular nucleus
PaVr	rostral subdivision of paraventricular nucleus
PaVc	caudal subdivision of paraventricular nucleus
Pin	pineal body
VTH	ventral thalamus
FF	nucleus of the field of Forel
ZI	zona incerta
ZId	zona incerta, dorsal division
ZIv	zona incerta, ventral division
EnP	endopeduncular nucleus
PSTh	parasubthalamic nucleus
R	reticular nucleus of thalamus
Rmc	magnocellular division of reticular nucleus
Rpc	parvocellular division of reticular nucleus (perireticular nucleus)
SubTH	subthalamus
STH	subthalamic nucleus
STHm	medial portion of STH
STHld	laterodorsal portion of STH
STHlv	lateroventral portion of STH
HTH	hypothalamus
HTHpo	preoptic region of HTH
PeVpo	periventricular nucleus, preoptic portion
DPe	dorsal periventricular nucleus
AVPe	anteroventral periventricular nucleus
AMPO	anteromedial preoptic nucleus
MPA	medial preoptic area
MPN	medial preoptic nucleus
LPA	lateral preoptic area
IMH	intermediate (sexually dimorphic) hypothalamic nuclei
MnPO	median preoptic nucleus
HTHso	supraoptic region of HTH
PeVso	periventricular nucleus, supraoptic portion
AHN	anterior hypothalamic nucleus

TABLE 3. *Continued*

AnHA		anterior hypothalamic area
PV		paraventricular nucleus of hypothalamus
PVd		descending division of paraventricular nucleus
PVmc		magnocellular division of paraventricular nucleus
PVpc		parvicellular division of paraventricular nucleus
PVpo		posterior division of paraventricular nucleus
UnN		uncinate nucleus
SCN		suprachiasmatic nucleus
SCNd		dorsal part of suprachiasmatic nucleus
SCNc		central part of suprachiasmatic nucleus
RCN		retrochiasmatic nucleus
SO		supraoptic nucleus
SOm		medial part of supraoptic nucleus
SOl		lateral part of supraoptic nucleus
LHAa		lateral hypothalamic area, anterior part
SuV		subventricular nucleus
SPZ		subparaventricular zone
HTHtub		tuberal region of HTH
PeVtub		periventricular nucleus, tuberal portion
JPLH		juxtaparaventricular lateral hypothalamic area
DHA		dorsal hypothalamic area
DMH		dorsomedial hypothalamic nucleus
DMHc		compact part of dorsomedial hypothalamic nucleus
DMHd		diffuse part of dorsomedial hypothalamic nucleus
VMH		ventromedial hypothalamic nucleus
VMHd		dorsal part of ventromedial hypothalamic nucleus
VMHv		ventral part of ventromedial hypothalamic nucleus
VMHc		central part of ventromedial hypothalamic nucleus
PMH		posteromedial hypothalamic nucleus
Arc		arcuate nucleus of hypothalamus
LT		lateral tuberal nuclei
LHAtub		lateral hypothalamic area, tuberal part
LHmc		magnocellular nucleus of lateral hypothalamic area
LHsc		accessory secretory cells of lateral hypothalamus
PalHy		pallidohypothalamic area
NCN		nanocellular hypothalamic nucleus
ME		median eminence
MEE		external portion of median eminence
MEI		internal portion of median eminence
HTHma		mammillary region of HTH
TM		tuberomammillary nucleus
SUM		supramammillary nucleus
MN		mammillary nucleus
MM		medial mammillary nucleus
MMl		lateral part of medial mammillary nucleus
MMm		medial part of medial mammillary nucleus
MMb		basal division of medial mammillary nucleus

TABLE 3. *Continued*

LM	lateral mammillary nucleus
PHN	posterior hypothalamic nucleus
LHAp	lateral hypothalamic area, posterior part
PeF	perifornical nucleus
PMN	premammillary nulceus
RMA	retromammillary area
Pit	pituitary body
FWM	white matter of forebrain
FCFT	forebrain commissural fiber tracts
ac	anterior commissure
cc	corpus callosum
ccr	rostrum of corpus callosum
ccg	genu of corpus callosum
ccg-mi	forceps minor (frontalis)
ccb	body of corpus callosum
ccbr	body of cc, rostral portion
ccbi	body of cc, intermediate portion
ccbc	body of cc, caudal portion
ccs	splenium of corpus callosum
ccs-ma	forceps major (occipitalis)
ccs-in	forceps inferior
ccrd	radiations of corpus callosum
tap	tapetum of corpus callosum
hac	habenular commissure
hic	hippocampal commissure
dhic	dorsal hippocampal commissure
vhic	ventral hippocampal commissure
smc	supramamillary commissure
FIFT	forebrain ipsilateral fiber tracts
alv	alveus
amtg	amygdalotegmental tract
ar	acoustic radiation
agb	angular bundle
al	ansa lenticularis
ap	ansa peduncularis
af	arcuate fasciculus
bx	bundle X
cb	cingulum bundle
cb-cx	cingulum bundle in cingulate cortex
cb-tx	cingulum bundle in temporal cortex
comb	comb fibers
cor	corona radiata
cor-a	anterior portion of corona radiata
cor-s	superior portion of corona radiata
cor-p	posterior portion of corona radiata
cbu-sc	corticobulbar tract, supracapsular part
cpa	corticopallidal tract

TABLE 3. *Continued*

cst		corticostriate tract
dpa		dentatopallidal tract
dib		diagonal band
dlf		dorsal longitudinal fasciculus
dob		dorsal occipital bundle
extC		external capsule
emlgp		external medullary lamina of globus pallidus
emlth		external medullary lamina of thalamus
extrC		extreme capsule
fim		fimbria
fx		fornix
fx-co		column of the fornix
fxc-r		column of the fornix, rostral portion
fxc-c		column of the fornix, caudal portion
fx-b		body of the fornix
fx-cr		crus of the fornix
hyhp		hypothalamo-hypophyseal tract
ilf		inferior longitudinal fasciculus
ithp		inferior thalamic peduncle
ic		internal capsule
aic		anterior limb of internal capsule
pfpf		prefrontopontine fibers
athf		anterior thalamic radiation
gic		genu of internal capsule
cbu-ic		corticobulbar fibers
cre		corticoreticular fibers
pic		posterior limb of internal capsule
lthp		lenticulothalamic portion
csp		corticospinal fibers
fpn		frontopontine fibers
sthr		superior thalamic radiation
cte		corticotectal fibers
cru		corticorubral fibers
relp		retrolenticular portion
pthr		posterior thalamic radiation
or-rl		optic radiation (geniculocalcarine tract)
ppn		parietopontine fibers
opn		occipitopontine fibers
oco		occipitocollicular fibers
sulp		sublenticular portion
ar-sl		auditory radiation
tepn		temporopontine fibers
imlgp		internal medullary lamina of globus pallidus
imlth		internal medullary lamina of thalamus
lls		lateral longitudinal stria
lf		lenticular fasciculus
mp		mammillary peduncle

TABLE 3. *Continued*

mtg		mammillotegmental tract
mtt		mammillothalamic tract
mcht		medial corticohypothalamic tract
mfb		medial forebrain bundle
mls		medial longitudinal stria
or-lp		Meyer's loop of optic radiation
milf		middle longitudinal fasciculus
npa		nigropallidal tract
nst		nigrostriate tract
off		occipitofrontal fasciculus
offi		inferior occipitofrontal fasciculus
offs		superior occipitofrontal fasciculus
olt		olfactory tract
ost		olfactory striae
lost		lateral olfactory stria
most		medial olfactory stria
ox		optic chiasm
on		optic nerve
or		optic radiation
ot		optic tract
opt		orbito-polar tract
pni		pallidonigral tract
ptg		pallidotegmental tract
pth		pallidothalamic tract
perf		perforant path
perp		perpendicular fasciculus
ponb		pontine bundle
rthp		rostral thalamic peduncle
sst		sagittal stratum
sste		external sagittal stratum
ssti		internal sagittal stratum
saf		short association fibers
sr		somatosensory radiation
szt		stratum zonale of thalamus
smt		stria medullaris of thalamus
st		stria terminalis
spa		striopallidal tract
sni		strionigral tract
sth		striothalamic tract
scf		subcallosal fasciculus
sthf		subthalamic fasciculus
sprs		superficial presubicular path
slf		superior longitudinal fasciculus
slf-m		superior longitudinal fasciculus, medial portion
slf-i		superior longitudinal fasciculus, intermediate portion
slf-l		superior longitudinal fasciculus, lateral portion
sox		supraoptic dicussation

TABLE 3. *Continued*

tpul	temporopulvinar bundle
thf	thalamic fasciculus
thpa	thalamopallidal tract
thst	thalamostriate tract
tuin	tuberoinfundibular path
unf	uncinate fasciculus
vamy	ventral amygdaloid efferent path
vof	vertical occipital fasciculus
FV	ventricles of forebrain
LV	lateral ventricles
aLV	anterior horn of lateral ventricle
bLV	body of lateral ventricle
xLV	atrium of lateral ventricle
pLV	posterior horn of lateral ventricle
iLV	inferior horn of lateral ventricle
olr	olfactory recess
3V	third ventricle
ifr3V	infundubular recess of 3V
por3V	preoptic recess of 3V
pir3V	pineal recess of 3V
spr3V	suprapineal recess of 3V
mmr3V	mammillary recess of 3V
IVF	interventricular foramen
FSS	surface structures of forebrain
CeS	cerebral sulci
PriS	primary sulci
cas	calcarine fissure (sulcus)
cas-r	rostral (common) portion of calcarine fissure
cas-c	caudal portion of calcarine fissure
cas-cs	superior ramus of caudal calcarine fissure
cas-ci	inferior ramus of caudal calcarine fissure
cals	callosal sulcus
cs	central sulcus
cis	cingulate sulcus
mr	marginal ramus of cingulate sulcus
csr	circular sulcus of Reil
csr-u	upper limiting sulcus
csr-l	lower limiting sulcus
cols	collateral sulcus
cols-r	collateral sulcus, rostral segment (rhinal sulcus, ventral part)
cols-c	collateral sulcus, caudal segment (medial occipitotemporal sulcus)
hf	hippocampal fissure
ips	intraparietal sulcus
las	lateral (sylvian) fissure (sulcus)
las-h	lateral fissure, horizontal (rostral) ramus
las-a	lateral fissure, ascending (middle) ramus
las-m	lateral fissure, main (caudal) ramus

TABLE 3. *Continued*

lof	longitudinal fissure
ots	occipitotemporal sulcus (lateral occipitotemporal sulcus)
ols	olfactory sulcus
ors	orbital sulcus
ors-m	medial orbital sulcus
ors-i	intermediate orbital sulcus
ors-p	posterior orbital sulcus
ors-l	lateral orbital sulcus
ors-t	transverse (arcuate) orbital sulcus
pos	parietooccipital fissure (sulcus)
pos-le	parietooccipital fissure, lateral extension
pocs	postcentral sulcus
prcs	precentral sulcus
sts	superior temporal sulcus
sts-a	superior temporal sulcus, mid-ascending branch
tranf	transverse cerebral fissure
SecS	secondary sulci
aos	anterior occipital sulcus
aos-d	anterior occipital sulcus, dorsal ramus
aos-v	anterior occipital sulcus, ventral ramus
ascs	anterior subcentral sulcus
ctfs	caudal transverse fusiform sulcus (posterior transverse collateral sulcus)
csin	central sulcus of insula
ds	diagonal sulcus
ers	endorhinal sulcus
fimd	fimbriodentate sulcus
fms	frontomarginal sulcus
fps	frontopolar sulcus
fps-d	dorsal frontopolar sulcus
fps-v	ventral frontopolar sulcus
ifs	inferior frontal sulcus
its	inferior temporal sulcus
imfs	intermediate frontal sulcus
ios	inferior occipital sulcus
itos	inferior transverse occipital sulcus
ans	angular sulcus
mcs	mid-cuneal sulcus
mffs	mid-fusiform sulcus (fusiform sulcus)
mos	middle (lateral) occipital sulcus
mligs	mid-lingual sulcus
mprcs	mid-precuneal sulcus
lus	lunate sulcus
mfs	medial frontal sulcus
pacs	paracentral sulcus
pacis	paracingulate sulcus
phligs	parahippocampo-ligual sulcus
pols	parolfactory sulcus

TABLE 3. *Continued*

pols-r		rostral parolfactory sulcus
pols-c		caudal parolfactory sulcus
prin		precentral sulcus of insula
poin		postcentral sulcus of insula
poscs		posterior subcentral sulcus
rs		rhinal sulcus (dorsal part)
rtfs		rostral transverse fusiform sulcus (posterior transverse collateral sulcus)
ros		rostral sulcus
ros-s		superior rostral sulcus
ros-i		inferior rostral sulcus
ss		semiannular sulcus
sps		subparietal (splenial) sulcus
sfs		superior frontal sulcus
spas		superior parietal sulcus
sms		supramarginal sulcus
tps		temporopolar sulcus
tps-m		medial temporopolar sulcus
tps-l		lateral temporopolar sulcus
trps		transverse parietal sulcus
tts		transverse temporal sulcus
atts		anterior transverse temporal sulcus
ptts		posterior transverse temporal sulcus
ims		intermediate transverse temporal sulcus
tts-le		lateral extension of transverse temporal sulcus
tros		transverse occipital sulcus
trs		triangular sulcus
us		uncal sulcus
CeG		cerebral gyri and lobules (**colors for this group are for online gyral version only**)
FroL		frontal lobe
PrCG		precentral gyrus
SFG		superior frontal gyrus
MFG		middle frontal gyrus
IFG		inferior frontal gyrus
IFGtr		inferior frontal gyrus, triangular part
IFGop		inferior frontal gyrus, opercular part
IFGor		inferior frontal gyrus, orbital part
ReG		gyrus rectus (straight gyrus)
MOrG		medial orbital gyrus
AOrG		anterior intermediate orbital gyrus
POrG		posterior intermediate orbital gyrus
LOrG		lateral orbital gyrus
PCLr		paracentral lobule, rostral part
PaCG		paracingulate gyrus
FrO		frontal operculum
OrO		orbital operculum
RoG		rostral gyrus
SRoG		superior rostral gyrus

TABLE 3. *Continued*

IRoG		inferior rostral gyrus
LOG		lateral olfactory gyrus
FMG		frontomarginal gyrus
FP		frontal pole
ParL		parietal lobe
PoCG		postcentral gyrus
SPL		supraparietal lobule
IPL		inferior parietal lobule
SMG		supramarginal gyrus
AnG		angular gyrus
PrCun		precuneus
PCLc		paracentral lobule, caudal part
PaO		parietal operculum
TemL		temporal lobe
STG		superior temporal gyrus
MTG		middle temporal gyrus
ITG		inferior temporal gyrus
FuGt		occipitotemporal (fusiform) gyrus, temporal part
PRG		perirhinal gyrus (rostral part of FuGt)
TTG		transverse temporal gyrus (Heschl's gyrus)
TTGr		rostral (anterior) transverse temporal gyrus
TTGc		caudal (posterior) transverse temporal gyrus
PLT		planum temporale
TP		temporal pole
PRL		perirhinal lobule
PLP		planum polare
OccL		occipital lobe
OP		occipital pole
OPR		occipitoparietal transition region
OTR		occipitotemporal transition region
Cun		cuneus
LiG		lingual gyrus (medial occipitotemporal gyrus)
FuGo		(lateral) occipitotemporal (fusiform) gyrus, occipital part
IOG		inferior occipital gyrus
SOG		superior occipital gyrus
InL		insular lobe
LIG		long insular gyri
SIG		short insular gyri
LimL		limbic lobe
CgG		cingulate gyrus
CgGr		cingulate gyrus, rostral (anterior) part
CgGc		cingulate gyrus, caudal (posterior) part
CgGrs		cingulate gyrus, retrospleninal part
IsCPH		cingulo-parahippocampal isthmus
SCG		subcallosal gyrus (parolfactory gyrus)
PTG		paraterminal gyrus
PHG		parahippocampal gyrus

TABLE 3. *Continued*

APH		anterior parahippocampal gyrus
PPH		posterior parahippocampal gyrus
UN		uncus of parahippocampal gyrus
AG		gyrus ambiens
BG		band of Giacomini
ILG		intralimbic gyrus
SLG		semilunar gyrus
HiF		hippocampal gyrus (formation)
HiH		head of hippocampus
HiD		digitations of hippocampus
HiB		body of hippocampus
HiT		tail of hippocampus
FaG		fasciolar gyrus
Retz		Retzius' gyrus
Subx		subicular complex
PrPir		prepiriform region
APS		anterior perforated substance
HaTr		habenular triangle
InF		infundibular stalk
LI		limen insula
MB		mammillary body
PrN		preoccipital notch
TPUJ		temporopolar uncal junction
TN		tentorial notch
TC		tuber cinereum
ASFV		adjoining structures of forebrain ventricles
CalA		calcar avis
ChoLV		choroid plexus of lateral ventricle
Cho3V		choroid plexus of 3V
ChoF		choroid fissure
ColE		collateral eminence
ColT		collateral trigone
hyths		hypothalamic sulcus
InTh		interthalamic adhesion (massa intermedia)
LaT		lamina terminalis
OVLT		organum vasculosum laminae terminalis
SFO		subfornical organ
Pell		septum pellucidum
cpell		cavum septi pellucidi
vip		velum interpositum
fbv		blood vessels of forebrain
M		midbrain (mesencephalon)
MGM		gray matter of midbrain
PTR		pretectal region
PTN		pretectal nuclear complex
DPT		dorsal (posterior/sublentiform) pretectal nucleus
MPT		medial pretectal nucleus

TABLE 3. *Continued*

NOP	nucleus of the optic tract (lentiform nucleus)
OPT	olivary pretectal nucleus
APT	anterior (ventral /principal) pretectal nucleus
APTc	anterior pretectal nucleus, compact division
APTr	anterior pretectal nucleus, reticular division
AOP	accessory nuclei of optic tract
AOPd	accessory nuclei of optic tract, dorsal nucleus (dorsal terminal nucleus)
AOPl	accessory nuclei of optic tract, lateral nucleus (lateral terminal nucleus)
AOPm	accessory nuclei of optic tract, medial nucleus (medial terminal nucleus)
MTg	midbrain tegmentum
MEN	efferent nuclei of the cranial nerves in the midbrain
EW	Edinger-Westphal nucleus (accessory oculomotor nucleus)
3N	oculomotor nucleus
3AM	anterior median oculomotor nucleus
3CC	caudal central oculomotor nucleus
3C	central oculomotor nucleus
3D	dorsal oculomotor nucleus
3M	medial oculomotor nucleus
3Vn	ventral oculomotor nucleus
4N	trochlear nucleus
S4N	supratrochlear nucleus
MAN	afferent nuclei of the cranial nerves in midbrain
Me5	mesencephalic trigeminal nucleus
PAG	periaqueductal gray substance
PAGD	periaqueductal gray substance, dorsolateral portion
PAGdm	periaqueductal gray substance,dorsomedial division
PAGdl	periaqueductal gray substance, dorsolateral division
PAGl	periaqueductal gray substance, lateral division
PAGvl	periaqueductal gray substance, ventrolateral division
PAGpl	periaqueductal gray substance, pleioglial division
PAGV	periaqueductal gray substance, ventral portion
DRc	cap of dorsal raphe nucleus
Dk	nucleus of Darkschewitsch
PC3	parvicellular oculomotor nucleus
Su3C	supraoculomotor cap
Su3	supraoculomotor nucleus
MRa	midbrain raphe nuclei
DR	dorsal raphe nucleus
DRC	dorsal raphe nucleus, caudal part
DRD	dorsal raphe nucleus, dorsal part
DRI	dorsal raphe nucleus, interfascicular part
DRL	dorsal raphe nucleus, lateral part
DRV	dorsal raphe nucleus, ventral part
DRVL	dorsal raphe nucleus, ventrolateral part
Lin	linear nucleus of the midbrain
CLiZ	caudal linear nucleus of the raphe
CLinAz	caudal linear nucleus of the raphe, azygos part

TABLE 3. *Continued*

CLinZ		caudal linear nucleus of the raphe, zygos part
RLin		rostral linear nucleus of the raphe
MnR		median raphe nucleus
PMnR		paramedian raphe nucleus
PDR		posterodorsal raphe nucleus
Rbd		rhabdoid nucleus
isRt		isthmic reticular formation
MRF		midbrain reticular formation
CnF		cuneiform nucleus
PrCnF		precuneiform area
U		nucleus U
PTg		pedunculopontine tegmental nucleus
PTgC		pedunculopontine tegmental nucleus, compact part
PTgD		pedunculopontine tegmental nucleus, dissipated part
SubCn		subcuneiform nucleus
Lth		lithoid nucleus
RN		red nucleus
RNdm		red nucleus, dorsomedial part
RNmc		red nucleus, magnocellular part
RNpc		red nucleus, parvicellular part
SN		substantia nigra
SNC		substantia nigra, compact part
SNCd		substantia nigra, compact part, dorsal subdivision
SNCm		substantia nigra, compact part, medial subdivision
SNCv		substantia nigra, compact part, ventral subdivision
SNL		substantia nigra, lateral part
SNR		substantia nigra, reticular part
VTR		ventral tegmental region of midbrain
VTA		ventral tegmental area
IF		interfascicular nucleus
PBP		parabrachial pigmented nucleus
PIF		parainterfascicular nucleus
PaN		paranigral nucleus
IP		interpeduncular nucleus
IPa		interpeduncular nucleus, apical subnucleus
IPc		interpeduncular nucleus, caudal subnucleus
IPdm		interpeduncular nucleus, dorsomedial subnucleus
IPi		interpeduncular nucleus, intermediate subnucleus
IPl		interpeduncular nucleus, lateral subnucleus
IPr		interpeduncular nucleus, rostral subnucleus
XMTg		other nuclei in midbrain tegmentum
CeMe		central mesencephalic nucleus
CTF		central tegmental field
DA8		dopamine cells A8
I3		interoculomotor nucleus
InC		interstitial nucleus of Cajal
Lt		lateral terminal nucleus of accessory optic tract

TABLE 3. *Continued*

MCPC		magnocellular nucleus of the posterior commissure
MA3		medial accessory oculomotor nucleus
MiTg		microcellular tegmental nucleus
p1Rt		p1 reticular formation
PaC		paracollicular tegmentum
PaP		parapeduncular nucleus
Pa4		paratrochlear nucleus
PP		peripeduncular nucleus
PDTg		posterodorsal tegmental nucleus
PrC		precommissural nucleus
PrEW		pre-Edinger-Westphal nucleus
RIs		retroisthmic nucleus
RRF		retrorubral field
SubB		subbrachial nucleus
MTc		midbrain tectum
SC		superior colliculus
SCS		superficial layer of superior colliculus
SCSon		optic nerve layer of superior colliculus
SCSg		superficial gray layer of superior colliculus
SCSw		superficial white layer of superior colliculus
SCSz		zonal layer of superior colliculus
SCI		intermediate layer of the superior colliculus
SCIg		intermediate gray layer of superior colliculus
SCIw		intermediate white layer of superior colliculus
SCD		deep layer of colliculus
SCDg		deep gray layer of superior colliculus
SCDw		deep white layer of superior colliculus
BrSC		nucleus of branchium of superior colliculus
IC		inferior colliculus
CxIC		cortex of inferior colliculus
CICd		dorsal cortex of inferior colliculus
CICe		external cortex of inferior colliculus
CIC		central nucleus of inferior colliculus
ICN		intercollicular nucleus
INPC		interstitial nucleus of posterior commissure
MxTZ		matrix layer of the tectal zone
BrIC		nucleus of the brachium of inferior colliculus
PBG		parabigeminal nucleus
Sag		sagulum nucleus
SCO		subcommissural organ
MWM		white matter of midbrain
bic		brachium of inferior colliculus
bsc		brachium of superior colliculus
ctg-m		central tegmental tract, midbrain portion
cpd		cerebral peduncle (crus cerebri)
cpn-m		corticopontine fibers, midbrain portion
fpn-m		frontal pontine fibers, midbrain portion

TABLE 3. *Continued*

potpn-m		parieto-occipito-temporal pontine fibers, midbrain portion
py-m		pyramidal tract, midbrain portion
cbu-m		corticobulbar tract, midbrain portion
cmic		commissure of inferior colliculus
cme		corticomesencephalic fibers
xrsp		decussation of rubrospinal tract
xscp		decussation of superior cerebellar peduncle
x4		decussation of trochlear nerve fibers
dlf-m		dorsal longitudinal fasciculus, midbrain portion
xdtg		dorsal tegmental decussation
dtth-m		dorsal trigeminothalamic tract, midbrain portion
fr		fasciculus retroflexus (habenuno-interpeduncular tract)
hysp-m		hypothalamospinal fibers, midbrain portion
iptg		interpedunculotegmental tract
issp-m		interstitiospinal tract, midbrain portion
ll-m		lateral lemniscus, midbrain portion
ml-m		medial lemniscus, midbrain portion
mlf-m		medial longitudinal fasciculus, midbrain portion
mtg-m		medial tegmental tract, midbrain portion
me5-m		mesencephalic trigeminal tract, midbrain portion
poc		posterior commissure
rubu-m		rubrobulbar (rubronuclear) tract, midbrain portion
rol-m		rubro-olivary tract, midbrain portion
rsp-m		rubrospinal tract, midbrain portion
sl-m		spinal lemniscus, midbrain portion
scp		superior cerebellar peduncle (brachium conjunctivum)
cbru		cerebellorubral tract
cbth		cerebellothalamic tract
dtth		dentatothalamic tract
geru		globose-emboliform-rubral tract
rucb		rubrocerebellar fibers
tcb		tectocerebellar fibers
vscb-m		ventral spinocerebellar tract, midbrain portion
tbu-m		tectobulbar tract, midbrain portion
tol		tecto-olivary fibers
tpn		tectopontine tract
tsp-m		tectospinal tract, midbrain portion
xvtg		ventral tegmental decussation
vtth-m		ventral trigeminothalamic tract, midbrain portion
wmtg		white matter of tegmentum
MV		ventricle of midbrain
Aq		cerebral aqueduct
MSS		surface structures of midbrain
fsmv		frenulum of the superior medullary velum
ipf		interpeduncular fossa
pops		posterior perforated substance
icr		infracollicular recess

TABLE 3. *Continued*

ocs	oculomotor sulcus
qgb	quadrigeminal body
r3	root of oculomotor nerve
r4	root of trochlear nerve
trill	trigone of lateral lemniscus (acoustic trigone)
H	hindbrain (rhombencephalon)
HGM	gray matter of the hindbrain
Met	metencephalon
CB	cerebellum
CBC	cerebellar cortex
CBV	cerebellar vermis
VeA	vermis, anterior lobe portion
VeAm	molecular layer of VeA
VeAp	Purkinje cell layer of VeA
VeAg	granular cell layer of VeA
VePo	vermis, posterior lobe portion
VePs	vermis, posterior lobe portion, superior part
VePsm	molecular layer of VePs
VePsp	Purkinje cell layer of VePs
VePsg	granular cell layer of VePs
VePi	vermis, posterior lobe portion, inferior part
VePim	molecular layer of VePi
VePip	Purkinje cell layer of VePi
VePig	granular cell layer of VePi
VeF	vermis, flocculonodular lobe portion (nodulus)
VeFm	molecular layer of VeF
VeFp	Purkinje cell layer of VeF
VeFg	granular cell layer of VeF
CBH	cerebellar hemisphere
CBPV	paravermis of cerebellum
PVA	paravermis, anterior lobe portion
PVAm	molecular layer of PVA
PVAp	Purkinje cell layer of PVA
PVAg	granular cell layer of PVA
PVP	paravermis, posterior lobe portion
PVPs	paravermis, posterior lobe portion, superior part
PVPsm	molecular layer of PVPs
PVPsp	Purkinje cell layer of PVPs
PVPsg	granular cell layer of PVPs
PVPi	paravermis, posterior lobe portion, inferior part
PVPim	molecular layer of PVPi
PVPip	Purkinje cell layer of PVPi
PVPig	granular cell layer of PVPi
PVF	paravermis, flocculonodular lobe portion
PVFm	molecular layer of PVF
PVFp	Purkinje cell layer of PVF
PVFg	granular cell layer of PVF

TABLE 3. *Continued*

CBL	lateral hemisphere of cerebellum
CBLA	lateral hemisphere, anterior lobe portion
CBLAm	molecular layer of CBLA
CBLAp	Purkinje cell layer of CBLA
CBLAg	granular cell layer of CBLA
CBLP	lateral hemisphere, posterior lobe portion
CBLPs	lateral hemisphere, posterior lobe portion, superior part
CBLPsm	molecular layer of CBLPs
CBLPsp	Purkinje cell layer of CBLPs
CBLPsg	granular cell layer of CBLPs
CBLPi	lateral hemisphere, posterior lobe portion, inferior part
CBLPim	molecular layer of CBLPi
CBLPip	Purkinje cell layer of CBLPi
CBLPig	granular cell layer of CBLPi
CBLF	lateral hemisphere, flocculonodular lobe portion
CBLFm	molecular layer of CBLF
CBLFp	Purkinje cell layer of CBLF
CBLFg	granular cell layer of CBLF
CbDN	cerebellar deep nuclei
DT	dentate (lateral) nucleus
DTlv	dentate nucleus, lateroventral part
DTmd	dentate nucleus, mediodorsal part
InP	interpositus (intermediate) nucleus
InPM	medial interpositus (globose) nucleus
InPL	lateral interpositus (emboliform) nucleus
Fas	fastigial (medial) nucleus
FasL	fastigial nucleus, lateral part
FasM	fastigial nucleus, medial part
BIcb	basal interstitial nucleus of cerebellum
Pn	pons
PnBa	basilar part of pons
PN	pontine nucleus
PNd	dorsal nucleus
PNdl	dorsolateral nucleus
PNdm	dorsomedial nucleus
PNl	lateral nucleus
PNm	median nucleus
PNpar	paramedian nucleus
PNped	peduncular nucleus
RTg	reticulotegmental nucleus
PnTg	pontine tegmentum
PnEN	efferent nuclei of cranial nerves in pons
6N	abducens nucleus
Acs7	accessory facial nucleus
7N	facial nucleus
7D	facial nucleus, dorsal subnucleus
7VI	facial nucleus, ventrointermediate subnucleus

TABLE 3. *Continued*

7VM	facial nucleus, ventromedial subnucleus
7SH	facial nucleus,stylohyoid part
7VL	facial nucleus, ventrolateral subnucleus
Lac	lacrimal nucleus
Mo5	motor nucleus of trigeminal nerve
Mo5lpt	motor nucleus of trigeminal nerve, lateral pterygoid part
Mo5ma	motor nucleus of trigeminal nerve, masseter part
Mo5mpt	motor nucleus of trigeminal nerve, medial pterygoid part
Mo5my	motor nucleus of trigeminal nerve, mylohyoid part
Mo5te	motor nucleus of trigeminal nerve, temporalis part
SuSV	superior salivatory nucleus
PnAN	afferent nuclei of cranial nerves in pons
8Co	cochlear nuclei
DCo	dorsal cochlear nucleus
GrCo	granular cell layer of cochlear nuclei
VCo	ventral cochlear nucleus
VCoR	ventral cochlear nucleus, rostral part
VCoC	ventral cochlear nucleus, caudal part
Me5-p	mesencephalic nucleus of trigeminal nerve, pontine part
Pr5	principal sensory nucleus of trigeminal nerve
Pr5dm	dorsomedial nucleus of Pr5
Pr5vl	ventrolateral nucleus of Pr5
Sp5o	spinal nucleus of trigeminal nerve, oral subnucleus
8Ve-p	vestibular nuclei in pons
LVe	lateral vestibular nucleus
LVeMC	lateral vestibular nucleus, magnocellular part
LVePC	lateral vestibular nucleus, parvicellular part
SuVe	superior vestibular nucleus
VTg	ventral tegmental nucleus
VTgR	ventral tegmental nucleus, rostral extension
VTgI	ventral tegmental nucleus, infrafascicular part
VTgP	ventral tegmental nucleus, principal part
VTgS	ventral tegmental nucleus, suprafascicular part
PnAR	auditory relay nuclei in pons
LLN	nuclei of lateral lemniscus
DLL	dorsal nucleus of lateral lemniscus
ILL	intermediate nucleus of lateral lemniscus
VLL	ventral nucleus of lateral lemniscus
TrZ	nucleus of trapezoid body
TrZl	lateral nucleus of trapezoid body
TrZm	medial nucleus of trapezoid body
TrZv	ventral nucleus of trapezoid body
SOC	superior olivary complex
POI	periolivary nuclei
LPOI	lateral periolivary nucleus
MPOI	medial periolivary nucleus
RO	retro-olivary cell group

TABLE 3. *Continued*

SOI	superior olivary nucleus
LSO	lateral superior olivary nucleus
MSO	medial superior olive
SPO	superior paraolivary nucleus
PrO	preolivary nucleus
PnRa	raphe pontis nucleus
DR-p	dorsal raphe nucleus
MnR-p	median raphe nucleus
PMnRt	paramedian raphe nucleus, reticular part
PRn	raphe pontis nucleus
RIP	raphe interpositus nucleus
PnRF	Pontine reticular formation
PB	parabrachial nuclei
LPB	lateral parabrachial nucleus
LPBc	lateral parabrachial nucleus, central part
LPBd	lateral parabrachial nucleus, dorsal part
LPBe	lateral parabrachial nucleus, external part
LPBs	lateral parabrachial nucleus, superior part
MPB	medial parabrachial nucleus
MPBe	medial parabrachial nucleus, external part
MPBm	medial parabrachial nucleus, medial part
SPP	subpeduncular pigmented nucleus
SPB	subparabrachial nucleus
PnRt	reticular nuclei of pons
PnC	pontine reticular nucleus, caudal part
PnO	pontine reticular nucleus, oral part
PLN	paralemniscal nucleus
PMn	paramedian reticular nucleus
RtTg	reticulotegmental nucleus
RtTgD	reticulotegmental nucleus, dorsal part
PnNA	group of noradrenergic neurons in pons
NC	nucleus coeruleus
SubC	subcoeruleus nucleus
SubCd	subcoeruleus nucleus, dorsal part
SubCv	subcoeruleus nucleus, ventral part
XPnTg	other nuclei in pontine tegmentum
Acs5	accessory trigeminal nucleus
AInS	alar interstitial nucleus
B9	B9 serotonin cells
Bar	Barrington's nucleus
PnCG	central gray of pons
CAT	central nucleus of acoustic tract
DTg	dorsal tegmental nucleus
DTgC	dorsal tegmental nucleus, central part
DTgP	dorsal tegmental nucleus, pericentral part
DMTg	dorsomedial tegmental area
PnE	ependyma and subependymal layers of pons

TABLE 3. *Continued*

EpC	epicoeruleus nucleus
PnG	pontine gamma nucleus
IIMLF	intermediate interstitial nucleus of medial longitudinal fasciculus
IMLF	interstitial nucleus of medial longitudinal fasciculus
I5	intertrigeminal nucleus
JxO	juxtaolivary nucleus
KF	Koelliker-Fuse nucleus
LDTg	laterodorsal tegmental nucleus
LDTgD	laterodorsal tegmental nucleus, dorsal part
LDTgV	laterodorsal tegmental nucleus, ventral part
NI	nucleus incertus
K	nucleus K
L	nucleus L
Pa6	paraabducens nucleus
PCuN	pericuneate nuclei
LPCu	lateral pericuneate nucleus
MPCu	medial pericuneate nucleus
PF7	perifacial zone
PnBi	pontobulbar nucleus, inferior part
P5	peritrigeminal zone
R7	retrofacial nucleus
RTz	retrotrapezoid nucleus
5N	trigeminal nuclei
VLTg	ventrolateral tegmental nucleus
SGe	supragenual nucleus
Mo	myelencephalon (medulla oblongata)
MoPy	pyramidal part of medulla oblongata
Ar	arcuate nucleus of medulla oblongata
Ct	conterminal nucleus
MoTg	tegmentum of medulla oblongata
MoEN	efferent nuclei of cranial nerves in the medulla oblongata
Amb	ambiguus nucleus
AmbC	ambiguus nucleus, compact part
AmbL	ambiguus nucleus, loose part
AmbSC	ambiguus nucleus, semicompact part
12N	hypoglossal nucleus
12GH	hypoglossal nucleus, geniohyoid part
12L	hypoglossal nucleus, lateral part
12M	hypoglossal nucleus, medial part
12V	hypoglossal nucleus, ventral part
InSV	inferior salivatory nucleus
10N	dorsal motor nucleus of the vagus (vagal nucleus)
10CaI	dorsal motor nucleus of vagus, caudointermediate part
10CeI	dorsal motor nucleus of vagus, centrointermediate part
10DI	dorsal motor nucleus of vagus, dorsointermediate part
10DR	dorsal motor nucleus of vagus, dorsorostral part
10F	dorsal motor nucleus of vagus, medial fringe

TABLE 3. *Continued*

10VI	dorsal motor nucleus of vagus, ventrointermediate part
10VR	dorsal motor nucleus of the vagus, ventrorostral part
MoAN	afferent nuclei of cranial nerves in medulla oblongata
Sol	solitary nucleus
SolC	solitary nucleus, commissural part
SolD	solitary nucleus, dorsal part
SolDL	solitary nucleus, dorsolateral part
SolG	solitary nucleus, gelatinous part
SolIM	solitary nucleus, intermediate part
SolI	solitary nucleus, interstitial part
SolM	solitary nucleus, medial part
SolPaC	solitary nucleus, paracommissural part
SolV	solitary nucleus, ventral part
SolVL	solitary nucleus, ventrolateral part
SSol	subsolitary nucleus
PSol	parasolitary nucleus
Sp5	spinal trigeminal nucleus
Sp5C	spinal trigeminal nucleus, caudal part
DM5	dorsomedial spinal trigeminal nucleus
Sp5ip	spinal trigeminal nucleus, interpolar part
8Ve	vestibular nuclei in medulla
I8	interstial nucleus of the vestibulocochlear nerve
MVe	medial vestibular nucleus
MVeMC	medial vestibular nucleus, magnocellular part
MVePC	medial vestibular nucleus, parvicellular part
EVe	nucleus of origin of vestibular efferents of vestibular nerve
SpVe	spinal (inferior) vestibular nucleus
PaVe	paravestibular nucleus
MoSR	sensory relay nuclei in medulla oblongata
ECu	external (accessory/lateral) cuneate nucleus
Cu	cuneate nucleus
CuR	cuneate nucleus, rotundus part
CuT	cuneate nucleus, triangular part
Gr	gracile nucleus
GrC	gracile nucleus, central part
GrR	gracile nucleus, rostral part (shell)
PrCbN	precerebellar nuclei
Crb	cribriform nucleus
DPMn	dorsal paramedian nucleus
CDPMn	caudal dorsal paramedian nucleus
ODPMn	rostral (oral) dorsal paramedian nucleus
IO	inferior olive
IODM	inferior olive, dorsomedial cell group
IOBe	inferior olive, beta nucleus
IOD	inferior olive, dorsal nucleus
IODC	inferior olive, dorsal nucleus, caudal part
IOM	inferior olive, medial nucleus

TABLE 3. *Continued*

IOK	Cap of Kooy of medial nucleus
IOA	subnucleus A of medial nucleus
IOB	subnucleus B of medial nucleus
IOC	subnucleus C of medial nucleus
IOPr	inferior olive, principal nucleus
IOVL	ventrolateral outgrowth of inferior olive
InM	intercalated nucleus of medulla
IPo	interpositus nucleus
PnbN	pontobulbar nucleus
PrH	prepositus hypoglossal nucleus
MoRF	medullary reticular formation
DRt	dorsal reticular nucleus
IRt	intermediate reticular nucleus
CVL	caudoventrolateral reticular nucleus
NA/A	noradrenaline/adrenaline cell group 1
RVRG	rostral ventral respiratory cell group
RVL	rostroventrolateral reticular nucleus of hindbrain
GiRt	gigantocellular reticular nuclei
GiRtA	alpha gigantocellular reticular nucleus
LPGi	lateral paragigantocellular nucleus
PGi	paragigantocellular nucleus
APGi	alpha part of paragigantocellular nucleus
DPGi	dorsal paragigantocellular nucleus
GiRtV	ventral gigantocellular reticular nucleus
LMRt	lateral reticular nuclei
LRt	lateral reticular nucleus (principal part)
LRtMC	lateral reticular nucleus, magnocellular part
LRtPC	lateral reticular nucleus, parvicellular part
LRtS5	lateral reticular nucleus, subtrigeminal part
Li	linear nucleus of hindbrain
MdD	medullary reticular nucleus, dorsal part (ventral reticular nucleus)
MdV	medullary reticular nucleus, ventral part (medial reticular nucleus)
PCRt	parvicellular reticular nucleus
PCRtA	alpha division of parvicellular reticular nucleus
MoRa	raphe nuclei in medulla oblongata
RMg	raphe magnus nucleus
ROb	raphe obscurus nucleus
RPa	raphe pallidus nucleus
NPRa	nucleus pararaphales
XMoTg	other nuclei in medullary tegmentum
Au	austral nucleus
BI	basal interstitial nucleus
Bo	Bötzinger complex
CGL	central glial substance
MoCG	central gray of medulla oblongata
DPO	dorsal periolivary nucleus
MoE	ependyma and subependymal layers of the medulla

TABLE 3. *Continued*

EL	endolemniscal nucleus
EF	epifascicular nucleus
IF12	interfascicular hypoglossal nucleus
IB	internal basal nucleus
Nt	notocuneate nucleus
Z	nucleus Z (posterodorsal subnucleus)
Y	nucleus Y
X	nucleus X (preaccessory cuneate nucleus)
Ro	nucleus of Roller
Pa5	paratrigeminal nucleus
PeCu	pericuneate nucleus
Pe5	peritrigeminal nucleus
PrBo	pre-Bötzinger complex
RAmb	retroambiguus nucleus
SSp	spinal accessory (supraspinal) nucleus
SuL	supralemniscal nucleus
HWM	white matter of hindbrain
ami	amiculum of the olive
af7	ascending fibers of the facial nerve
ctg	central tegmental tract
cpn	cortico-pontine fibers, pontine part
cuf	cuneate fasciculus
xml	decussation of medial lemniscus
das	dorsal acoustic stria
def	dorsal external fibers
dlf-h	dorsal longitudinal fasciculus
dtgth	dorsal trigeminothalamic tract
eaf	external arcuate fibers
g7	genu of the facial nerve
gr	gracile fasciculus
hio	hilus of the inferior olive
hysp	hypothalamospinal tract
icp	inferior cerebellar peduncle
rsf	restiform body
cbrf	cerebelloreticular fibers
cbvf	cerebellovestibular fibers
cucb	cuneocerebellar tract
dsc	dorsal spinocerebellar tract
ocb	olivocerebellar tract
rcbtm	reticulocerebellar tract, medullary division
sct	spinocerebellar tract
jx	juxtarestiform body
fasr	fastigial reticular tract
fasv	fastigial vestibular tract
tgcb	trigeminocerebellar tract
vecb	vestibulocerebellar tract
ias	intermediate acoustic stria

TABLE 3. *Continued*

iaf		internal arcuate fibers
issp		interstitiospinal tract
lbrs		lateral bulboreticulospinal tract
lcs		lateral corticospinal tract
ll		lateral lemniscus
lvs		lateral vestibulospinal tract
lfpn		longitudinal fasciculus of the pons
ml		medial lemniscus
mlf		medial longitudinal fasciculus
metg		medial tegmental tract
mvet		medial vestibulospinal tract
me5		mesencephalic trigeminal tract
mcp		middle cerebellar peduncle
pncb		pontocerebellar tract
rctp		reticulocerebellar tract, pontine division
olcob		olivocochlear bundle
xpy		pyramidal decussation
py		pyramidal tract
cbu-h		corticobulbar tract
cre-h		corticoreticular tract
csp-h		corticospinal tract
rsp		raphespinal tract
lrsp		lateral raphespinal tract
vrsp		ventral raphespinal tract
rbb		rubrobulbar tract
rol		rubro-olivary tract
rusp		rubrospinal tract
sol		solitary tract
slh		spinal lemniscus in hindbrain
spb		spinobulbar tract
sphy		spinohypothalamic tract
spme		spinomesencephalic tract
spre		spinoreticular tract
spth		spinothalamic tract
spve		spinovestibular tract
tbu		tectobulbar tract
sp5		spinal trigeminal tract
spol		spino-olivary tract
sm4V		stria medulares of the fourth ventricle
tsp		tectospinal tract
tfp		transverse fibers of pons
tz		trapezoid body
tri5		trigeminothalamic tract
ubcb		uncinate (hooked) bundle of cerebellum
vcsp		ventral corticospinal tract
vexf		ventral external fibers
vresp		ventral reticulospinal tract

TABLE 3. *Continued*

vscb		ventral spinocerebellar tract
vtg		ventral tegmental tract
vtth		ventral trigeminothalamic tract
veme		vestibulomesencephalic tract
HV		ventricles of hindbrain
4V		fourth ventricle
4Vro		roof of fourth ventricle
lr4V		lateral recess of fourth ventricle
4Vfl		floor of fourth ventricle (rhomboid fossa)
cec		central canal of medulla oblongata
HSS		surface structures of hindbrain
CbSS		surface structures of cerebellum
cbf		cerebellar fissures
prcf		precentral (postlingual) fissure
pocf		postcentral (preculminate) fissure
icf		intraculminate fissure
prif		primary (anterior superior) fissure
psf		posterior superior (postclival) fissure
hof		horizontal (intercrural) fissure
apf		ansoparamedian fissure
prpy		prepyramidal (prebiventral) fissure
ibif		intravbiventral fissure
popy		secondary (post pyramidal) fissure
polf		posterolateral (postnodular) fissure
CBLL		cerebellar lobes and lobules
ACb		anterior lobe
CbI		lobule I (lingula)
CbII		lobule II (central lobule and wing, anterior part)
CbIII		lobule III (central lobule and wing, posterior part)
CbIV		lobule IV (culmen and quadrangular lobule, anterior part)
CbV		lobule V (culmen and quadrangular lobule, posterior part)
PCb		posterior lobe
CbVI		lobule VI (declive and simplex lobule)
CbVIIa1		lobule VIIAf/crus I (folium and superior semilunar lobule)
CbVIIa2		lobule VIIAt/crus II (tuber and inferior semilunar lobule)
CbVIIb		lobule VIIB (gracile lobule)
CbVIIIa		lobule VIIIA (pyramis and biventral lobule, anterior part)
CbVIIIb		lobule VIIIB (pyramis and biventral lobule, posterior part)
CbIX		lobule IX (uvula and tonsil)
FNCb		flocculonodular lobe
CbX		lobule X (nodulus and flocculus)
PnSS		surface structures of pons
bas		basilar sulcus
IsRh		isthmus of rhombencephalon
pbr		parabrachial recess
pmed		pontomedullary sulcus
pmes		pontomesencephalic sulcus

TABLE 3. *Continued*

r6		root of abducens nerve
r7		root of facial nerve
r7m		motor root of facial nerve
r7in		root of intermediate nerve
r5		root of trigeminal nerve
r5m		motor root of trigeminal nerve
r5s		sensory root of trigeminal nerve
r8		root of vestibulocochlear nerve
r8co		cochlear root of vestibulocochlear nerve
r8ve		vestibular root of vestibulocochlear nerve
rmv		rostral (anterior) medullary velum
AS4V		adjoining structures of fourth ventricle
AP		area postrema
Cho4V		choroid plexus of the fourth ventricle
FaC		facial colliculus
FovI		fovea inferior
FovS		fovea superior
FnS		funiculus separans
12Tr		hypoglossal trigone
la4V		lateral aperture (foramen of Luschka)
LC		locus coeruleus
MEm		medial eminence
ma4V		median aperture (foramen of Magendie)
MSul		median sulcus
Obx		obex
SulL		sulcus limitans
Tae		taenia cinerea
10Tr		vagal trigone
MOSS		surface structures of medulla
alms		anterolateral medullary sulcus
pros		preolivary sulcus
cutu		cuneate tubercle
dmms		dorsal (posterior) median medullary sulcus
fce		foramen caecum
grtu		gracile tubercle (clava)
imv		inferior (caudal) medullary velum
dims		dorsal intermedite medullary sulcus
dlms		dorsal lateral medullary sulcus
posos		postolivary sulcus
r11		root of accessory nerve
r11cr		cranial root of accessory nerve
r11sp		spinal root of accessory nerve
r12		root of hypoglossal nerve
r9		root of glossopharyngeal nerve
r10		root of vagus nerve
vmms		ventral (anterior) median medullary sulcus
SpC		spinal cord

TABLE 3. *Continued*

SGM		gray matter of spinal cord
SpI		laminar I of spinal cord
SpII		laminar II of spinal cord
SpIII-IV		laminar III and IV of spinal cord
SpV-VI		laminar V and VI of spinal cord
SpVII		laminar VII of spinal cord
CeCv		central cervical nucleus of spinal cord
SpVIII		laminar VIII of spinal cord
SpIX		laminar IX of spinal cord
SpX		laminar X of spinal cord
SWM		white matter of spinal cord
dfs		dorsal fasciculus of spinal cord
lfs		lateral fasciculus of spinal cord
polt		posterior lateral tract of spinal cord
vfs		ventral fasciculus of spinal cord
SV		ventricle of spinal cord
cces		central canal and ependyma of spinal cord
SSS		surface structures of spinal cord
rsn		roots of spinal nerves
vmss		ventral (anterior) median spinal sulcus

Figure 16. Anteroposterior position of the 106 annotated plates shown in Figure 17. Major macroscopic landmarks (sulci and gyri) on the medial aspect of the left hemisphere are indicated (flipped to show the plate levels (plates 1–106) in an anterior-to-posterior order). General locations of slabs 1–8 were also marked at the top. Note that in slabs 4–7, only the alternative plates were indicated, to avoid busy lines. For abbreviations see Table 3. Scale bar = 2 cm.

Figure 17. Human brain atlas plates. 106 plates with matching histological sections are displayed in anterior-to-posterior (A-P) order. The matching histological images include 50 Nissl-stained, and 50 NFP- and 6 PV-immunostained sections. The 106 plate images, corresponding to the A-P positions delineated in Figure 16, combine the cortical annotation of modified Brodmann areas and traditional gyri and sulci. At each level, a color-coded atlas plate ("a" series; 1a–106a) and a histological image ("b" series; 1b–106b) are presented. The inset diagram at the top right corner of each atlas plate shows the A-P position (red line) of that plate on a schematic representation of the whole hemisphere based on MRI. The green lettering along the cortical surface indicates cortical sulci (lower case, often with black arrowheads) and gyri (upper case), which were generally defined by adjacent sulci. Modified Brodmann areas were labeled within the cortical gray matter with differential color coding. In plates containing cerebellar cortex, alternative plates were annotated for three cerebellar cortical zones (vermis, paravermis, and lateral hemisphere) and 10 lobules (lobules I–X), respectively. Other subcortical structures were also labeled with differential color coding. The general locations of most white matter tracts are indicated by a circled "W". Fiber tracts with clear boundaries, such as ac, mtt, ot, sste/or, fx, fr, scp, py, and ml, were outlined by black lines without color code (white). The parcellation and subdivisions of different brain regions as well as the parent–daughter relationship and abbreviation of each structure are detailed in Table 3. Note that two separate versions of this atlas for modified Brodmann areas and traditional gyri and sulci, respectively, are available in the online version of this atlas (www.brainspan.org or http://brainspan.org/static/atlas). For abbreviations see Table 3. Scale bar = 5 mm (at levels 1b–106b).

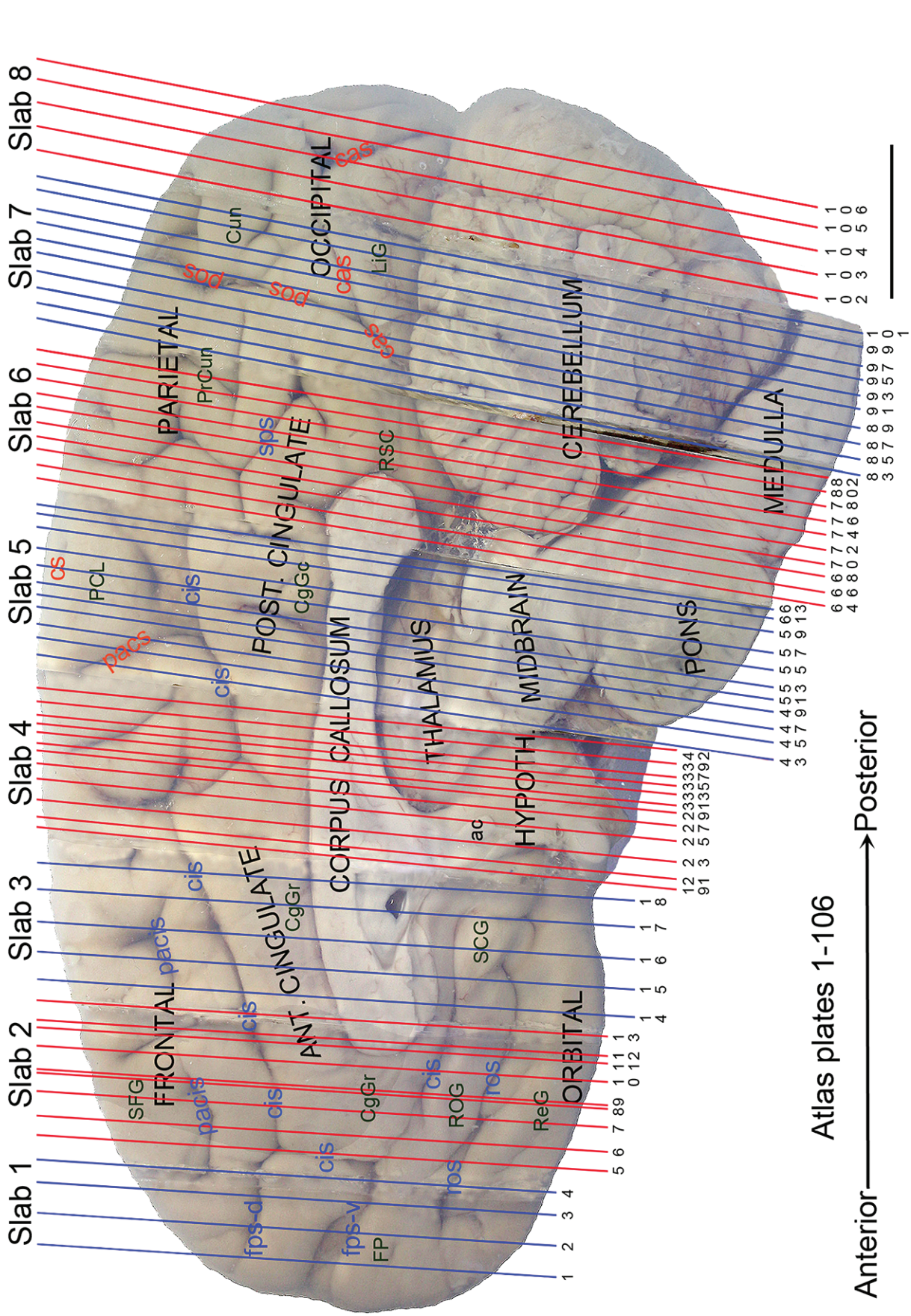
Slab 1
Slab 2
Slab 3
Slab 4
Slab 5
Slab 6
Slab 7
Slab 8
SFG
FRONTAL
pacis
cis
fps-d
fps-v
FP
ros
ROG
ReG
ORBITAL
CgGr
ANT. CINGULATE
CORPUS CALLOSUM
ac
SCG
THALAMUS
HYPOTH.
MIDBRAIN
PONS
MEDULLA
CEREBELLUM
RSC
POST. CINGULATE
CgGc
cs
PCL
PARIETAL
PrCun
sps
sod
Cun
cas
LiG
OCCIPITAL
Anterior
Atlas plates 1-106
Posterior

Figure 16.

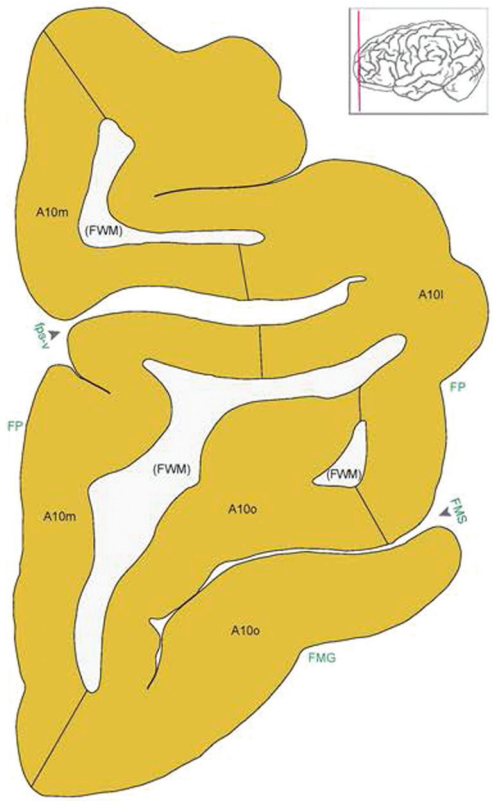

Figure 17. Level 1a (01_111)

Link to online high resolution atlas plate
Link to online high resolution atlas plate (Nissl)

Figure 17. Level 1b (NFP (SMI-32))

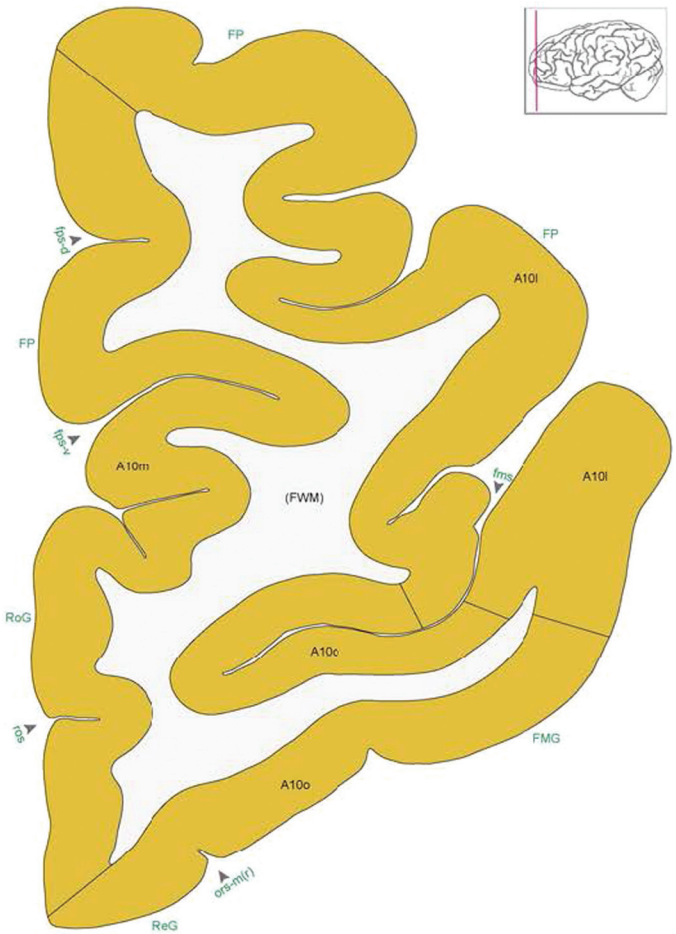

Figure 17. Level 2a (01_179)

Link to online high resolution atlas plate
Link to online high resolution atlas plate (Nissl)

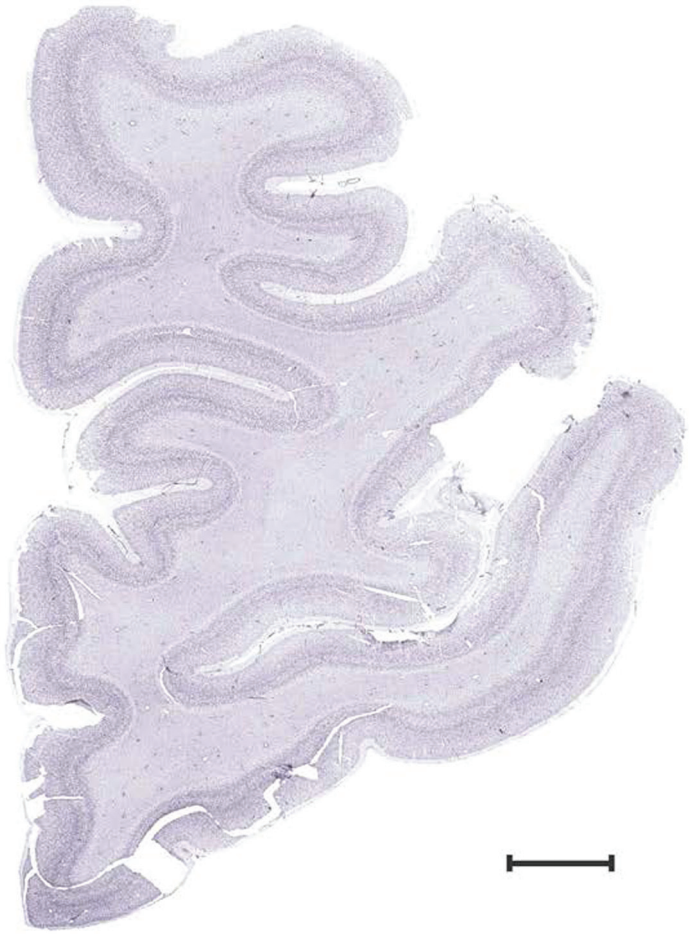

Figure 17. Level 2b (Nissl)

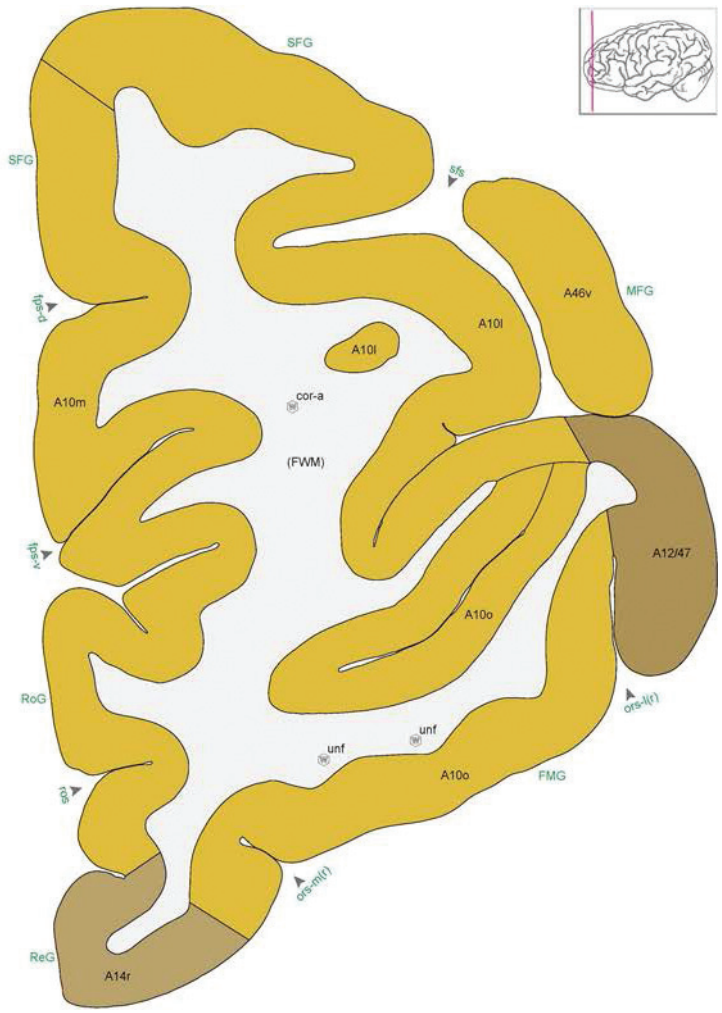

Figure 17. Level 3a (01_247)

Link to online high resolution atlas plate
Link to online high resolution atlas plate (Nissl)

Figure 17. Level 3b (NFP (SMI-32))

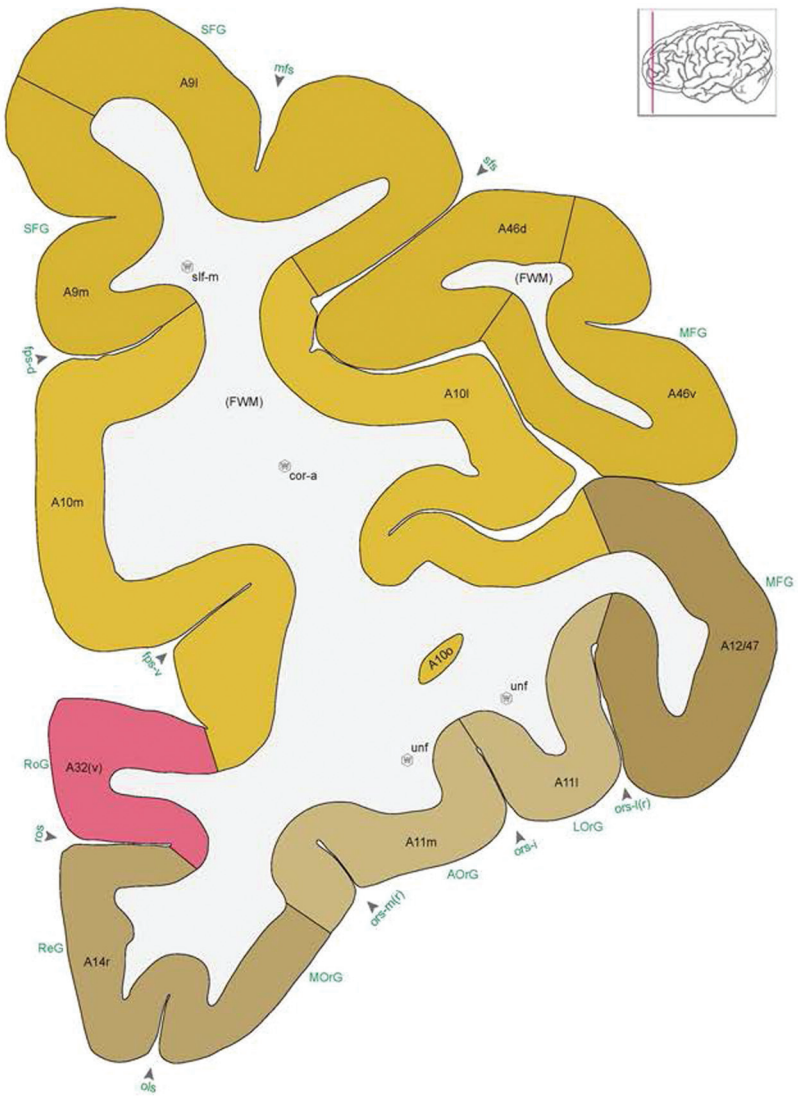

Figure 17. Level 4a (01_307)

Link to online high resolution atlas plate
Link to online high resolution atlas plate (Nissl)

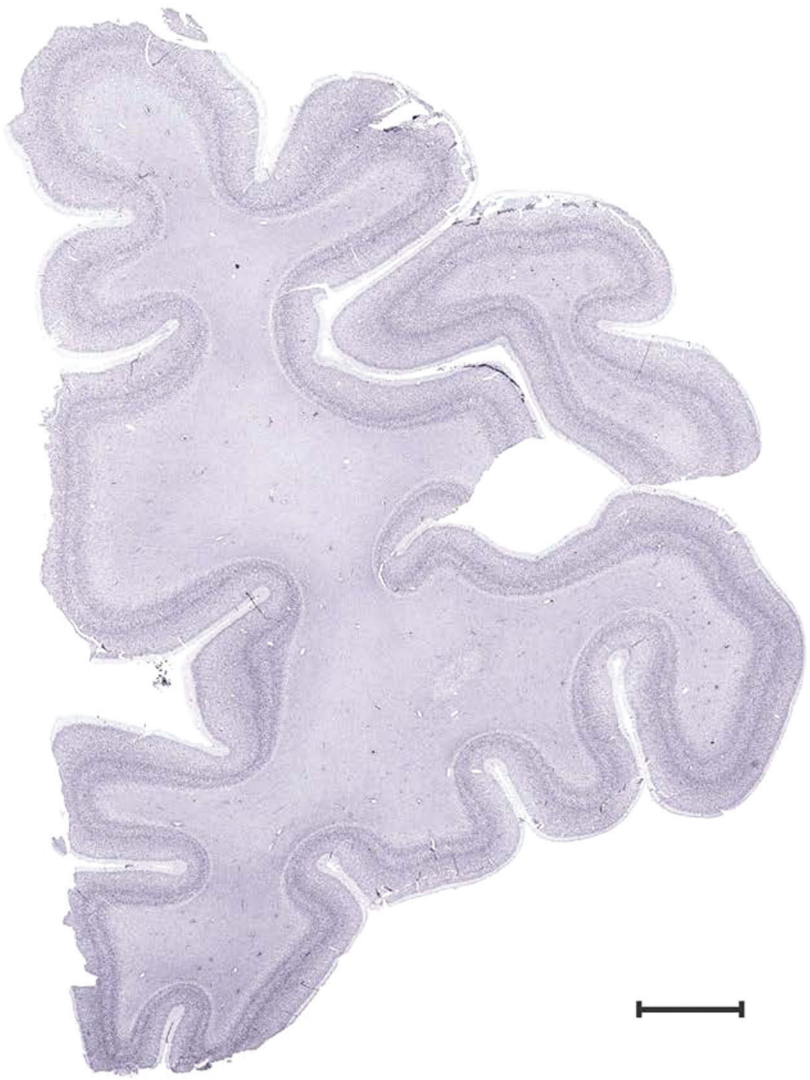

Figure 17. Level 4b (Nissl)

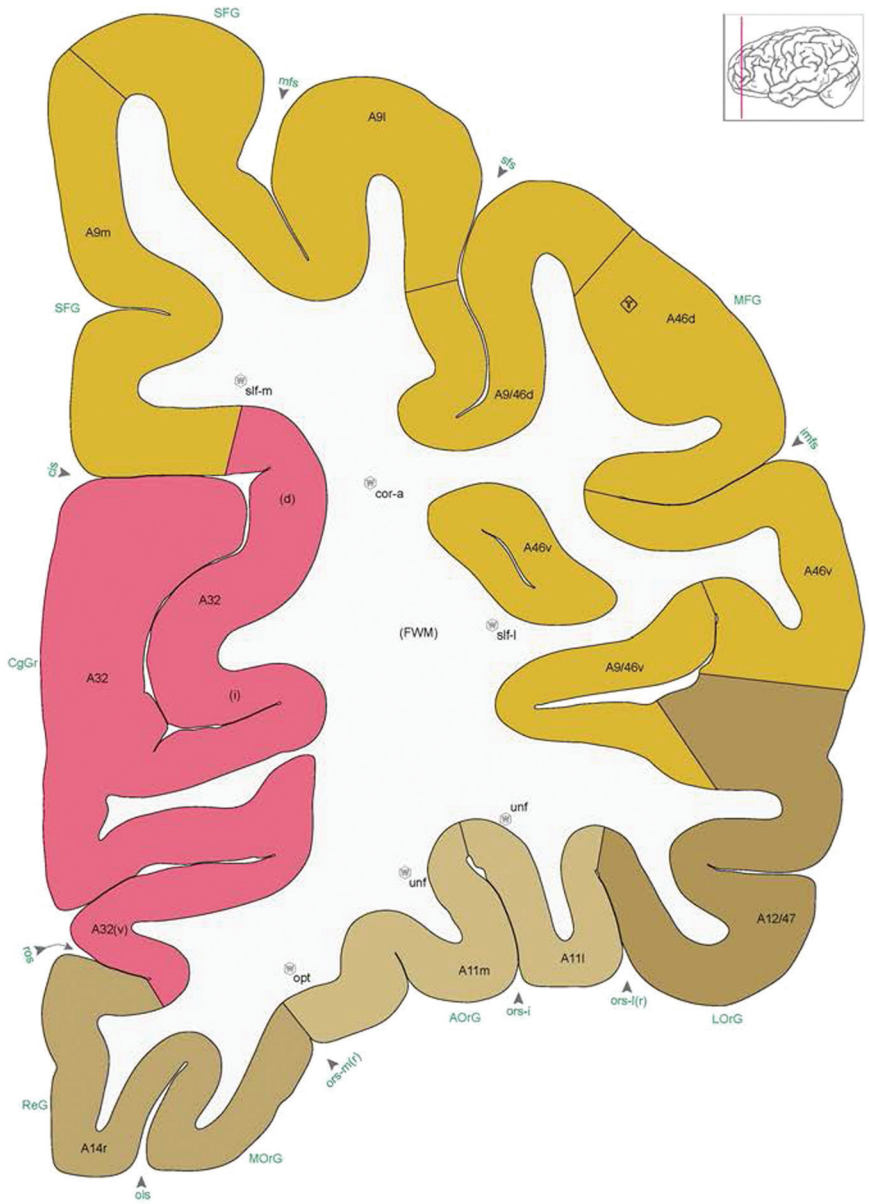

Figure 17. Level 5a (02_111)

Link to online high resolution atlas plate
Link to online high resolution atlas plate (Nissl)

Figure 17. Level 5b (NFP (SMI-32))

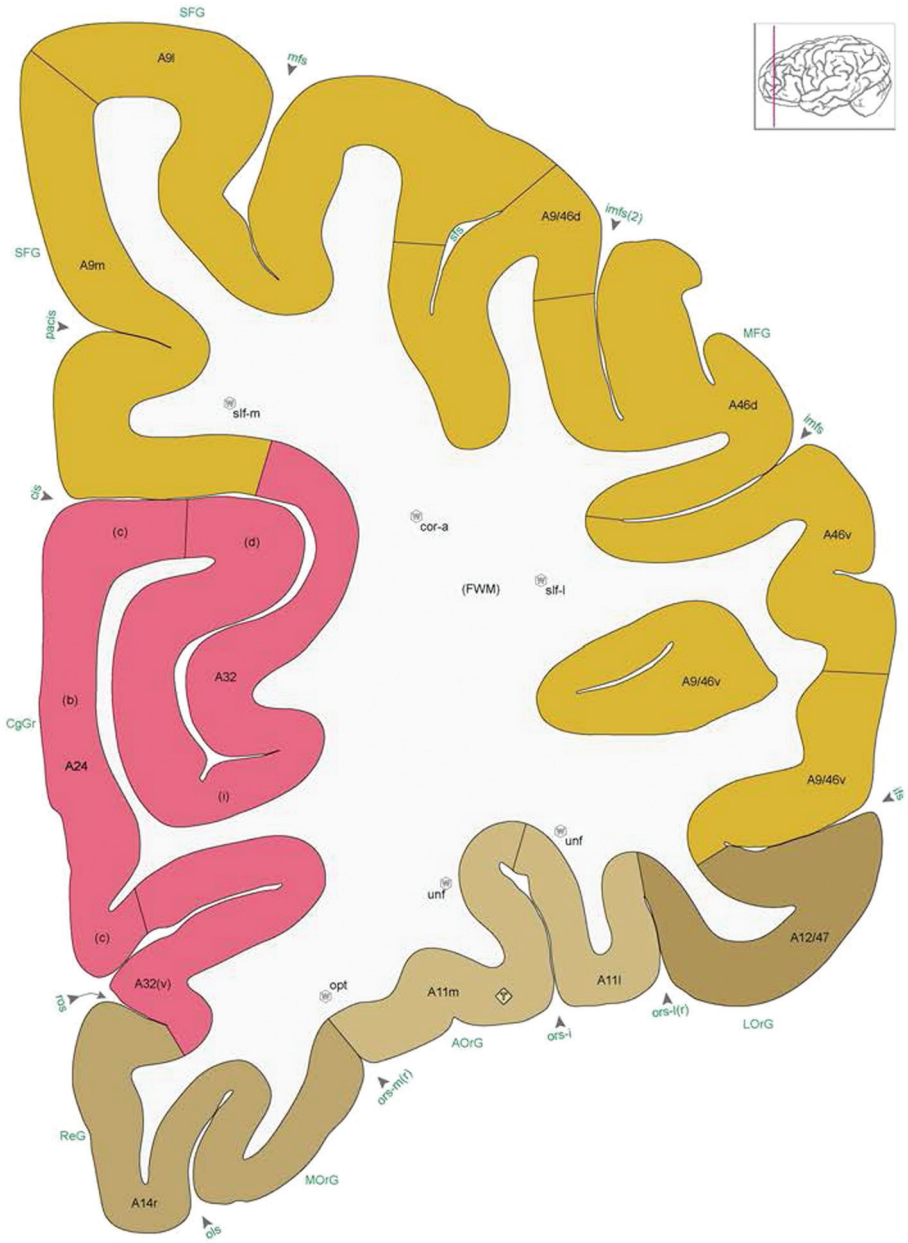

Figure 17. Level 6a (02_111)

Link to online high resolution atlas plate
Link to online high resolution atlas plate (Nissl)

Figure 17. Level 6b (NFP (SMI-32))

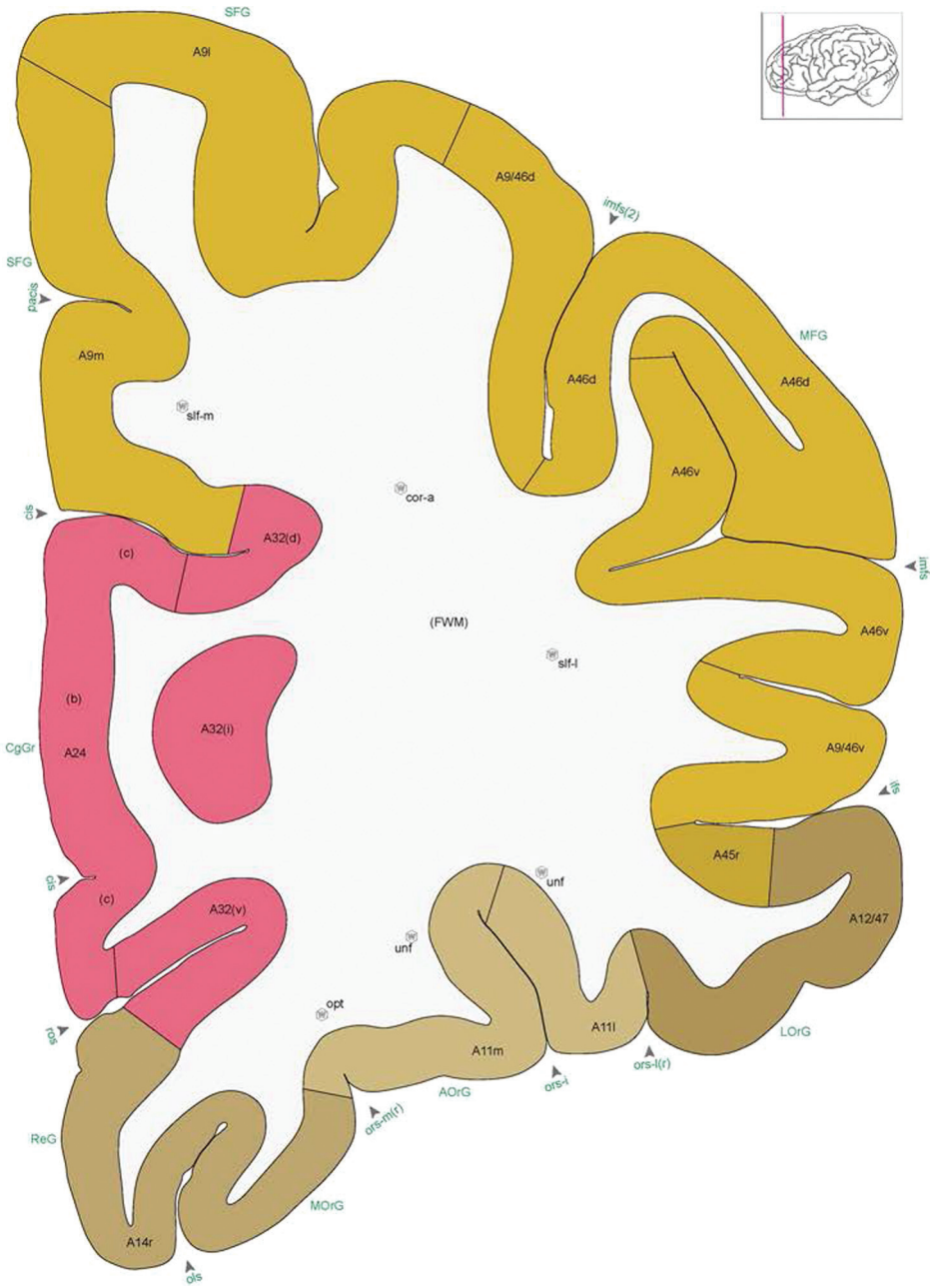

Figure 17. Level 7a (02_175)

Link to online high resolution atlas plate
Link to online high resolution atlas plate (Nissl)

Figure 17. Level 7b (Nissl)

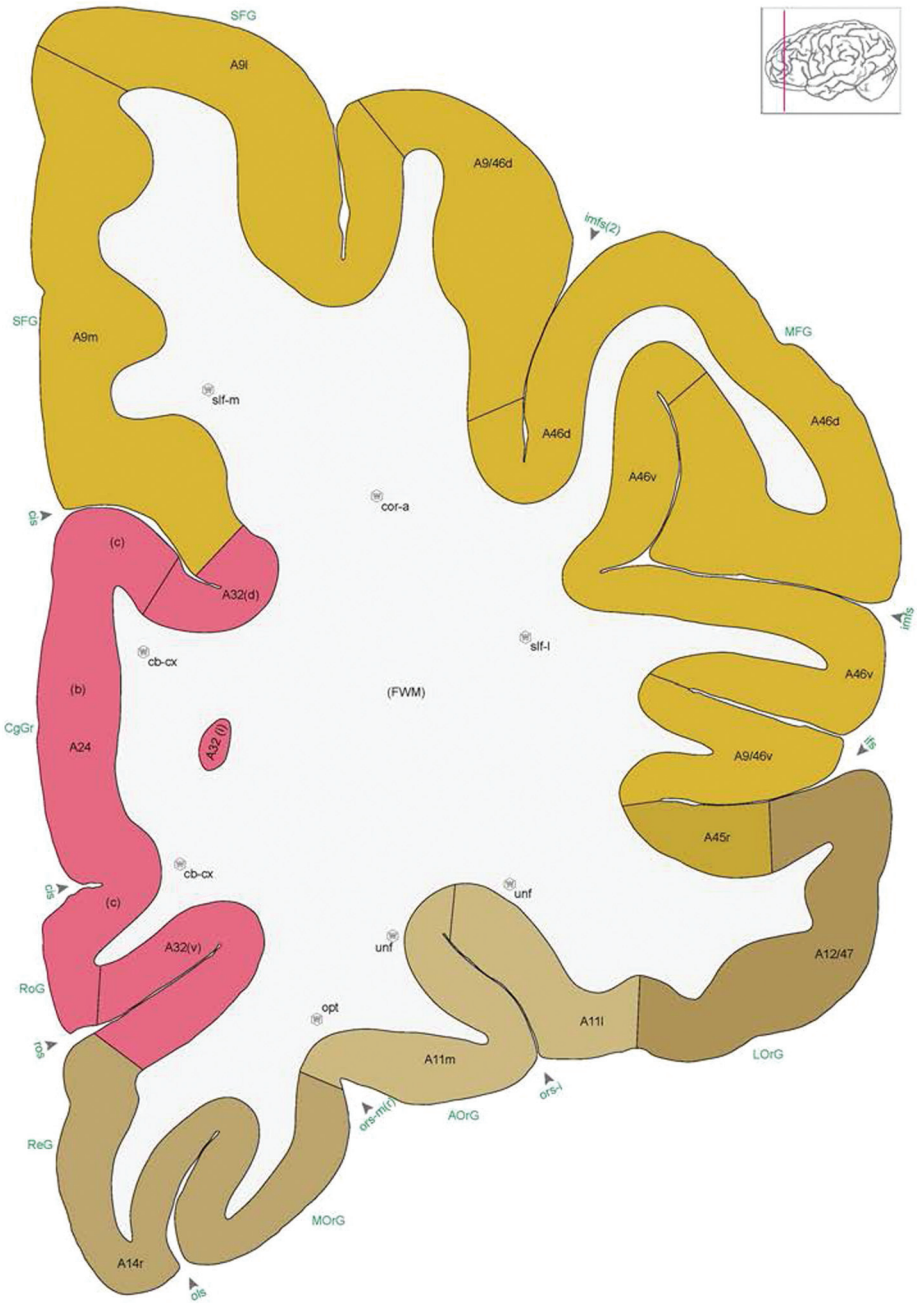

Figure 17. Level 8a (02_219)

Link to online high resolution atlas plate
Link to online high resolution atlas plate (Nissl)

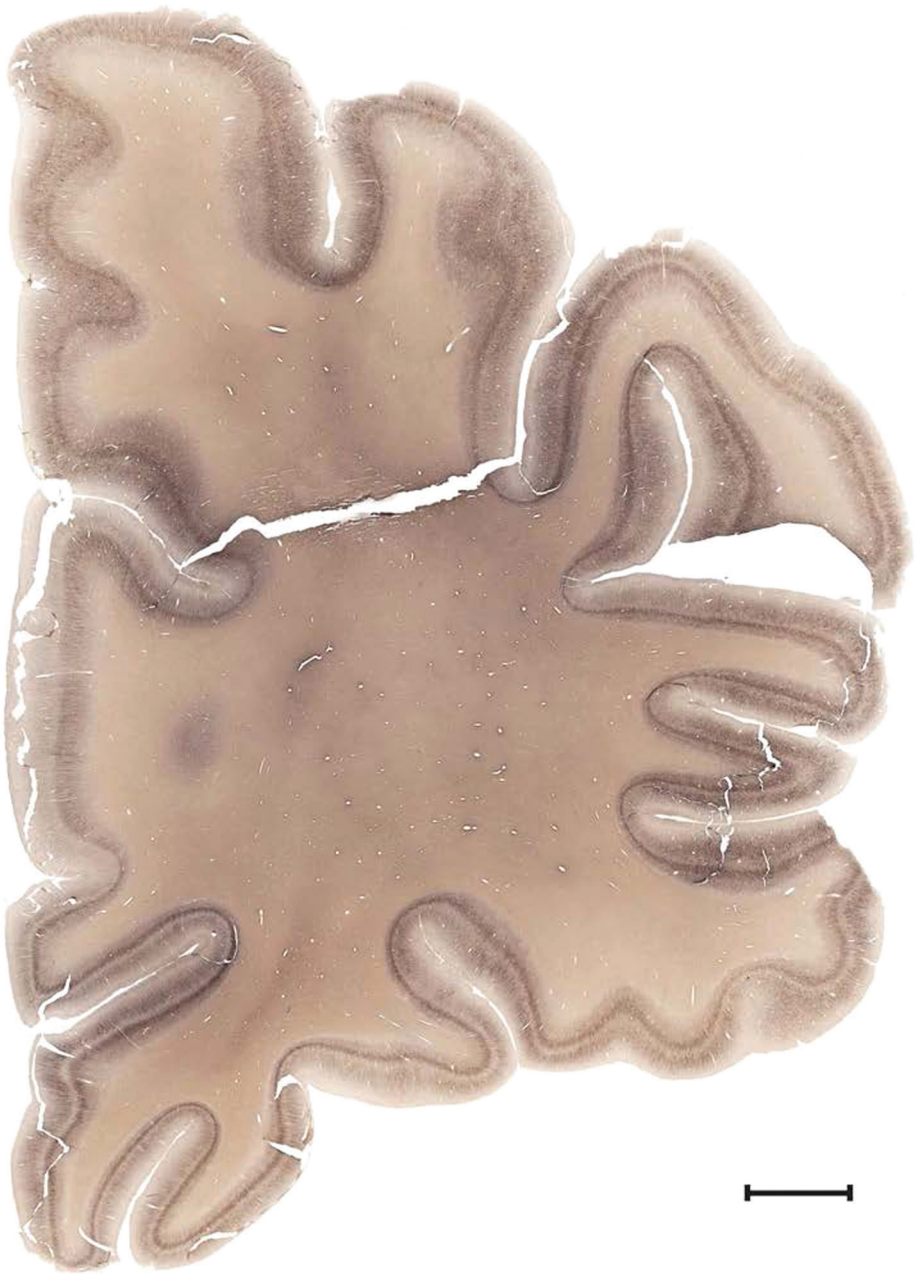

Figure 17. Level 8b (NFP (SMI-32))

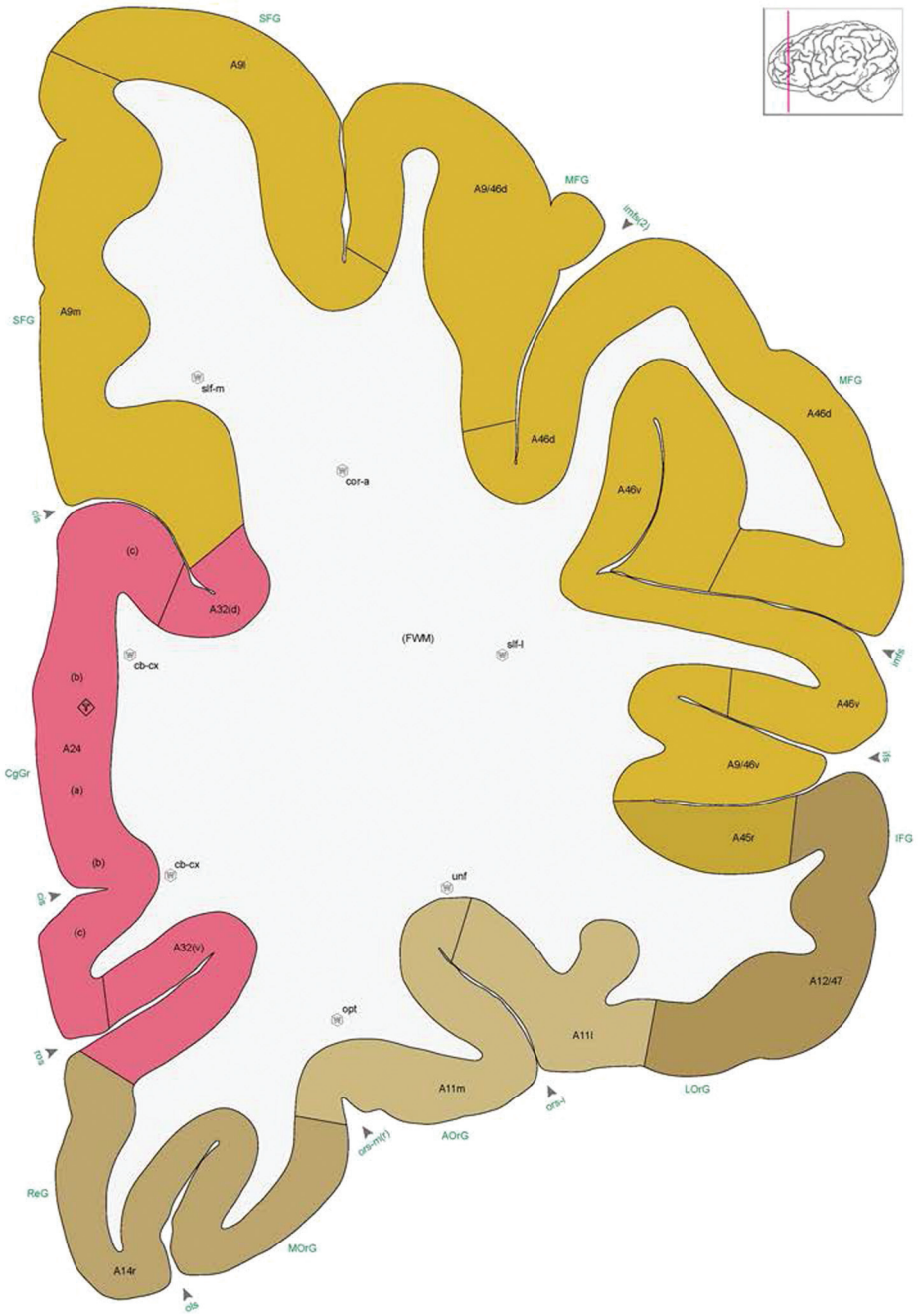

Figure 17. Level 9a (02_231)

Link to online high resolution atlas plate
Link to online high resolution atlas plate (Nissl)

Figure 17. Level 9b (NFP (SMI-32))

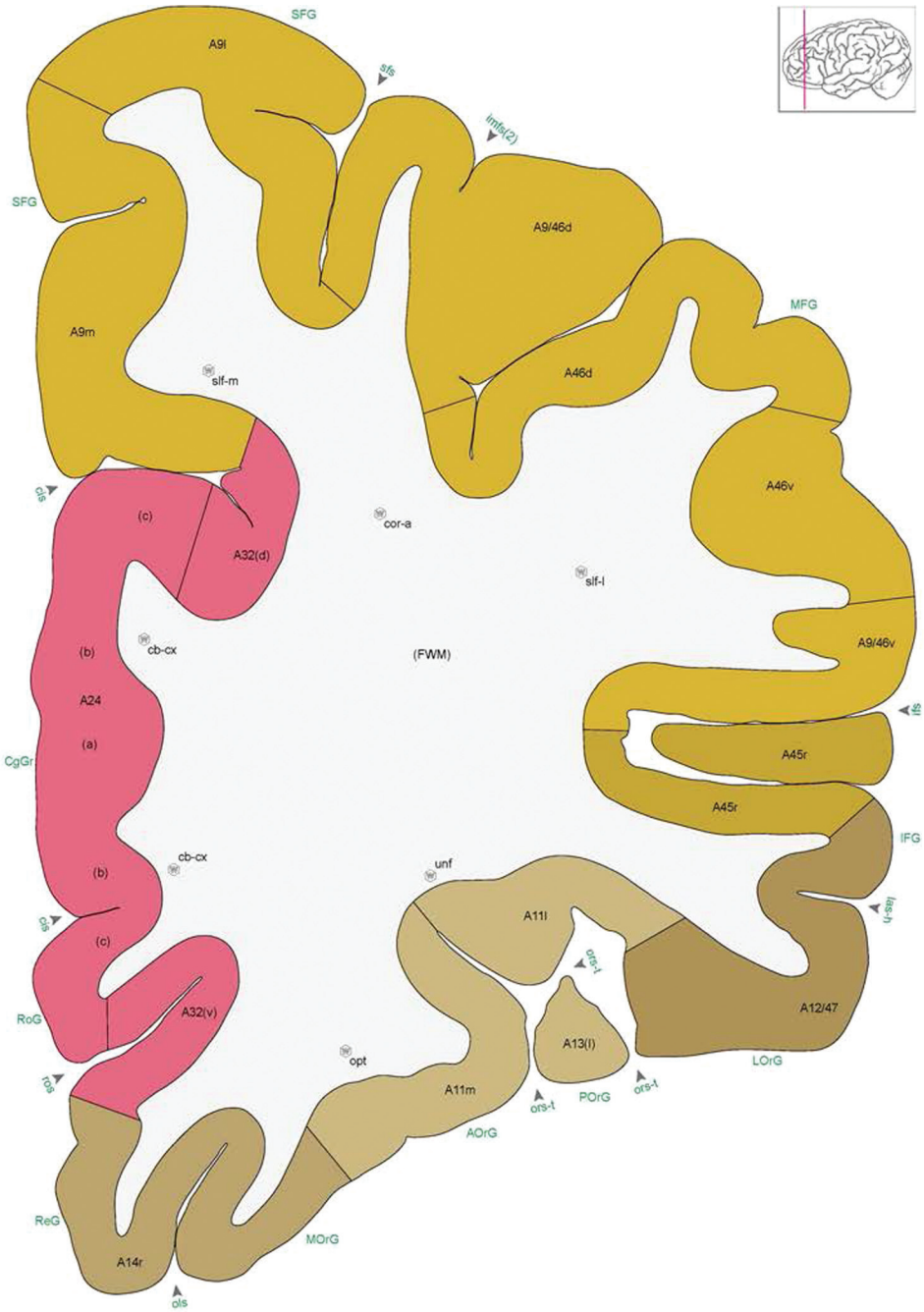

Figure 17. Level 10a (02_295)

Link to online high resolution atlas plate
Link to online high resolution atlas plate (Nissl)

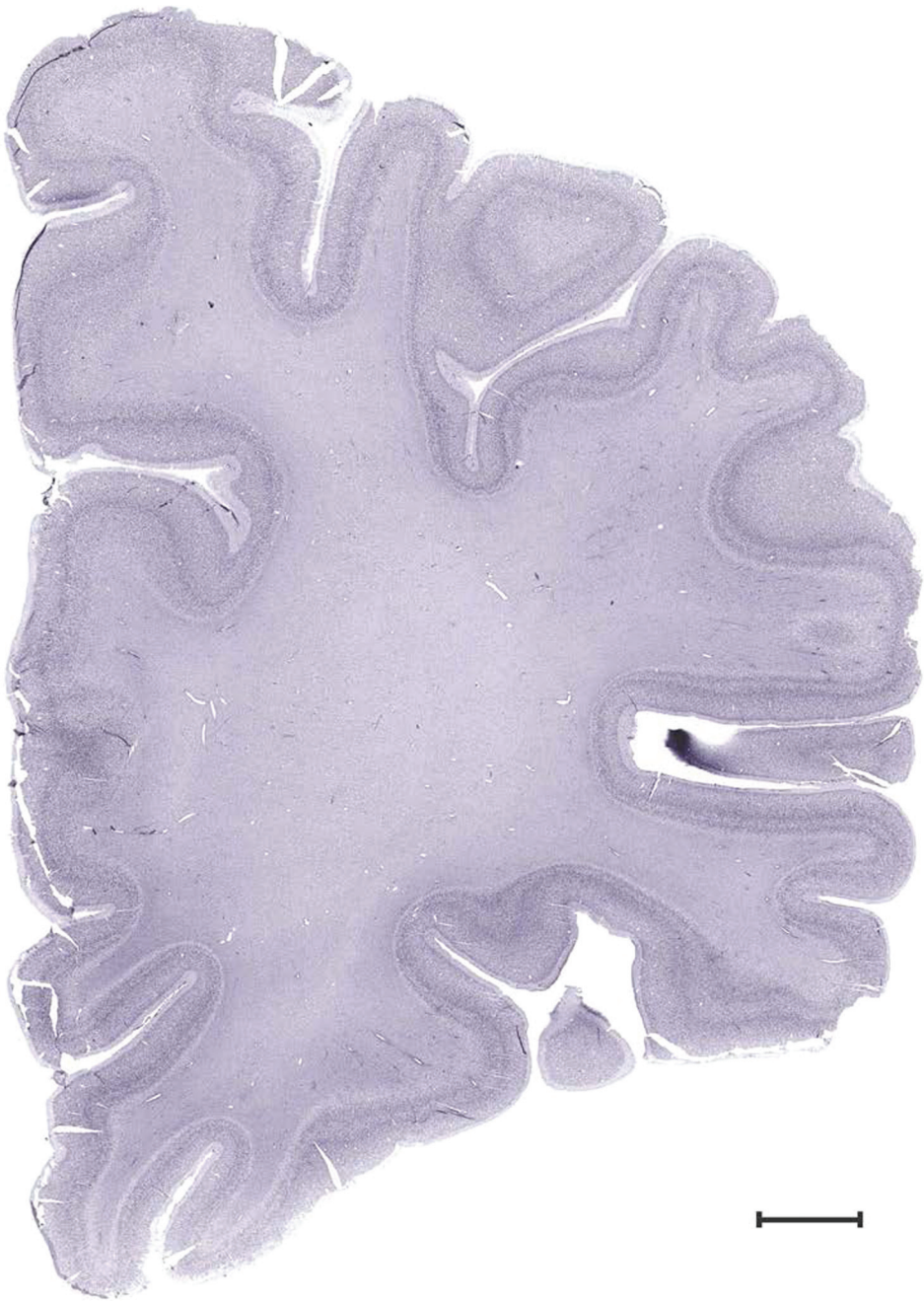

Figure 17. Level 10b (Nissl)

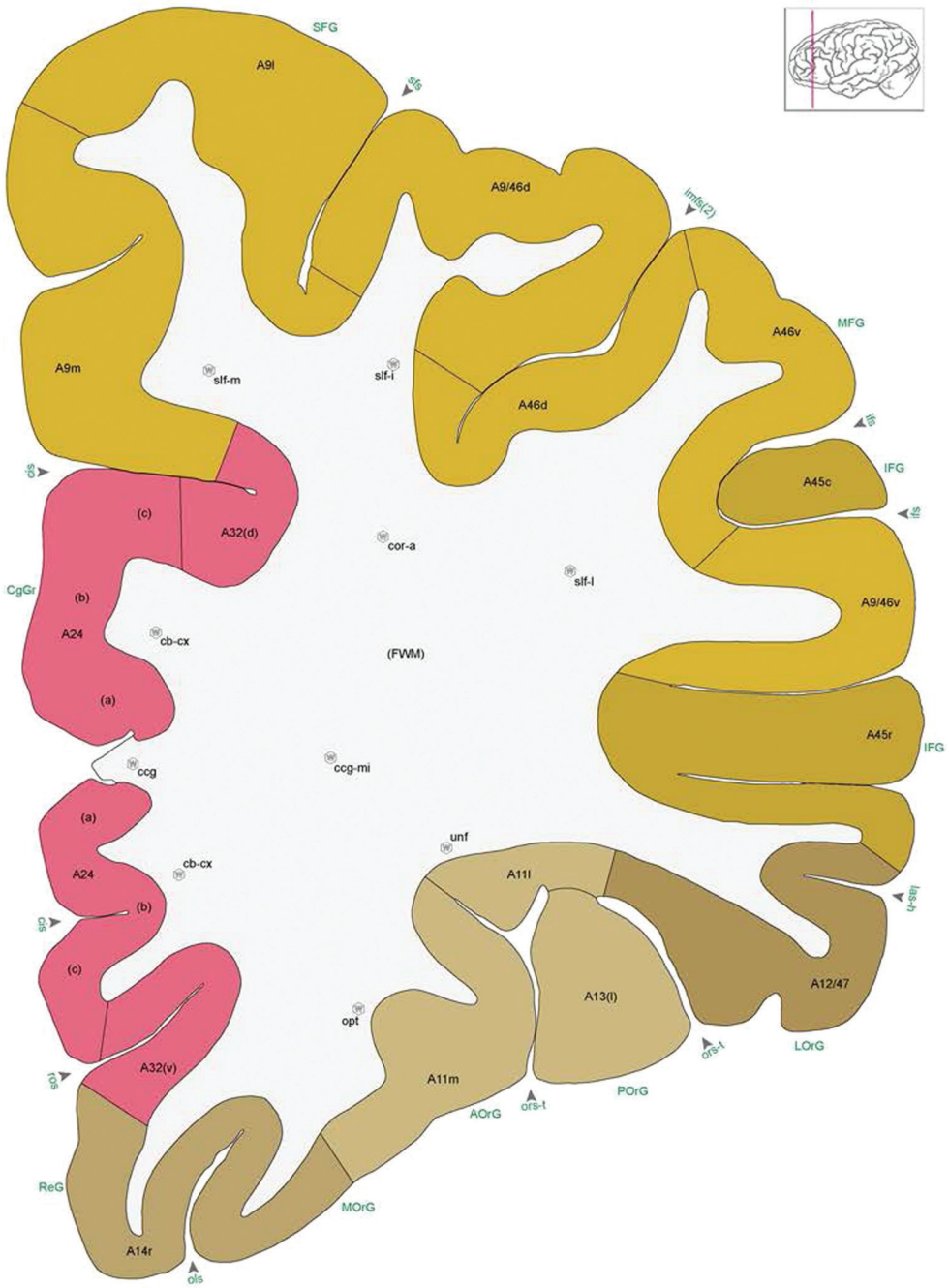

Figure 17. Level 11a (02_335)

Link to online high resolution atlas plate
Link to online high resolution atlas plate (Nissl)

Figure 17. Level 11b (NFP (SMI-32))

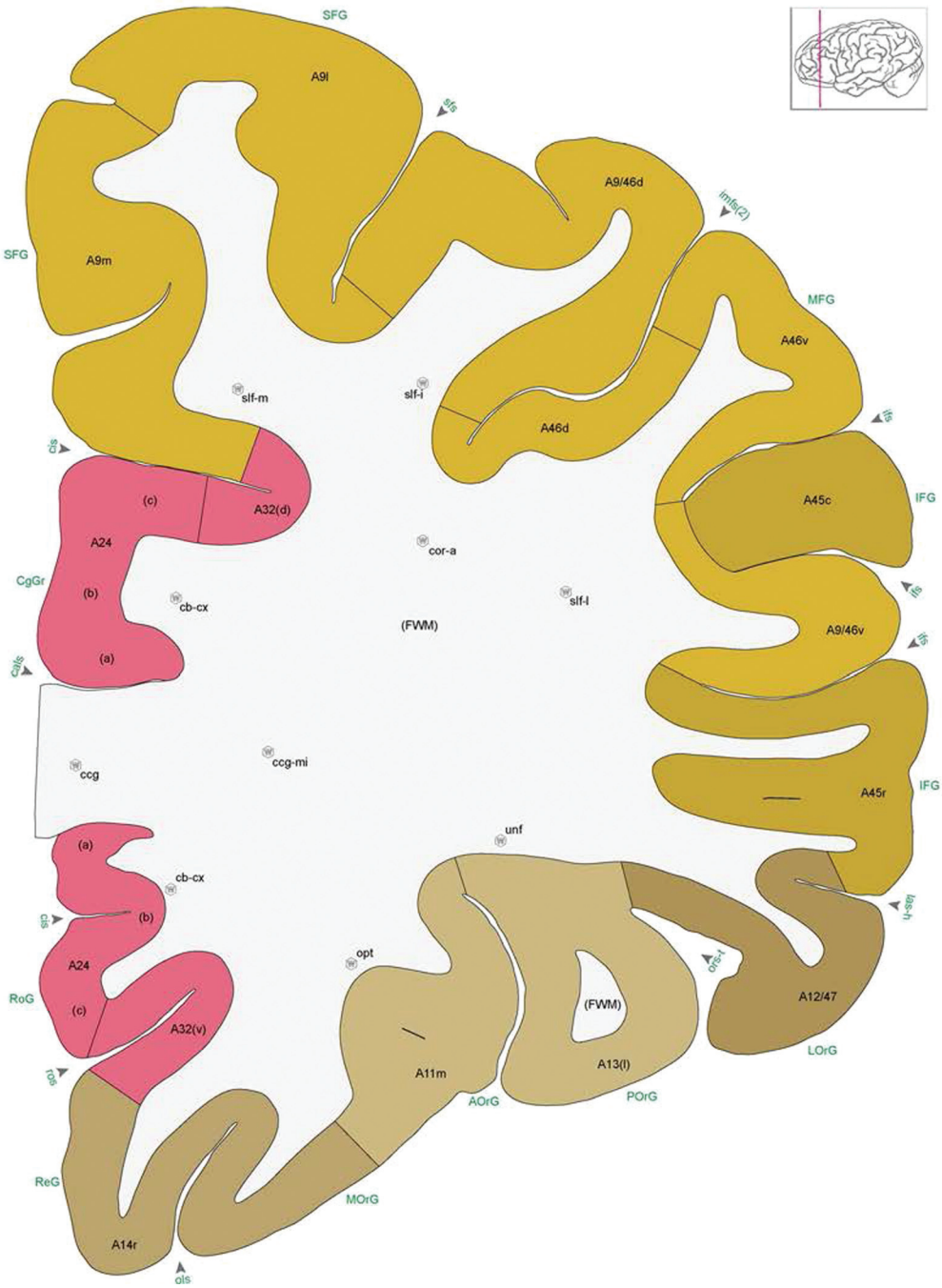

Figure 17. Level 12a (02_359)

Link to online high resolution atlas plate
Link to online high resolution atlas plate (Nissl)

Figure 17. Level 12b (NFP (SMI-32))

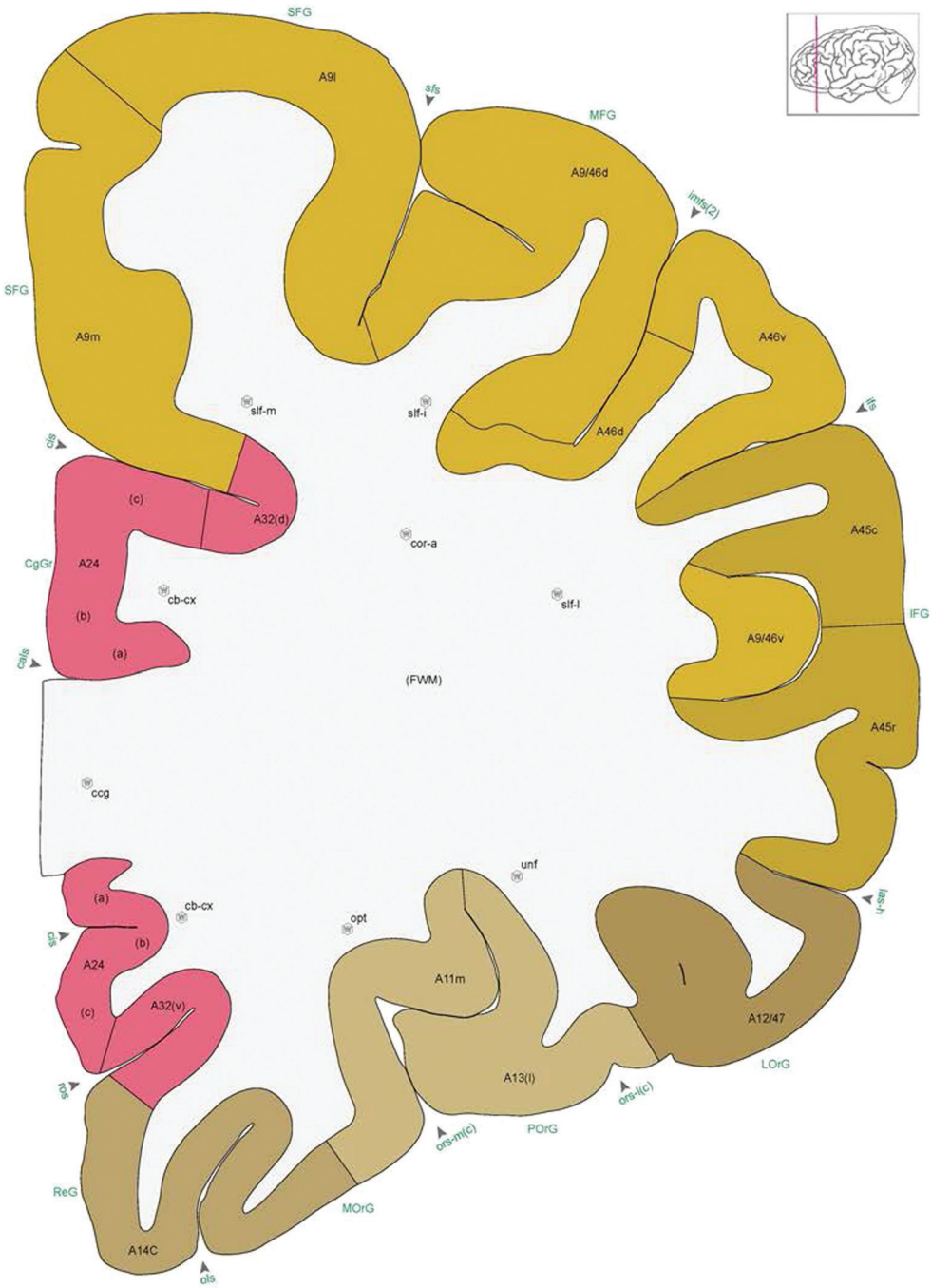

Figure 17. Level 13a (02_407)

Link to online high resolution atlas plate
Link to online high resolution atlas plate (Nissl)

Figure 17. Level 13b (Nissl)

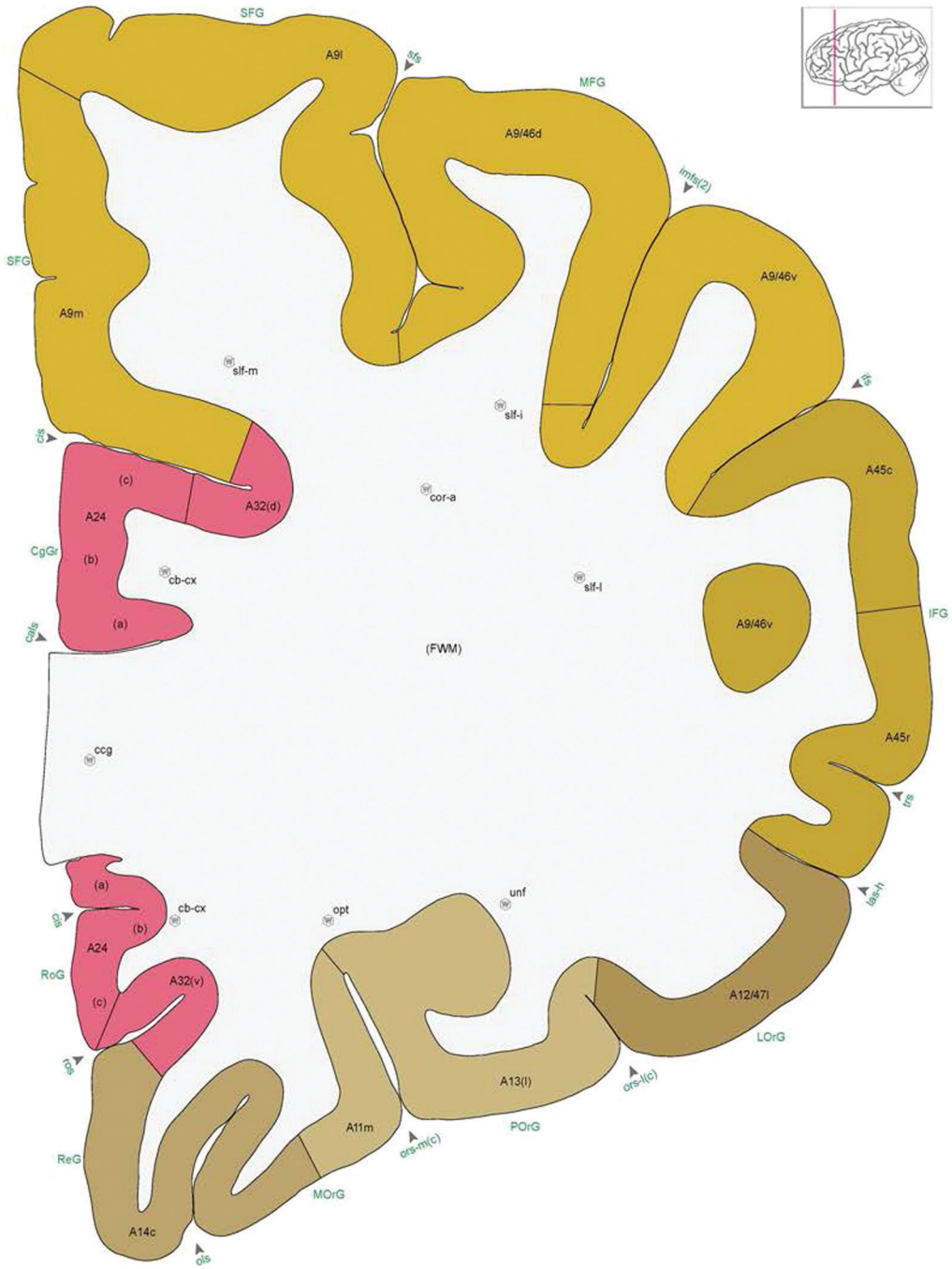

Figure 17. Level 14a (03_031)

Link to online high resolution atlas plate
Link to online high resolution atlas plate (Nissl)

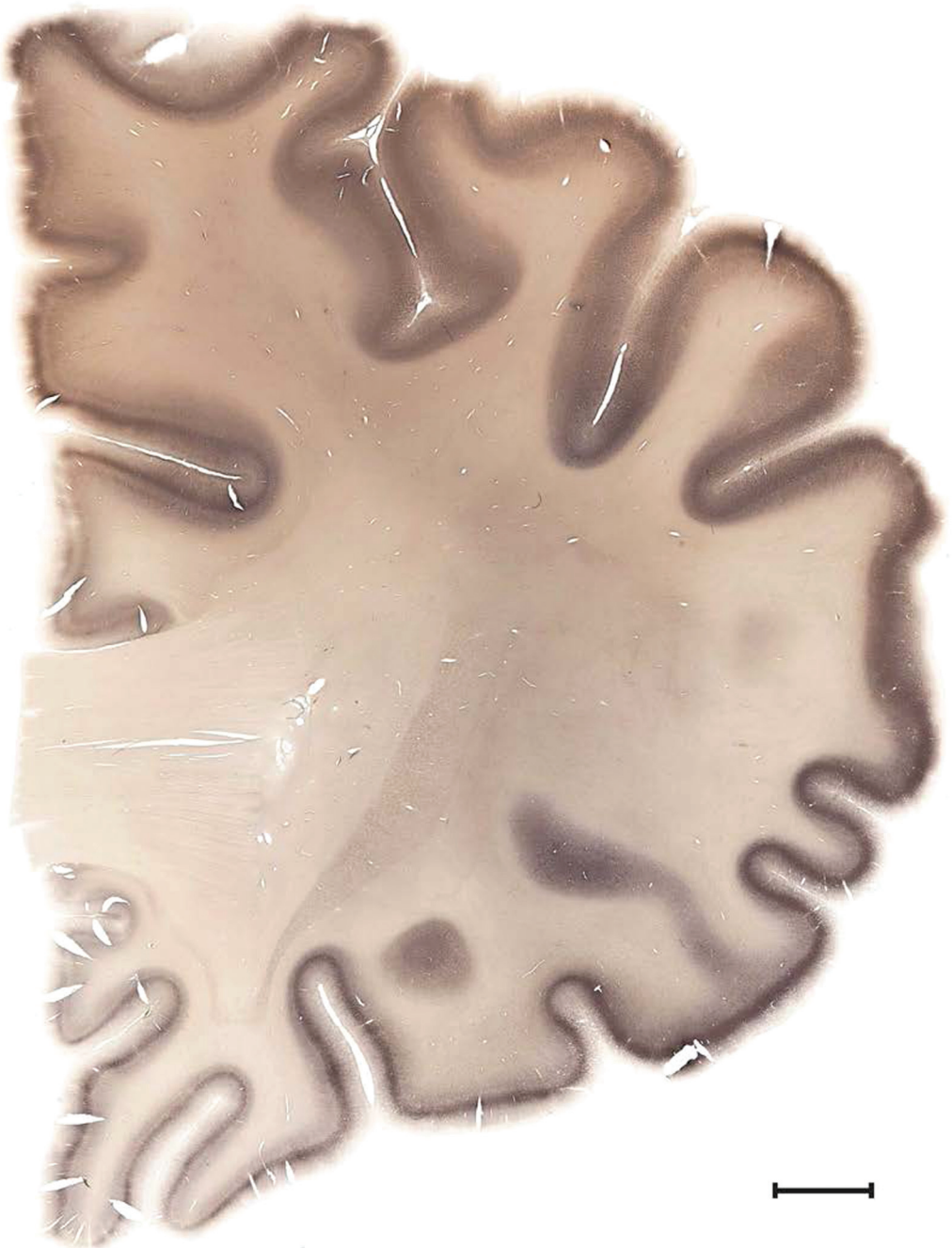

Figure 17. Level 14b (Parvalbumin)

Figure 17. Level 15a (03_095)

Link to online high resolution atlas plate
Link to online high resolution atlas plate (Nissl)

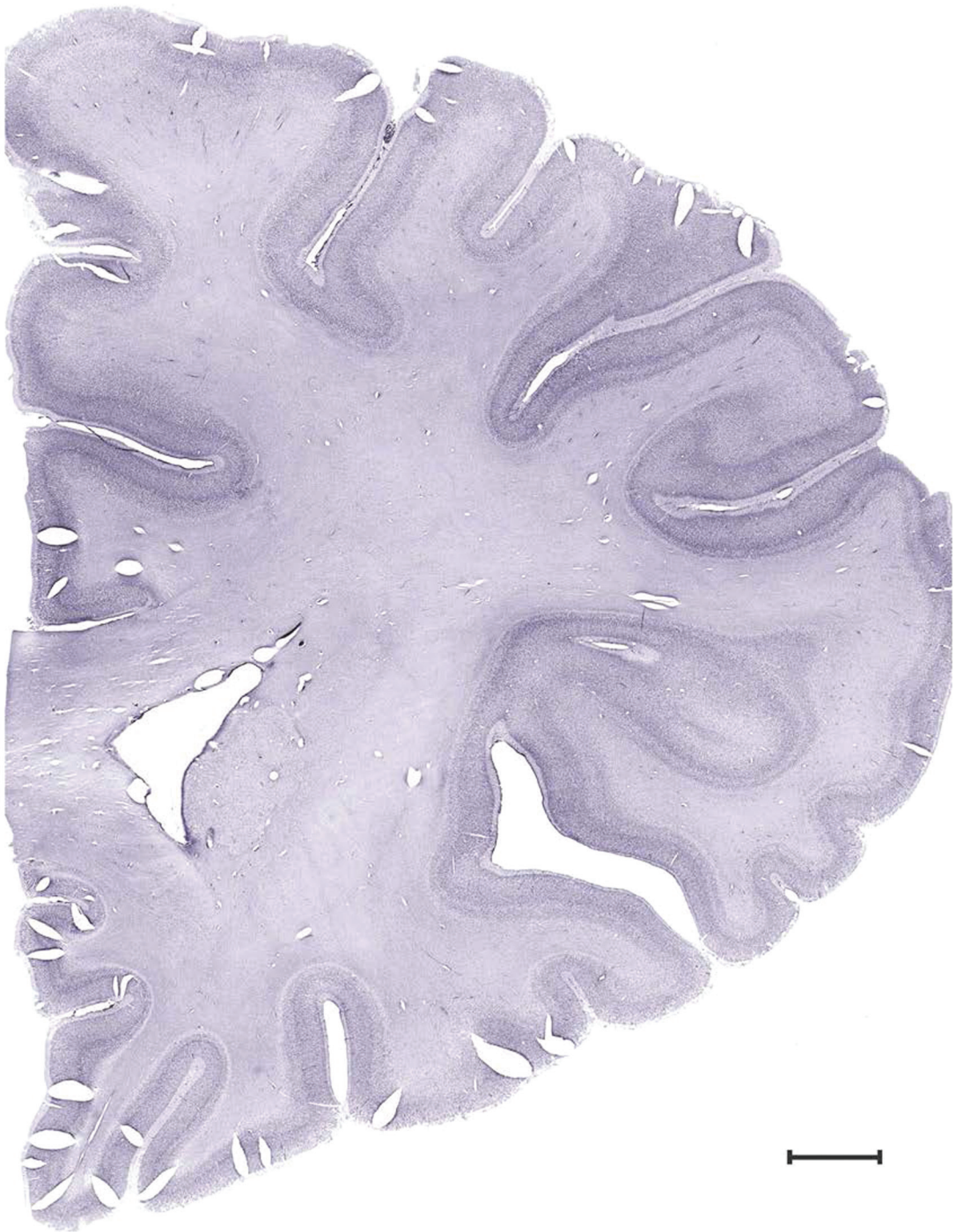

Figure 17. Level 15b (Nissl)

Figure 17. Level 16a (03_159)

Link to online high resolution atlas plate
Link to online high resolution atlas plate (Nissl)

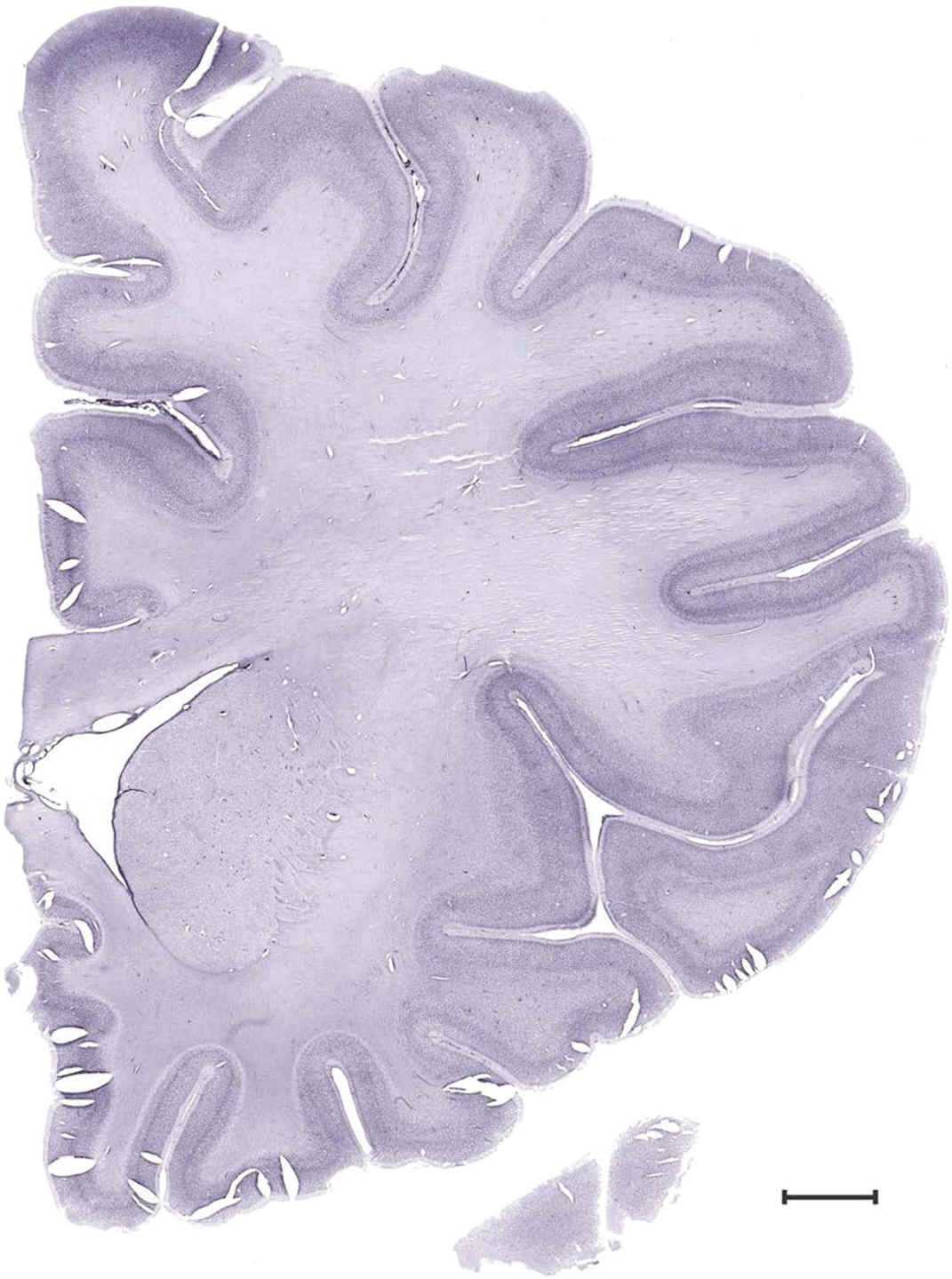

Figure 17. Level 16b (Nissl)

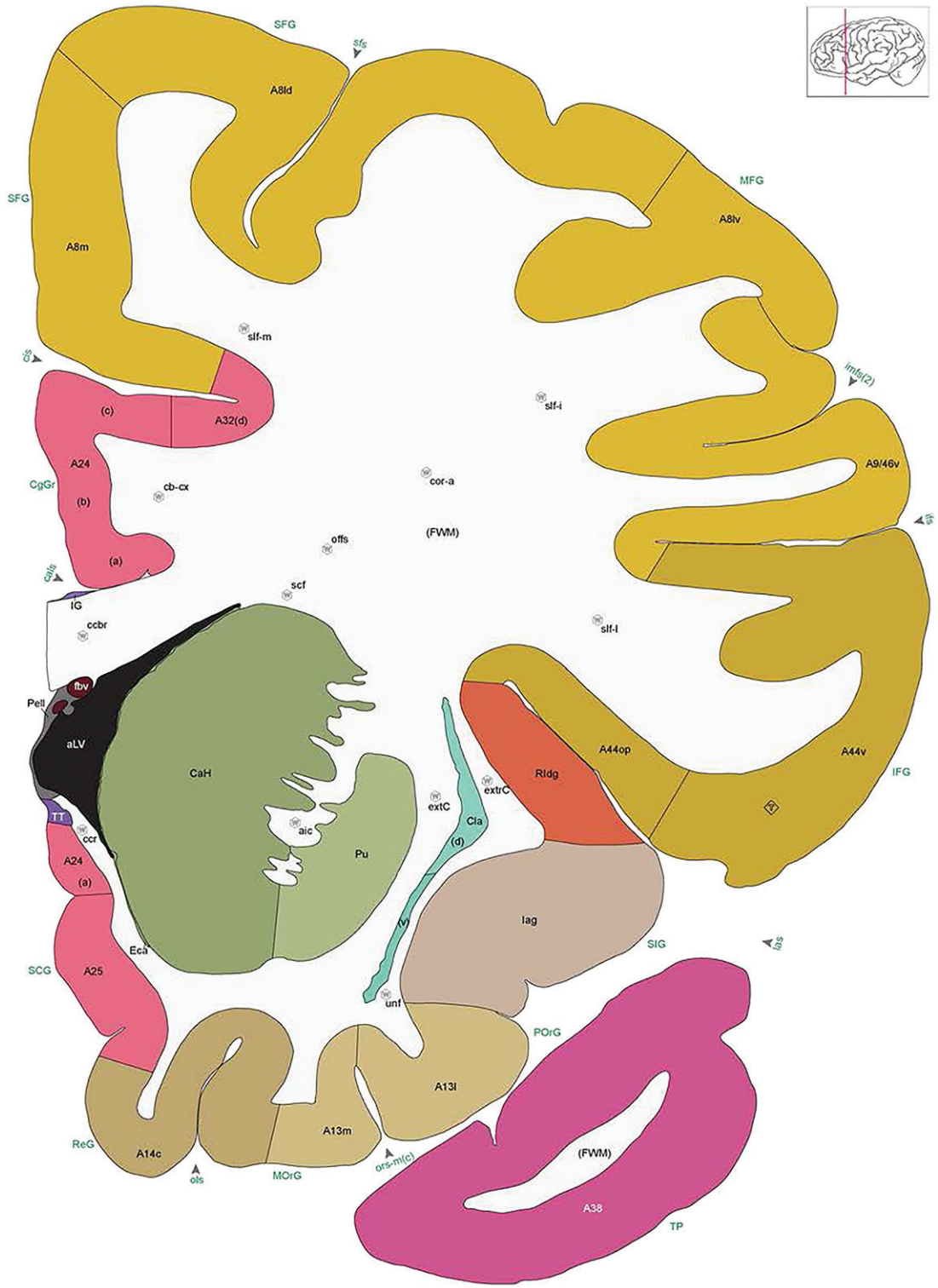

Figure 17. Level 17a (03_227)

Link to online high resolution atlas plate
Link to online high resolution atlas plate (Nissl)

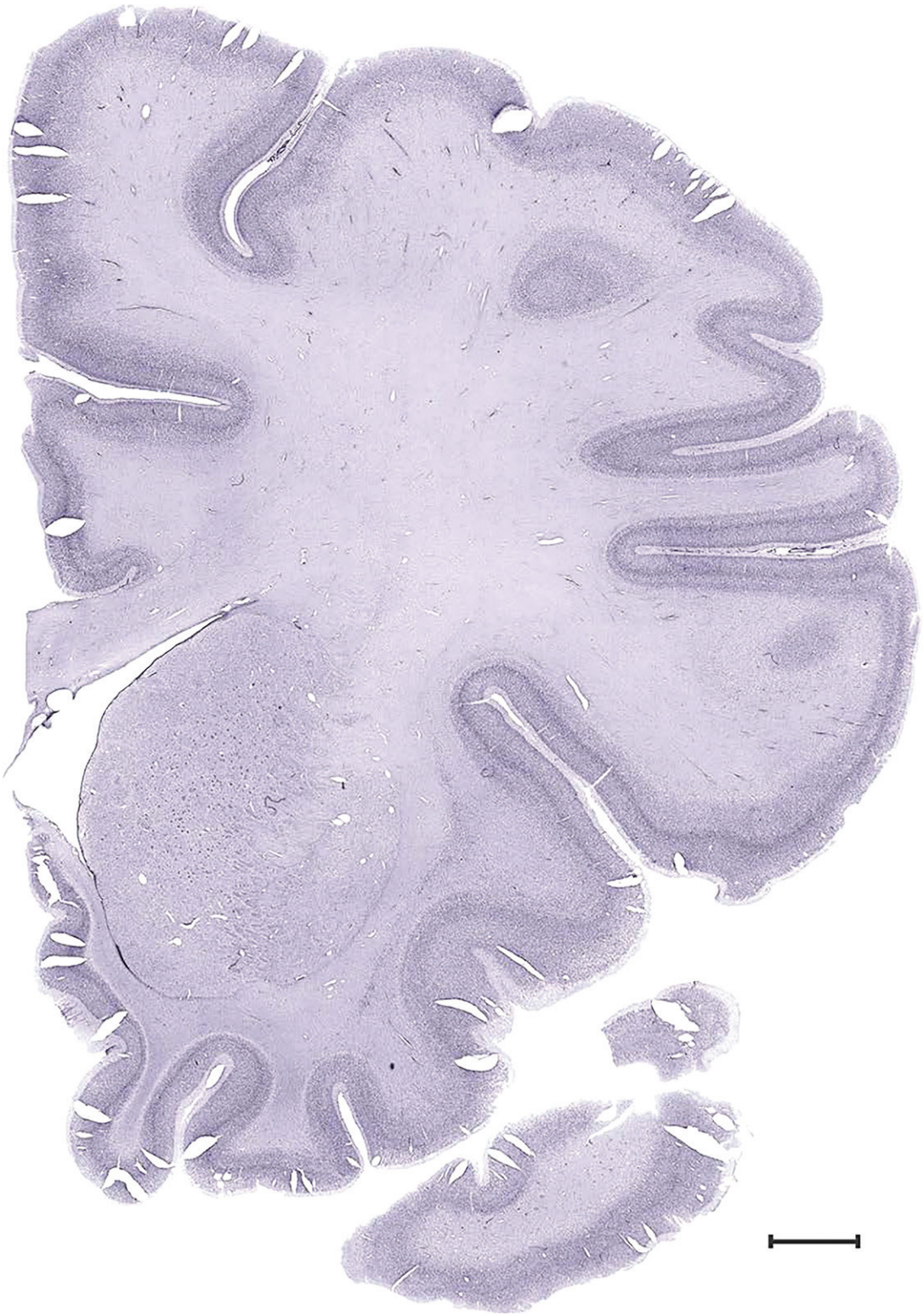

Figure 17. Level 17b (Nissl)

Figure 17. Level 18a (03_291)

Link to online high resolution atlas plate
Link to online high resolution atlas plate (Nissl)

Figure 17. Level 18b (Nissl)

Figure 17. Level 19a (04_035)

Link to online high resolution atlas plate
Link to online high resolution atlas plate (Nissl)

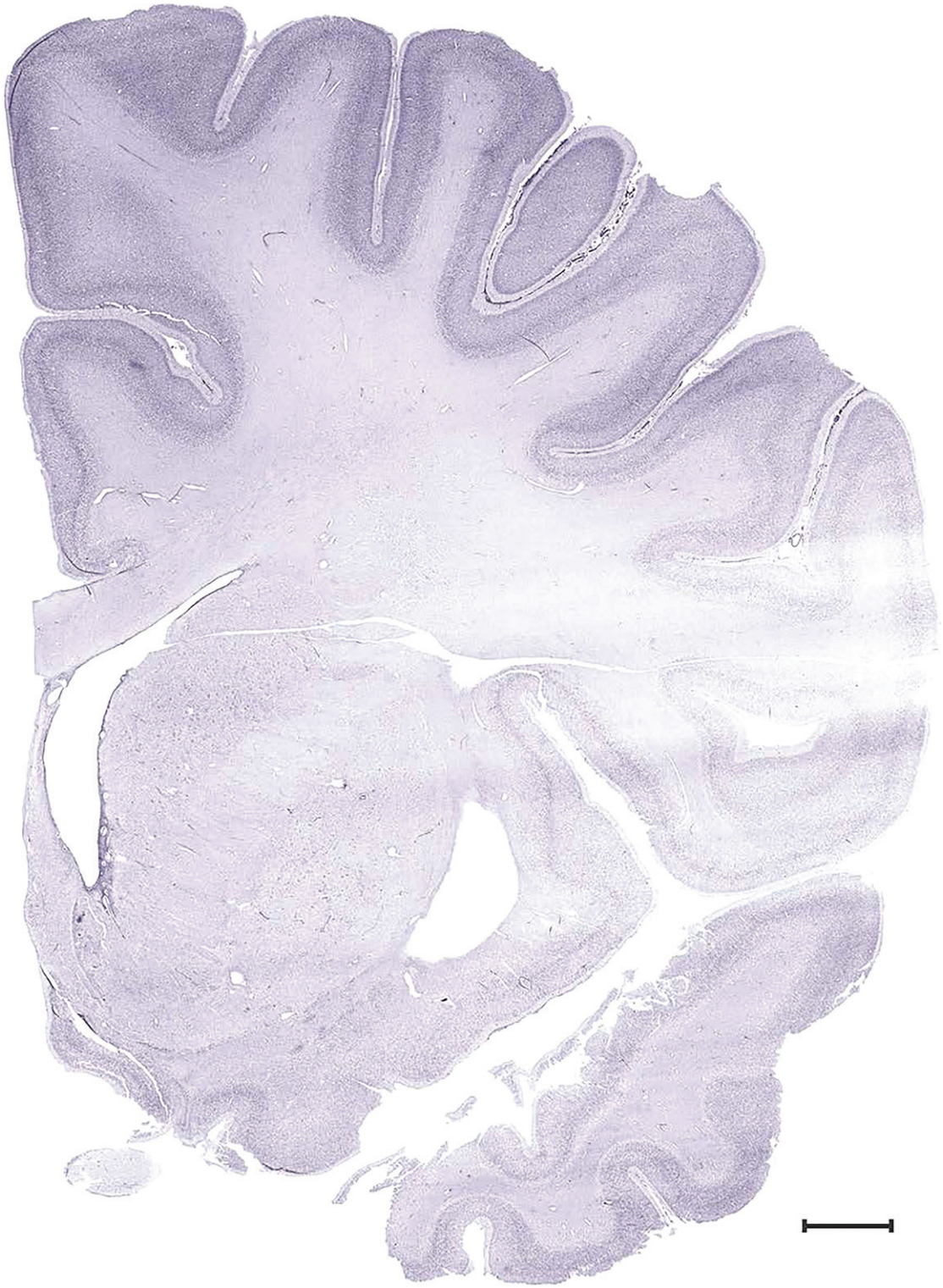

Figure 17. Level 19b (Nissl)

Figure 17. Level 20a (04_051)

Link to online high resolution atlas plate
Link to online high resolution atlas plate (Nissl)

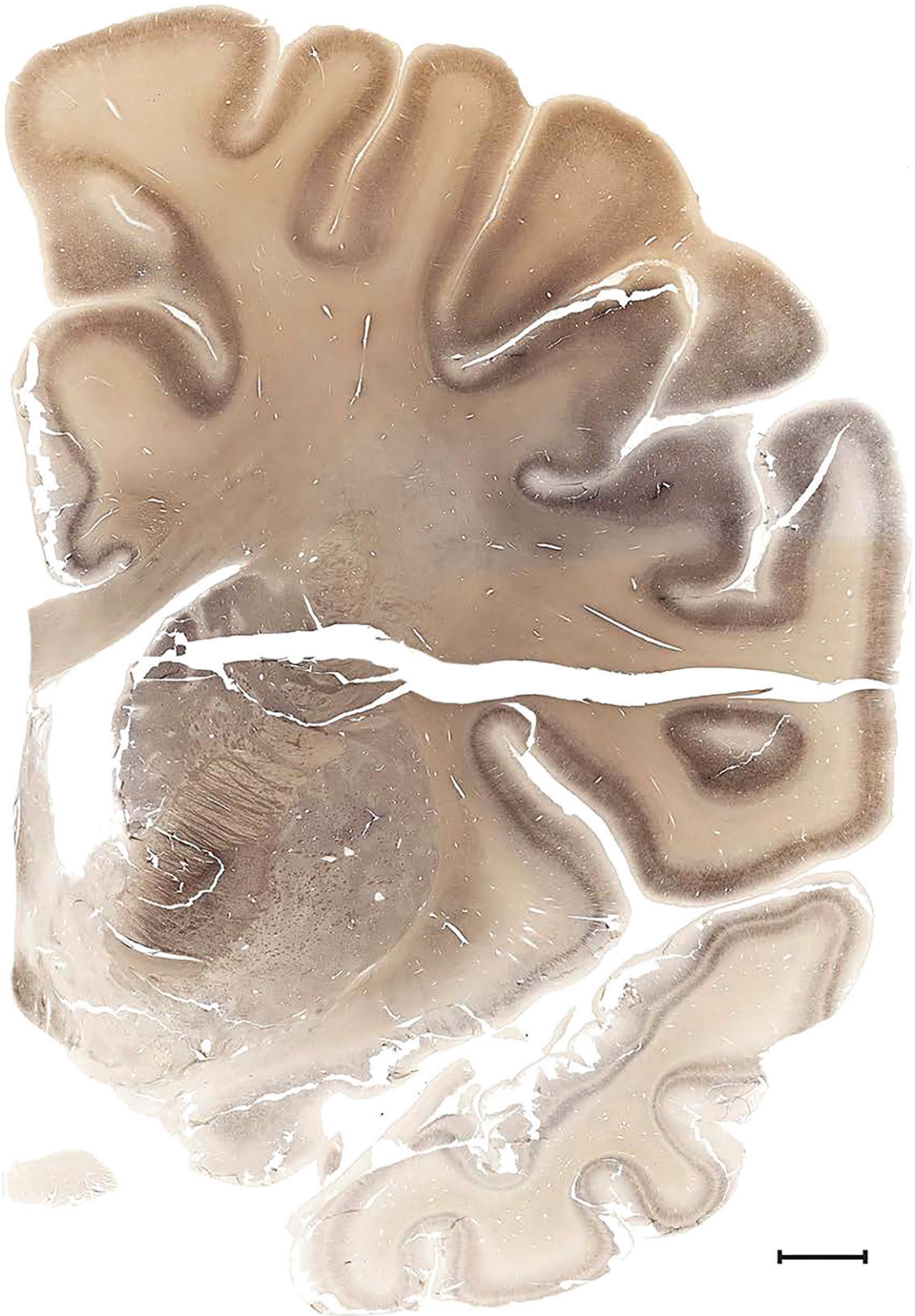

Figure 17. Level 20b (NFP (SMI-32))

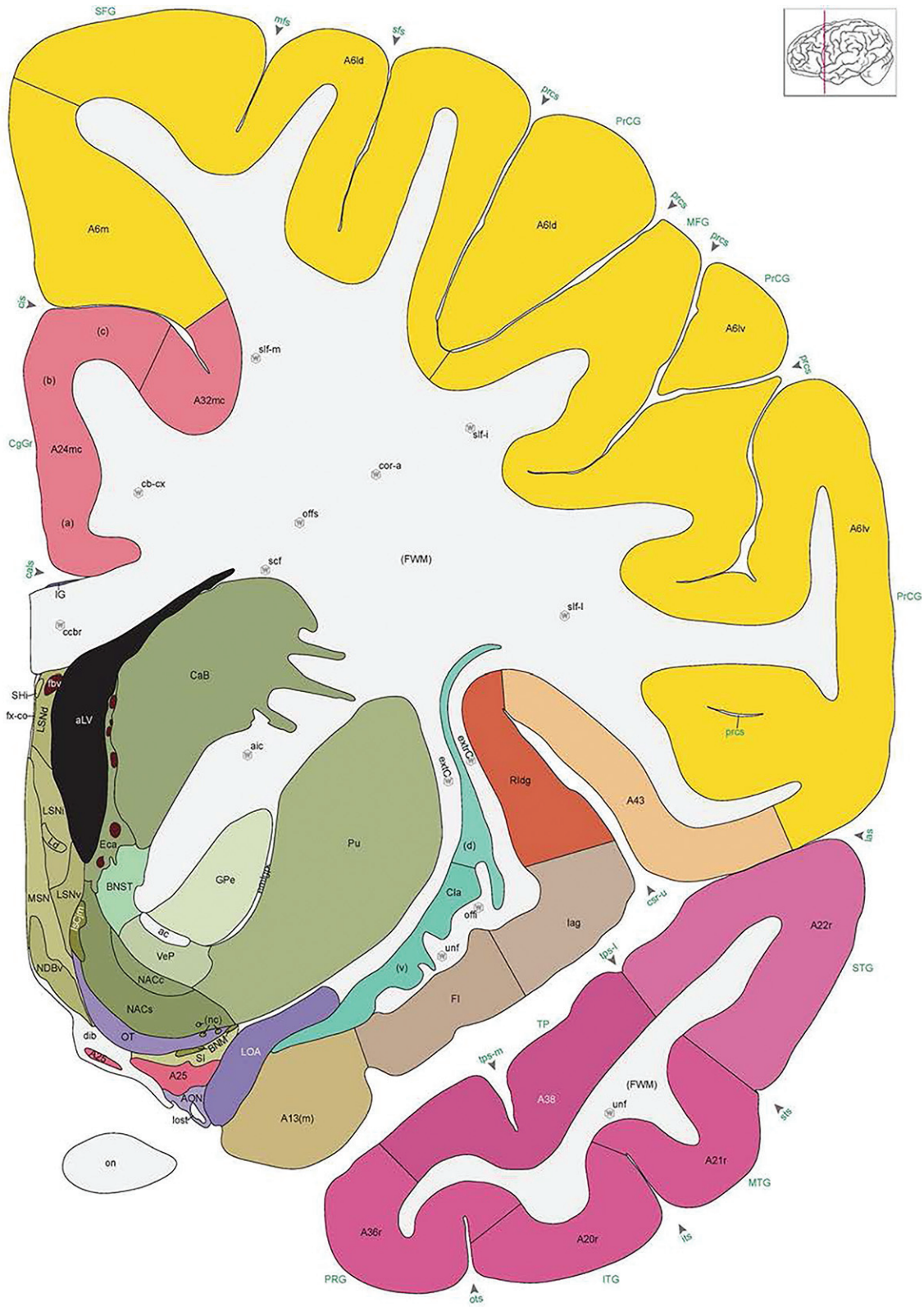

Figure 17. Level 21a (04_059)

Link to online high resolution atlas plate
Link to online high resolution atlas plate (Nissl)

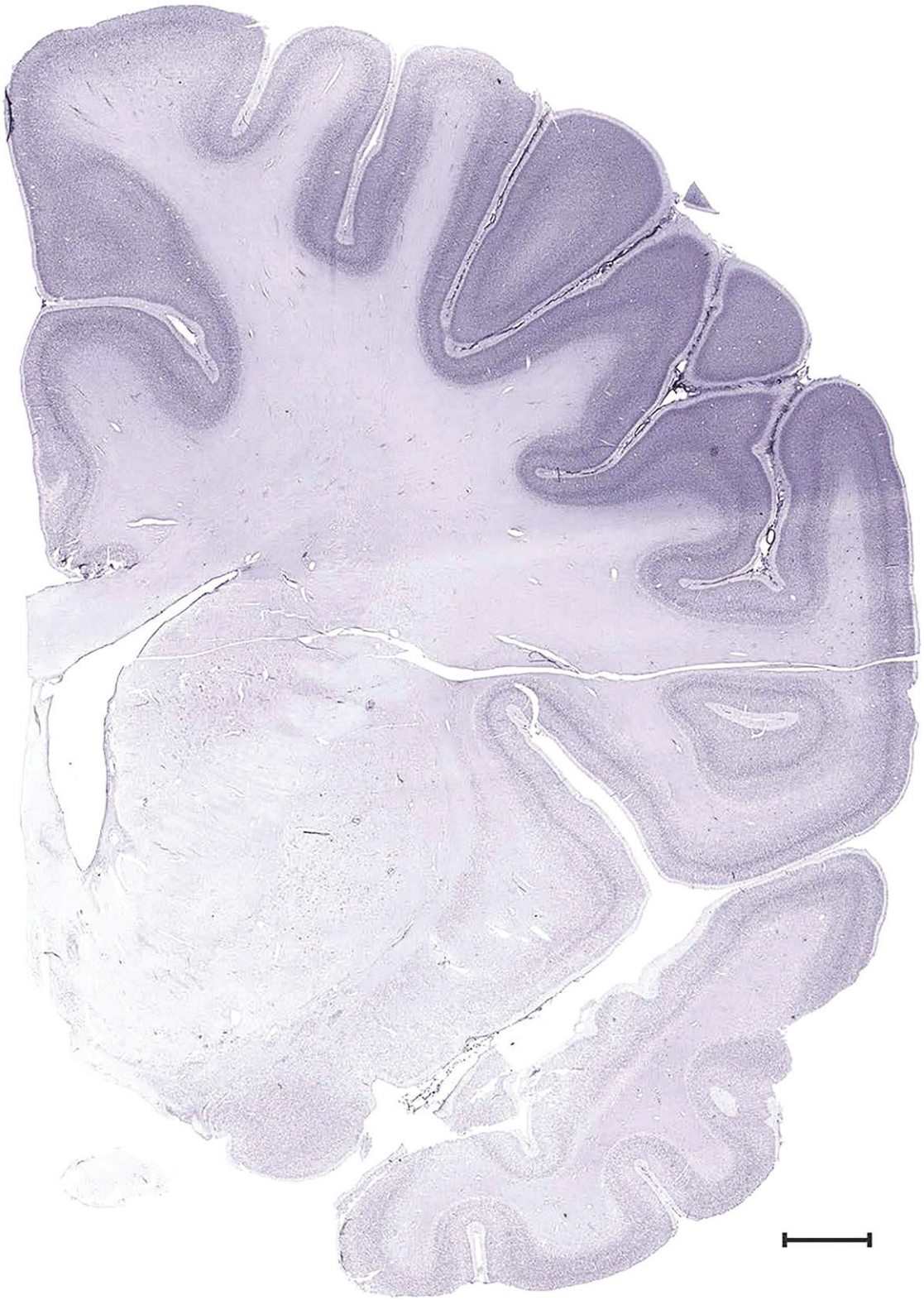

Figure 17. Level 21b (Nissl)

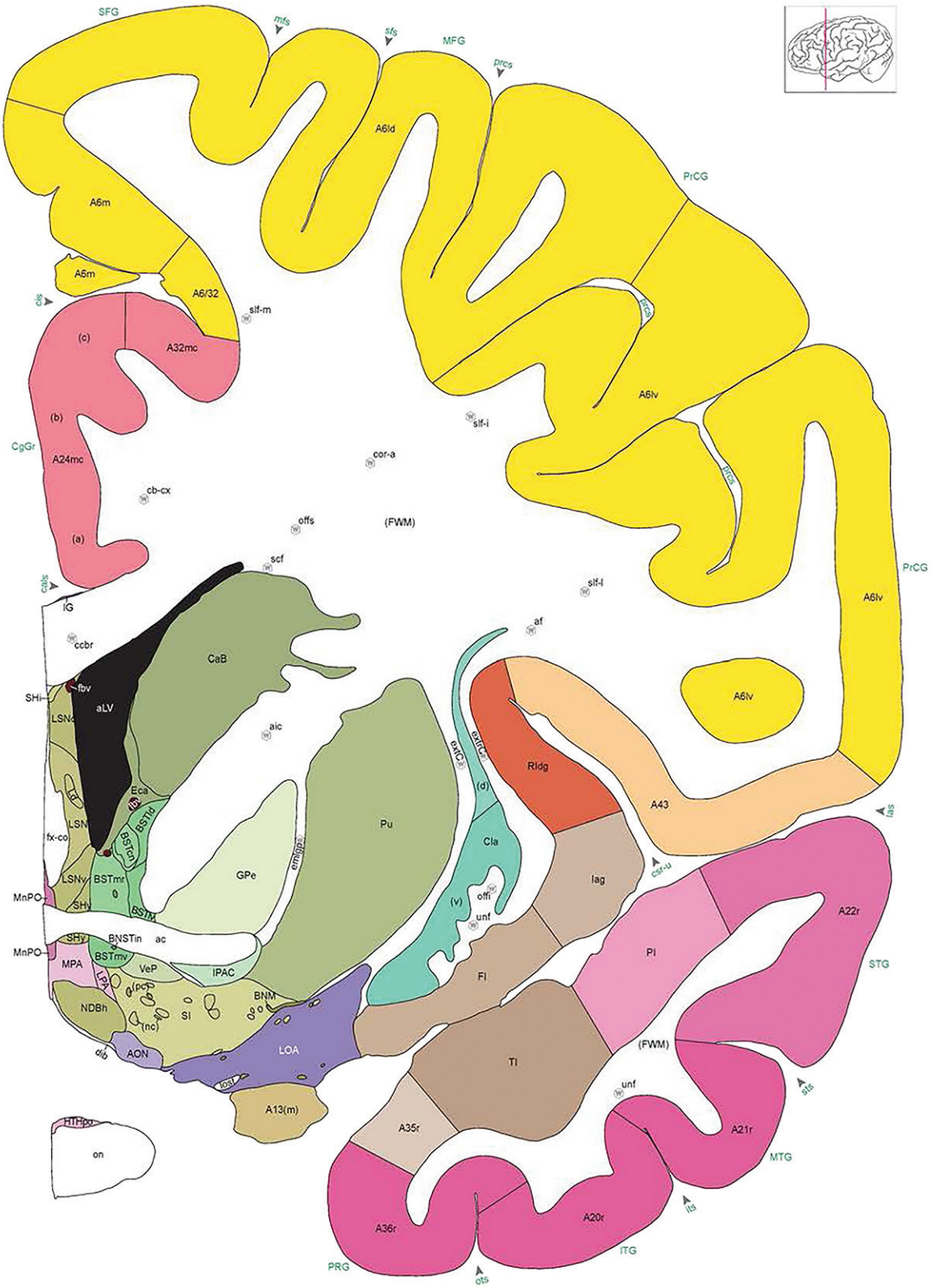

Figure 17. Level 22a (04_083)

Link to online high resolution atlas plate
Link to online high resolution atlas plate (Nissl)

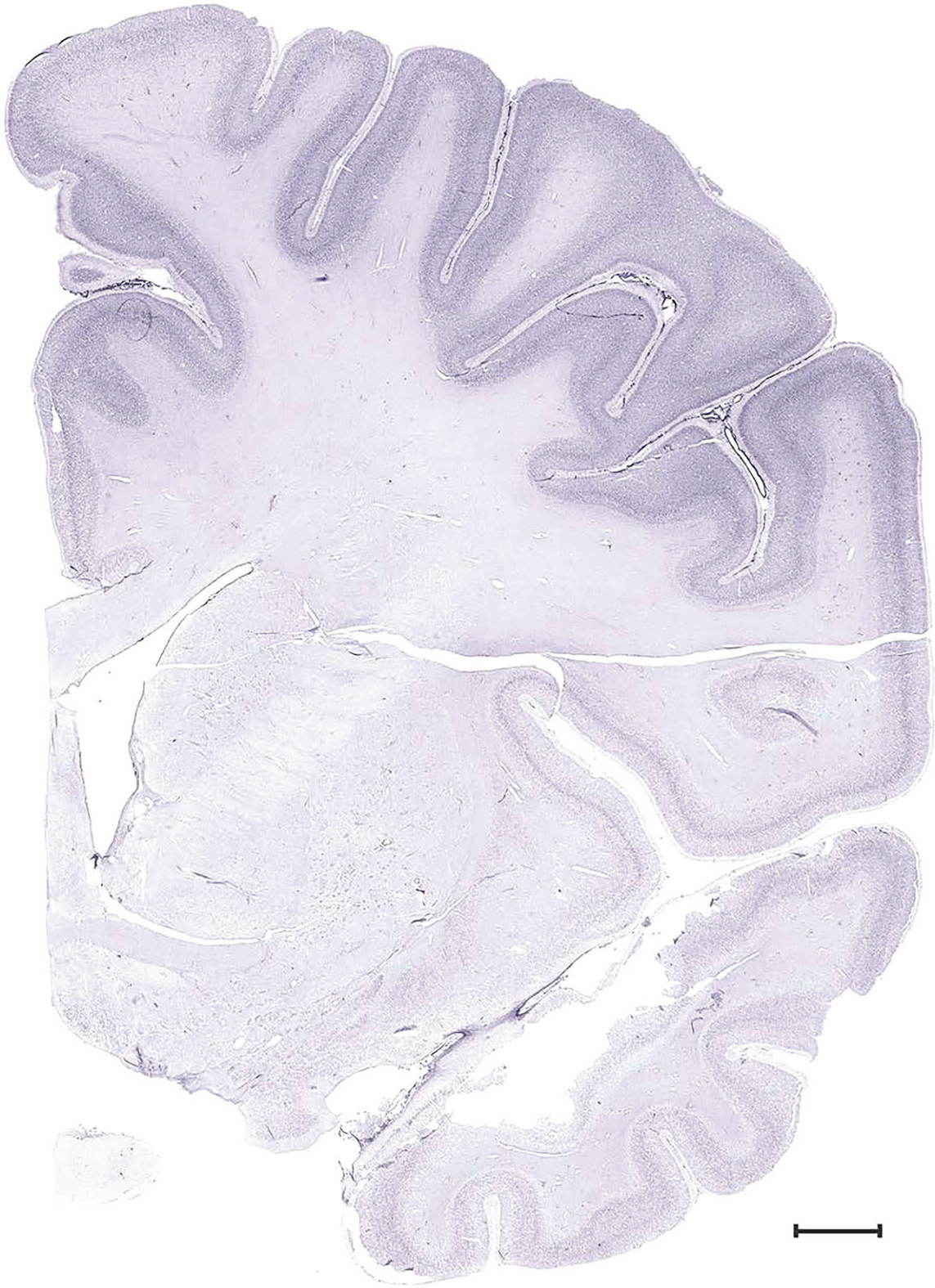

Figure 17. Level 22b (Nissl)

Figure 17. Level 23a (04_095)

Link to online high resolution atlas plate
Link to online high resolution atlas plate (Nissl)

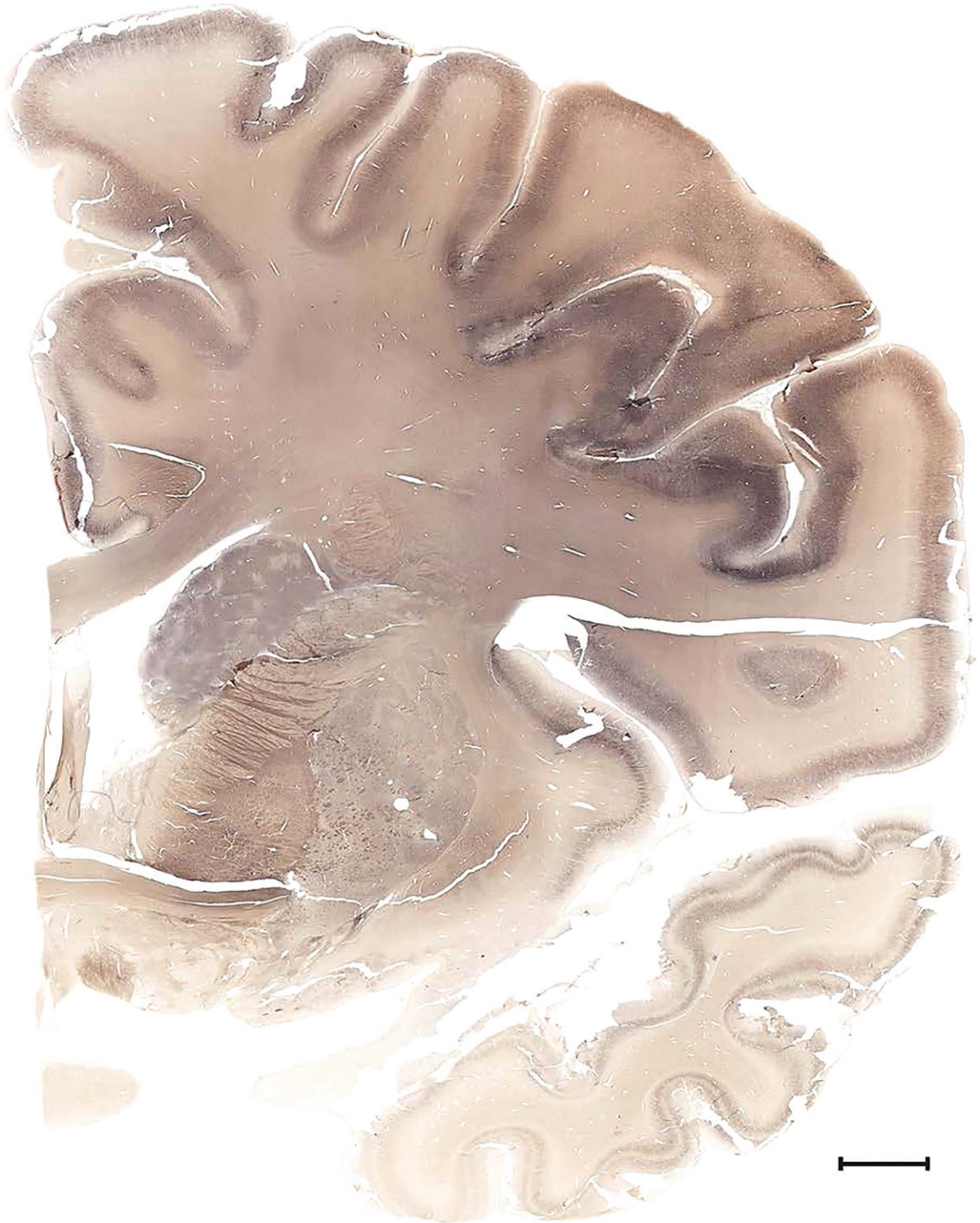

Figure 17. Level 23b (NFP (SMI-32))

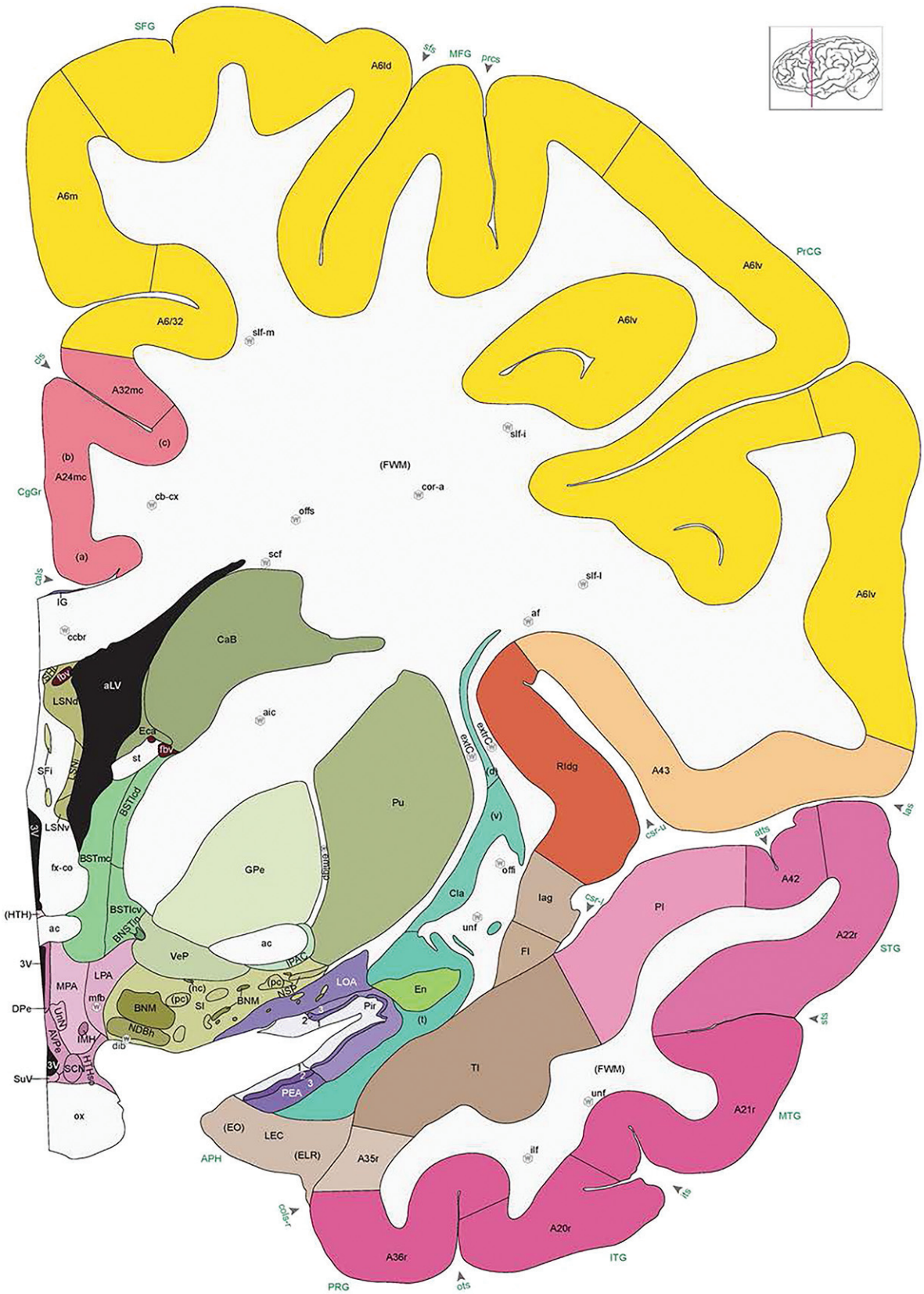

Figure 17. Level 24a (04_115)

Link to online high resolution atlas plate
Link to online high resolution atlas plate (Nissl)

Figure 17. Level 24b (Nissl)

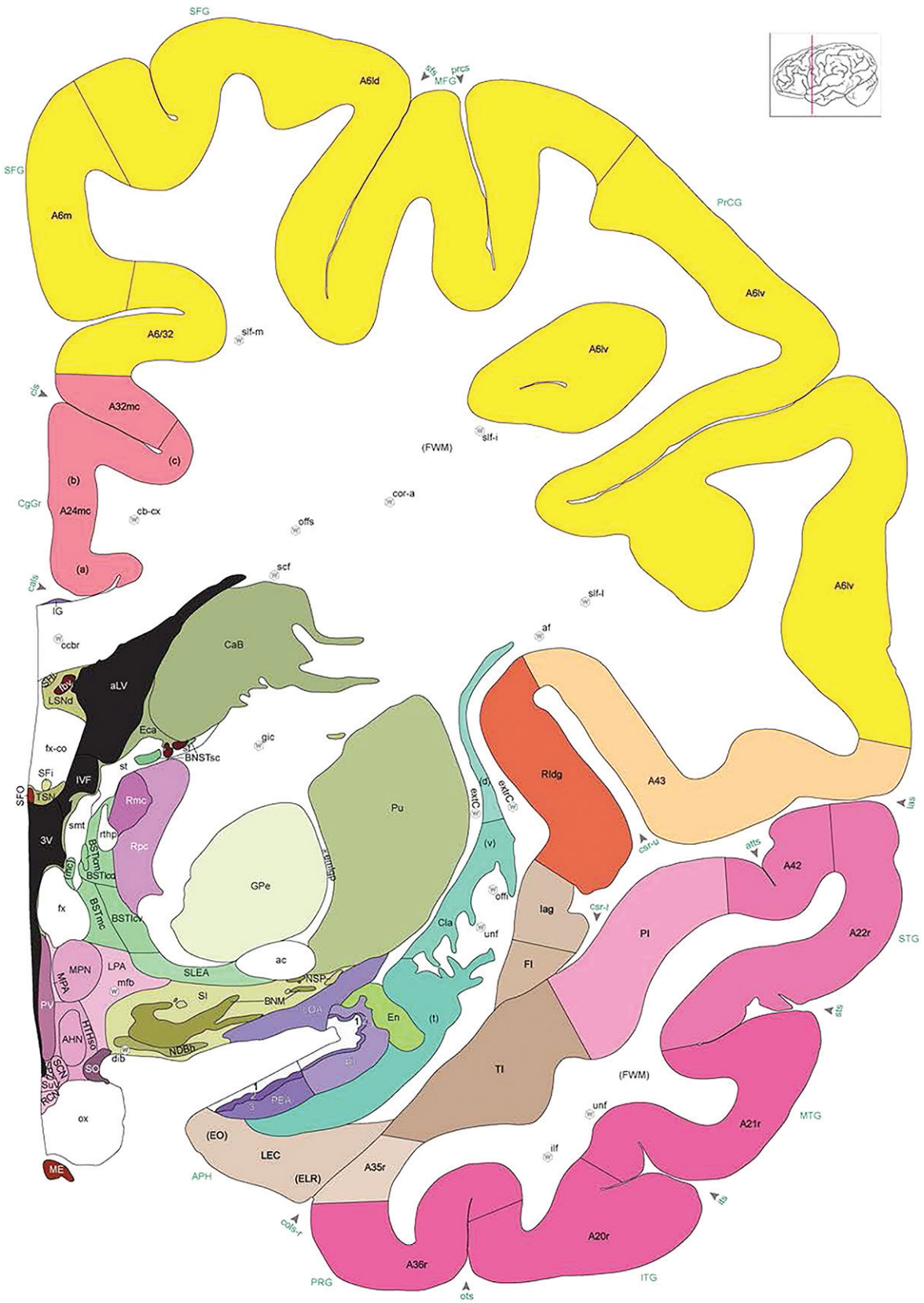

Figure 17. Level 25a (04_135)

Link to online high resolution atlas plate
Link to online high resolution atlas plate (Nissl)

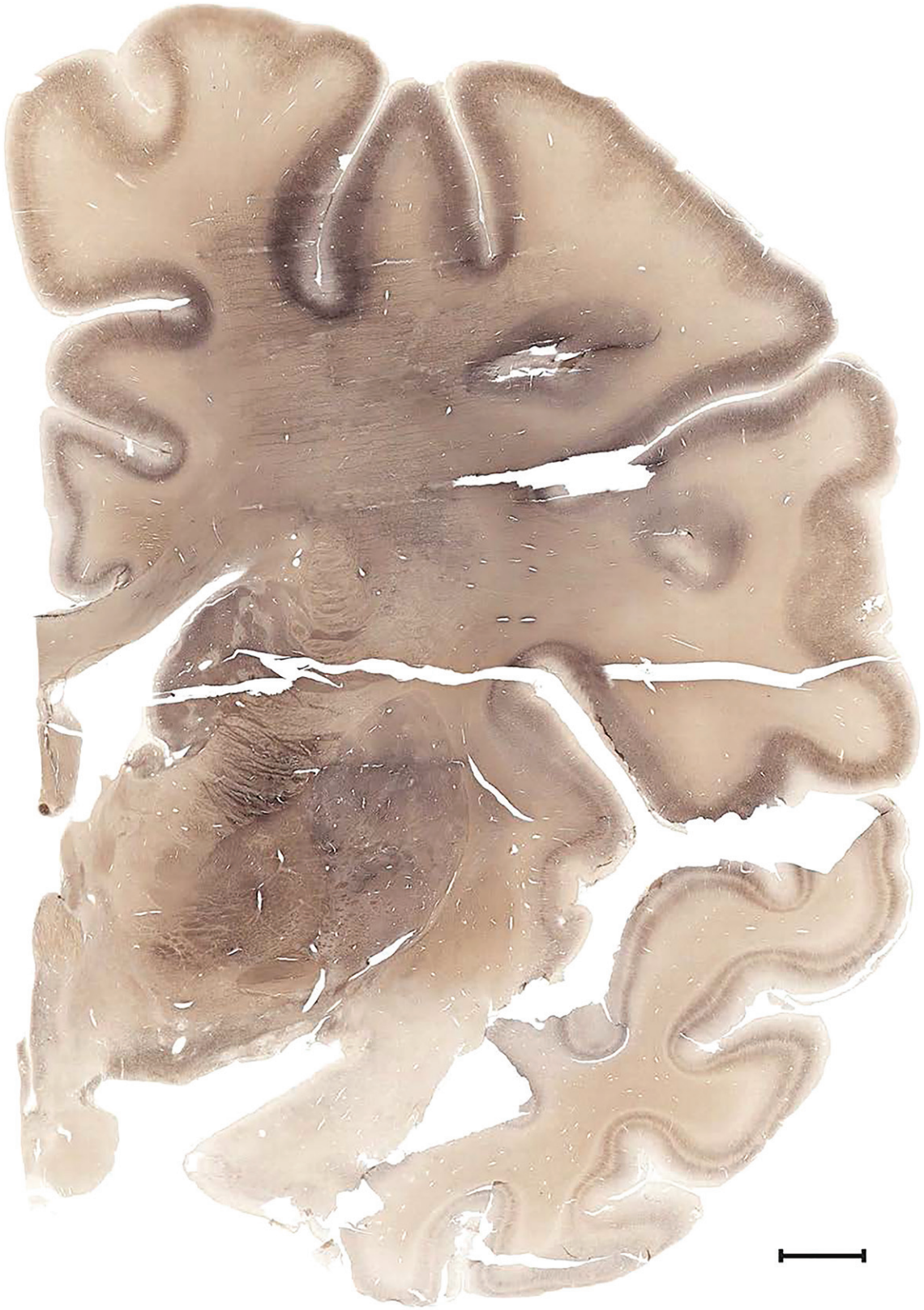

Figure 17. Level 25b (NFP (SMI-32))

Figure 17. Level 26a (04_147)

Link to online high resolution atlas plate
Link to online high resolution atlas plate (Nissl)

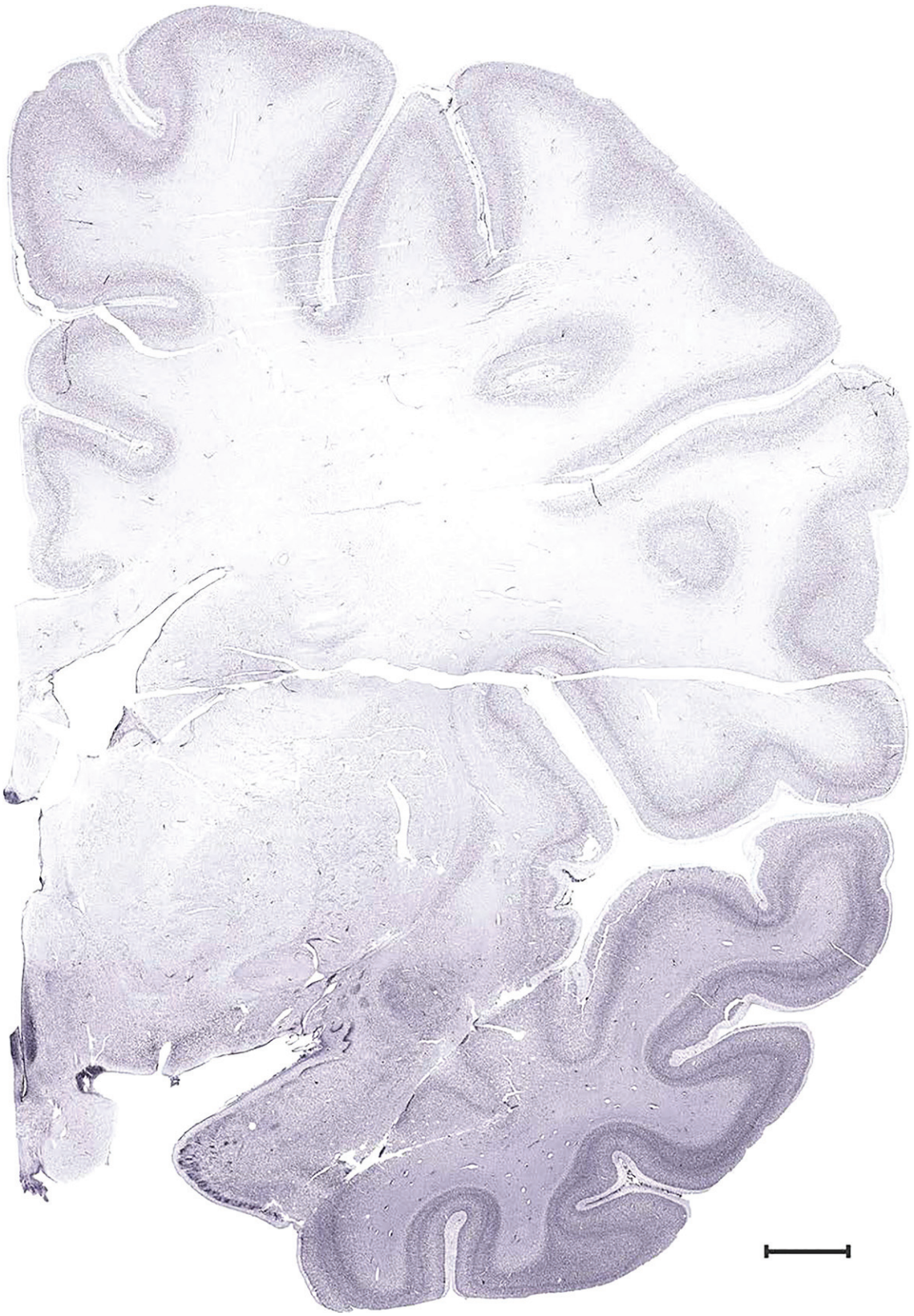

Figure 17. Level 26b (Nissl)

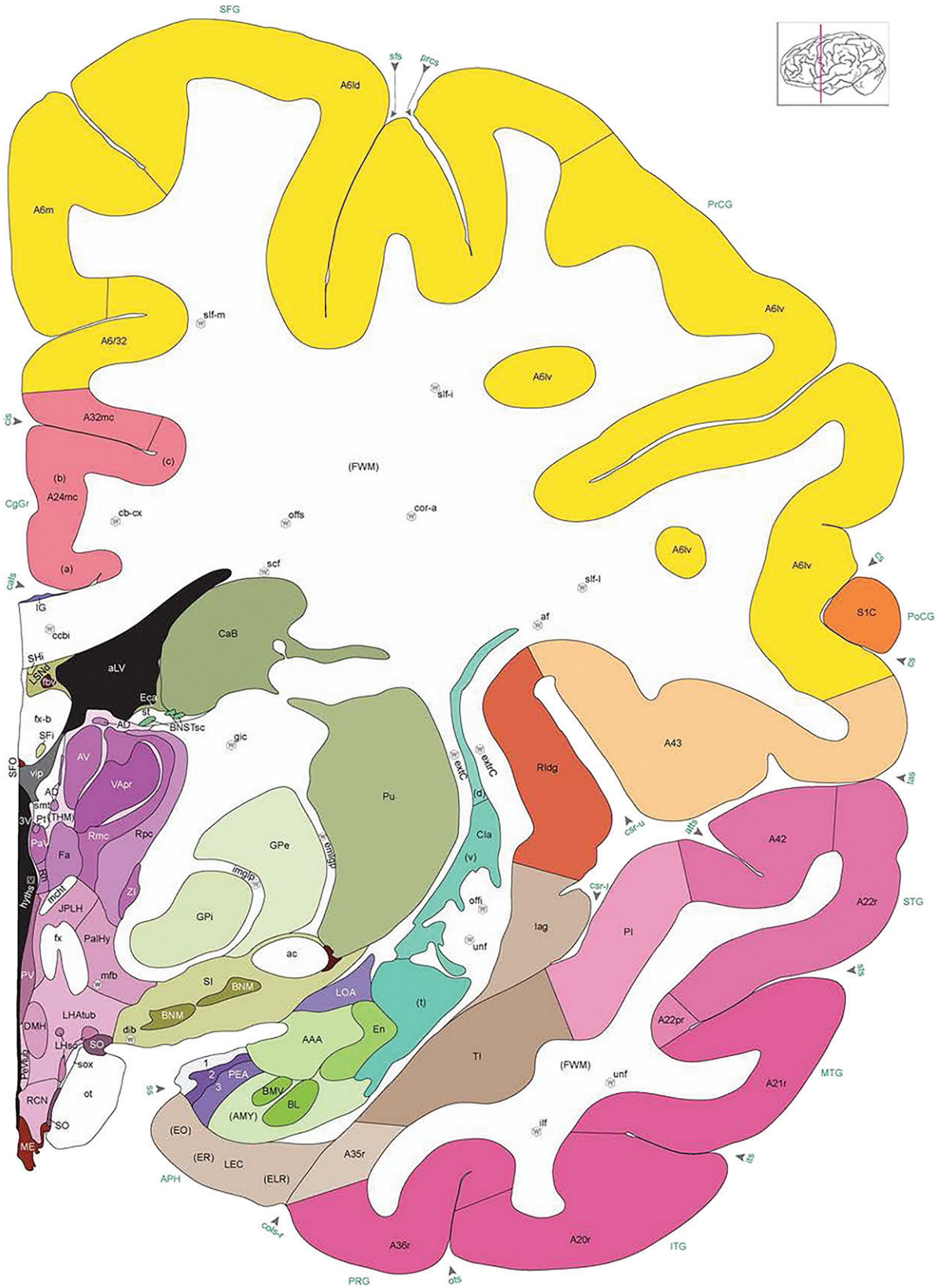

Figure 17. Level 27a (04_167)

Link to online high resolution atlas plate
Link to online high resolution atlas plate (Nissl)

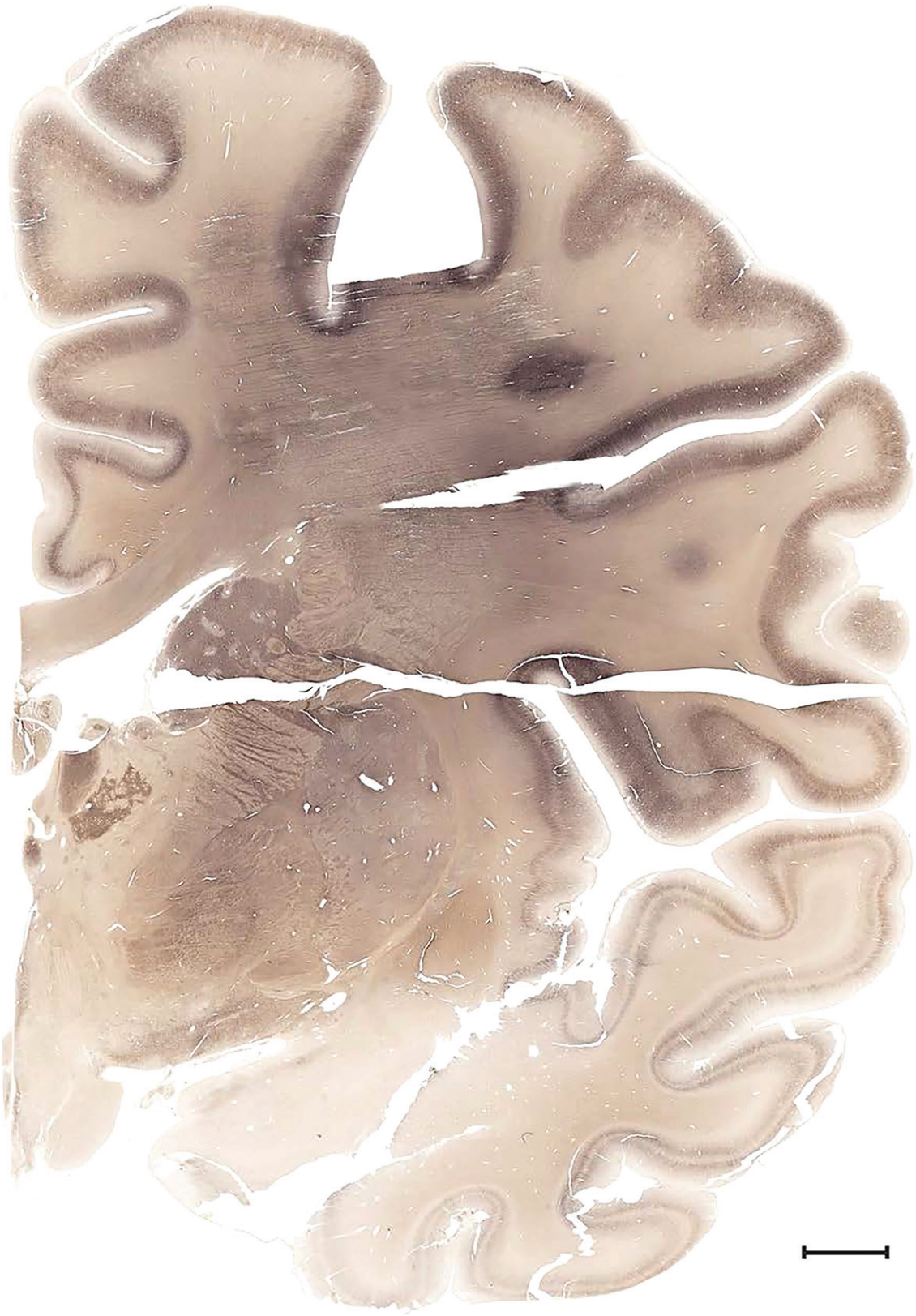

Figure 17. Level 27b (NFP (SMI-32))

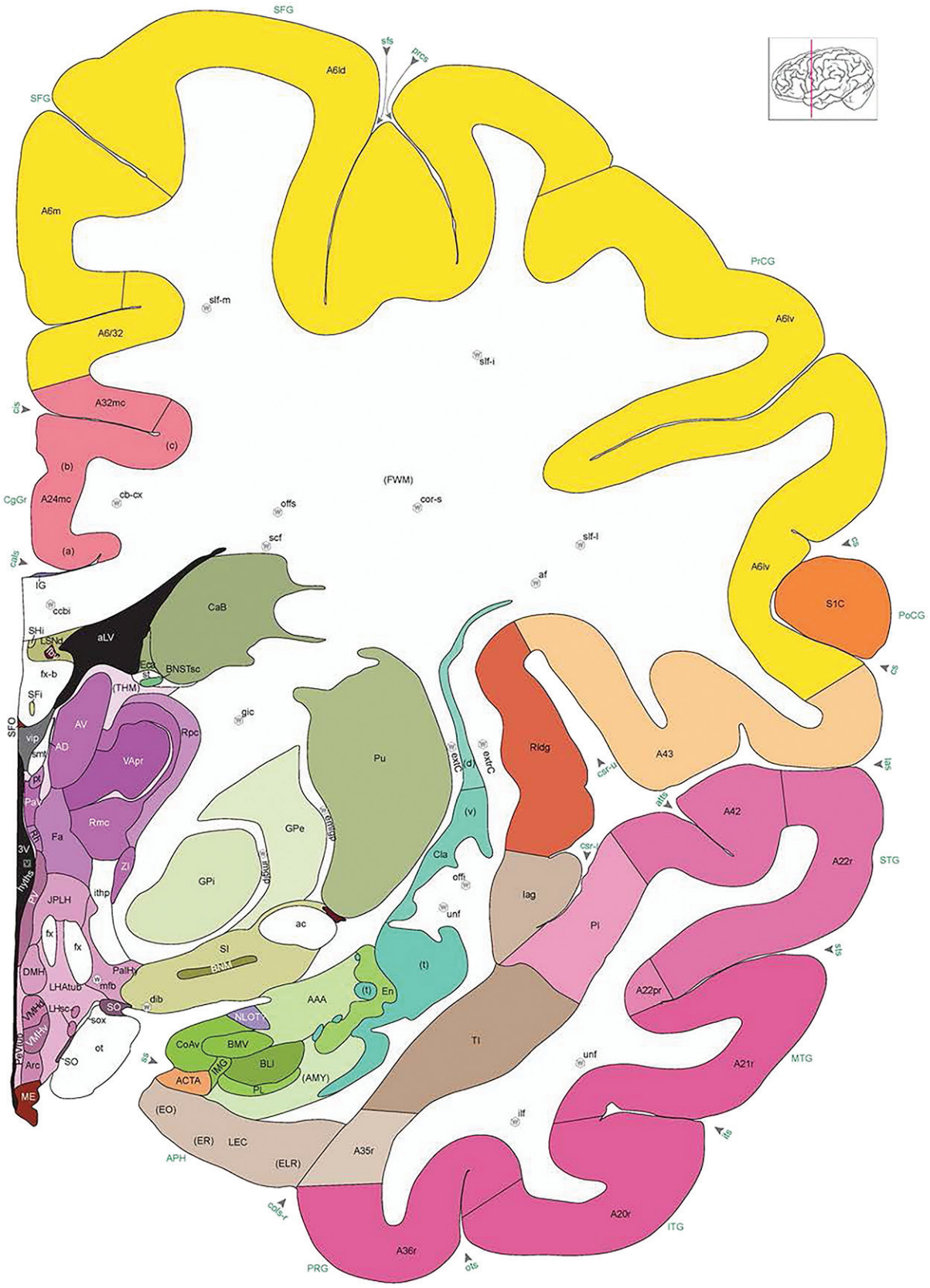

Figure 17. Level 28a (04_179)

Link to online high resolution atlas plate
Link to online high resolution atlas plate (Nissl)

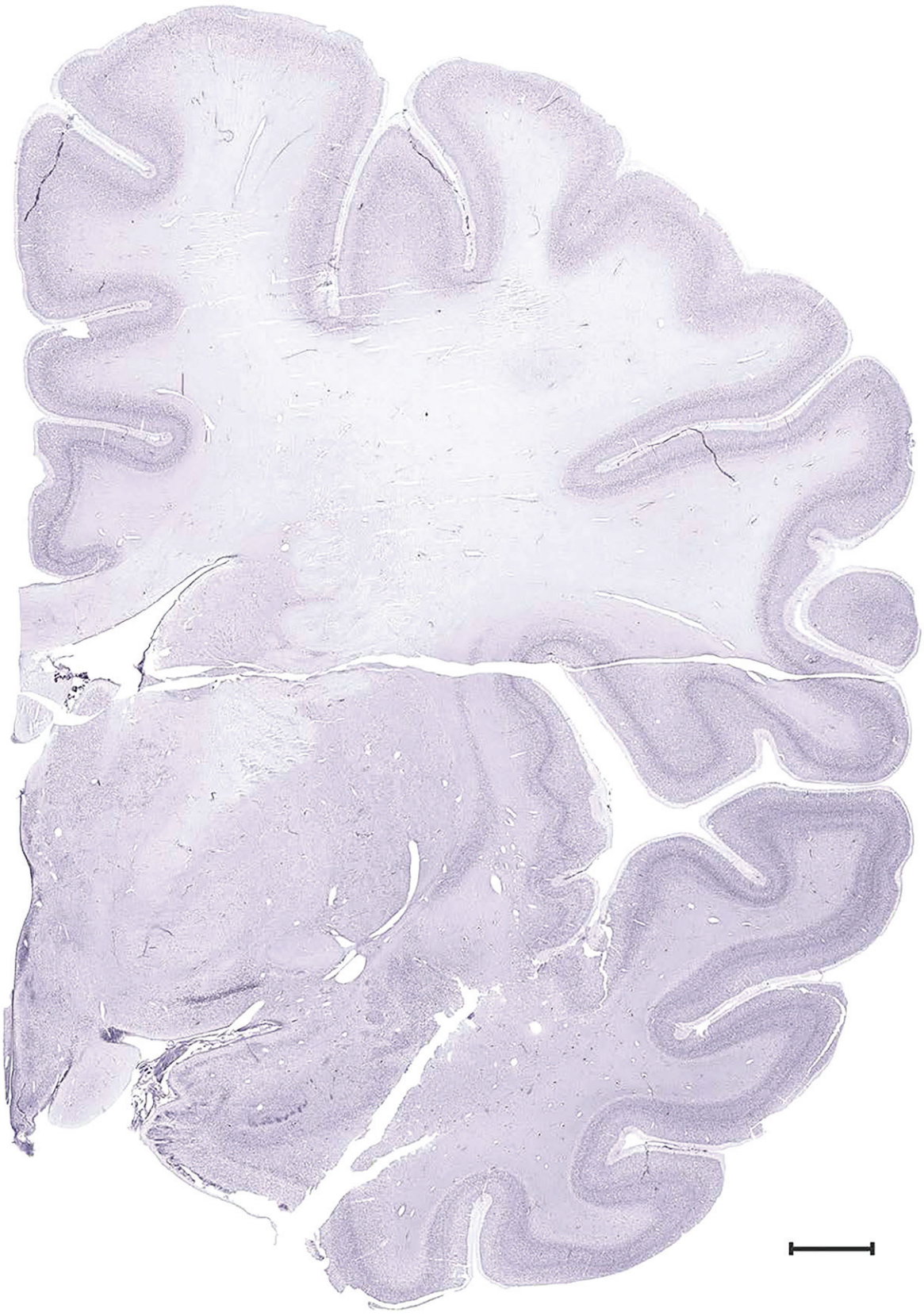

Figure 17. Level 28b (Nissl)

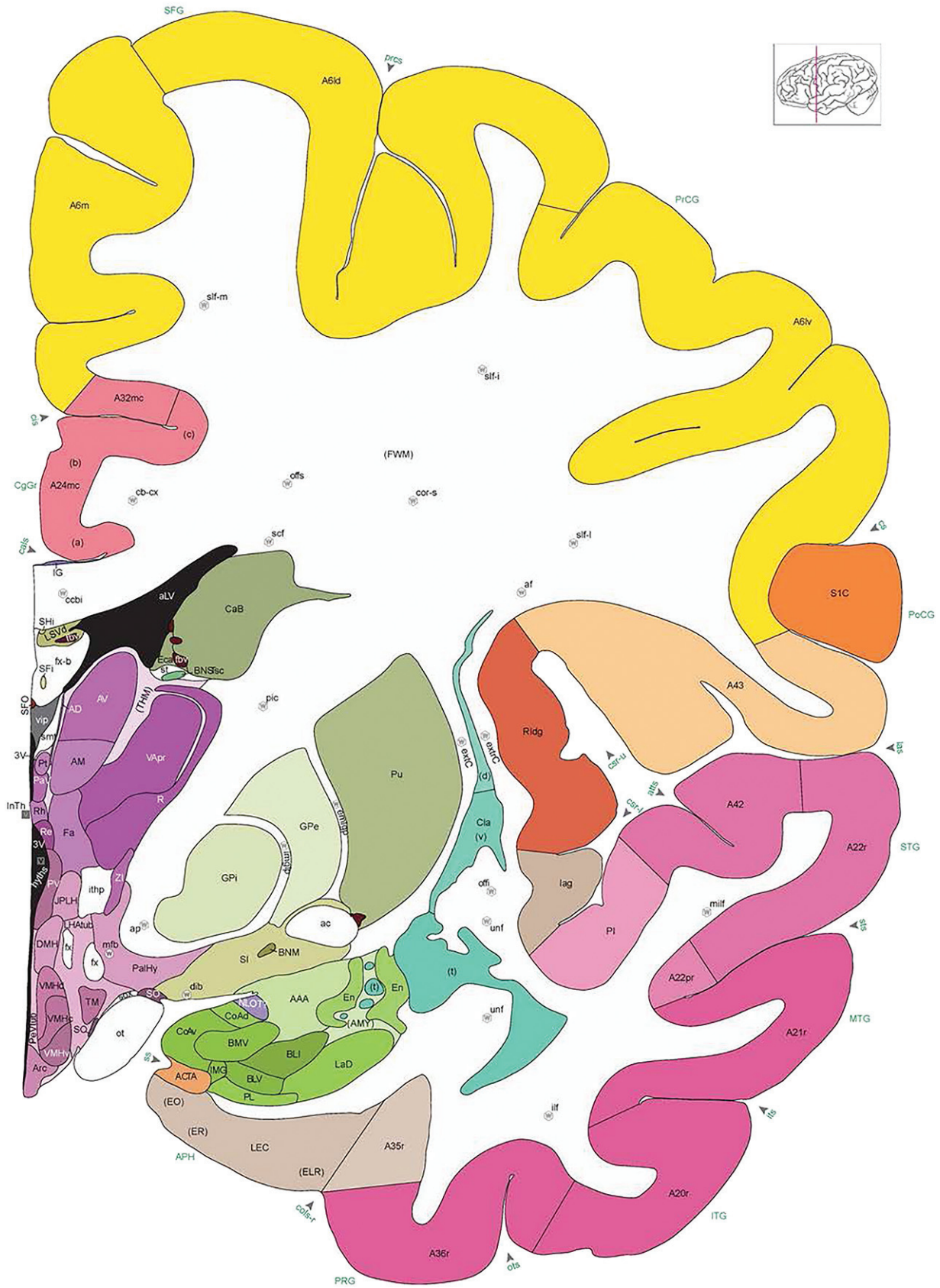

Figure 17. Level 29a (04_195)

Link to online high resolution atlas plate
Link to online high resolution atlas plate (Nissl)

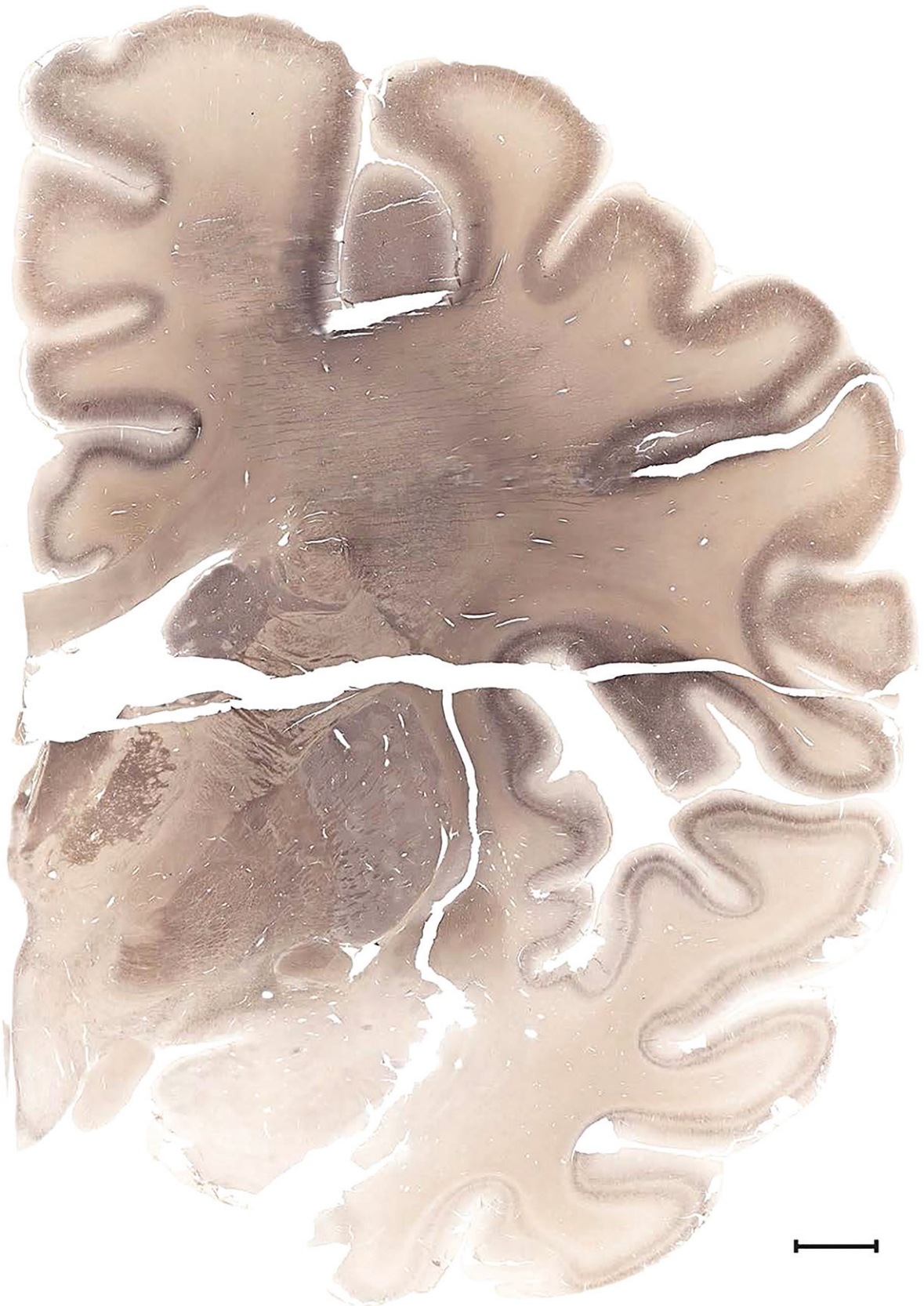

Figure 17. Level 29b (NFP (SMI-32))

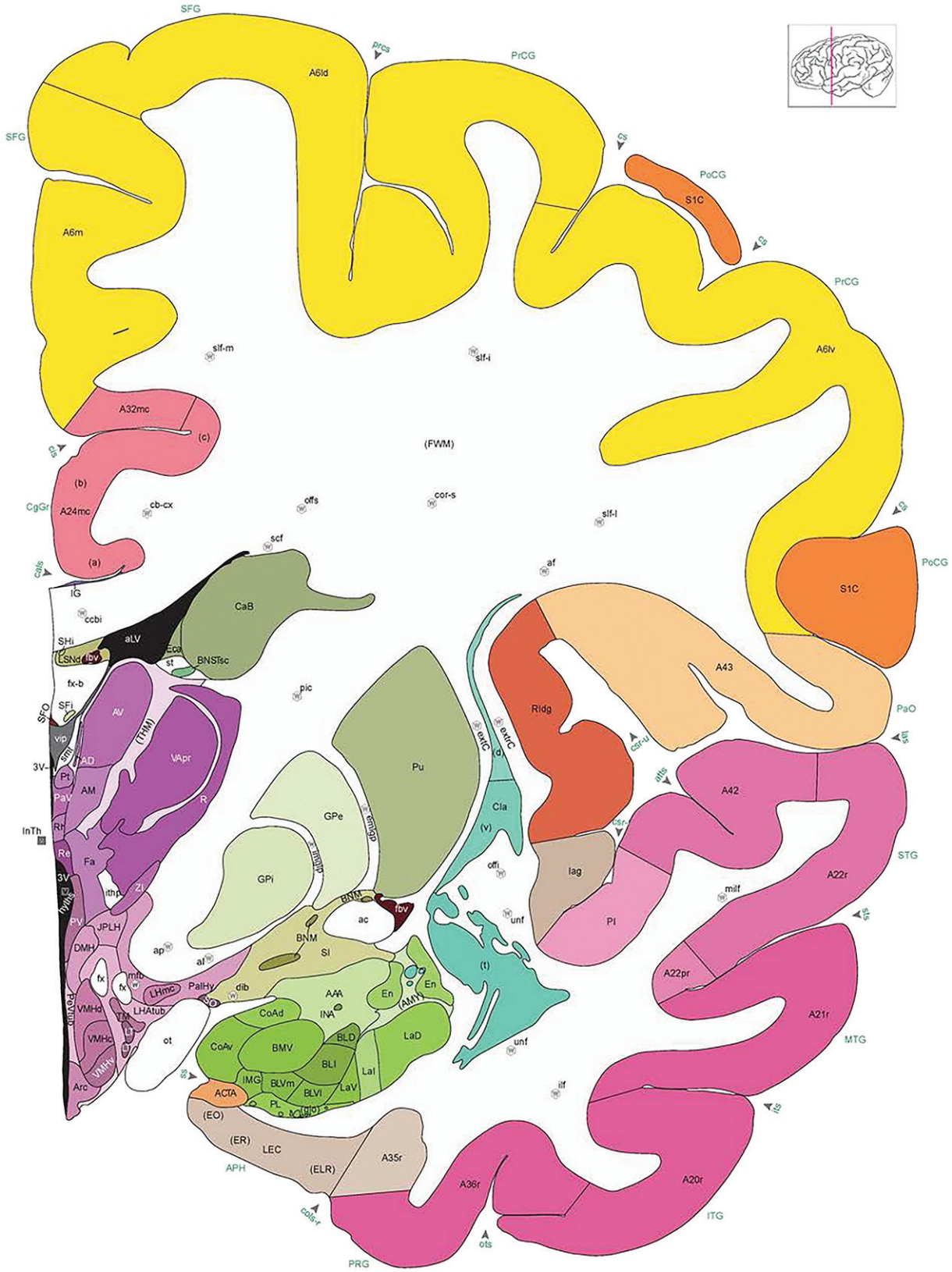

Figure 17. Level 30a (04_207)

Link to online high resolution atlas plate
Link to online high resolution atlas plate (Nissl)

Figure 17. Level 30b (Nissl)

Figure 17. Level 31a (04_215)

Link to online high resolution atlas plate
Link to online high resolution atlas plate (Nissl)

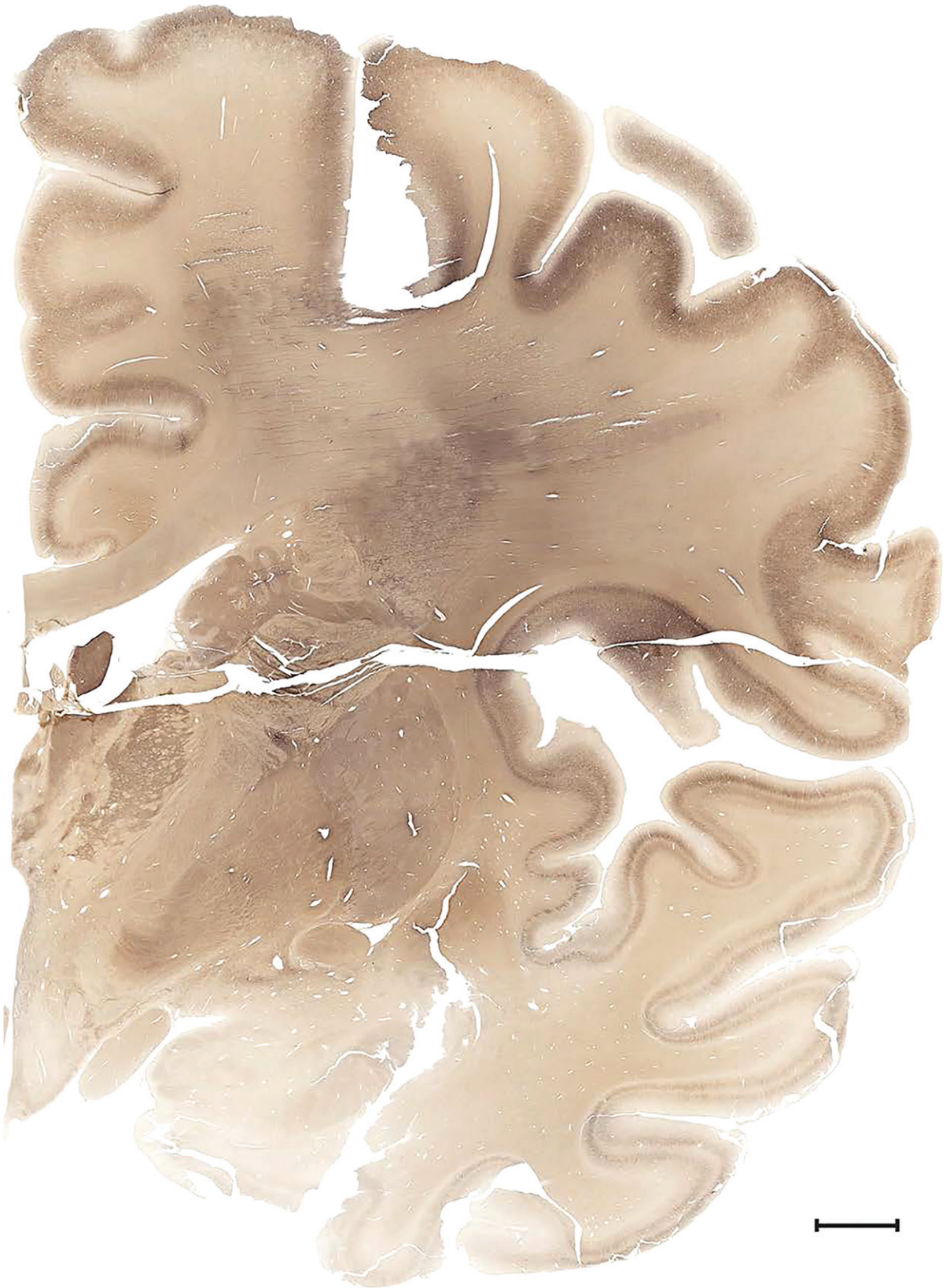

Figure 17. Level 31b (NFP (SMI-32))

Figure 17. Level 32a (04_231)

Link to online high resolution atlas plate
Link to online high resolution atlas plate (Nissl)

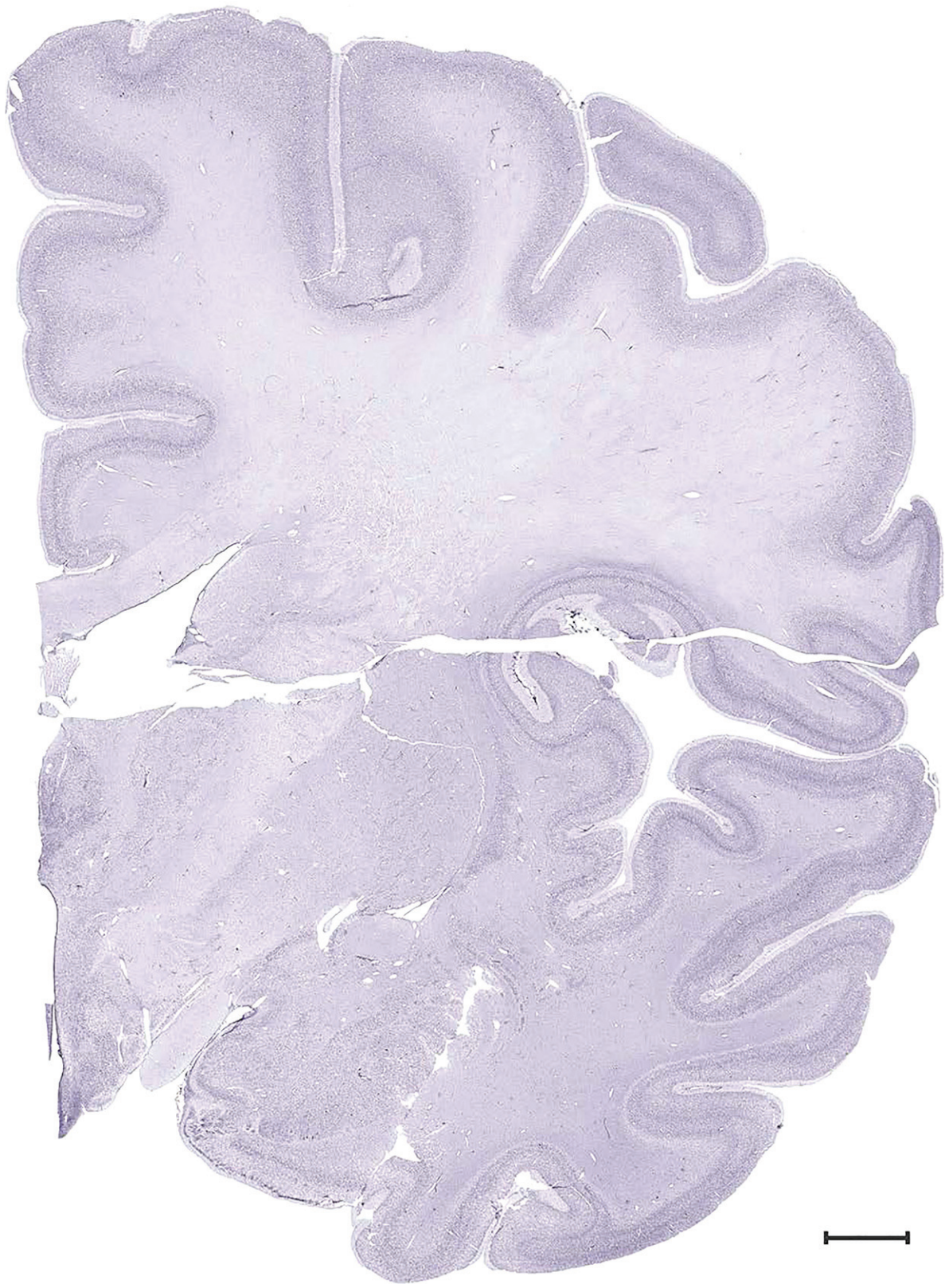

Figure 17. Level 32b (Nissl)

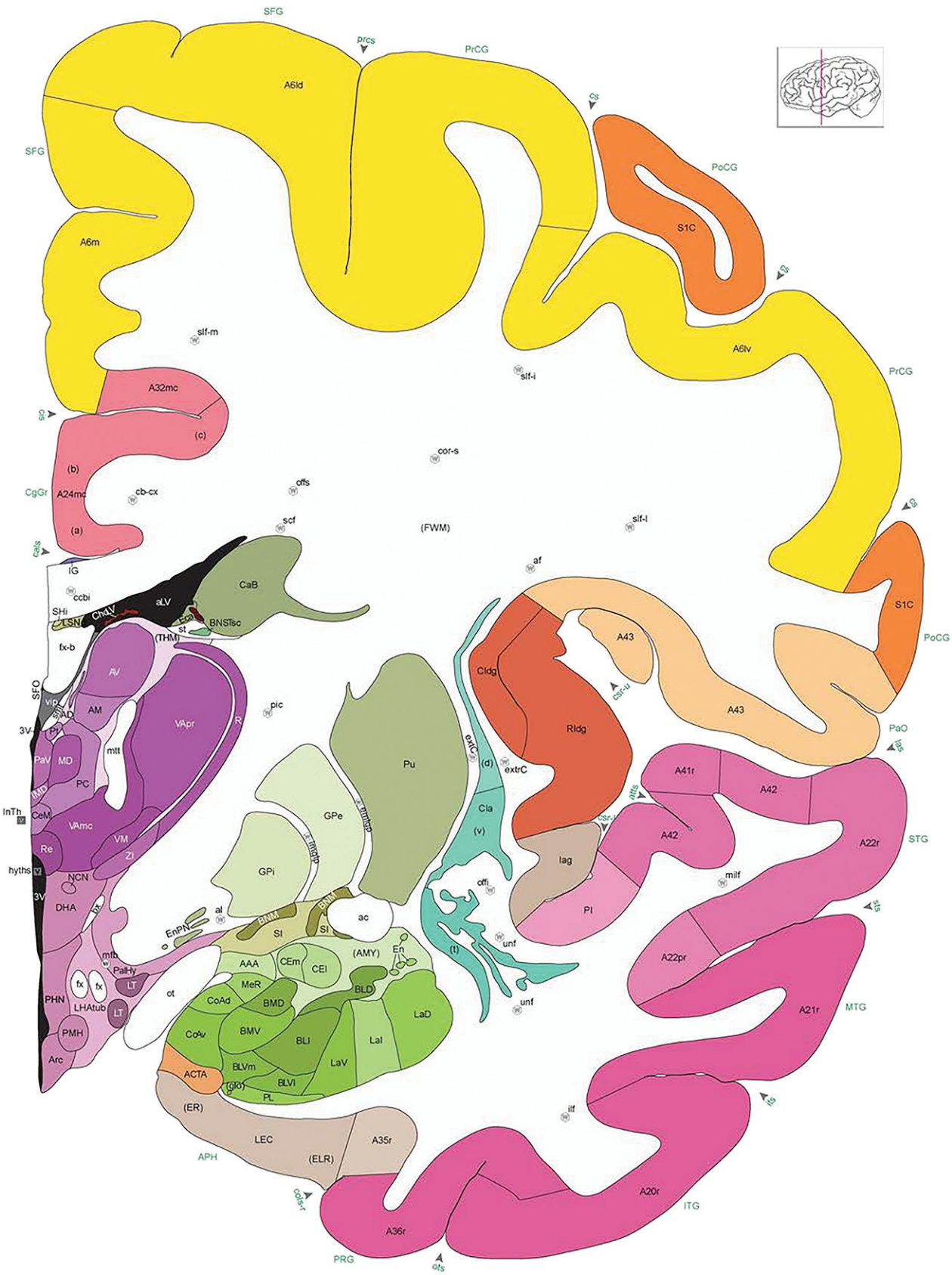

Figure 17. Level 33a (04_239)

Link to online high resolution atlas plate
Link to online high resolution atlas plate (Nissl)

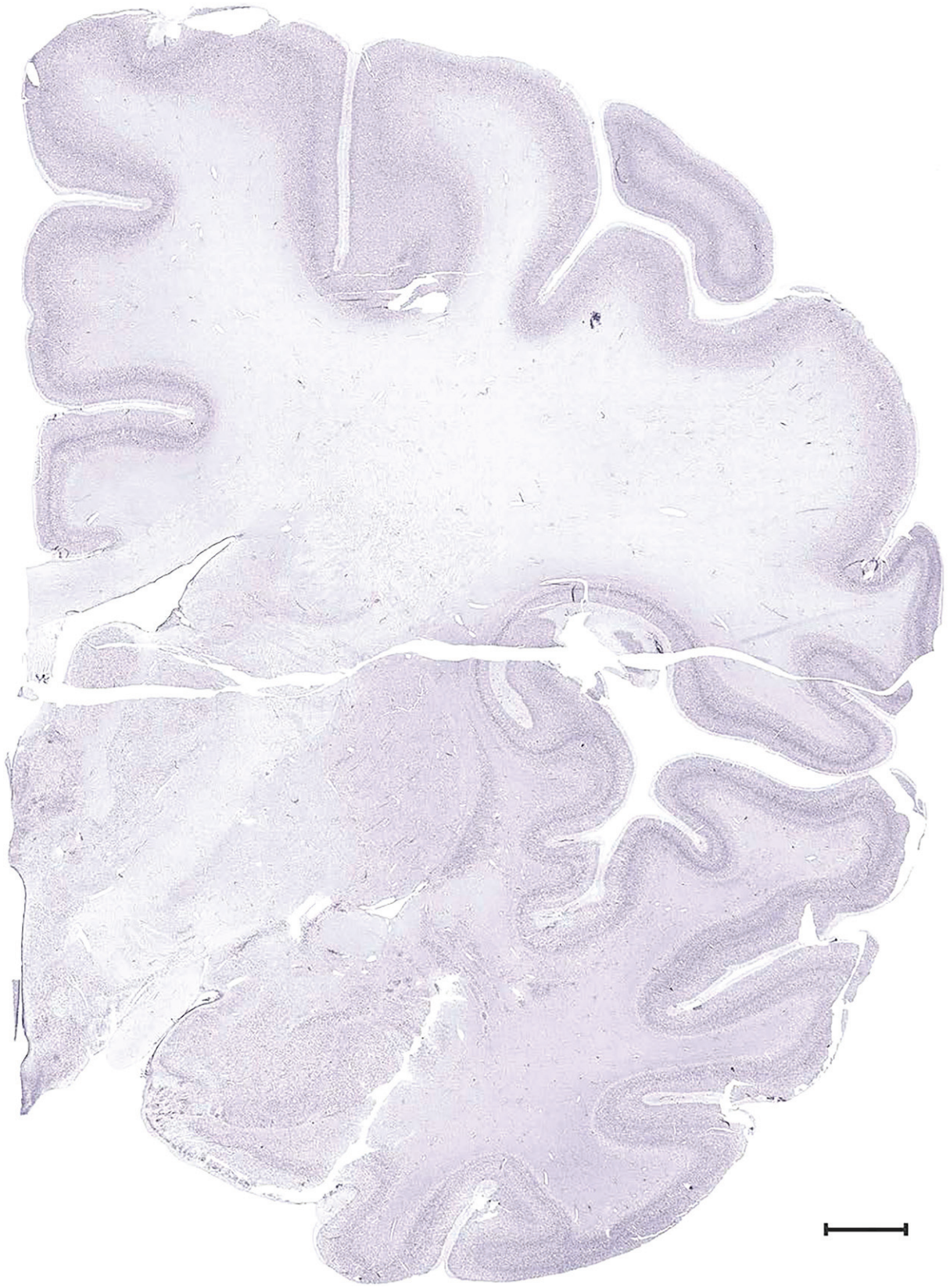

Figure 17. Level 33b (Nissl)

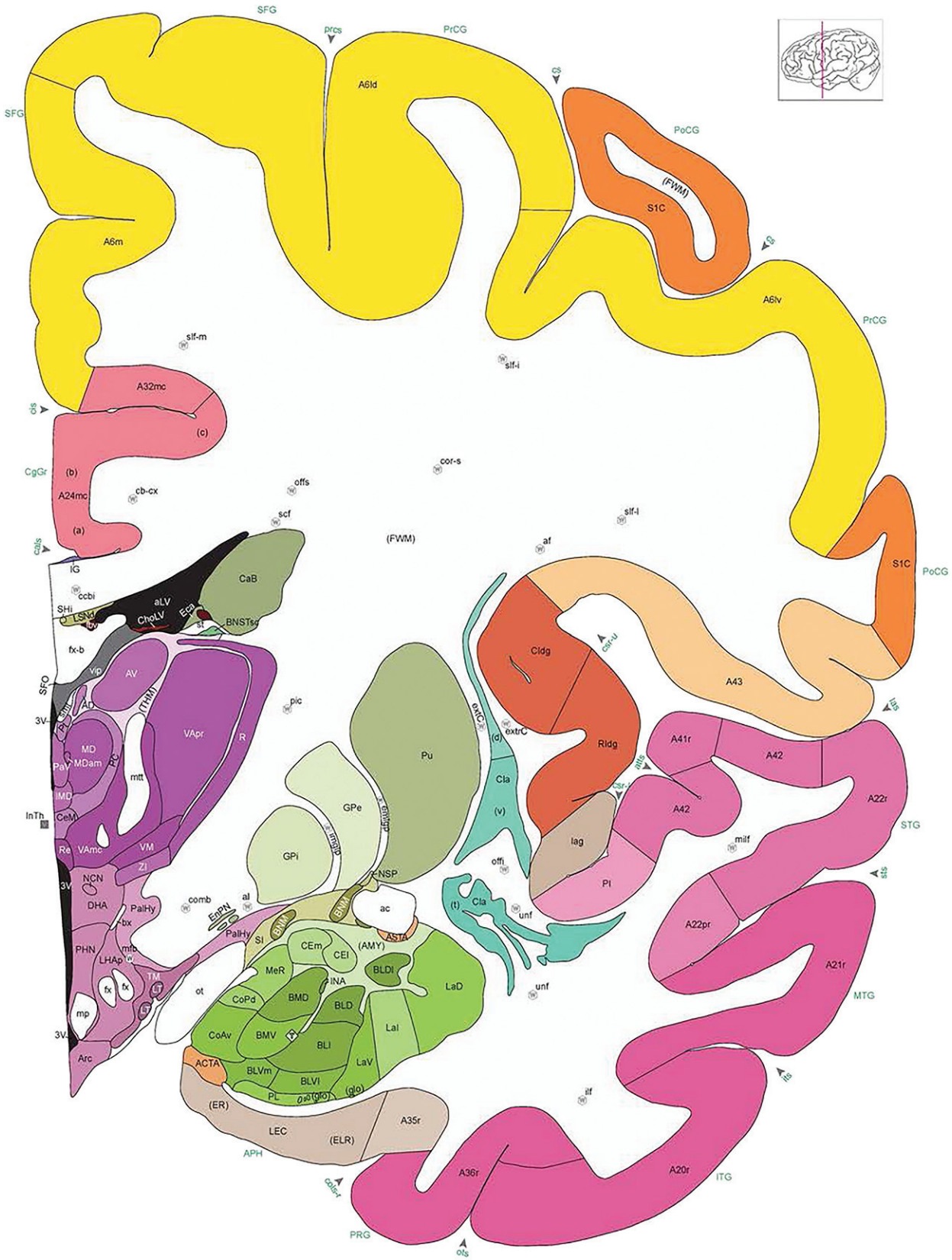

Figure 17. Level 34a (04_251)

Link to online high resolution atlas plate
Link to online high resolution atlas plate (Nissl)

Figure 17. Level 34b (Nissl)

Figure 17. Level 35a (04_259)

Link to online high resolution atlas plate
Link to online high resolution atlas plate (Nissl)

Figure 17. Level 35b (NFP (SMI-32))

Figure 17. Level 36a (04_267)

Link to online high resolution atlas plate
Link to online high resolution atlas plate (Nissl)

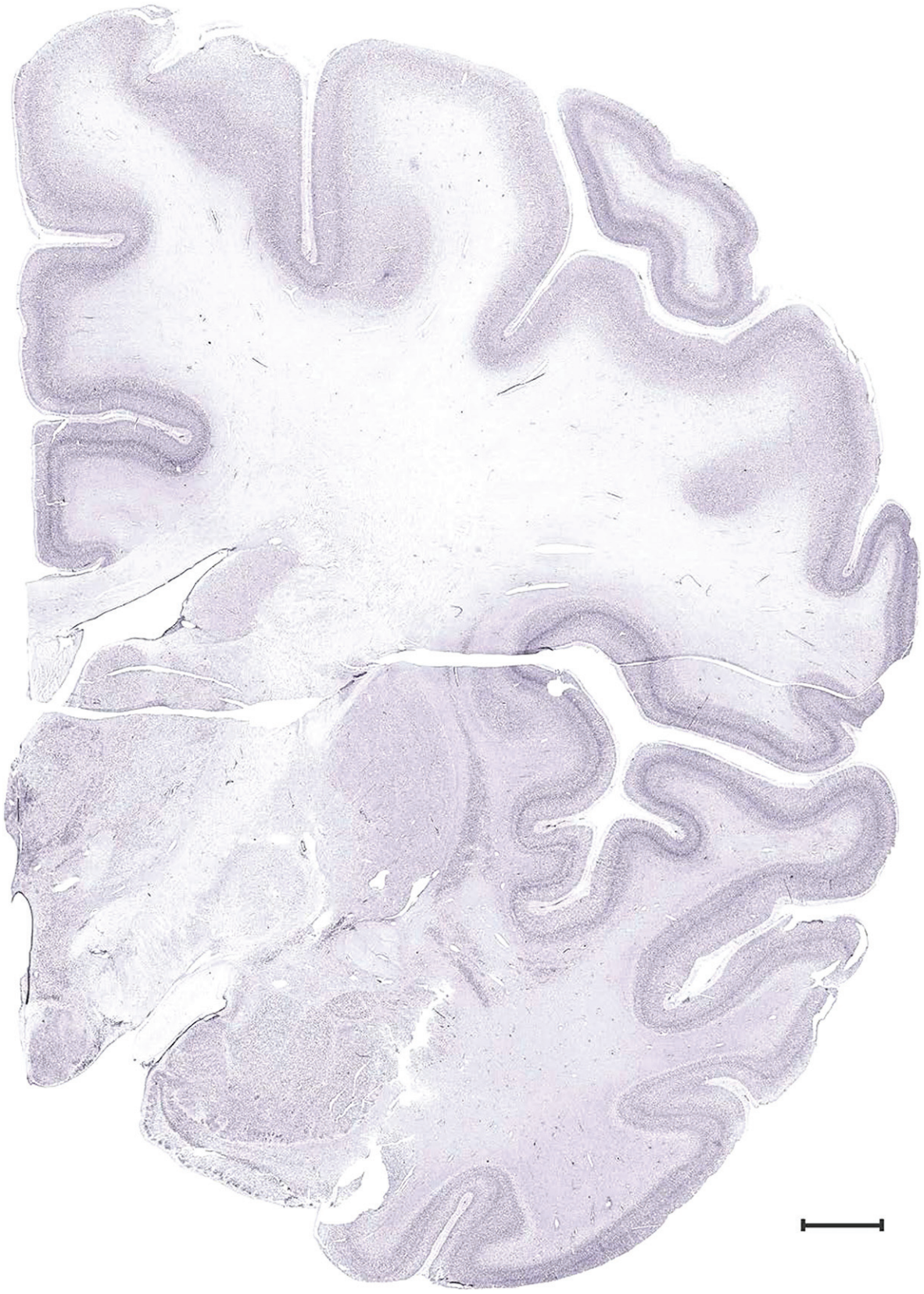

Figure 17. Level 36b (Nissl)

Figure 17. Level 37a (04_279)

Link to online high resolution atlas plate
Link to online high resolution atlas plate (Nissl)

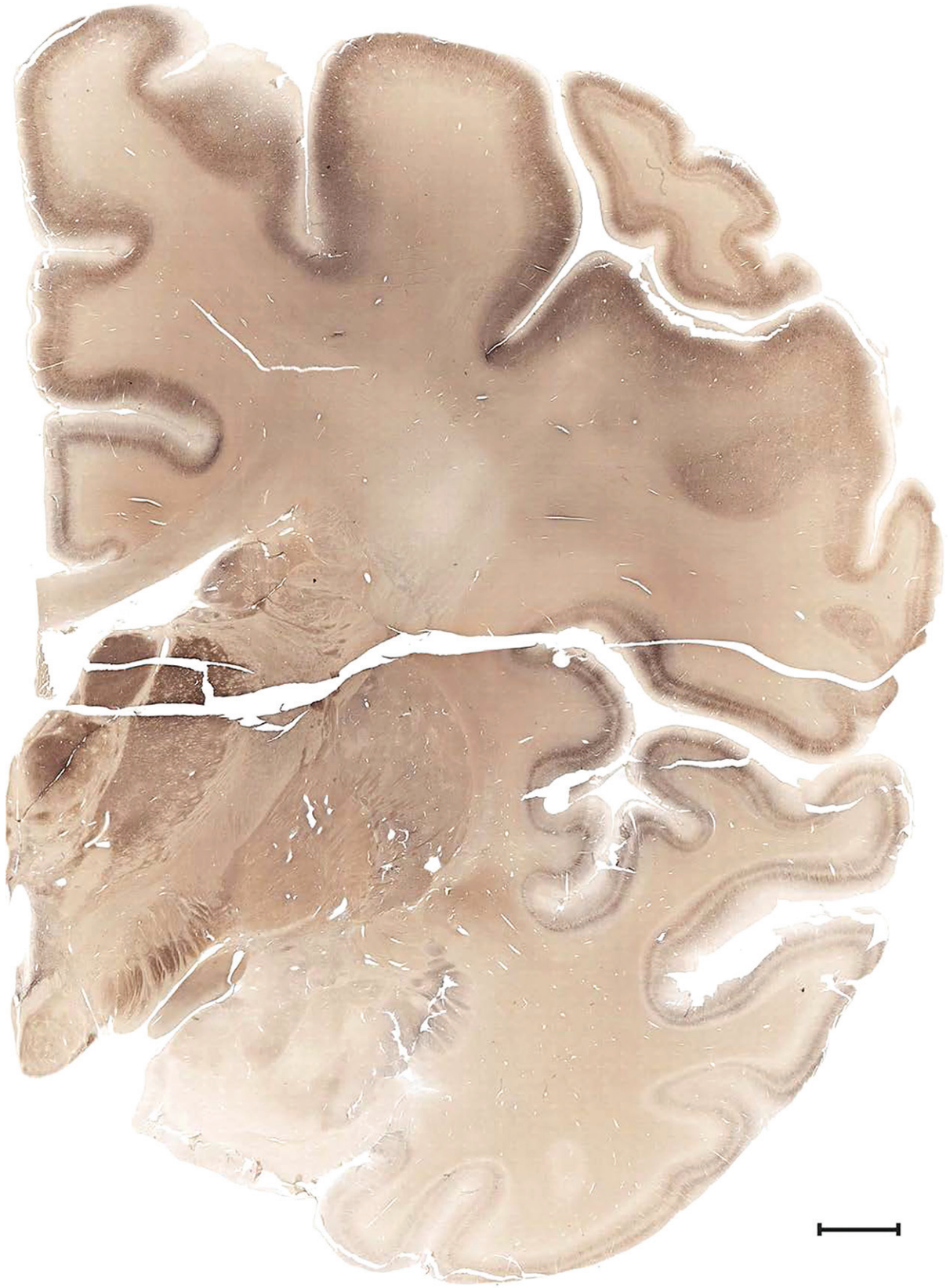

Figure 17. Level 37b (NFP (SMI-32))

Figure 17. Level 38a (04_291)

Link to online high resolution atlas plate
Link to online high resolution atlas plate (Nissl)

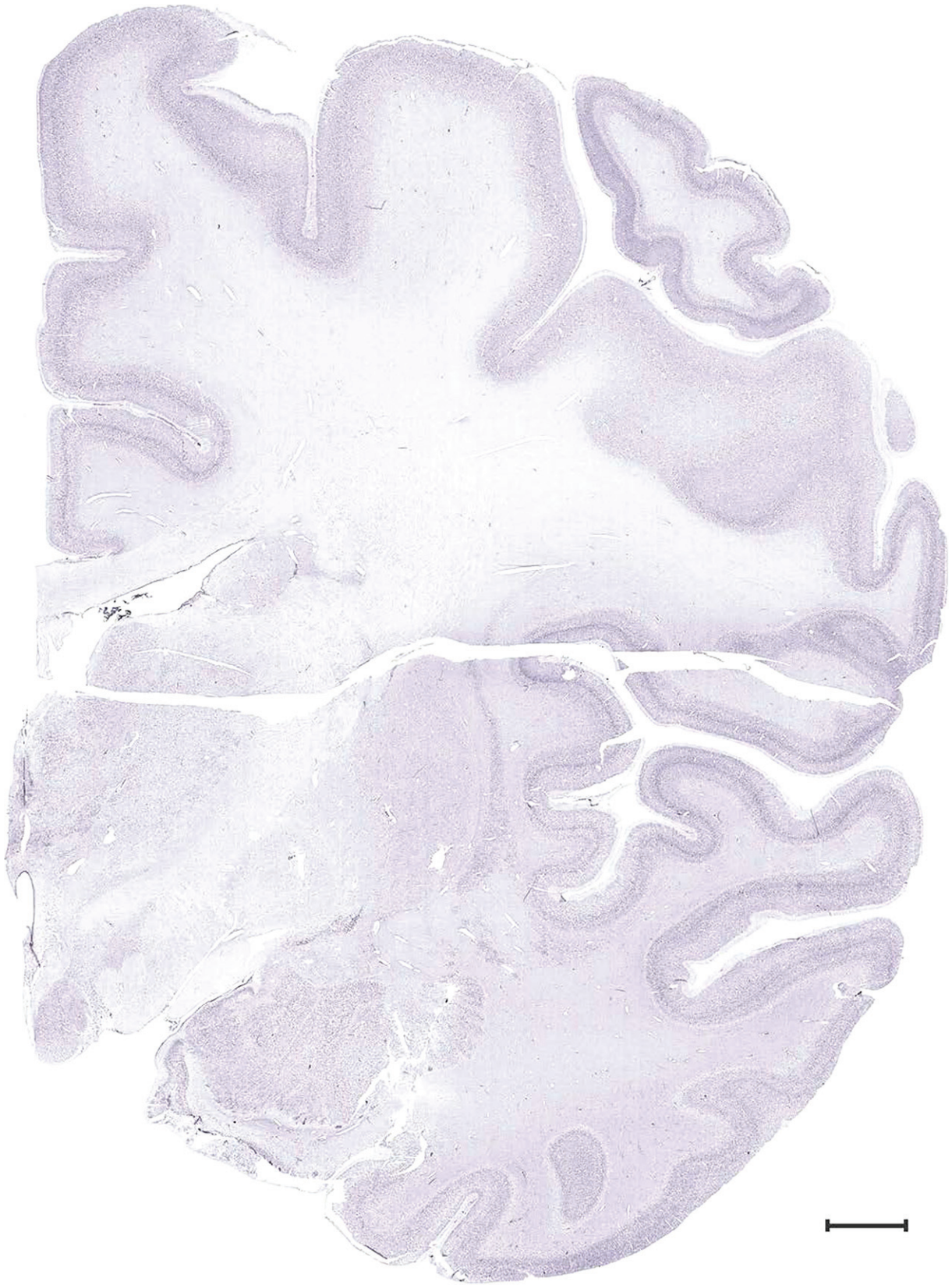

Figure 17. Level 38b (Nissl)

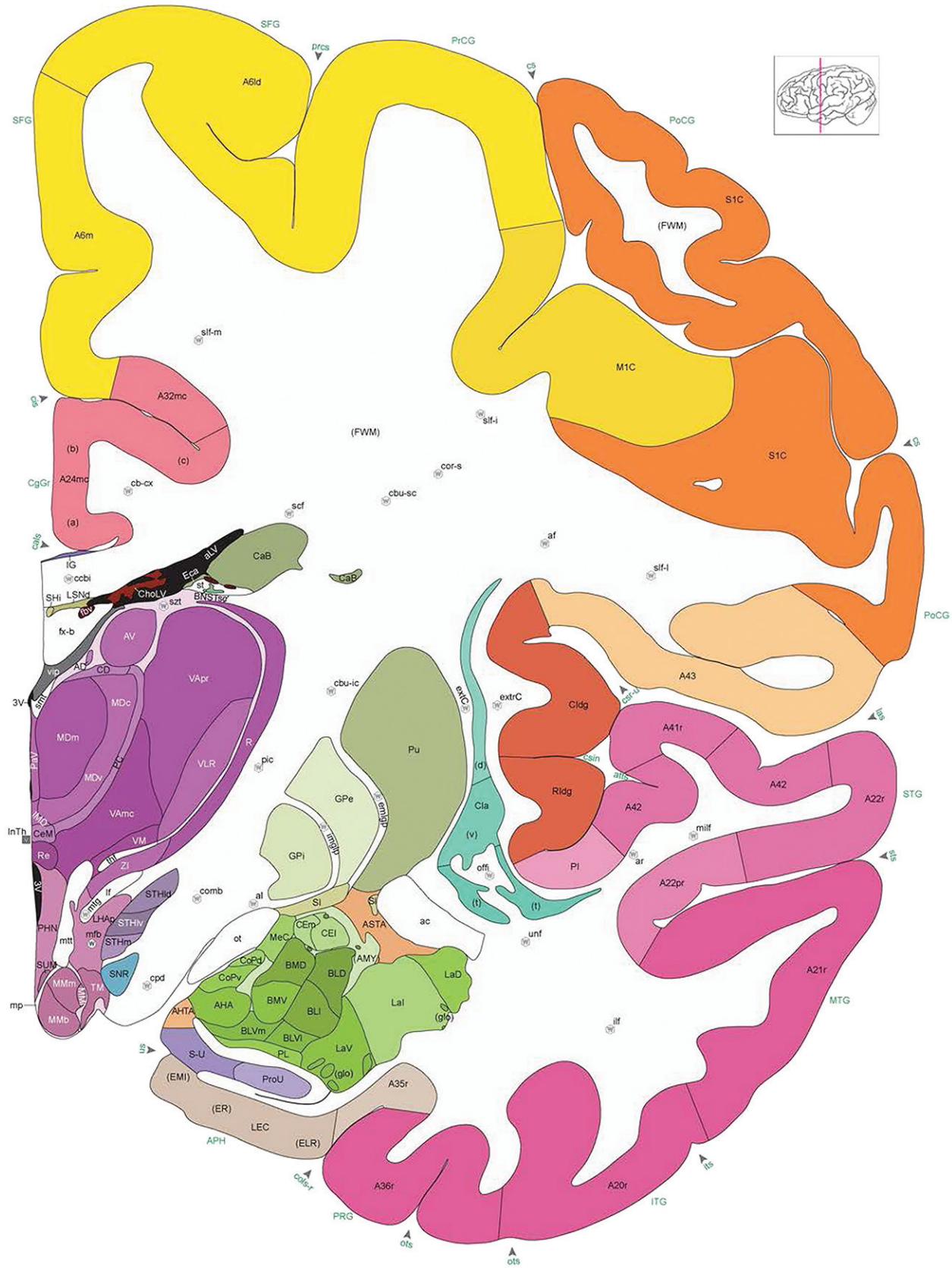

Figure 17. Level 39a (04_307)

Link to online high resolution atlas plate
Link to online high resolution atlas plate (Nissl)

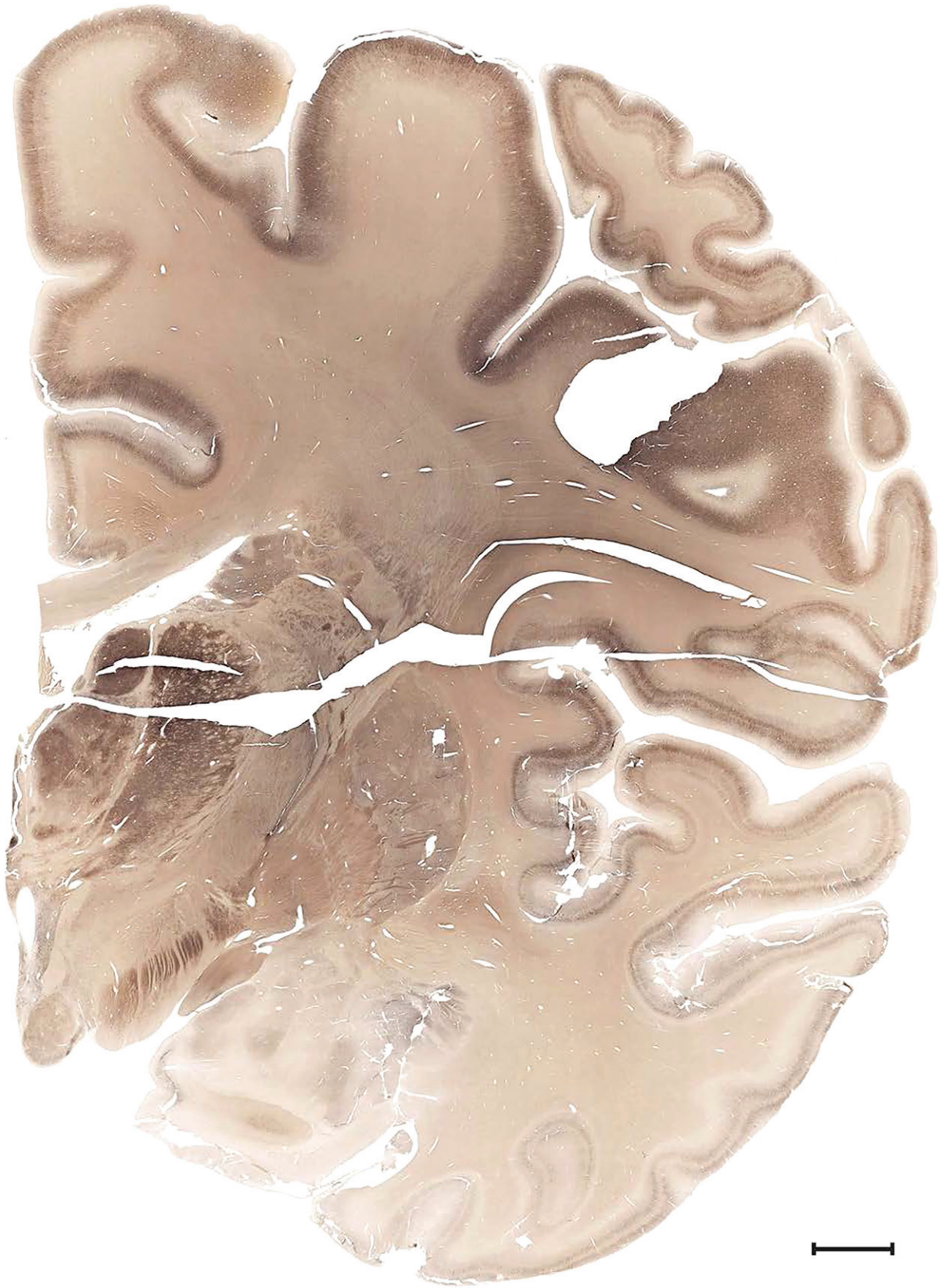

Figure 17. Level 39b (NFP (SMI-32))

Figure 17. Level 40a (04_315)

Link to online high resolution atlas plate
Link to online high resolution atlas plate (Nissl)

Figure 17. Level 40b (Nissl)

Figure 17. Level 41a (04_327)

Link to online high resolution atlas plate
Link to online high resolution atlas plate (Nissl)

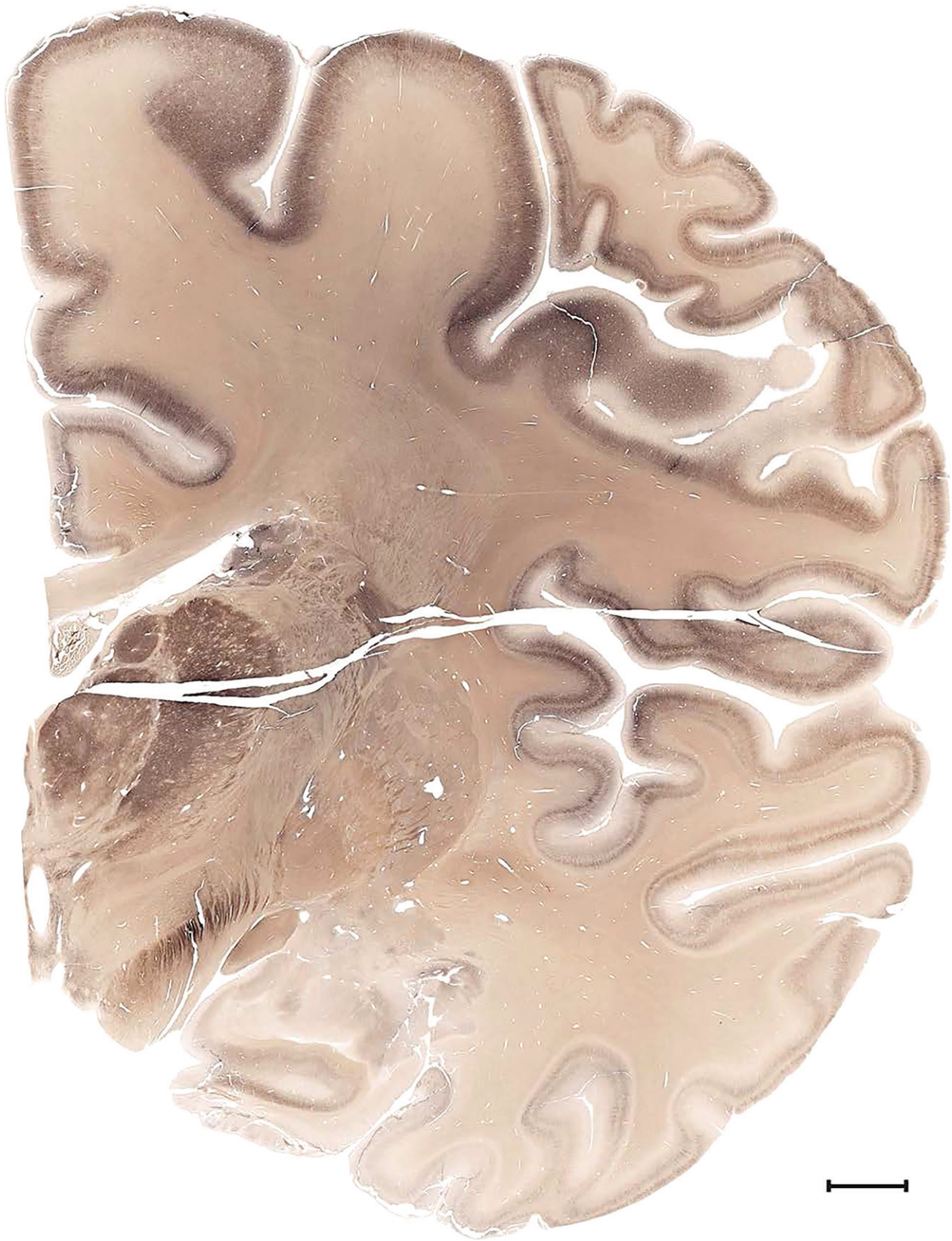

Figure 17. Level 41b (NFP (SMI-32))

Figure 17. Level 42a (04_335)

Link to online high resolution atlas plate
Link to online high resolution atlas plate (Nissl)

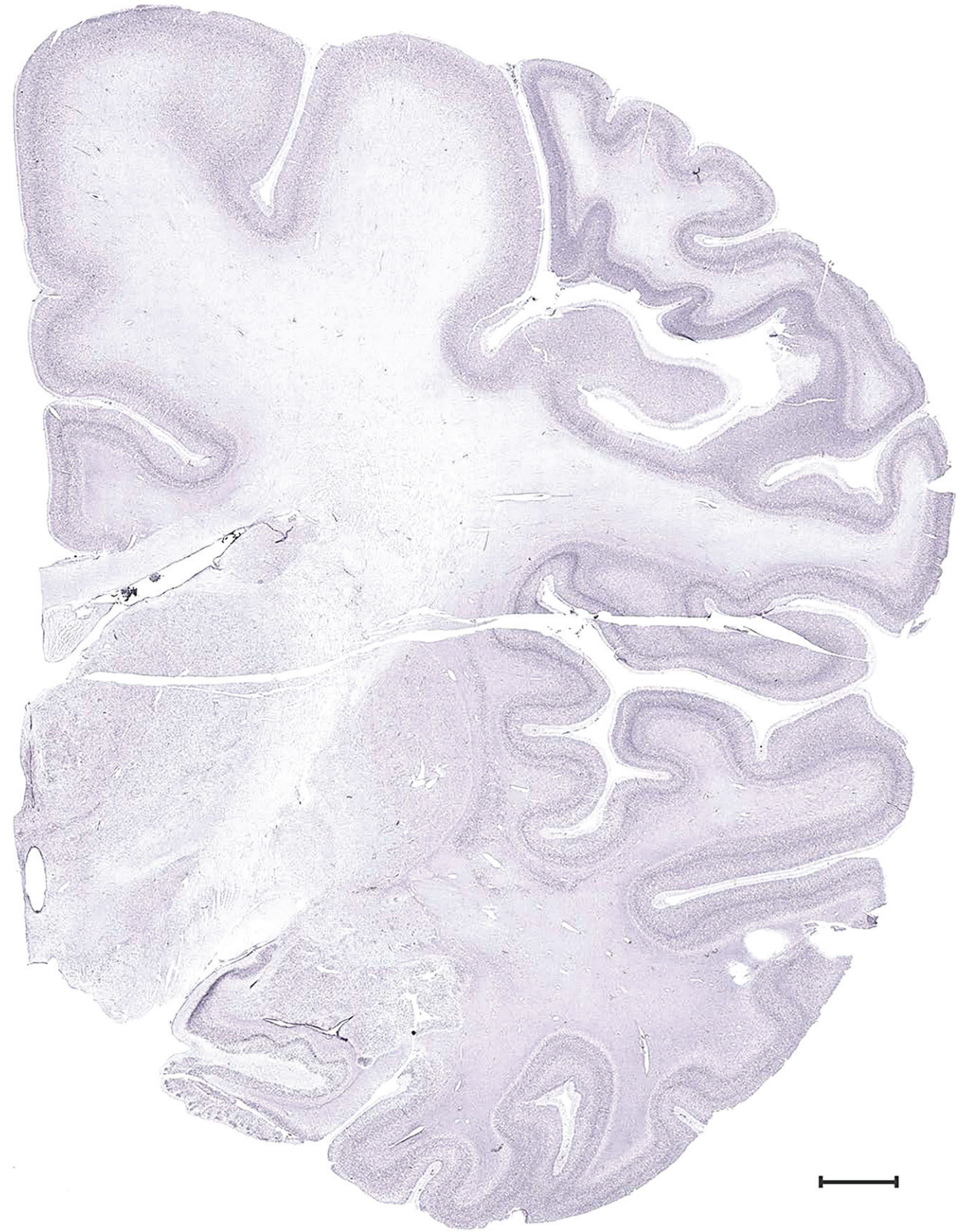

Figure 17. Level 42b (Nissls)

Figure 17. Level 43a (05_031)

Link to online high resolution atlas plate
Link to online high resolution atlas plate (Nissl)

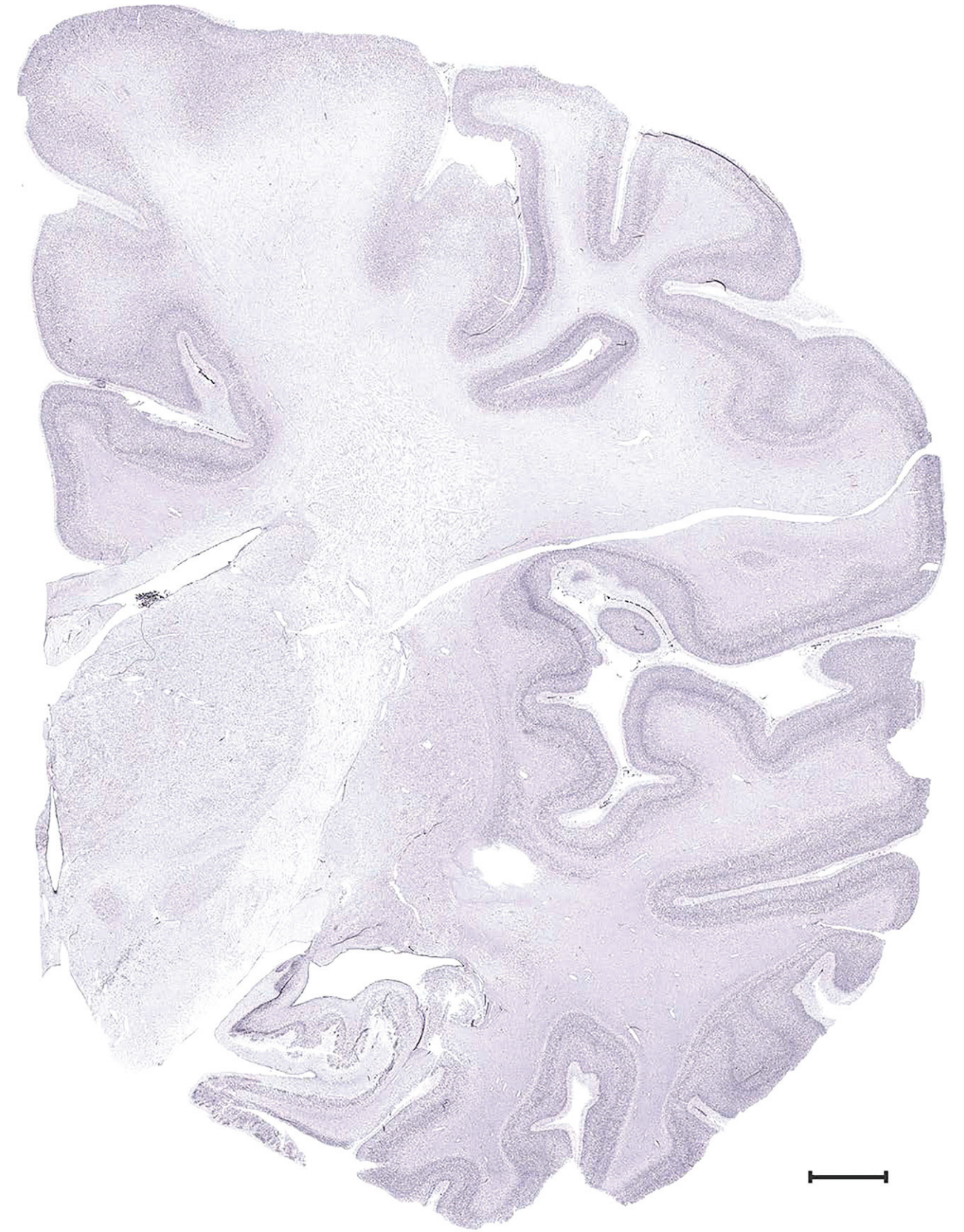

Figure 17. Level 43b (Nissl)

Figure 17. Level 44a (05_047)

Link to online high resolution atlas plate
Link to online high resolution atlas plate (Nissl)

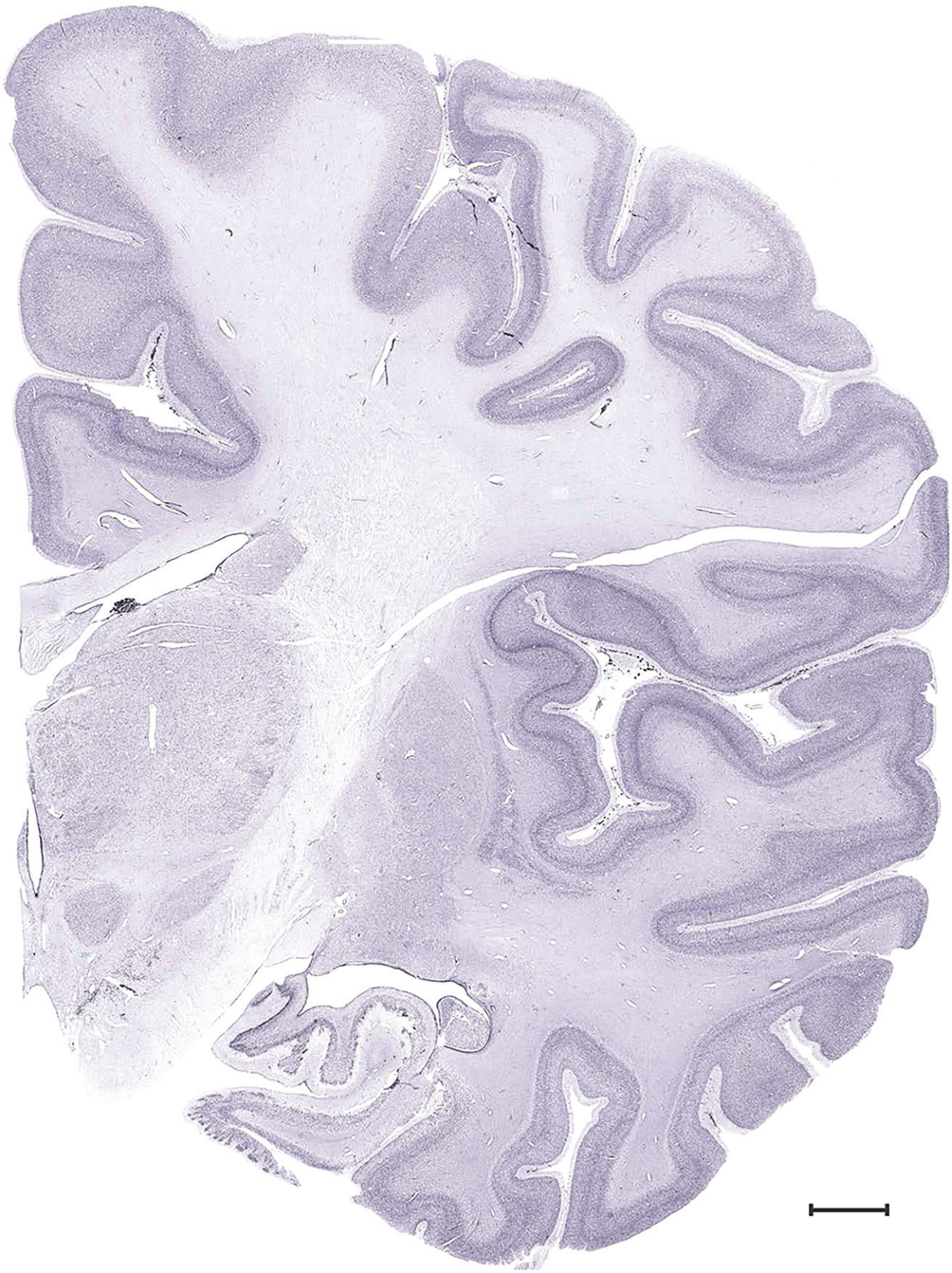

Figure 17. Level 44b (Nissl)

Figure 17. Level 45a (05_063)

Link to online high resolution atlas plate
Link to online high resolution atlas plate (Nissl)

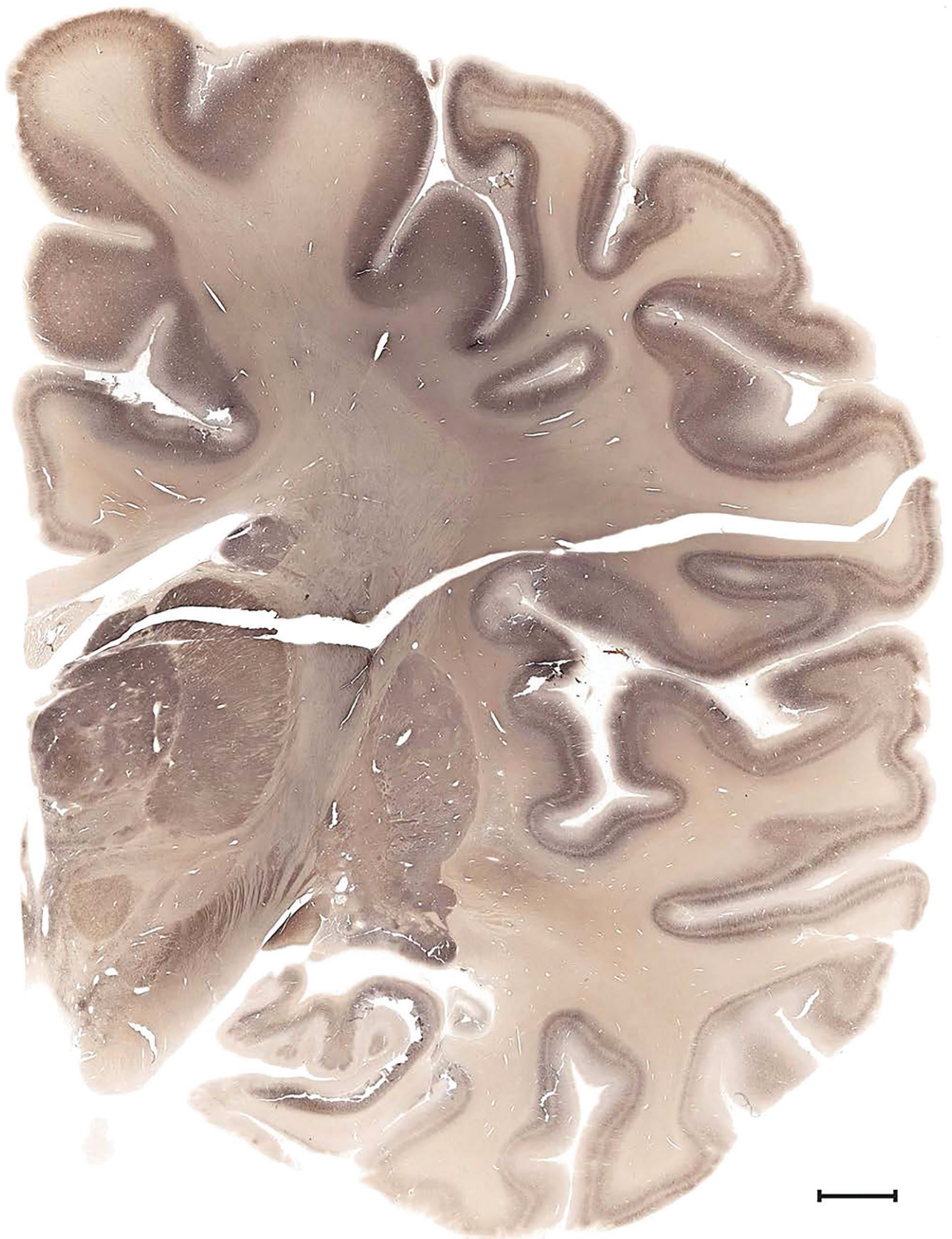

Figure 17. Level 45b (NFP (SMI-32))

Figure 17. Level 46a (05_079)

Link to online high resolution atlas plate
Link to online high resolution atlas plate (Nissl)

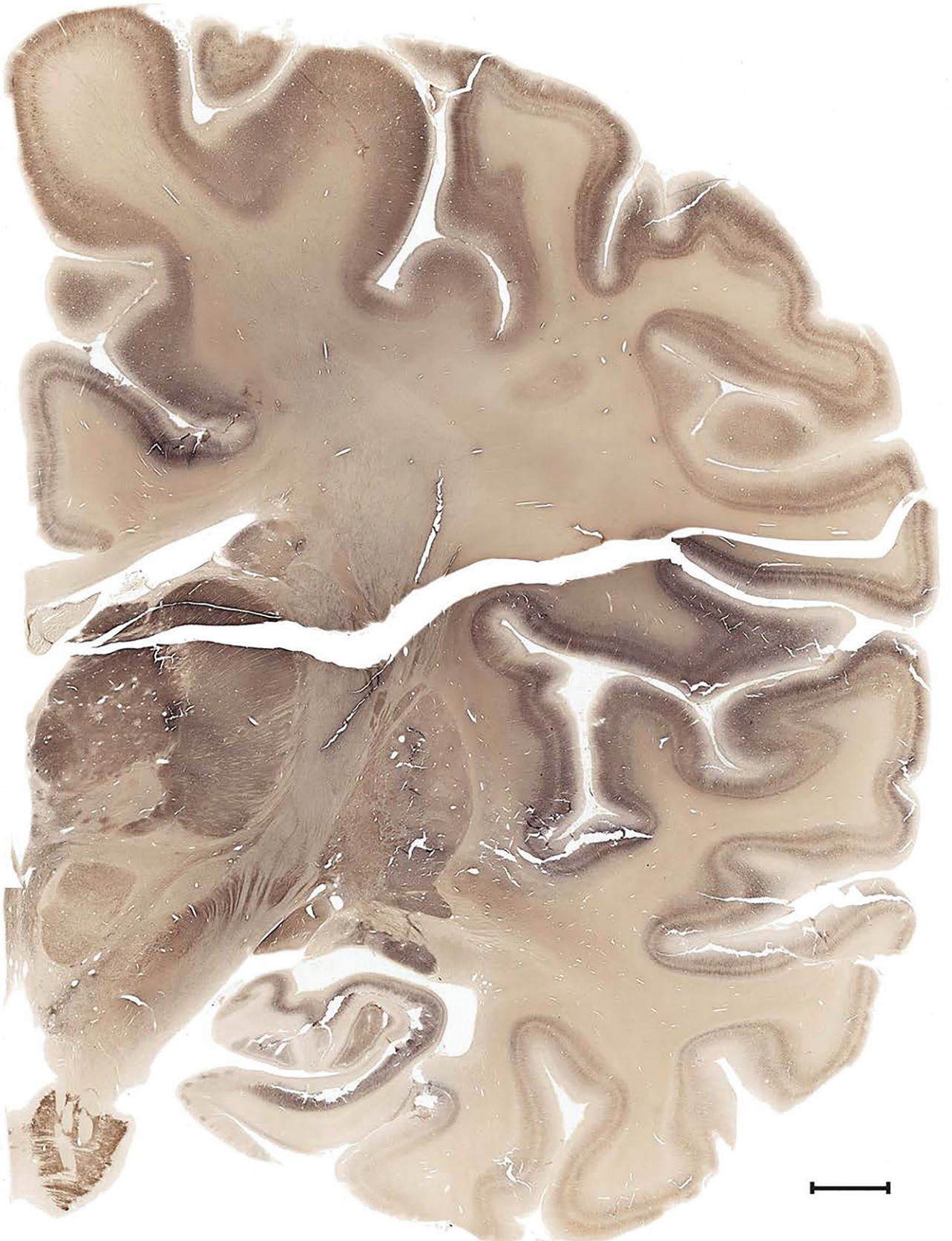

Figure 17. Level 46b (NFP (SMI-32))

Figure 17. Level 47a (05_091)

Link to online high resolution atlas plate
Link to online high resolution atlas plate (Nissl)

Figure 17. Level 47b (NFP (SMI-32))

Figure 17. Level 48a (05_103)

Link to online high resolution atlas plate
Link to online high resolution atlas plate (Nissl)

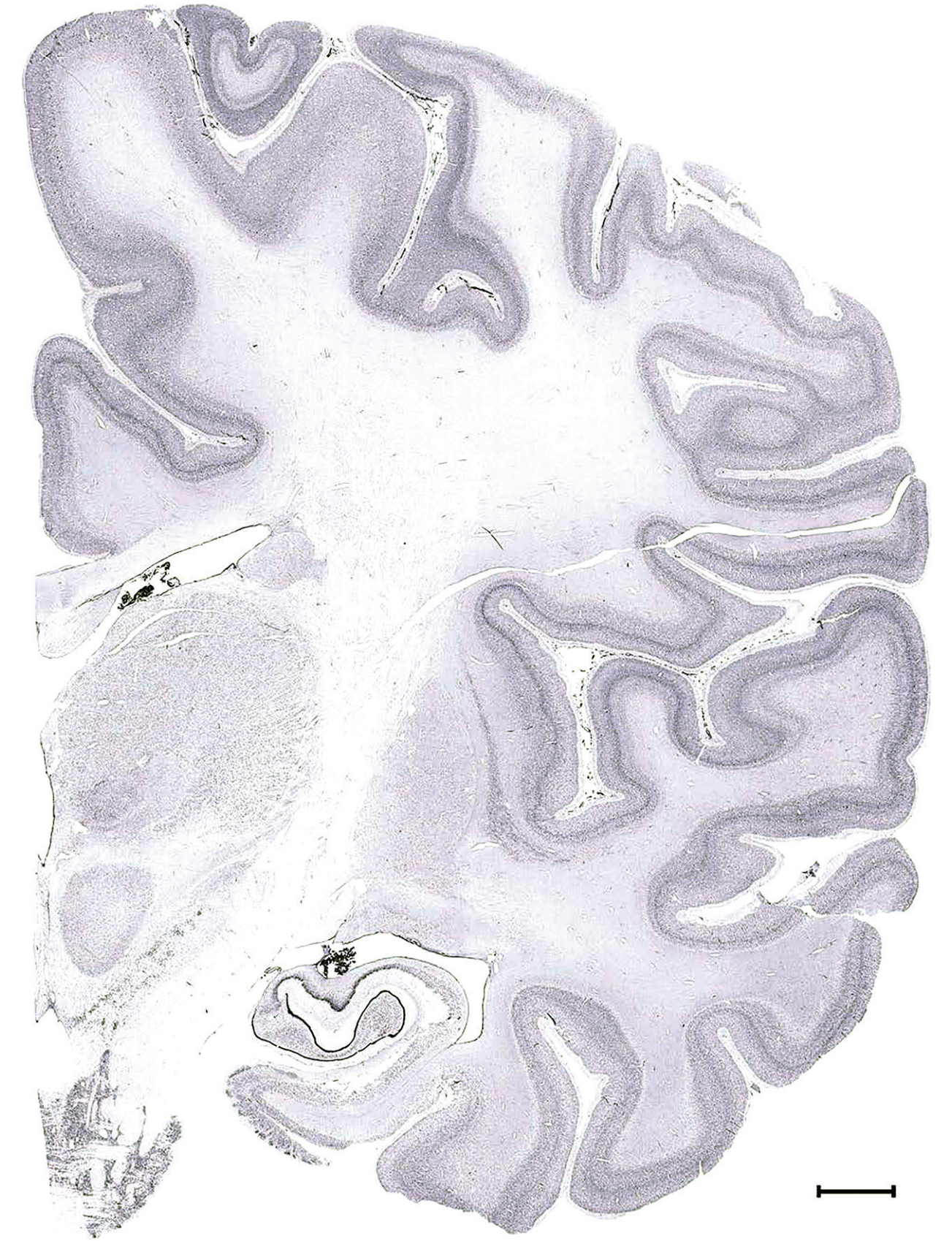

Figure 17. Level 48b (Nissl)

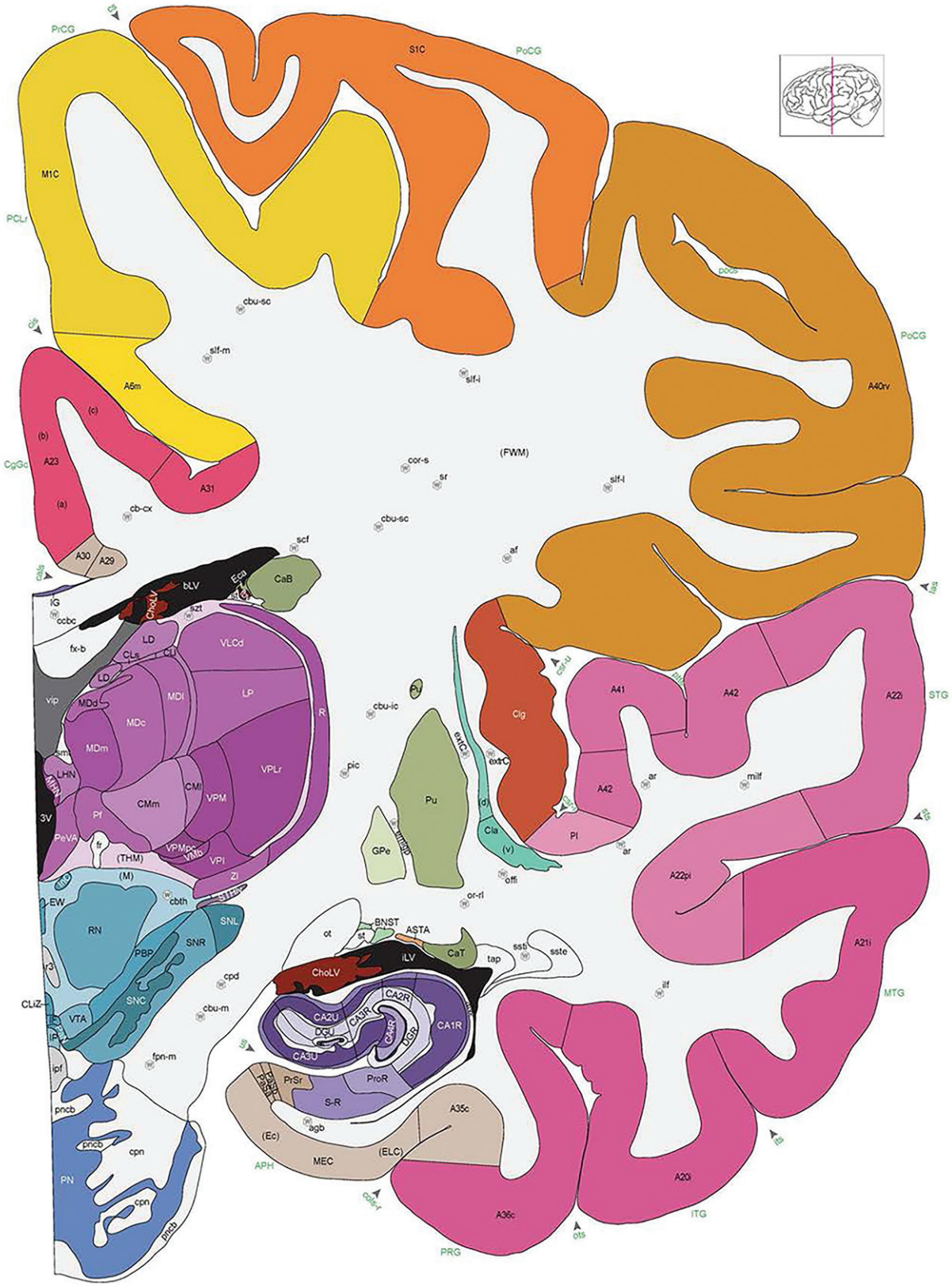

Figure 17. Level 49a (05_123)

Link to online high resolution atlas plate
Link to online high resolution atlas plate (Nissl)

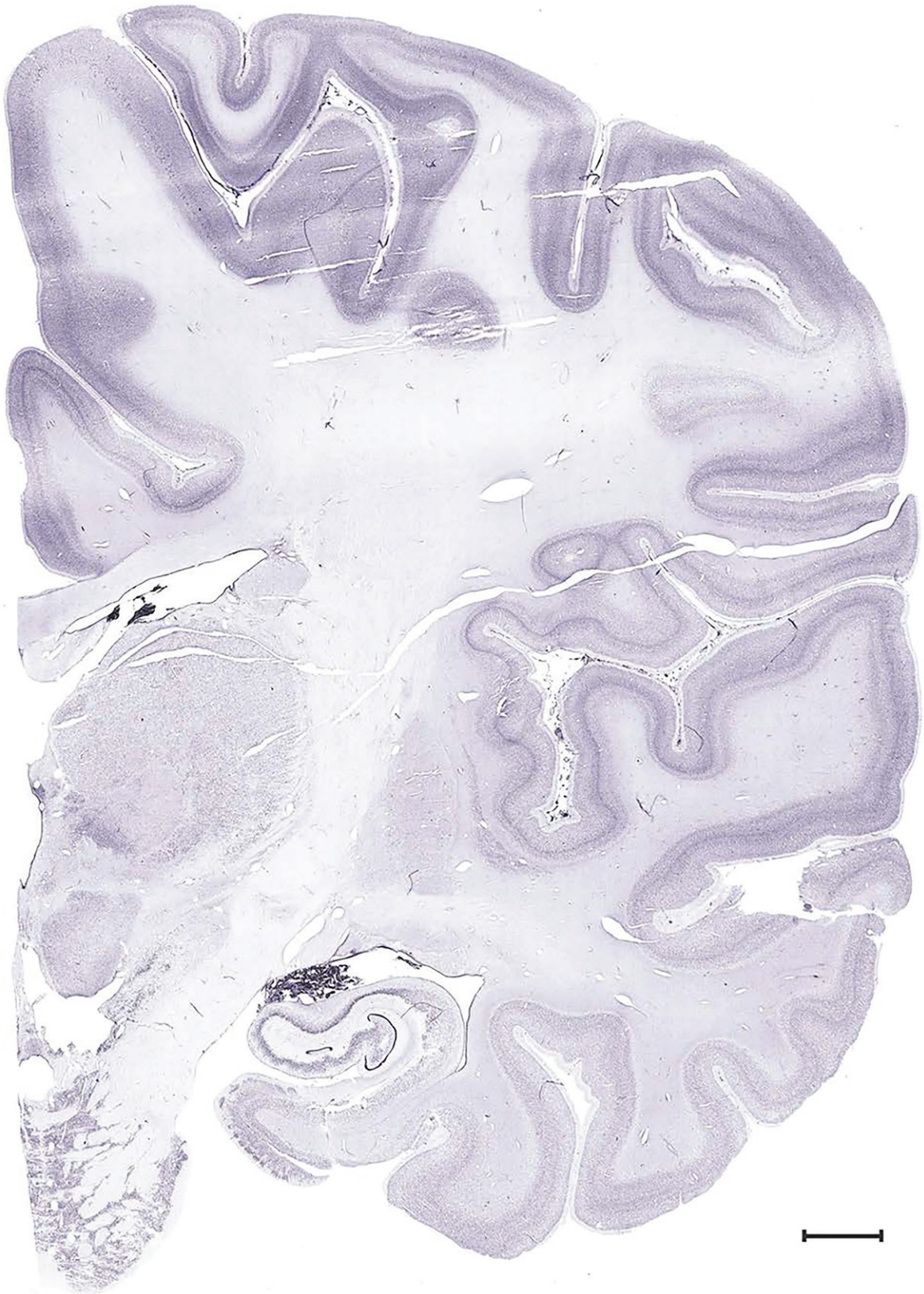

Figure 17. Level 49b (Nissl)

Figure 17. Level 50a (05_135)

Link to online high resolution atlas plate
Link to online high resolution atlas plate (Nissl)

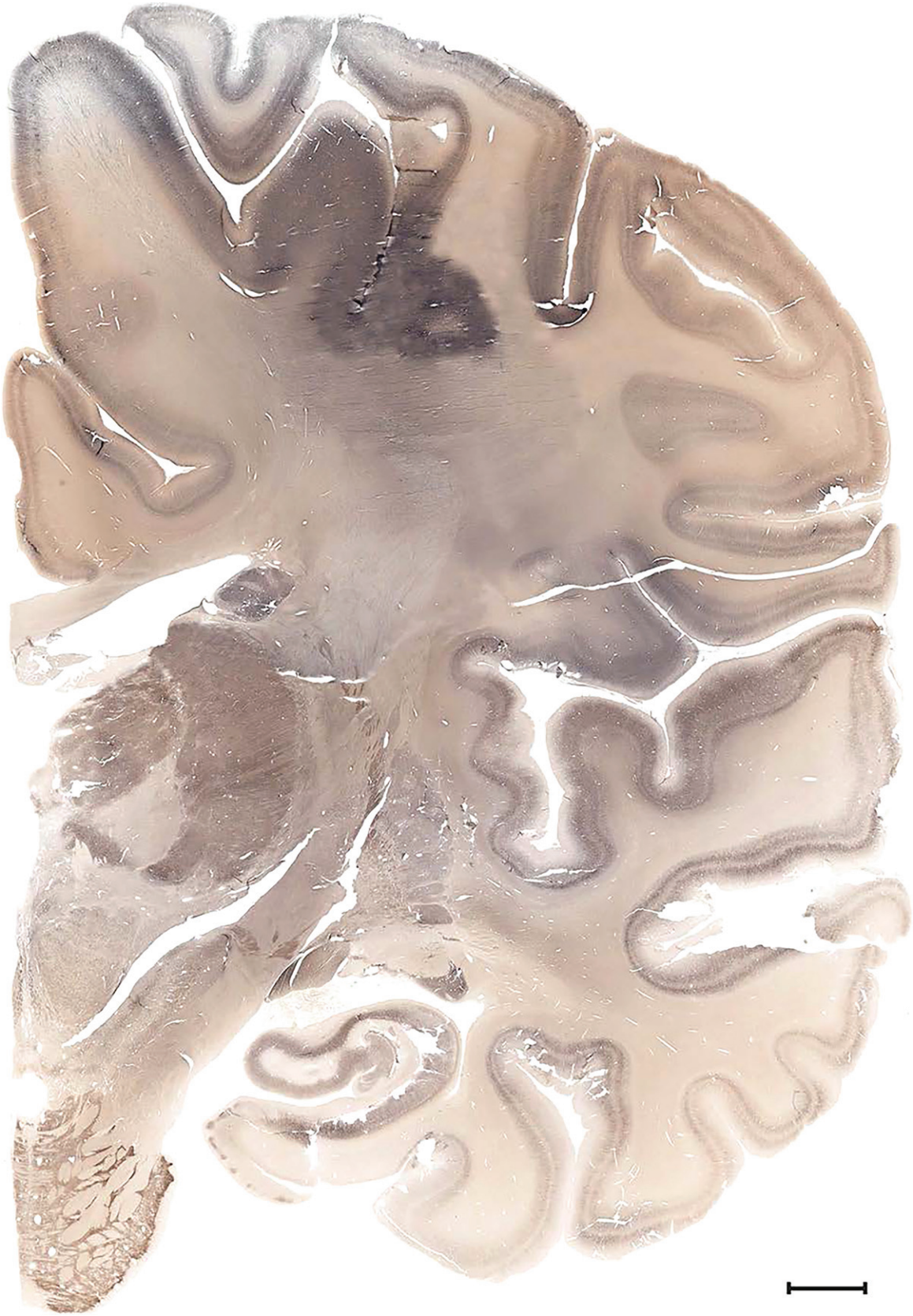

Figure 17. Level 50b (NFP (SMI-32))

Figure 17. Level 51a (05_147)

Link to online high resolution atlas plate
Link to online high resolution atlas plate (Nissl)

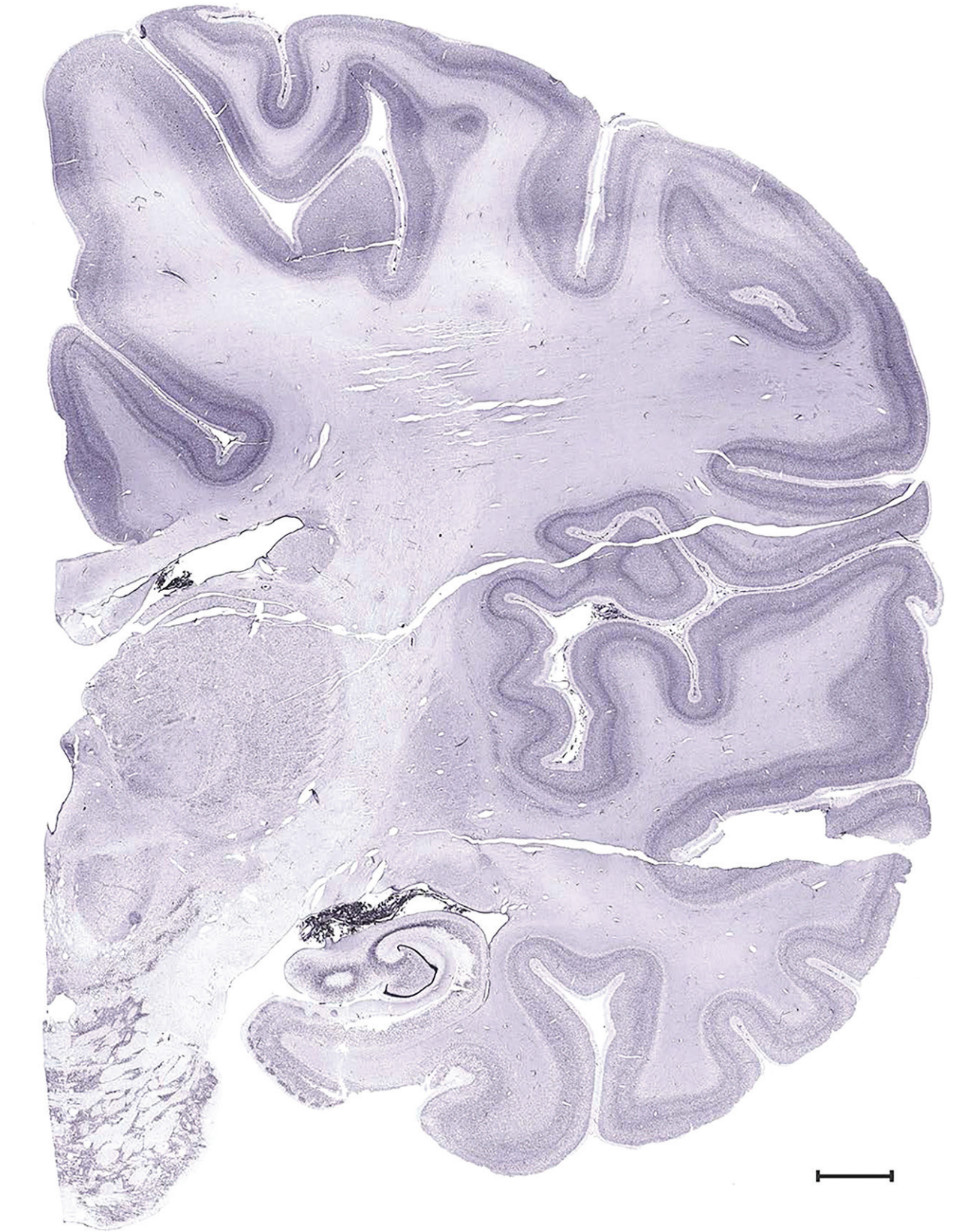

Figure 17. Level 51b (Nissl)

Figure 17. Level 52a (05_159)

Link to online high resolution atlas plate
Link to online high resolution atlas plate (Nissl)

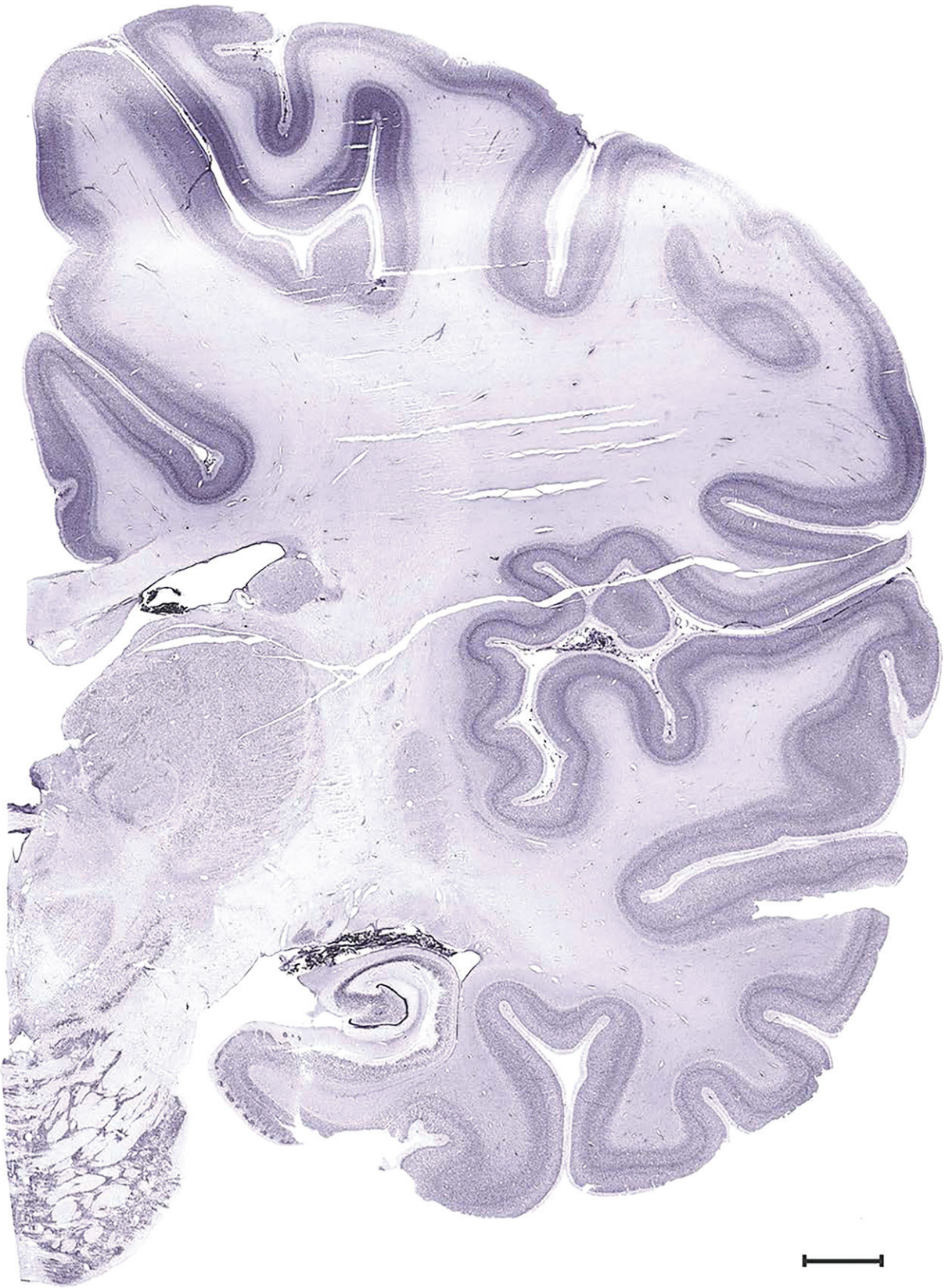

Figure 17. Level 52b (Nissl)

Figure 17. Level 53a (05_171)

Link to online high resolution atlas plate
Link to online high resolution atlas plate (Nissl)

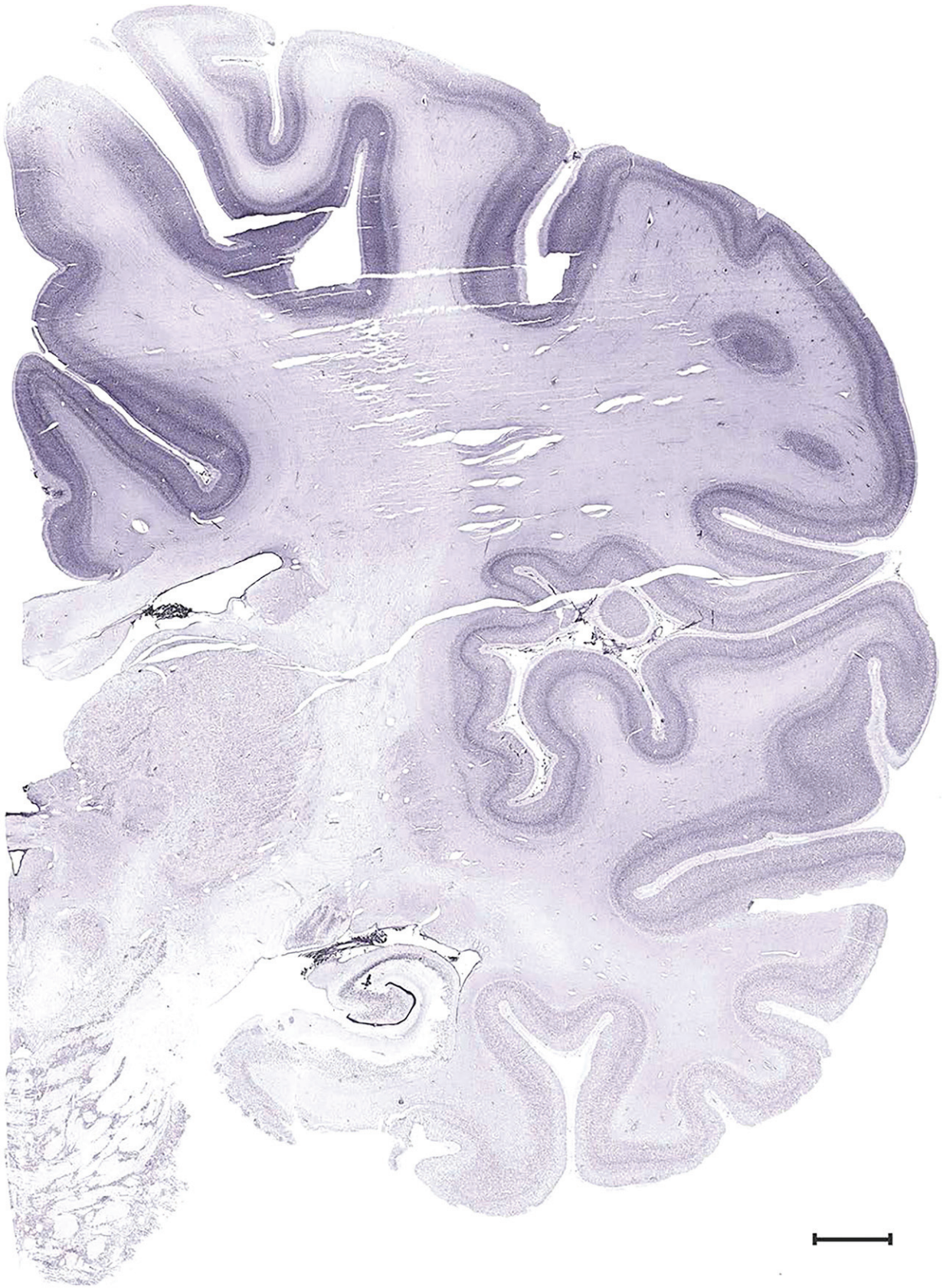

Figure 17. Level 53b (Nissl)

Figure 17. Level 54a (05_187)

Link to online high resolution atlas plate
Link to online high resolution atlas plate (Nissl)

Figure 17. Level 54b (NFP (SMI-32))

Figure 17. Level 55a (05_203)

Link to online high resolution atlas plate
Link to online high resolution atlas plate (Nissl)

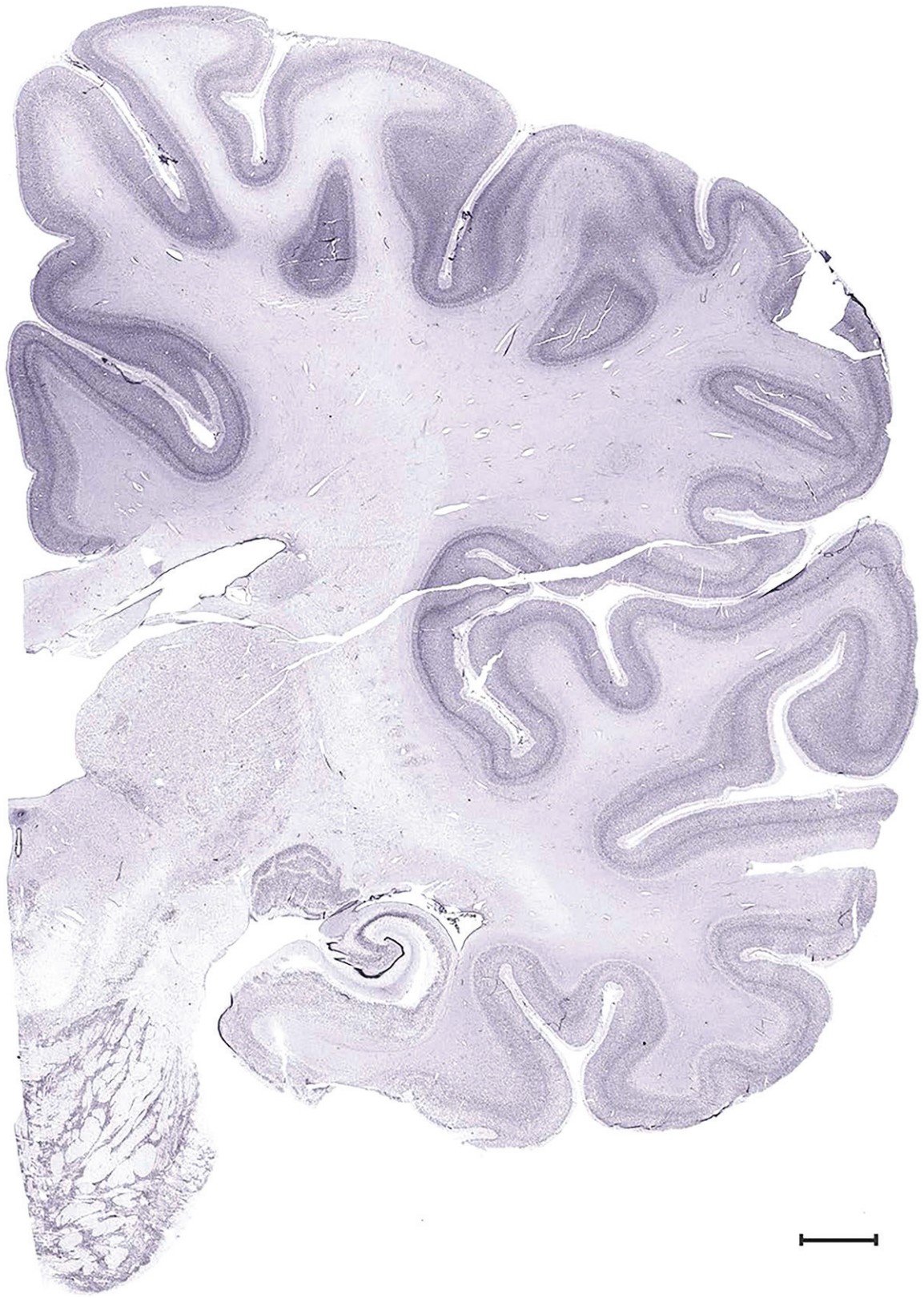

Figure 17. Level 55b (Nissl)

Figure 17. Level 56a (05_223)

Link to online high resolution atlas plate
Link to online high resolution atlas plate (Nissl)

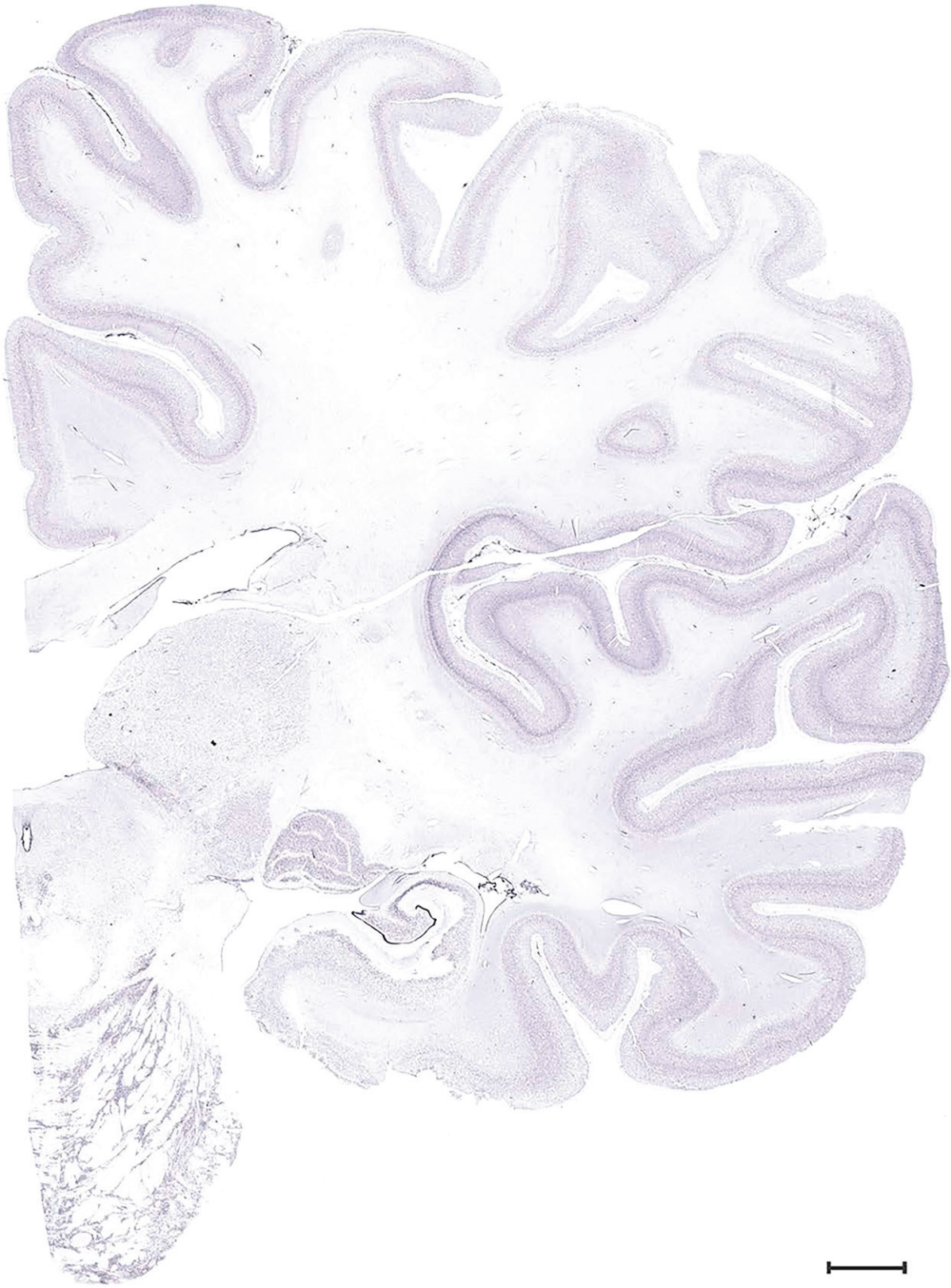

Figure 17. Level 56b (Nissl)

Figure 17. Level 57a (05_235)

Link to online high resolution atlas plate
Link to online high resolution atlas plate (Nissl)

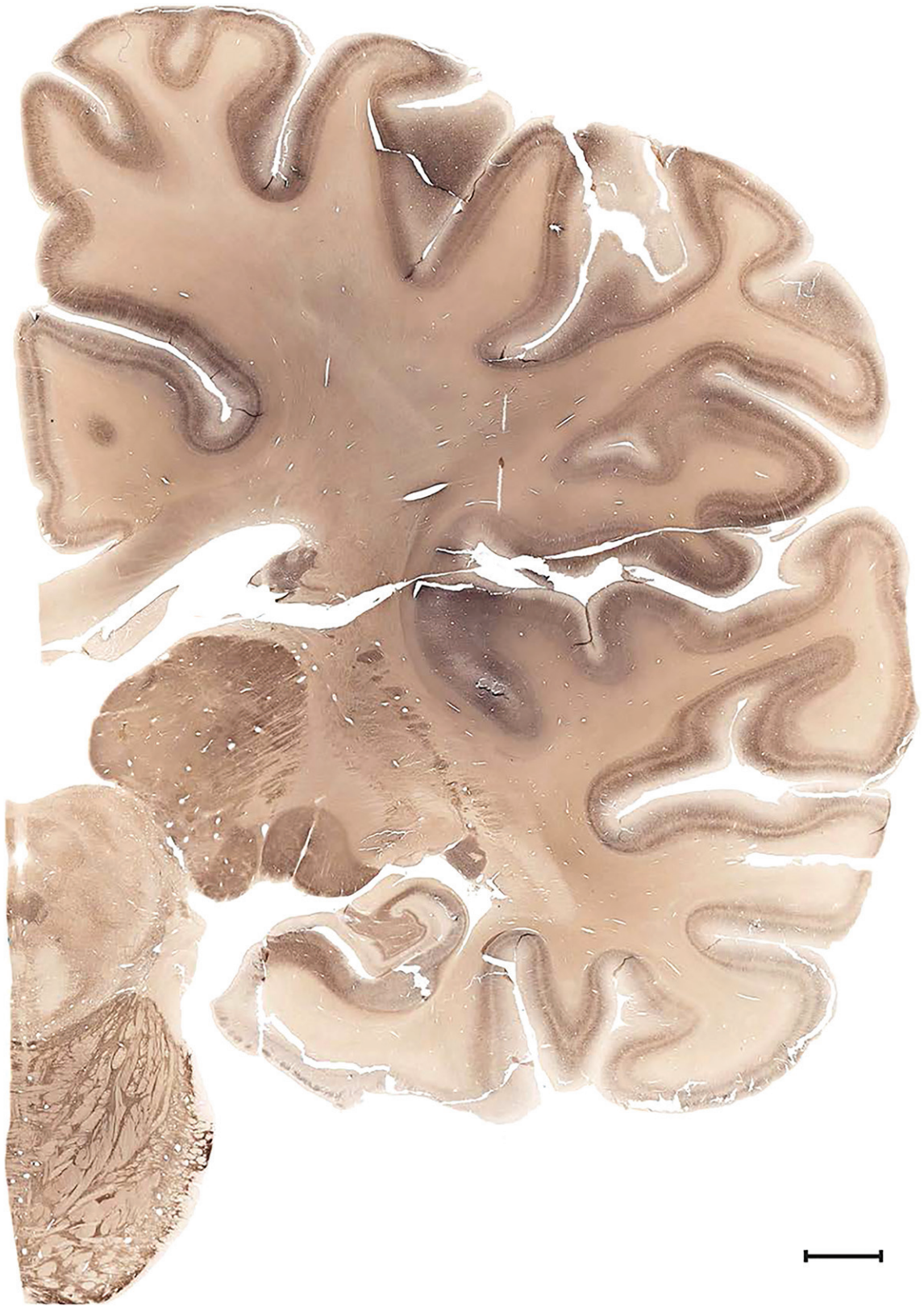

Figure 17. Level 57b (NFP (SMI-32))

Figure 17. Level 58a (05_255)

Link to online high resolution atlas plate
Link to online high resolution atlas plate (Nissl)

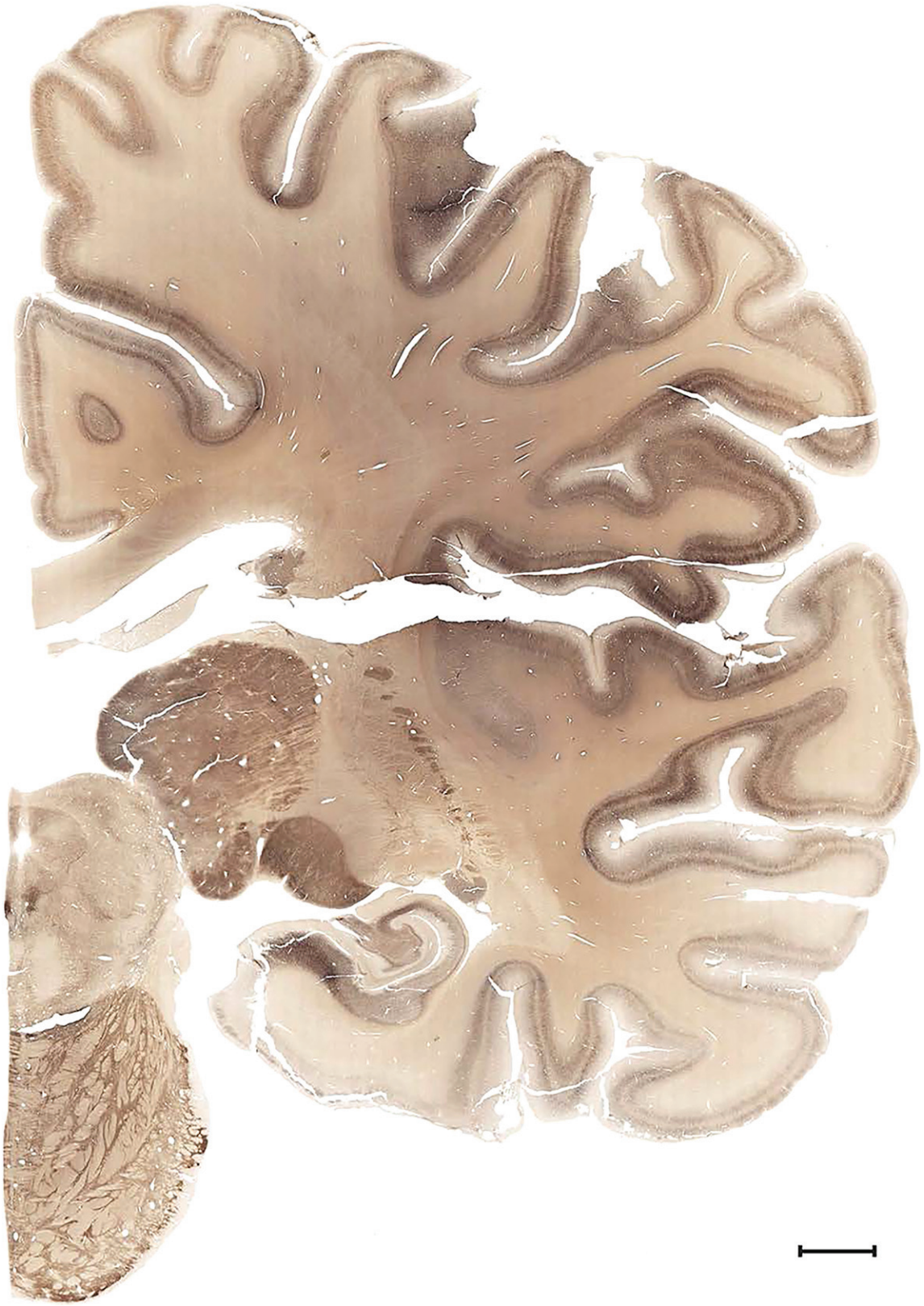

Figure 17. Level 58b (NFP (SMI-32))

Figure 17. Level 59a (05_275)

Link to online high resolution atlas plate
Link to online high resolution atlas plate (Nissl)

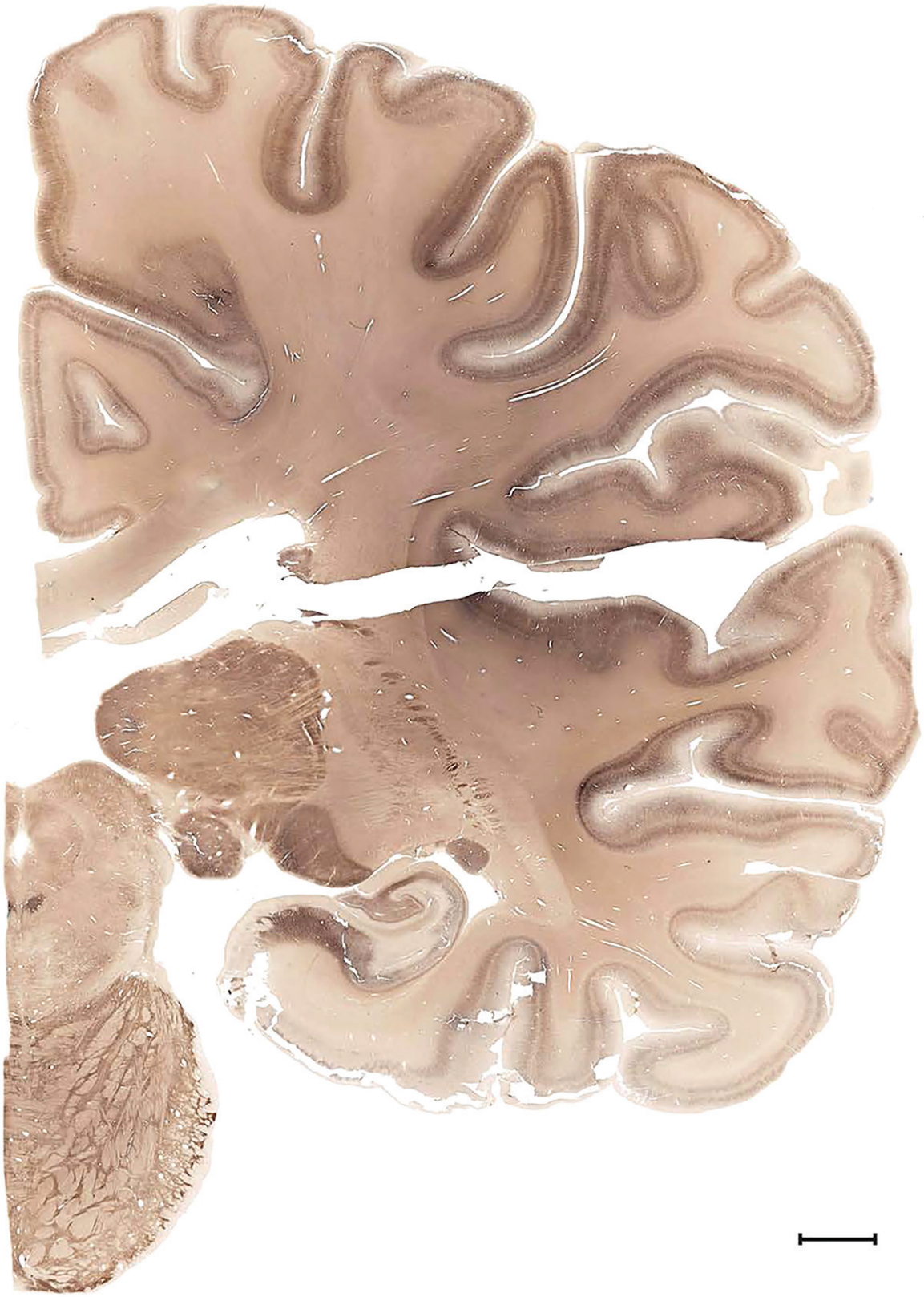

Figure 17. Level 59b (NFP (SMI-32))

Figure 17. Level 60a (05_287)

Link to online high resolution atlas plate
Link to online high resolution atlas plate (Nissl)

Figure 17. Level 60b (NFP (SMI-32))

Figure 17. Level 61a (05_303)

Link to online high resolution atlas plate
Link to online high resolution atlas plate (Nissl)

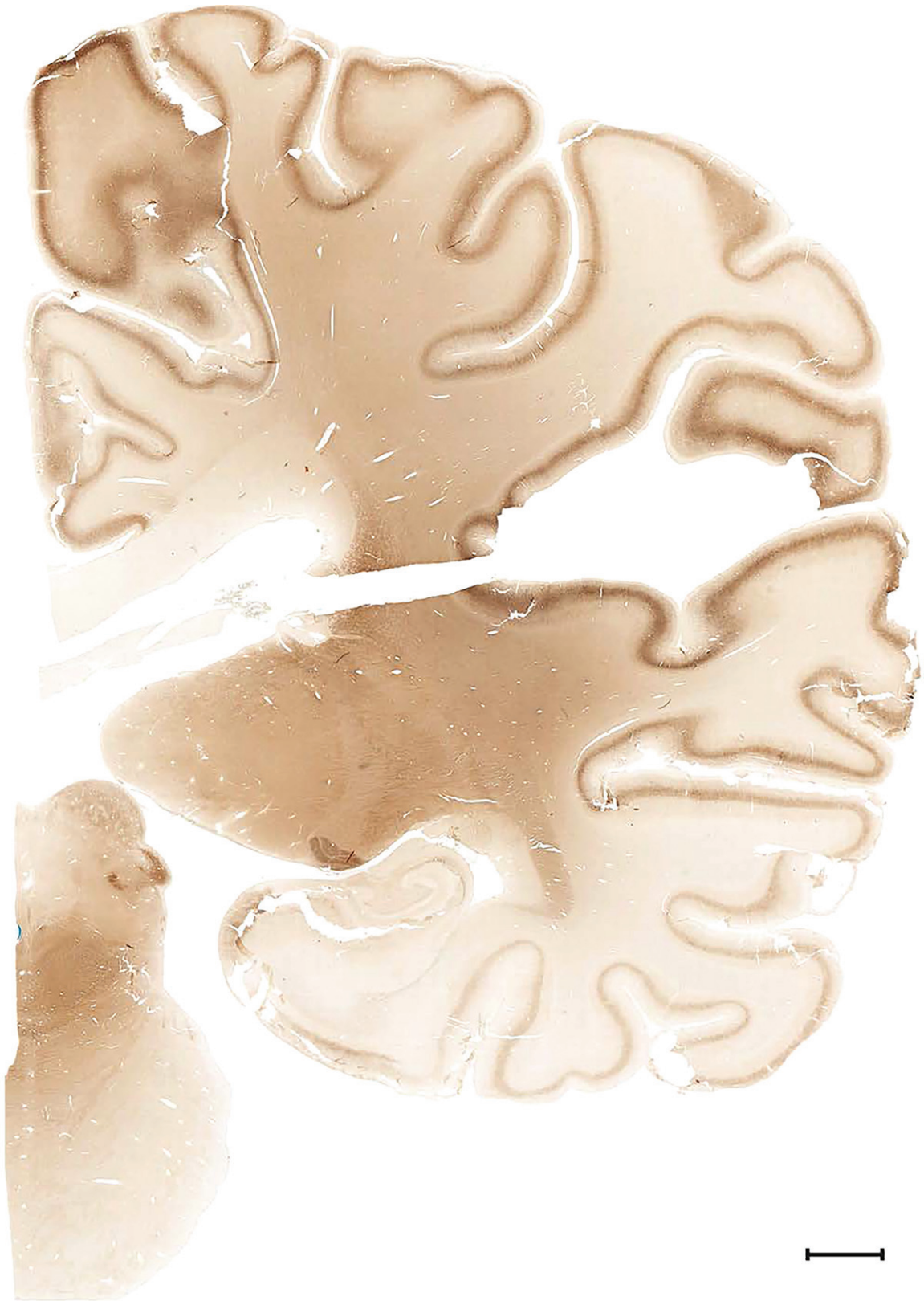

Figure 17. Level 61b (Parvalbumin)

Figure 17. Level 62a (05_311)

Link to online high resolution atlas plate
Link to online high resolution atlas plate (Nissl)

Figure 17. Level 62b (NFP (SMI-32))

Figure 17. Level 63a (05_323)

Link to online high resolution atlas plate
Link to online high resolution atlas plate (Nissl)

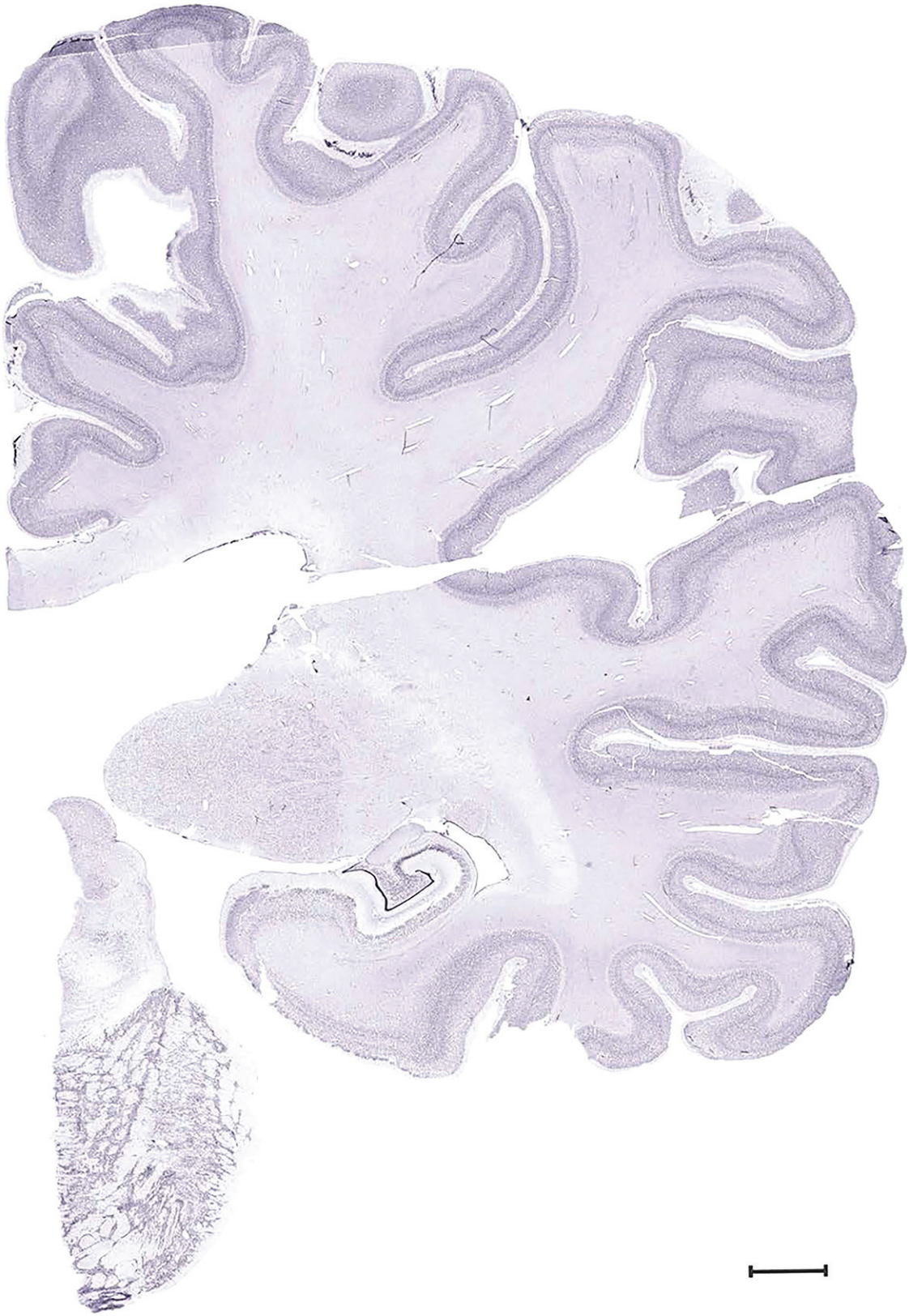

Figure 17. Level 63b (Nissl)

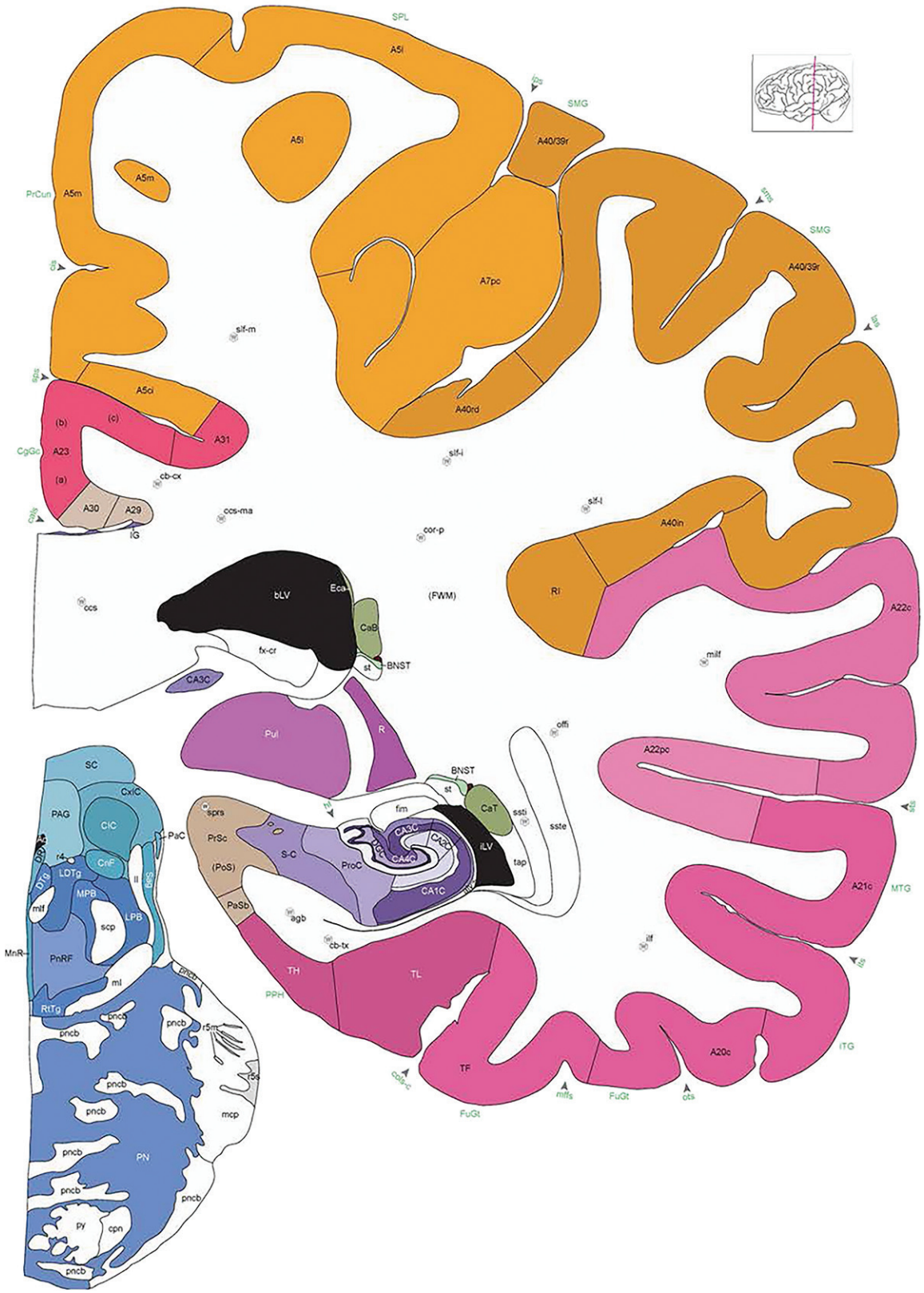

Figure 17. Level 64a (06_035)

Link to online high resolution atlas plate
Link to online high resolution atlas plate (Nissl)

Figure 17. Level 64b (Parvalbumin)

Figure 17. Level 65a (05_047)

Link to online high resolution atlas plate
Link to online high resolution atlas plate (Nissl)

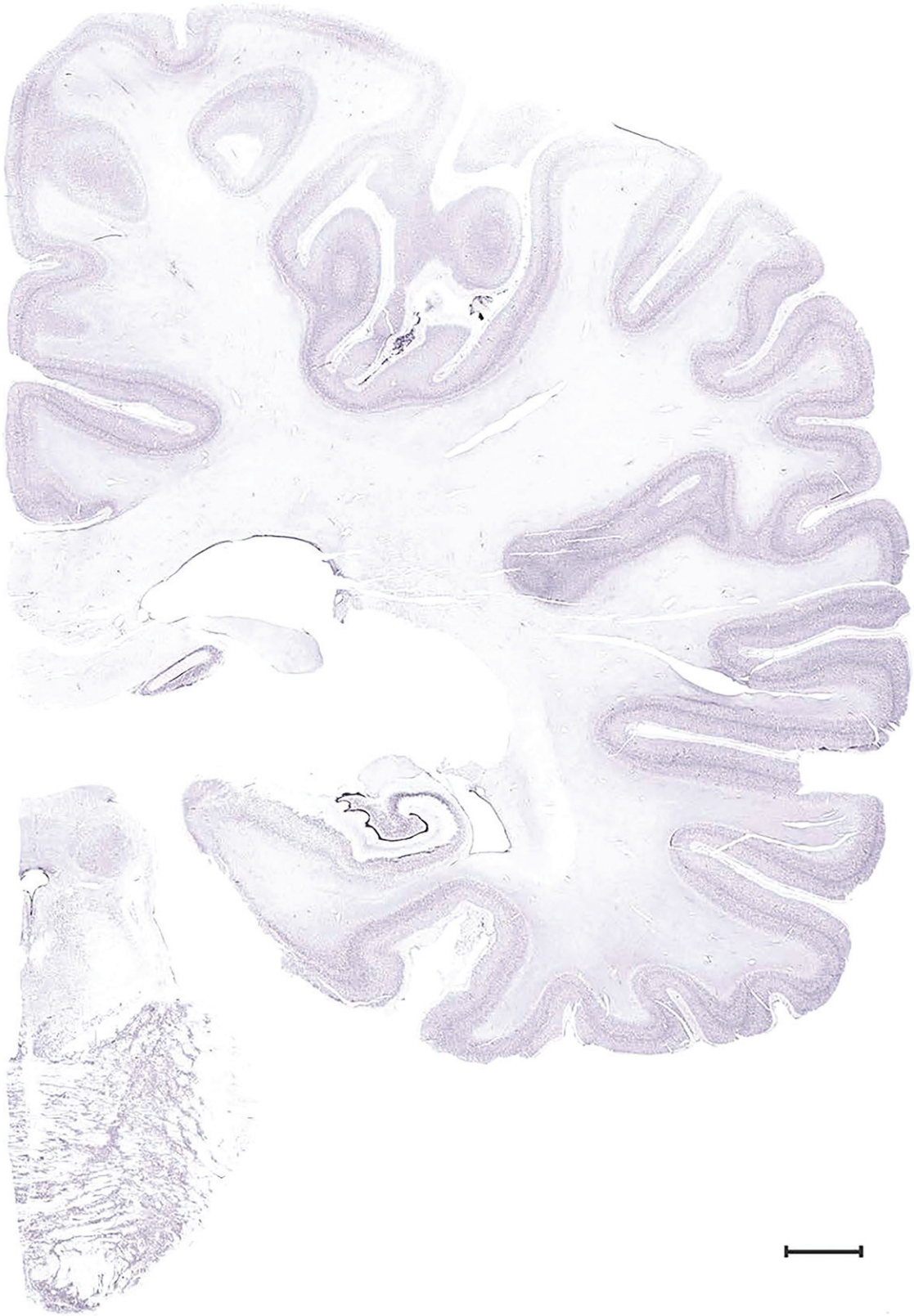

Figure 17. Level 65b (Nissl)

Figure 17. Level 66a (06_063)

Link to online high resolution atlas plate
Link to online high resolution atlas plate (Nissl)

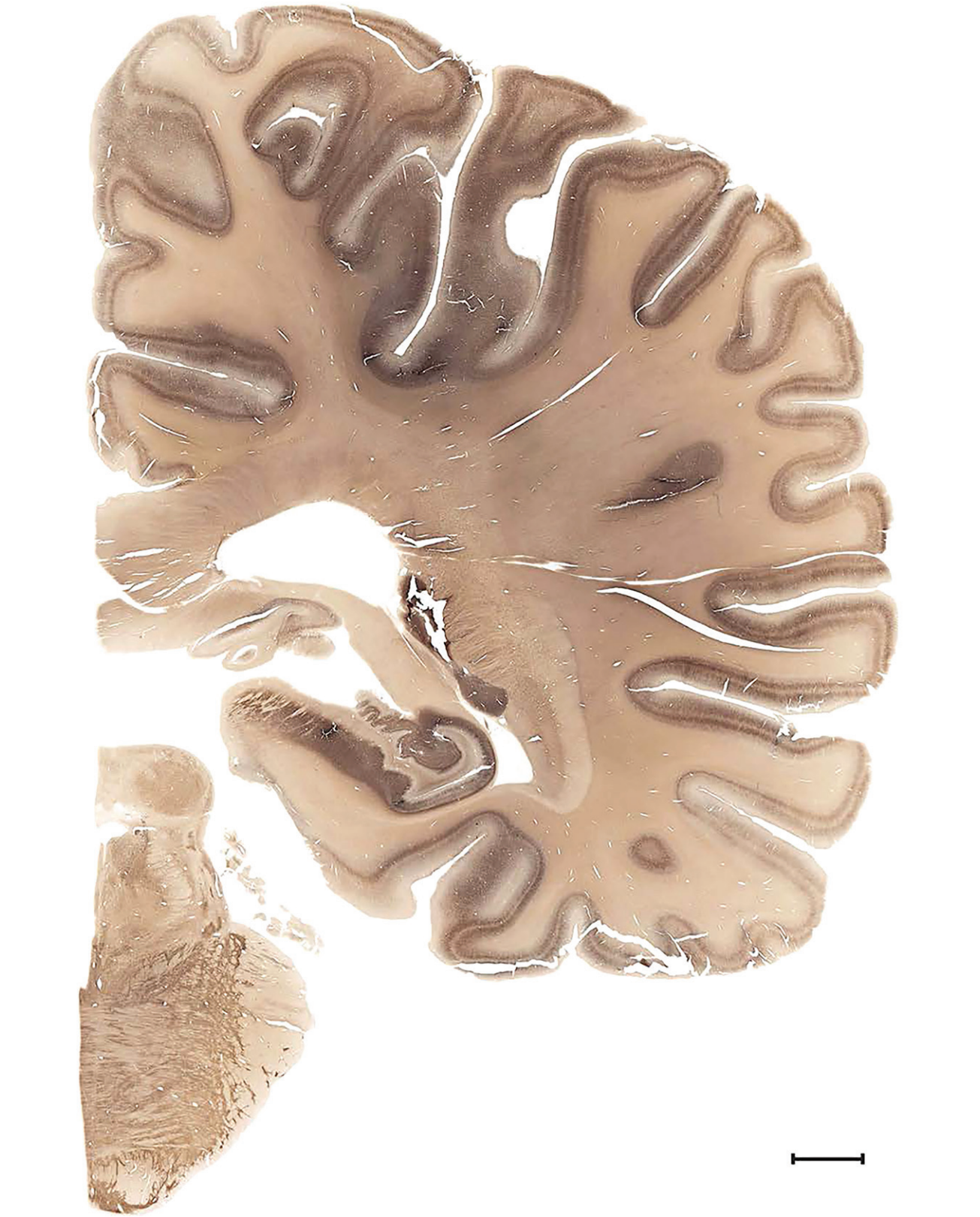

Figure 17. Level 66b (NFP (SMI-32))

Figure 17. Level 67a (06_083)

Link to online high resolution atlas plate
Link to online high resolution atlas plate (Nissl)

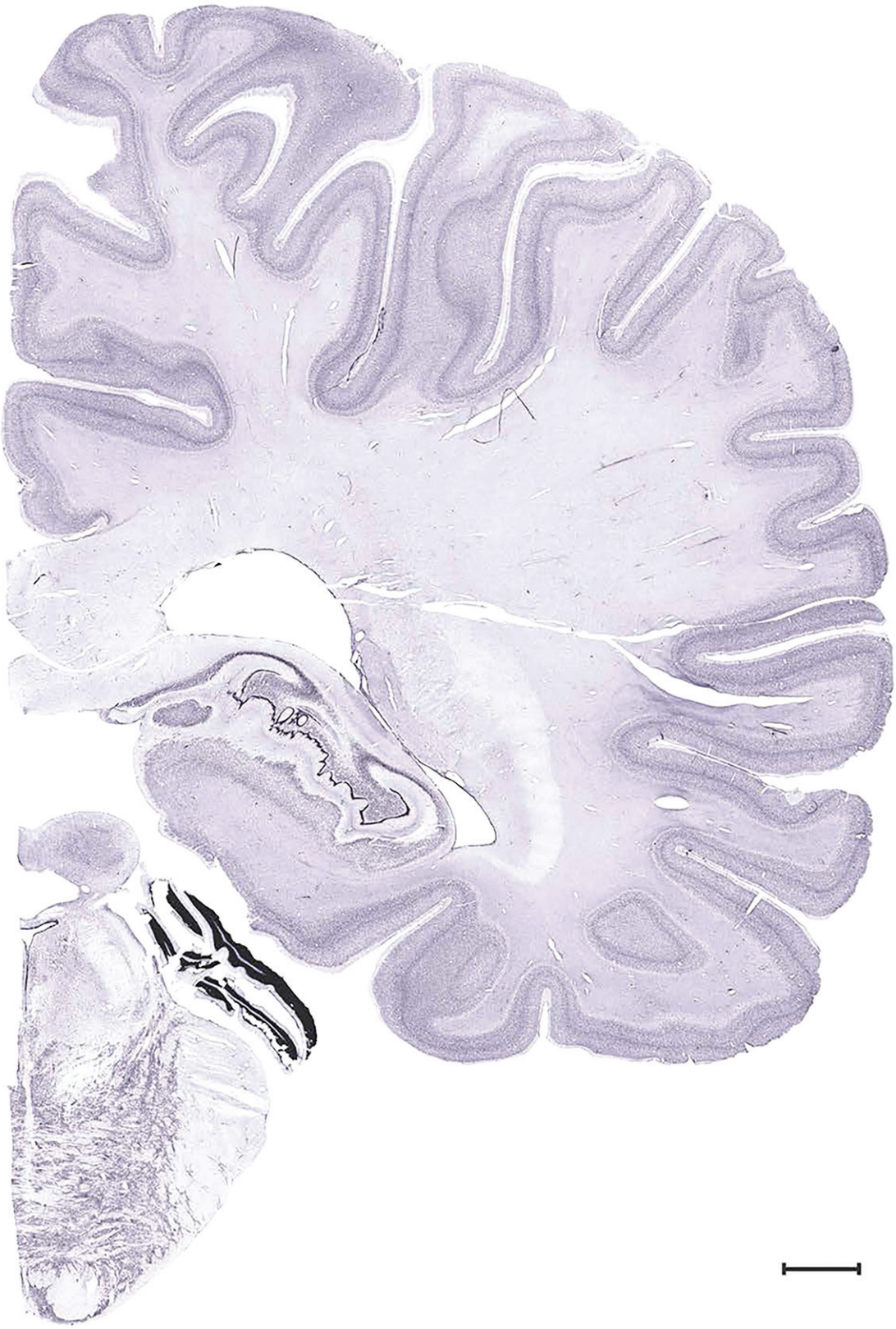

Figure 17. Level 67b (Nissl)

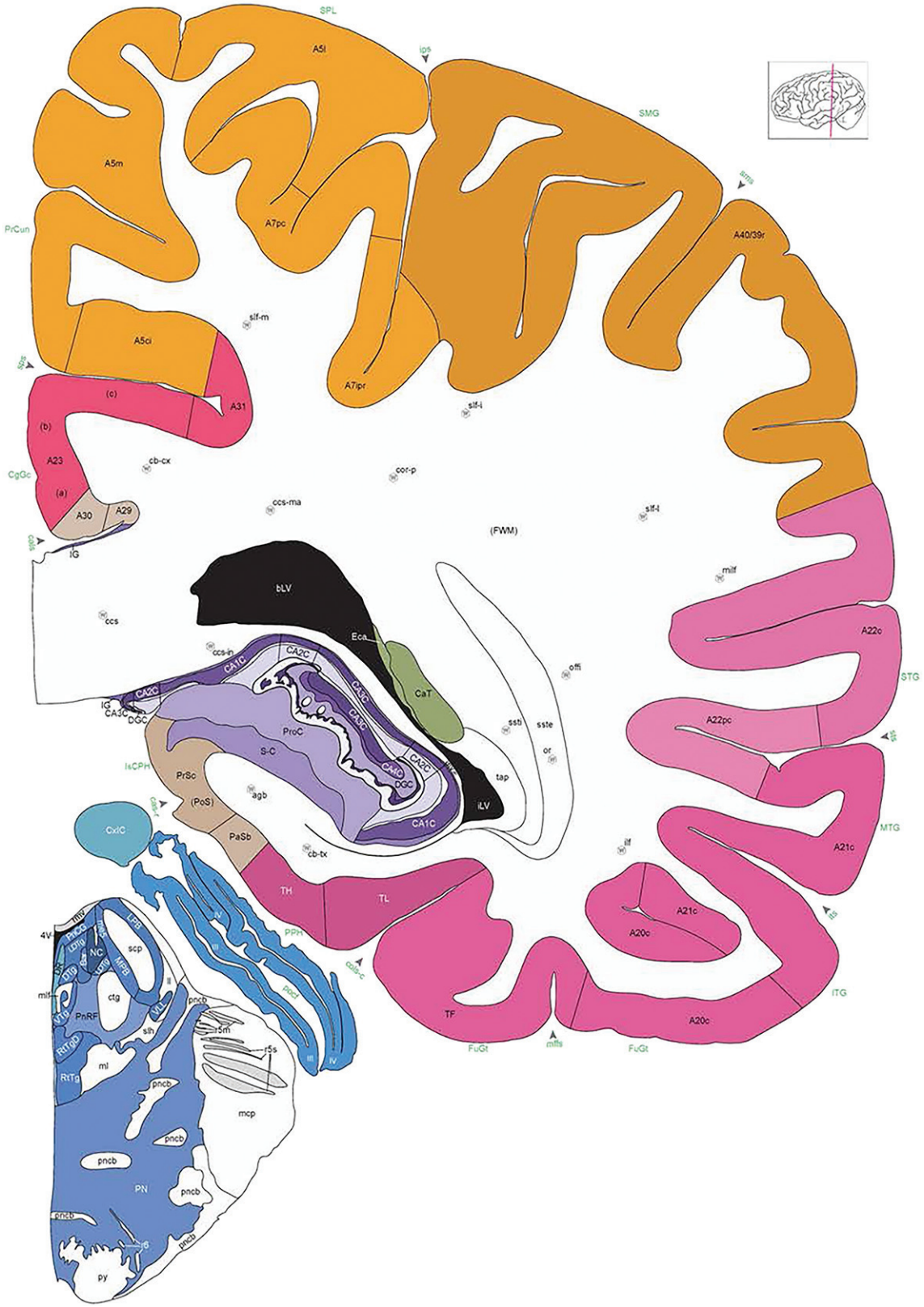

Figure 17. Level 68a (06_095)

Link to online high resolution atlas plate
Link to online high resolution atlas plate (Nissl)

Figure 17. Level 68b (NFP (SMI-32))

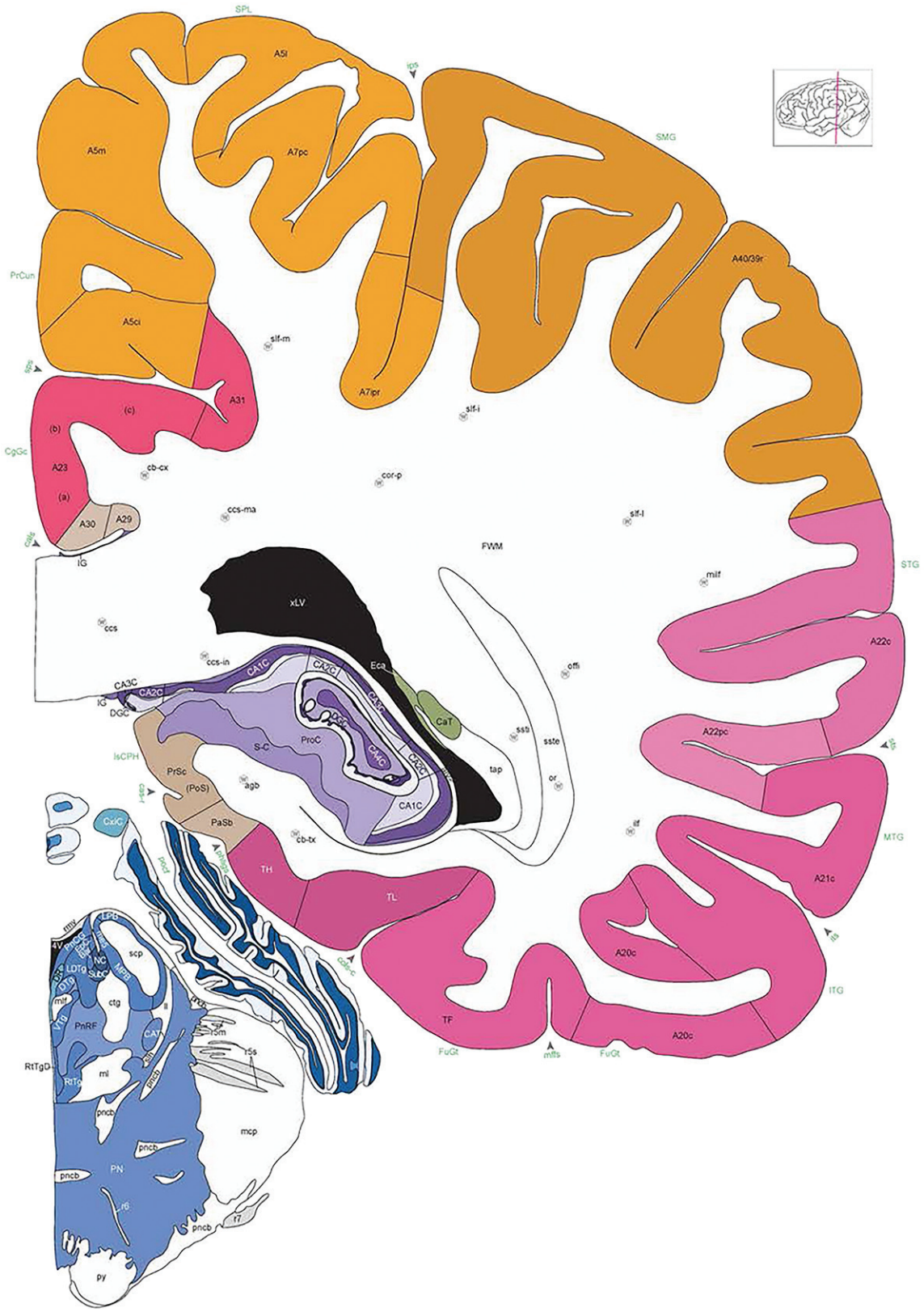

Figure 17. Level 69a (06_107)

Link to online high resolution atlas plate
Link to online high resolution atlas plate (Nissl)

Figure 17. Level 69b (Parvalbumin)

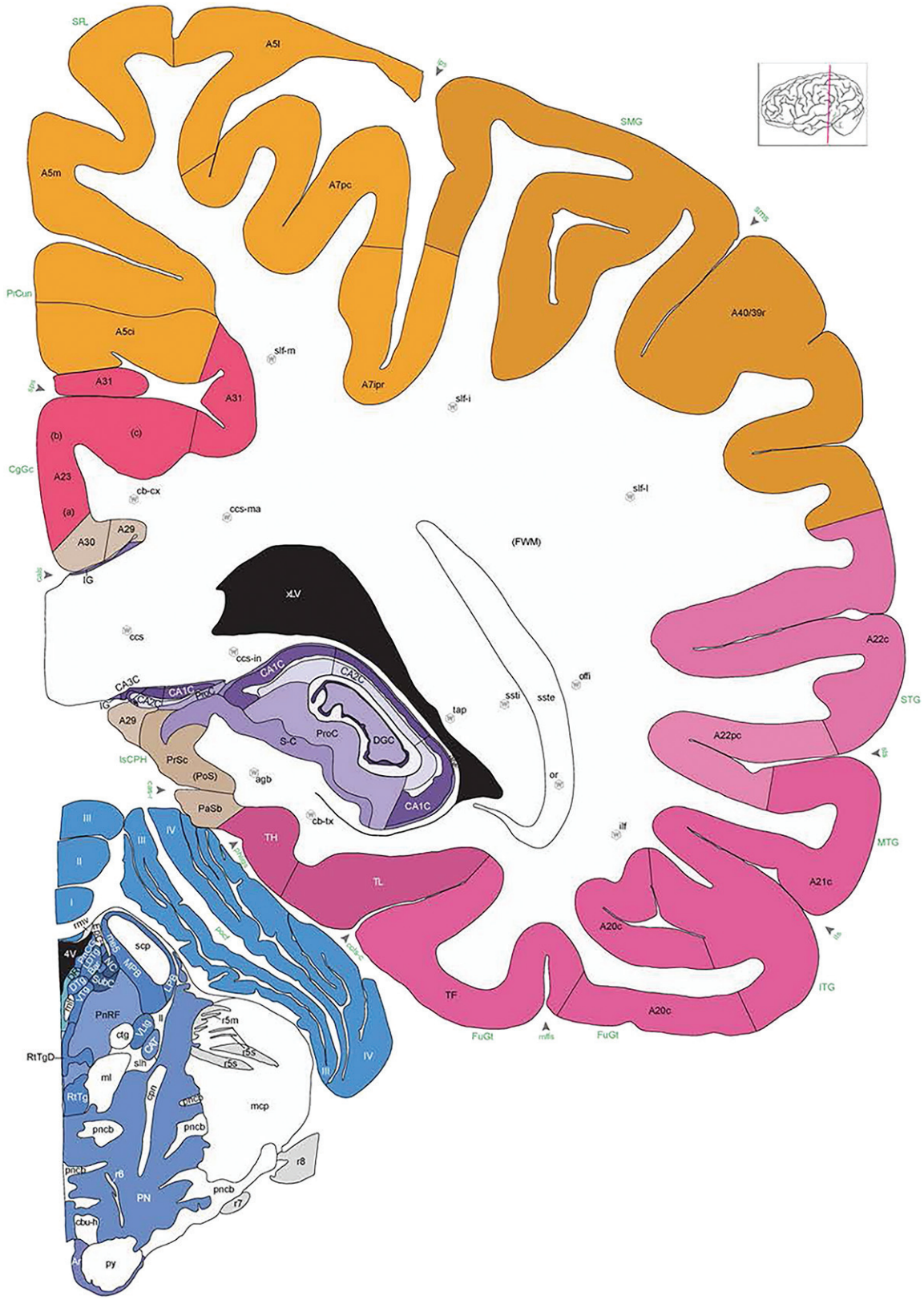

Figure 17. Level 70a (06_119)

Link to online high resolution atlas plate
Link to online high resolution atlas plate (Nissl)

Figure 17. Level 70b (NFP (SMI-32))

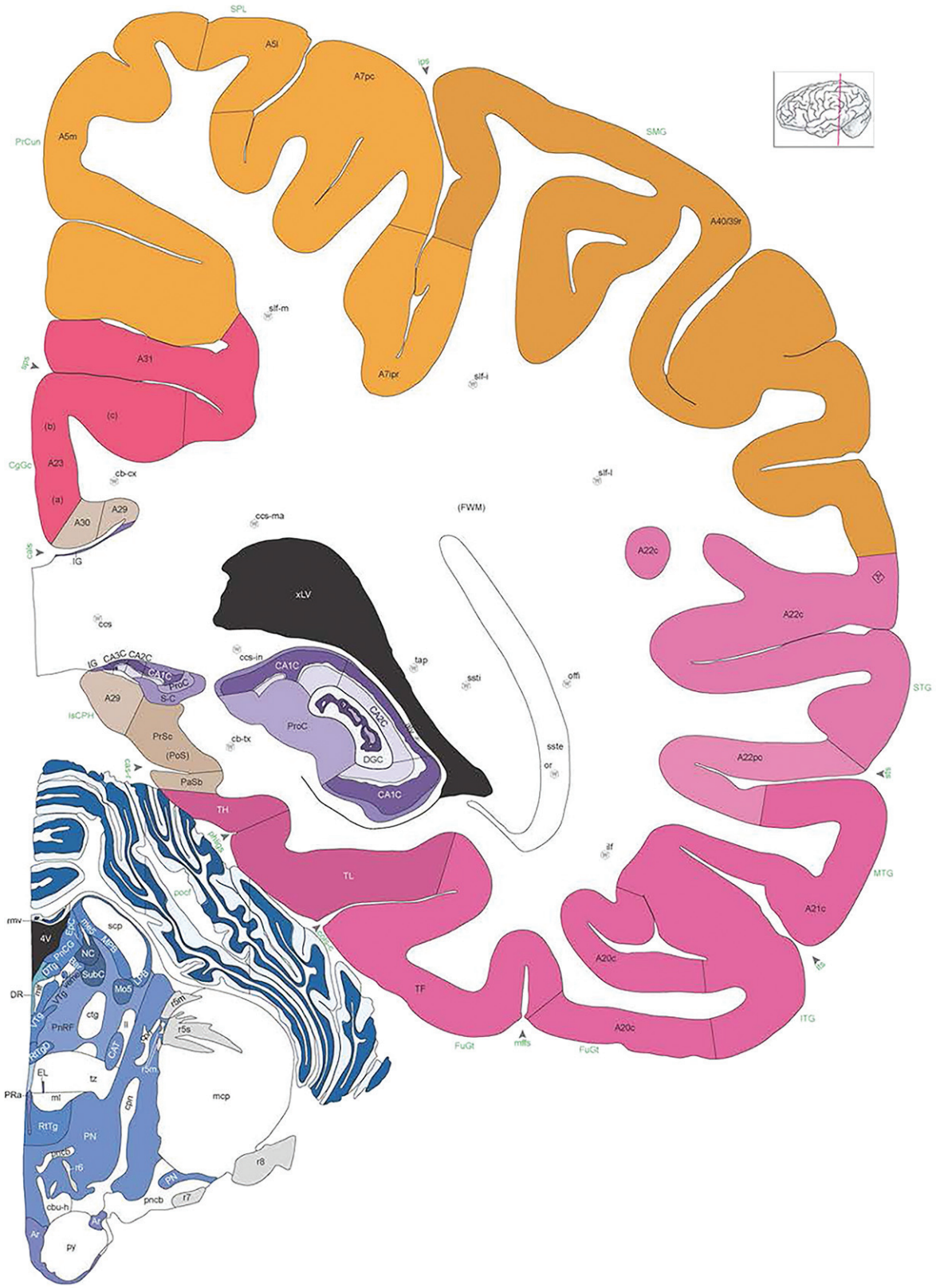

Figure 17. Level 71a (06_131)

Link to online high resolution atlas plate
Link to online high resolution atlas plate (Nissl)

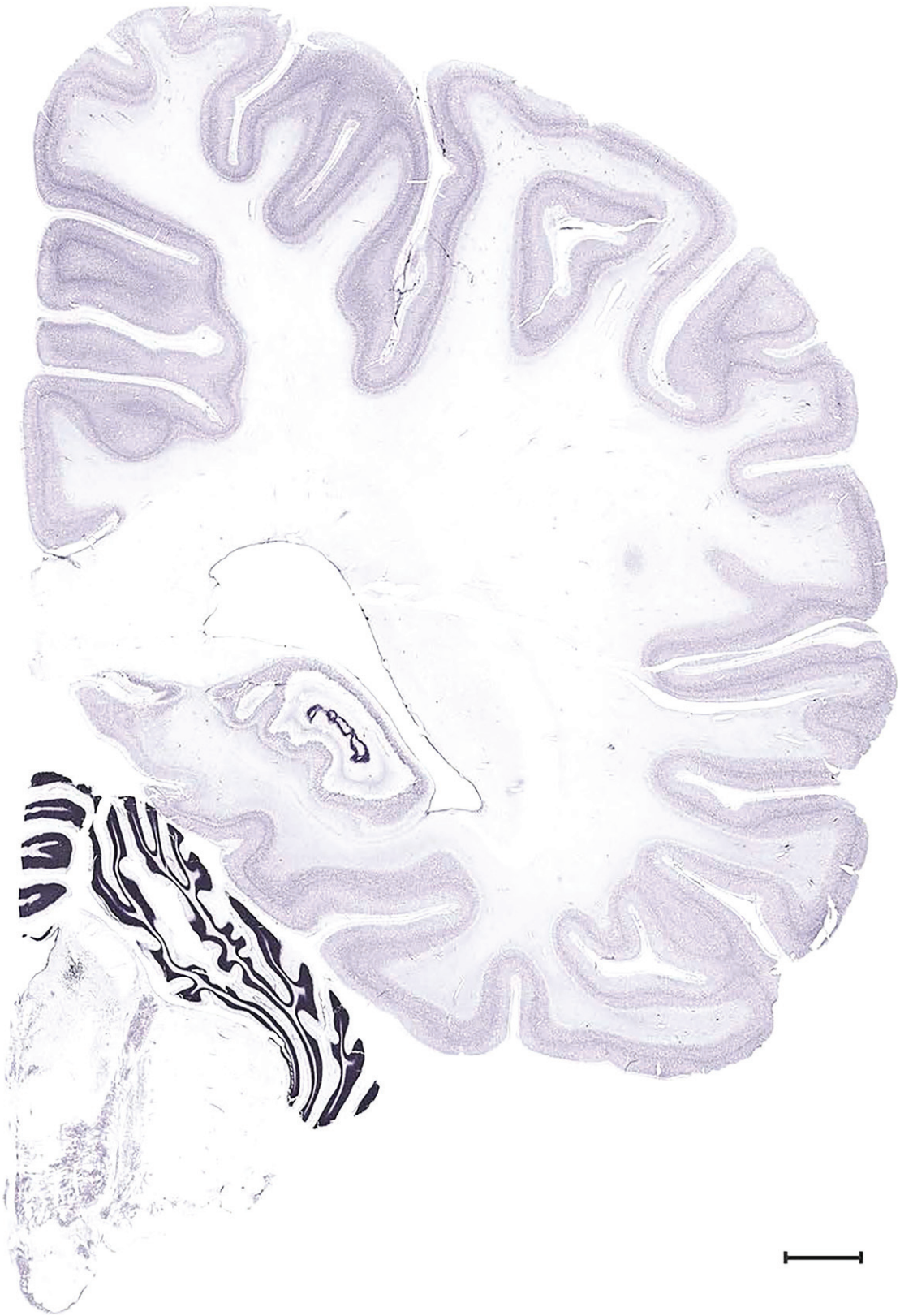

Figure 17. Level 71b (Nissl)

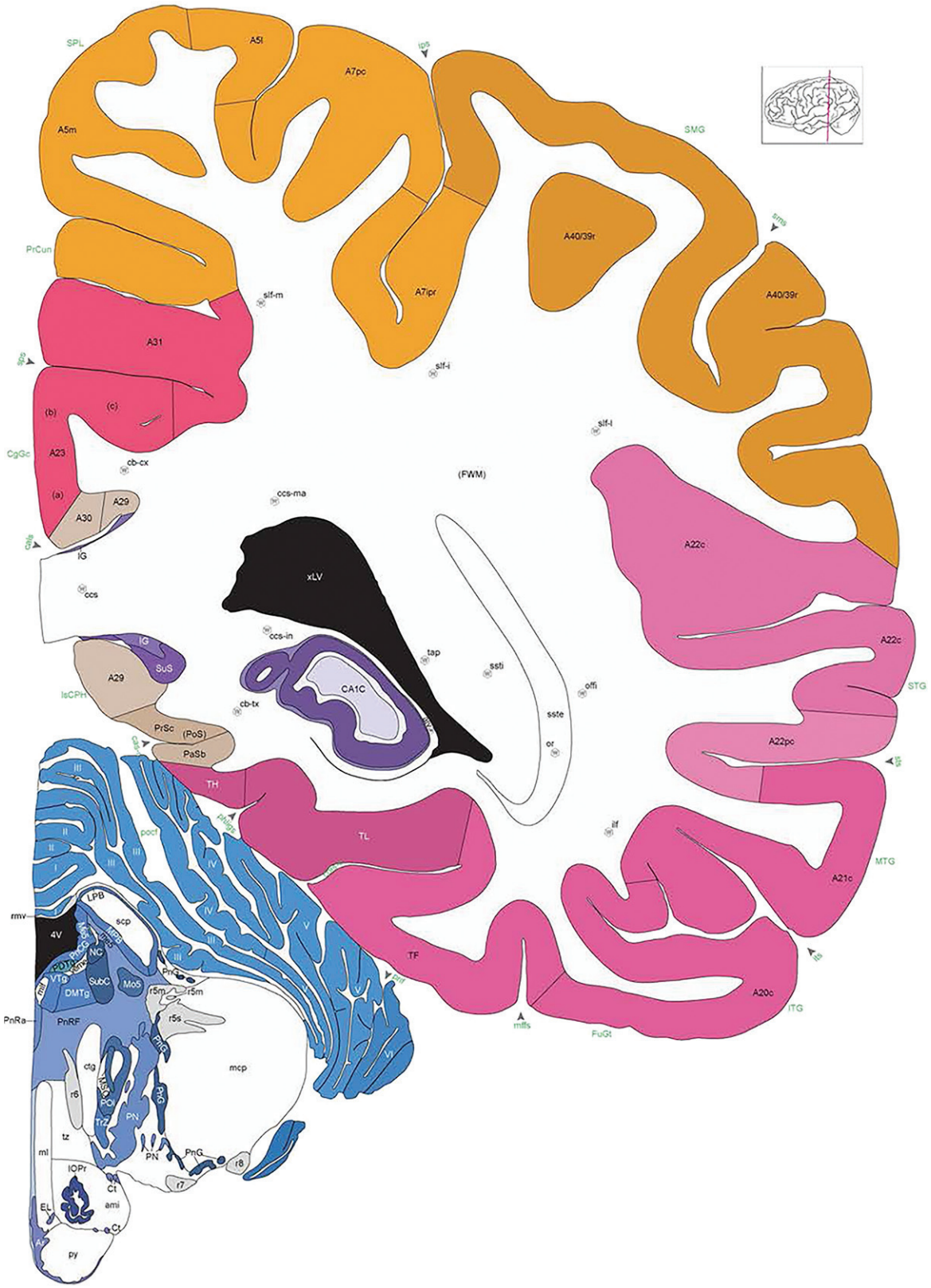

Figure 17. Level 72a (06_147)

Link to online high resolution atlas plate
Link to online high resolution atlas plate (Nissl)

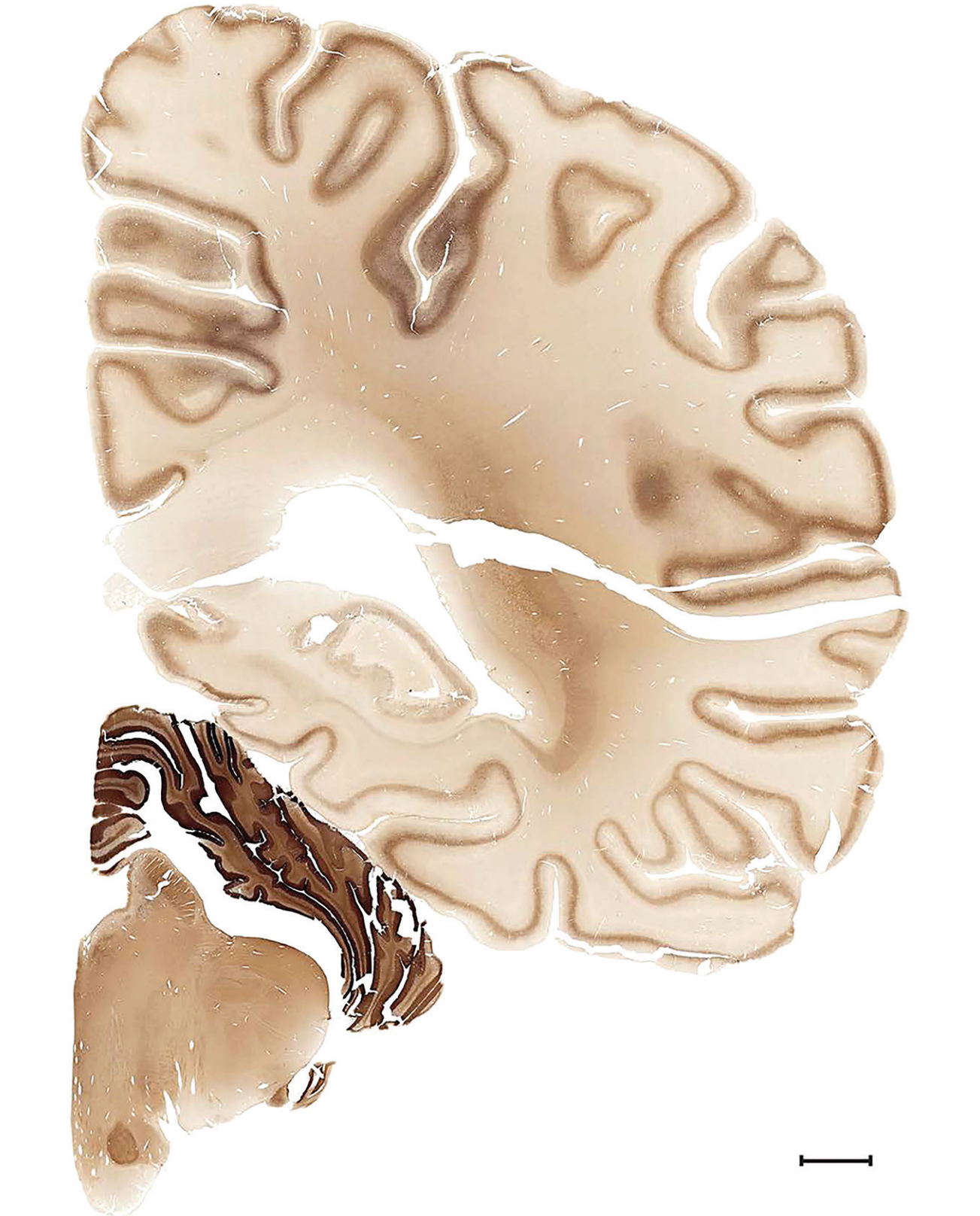

Figure 17. Level 72b (Parvalbumin)

Figure 17. Level 73a (06_159)

Link to online high resolution atlas plate
Link to online high resolution atlas plate (Nissl)

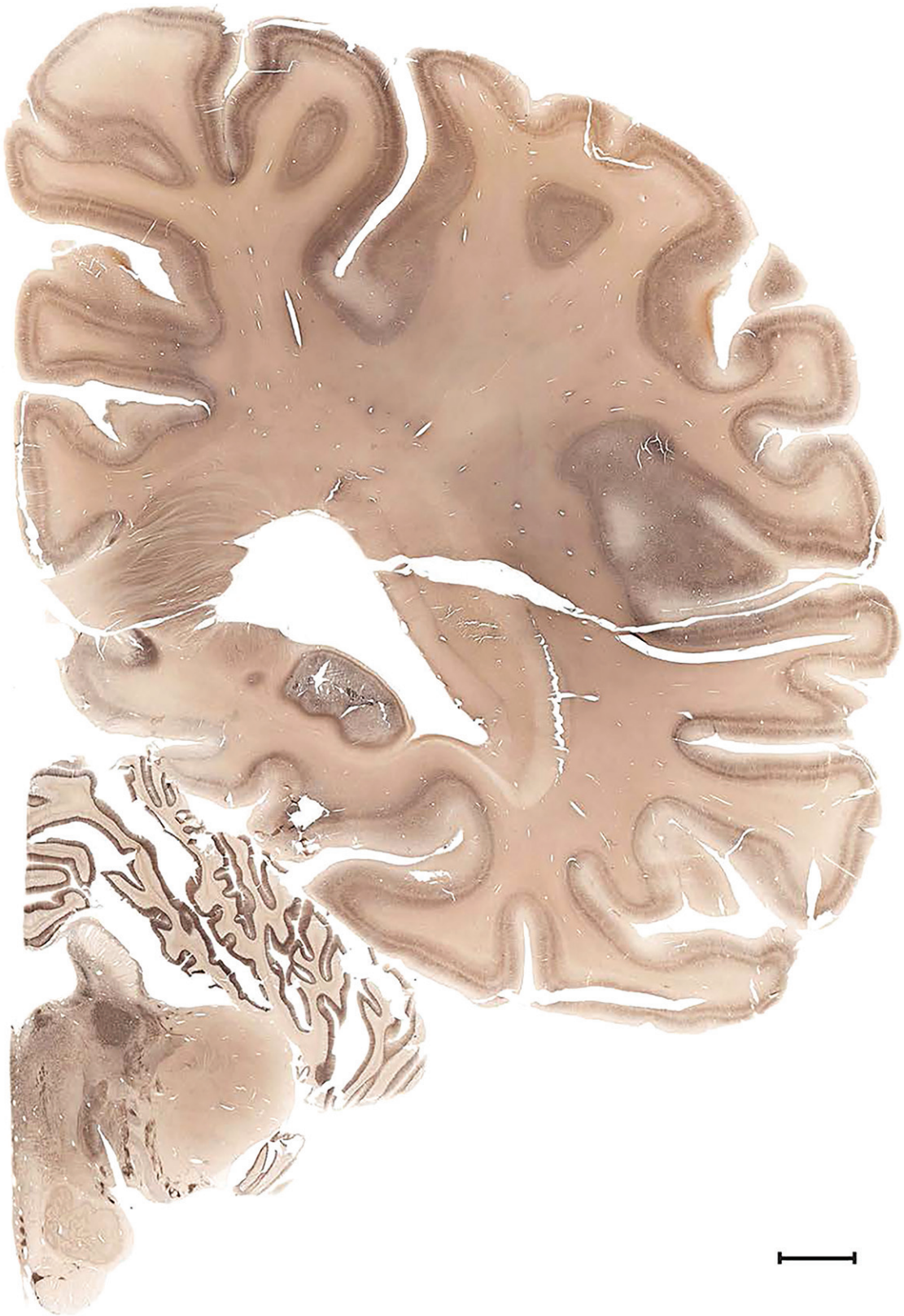

Figure 17. Level 73b (NFP (SMI-32))

Figure 17. Level 74a (06_179)

Link to online high resolution atlas plate
Link to online high resolution atlas plate (Nissl)

Figure 17. Level 74b (NFP (SMI-32))

Figure 17. Level 75a (06_195)

Link to online high resolution atlas plate
Link to online high resolution atlas plate (Nissl)

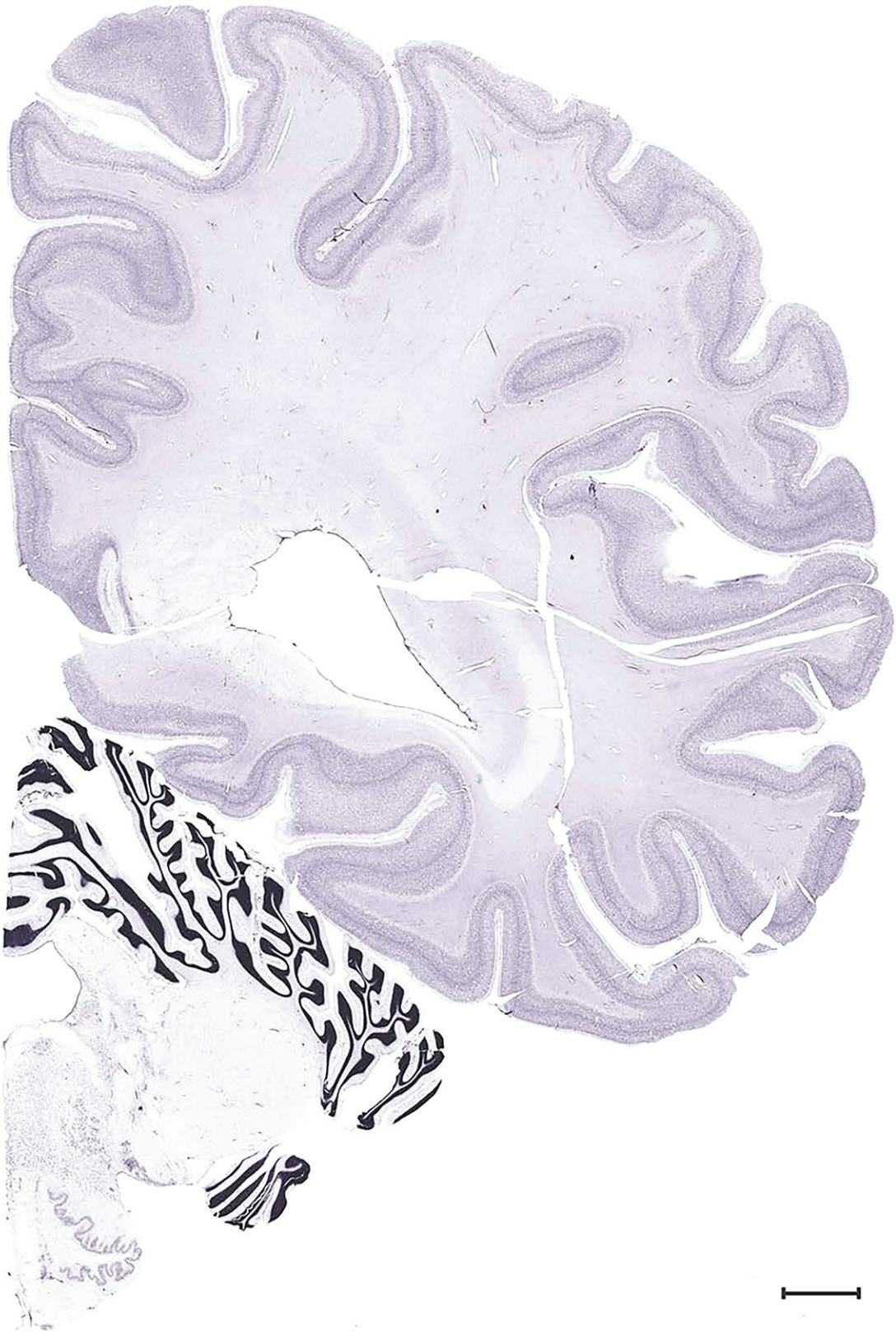

Figure 17. Level 75b (Nissl)

Figure 17. Level 76a (06_207)

Link to online high resolution atlas plate
Link to online high resolution atlas plate (Nissl)

Figure 17. Level 76b (NFP (SMI-32))

Figure 17. Level 77a (06_223)

Link to online high resolution atlas plate
Link to online high resolution atlas plate (Nissl)

Figure 17. Level 77b (Parvalbumin)

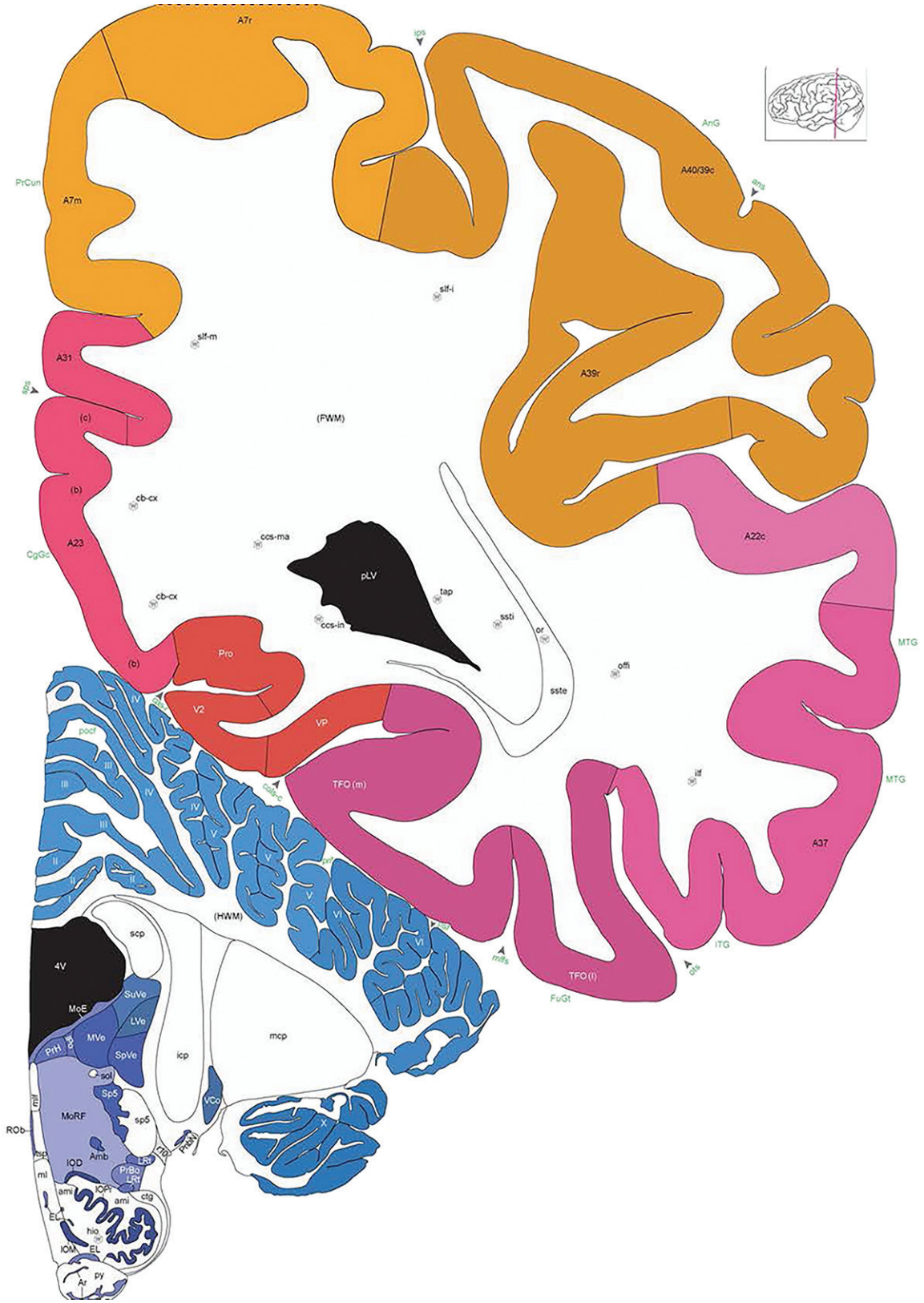

Figure 17. Level 78a (06_239)

Link to online high resolution atlas plate
Link to online high resolution atlas plate (Nissl)

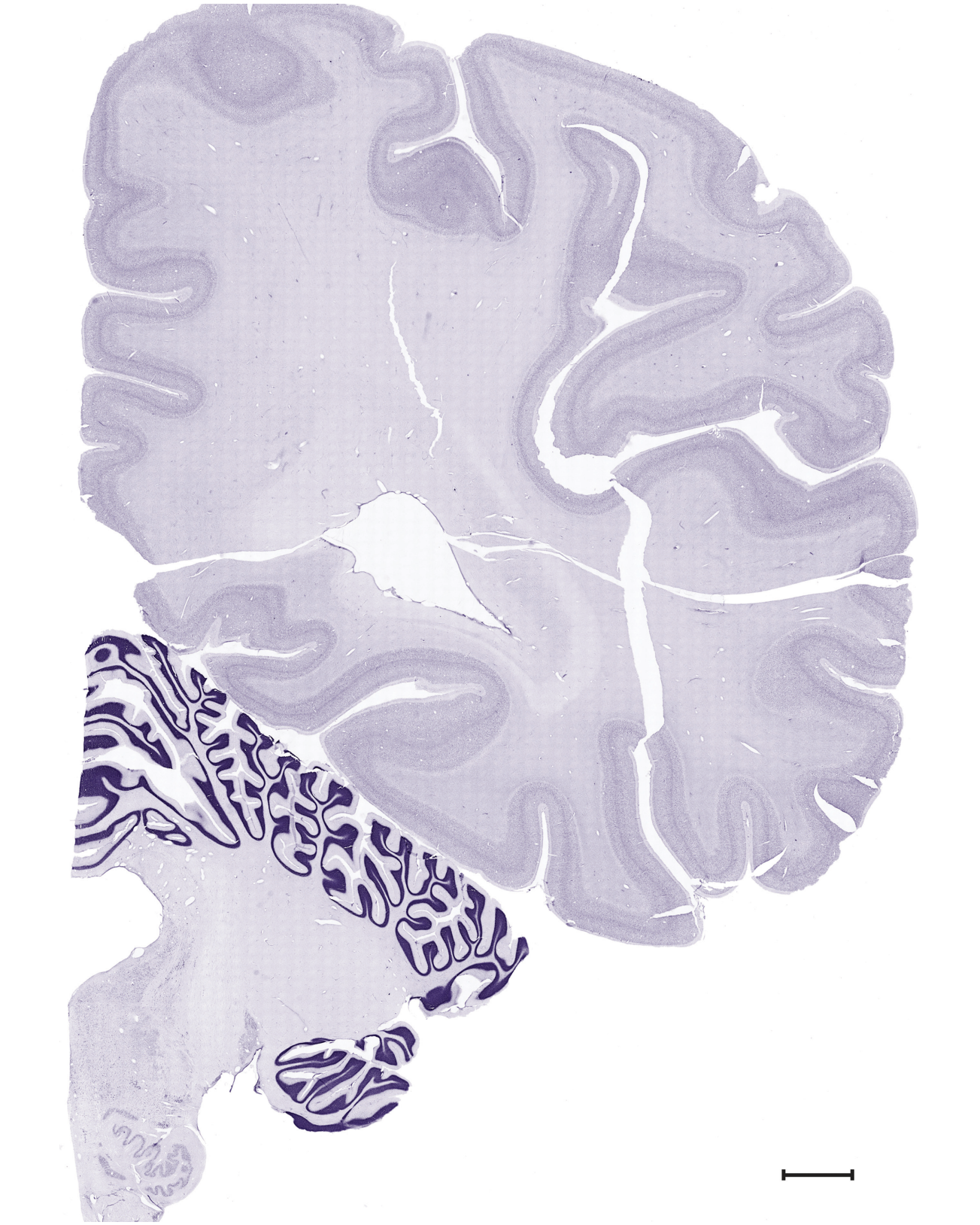

Figure 17. Level 78b (Nissl)

Figure 17. Level 79a (06_255)

Link to online high resolution atlas plate
Link to online high resolution atlas plate (Nissl)

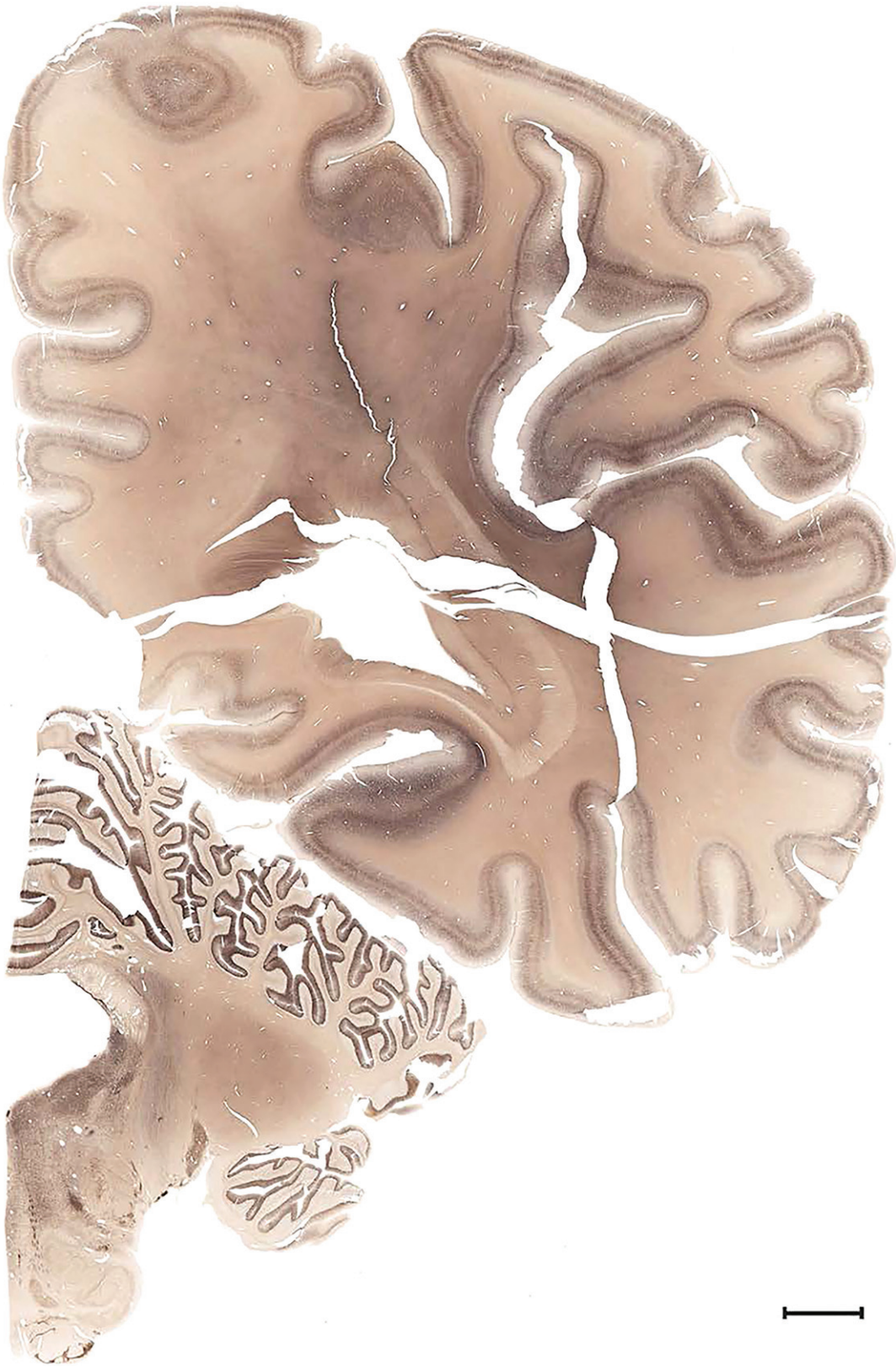

Figure 17. Level 79b (NFP (SMI-32))

Figure 17. Level 80a (06_271)

Link to online high resolution atlas plate
Link to online high resolution atlas plate (Nissl)

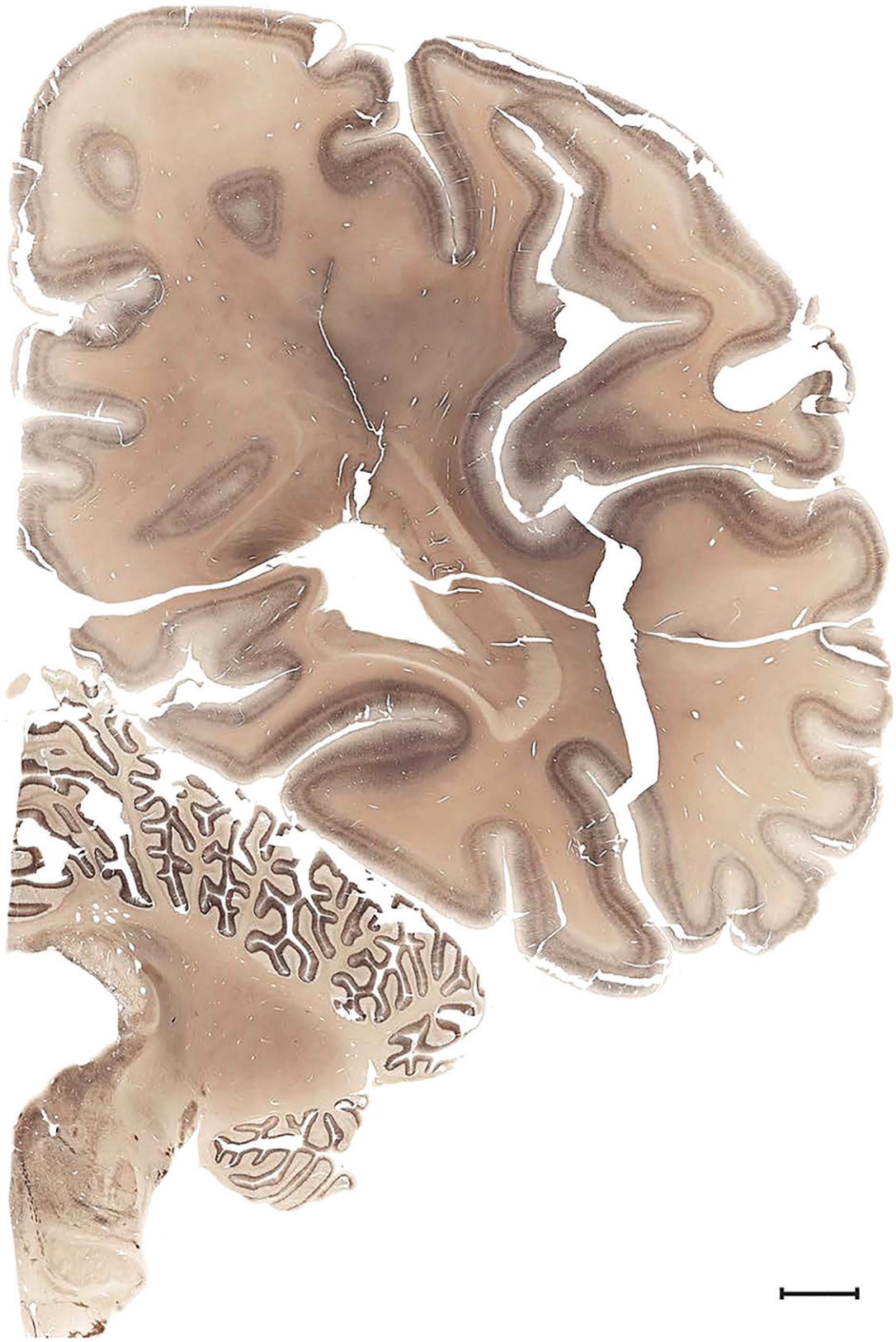

Figure 17. Level 80b (NFP (SMI-32))

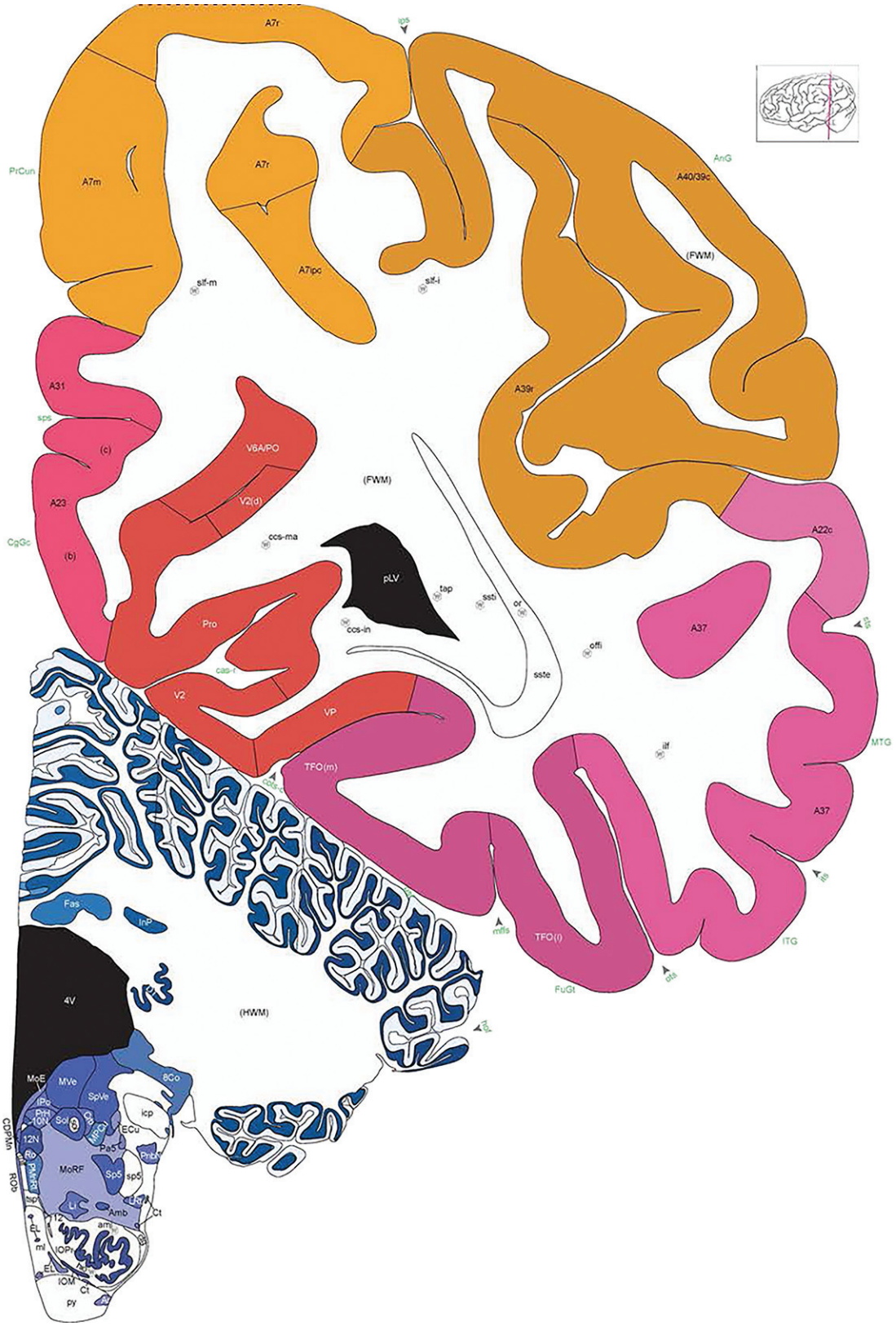

Figure 17. Level 81a (06_291)

Link to online high resolution atlas plate
Link to online high resolution atlas plate (Nissl)

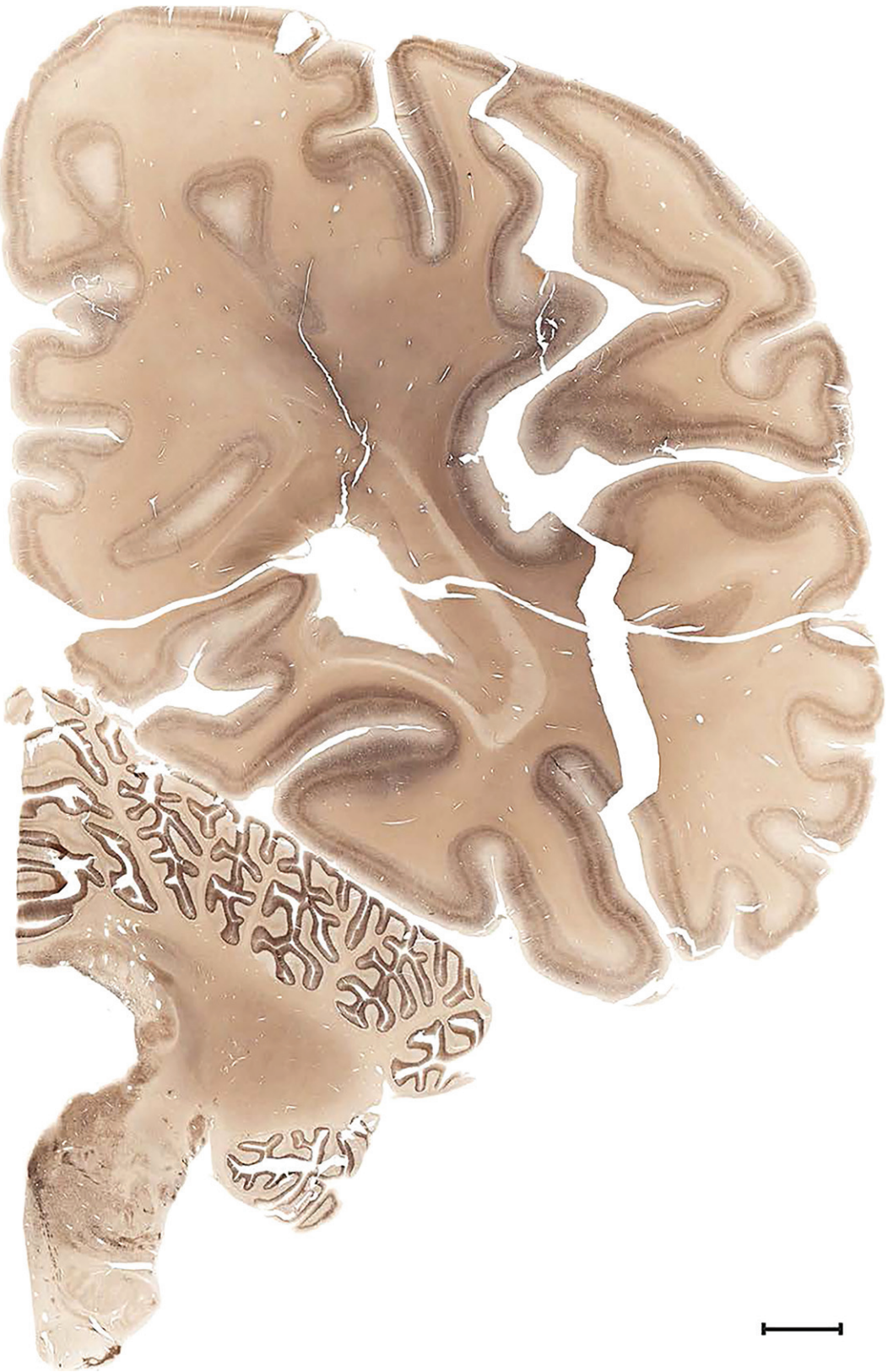

Figure 17. Level 81b (NFP (SMI-32))

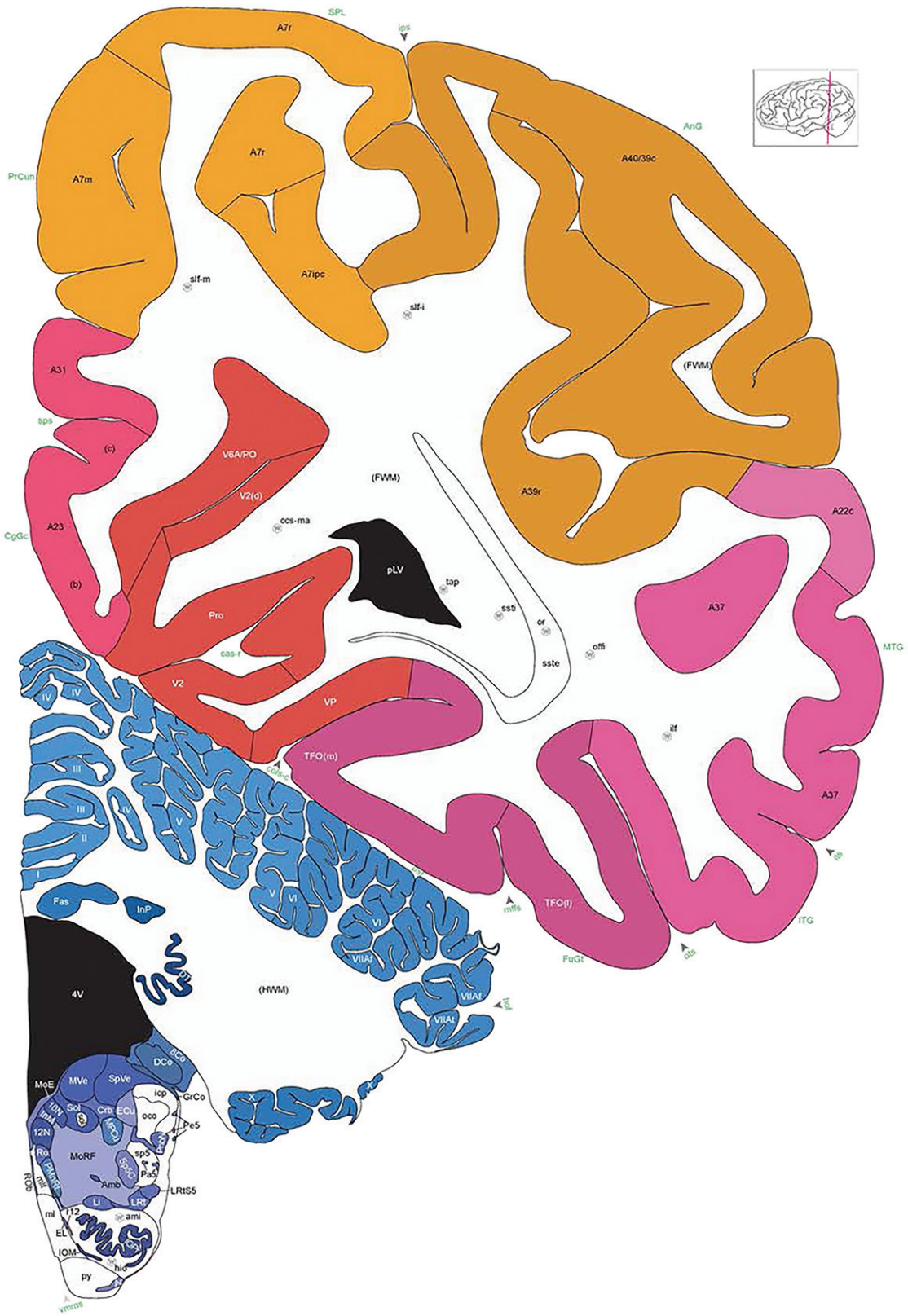

Figure 17. Level 82a (06_299)

Link to online high resolution atlas plate
Link to online high resolution atlas plate (Nissl)

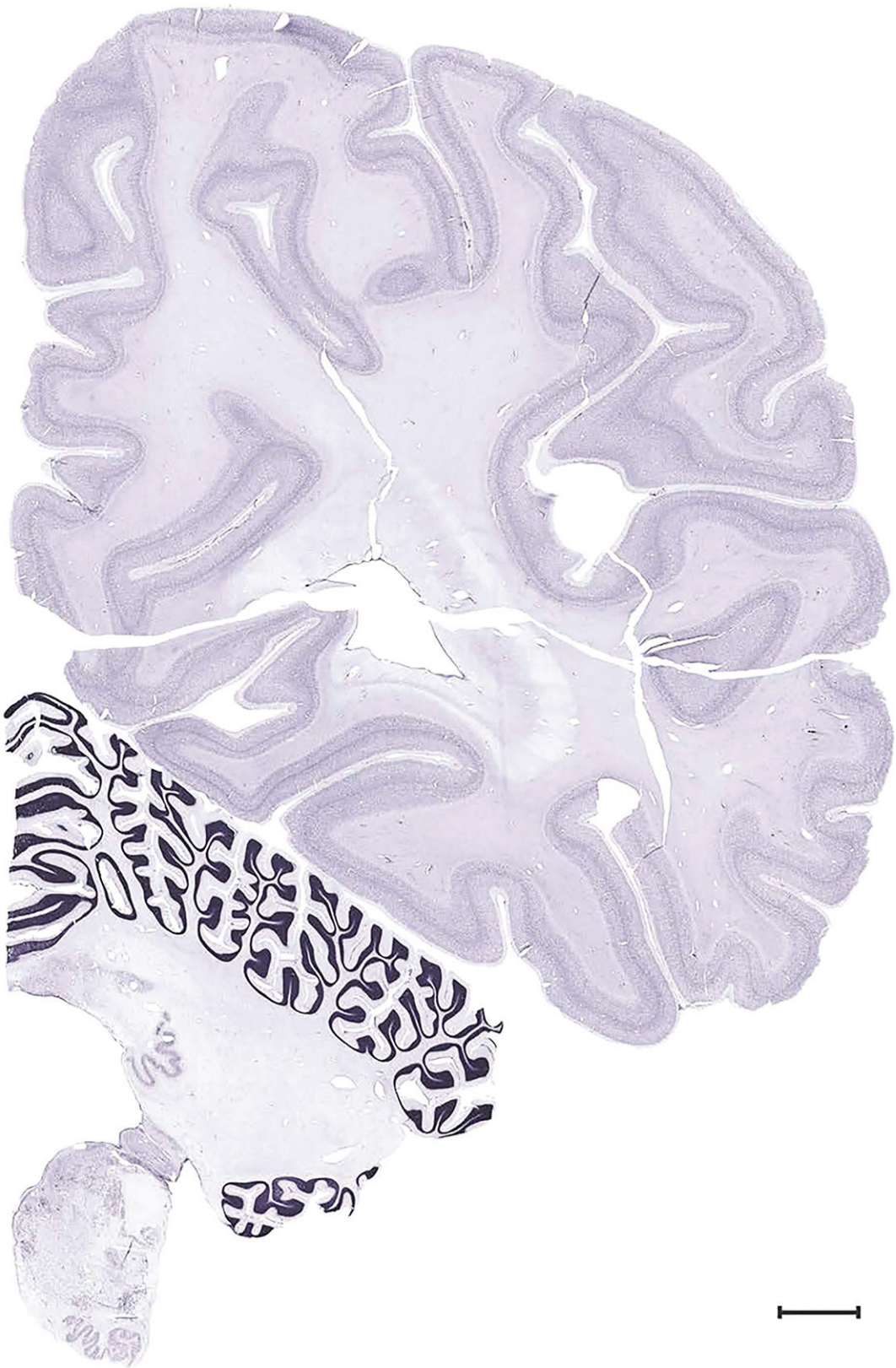

Figure 17. Level 82b (Nissl)

Figure 17. Level 83a (07_027)

Link to online high resolution atlas plate
Link to online high resolution atlas plate (Nissl)

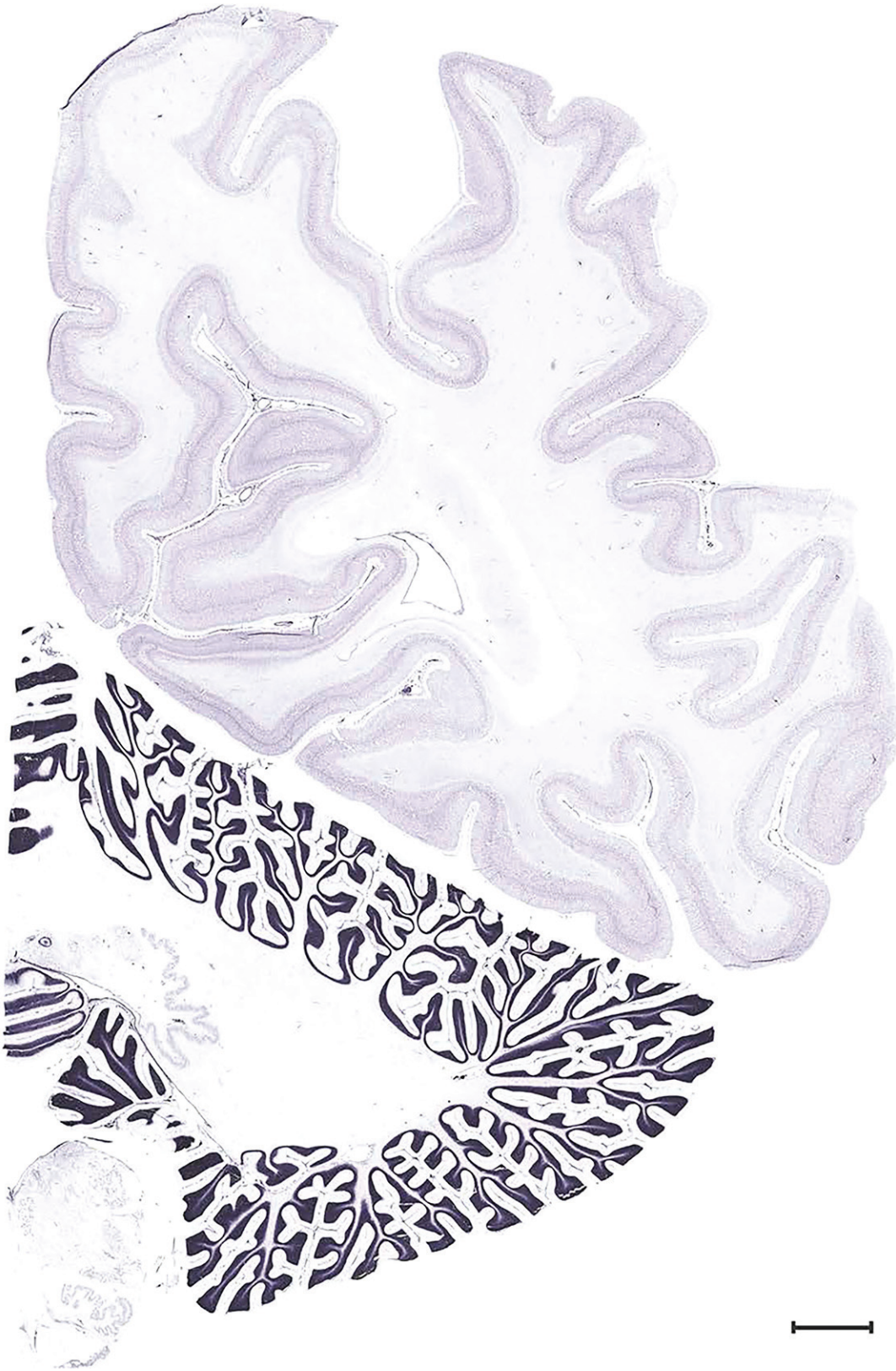

Figure 17. Level 83b (Nissl)

Figure 17. Level 84a (07_043)

Link to online high resolution atlas plate
Link to online high resolution atlas plate (Nissl)

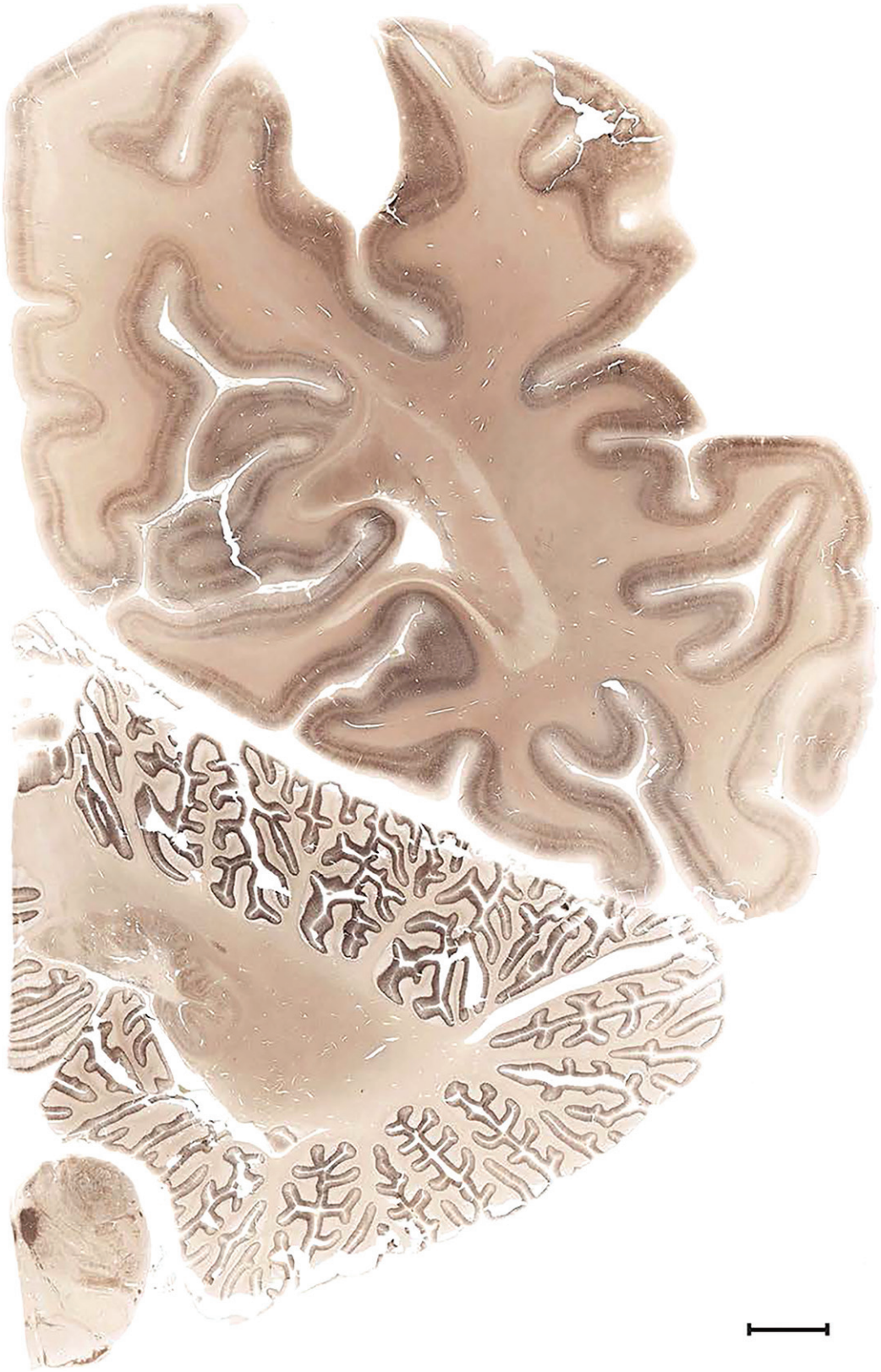

Figure 17. Level 84b (NFP (SMI-32))

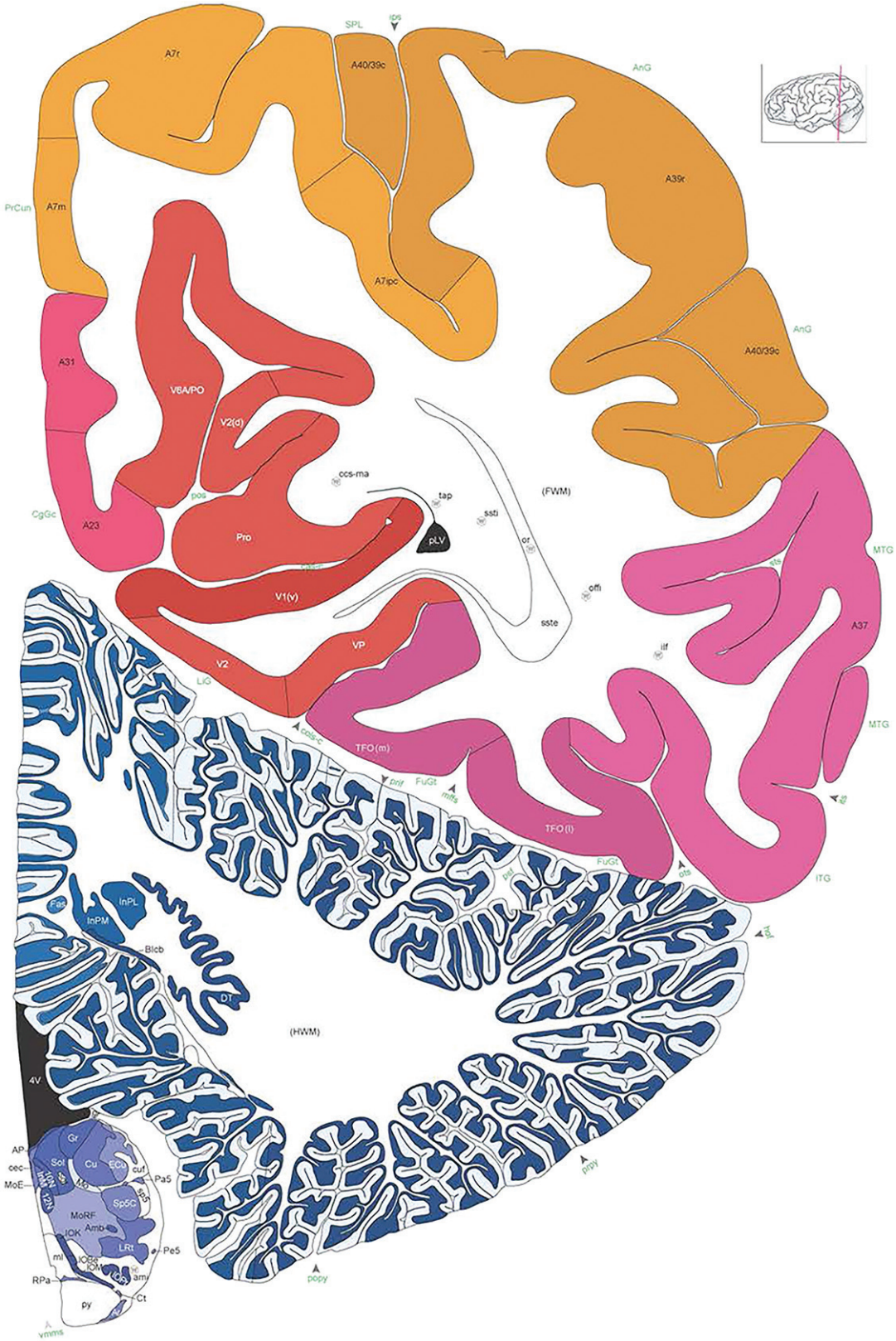

Figure 17. Level 85a (07_059)

Link to online high resolution atlas plate
Link to online high resolution atlas plate (Nissl)

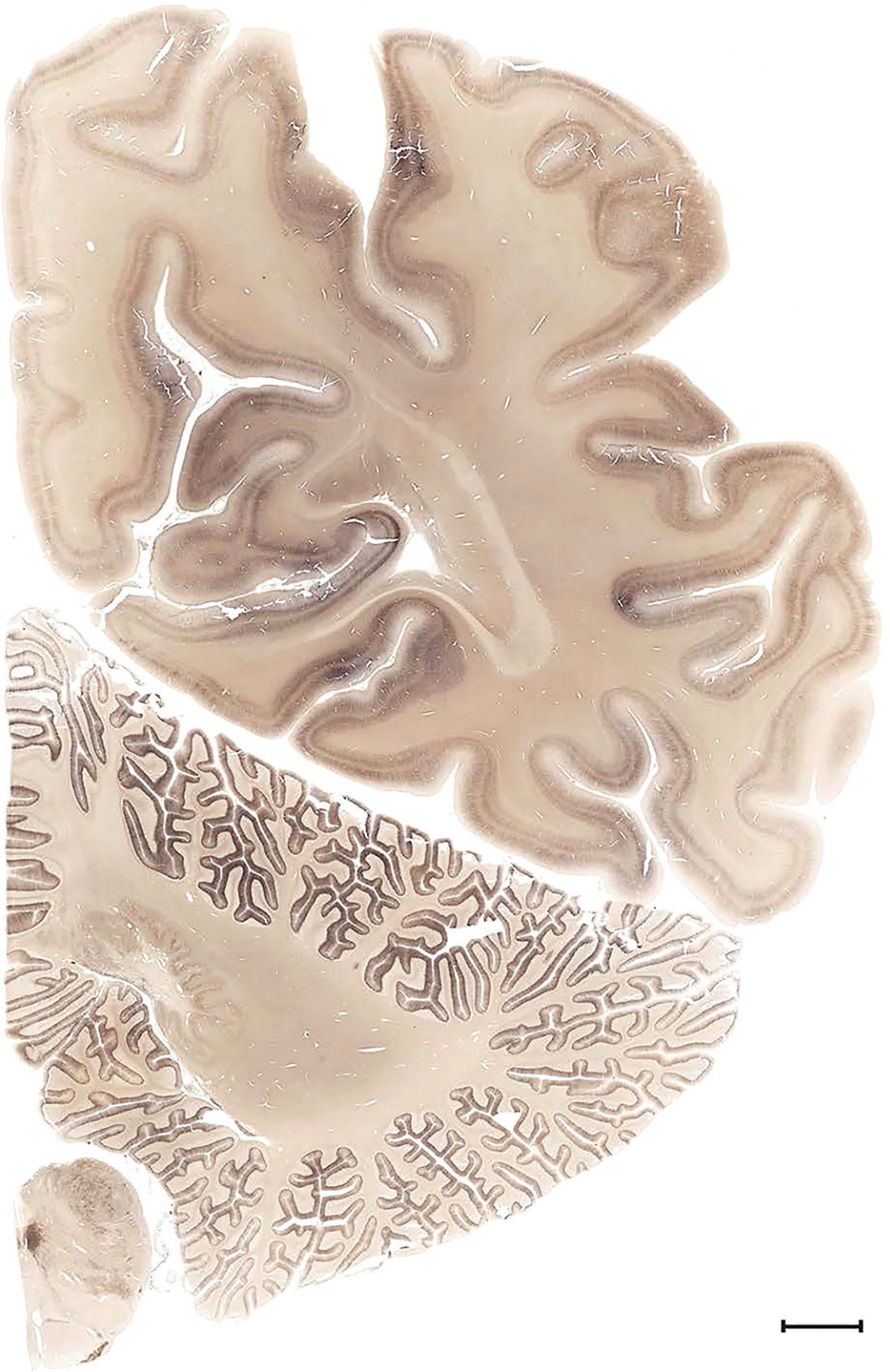

Figure 17. Level 85b (NFP (SMI-32))

Figure 17. Level 86a (07_075)

Link to online high resolution atlas plate
Link to online high resolution atlas plate (Nissl)

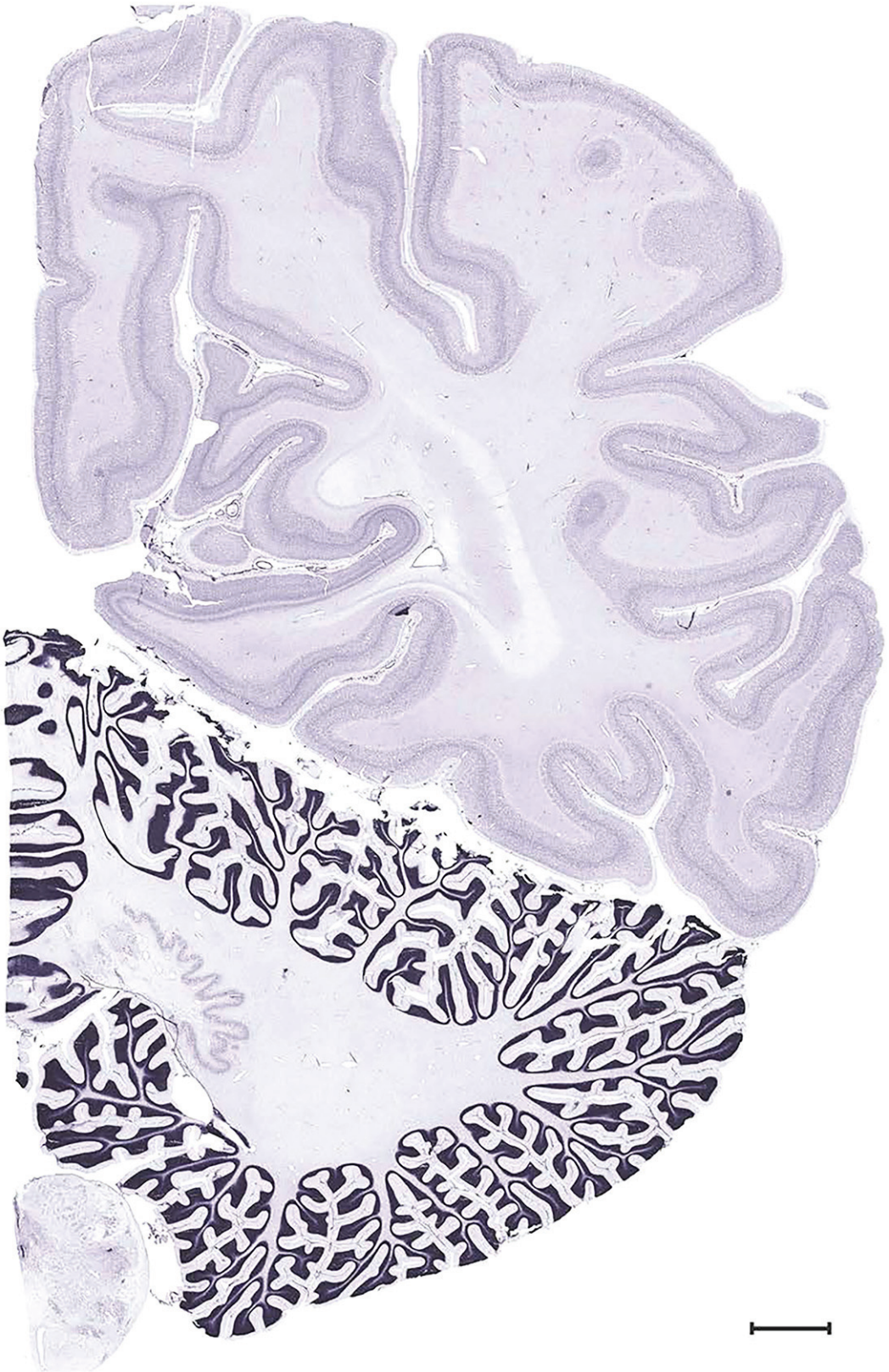

Figure 17. Level 86b (Nissl)

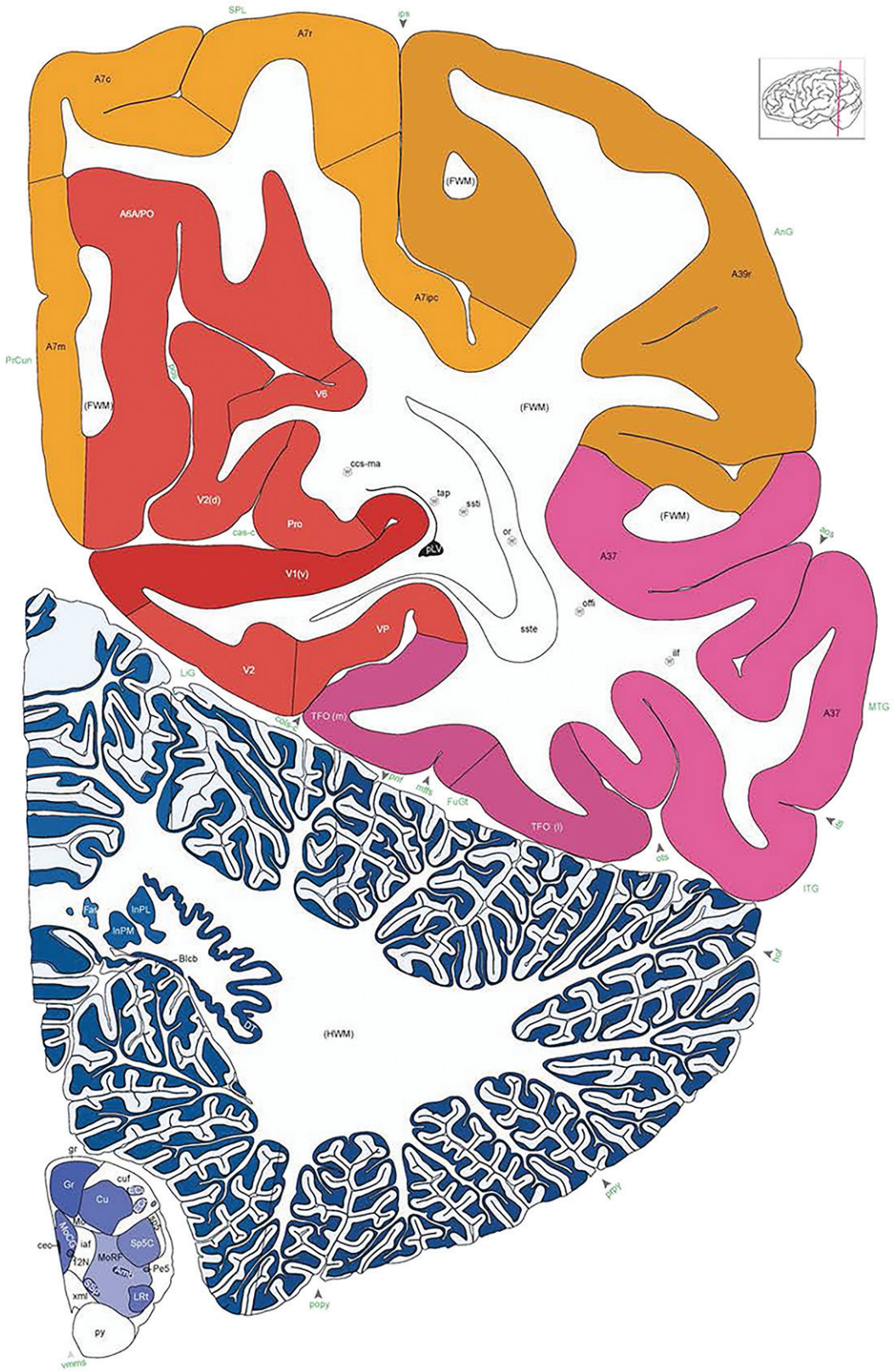

Figure 17. Level 87a (07_091)

Link to online high resolution atlas plate
Link to online high resolution atlas plate (Nissl)

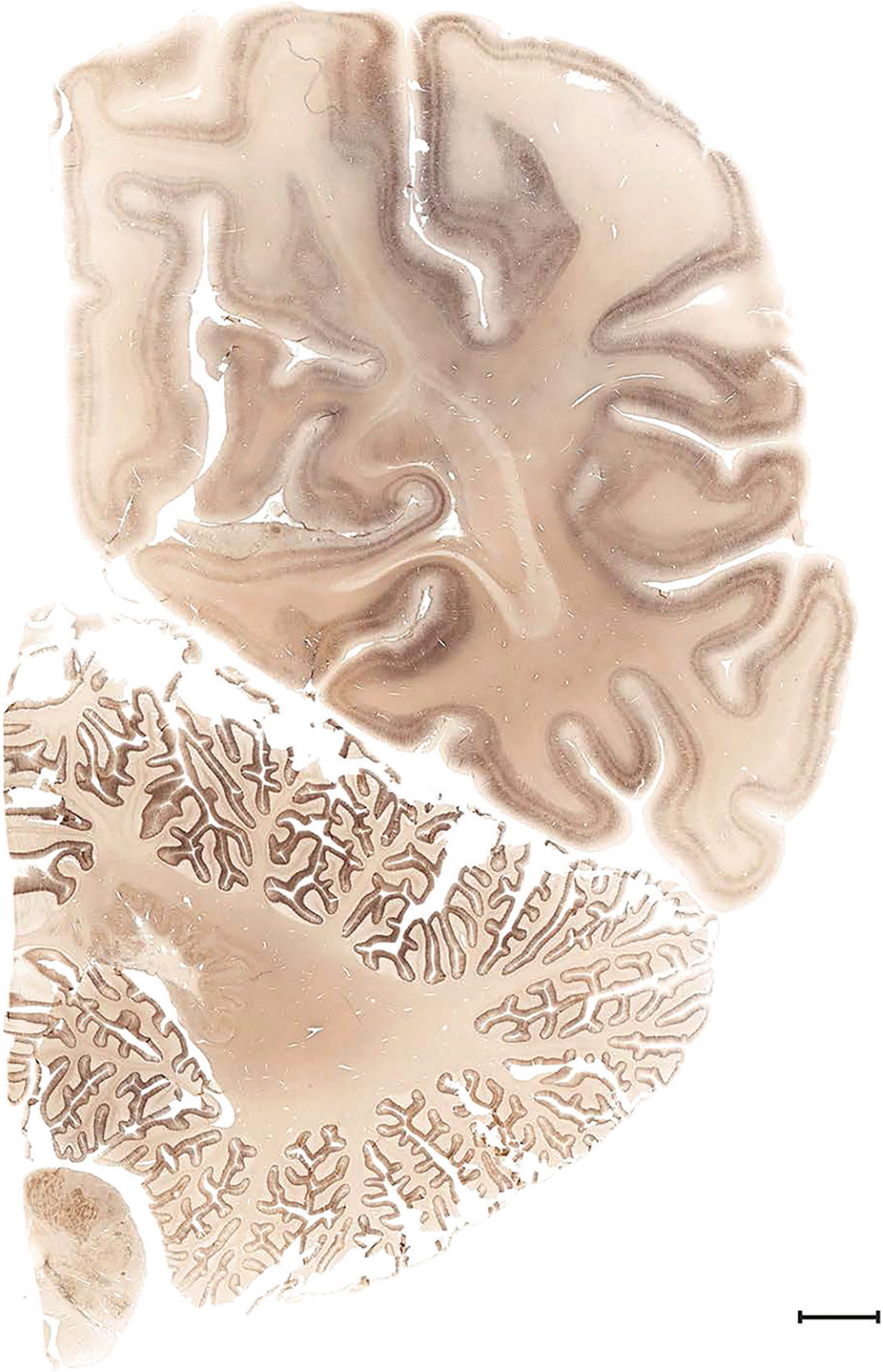

Figure 17. Level 87b (NFP (SMI-32))

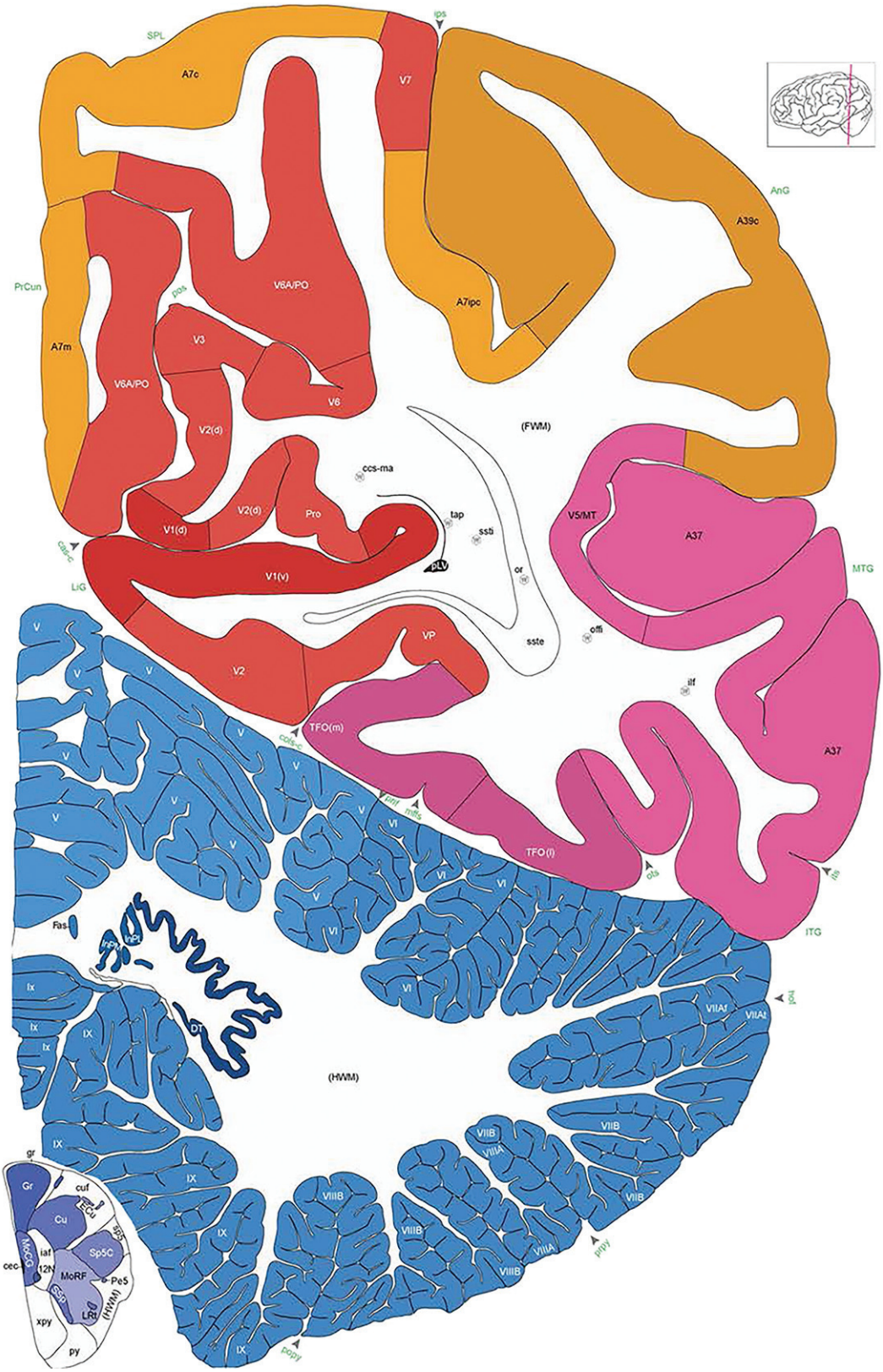

Figure 17. Level 88a (07_111)

Link to online high resolution atlas plate
Link to online high resolution atlas plate (Nissl)

Figure 17. Level 88b (NFP (SMI-32))

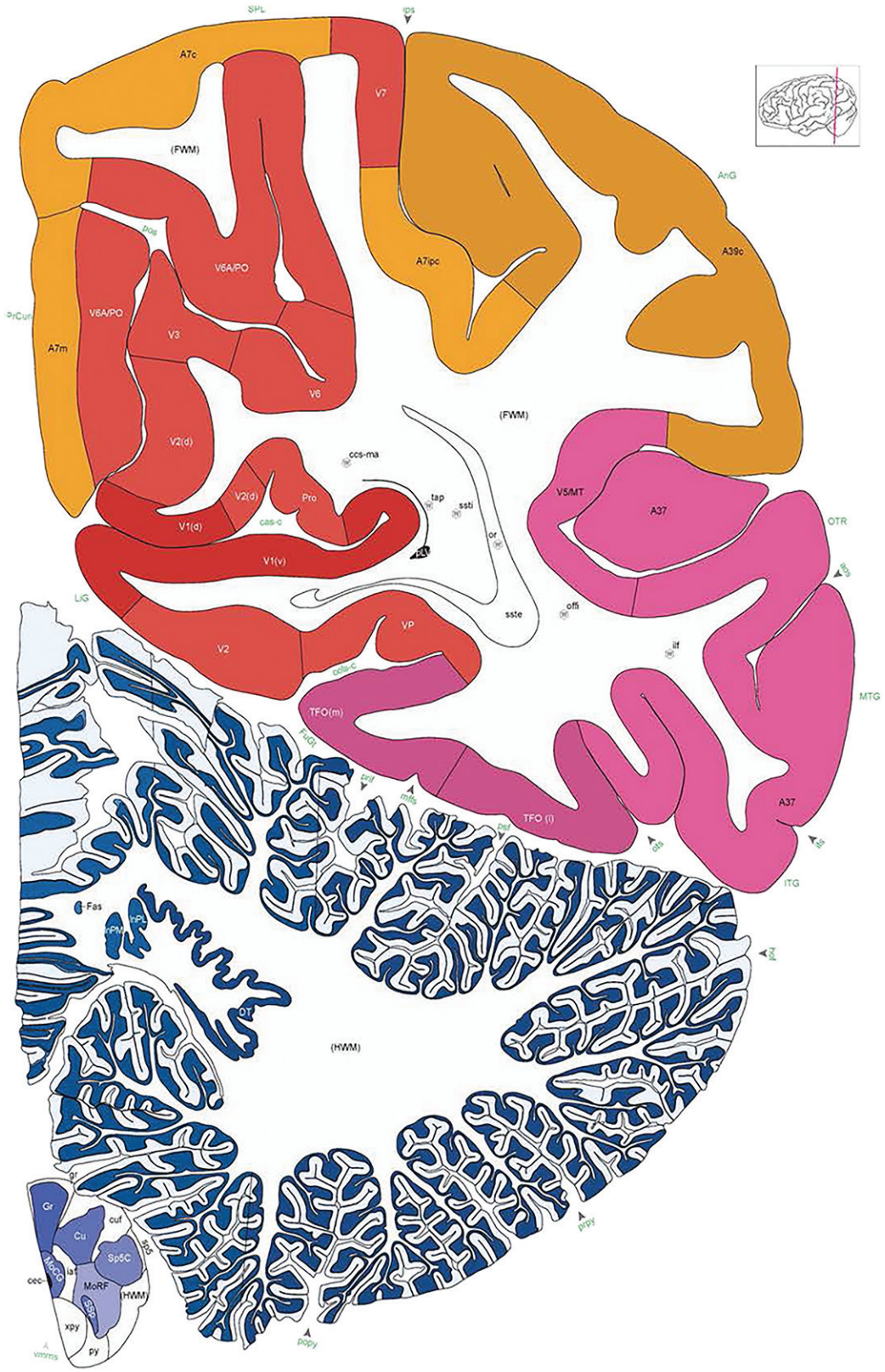

Figure 17. Level 89a (07_123)

Link to online high resolution atlas plate
Link to online high resolution atlas plate (Nissl)

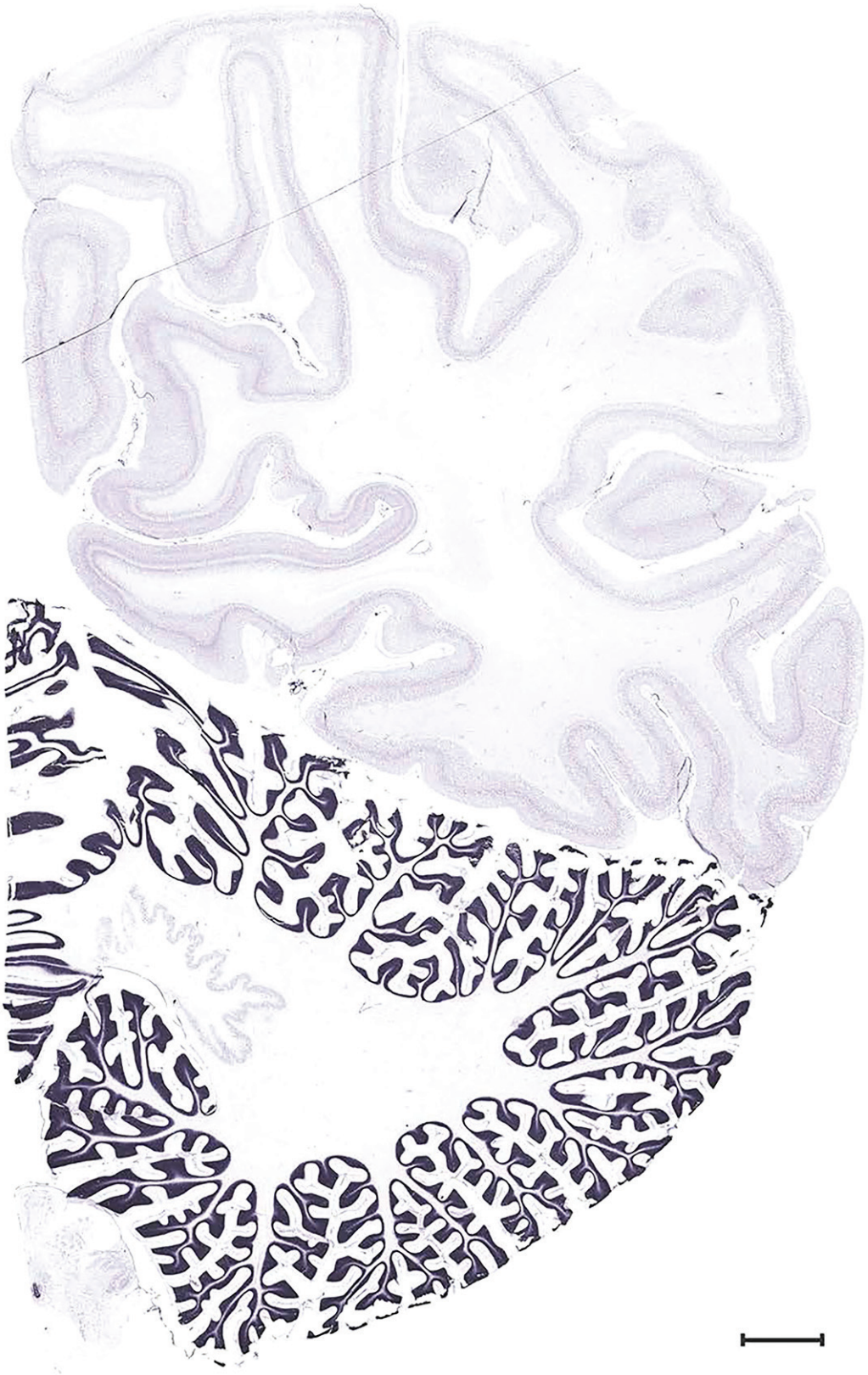

Figure 17. Level 89b (Nissl)

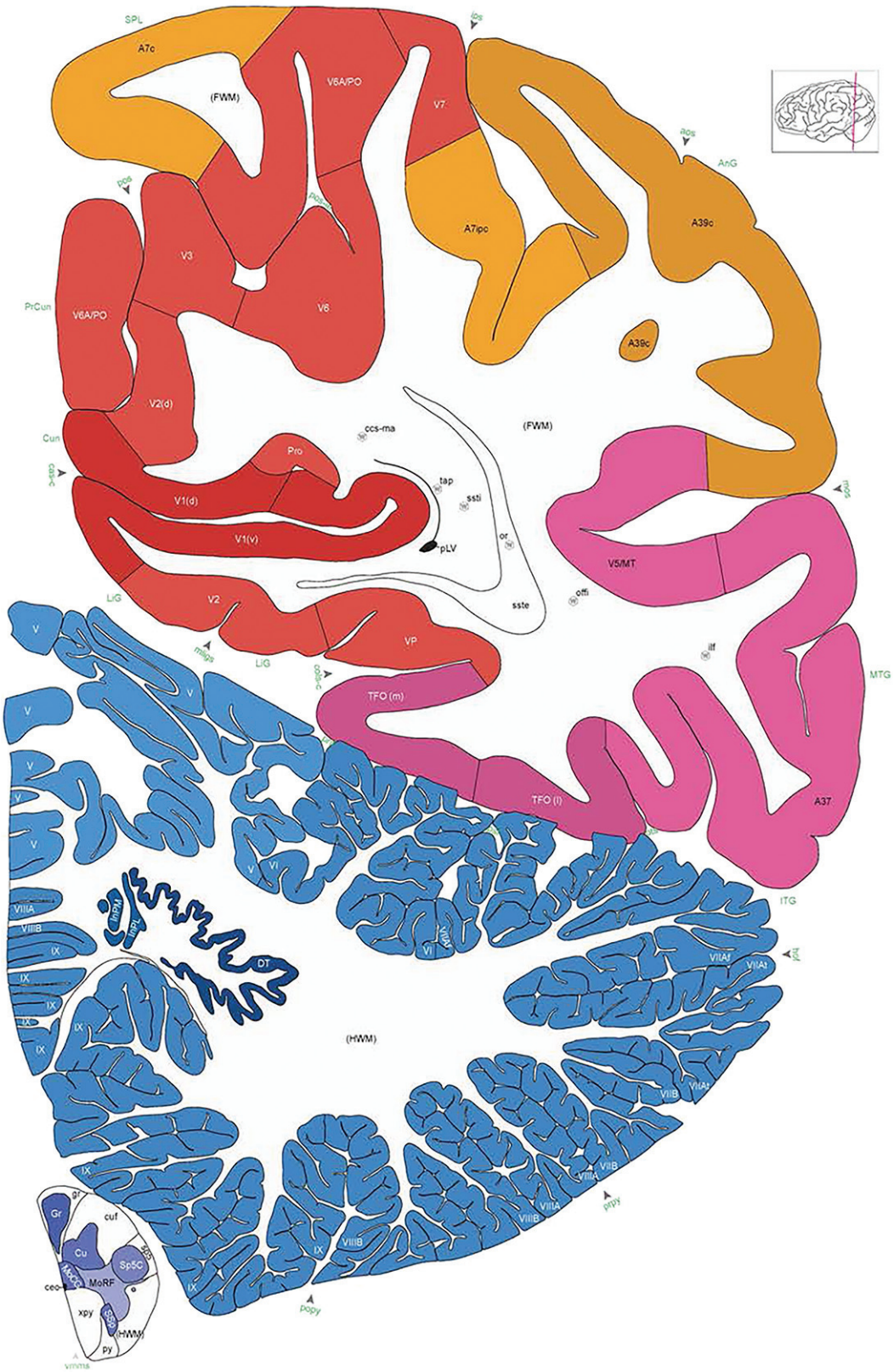

Figure 17. Level 90a (07_147)

Link to online high resolution atlas plate
Link to online high resolution atlas plate (Nissl)

Figure 17. Level 90b (NFP (SMI-32))

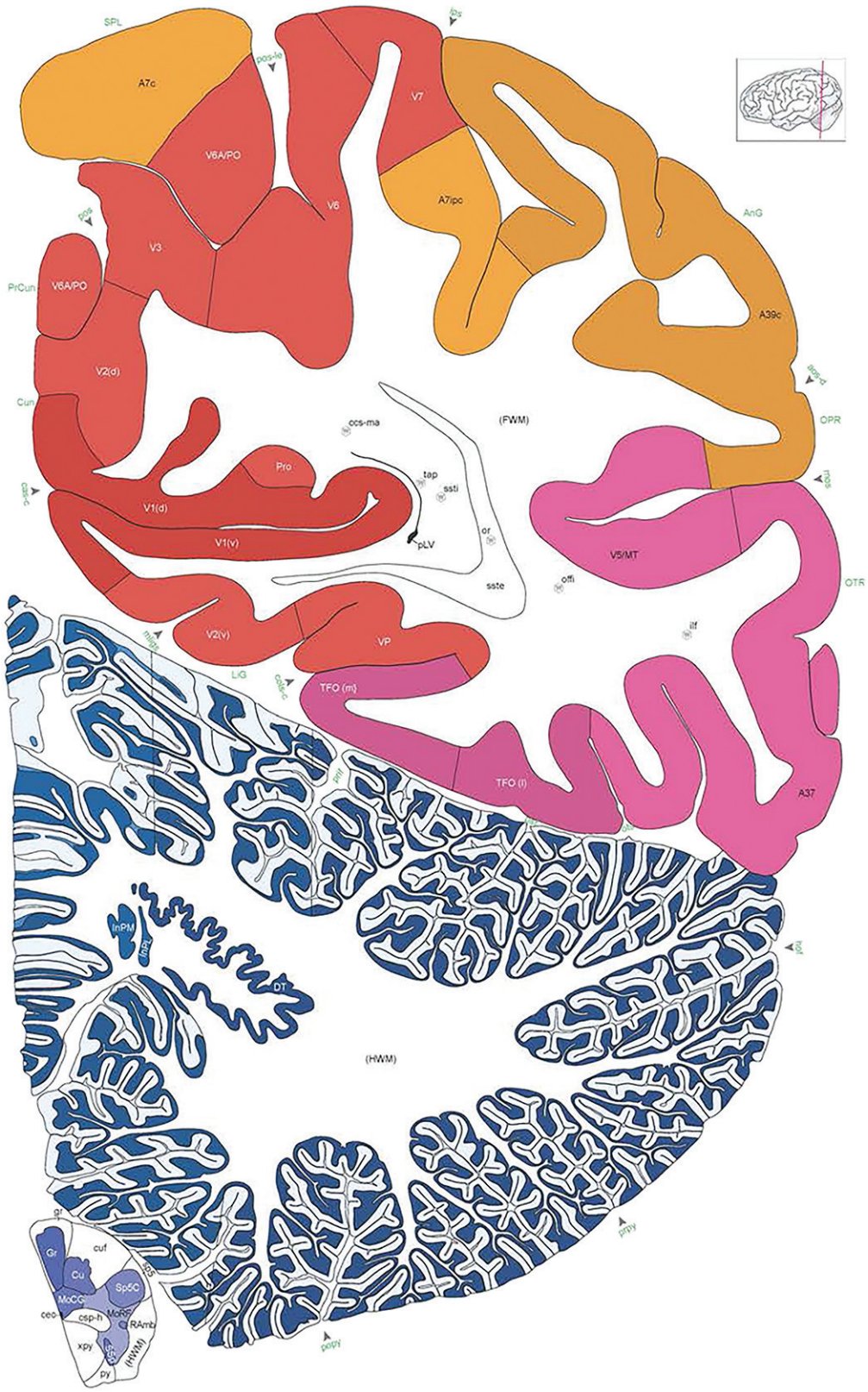

Figure 17. Level 91a (07_163)

Link to online high resolution atlas plate
Link to online high resolution atlas plate (Nissl)

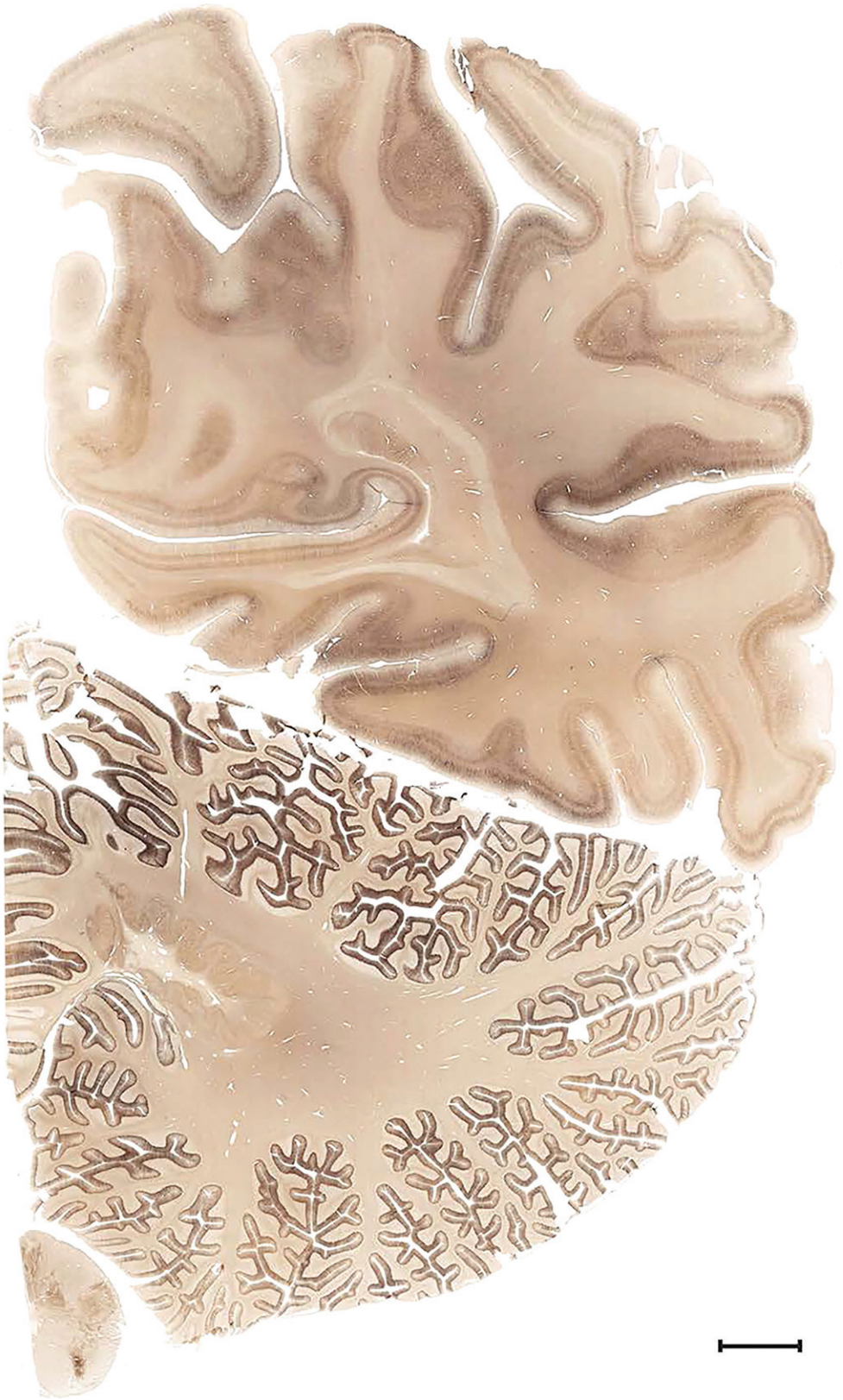

Figure 17. Level 91b (NFP (SMI-32))

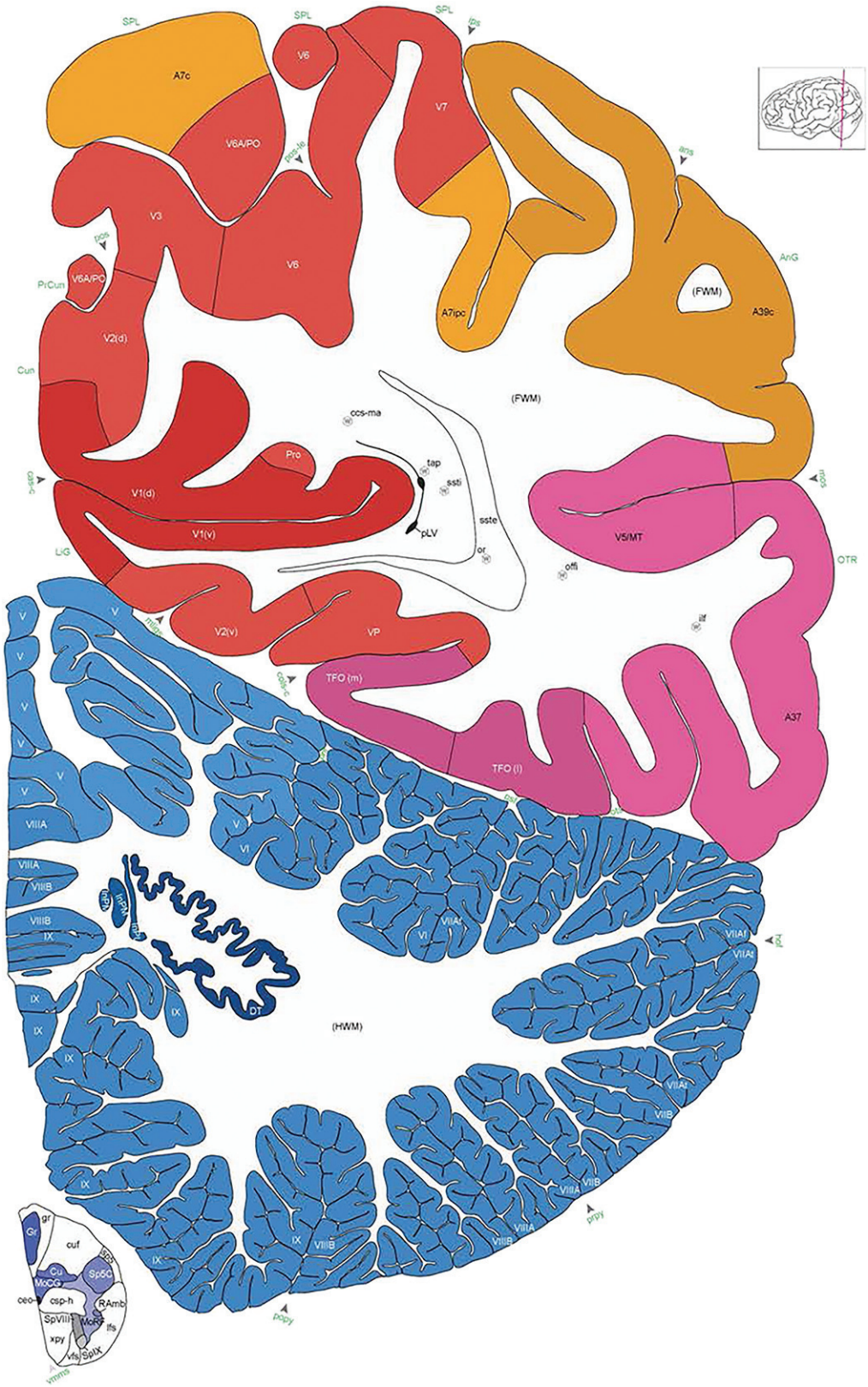

Figure 17. Level 92a (07_171)

Link to online high resolution atlas plate
Link to online high resolution atlas plate (Nissl)

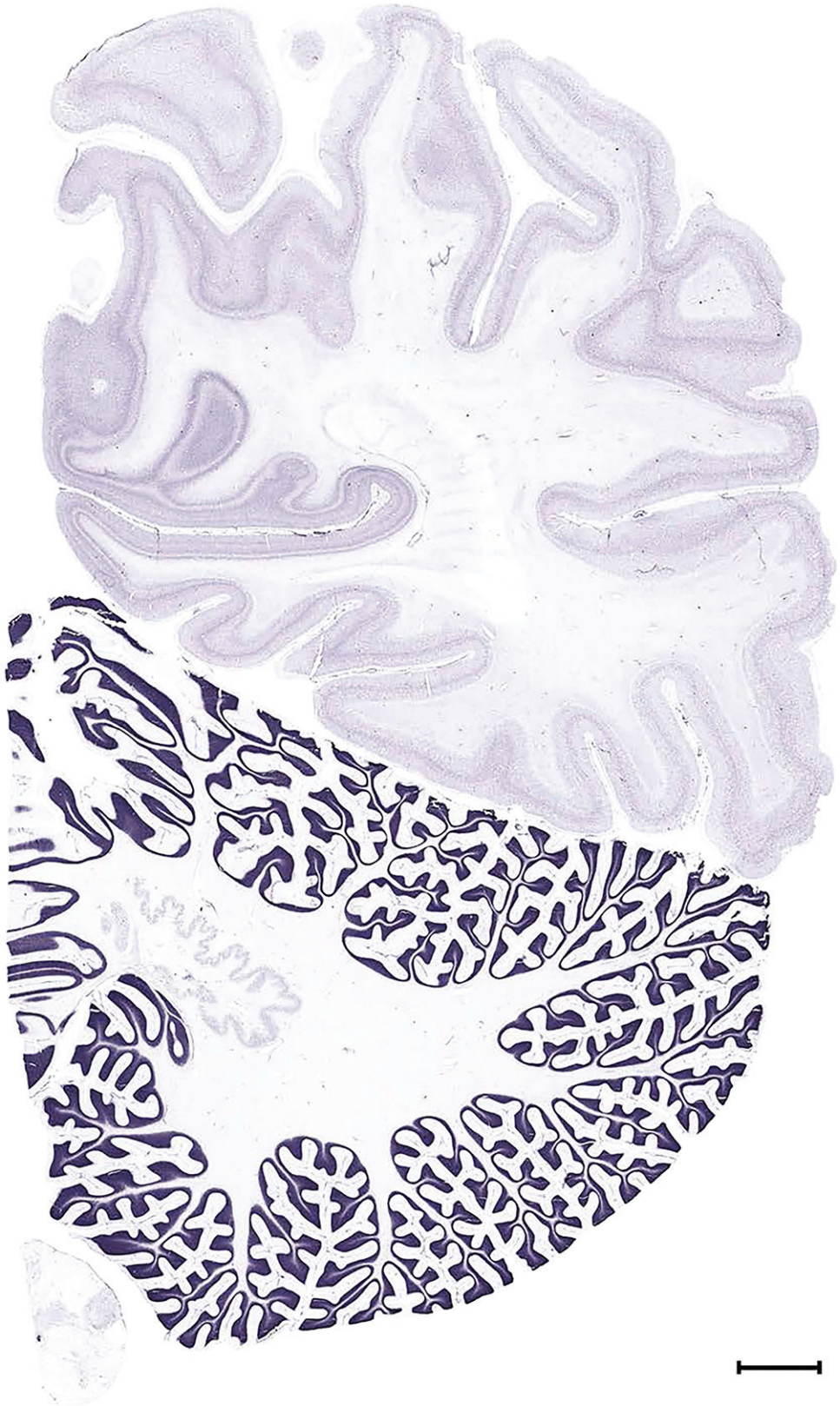

Figure 17. Level 92b (Nissl)

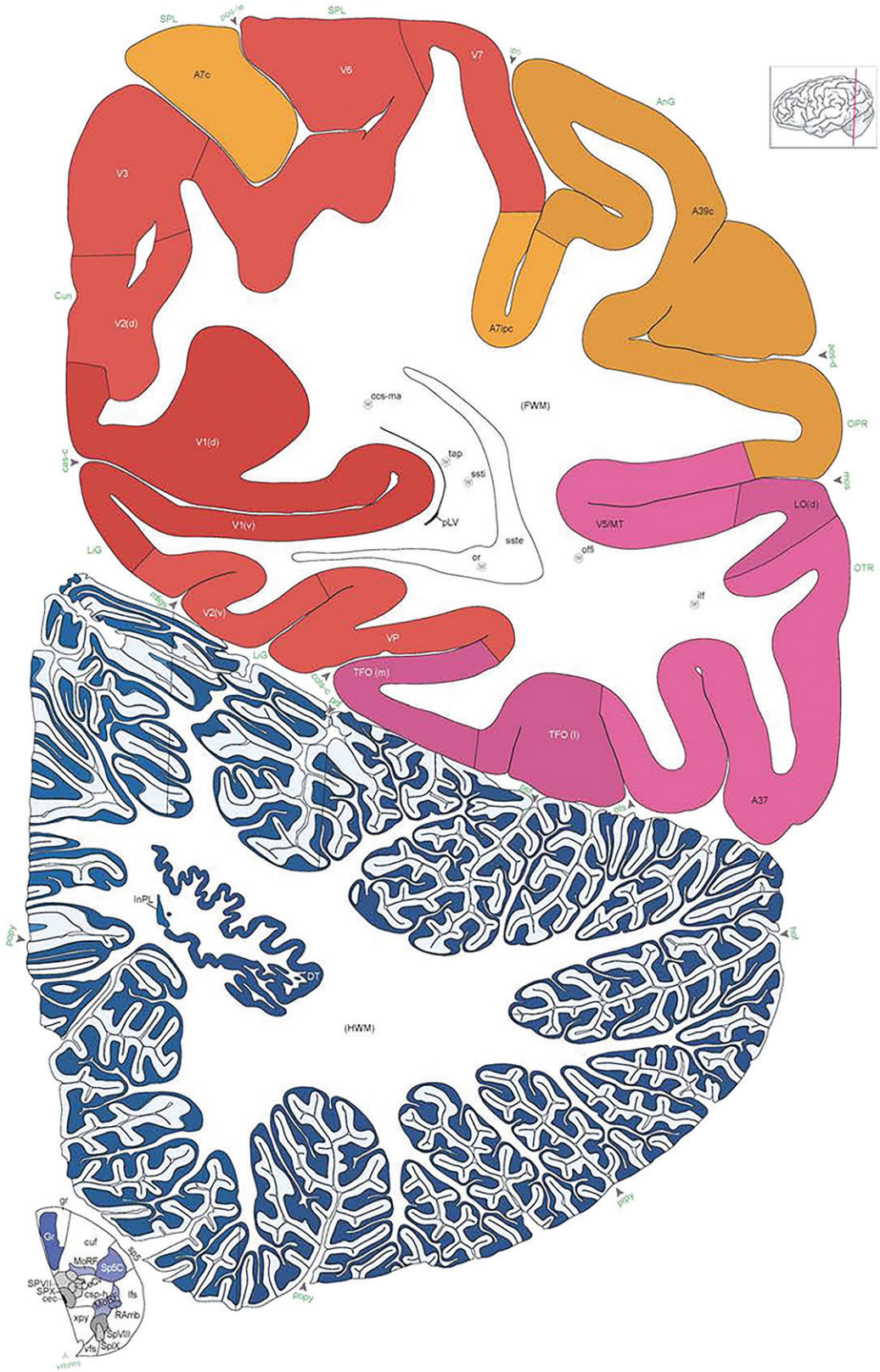

Figure 17. Level 93a (07_191)

Link to online high resolution atlas plate
Link to online high resolution atlas plate (Nissl)

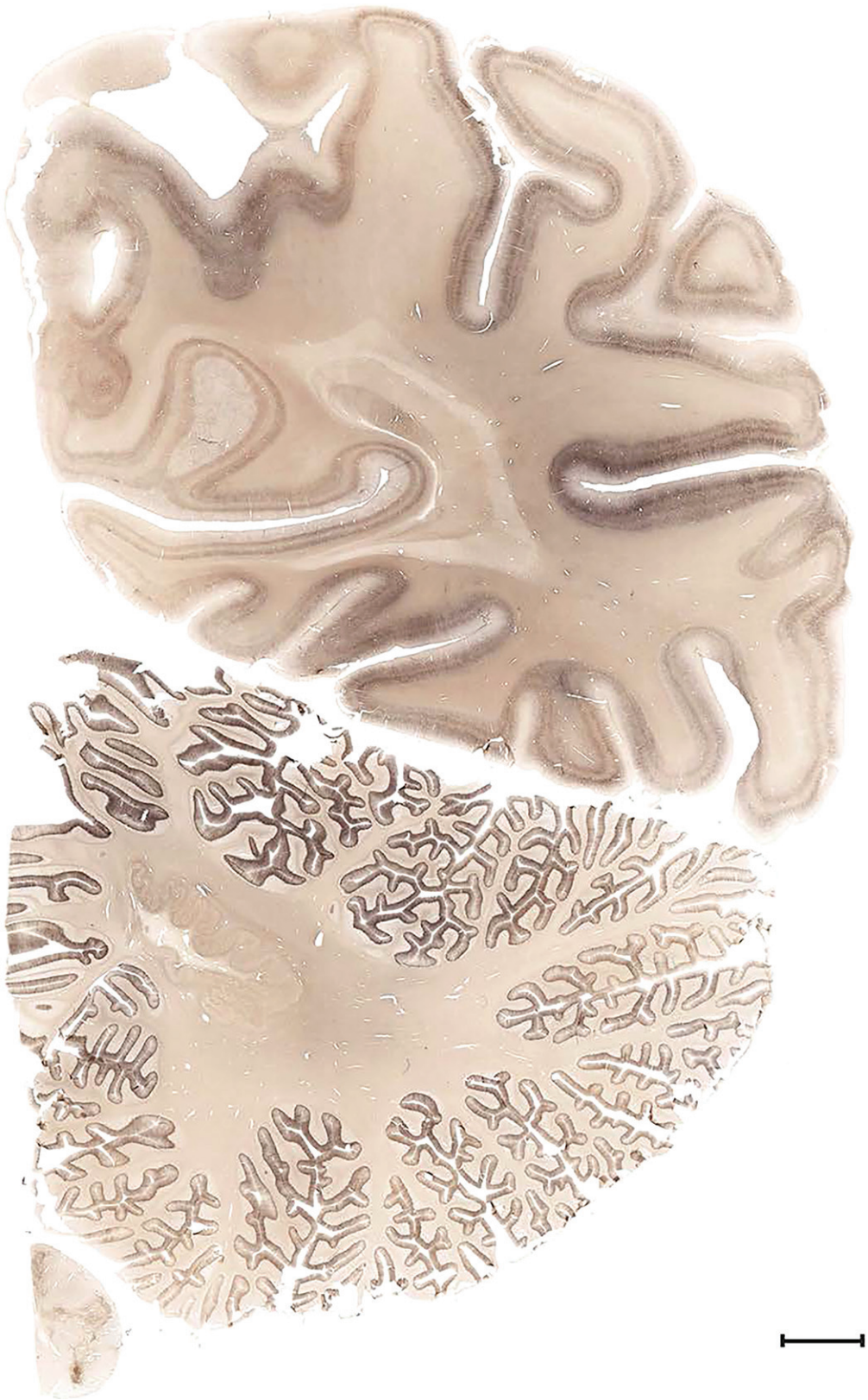

Figure 17. Level 93b (NFP (SMI-32))

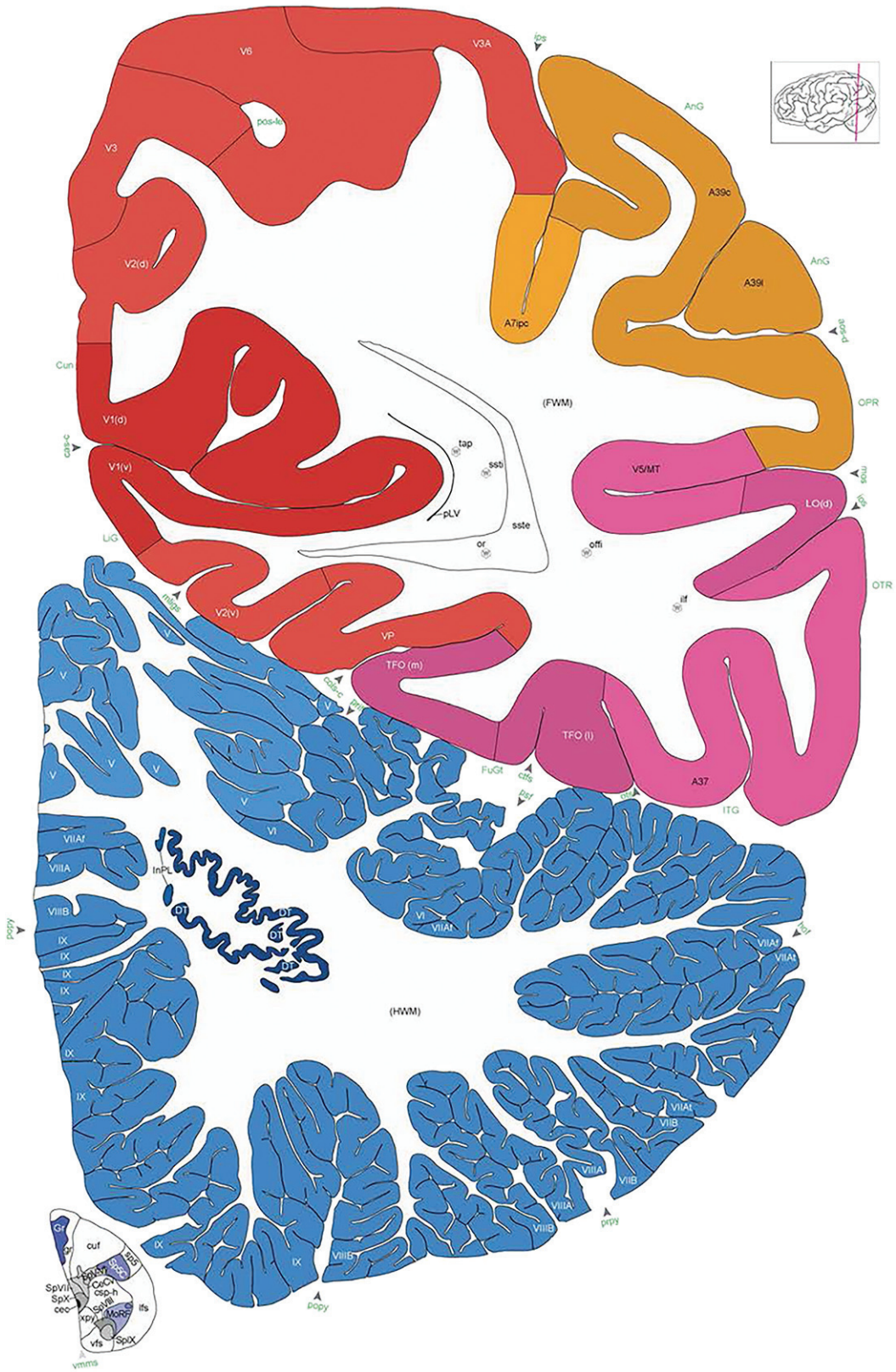

Figure 17. Level 94a (07_207)

Link to online high resolution atlas plate
Link to online high resolution atlas plate (Nissl)

Figure 17. Level 94b (NFP (SMI-32))

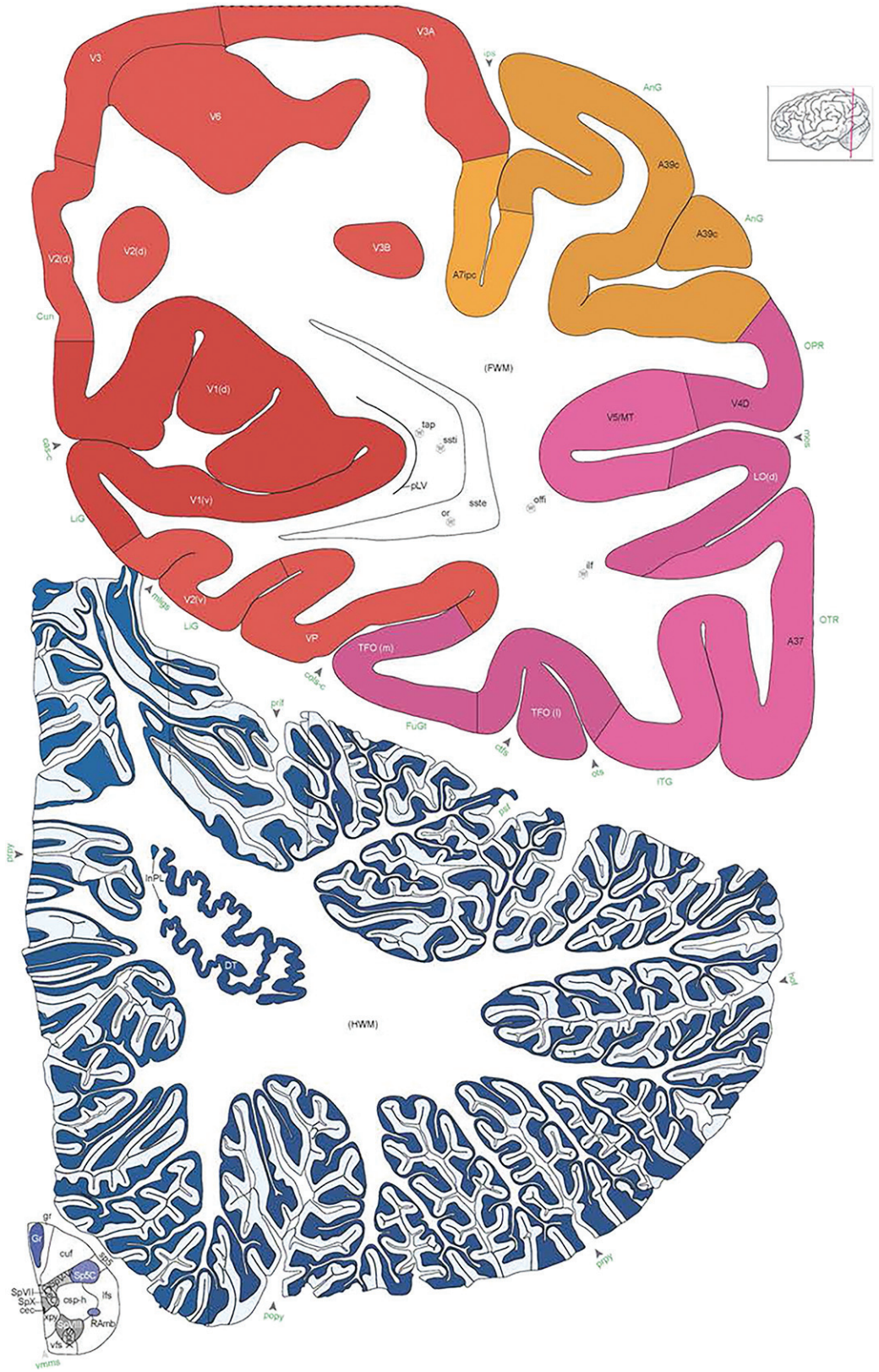

Figure 17. Level 95a (07_223)

Link to online high resolution atlas plate
Link to online high resolution atlas plate (Nissl)

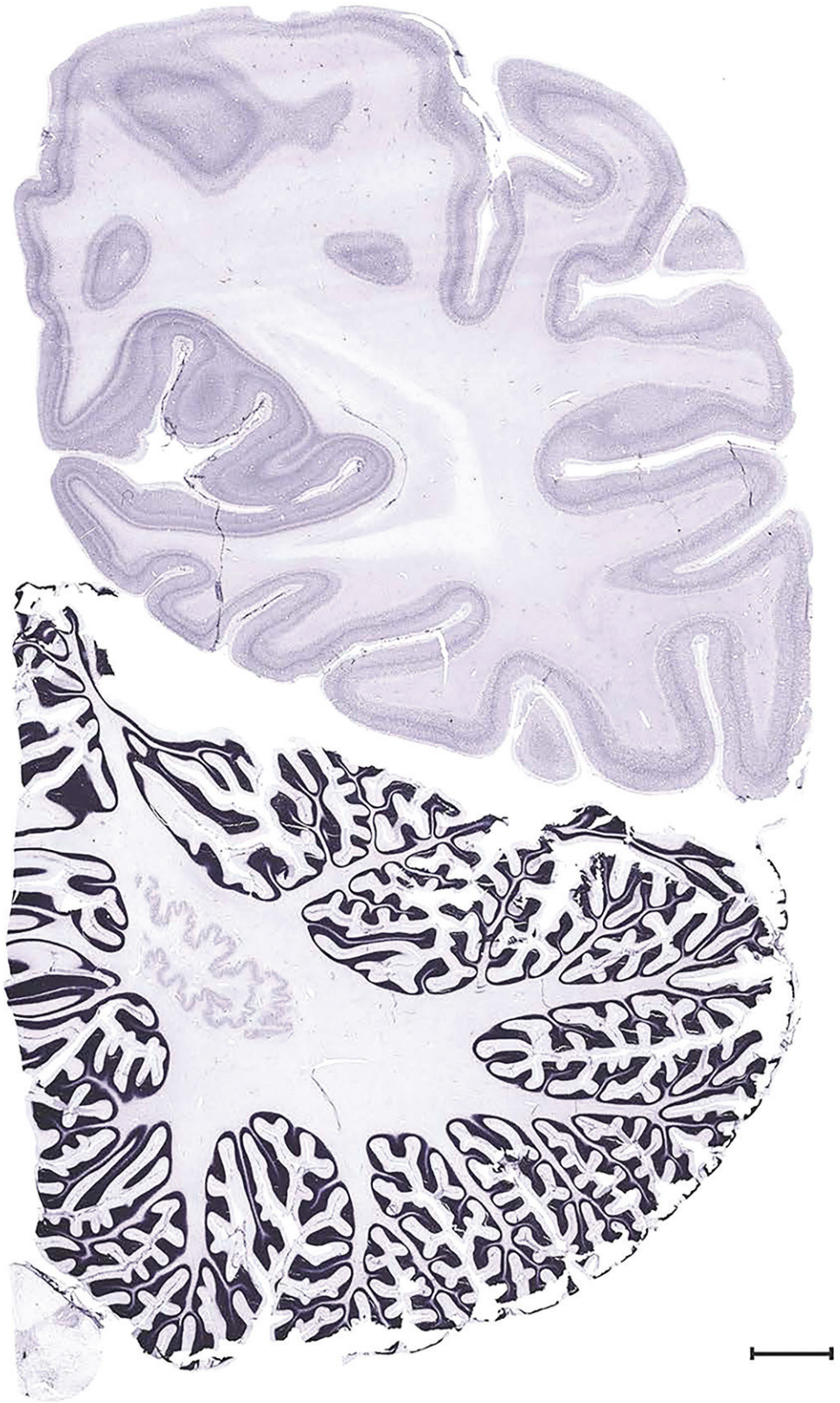

Figure 17. Level 95b (Nissl)

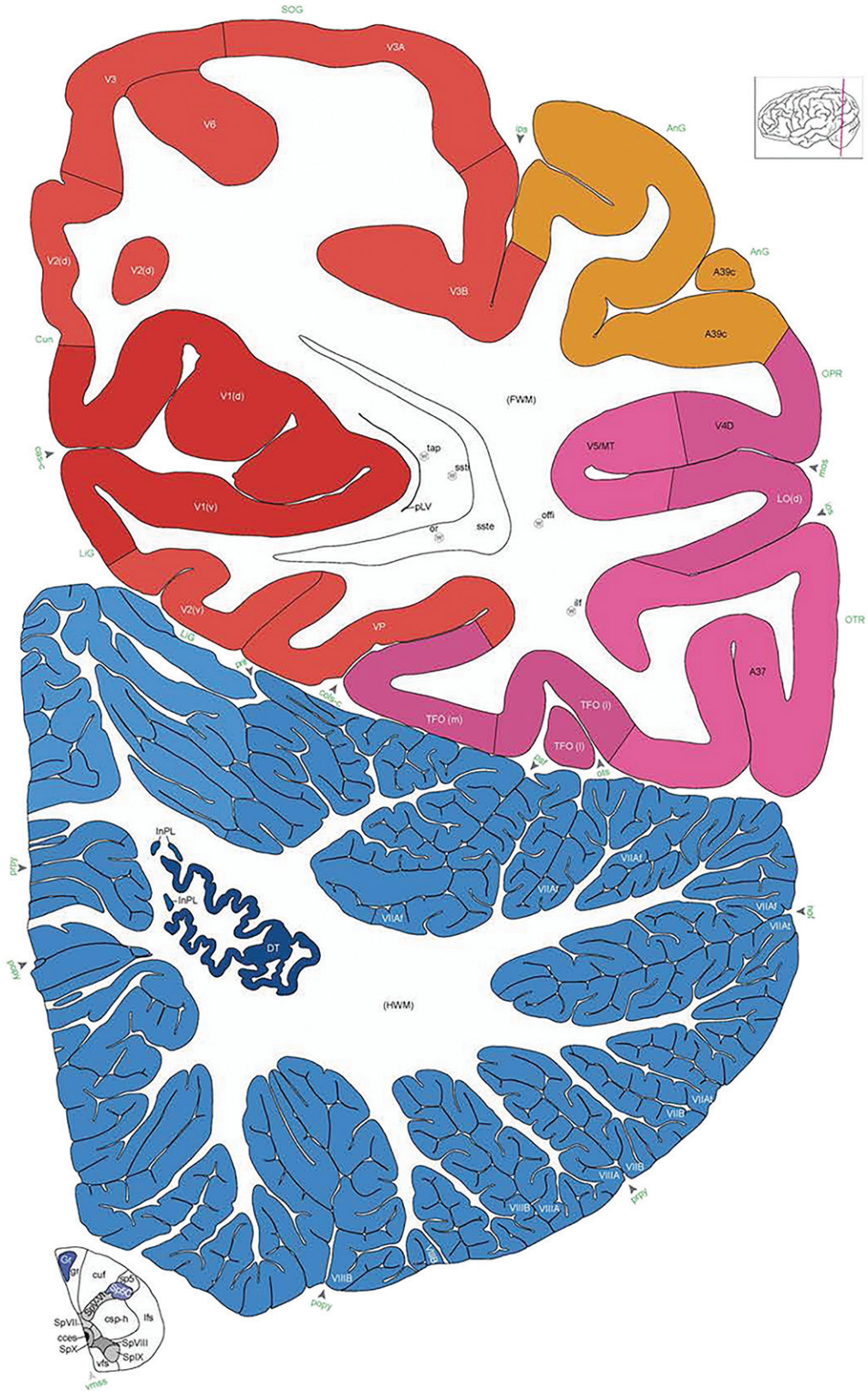

Figure 17. Level 96a (07_235)

Link to online high resolution atlas plate
Link to online high resolution atlas plate (Nissl)

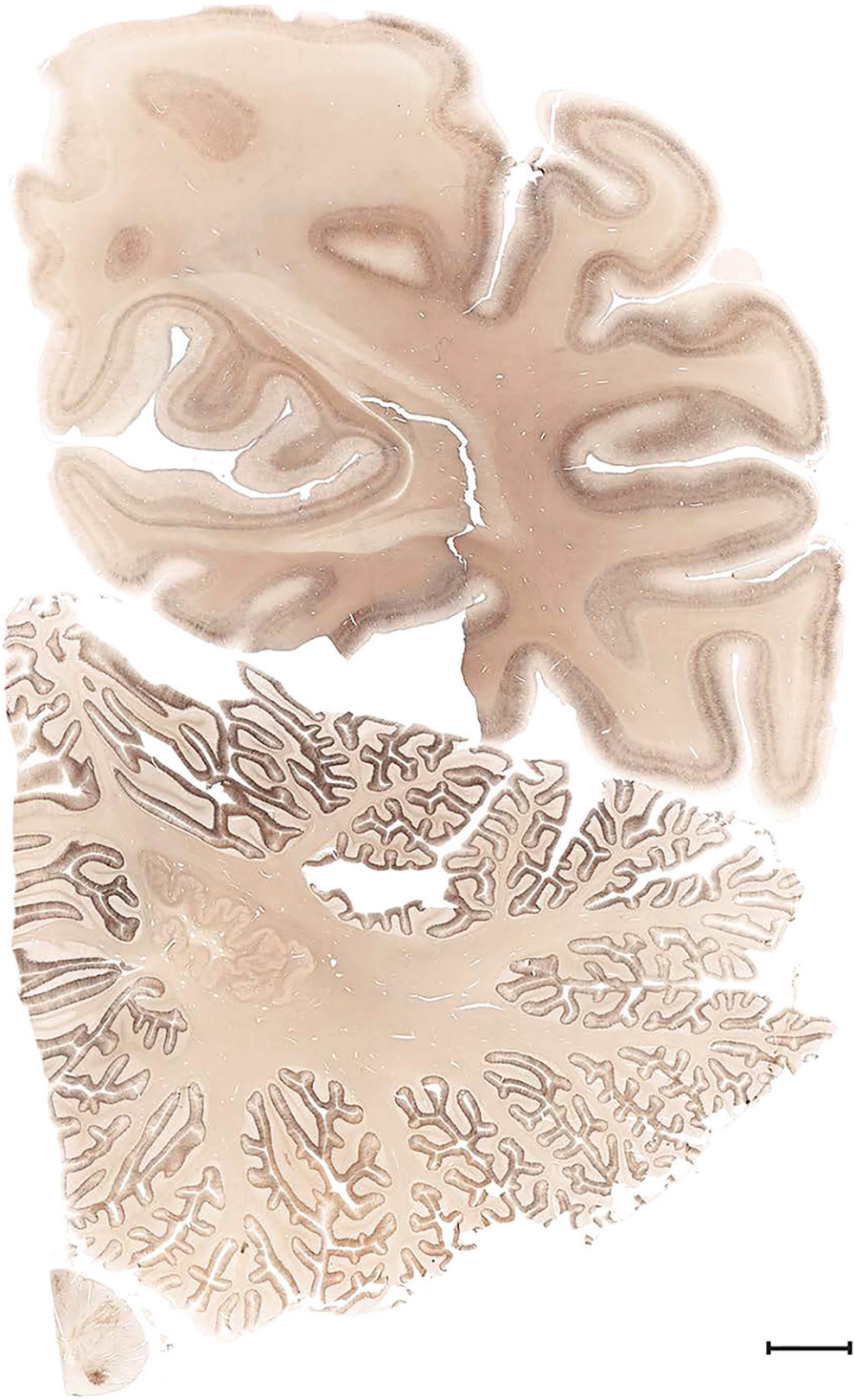

Figure 17. Level 96b (NFP (SMI-32))

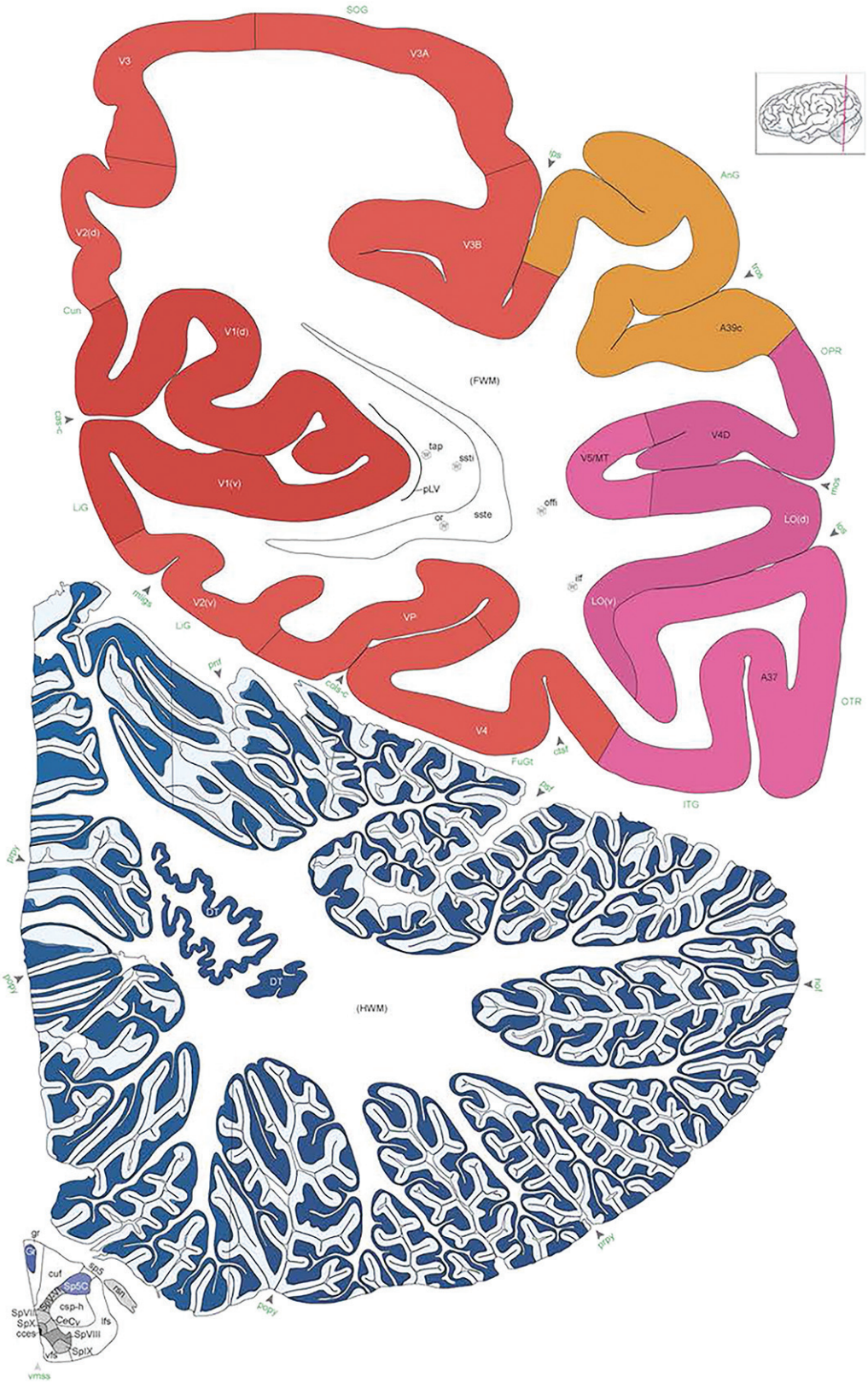

Figure 17. Level 97a (07_251)

Link to online high resolution atlas plate
Link to online high resolution atlas plate (Nissl)

Figure 17. Level 97b (Nissl)

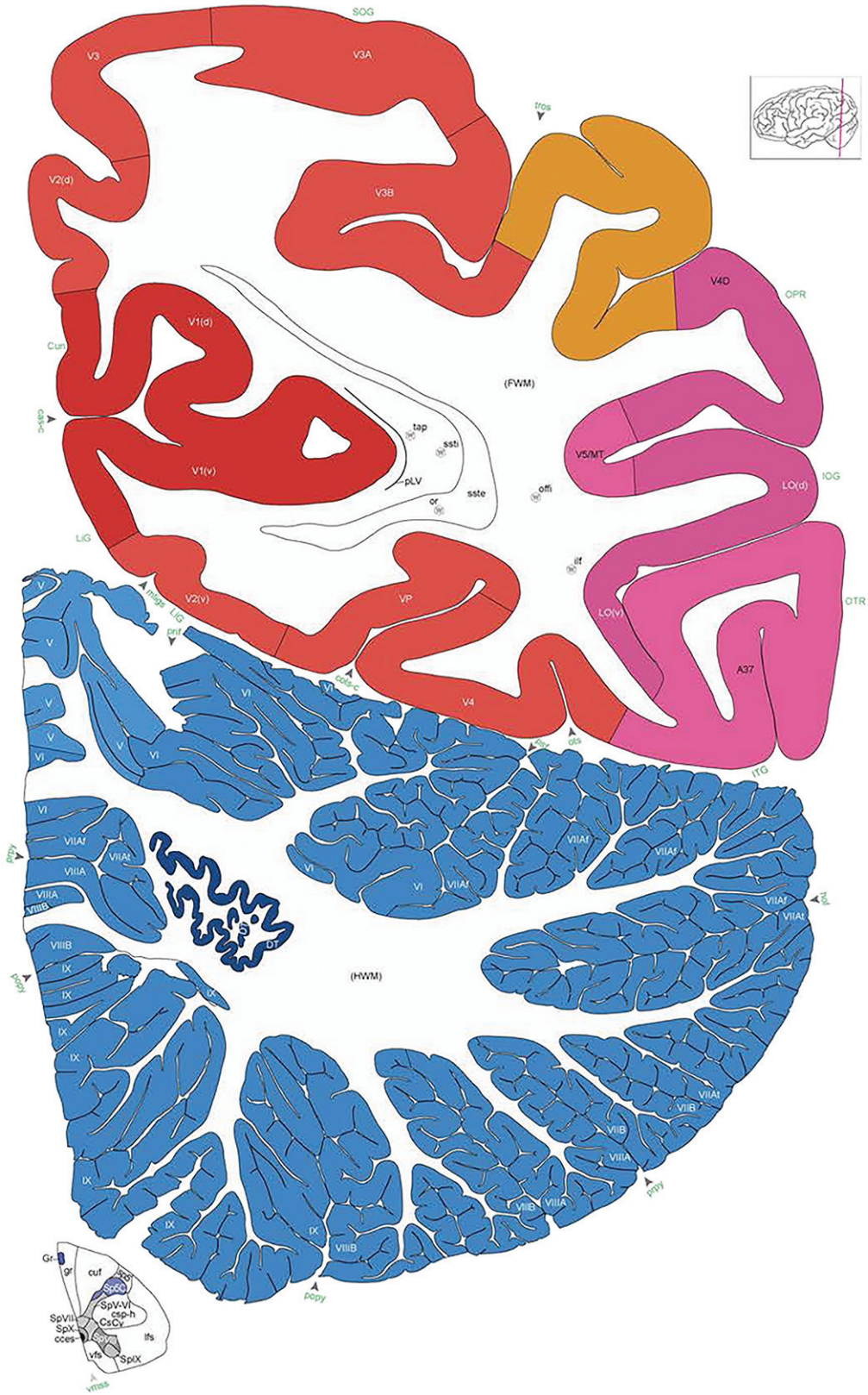

Figure 17. Level 98a (07_267)

Link to online high resolution atlas plate
Link to online high resolution atlas plate (Nissl)

Figure 17. Level 98b (NFP (SMI-32))

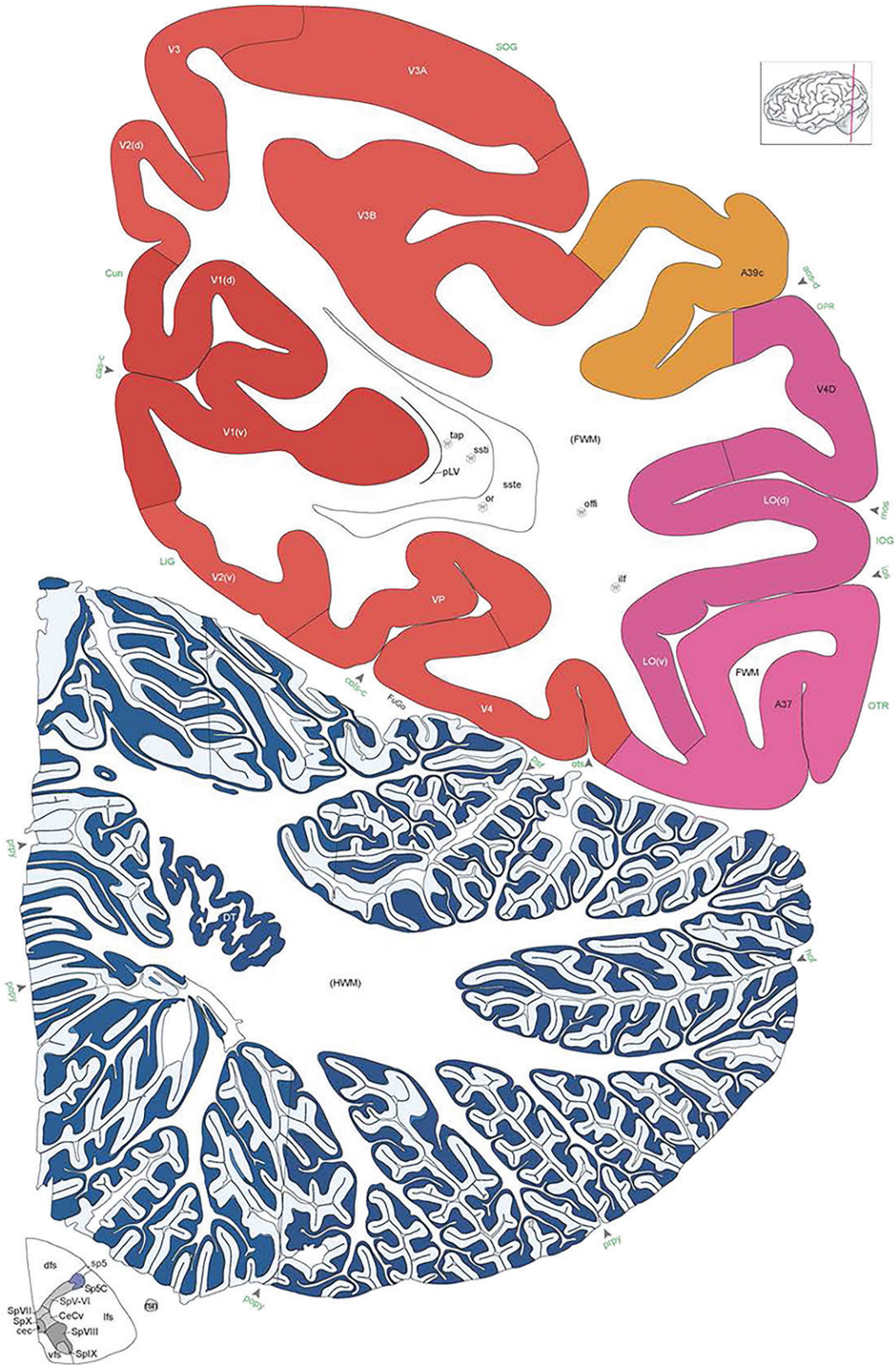

Figure 17. Level 99a (07_287)

Link to online high resolution atlas plate
Link to online high resolution atlas plate (Nissl)

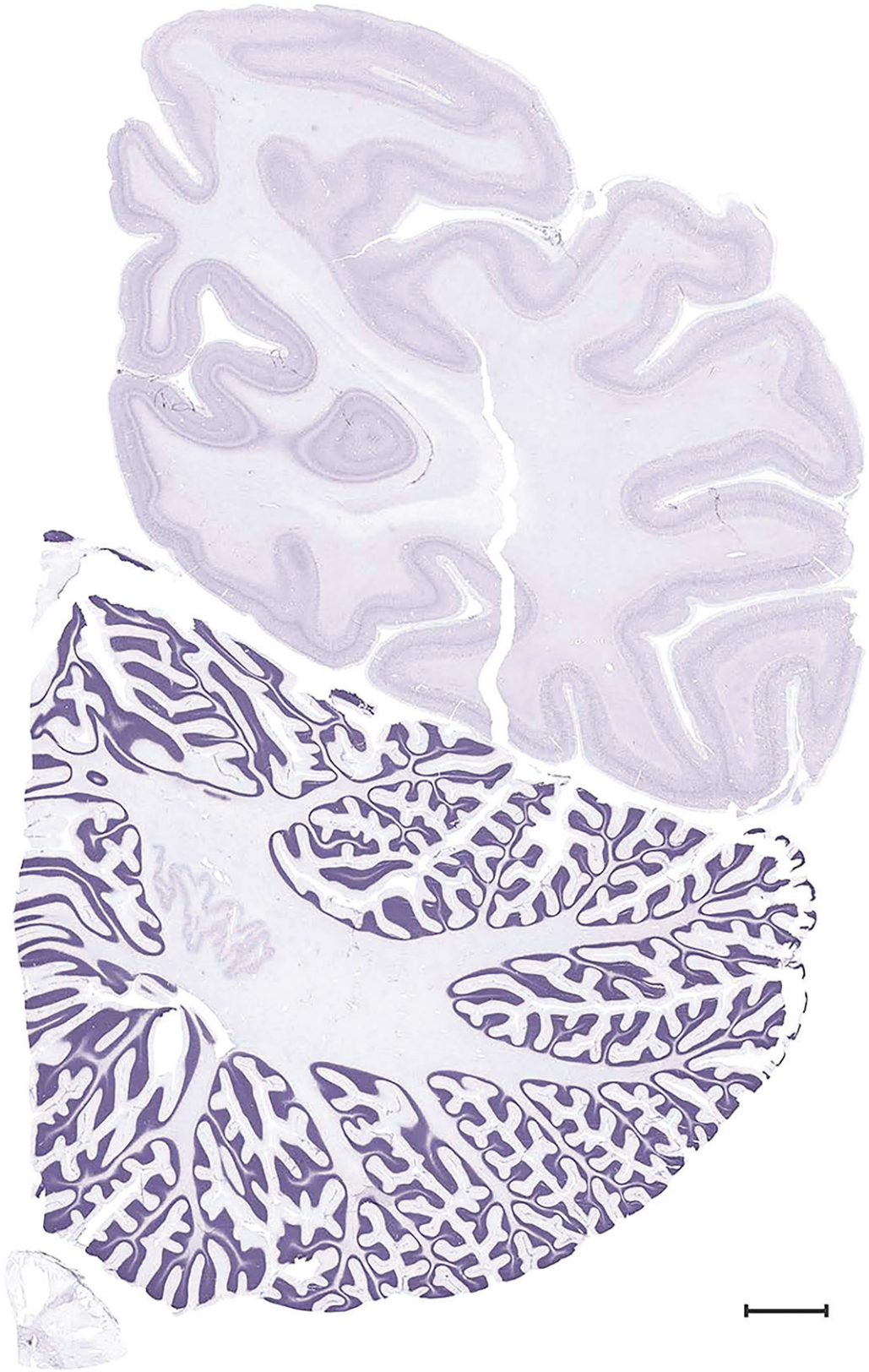

Figure 17. Level 99b (Nissl)

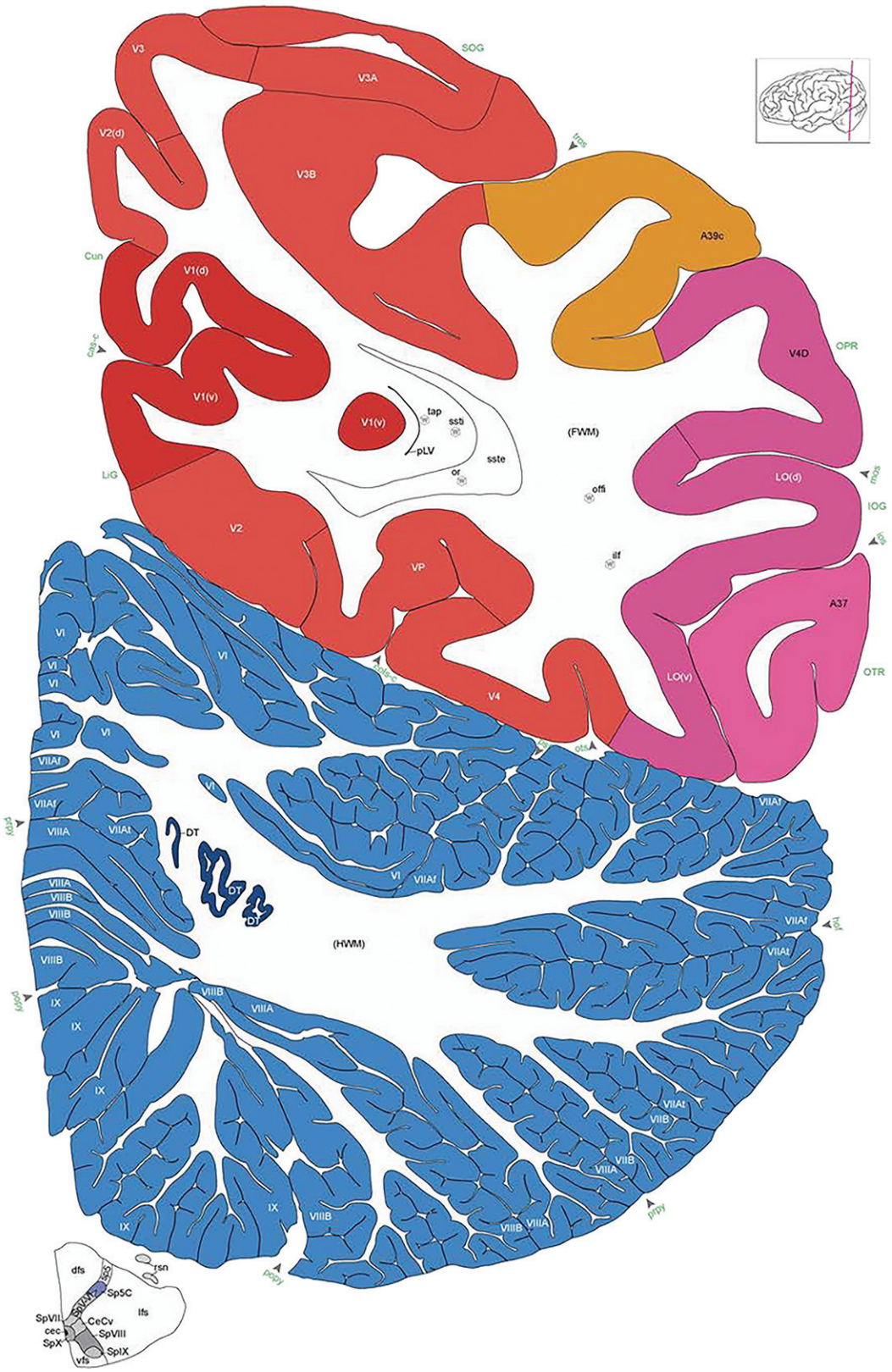

Figure 17. Level 100a (07_299)

Link to online high resolution atlas plate
Link to online high resolution atlas plate (Nissl)

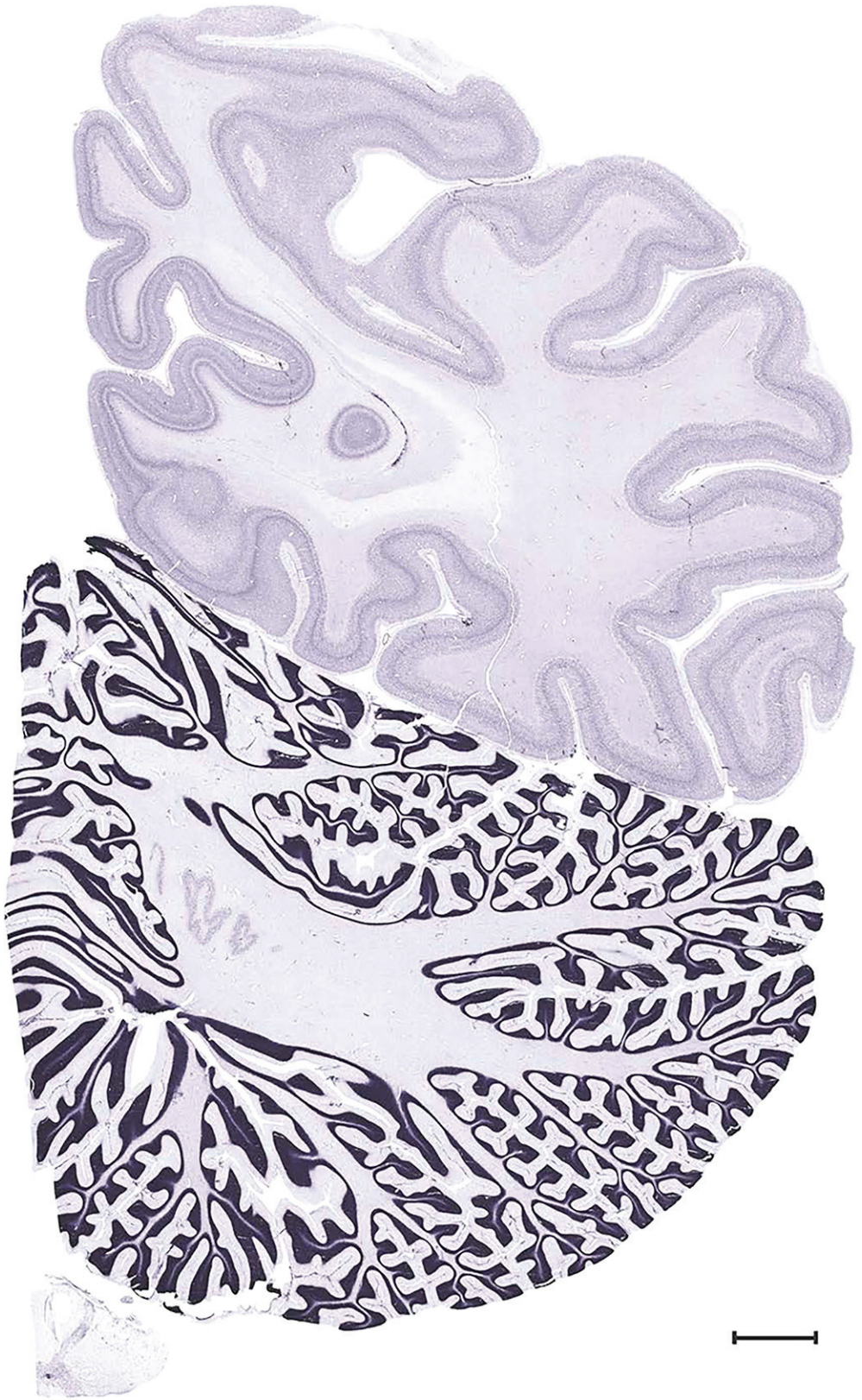

Figure 17. Level 100b (Nissl)

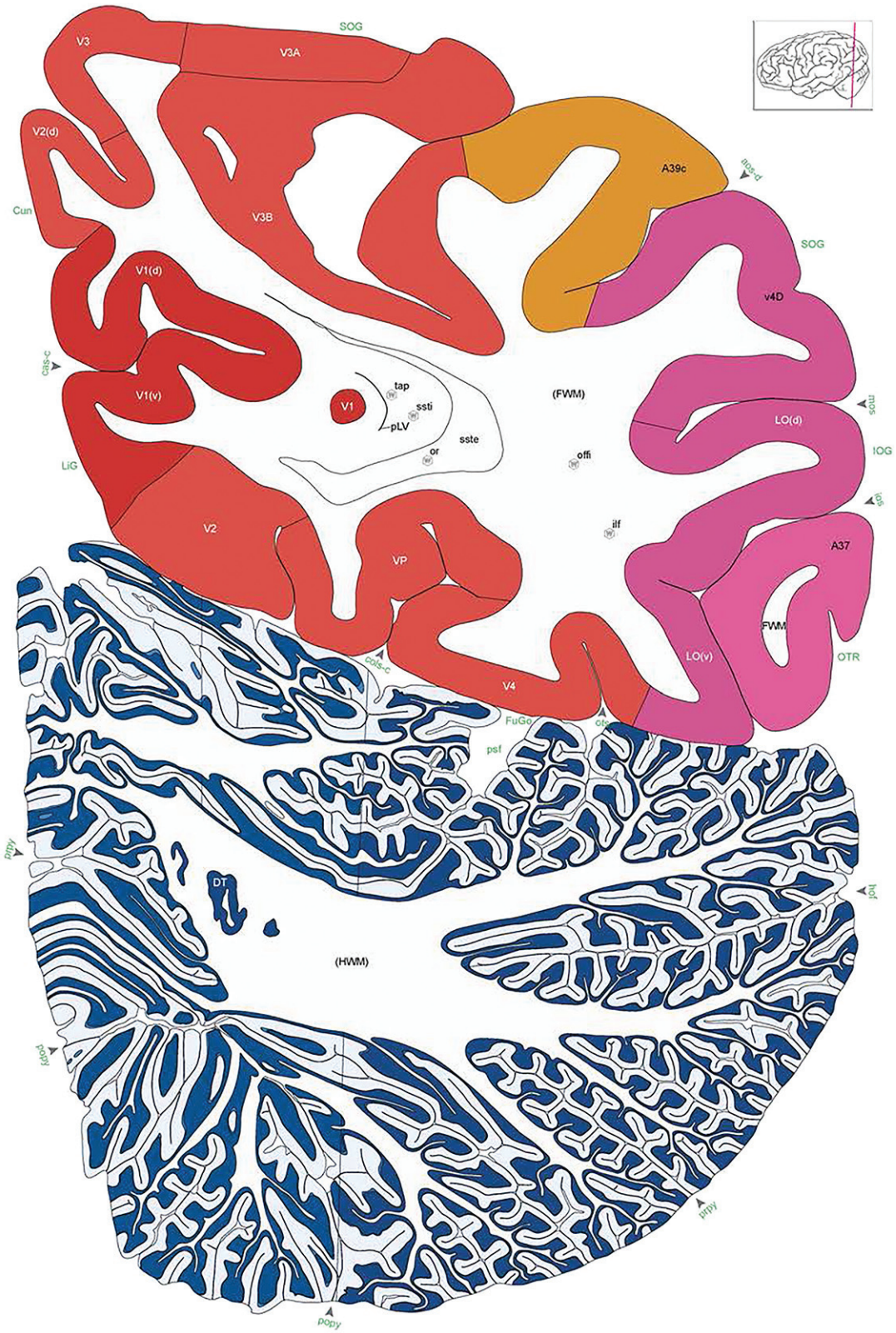

Figure 17. Level 101a (07_315)

Link to online high resolution atlas plate
Link to online high resolution atlas plate (Nissl)

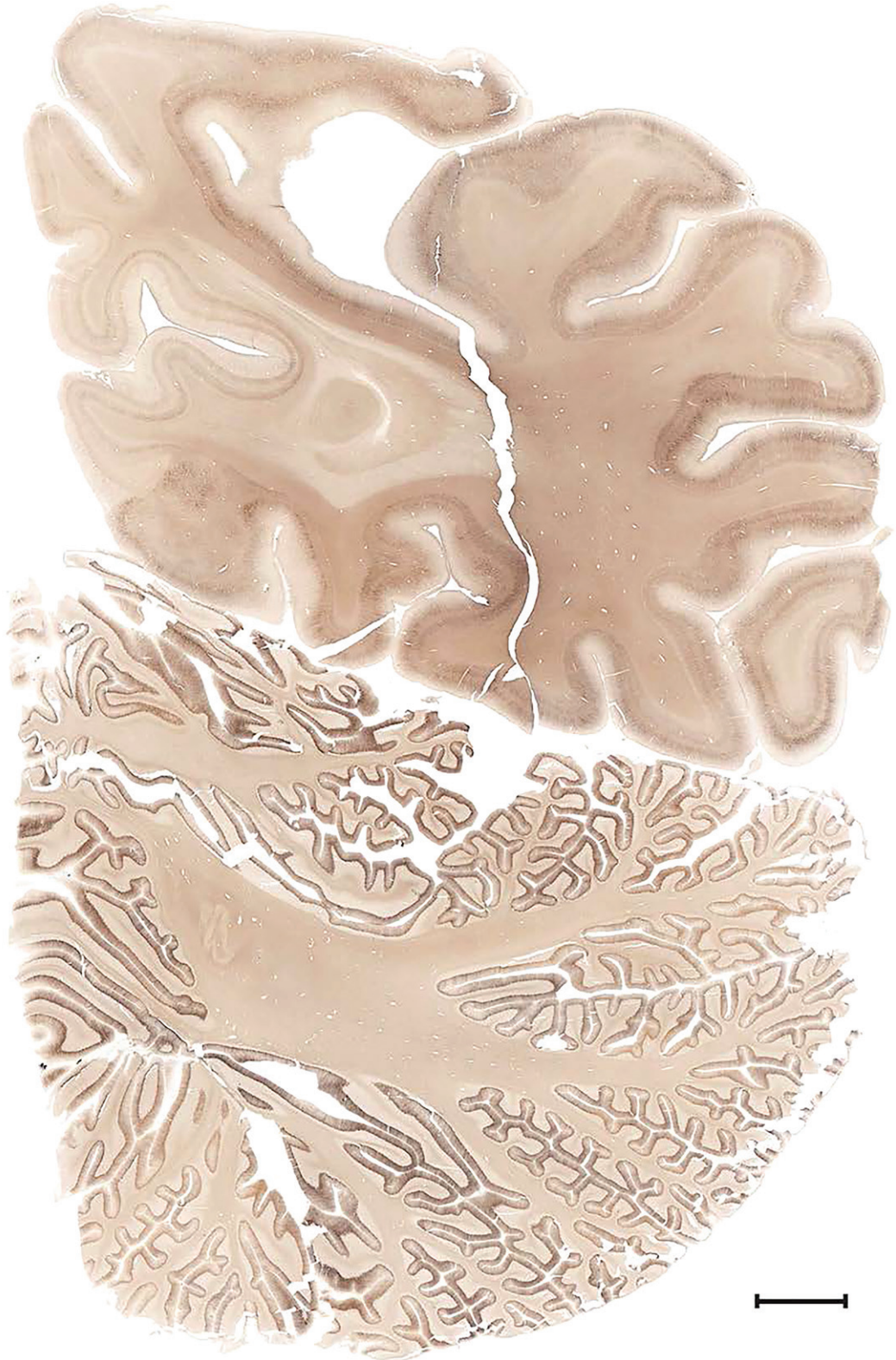

Figure 17. Level 101b (NFP (SMI-32))

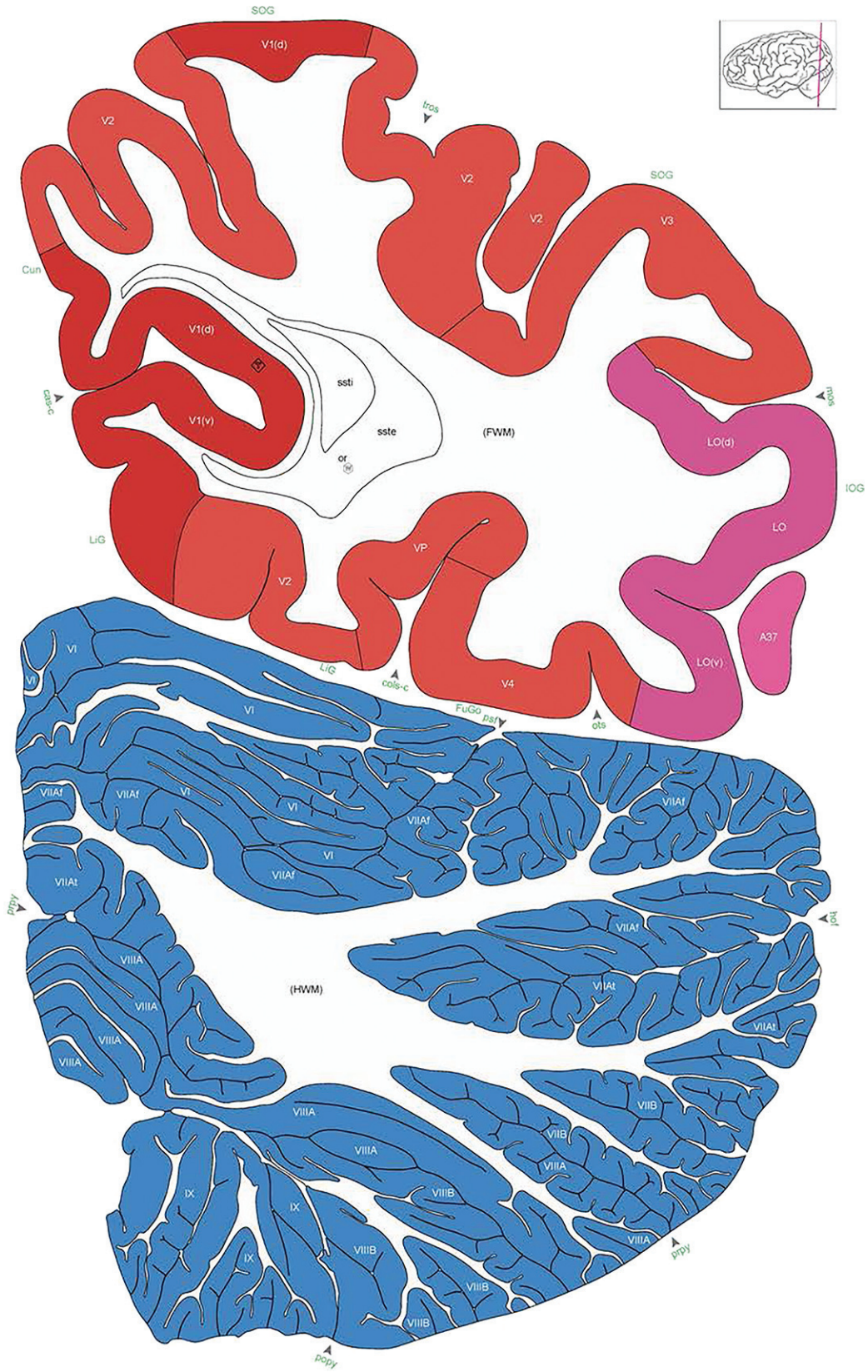

Figure 17. Level 102a (08_039)

Link to online high resolution atlas plate
Link to online high resolution atlas plate (Nissl)

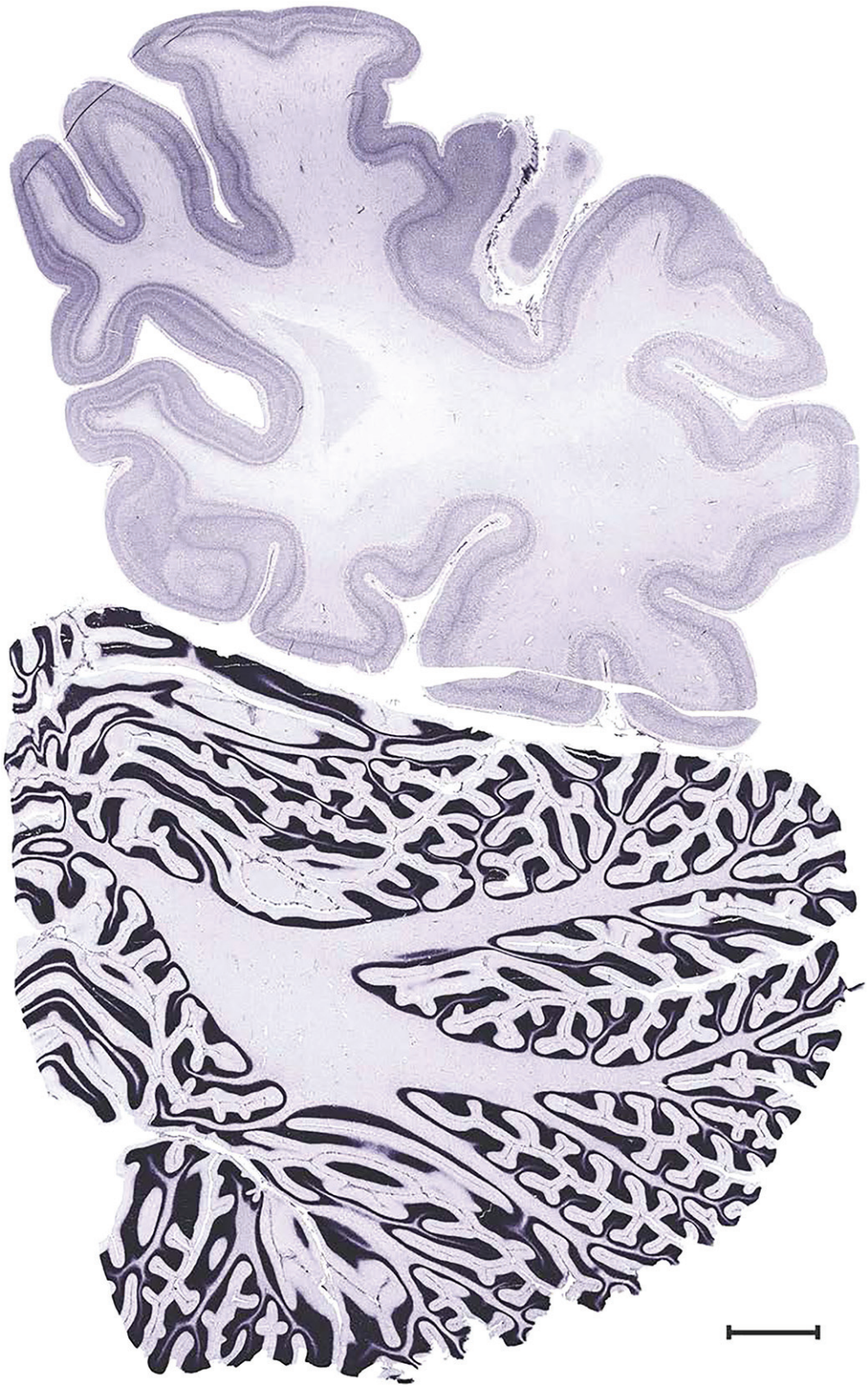

Figure 17. Level 102b (Nissl)

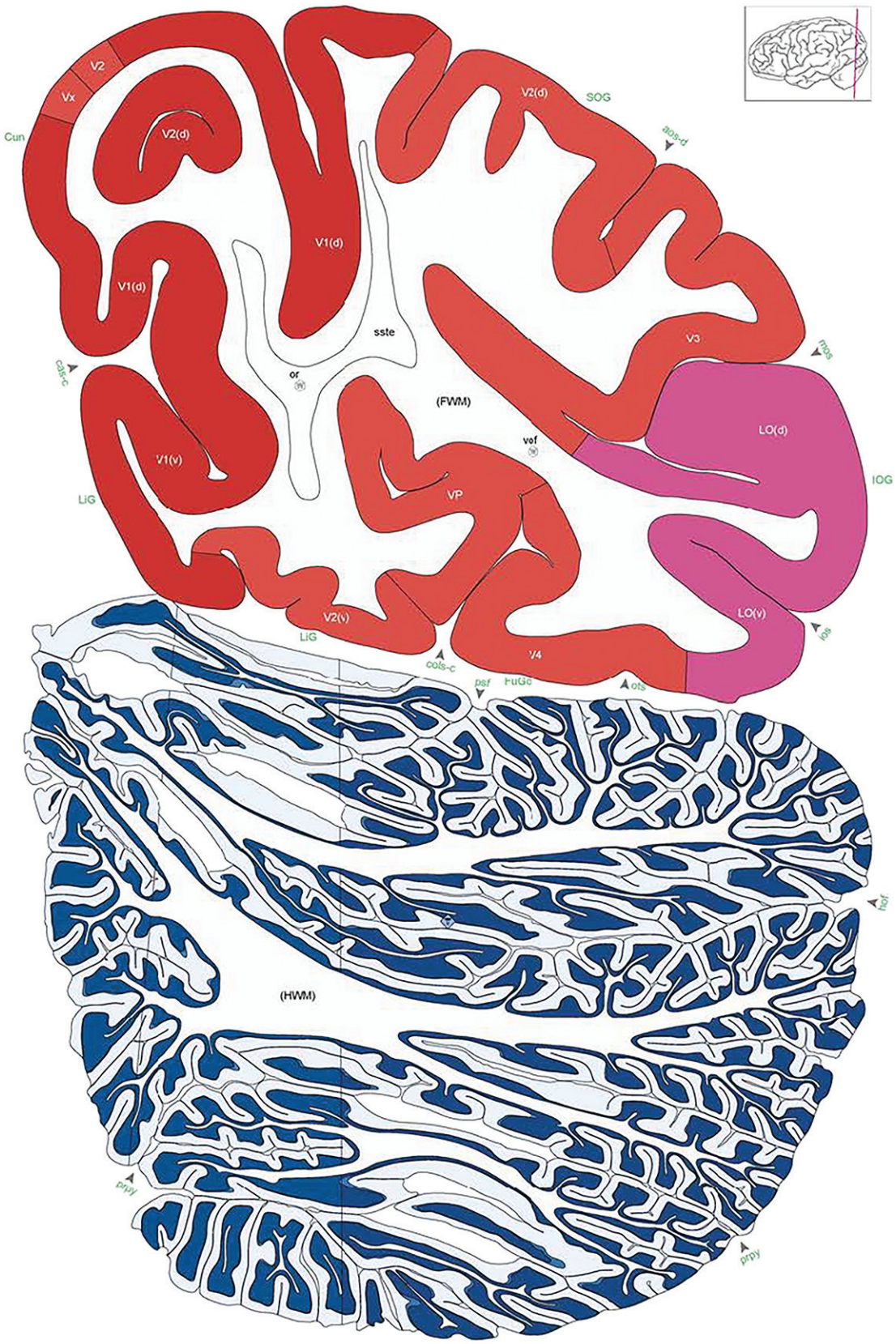

Figure 17. Level 103a (08_103)

Link to online high resolution atlas plate
Link to online high resolution atlas plate (Nissl)

Figure 17. Level 103b (NFP (SMI-32))

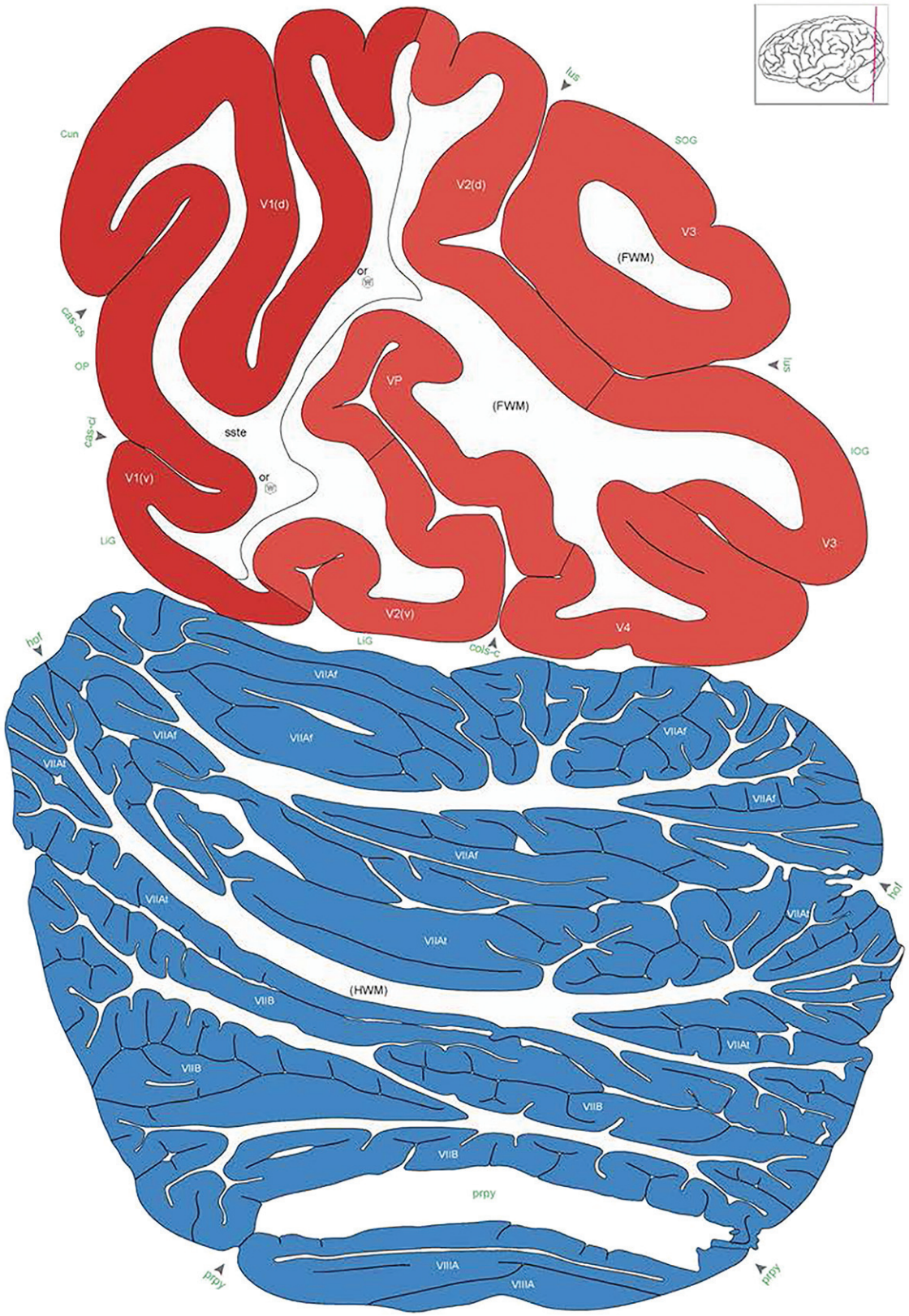

Figure 17. Level 104a (08_167)

Link to online high resolution atlas plate
Link to online high resolution atlas plate (Nissl)

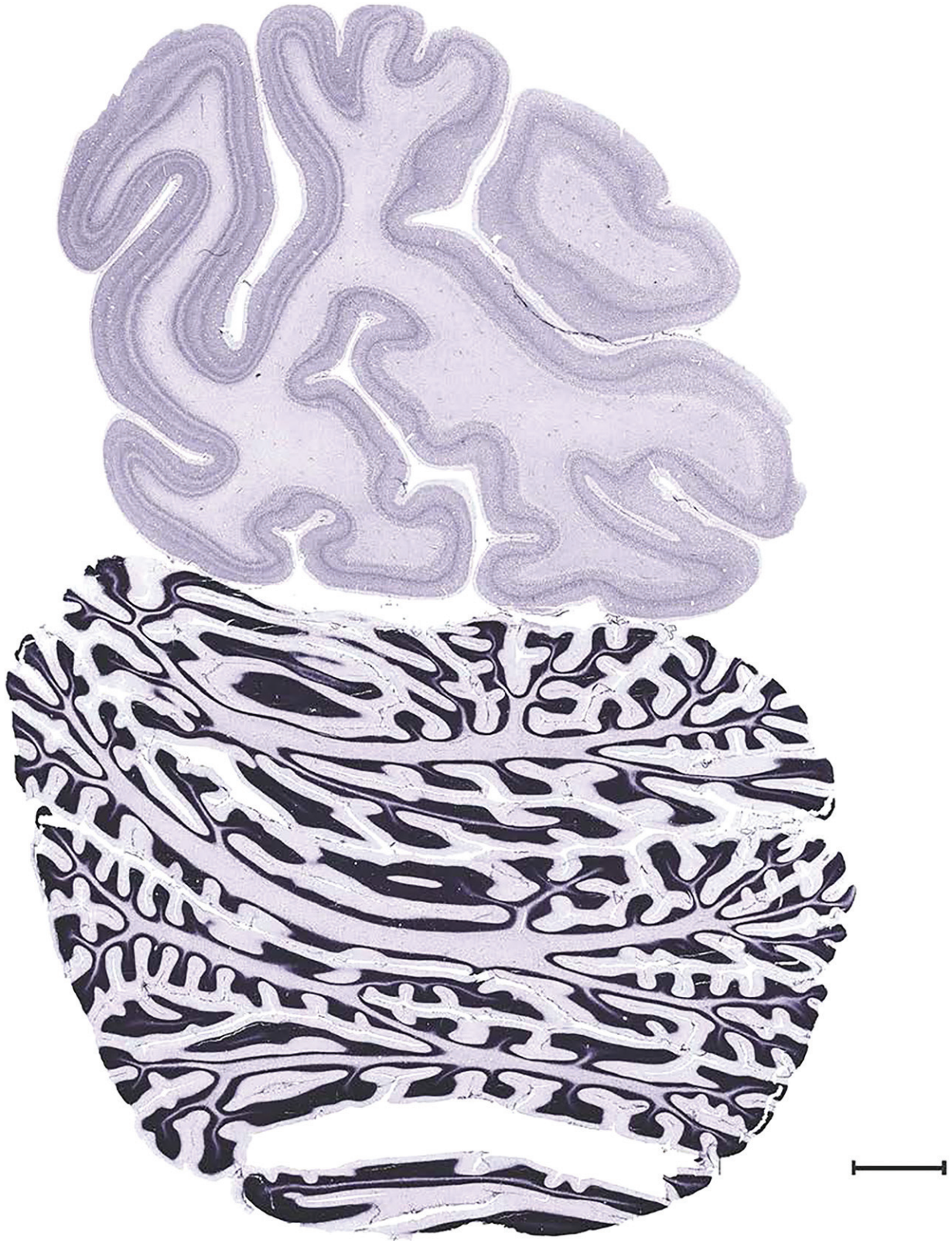

Figure 17. Level 104b (Nissl)

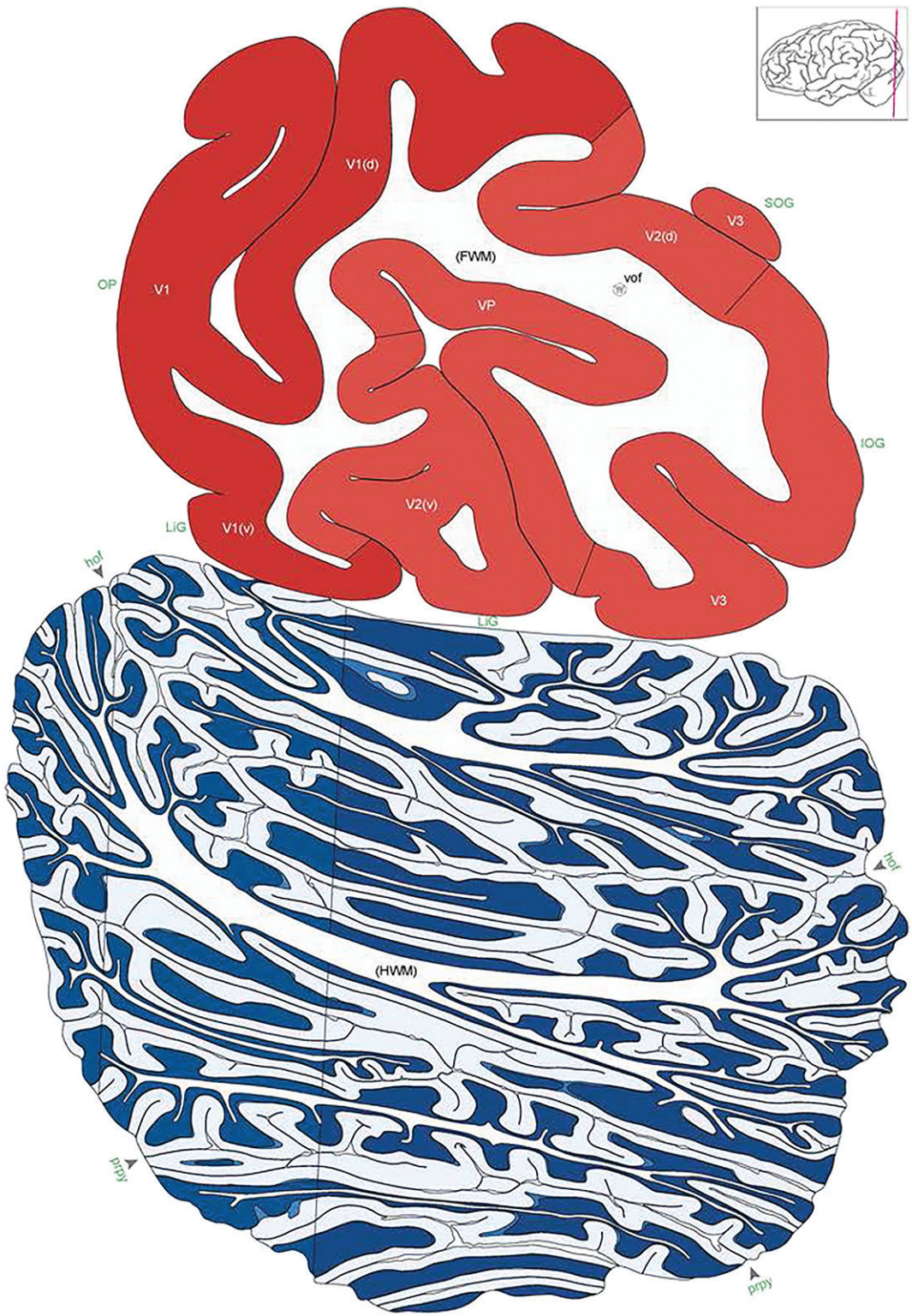

Figure 17. Level 105a (08_231)

Link to online high resolution atlas plate
Link to online high resolution atlas plate (Nissl)

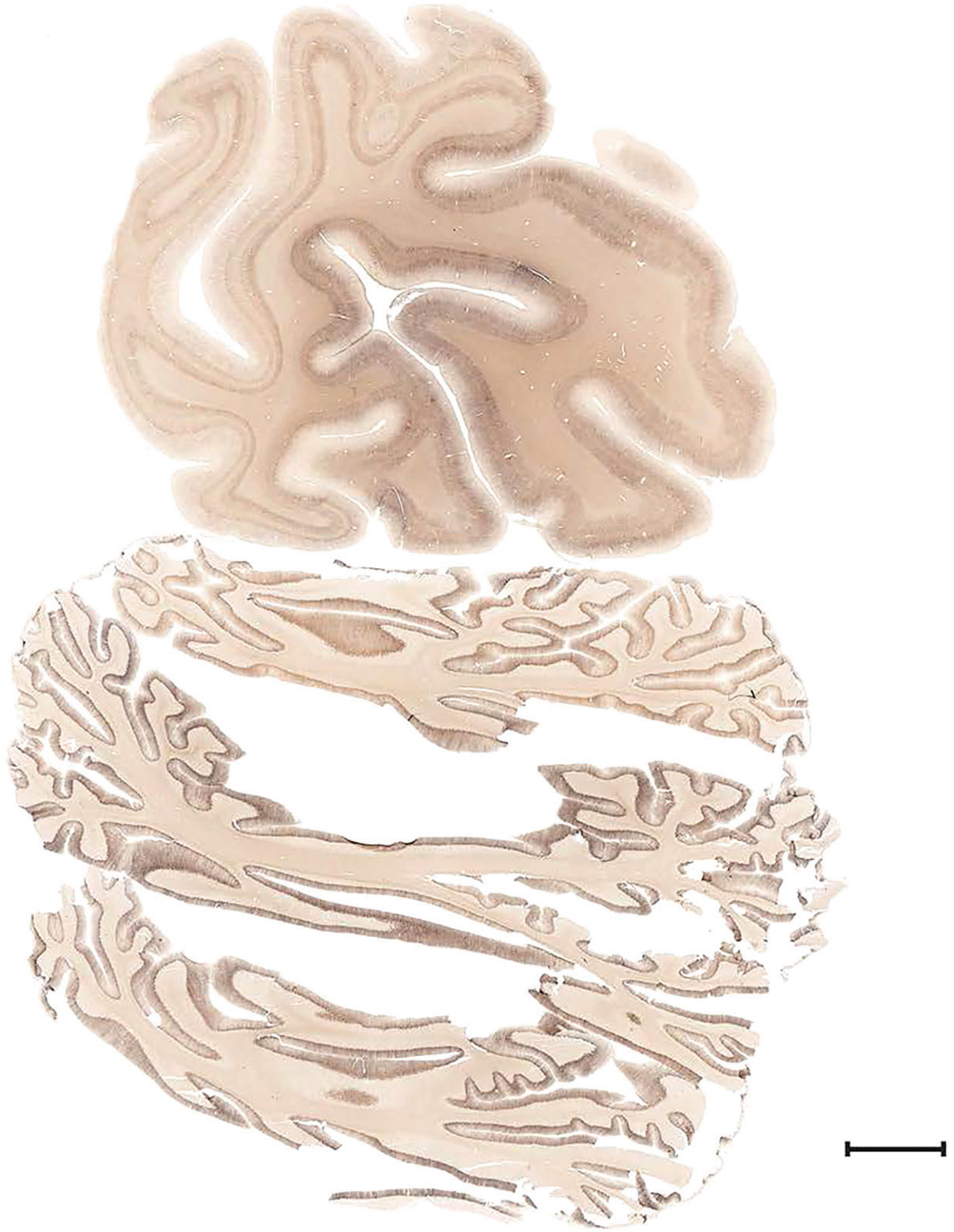

Figure 17. Level 105b (NFP (SMI-32))

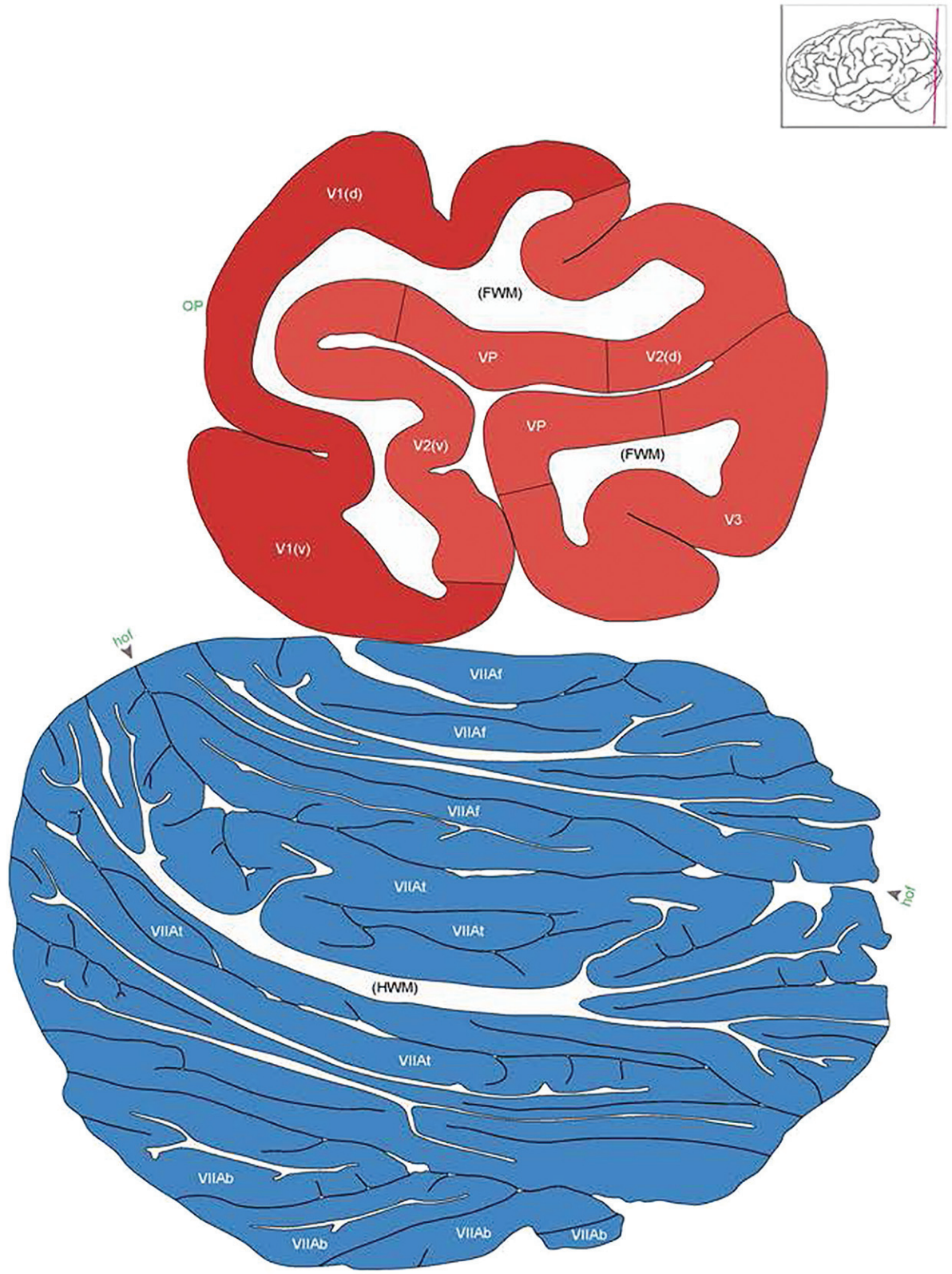

Figure 17. Level 106a (08_291)

Link to online high resolution atlas plate
Link to online high resolution atlas plate (Nissl)

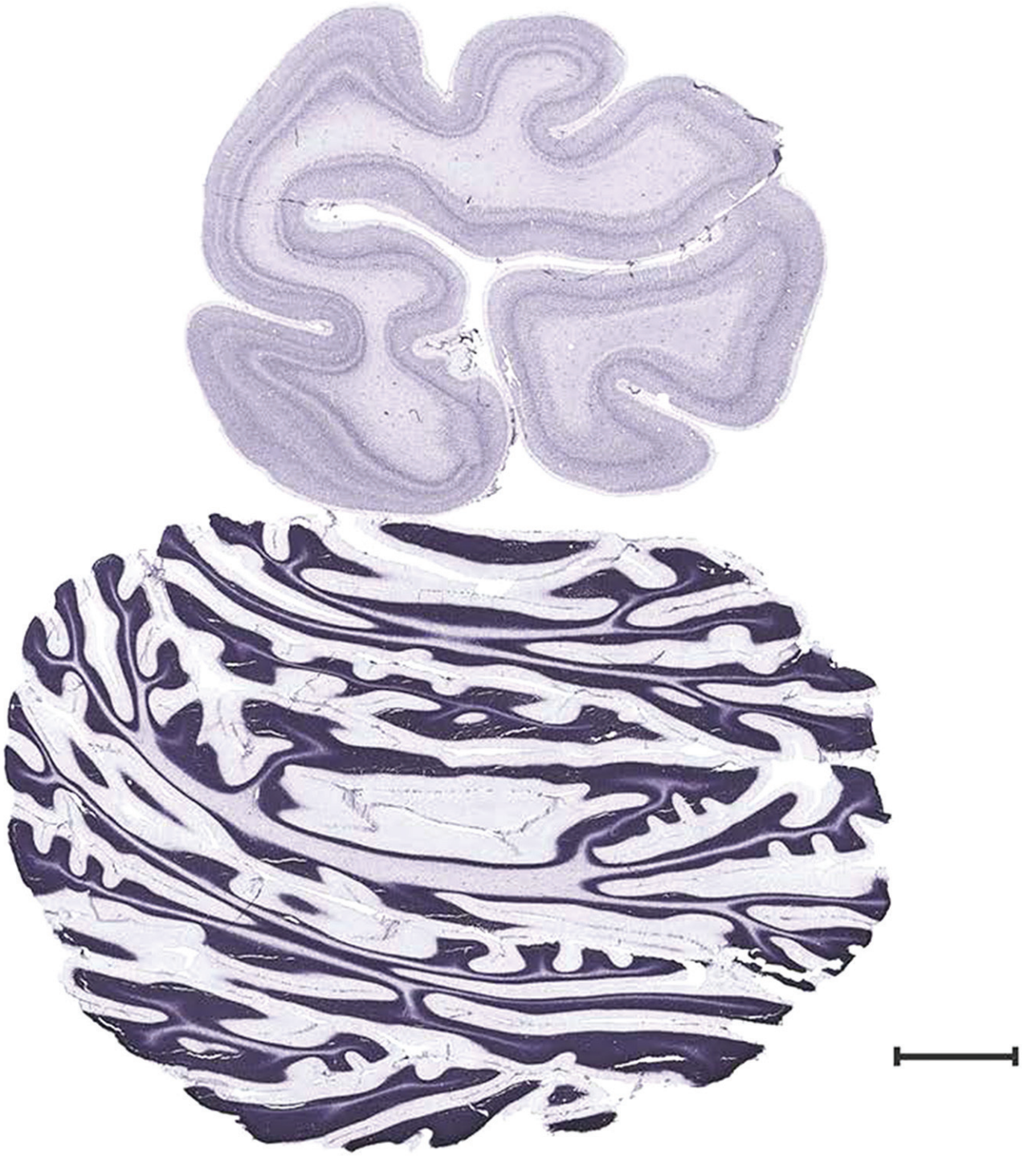

Figure 17. Level 106b (Nissl)

Figure 18. Gross anatomy of the left hemisphere and anteroposterior position of the 76 annotated MRI images shown in Figure 19. Main macroscopic landmarks (sulci and gyri) on dorsal (**A**), lateral (**B**), and ventral (**C**) aspects of the left hemisphere are indicated. The A-P locations (levels 1–76) of the 76 MRI images are marked with black lines 1–76 in B. * and # indicate two corresponding regions. For abbreviations see Table 3. Scale bar = 2 cm in A (applies to A–C).

Figure 19. MRI and DWI plates from the same brain. Left column: Seventy-six sequential 7T MRI slices from the same left hemisphere as the atlas shown in Figure 17 were annotated according to the atlas plates in Figure 17. The interval between each slice is 2 mm. The MRI images were annotated for easily predicted and/or identified structures through correspondence to the annotated histological atlas. Several clearly delineated fiber tracts are annotated as well, including the optic radiation ("or" at levels 42–69) and somatosensory radiation ('sr" at levels 38–46). For abbreviations see Table 3. Right column: Top panel shows colorized fractional anisotropy (FA) maps of the corresponding plane of section in the DWI dataset, representing the primary eigenvectors of the diffusion tensor data overlaid on the FA map. Bottom panel shows tractography images created in TrackVis showing all tracts passing through the represented plane of section (90% of tracts omitted with only tracts longer than 20 mm displayed). Scale bars = 5 mm.

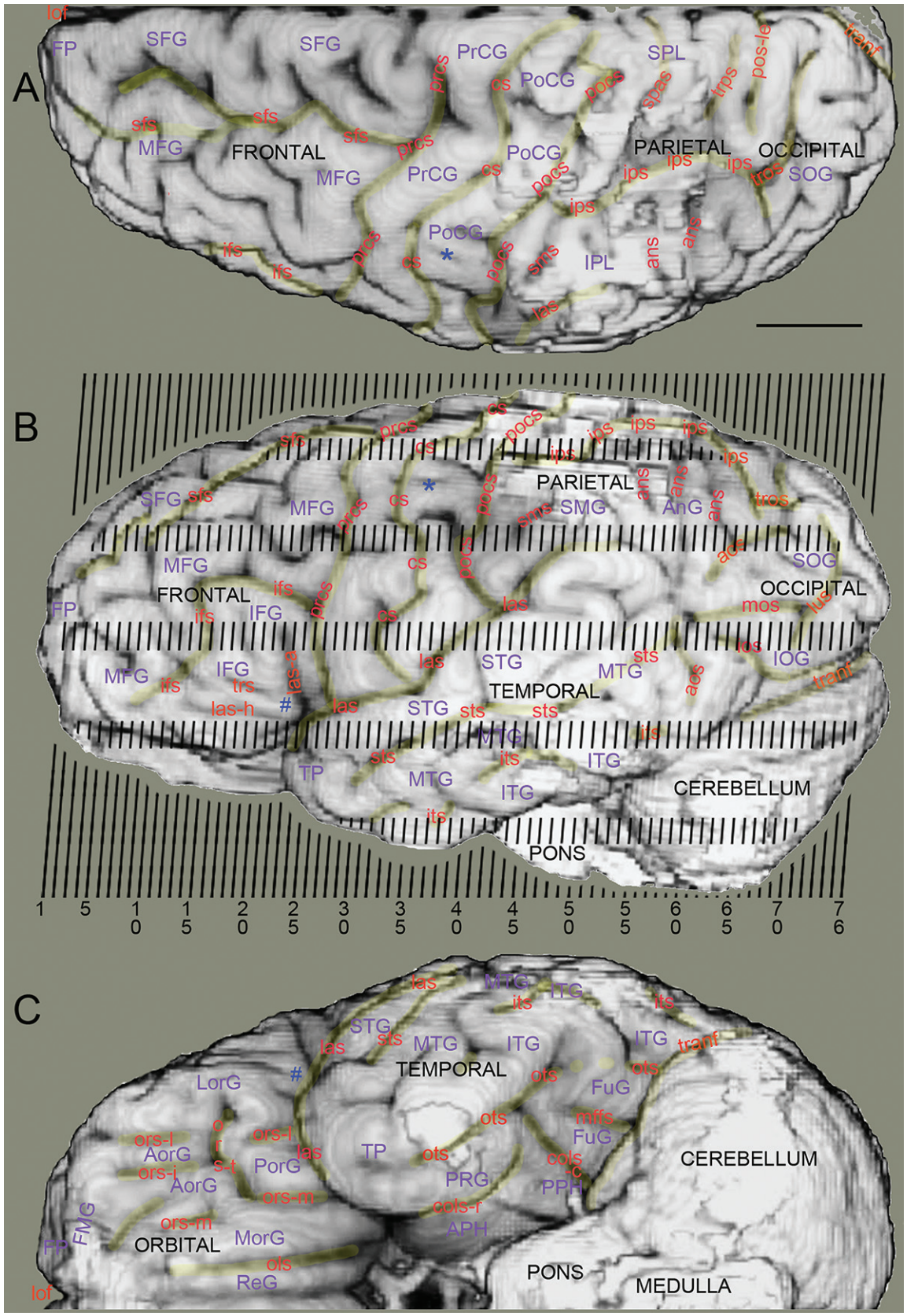
A
lof
FP
SFG
SFG
PrCG
SPL
pos-le
tranf
prcs
cs
PoCG
pocs
spas
trps
sfs
sfs
MFG
FRONTAL
sfs
prcs
PoCG
PARIETAL
OCCIPITAL
MFG
PrCG
cs
pocs
ips
ips
ips
tros
SOG
ips
PoCG
ifs
ifs
prcs
cs
*
pocs
sms
IPL
ans
ans
las
B
cs
prcs
pocs
ips
ips
ips
sfs
ds
ips
ips
PARIETAL
*
ans
ans
SFG
sfs
MFG
prcs
cs
pocs
sms
SMG
AnG
ans
tros
acs
SOG
MFG
cs
pocs
OCCIPITAL
FRONTAL
ifs
prcs
mos
tus
FP
ifs
IFG
cs
las
las
STG
sts
MTG
tos
IOG
MFG
IFG
las-a
las
STG
TEMPORAL
acs
tranf
ifs
trs
las-h
#
las
STG
sts
sts
MTG
its
its
sts
its
ITG
TP
MTG
ITG
CEREBELLUM
its
PONS
1 5 1 0 1 5 2 0 2 5 3 0 3 5 4 0 4 5 5 0 5 5 6 0 6 5 7 0 7 6
C
las
MTG
ITG
its
its
STG
las
sts
MTG
ITG
ITG
tranf
TEMPORAL
#
ots
ots
LorG
FuG
ots
mifs
FuG
ors-l
o
r
s-t
ors-l
AorG
las
TP
ots
cols
-c
CEREBELLUM
ors-l
AorG
PorG
PRG
PPH
ors-m
cols-r
FMG
ors-m
APH
FP
ORBITAL
MorG
ols
PONS
MEDULLA
lof
ReG

Figure 18.

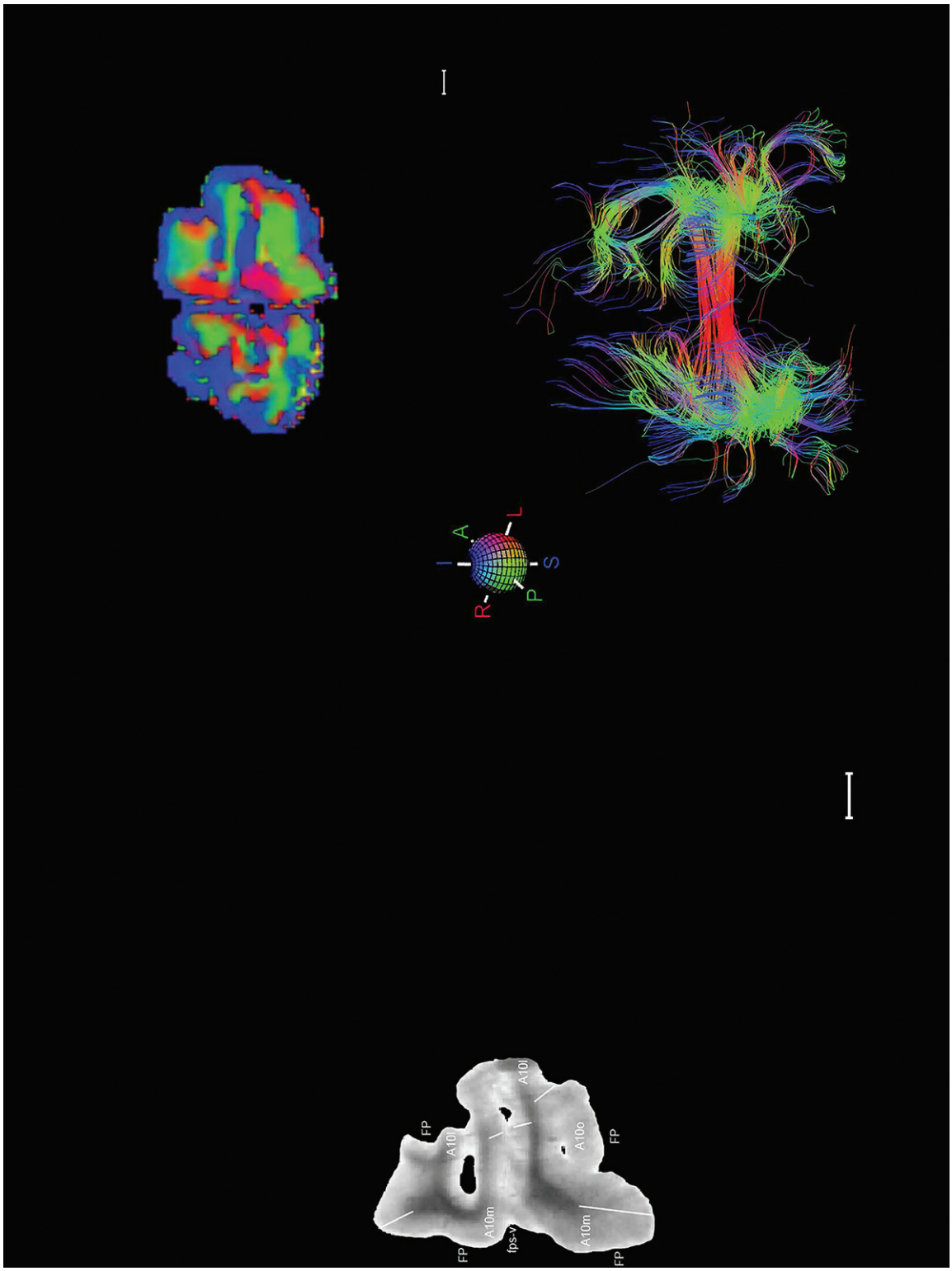

Figure 19. Level 01

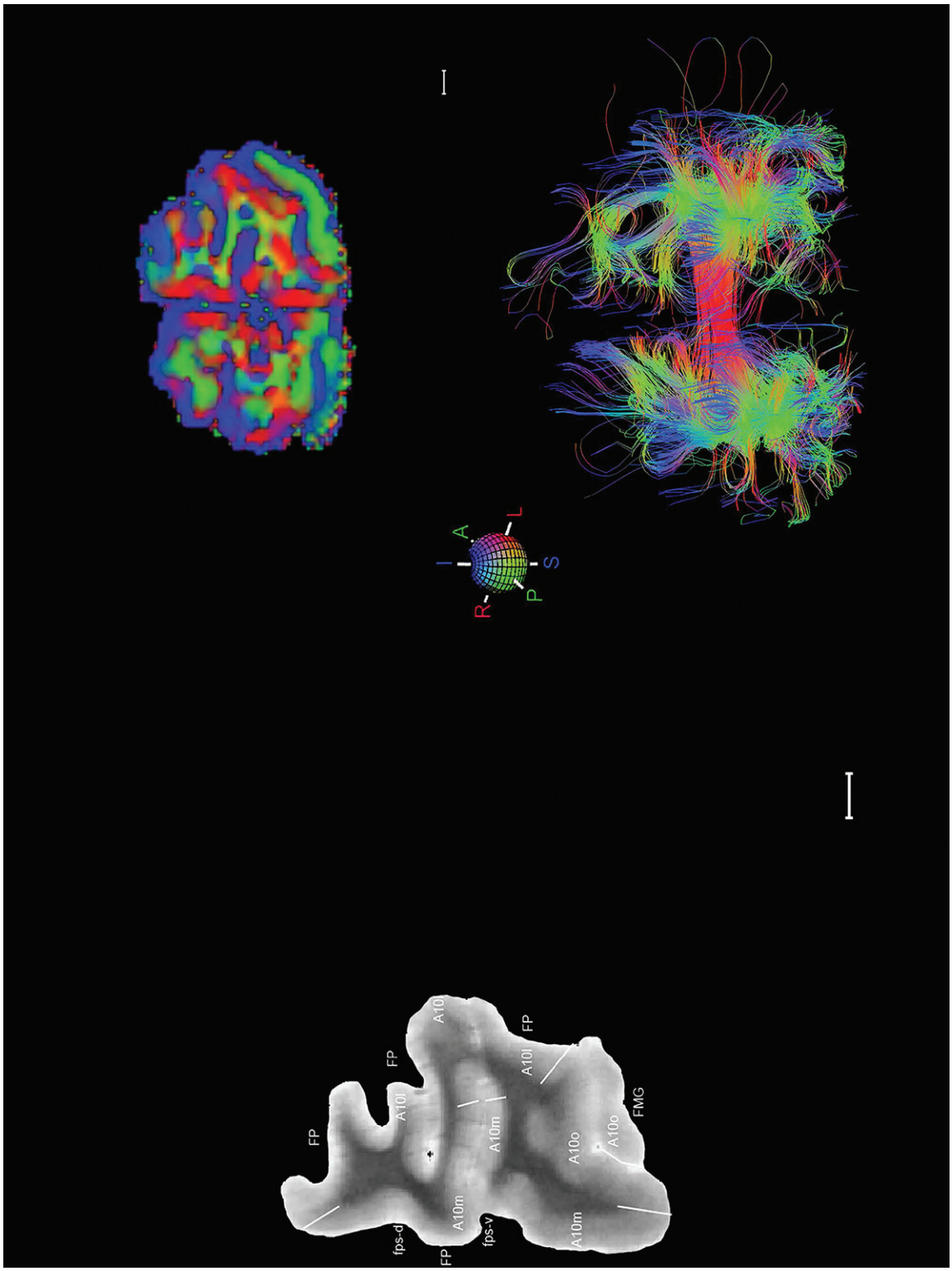

Figure 19. Level 02

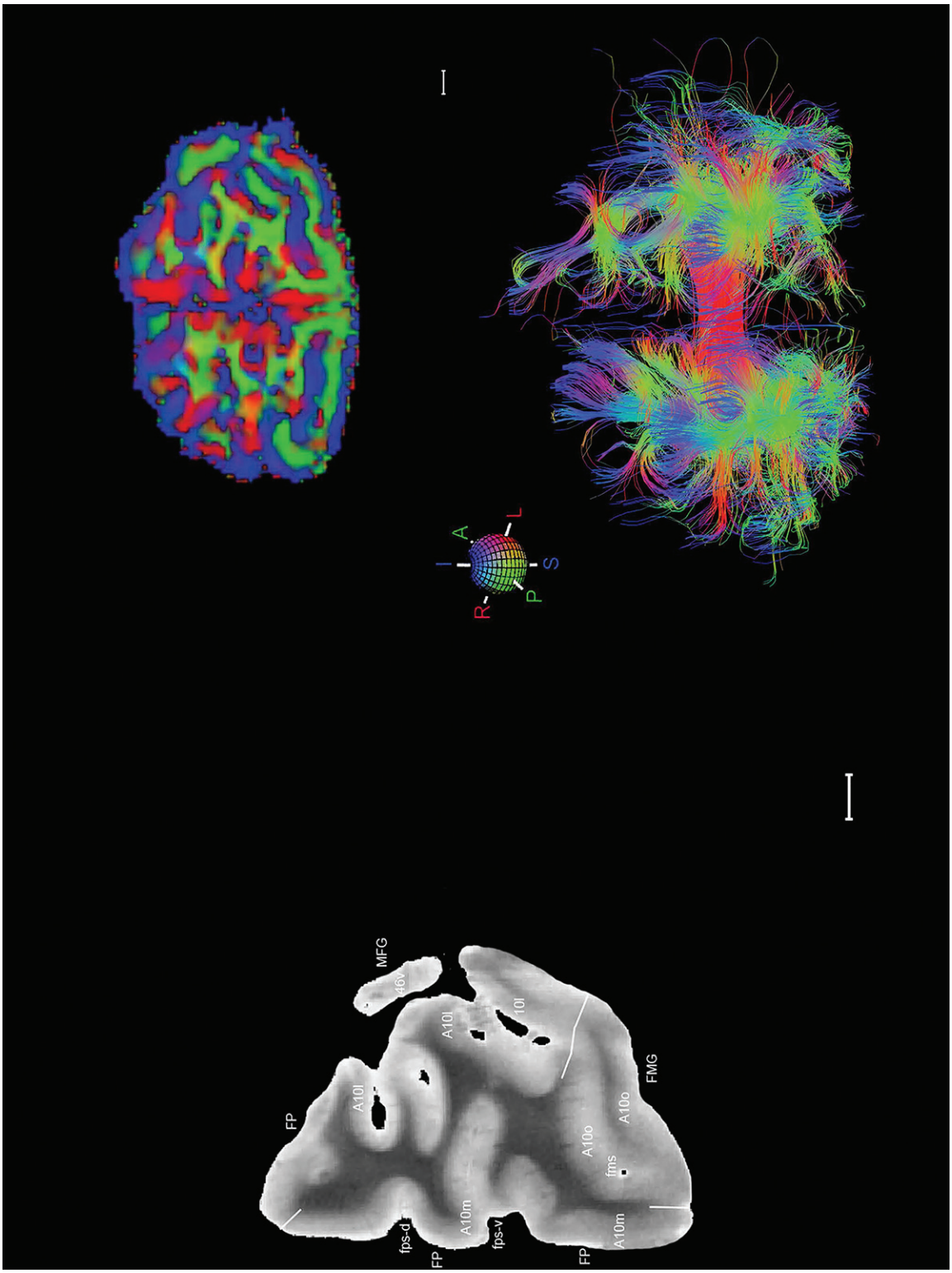

Figure 19. Level 03

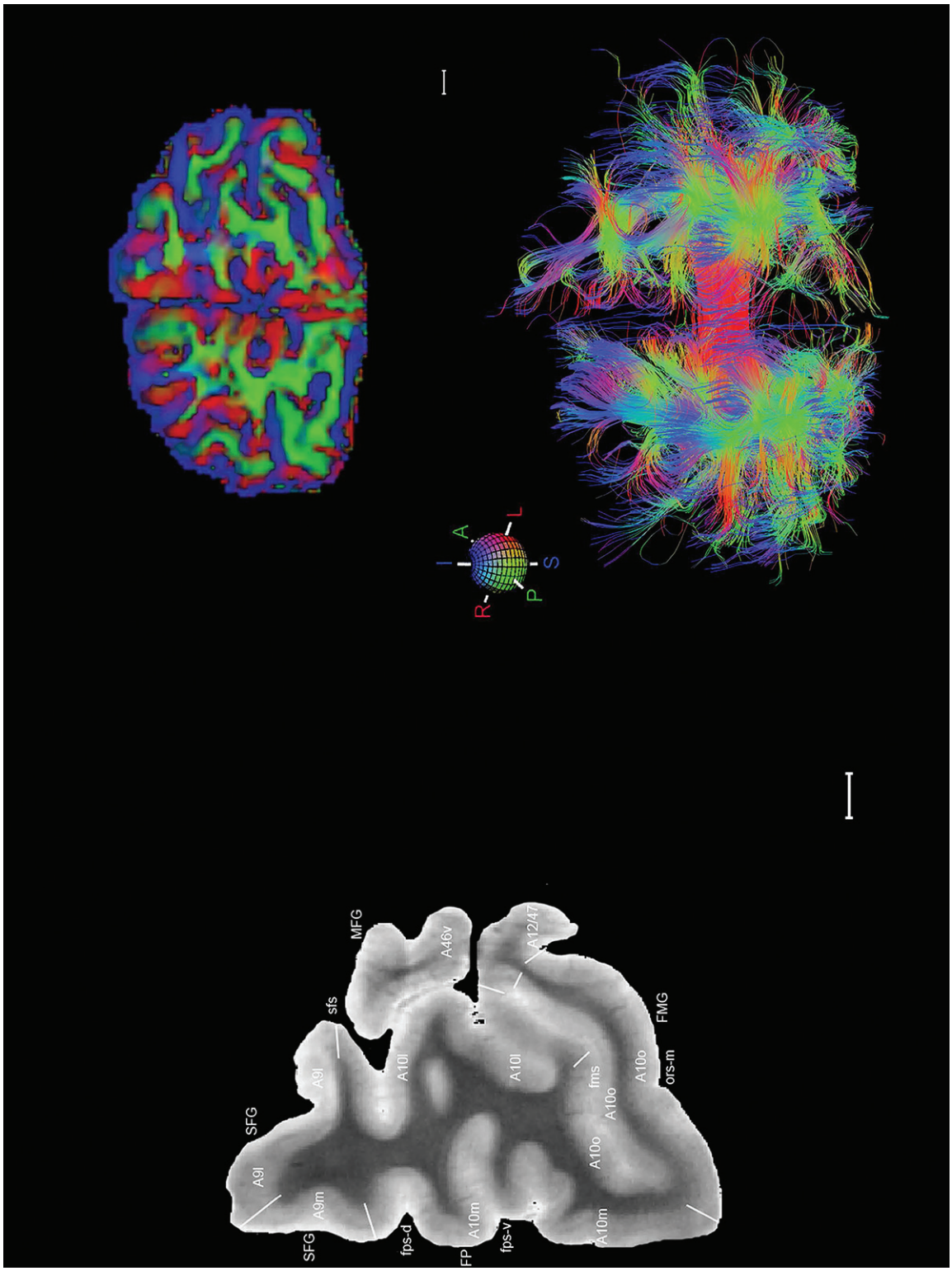

Figure 19. Level 04

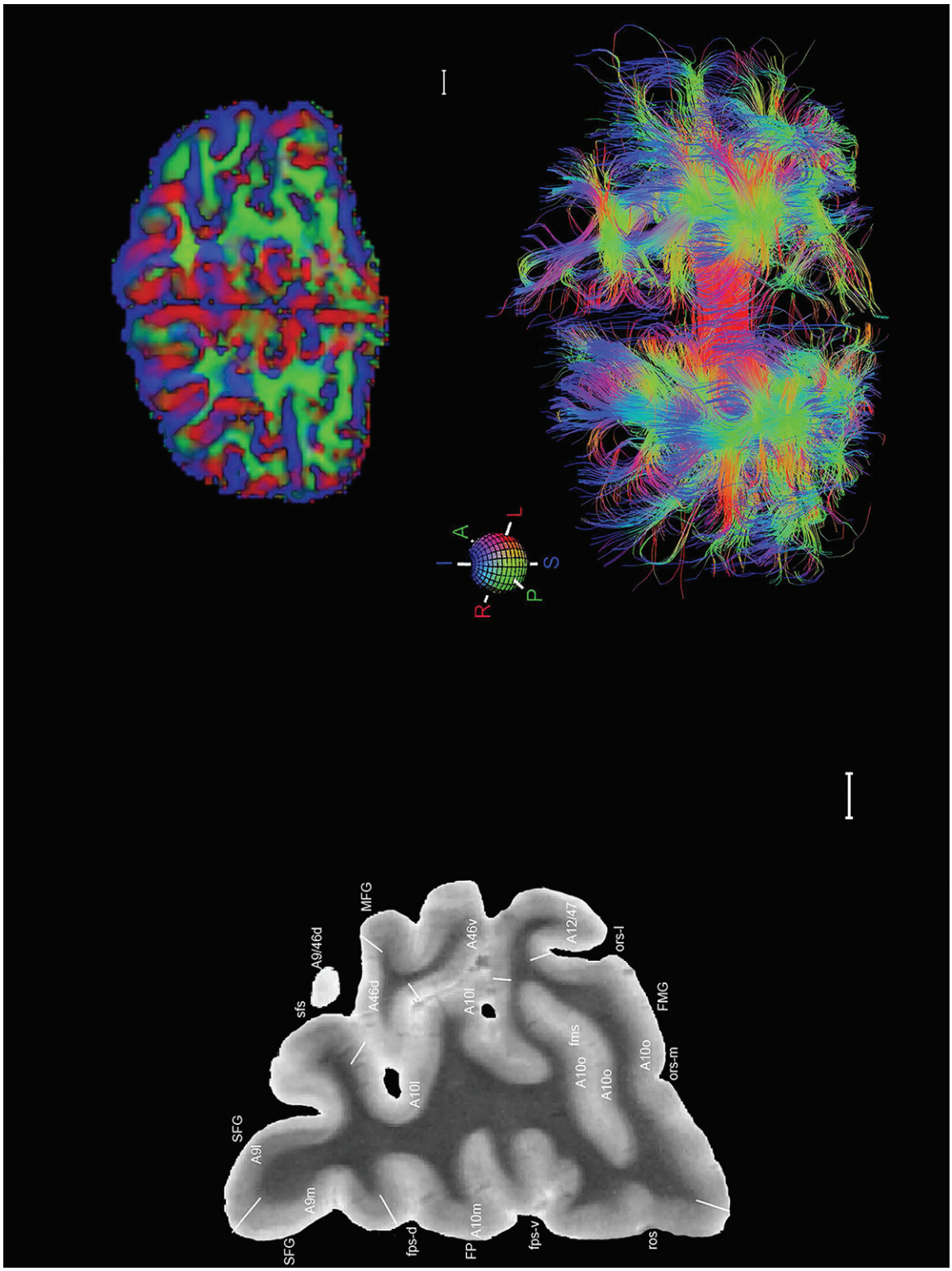

Figure 19. Level 05

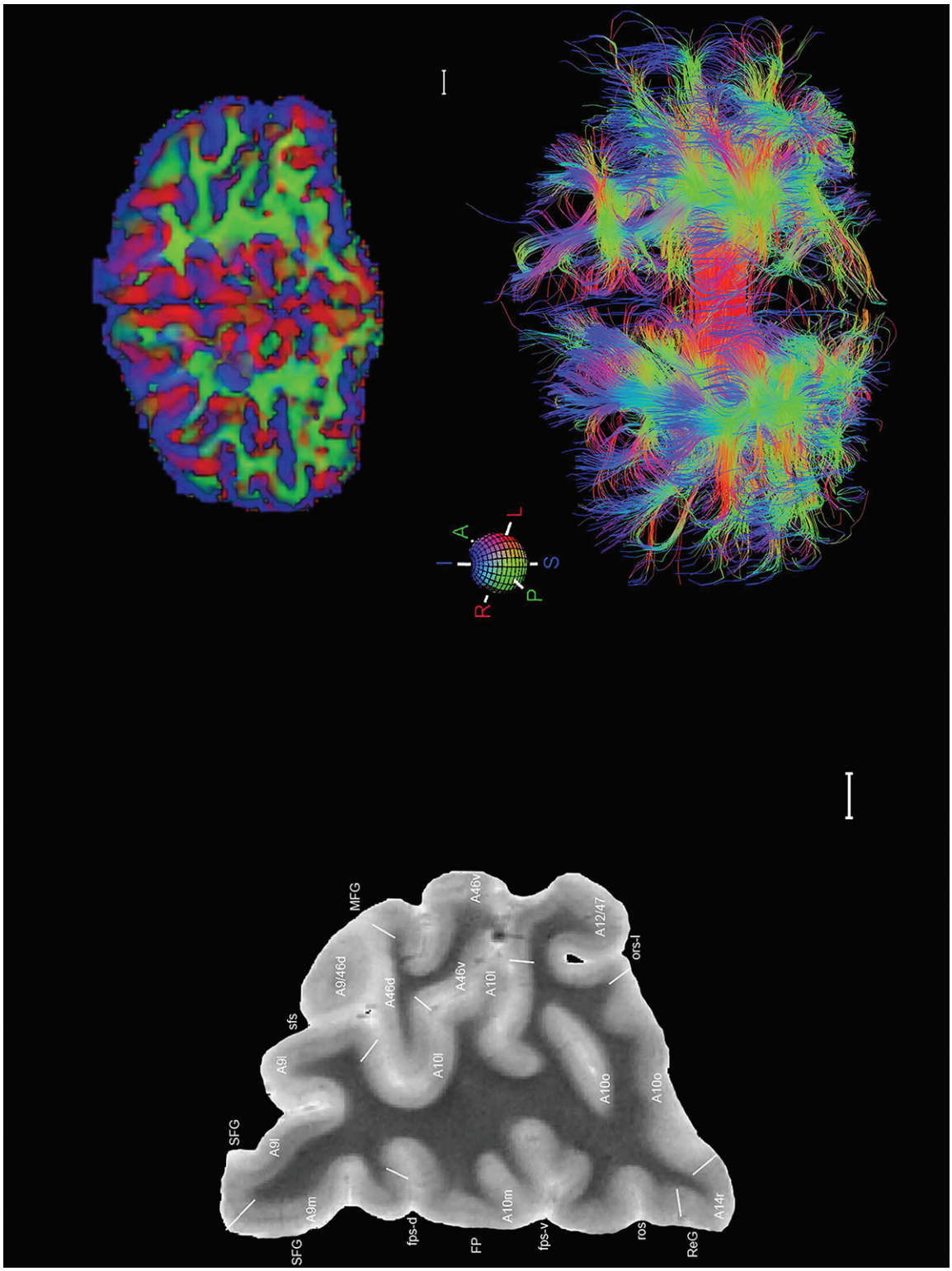

Figure 19. Level 06

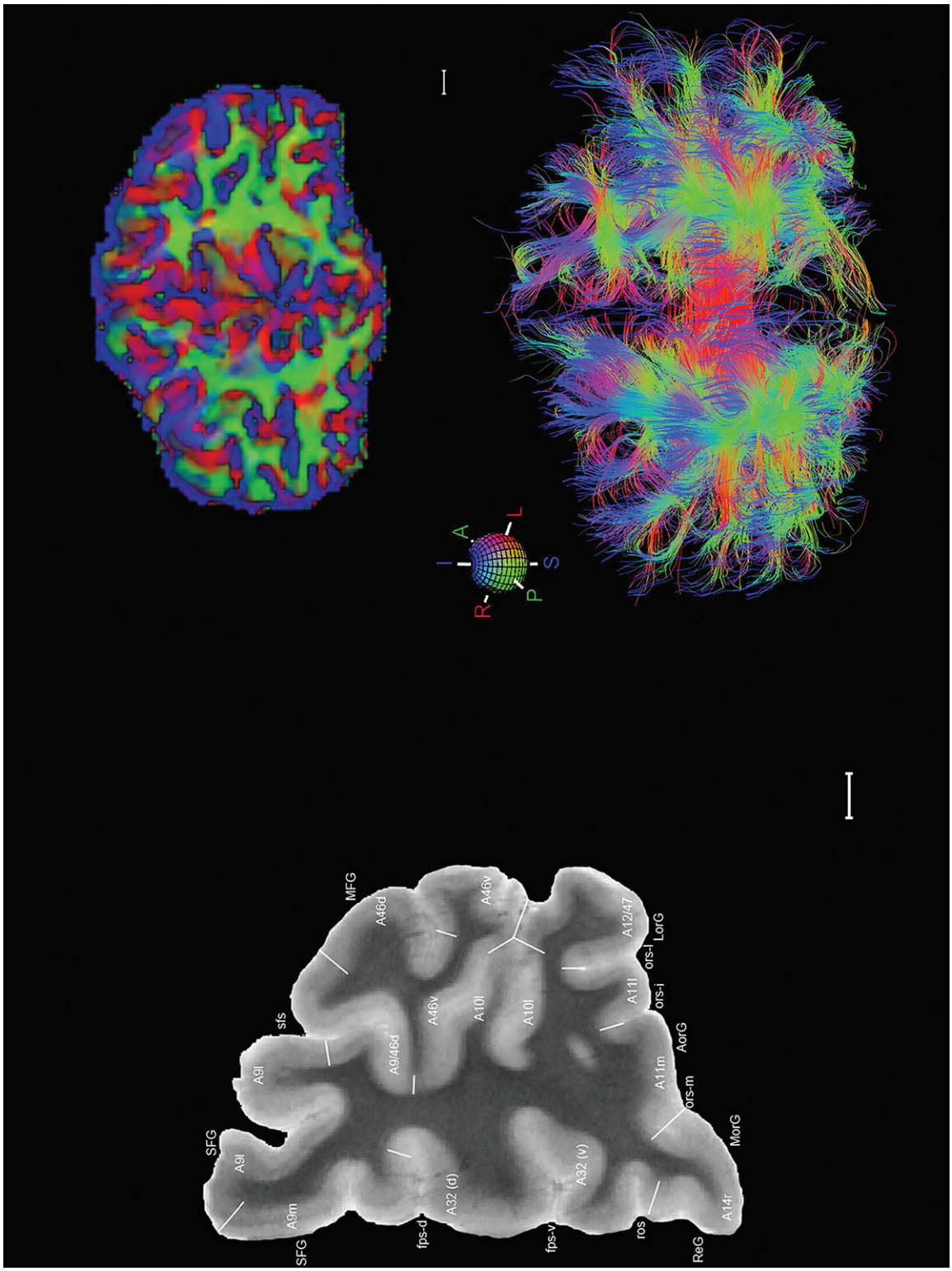

Figure 19. Level 07

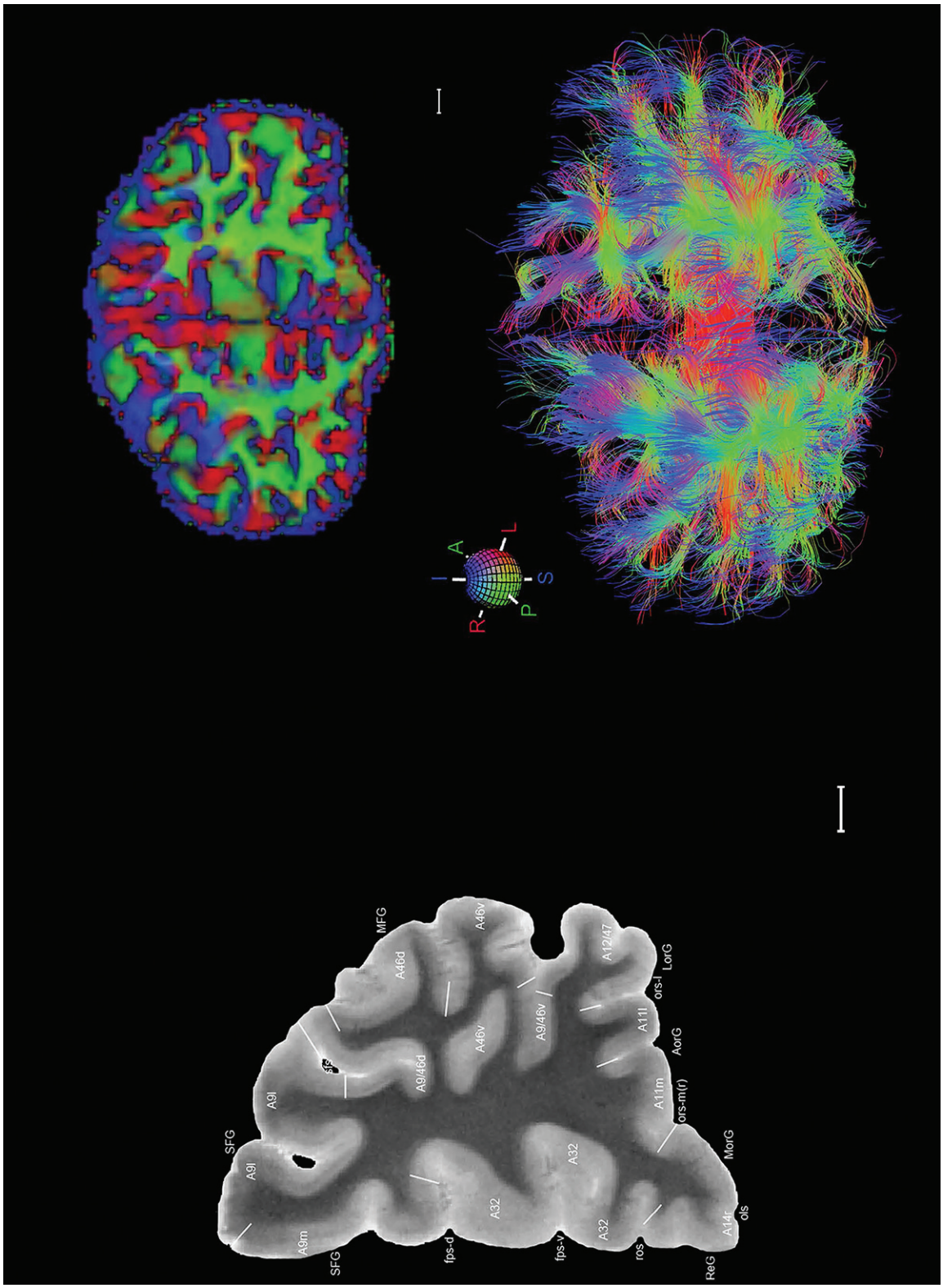

Figure 19. Level 08

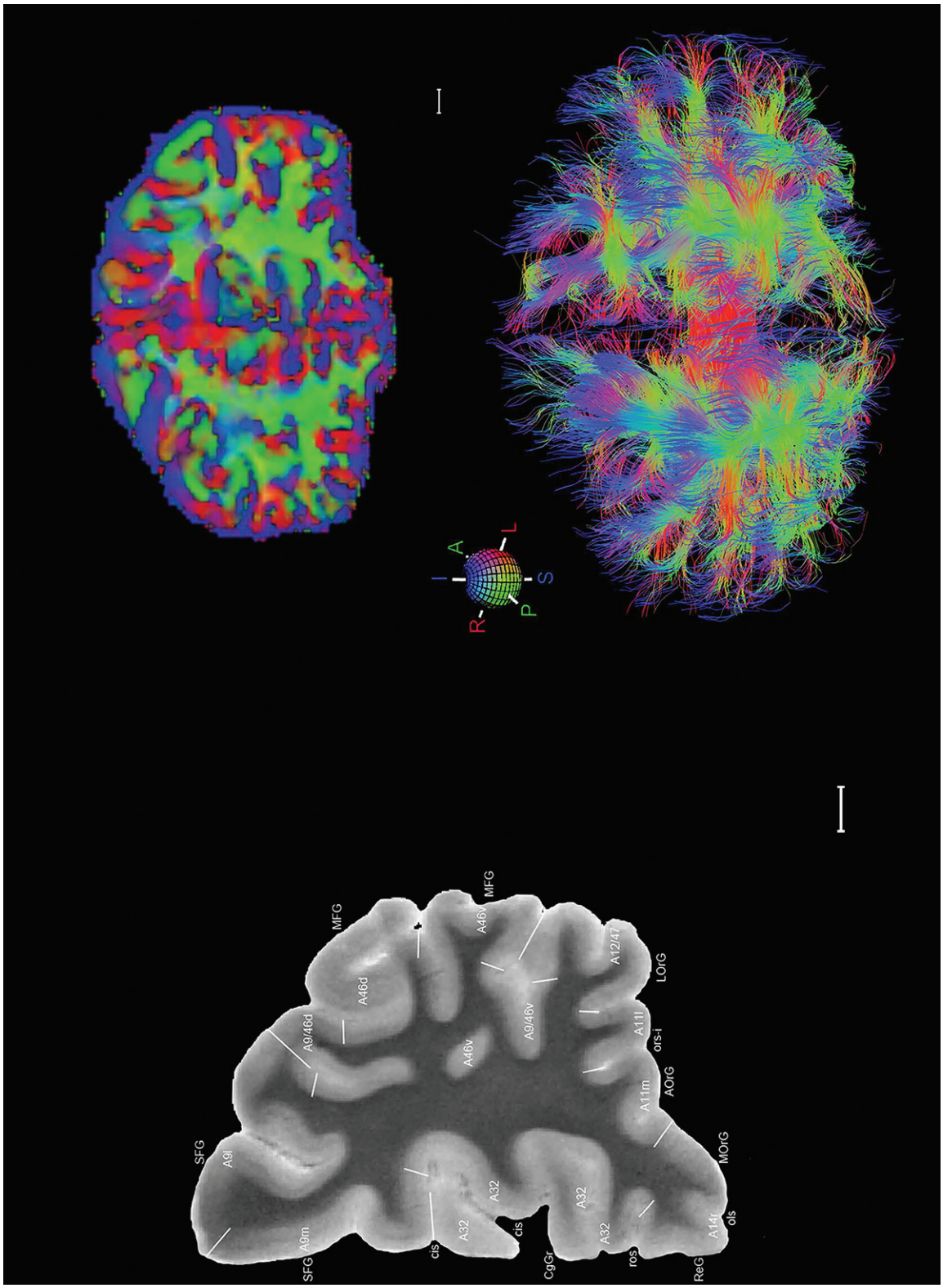

Figure 19. Level 09

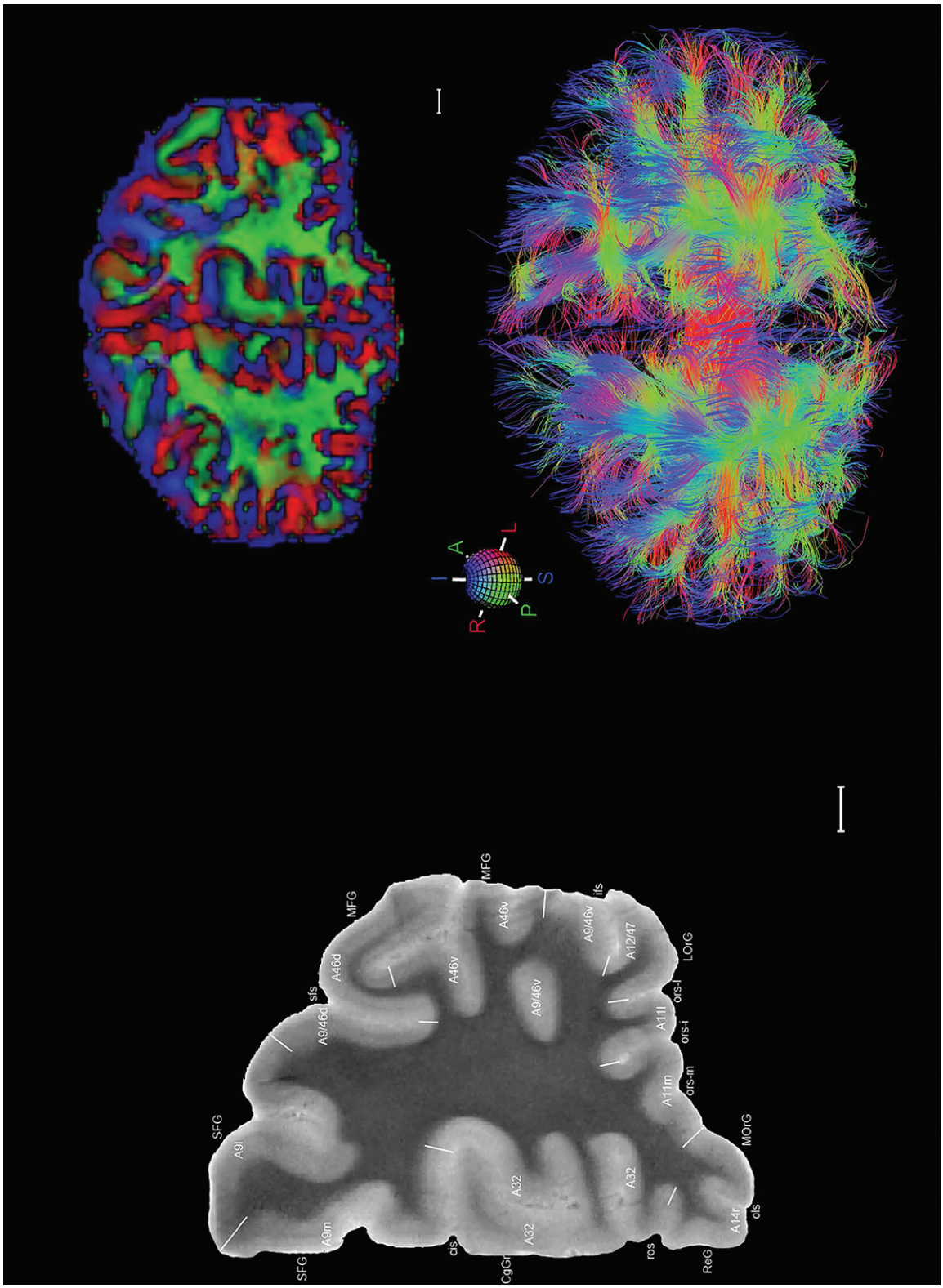

Figure 19. Level 10

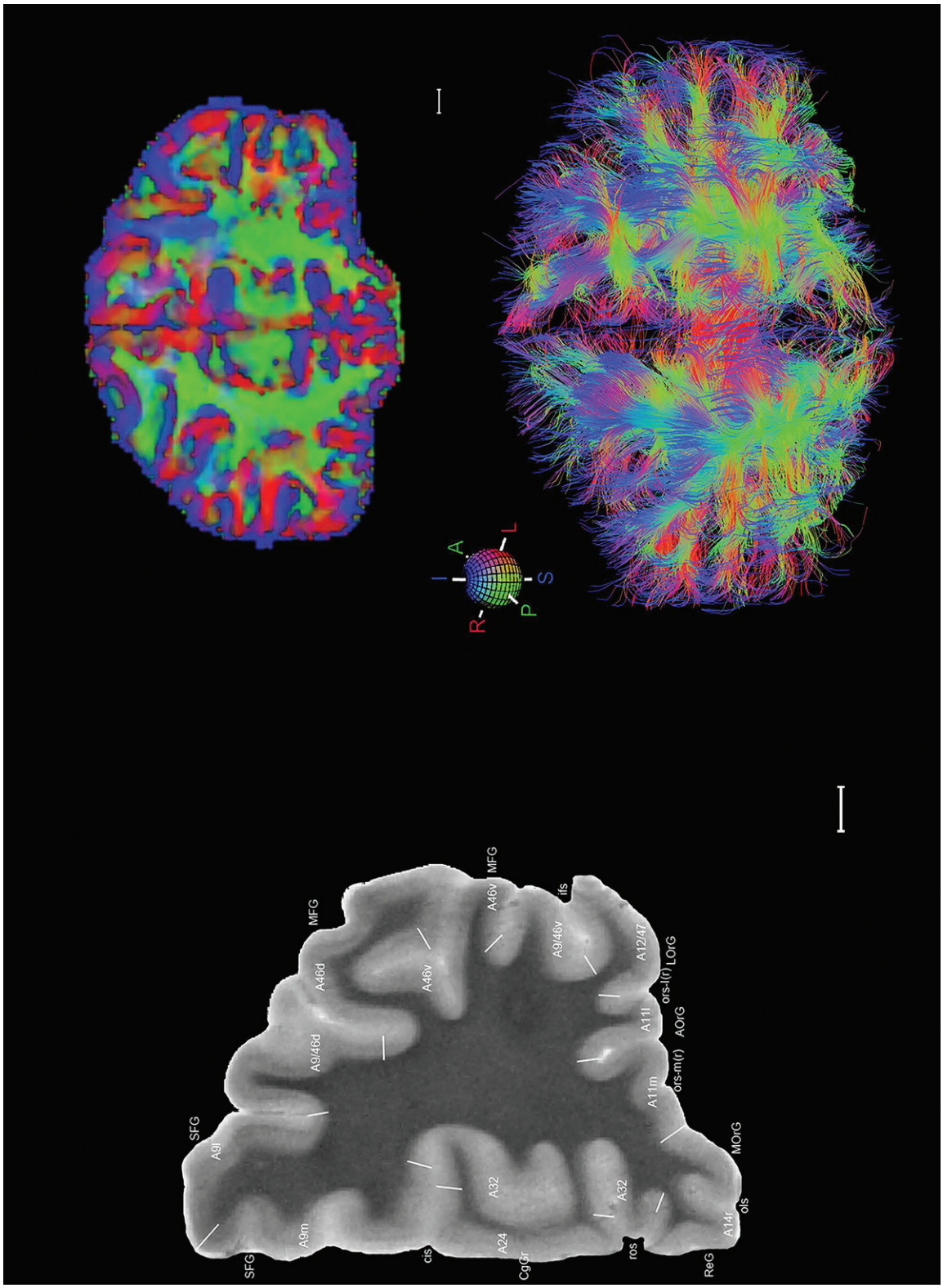

Figure 19. Level 11

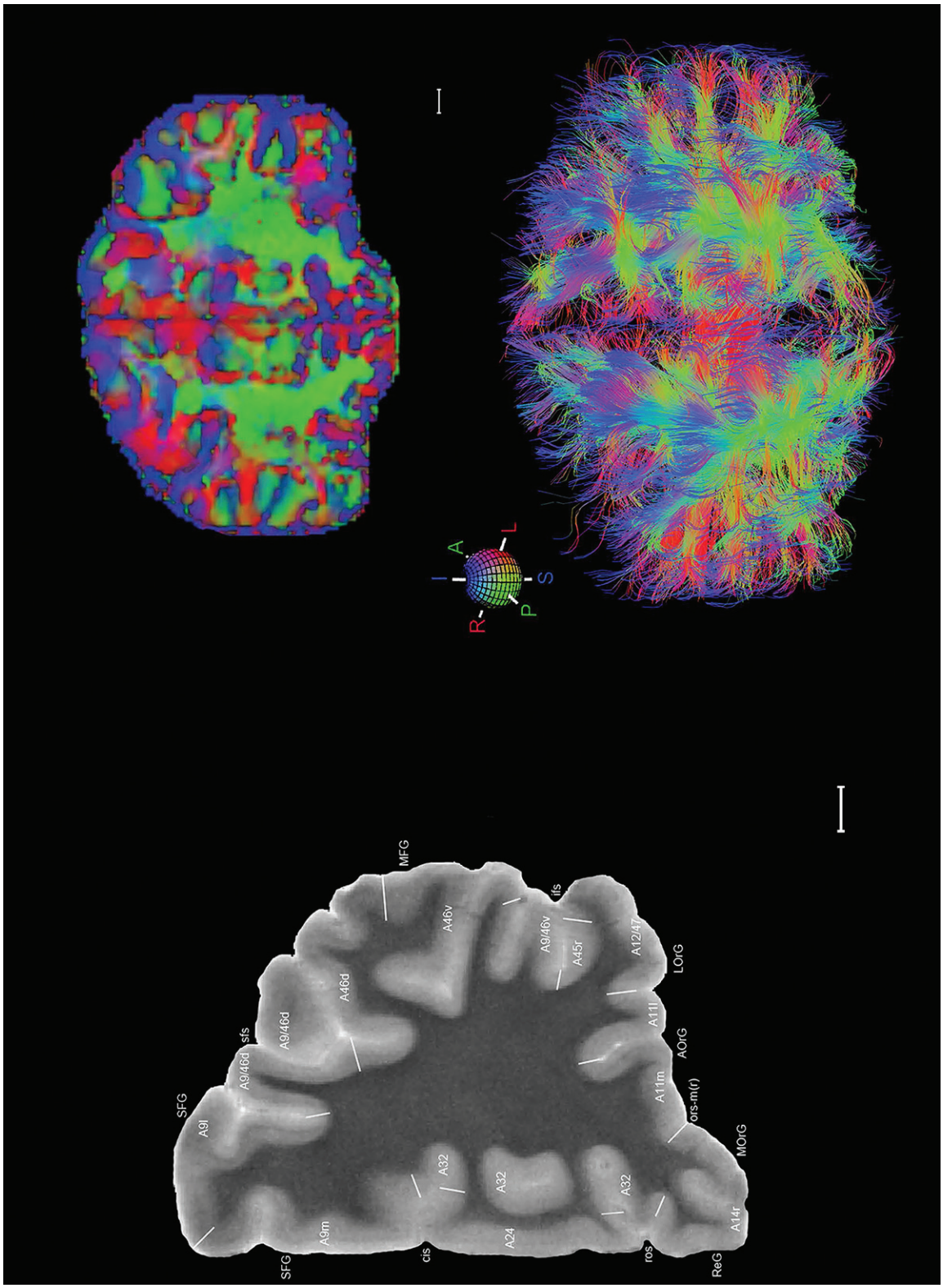

Figure 19. Level 12

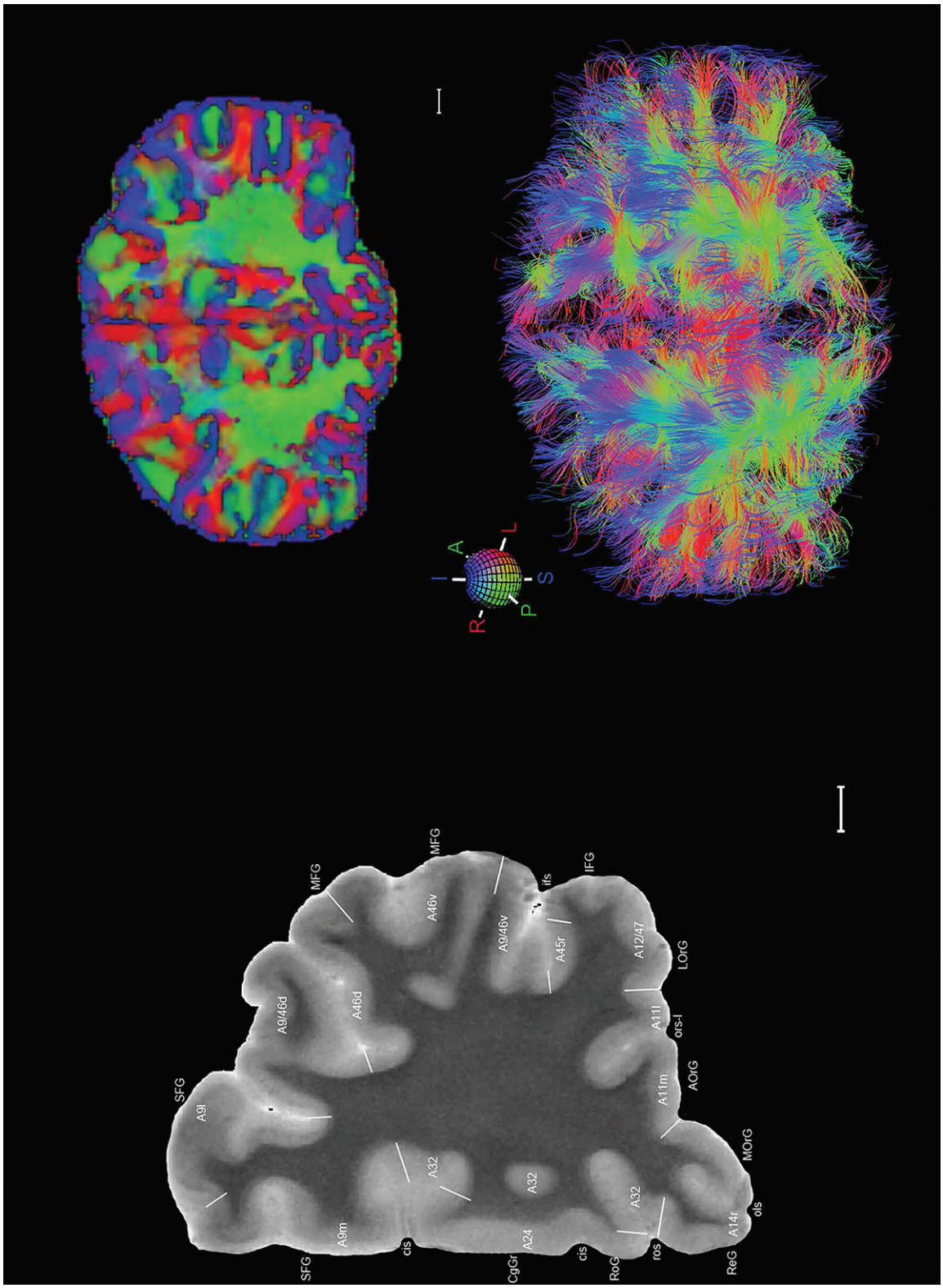

Figure 19. Level 13

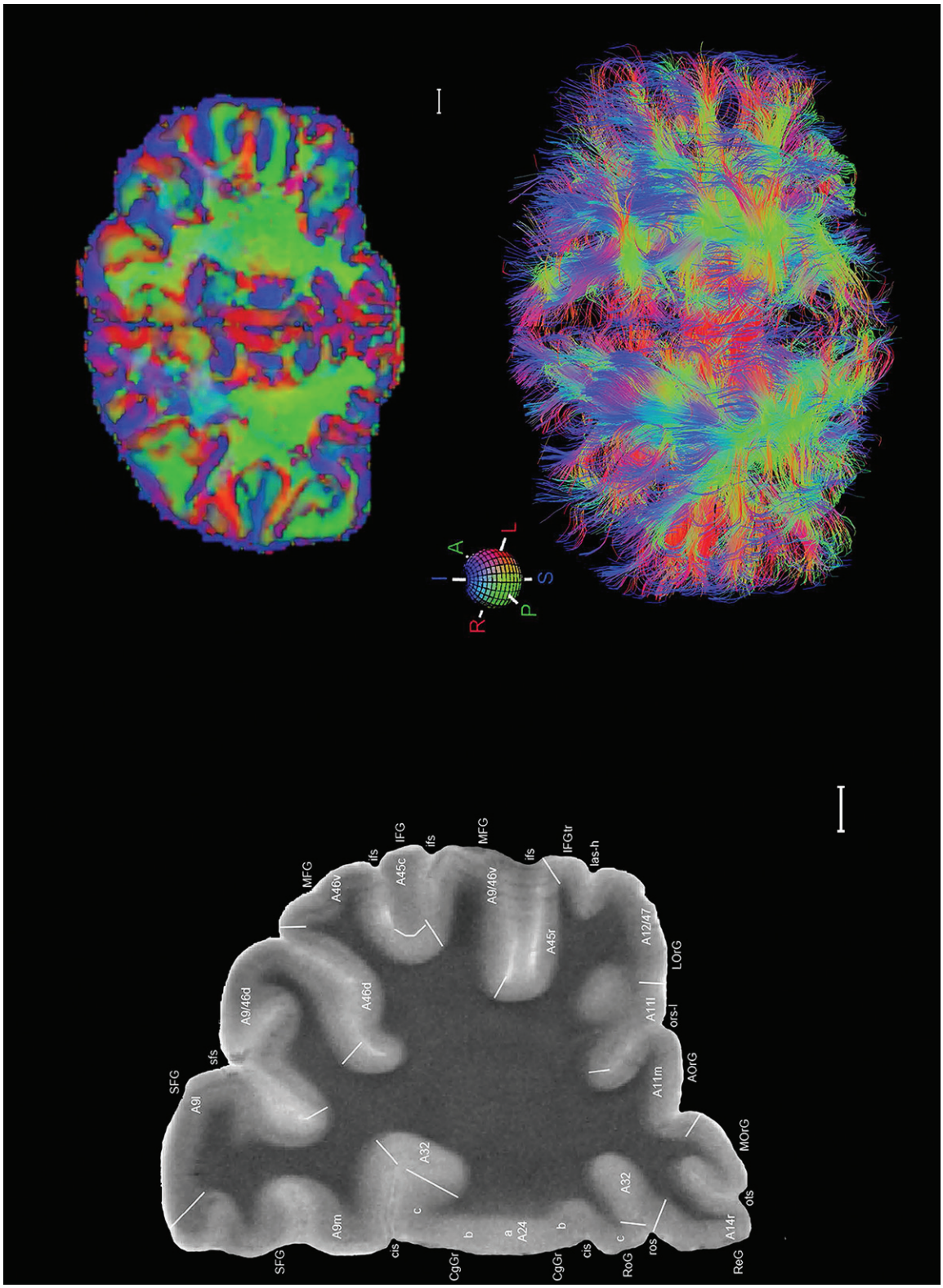

Figure 19. Level 14

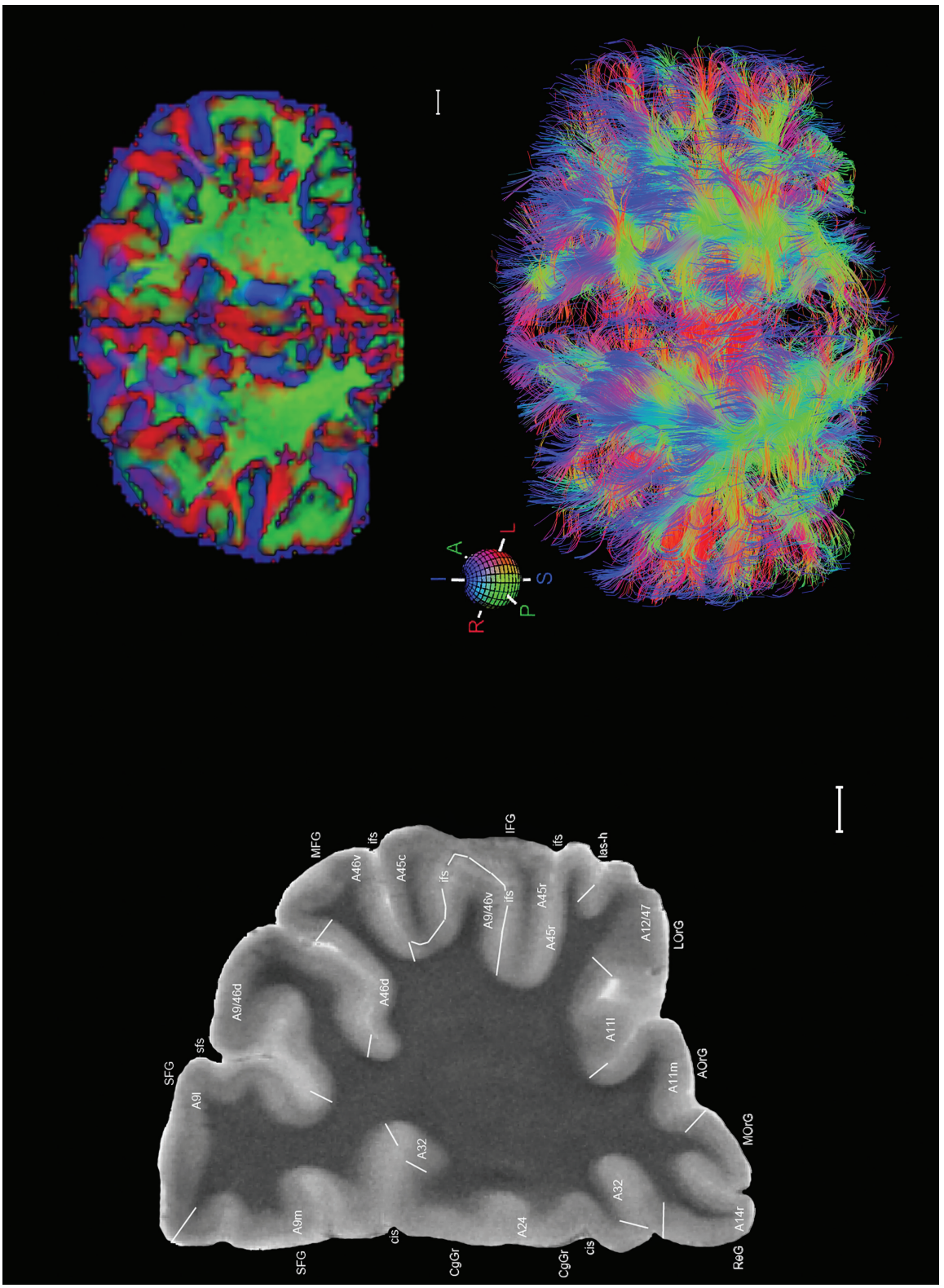

Figure 19. Level 15

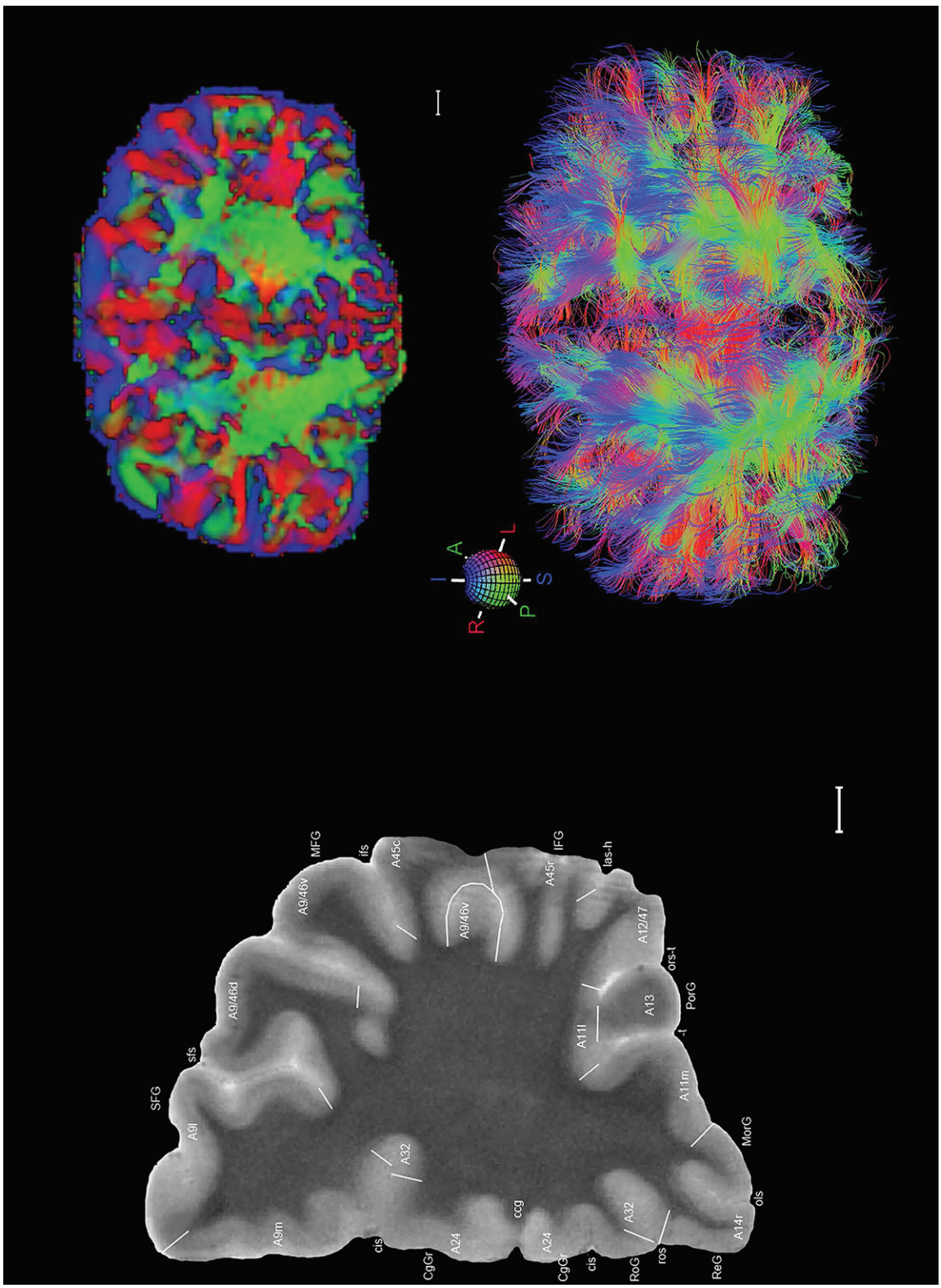

Figure 19. Level 16

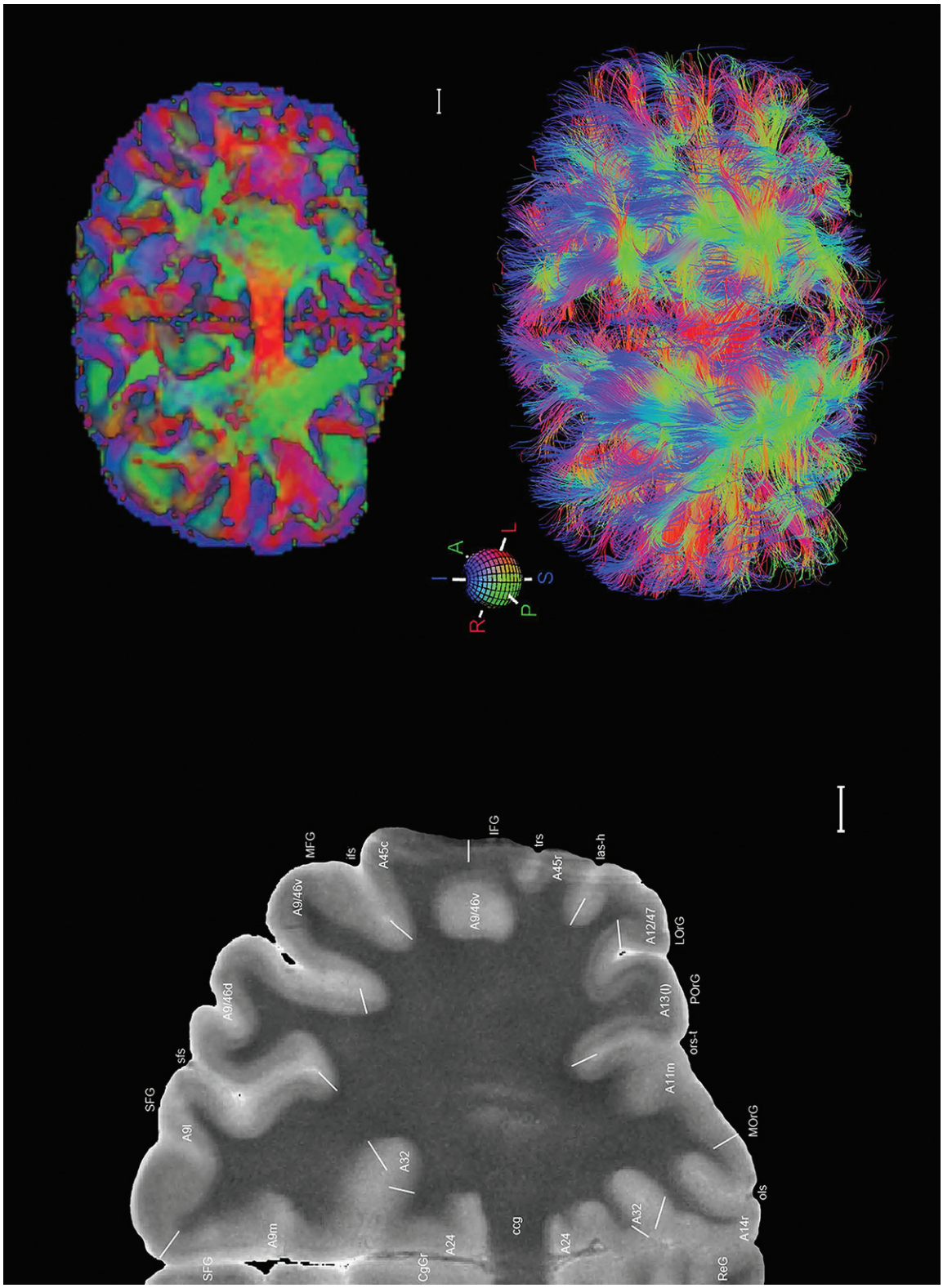

Figure 19. Level 17

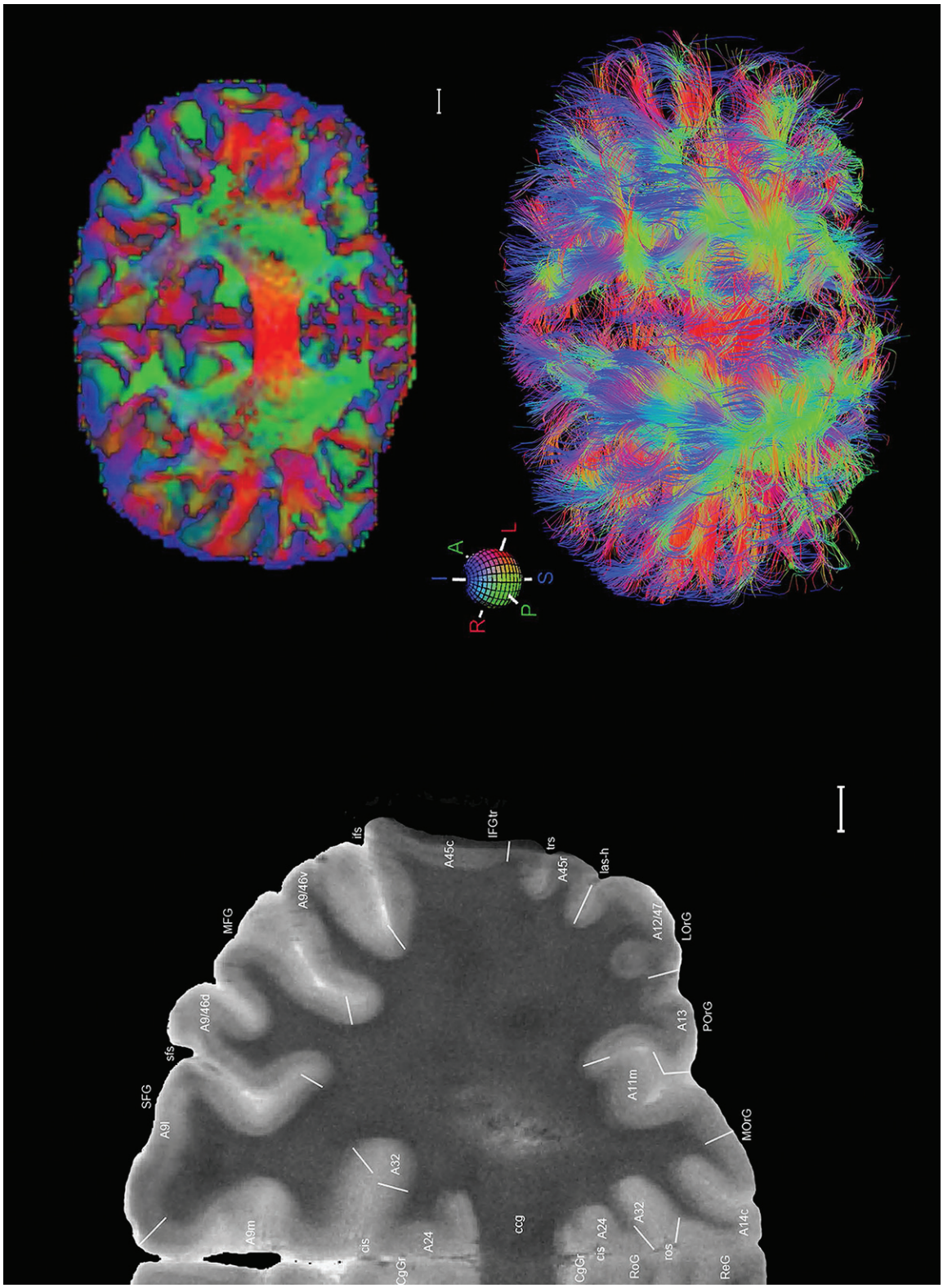

Figure 19. Level 18

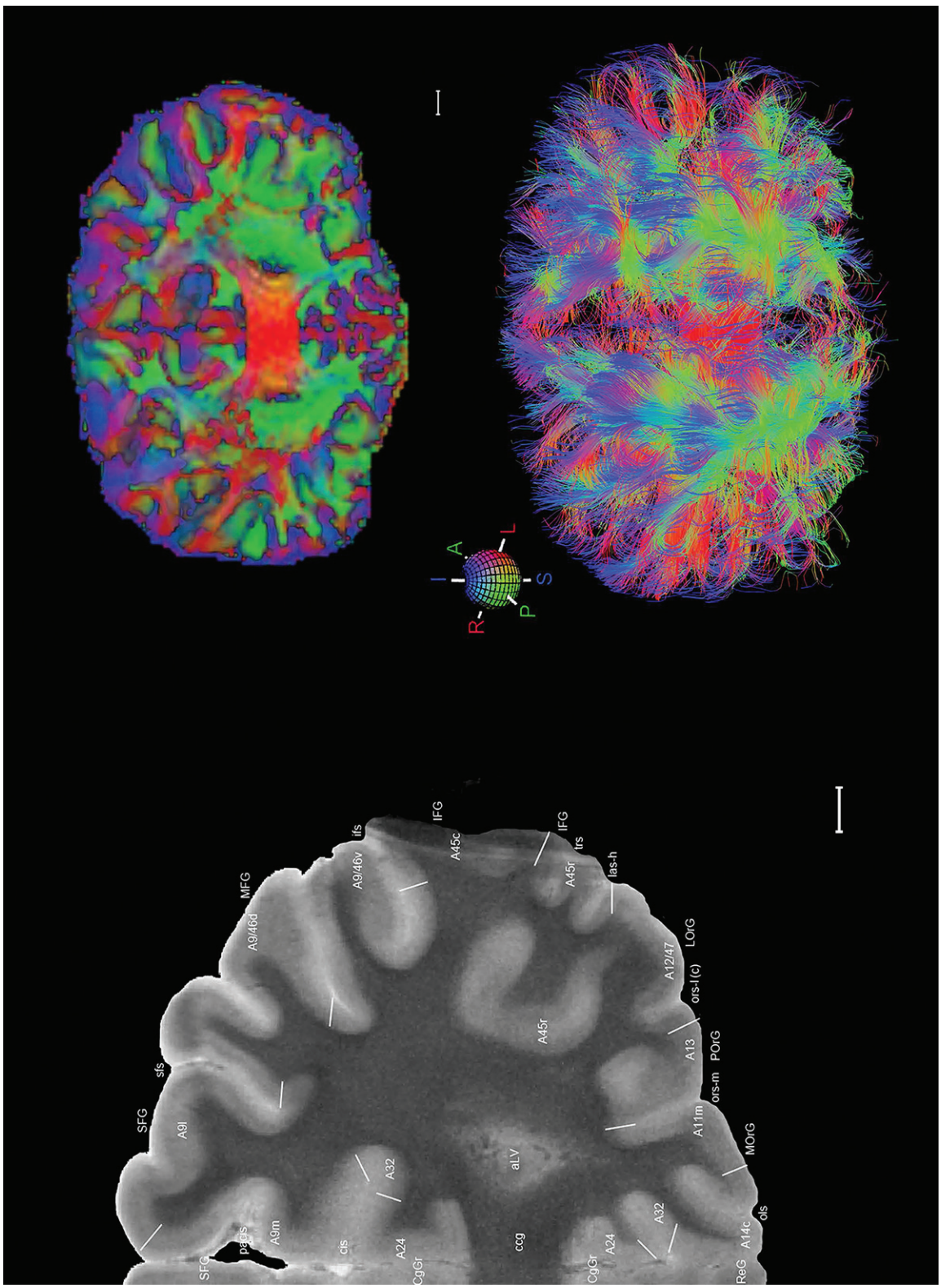

Figure 19. Level 19

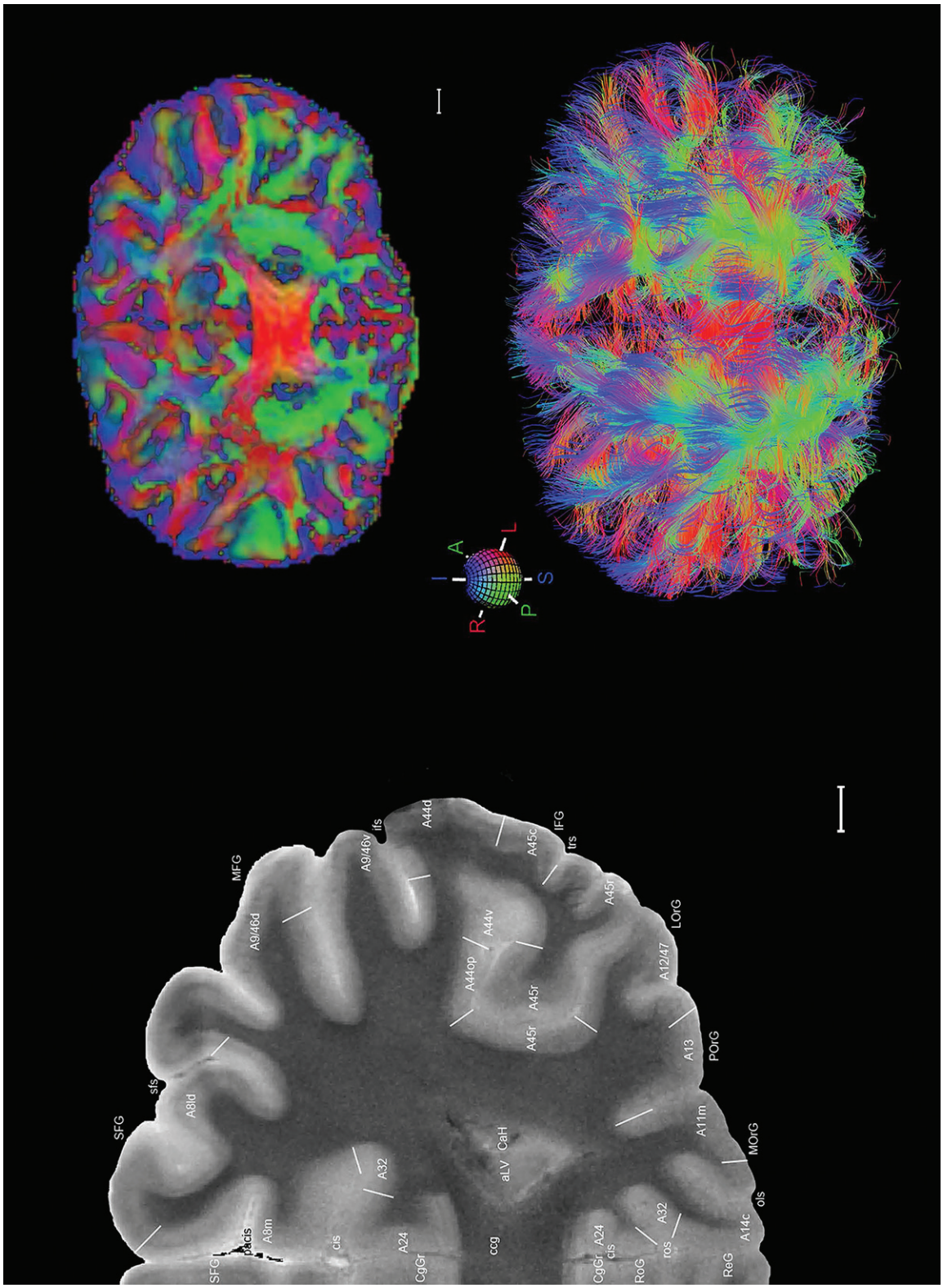

Figure 19. Level 20

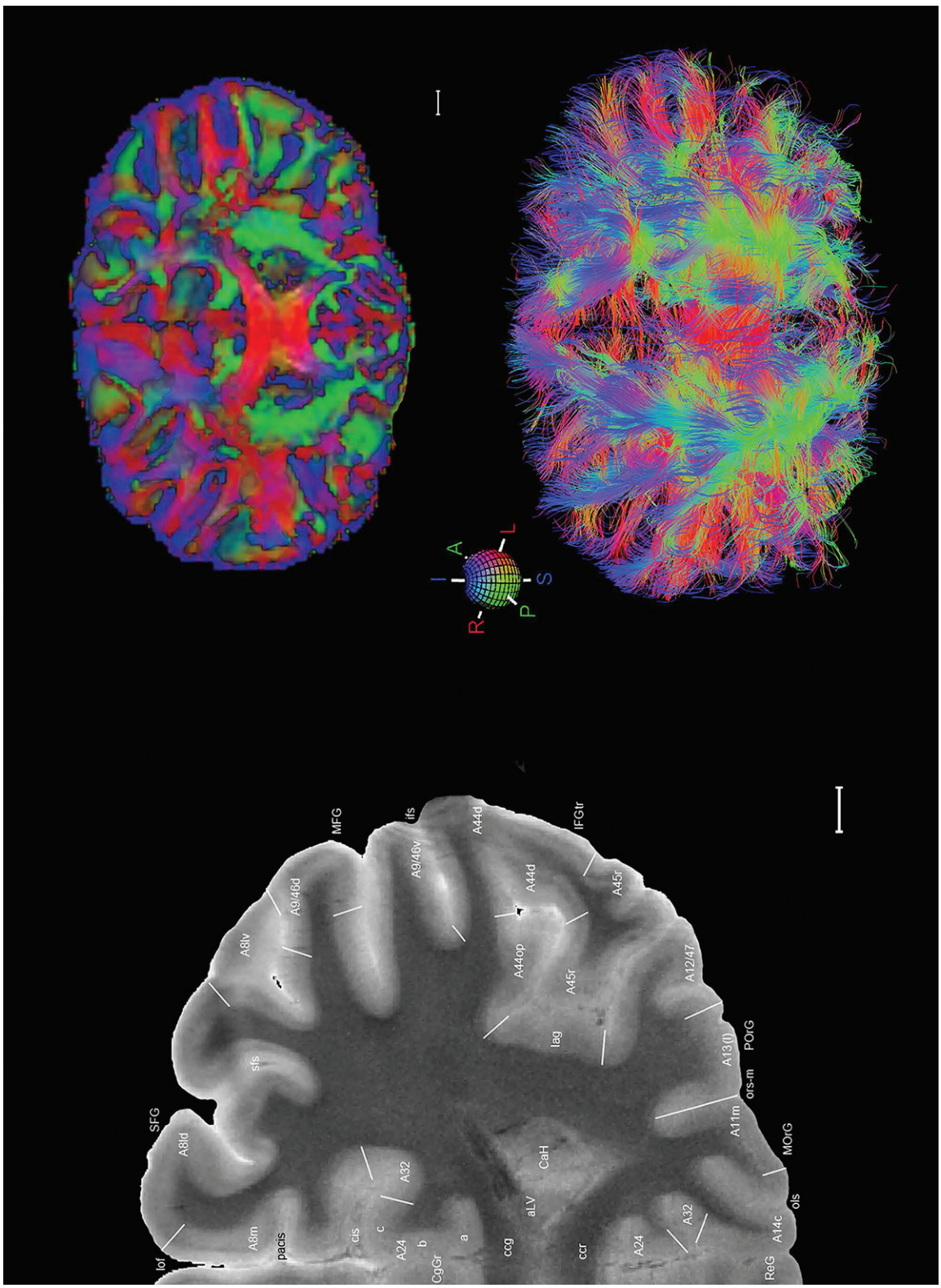

Figure 19. Level 21

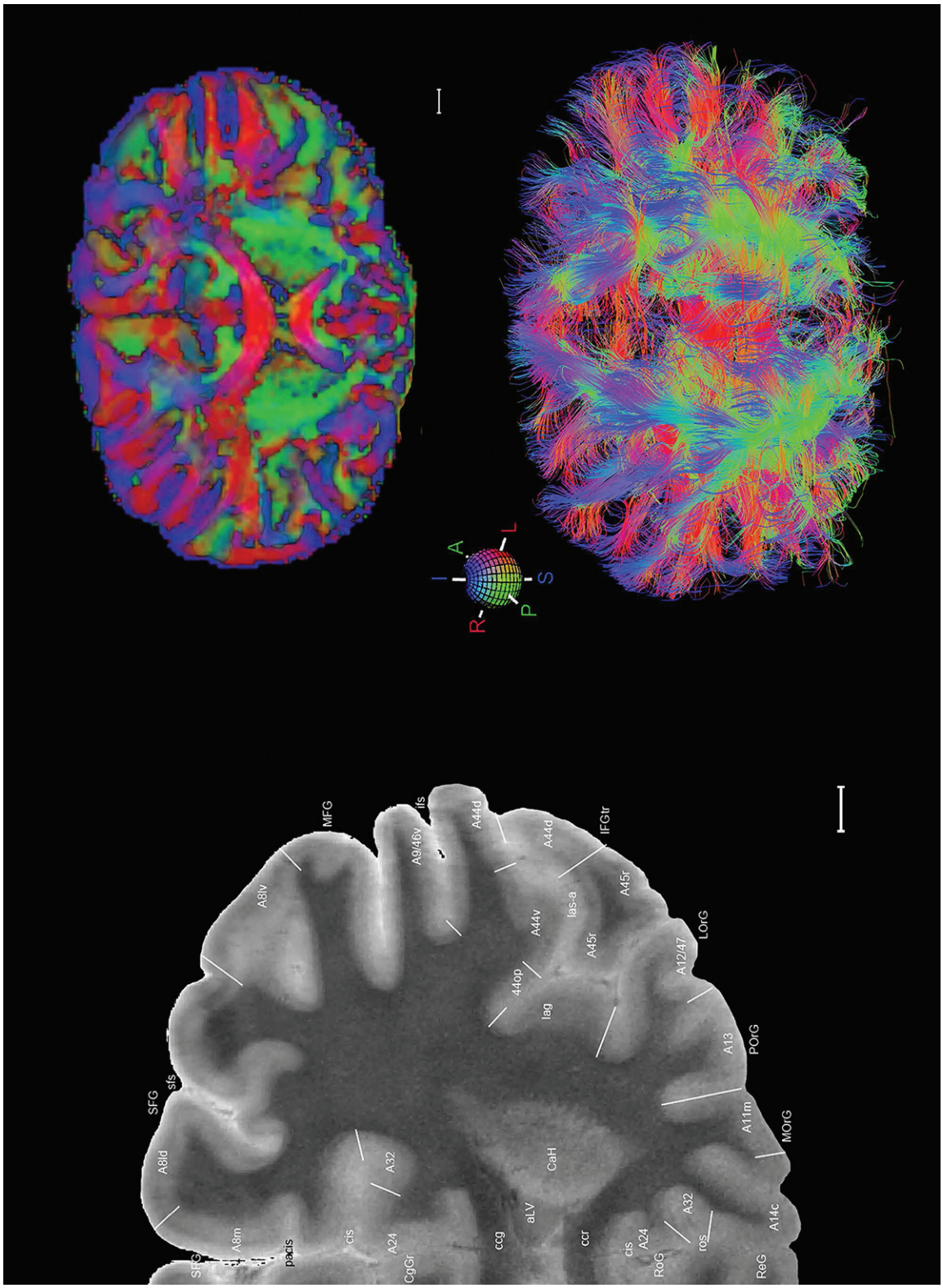

Figure 19. Level 22

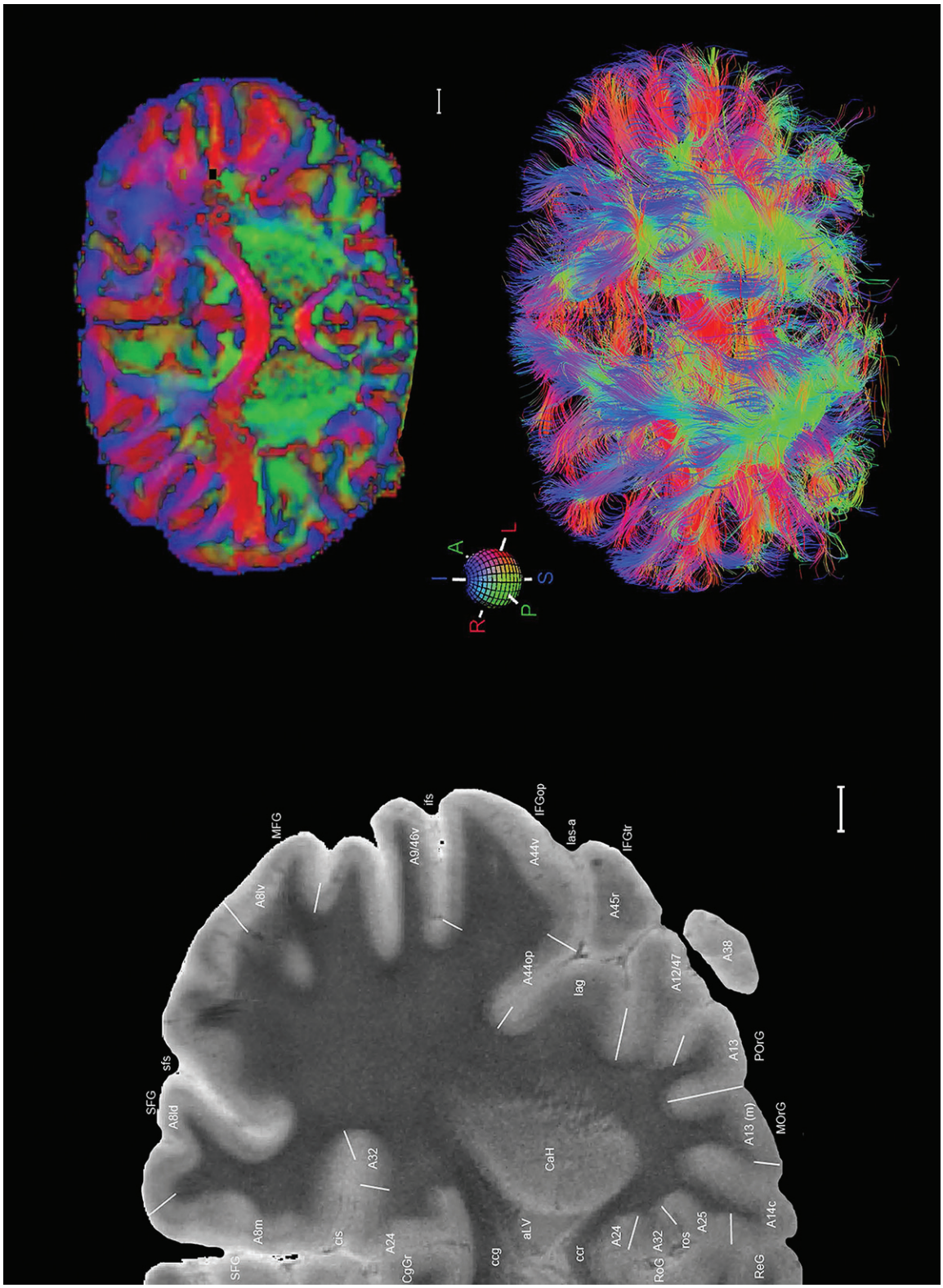

Figure 19. Level 23

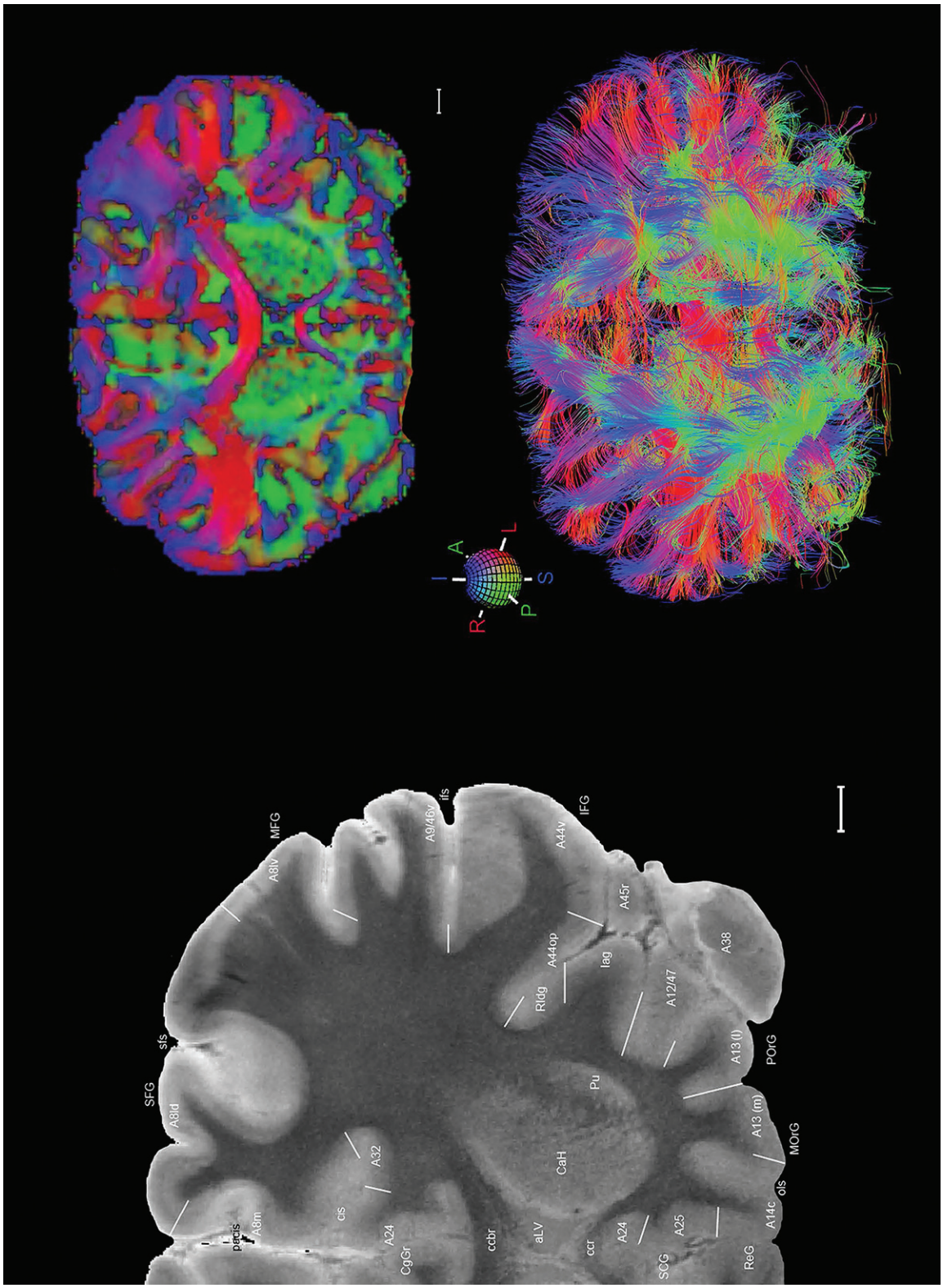

Figure 19. Level 24

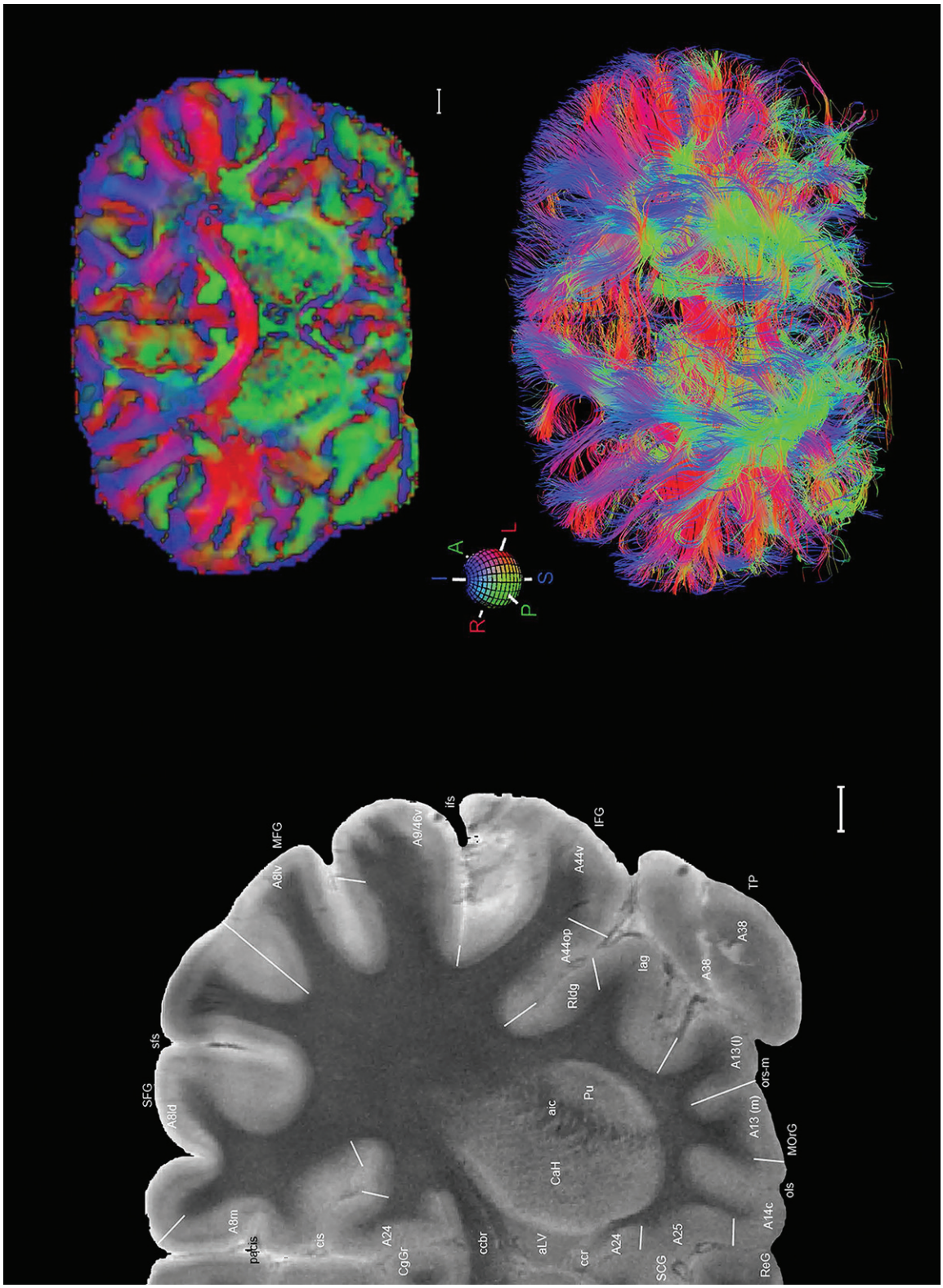

Figure 19. Level 25

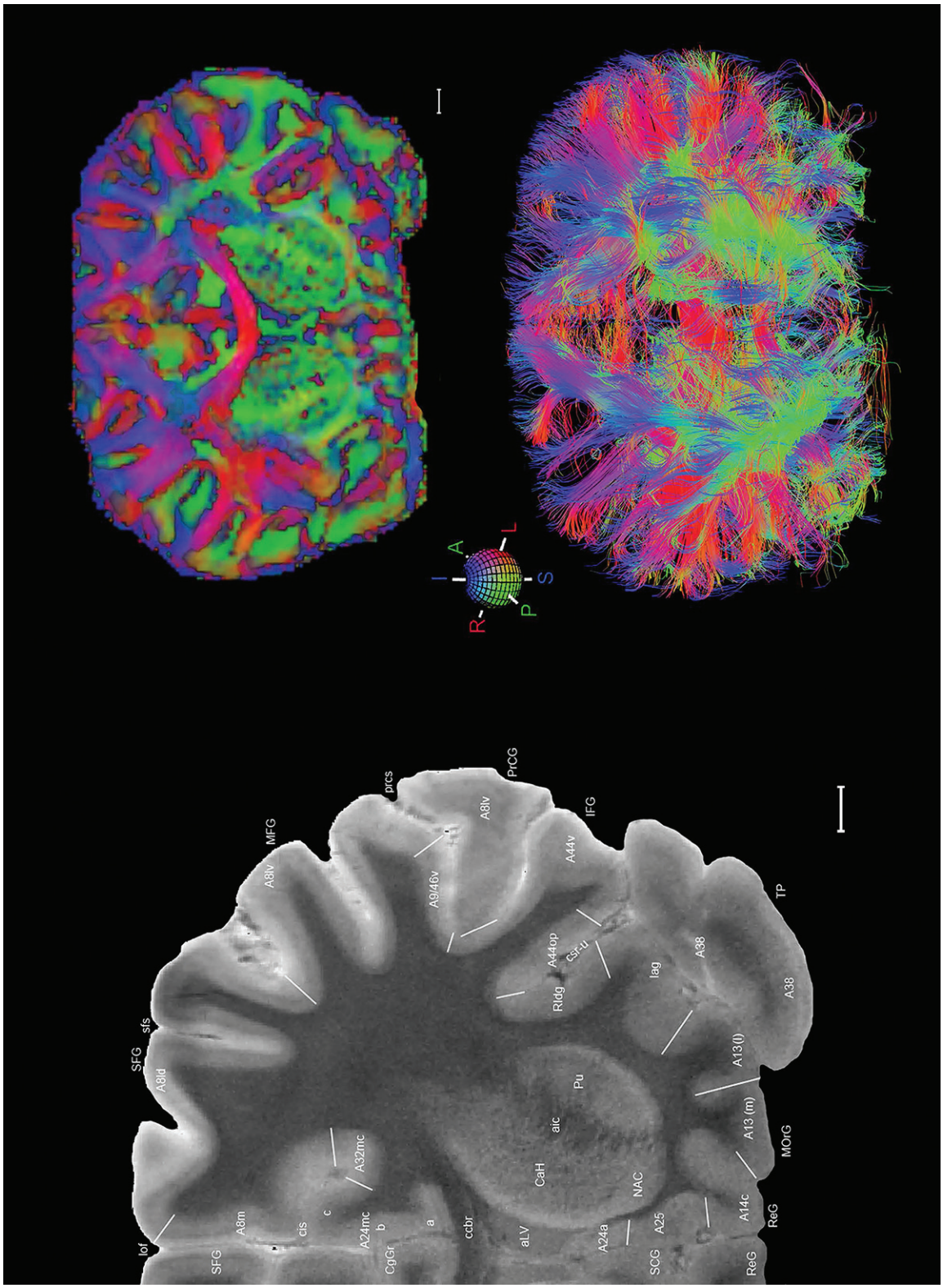

Figure 19. Level 26

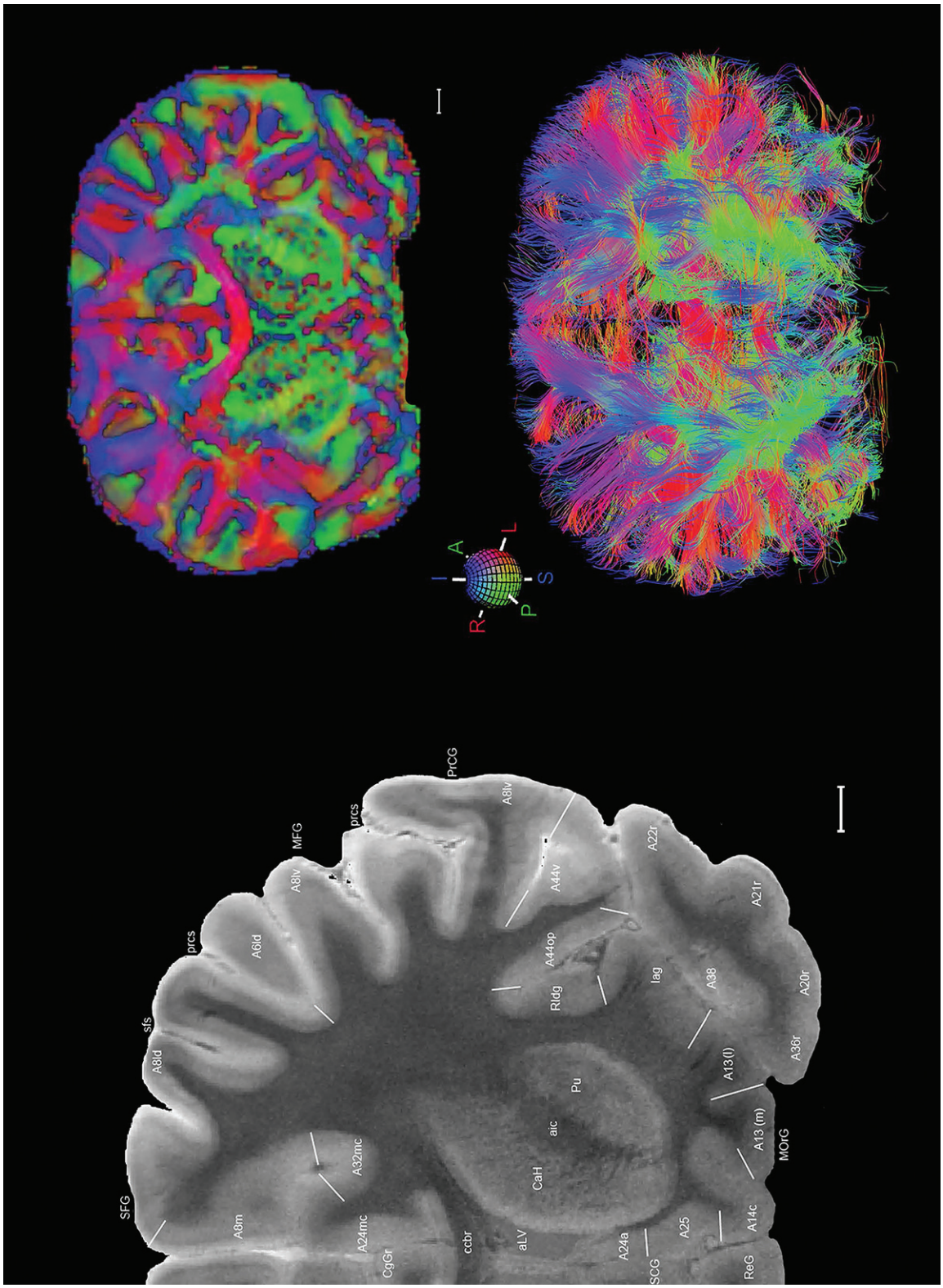

Figure 19. Level 27

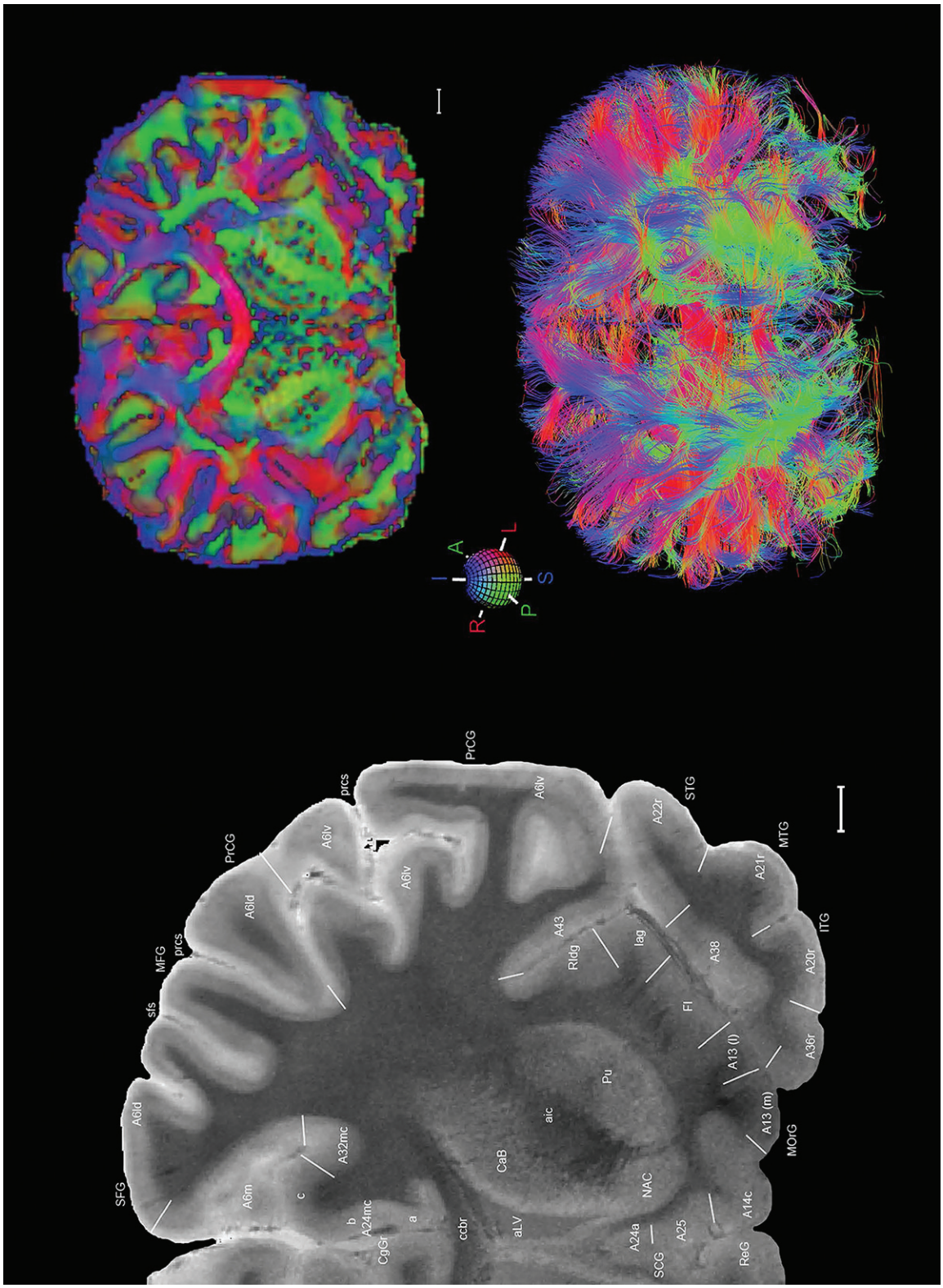

Figure 19. Level 28

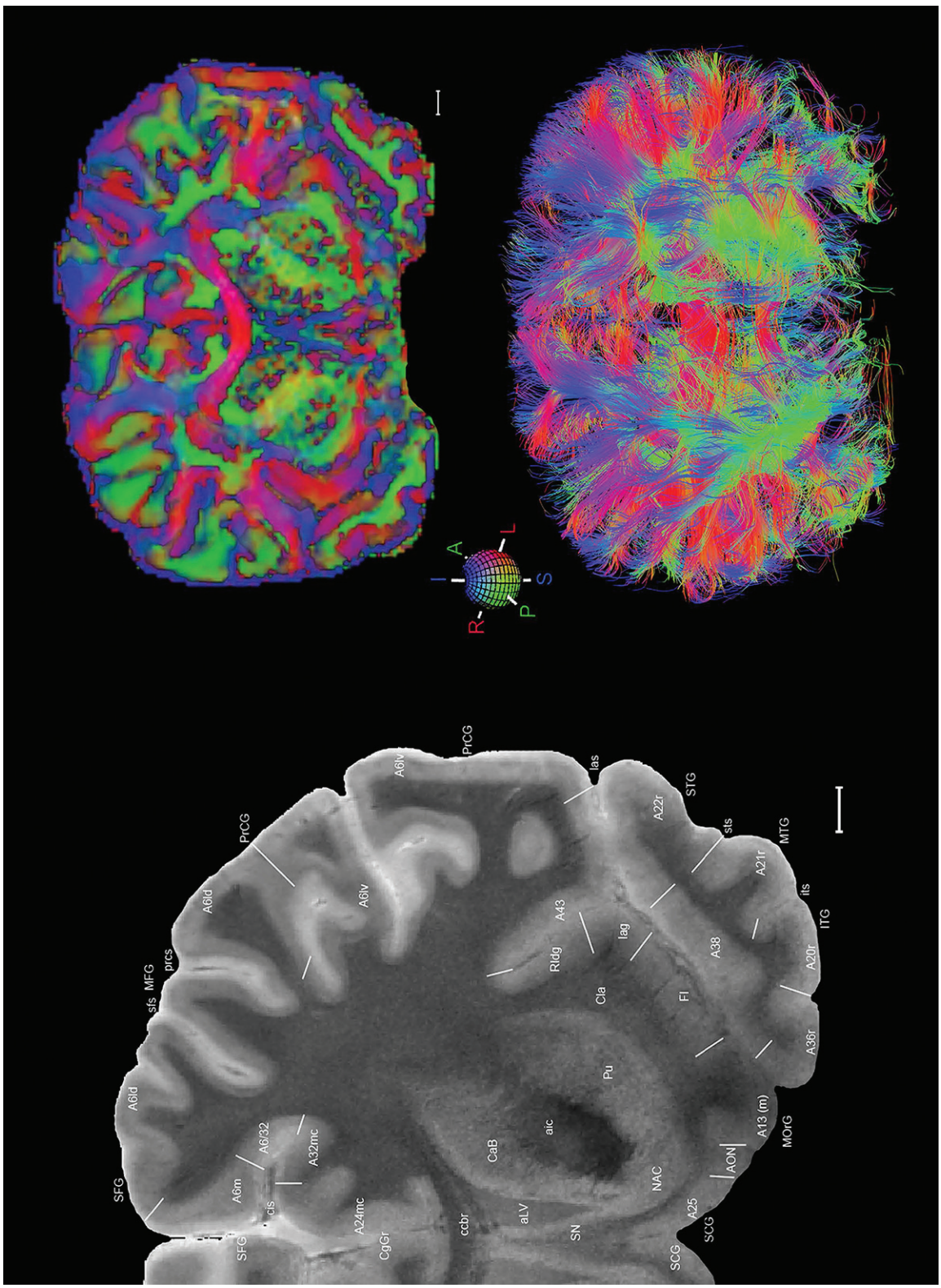

Figure 19. Level 29

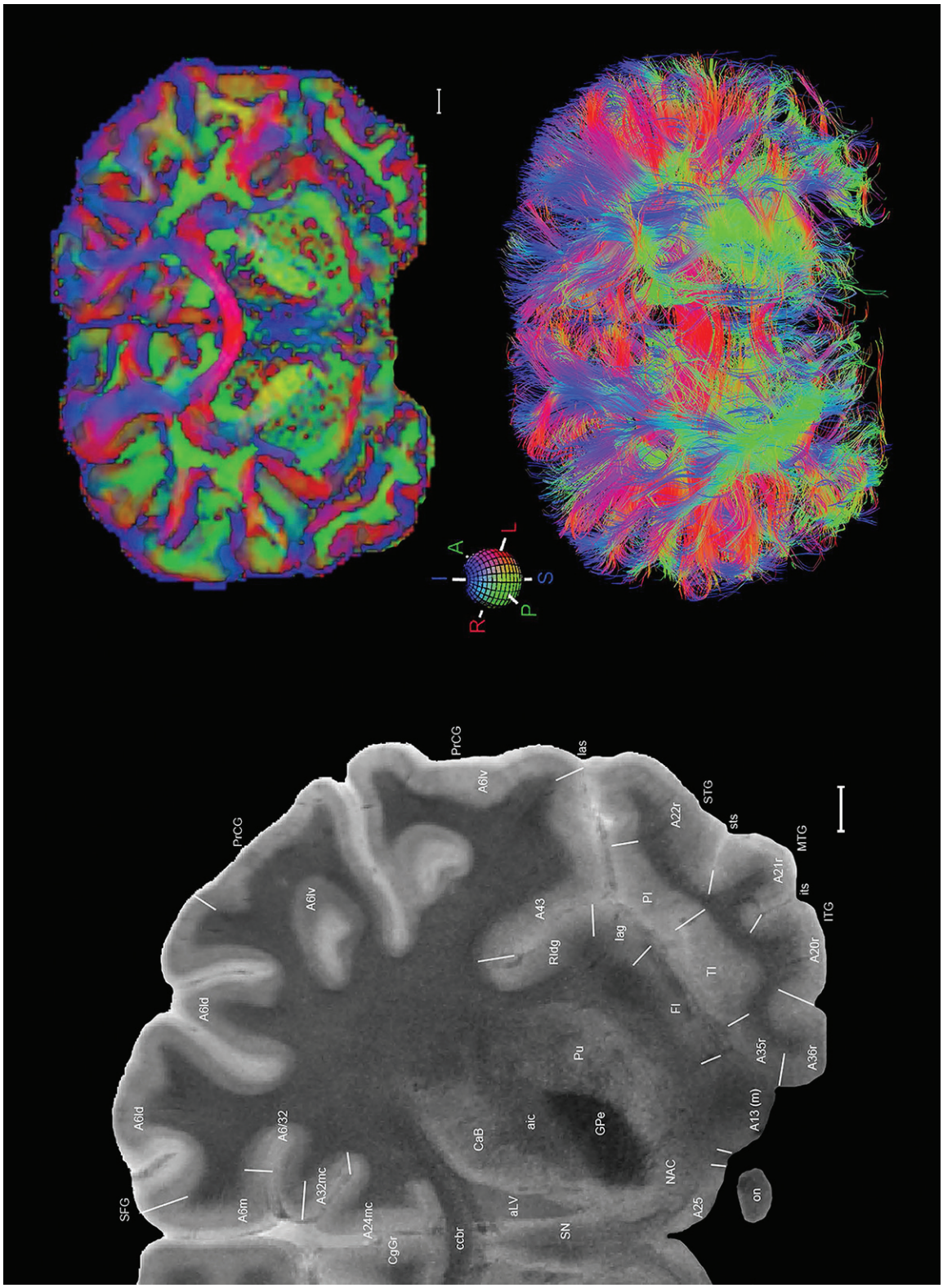

Figure 19. Level 30

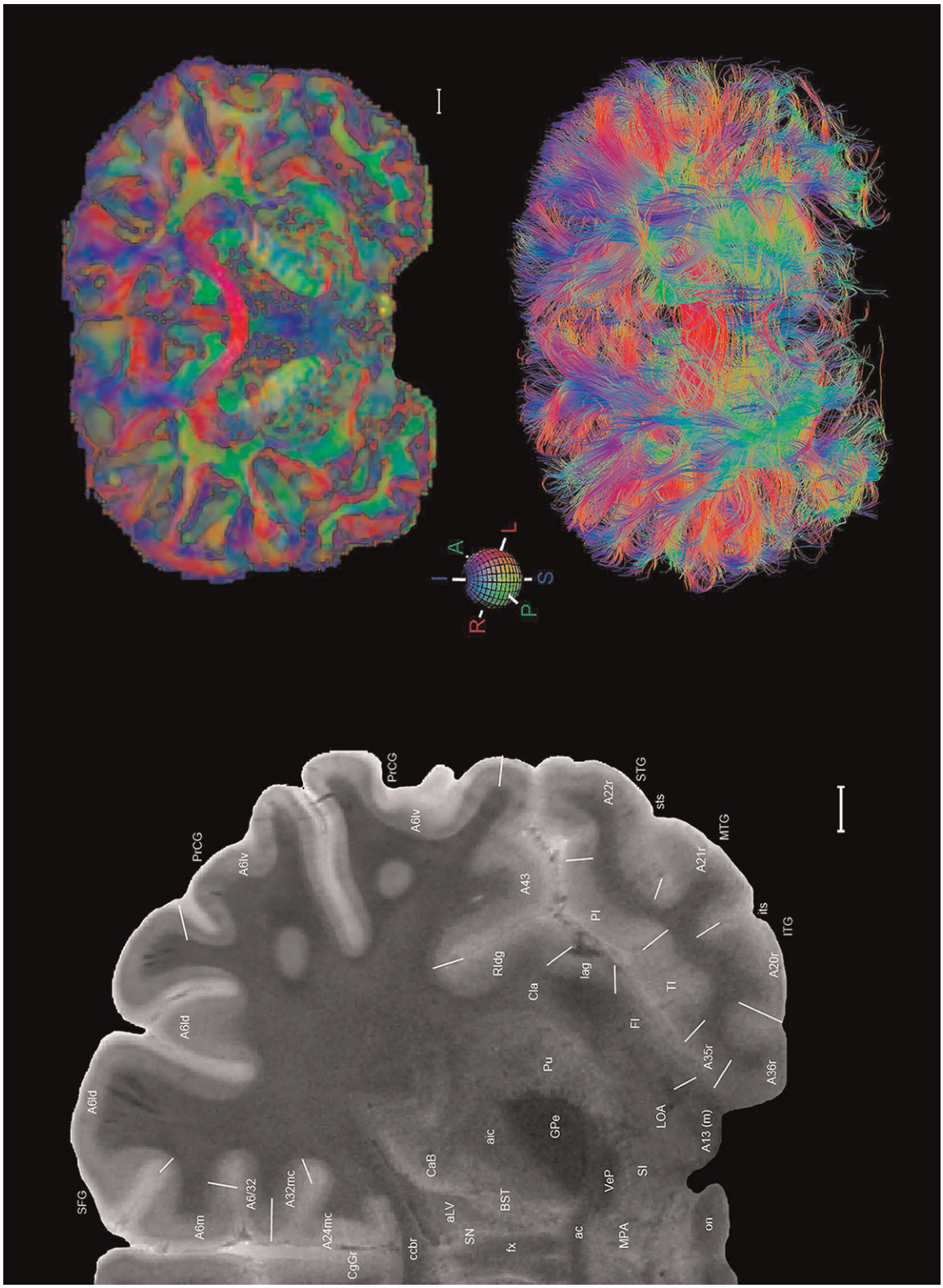

Figure 19. Level 31

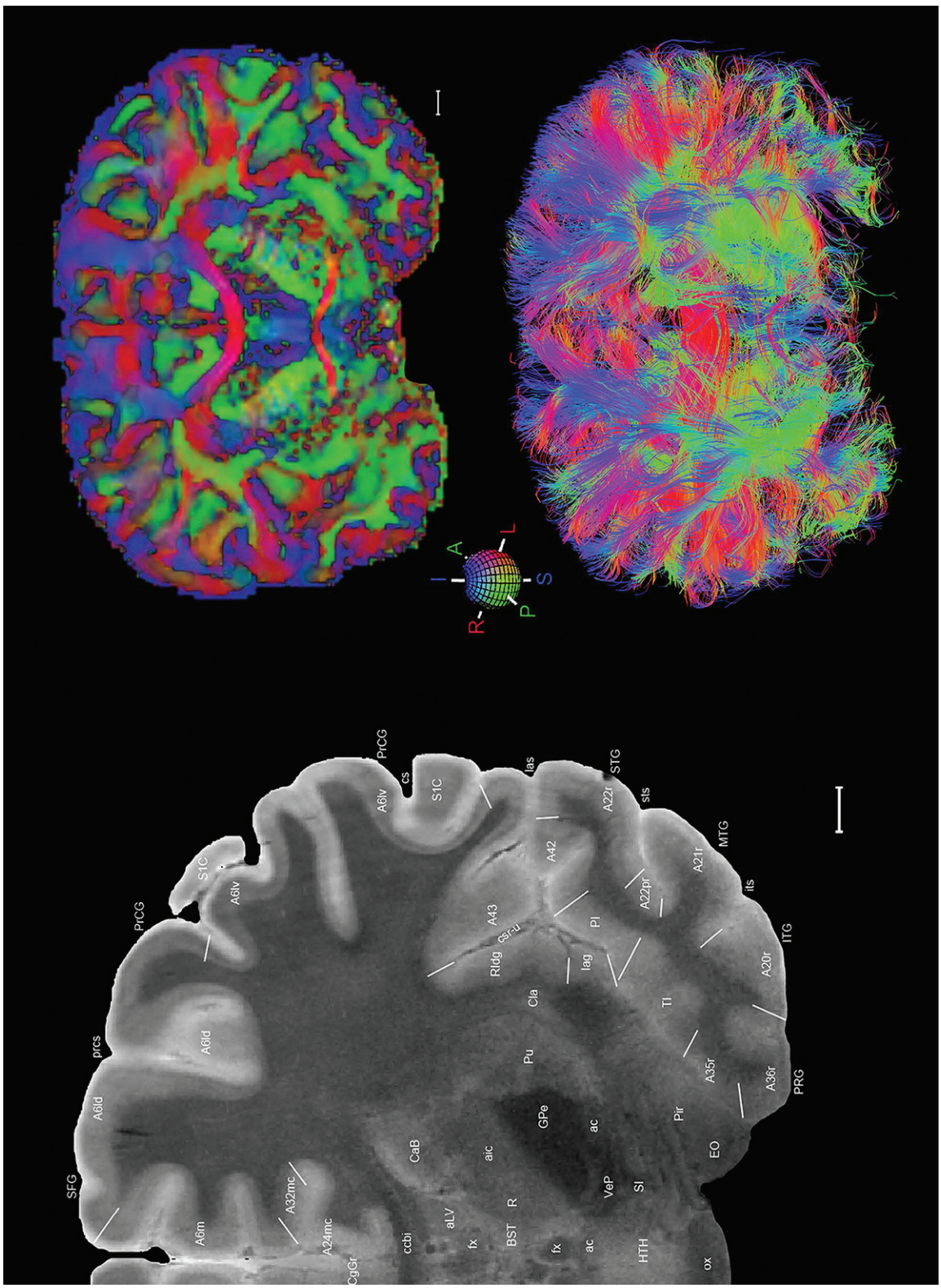

Figure 19. Level 32

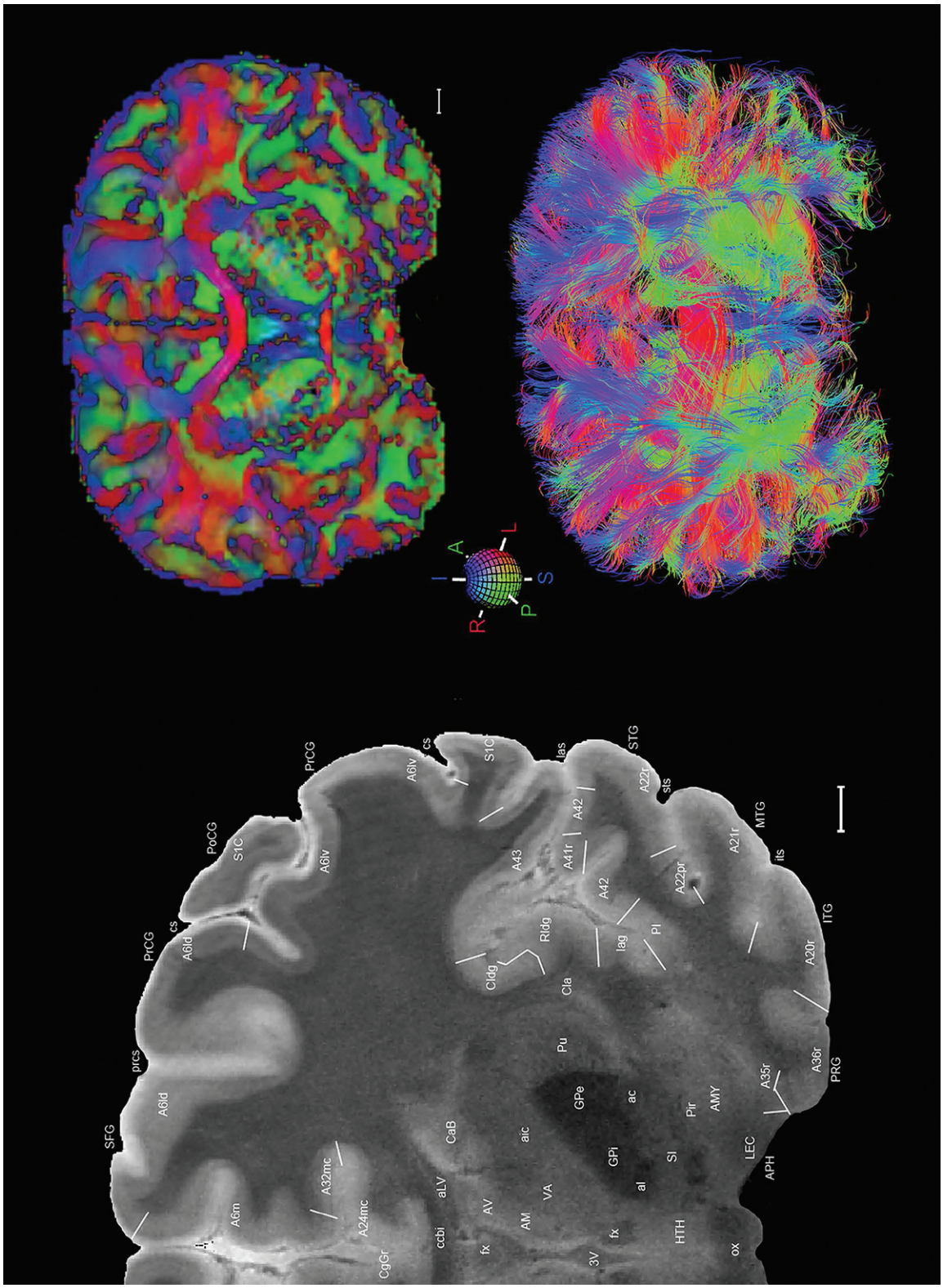

Figure 19. Level 33

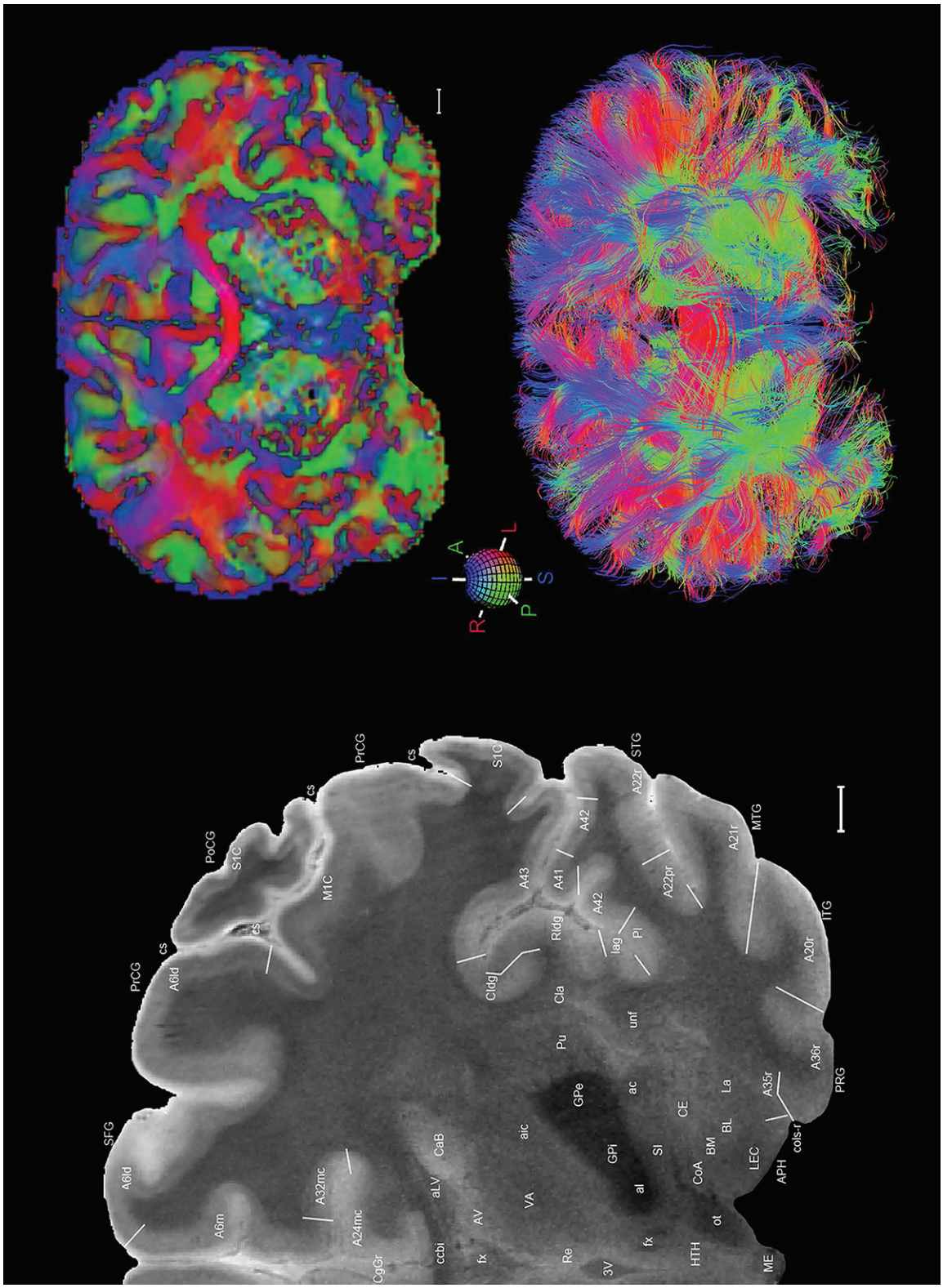

Figure 19. Level 34

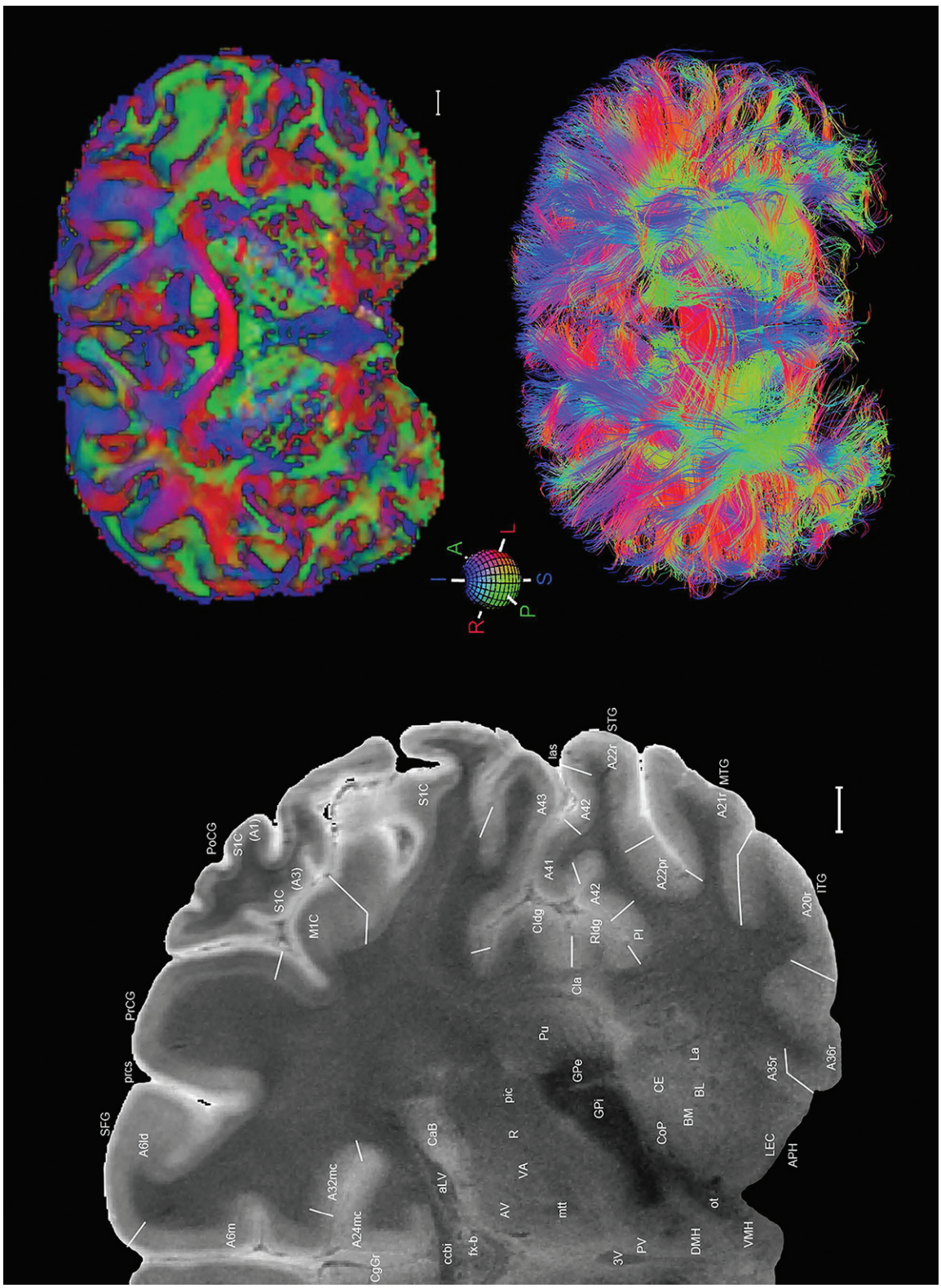

Figure 19. Level 35

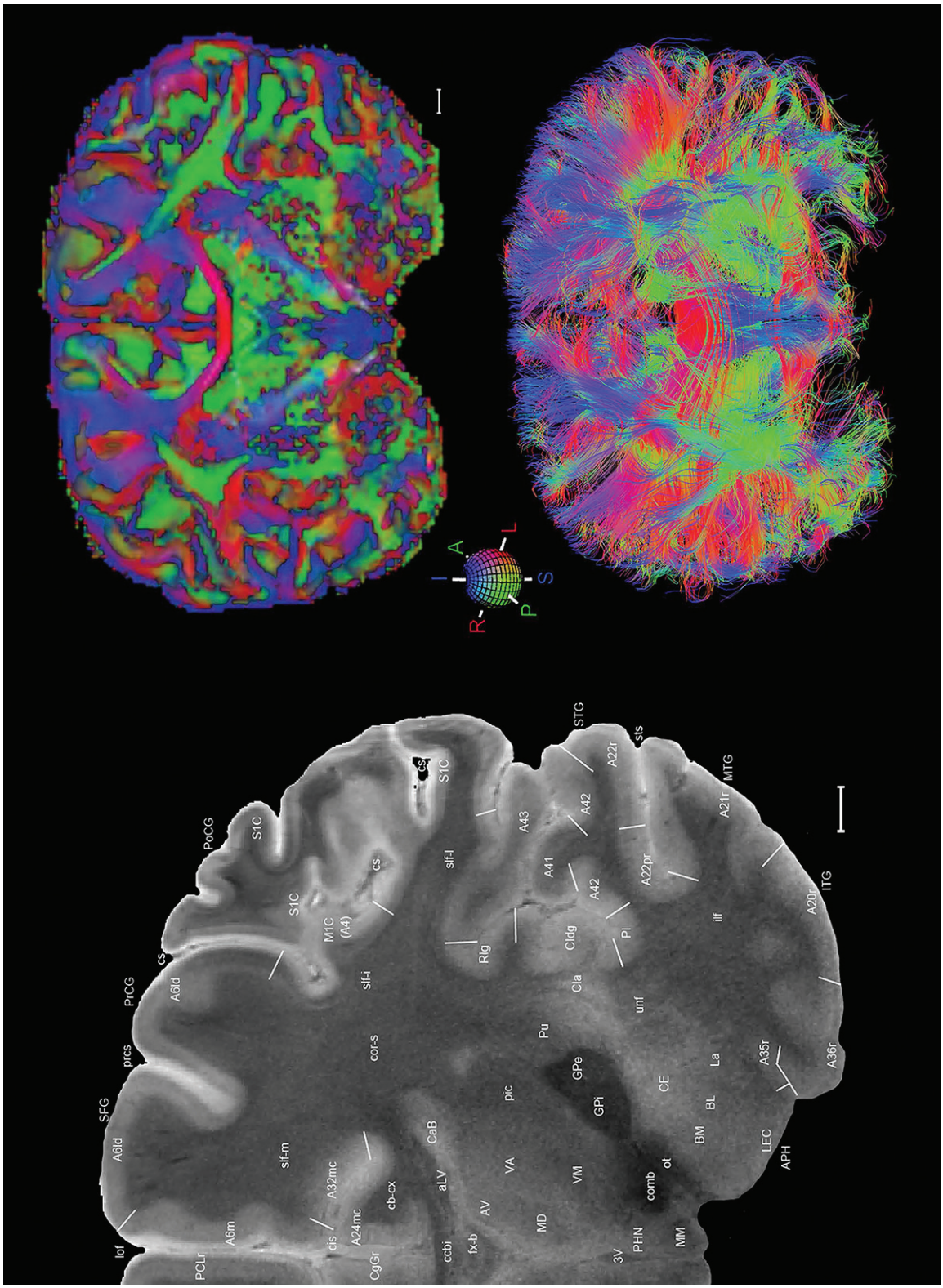

Figure 19. Level 36

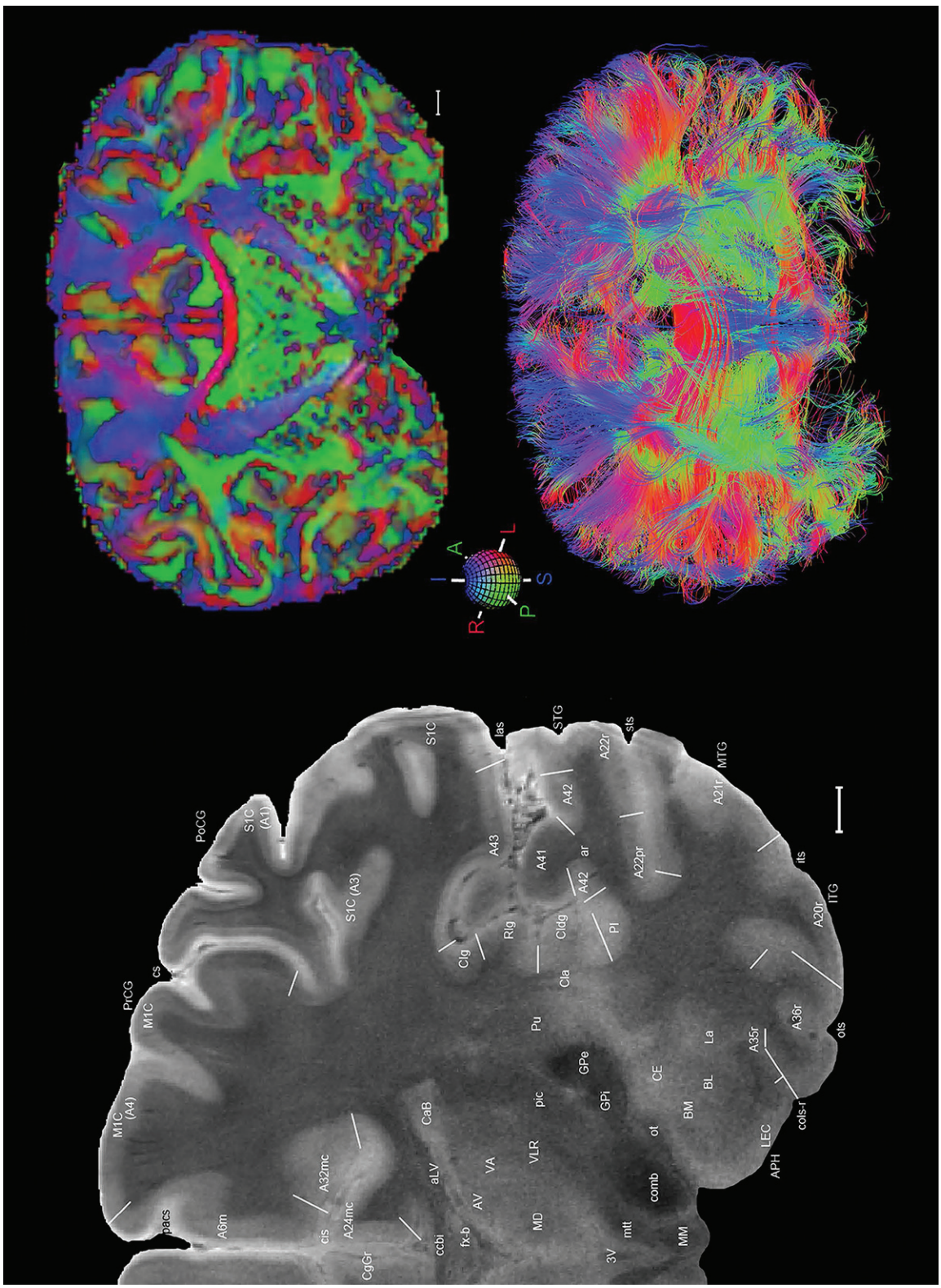

Figure 19. Level 37

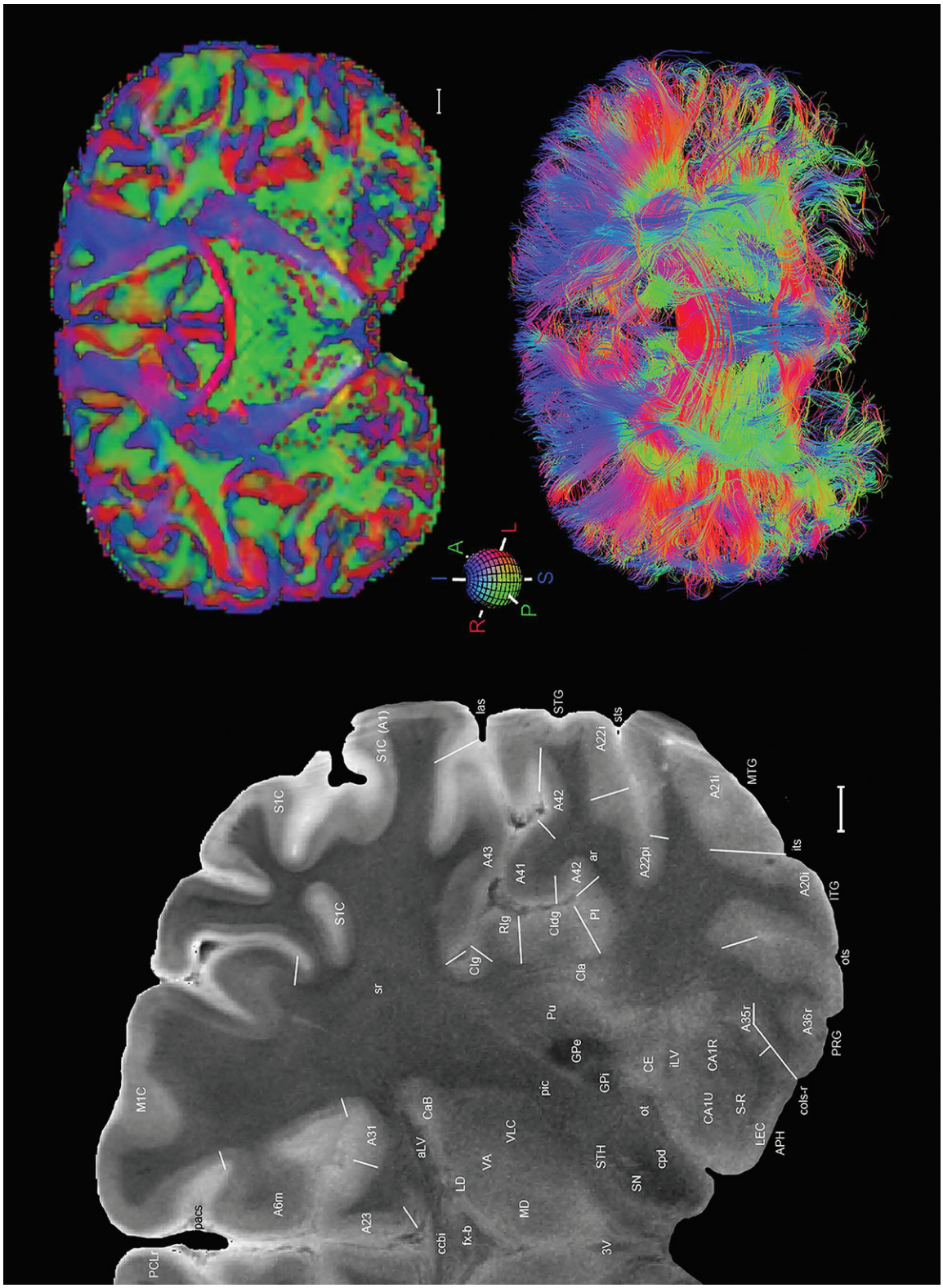

Figure 19. Level 38

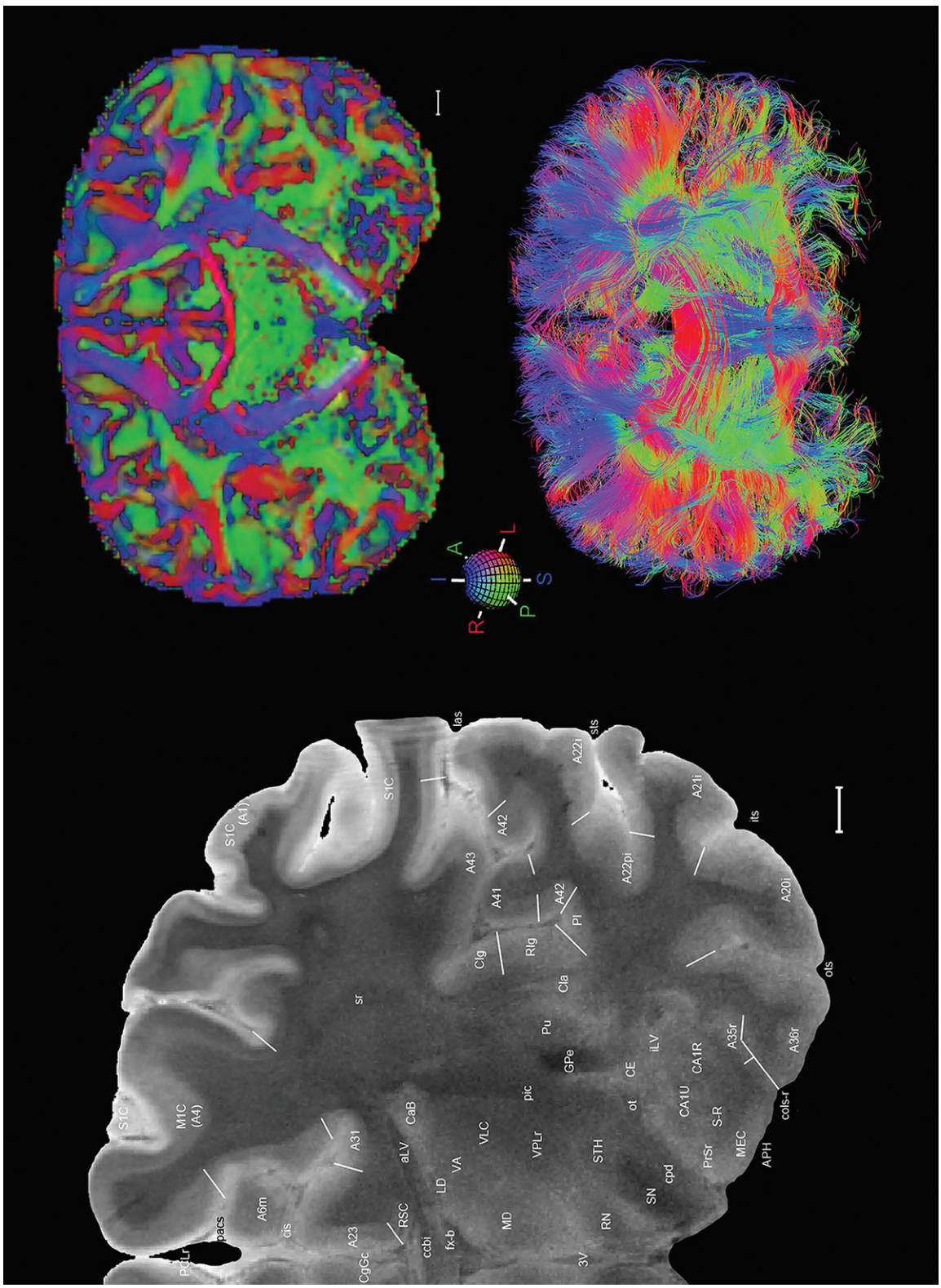

Figure 19. Level 39

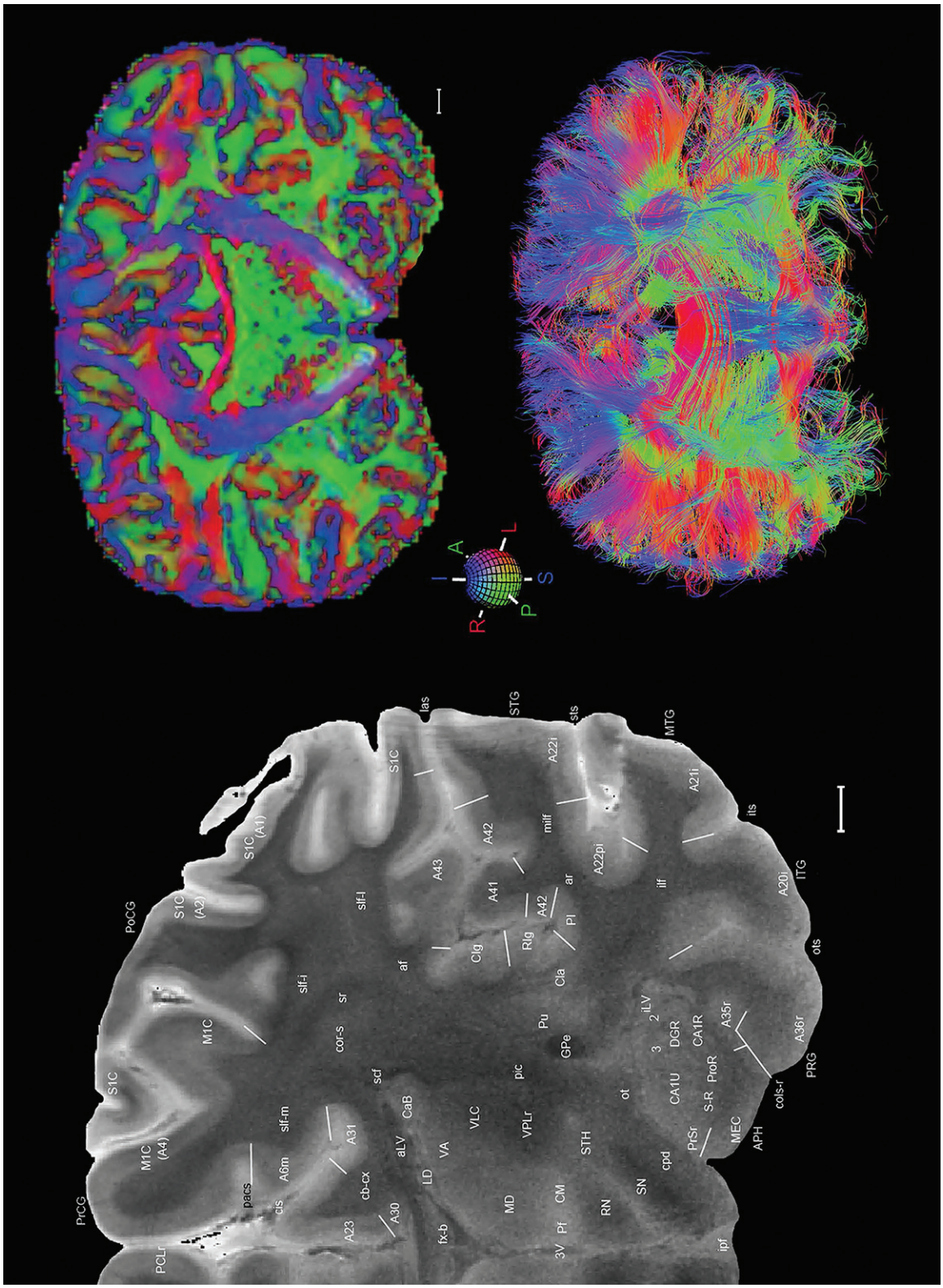

Figure 19. Level 40

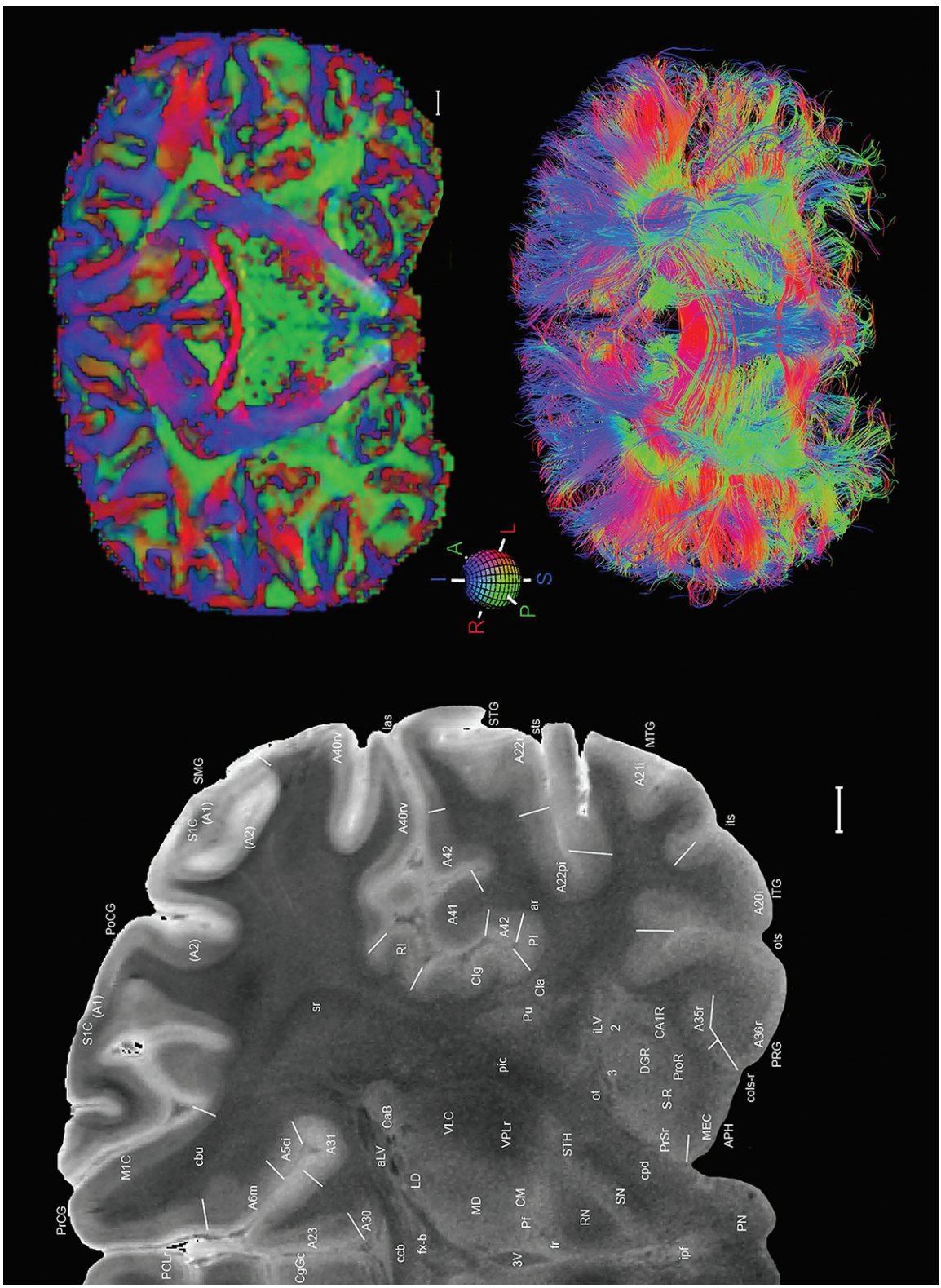

Figure 19. Level 41

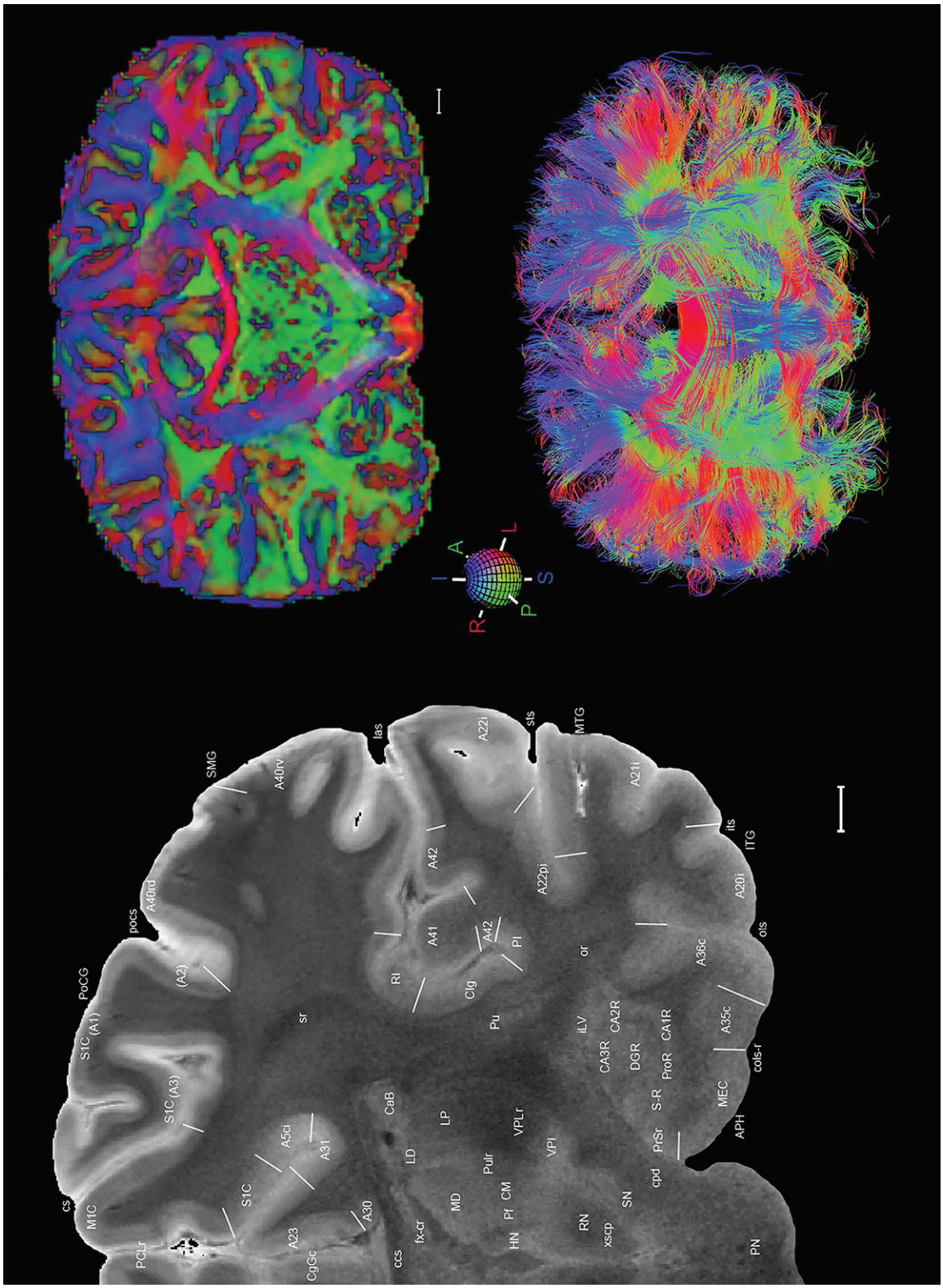

Figure 19. Level 42

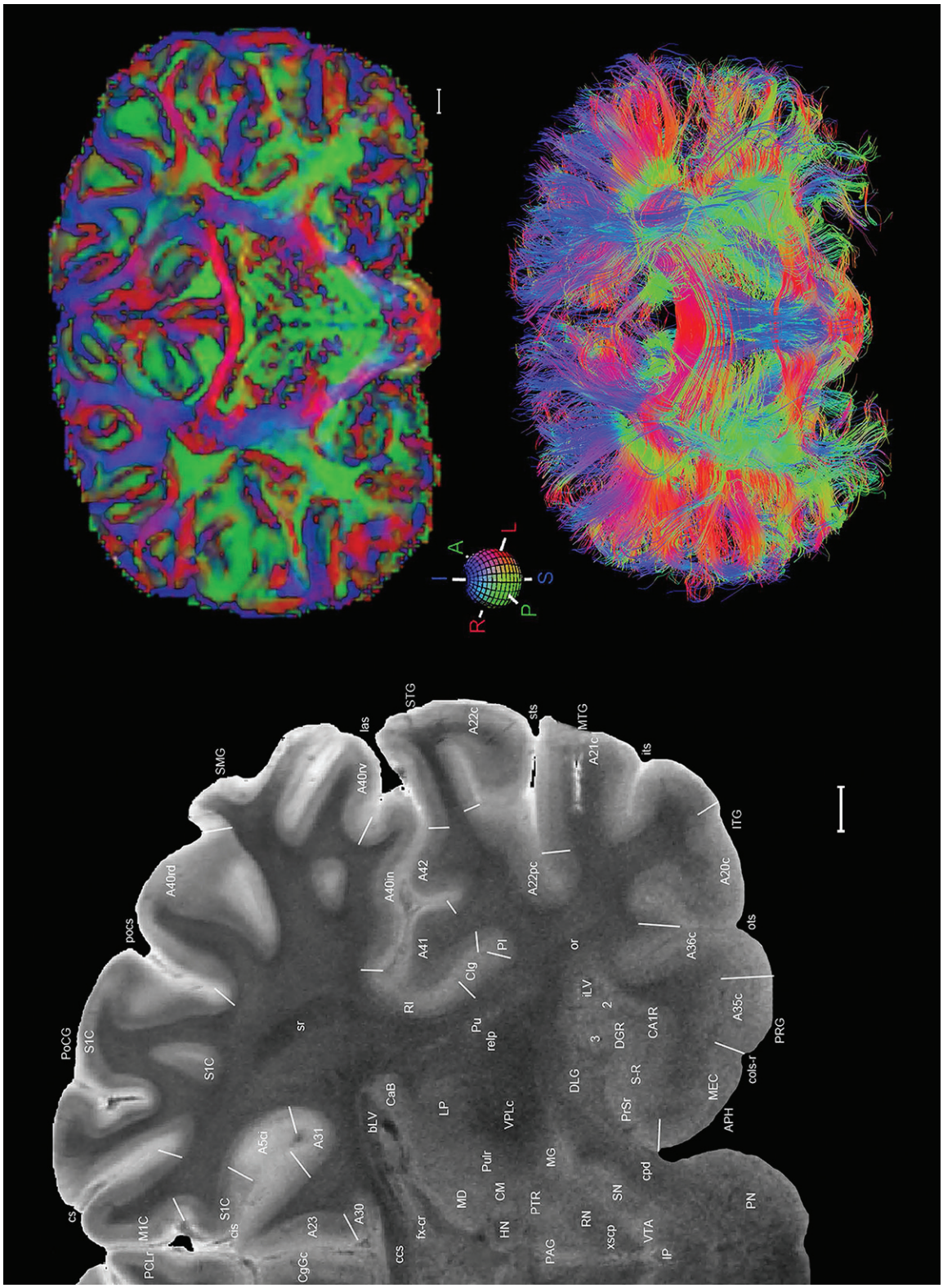

Figure 19. Level 43

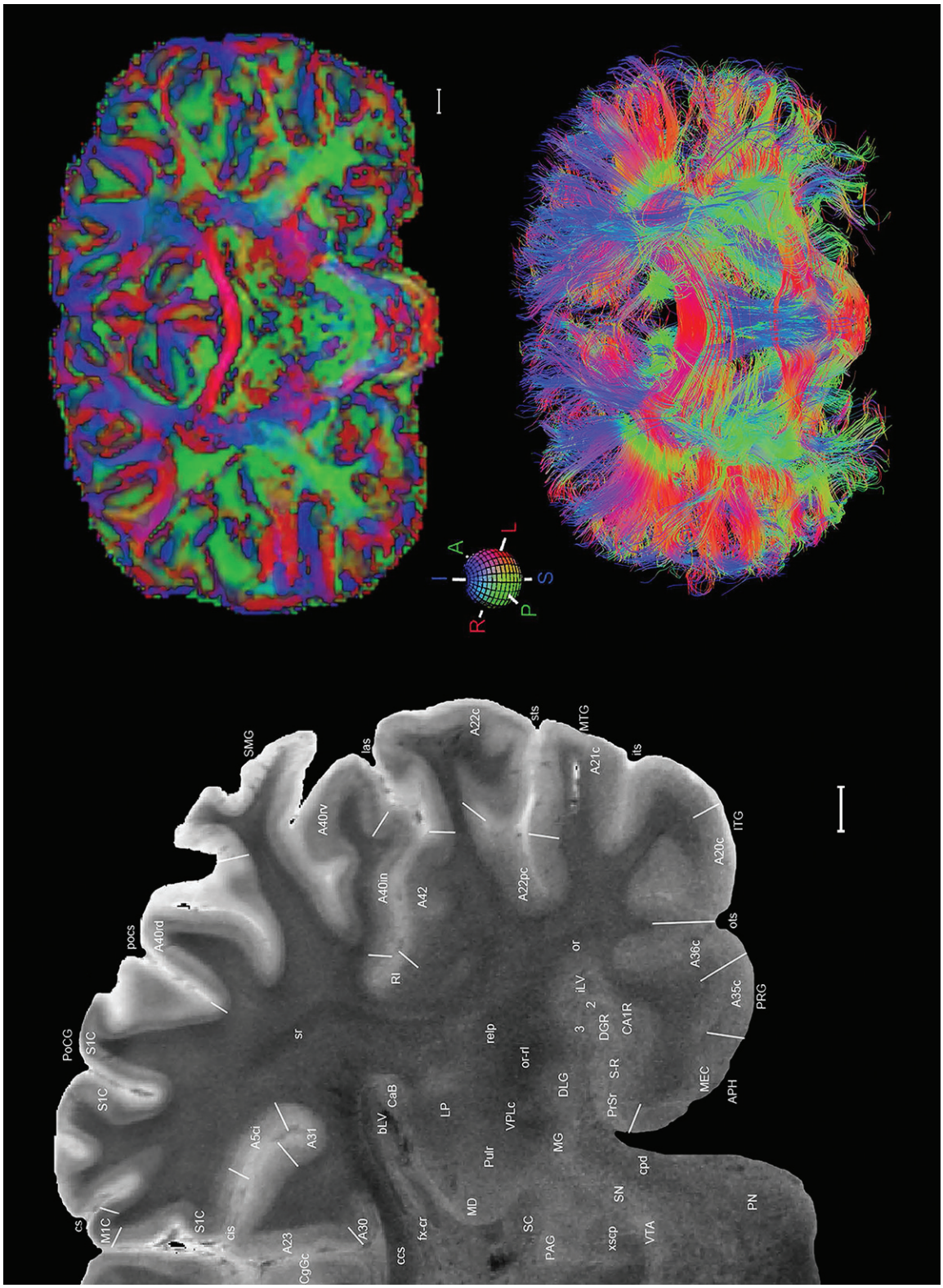

Figure 19. Level 44

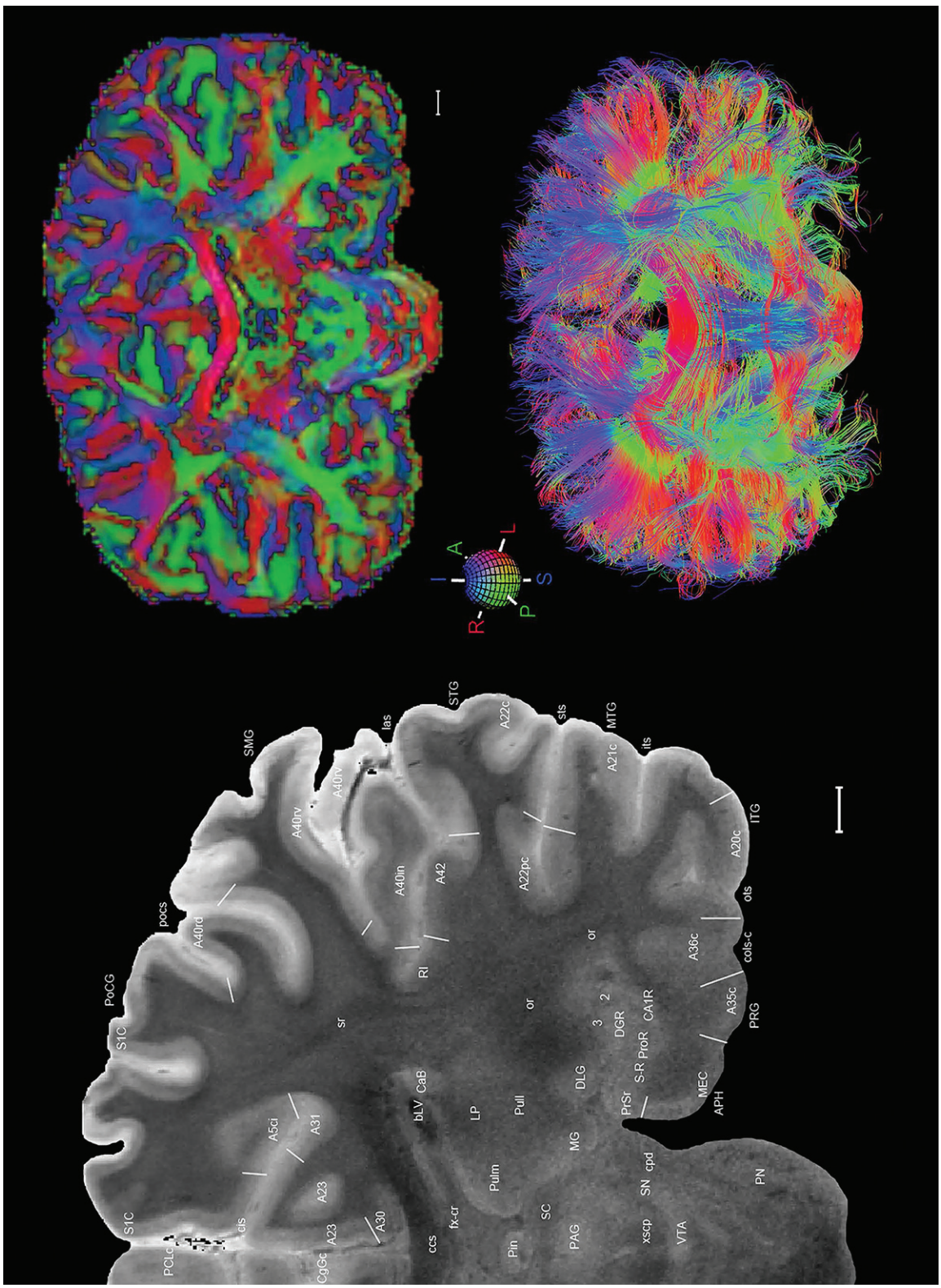

Figure 19. Level 45

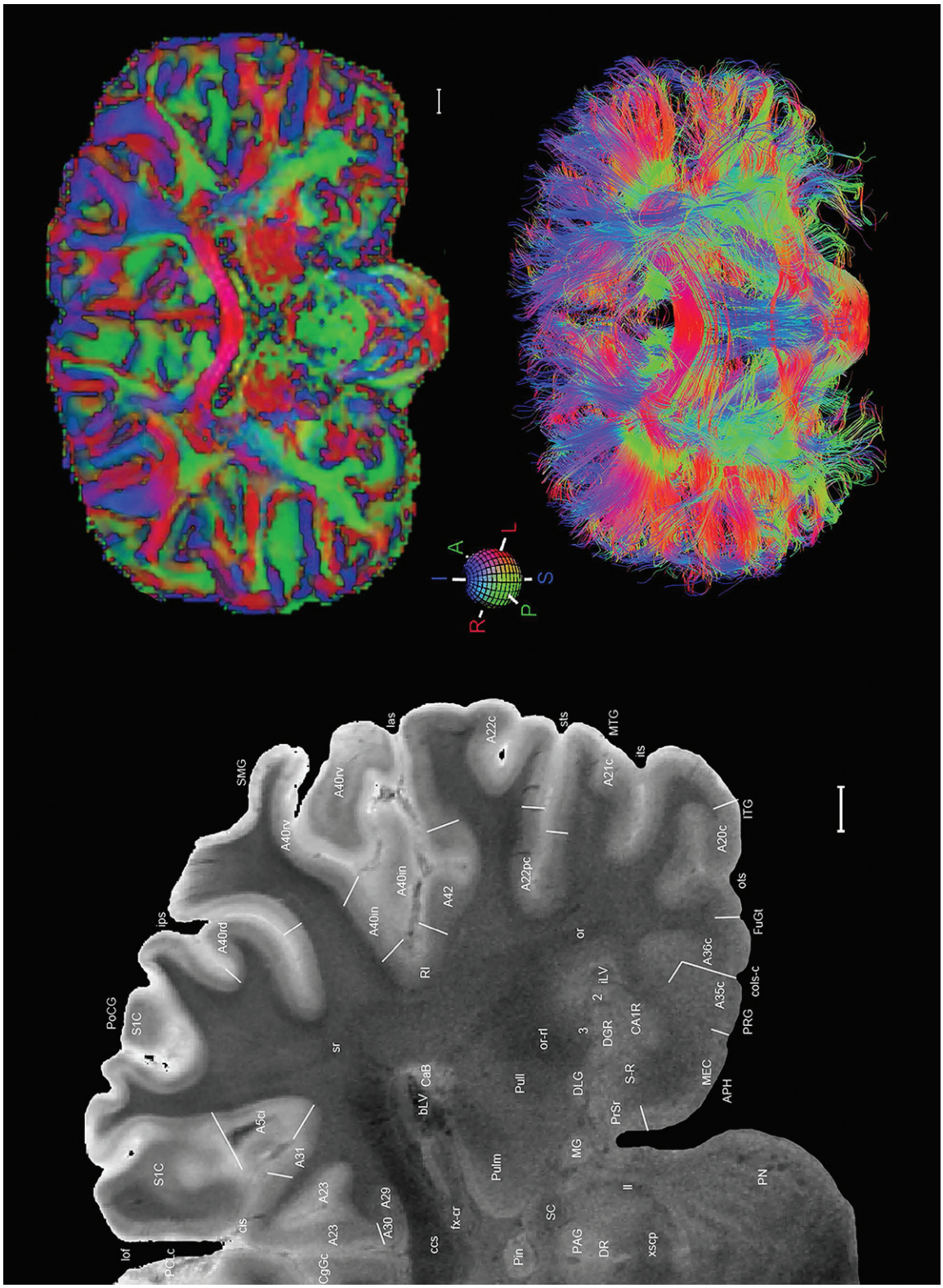

Figure 19. Level 46

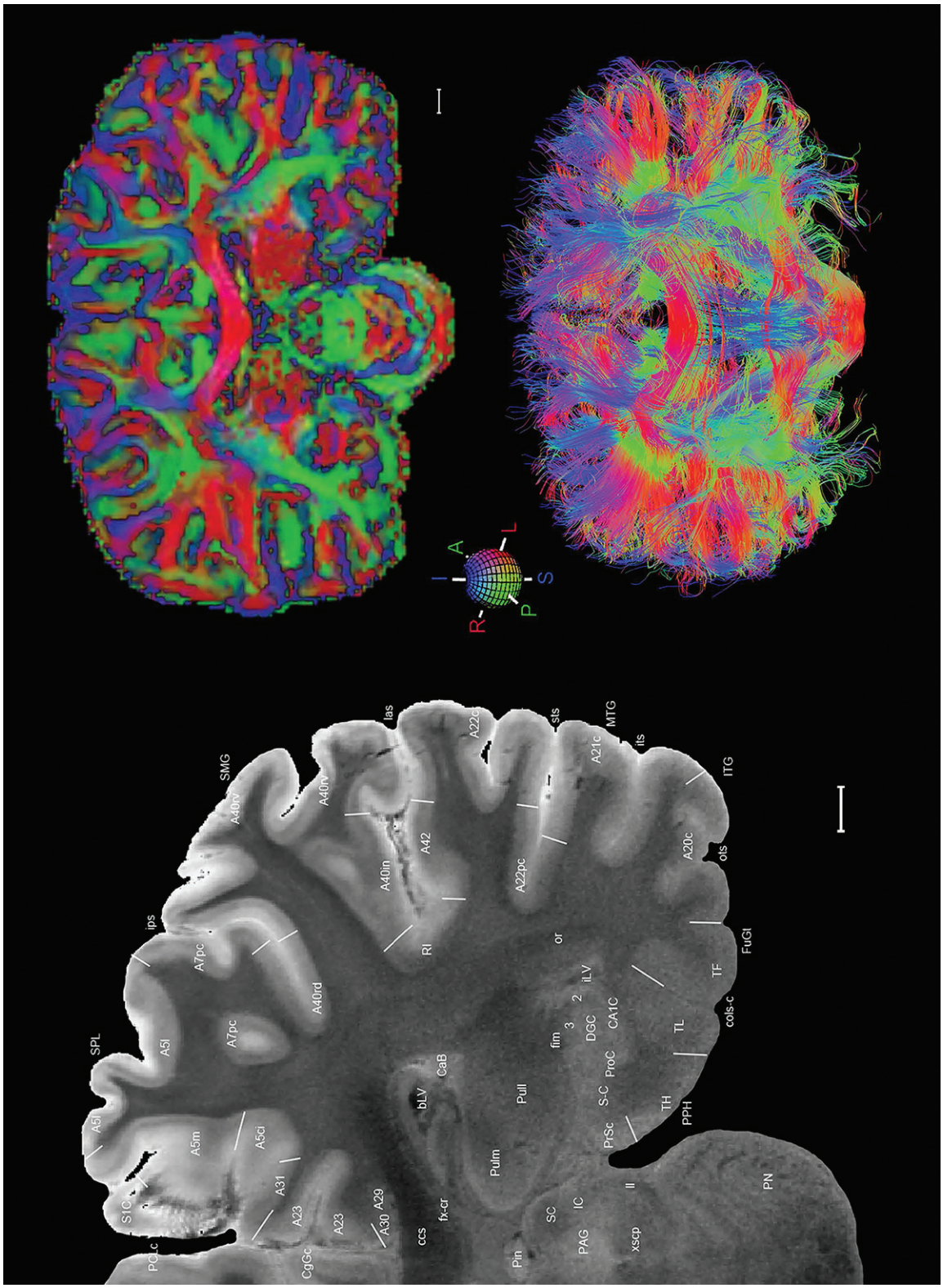

Figure 19. Level 47

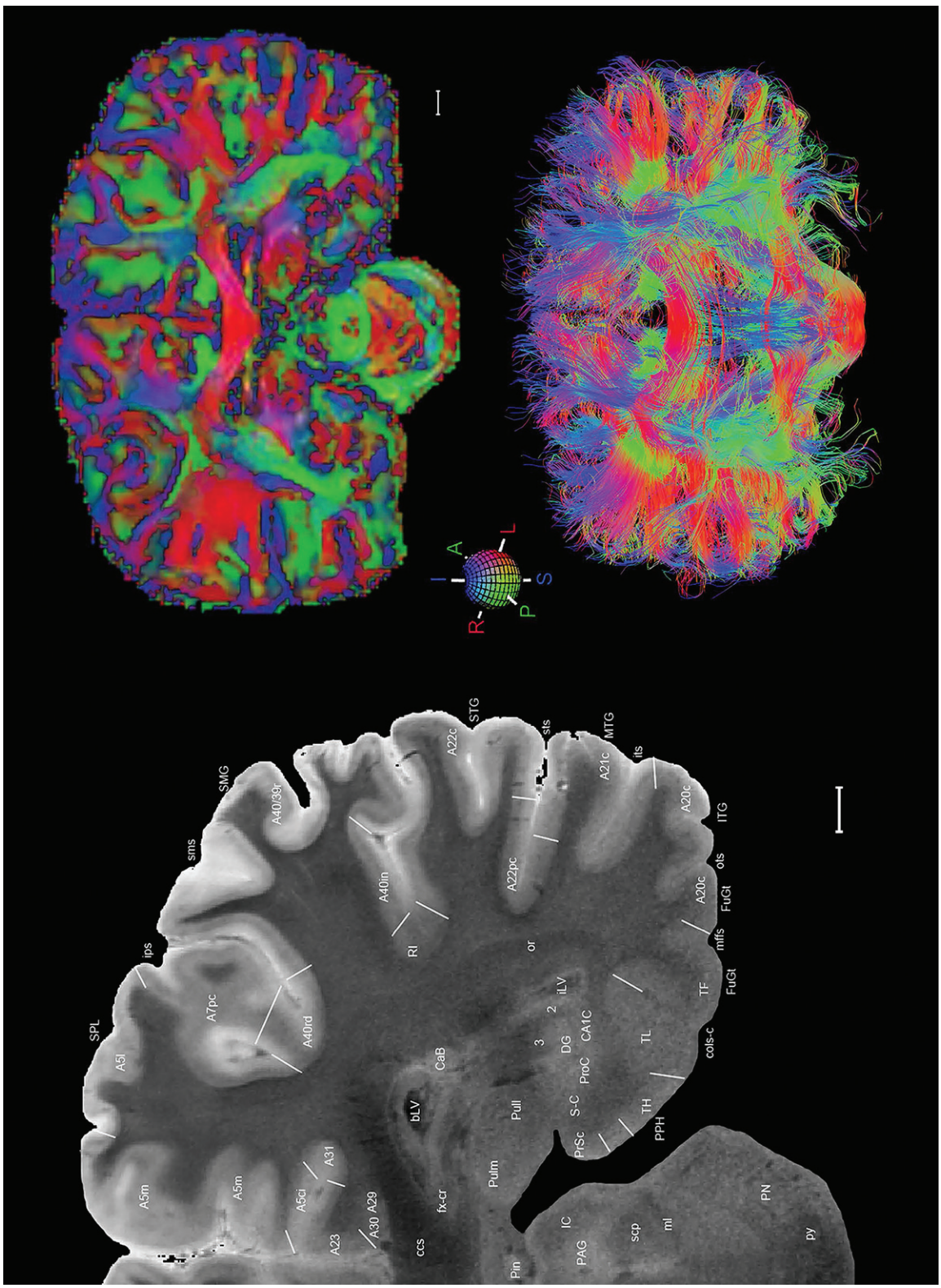

Figure 19. Level 48

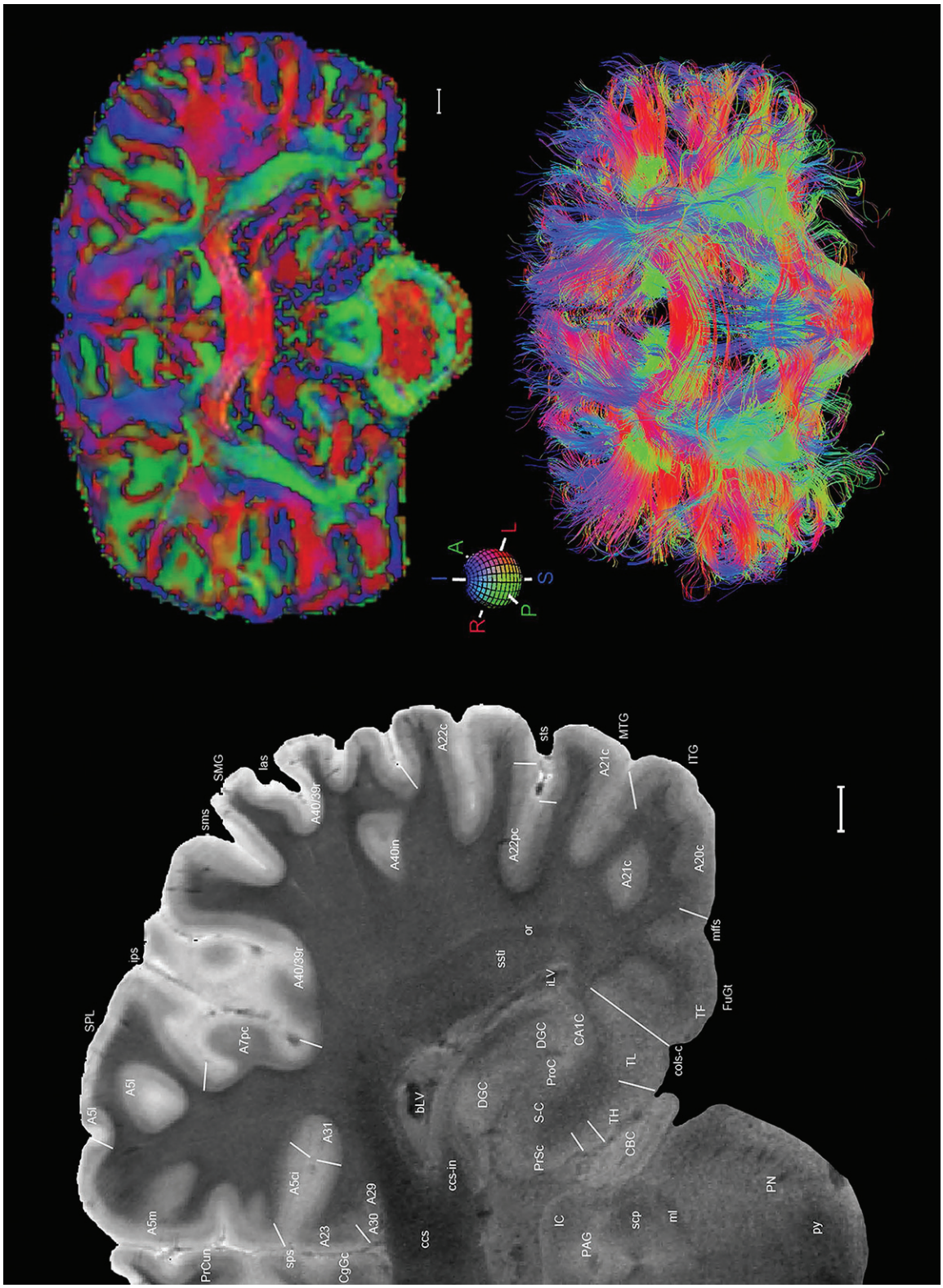

Figure 19. Level 49

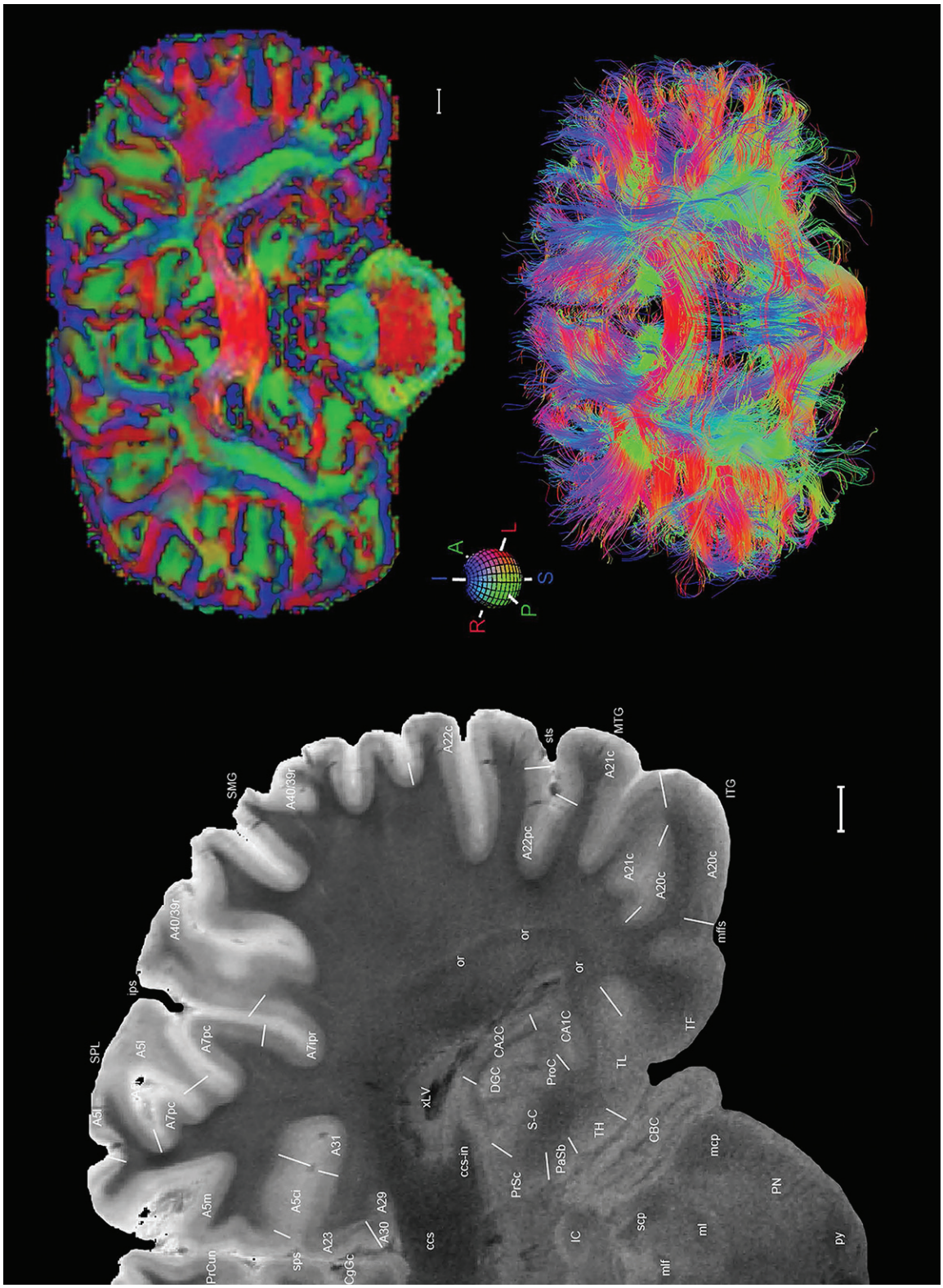

Figure 19. Level 50

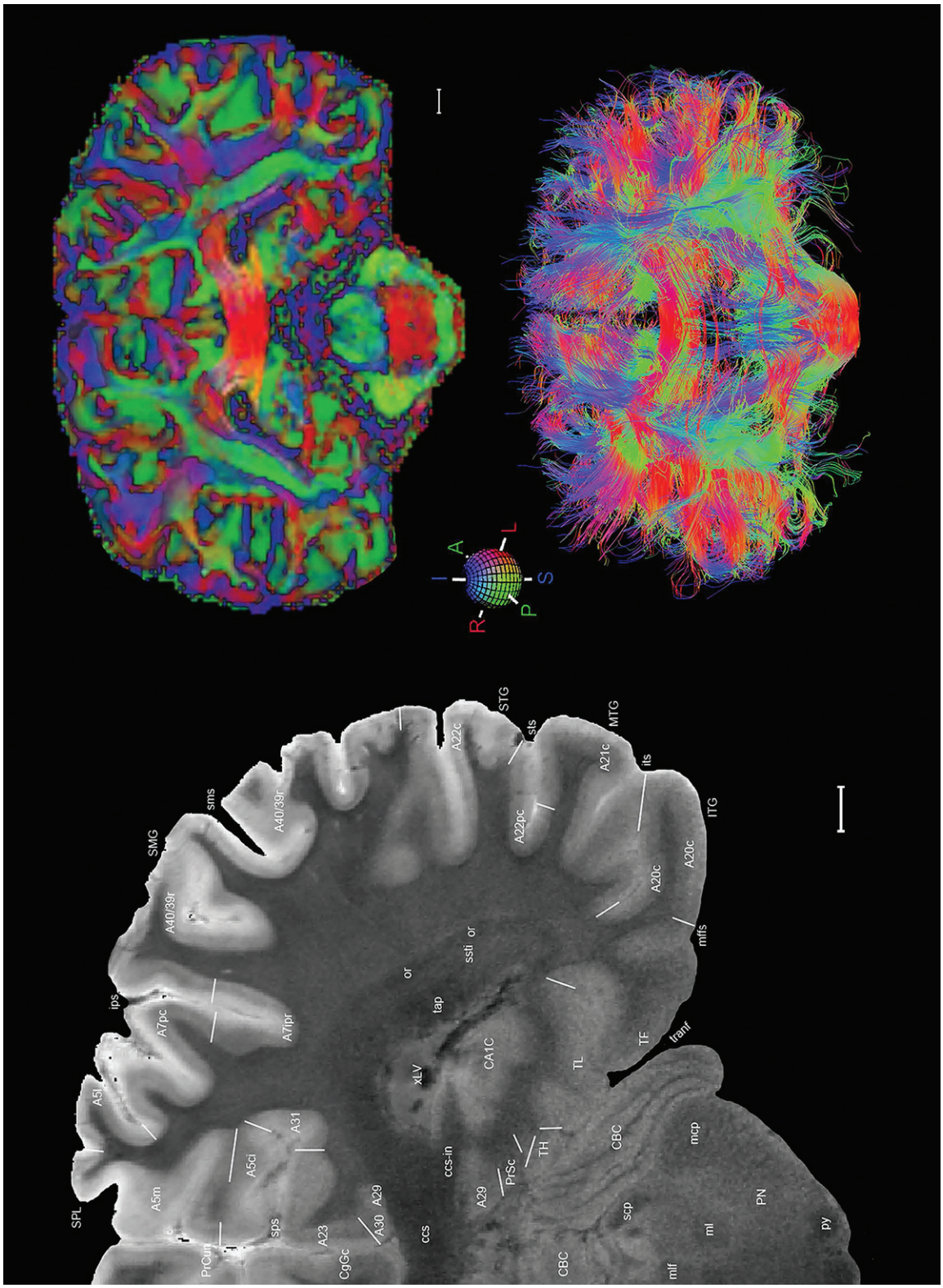

Figure 19. Level 51

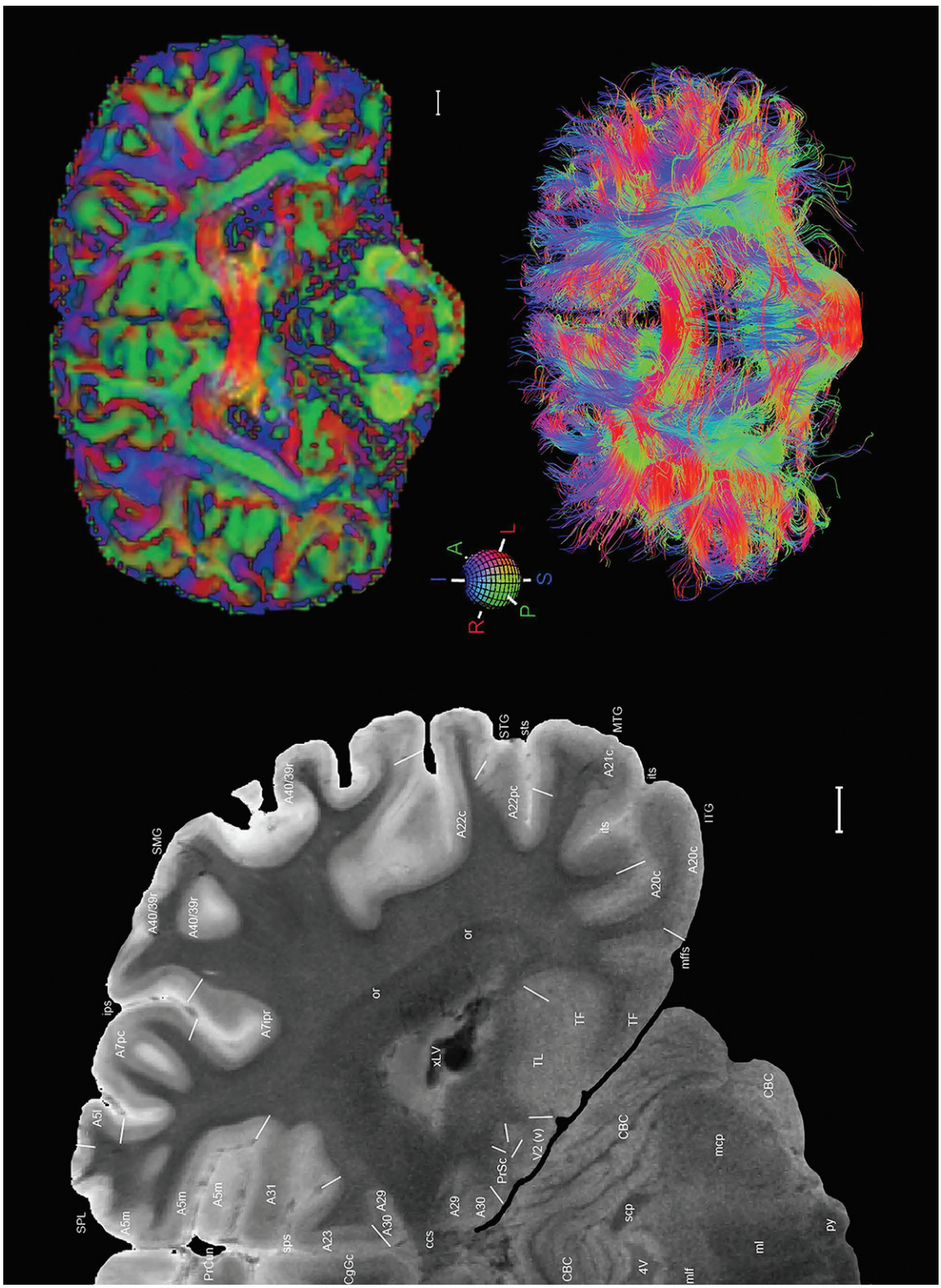

Figure 19. Level 52

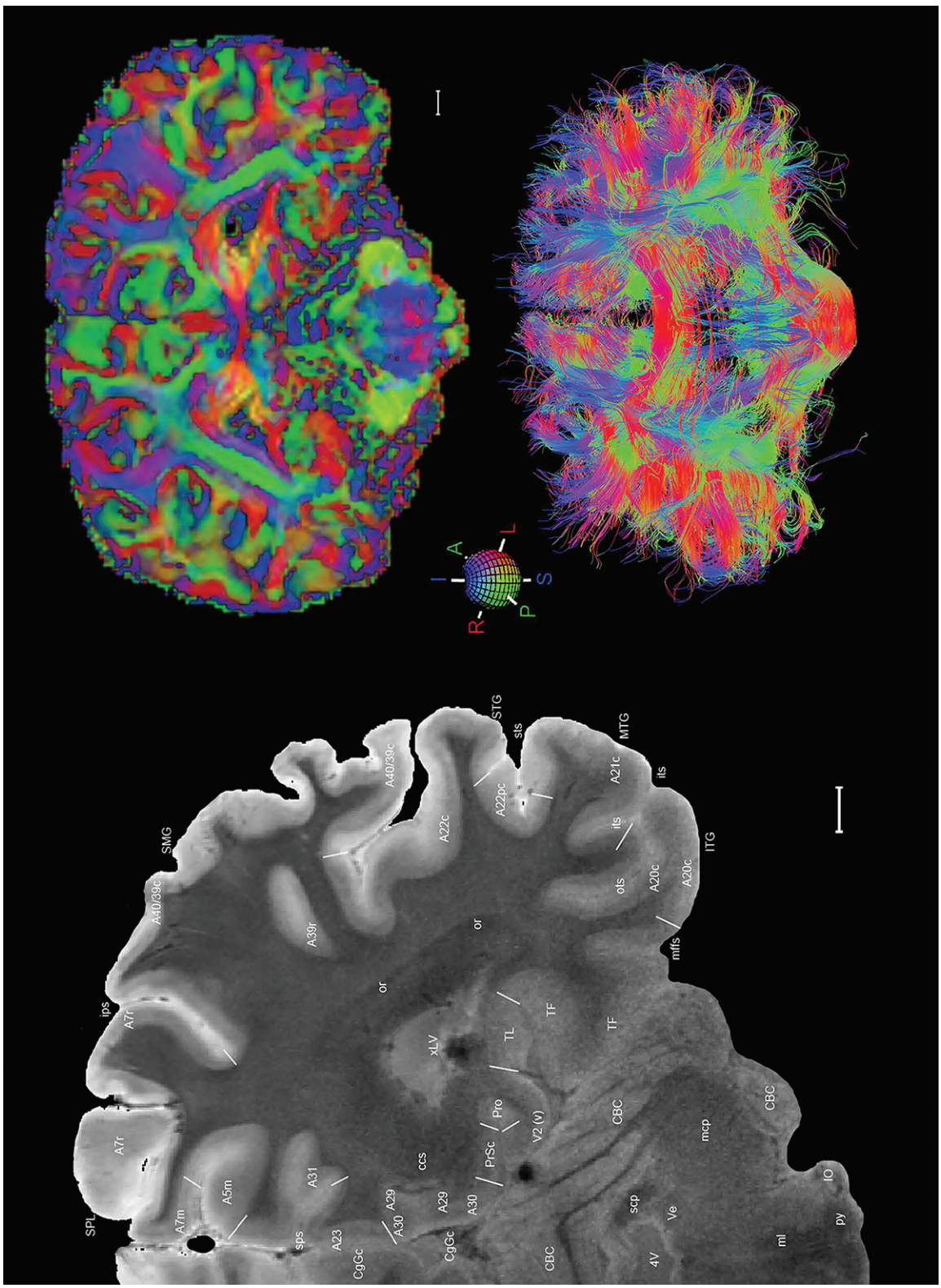

Figure 19. Level 53

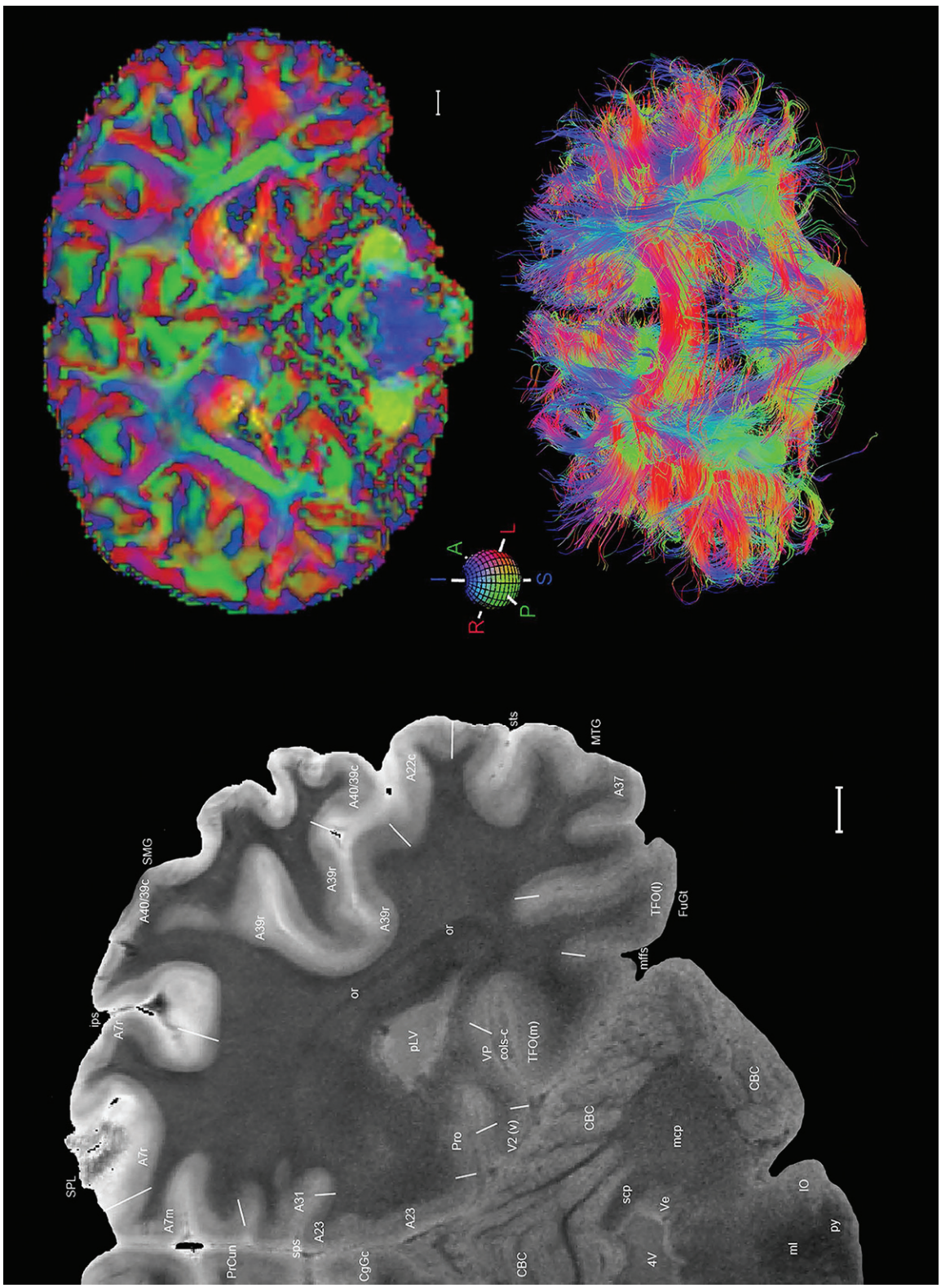

Figure 19. Level 54

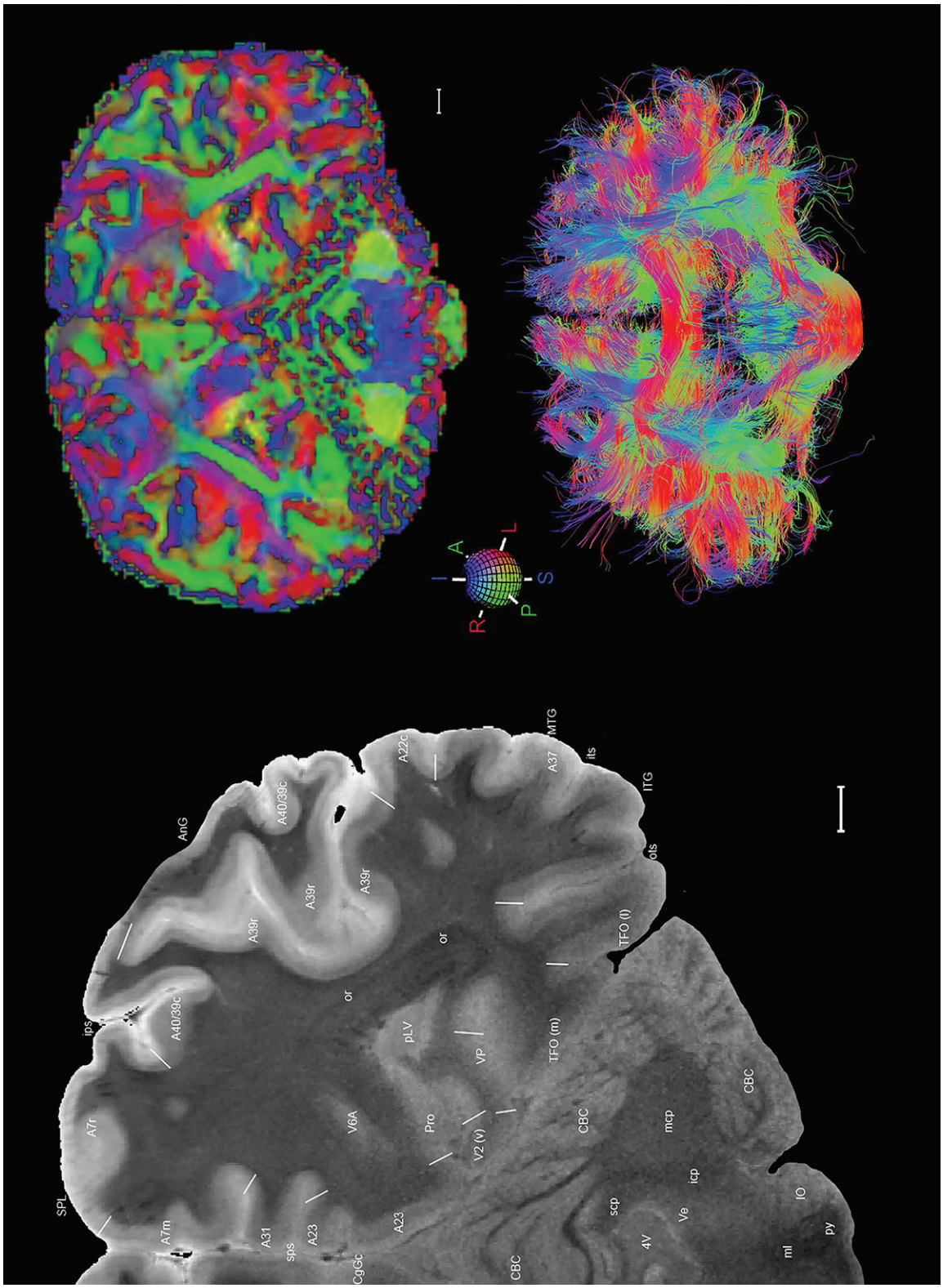

Figure 19. Level 55

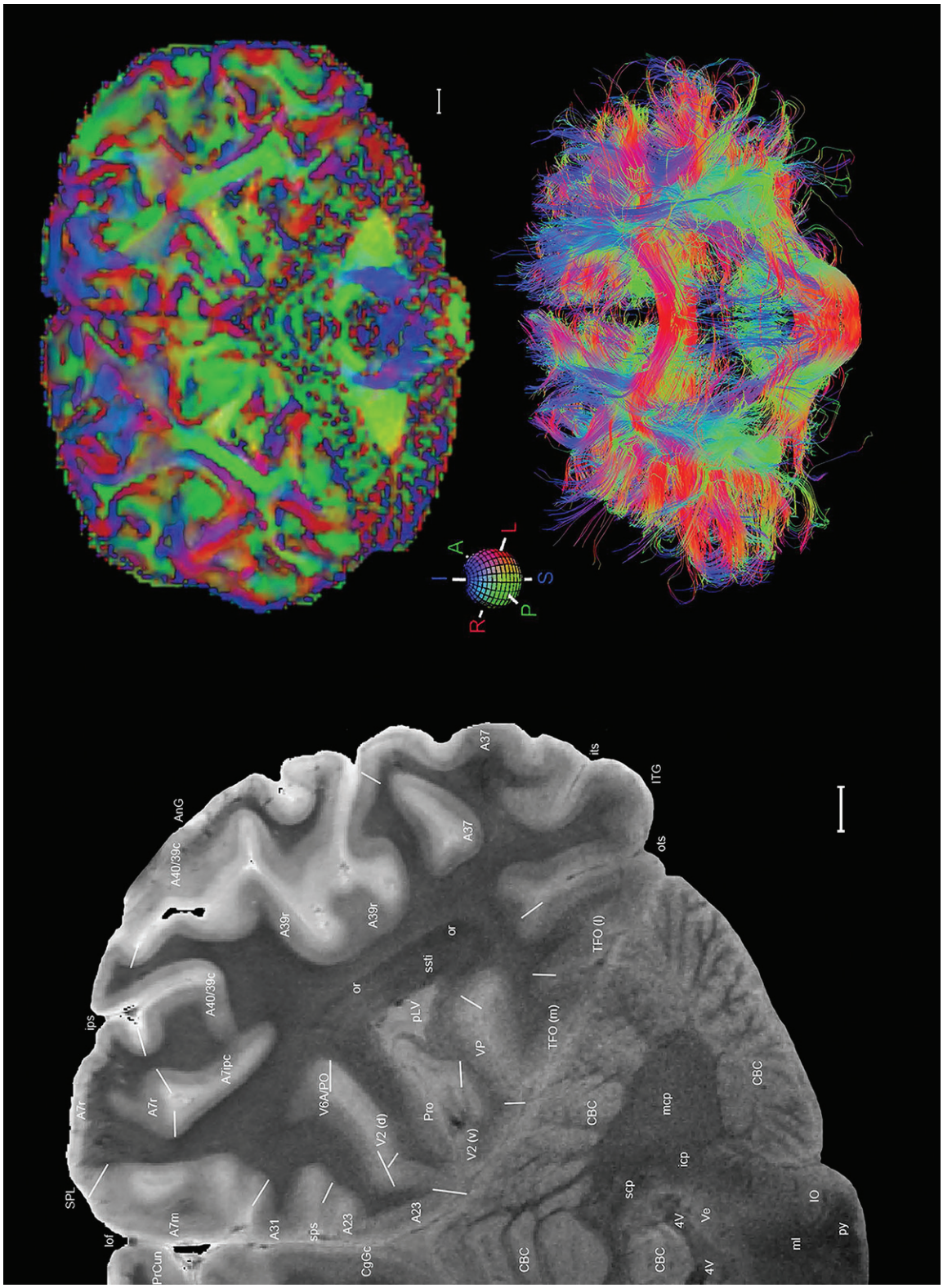

Figure 19. Level 56

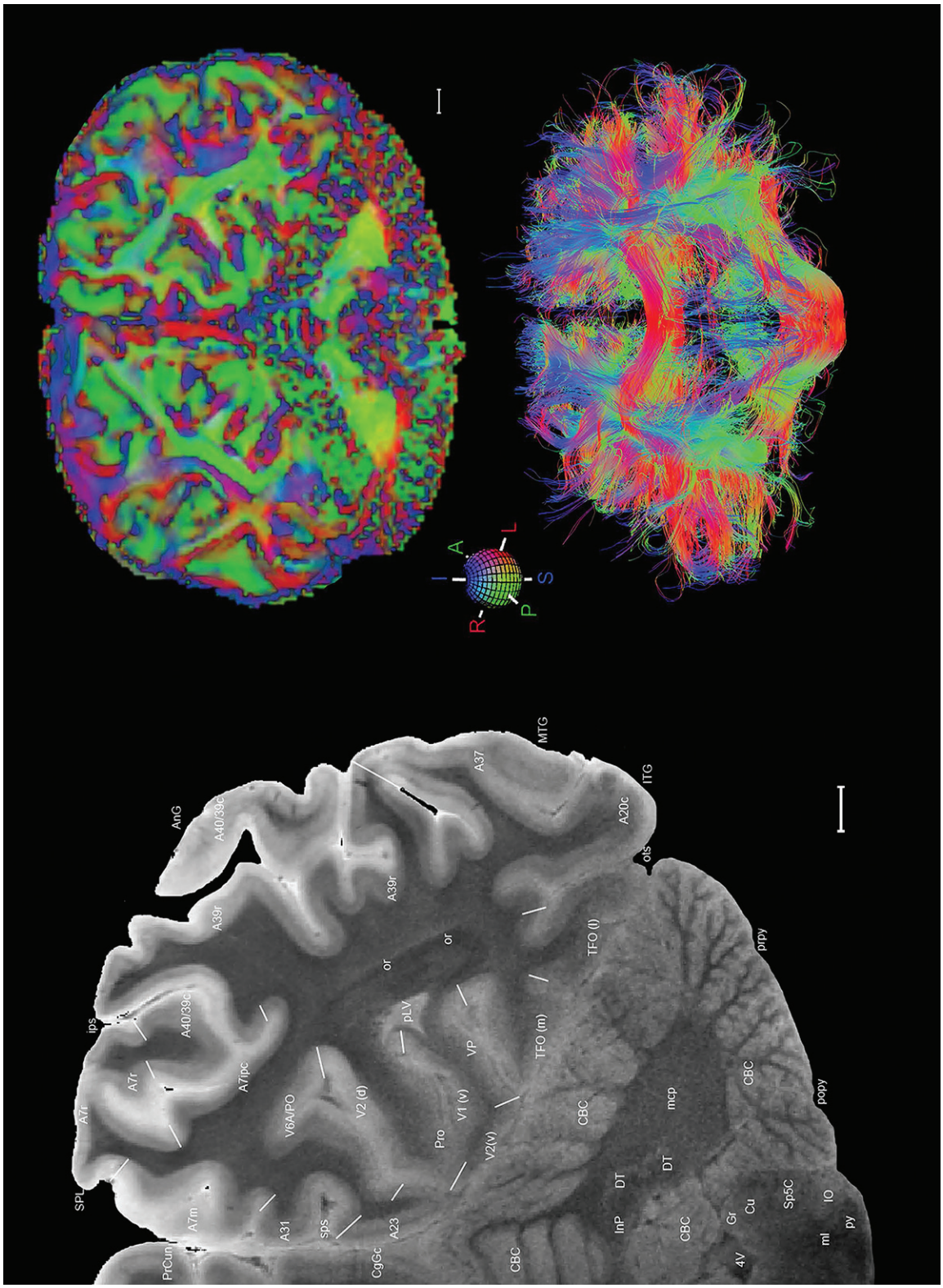

Figure 19. Level 57

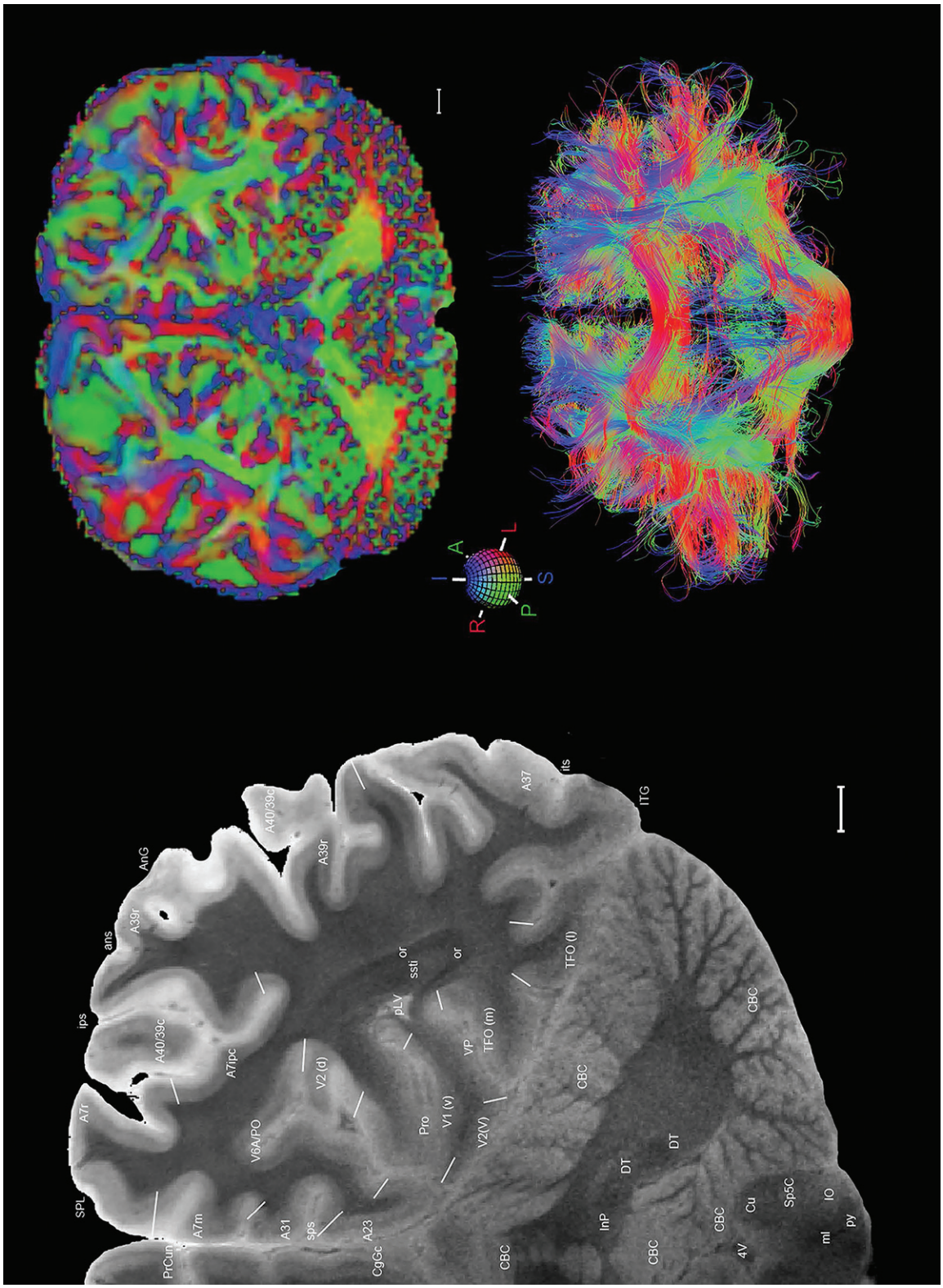

Figure 19. Level 58

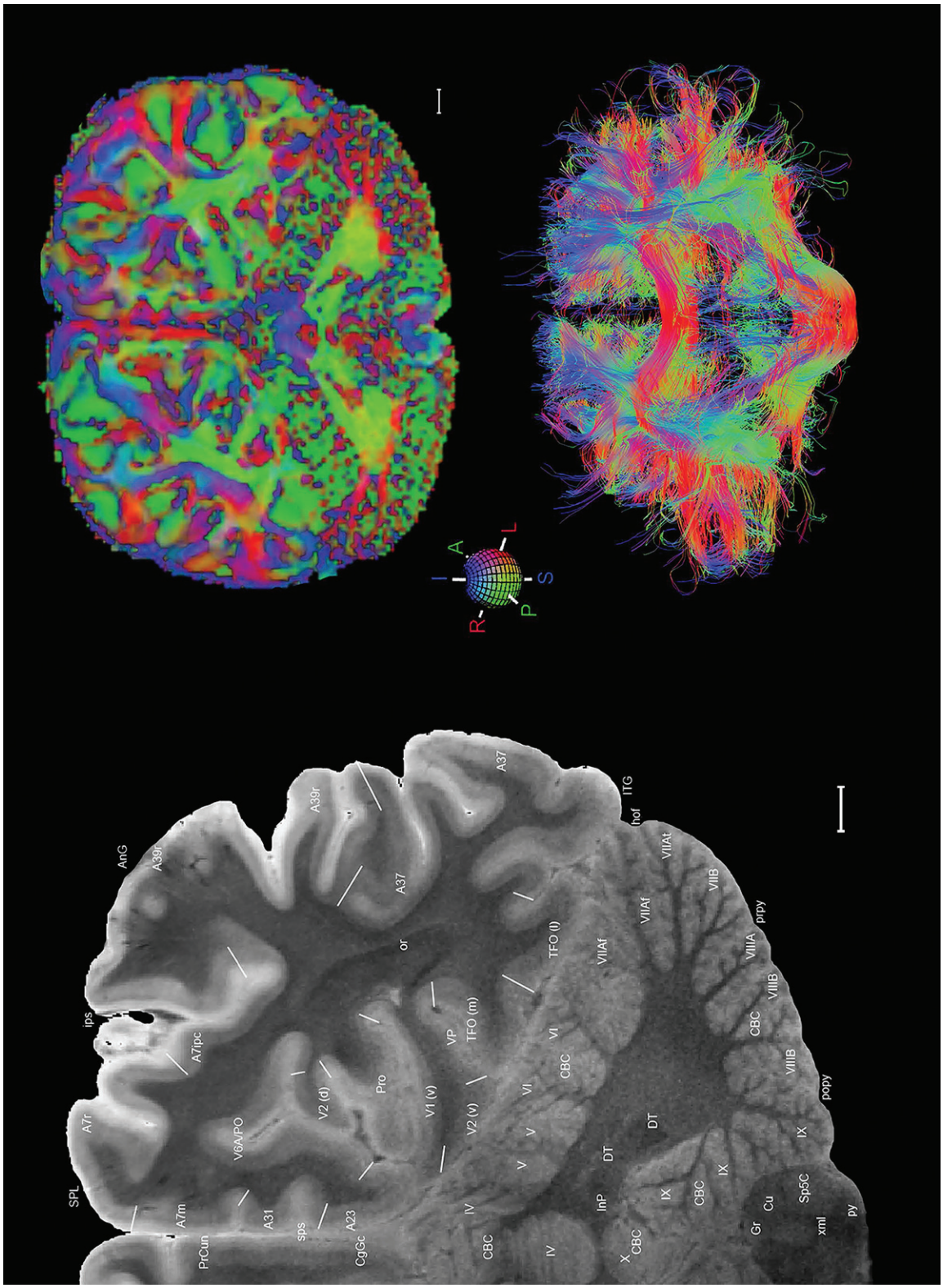

Figure 19. Level 59

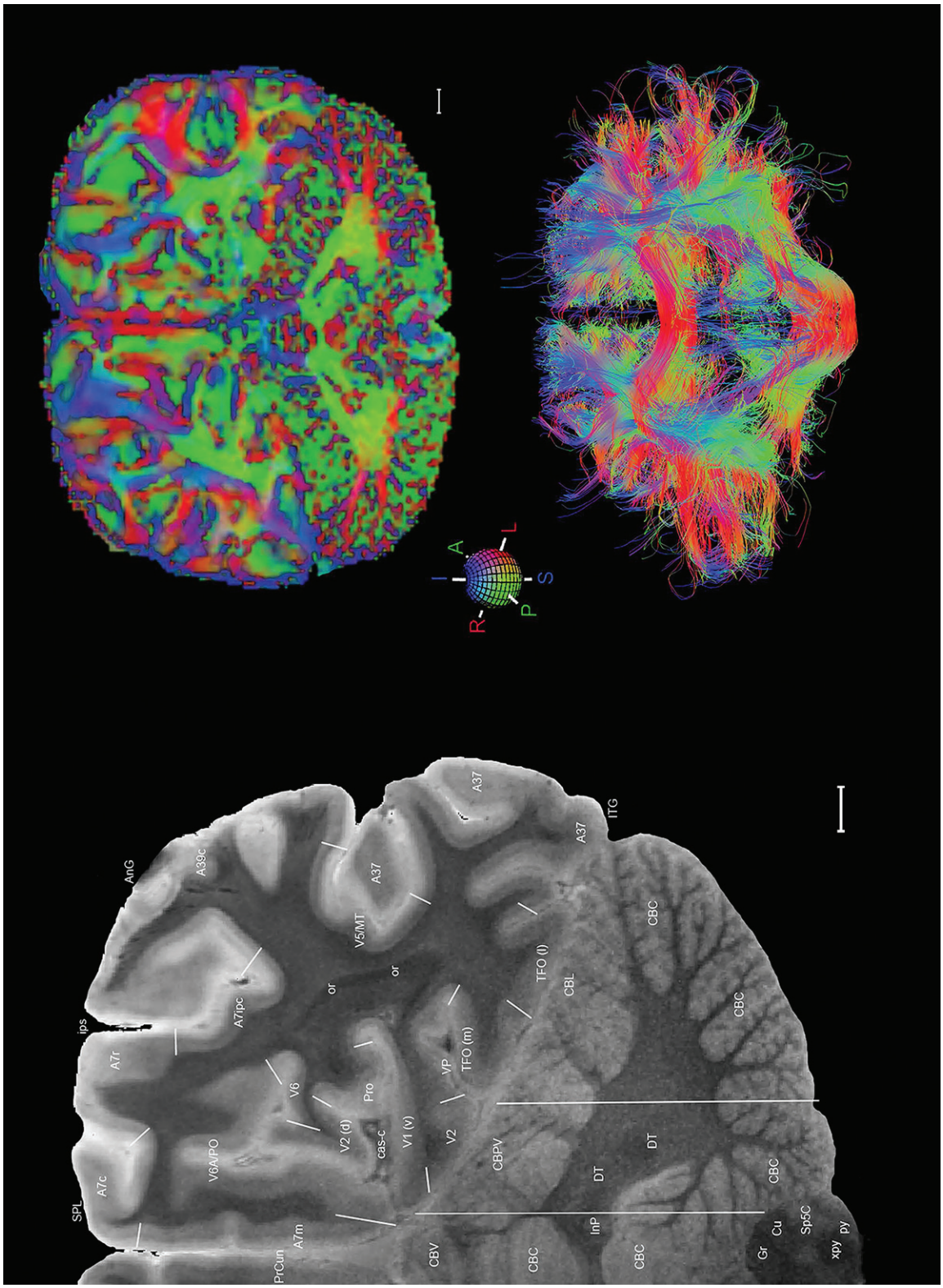

Figure 19. Level 60

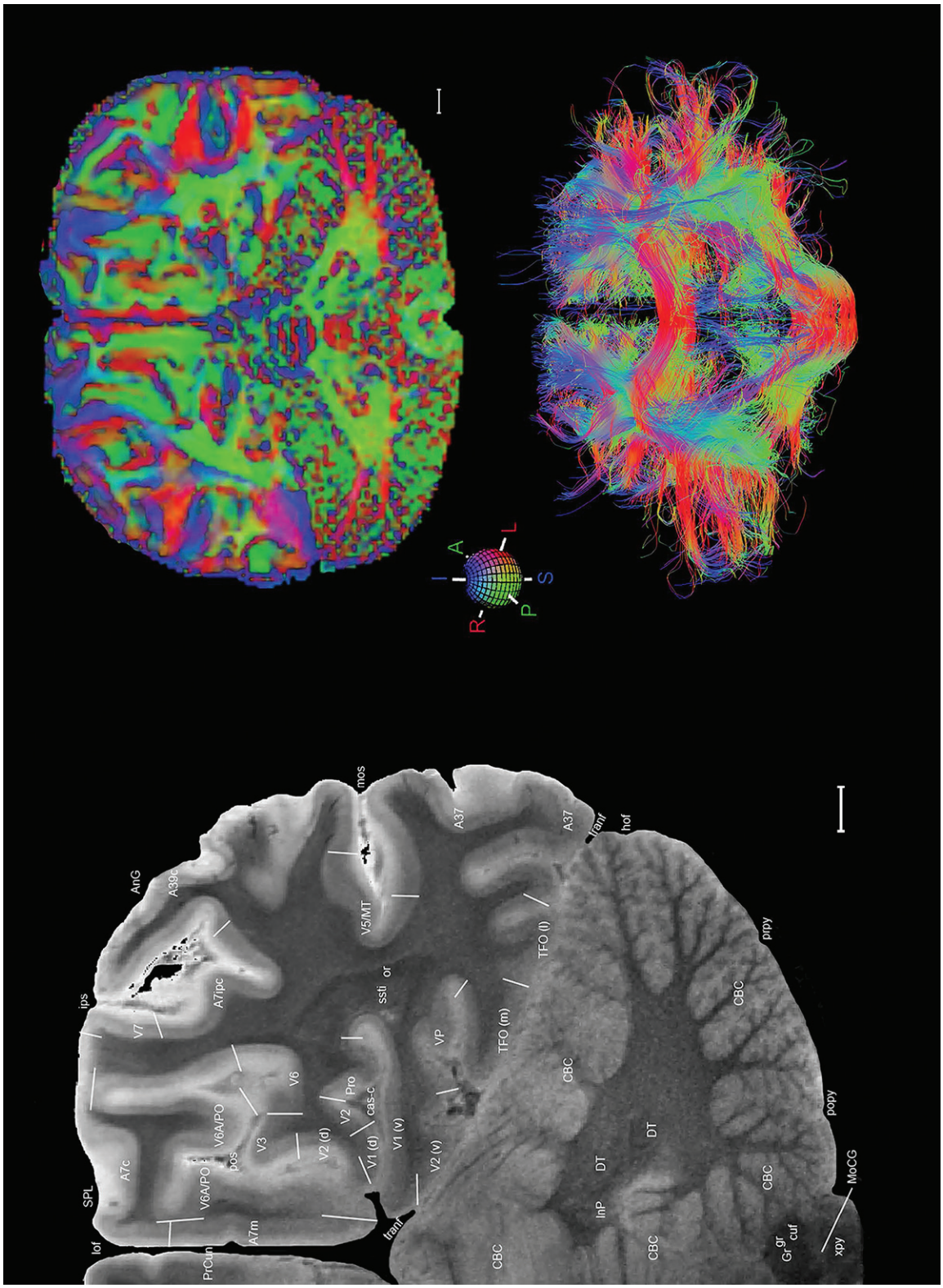

Figure 19. Level 61

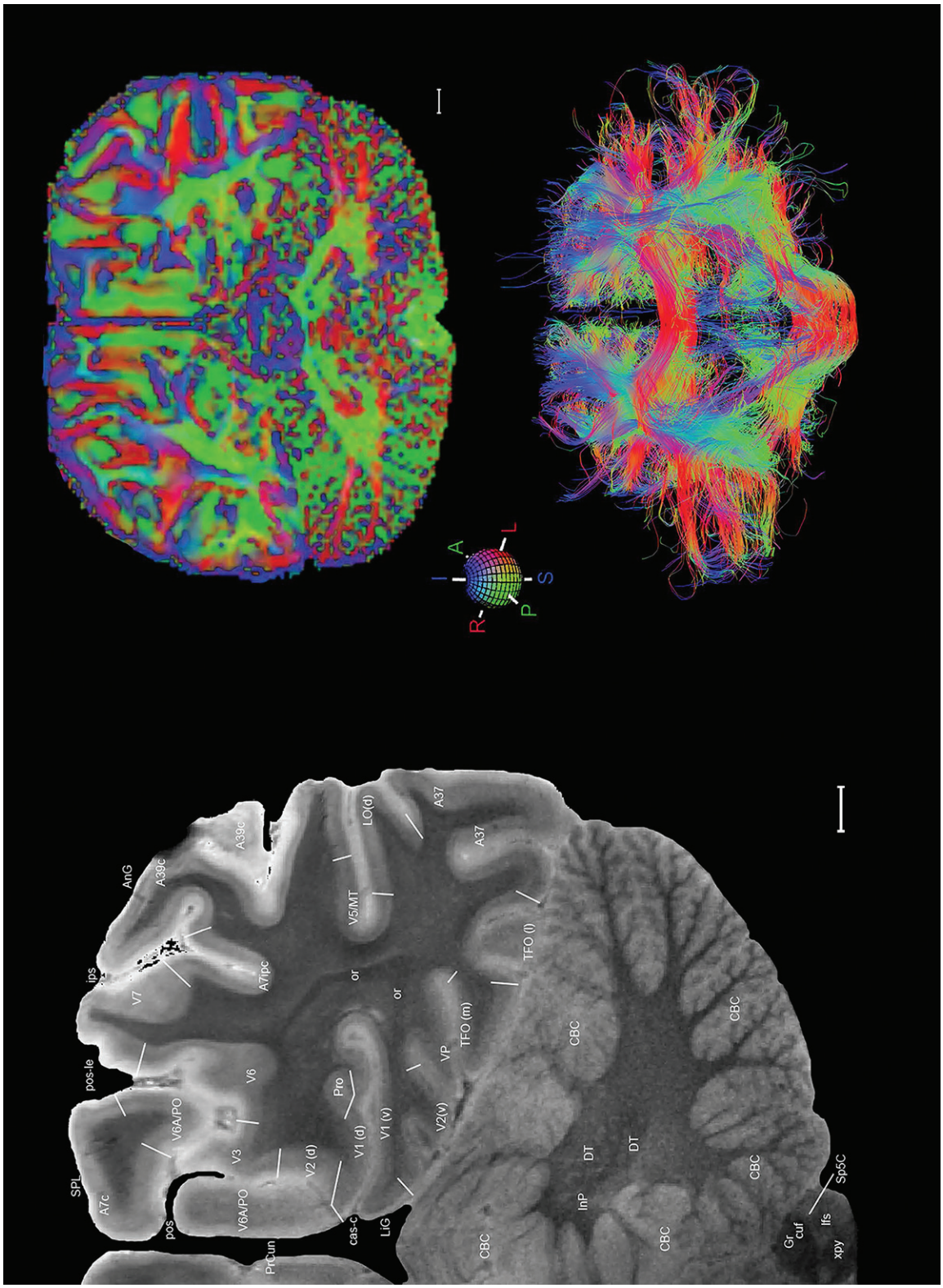

Figure 19. Level 62

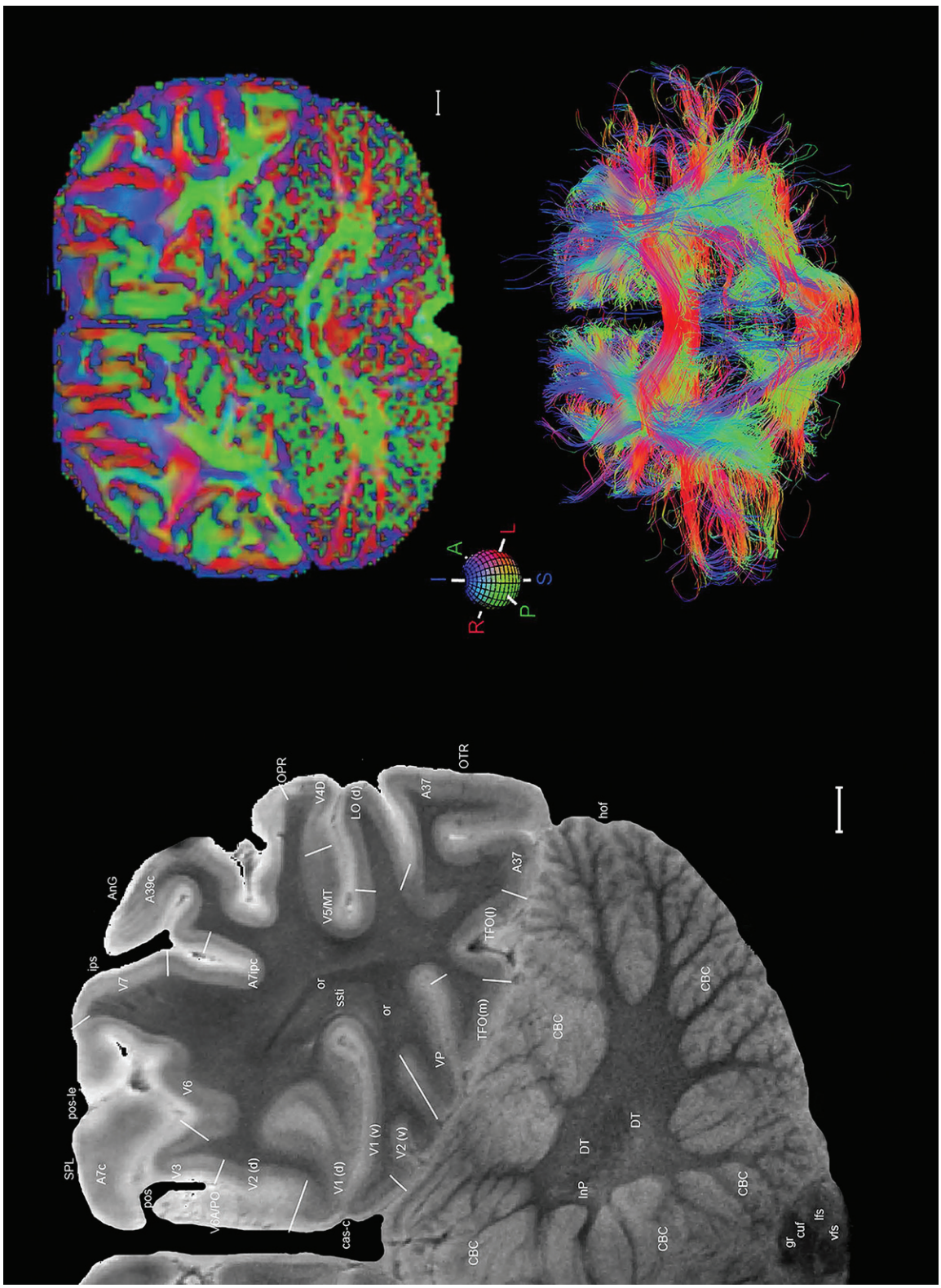

Figure 19. Level 63

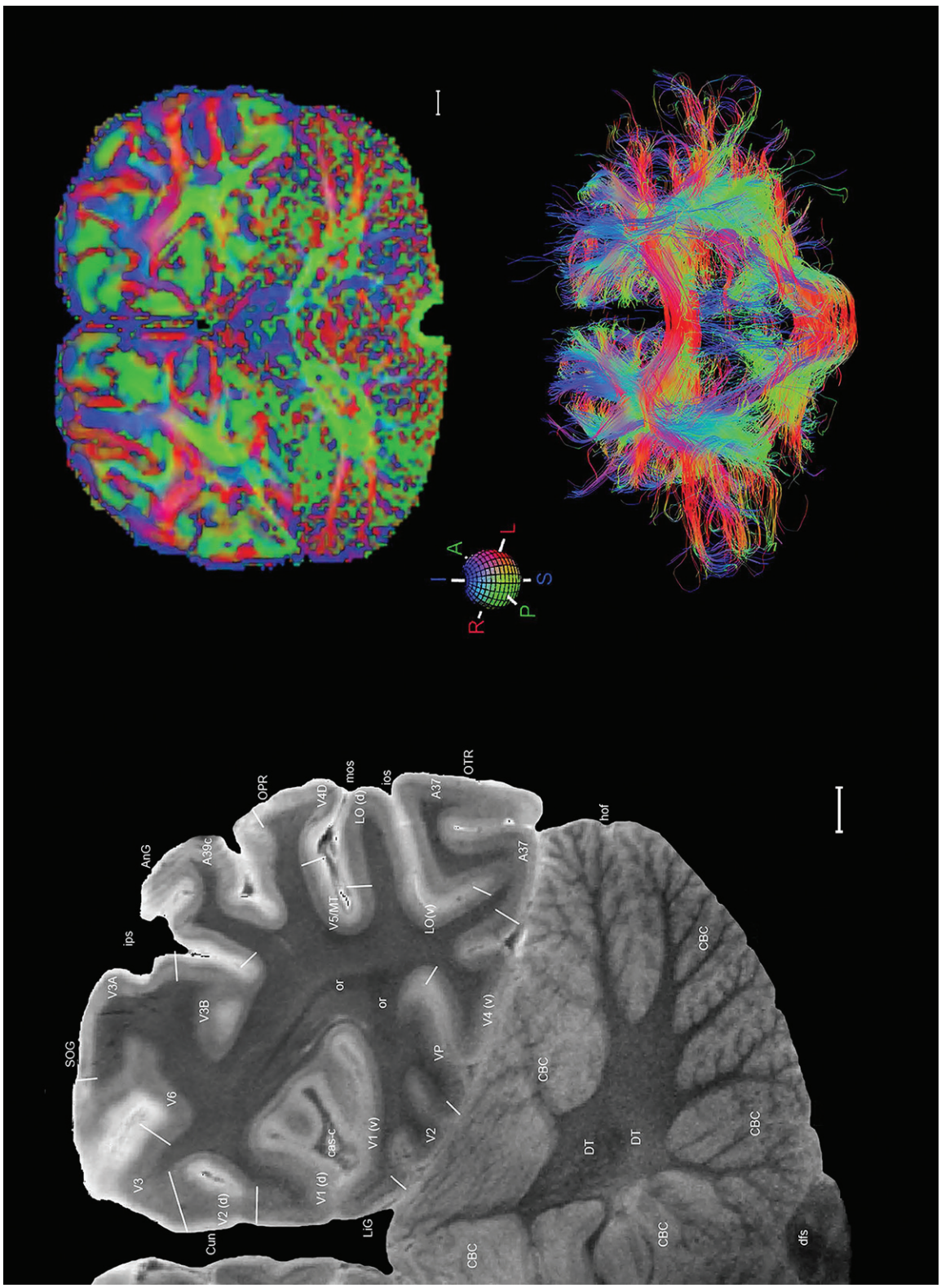

Figure 19. Level 64

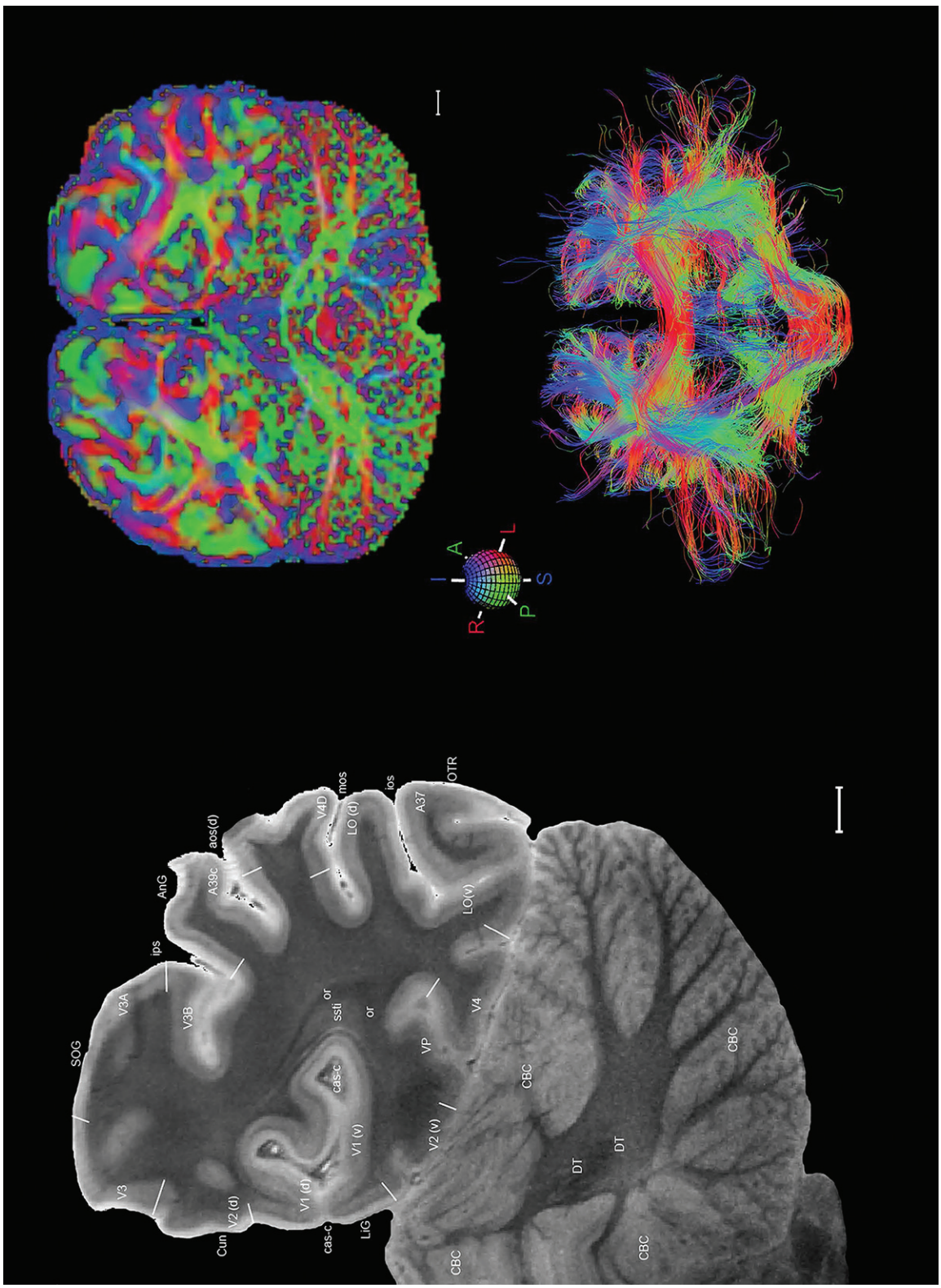

Figure 19. Level 65

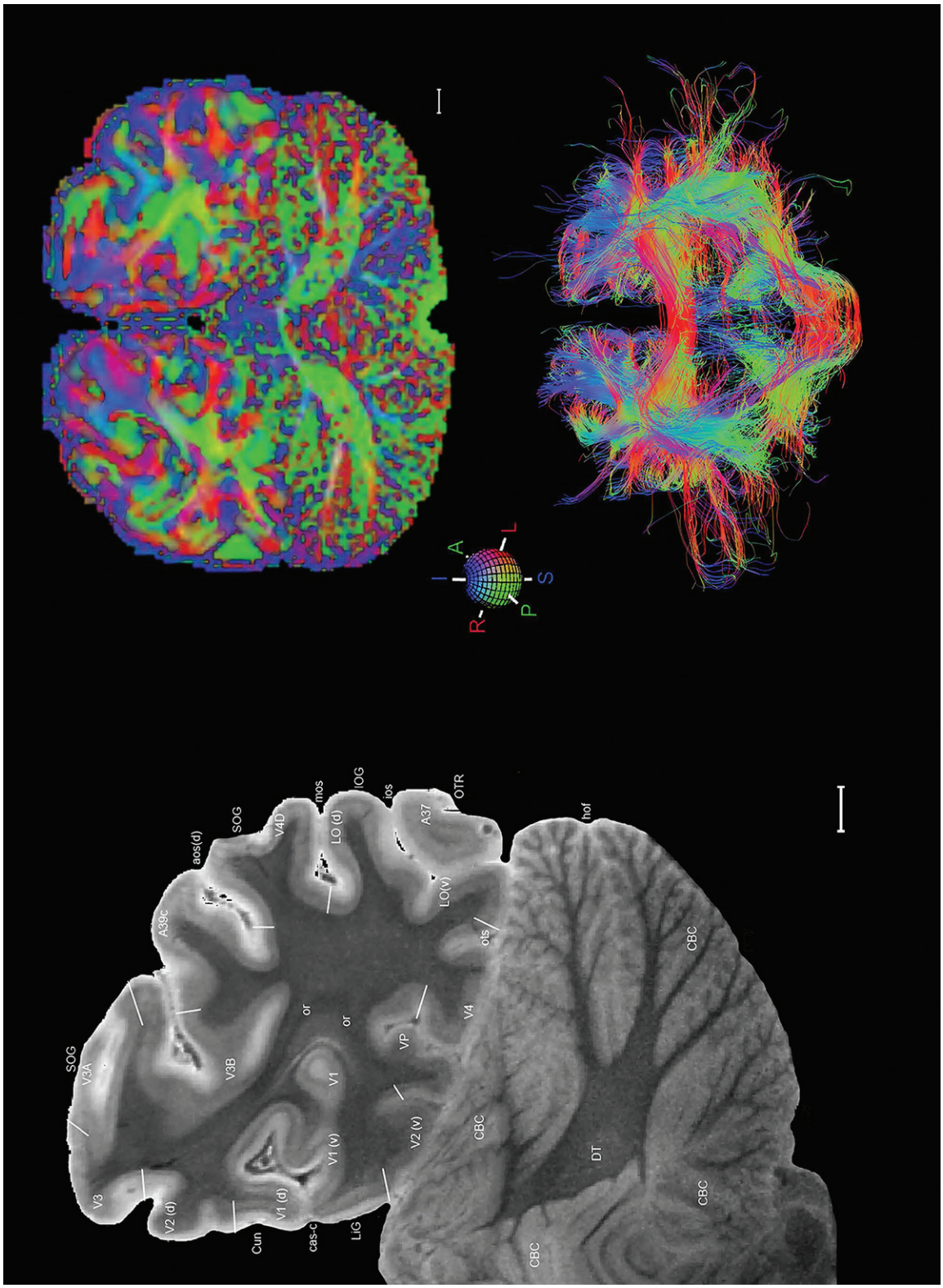

Figure 19. Level 66

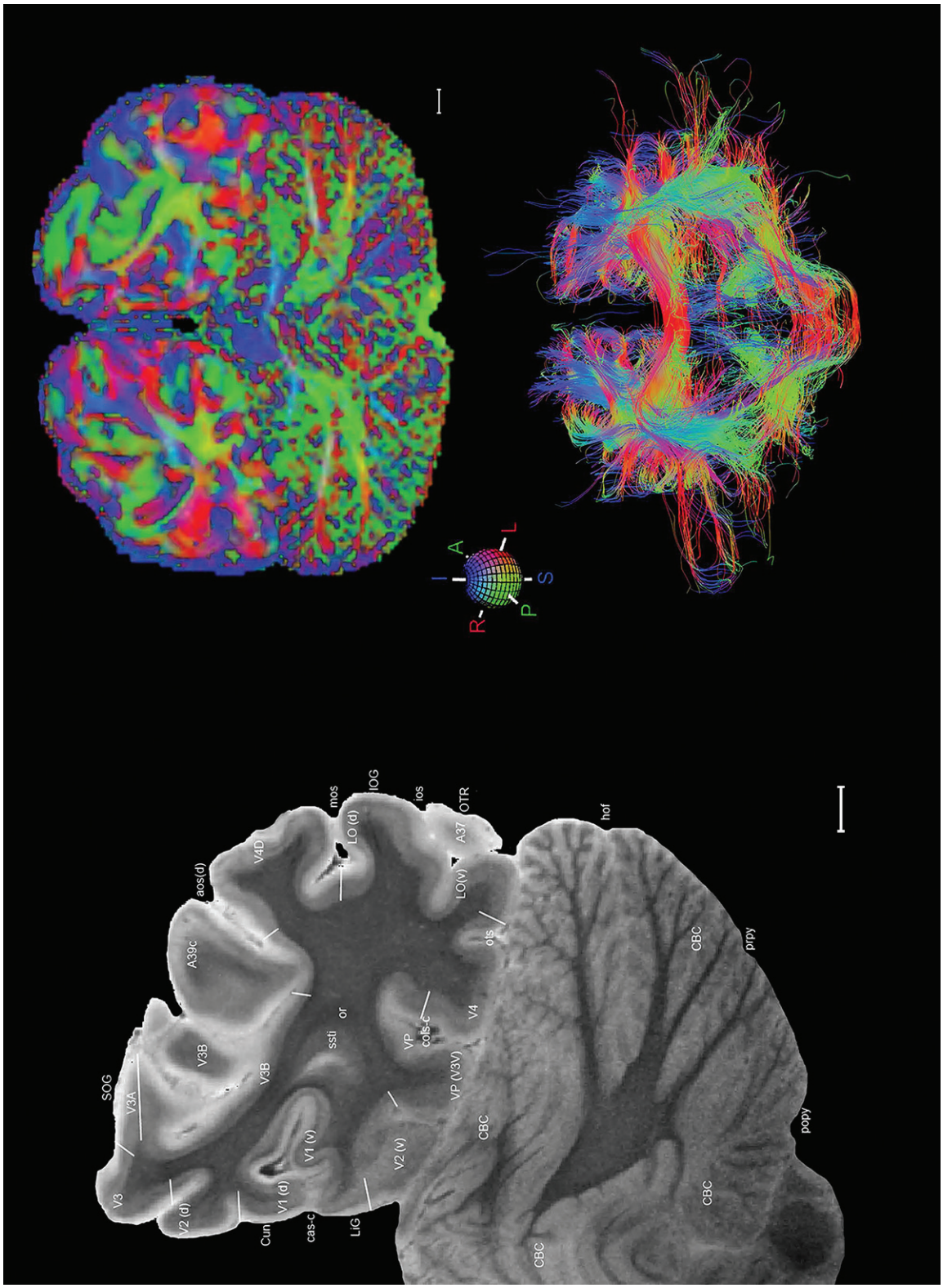

Figure 19. Level 67

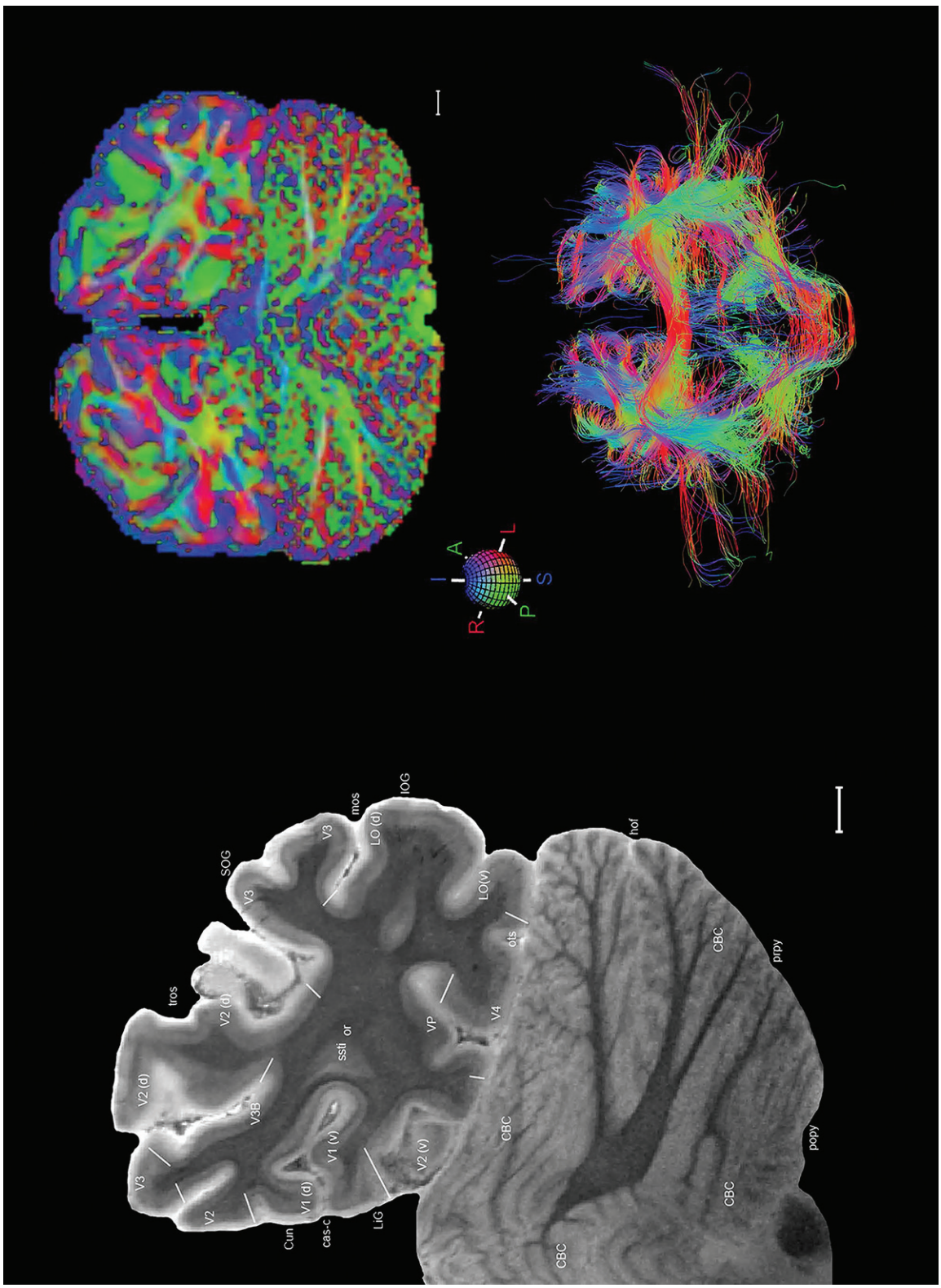

Figure 19. Level 68

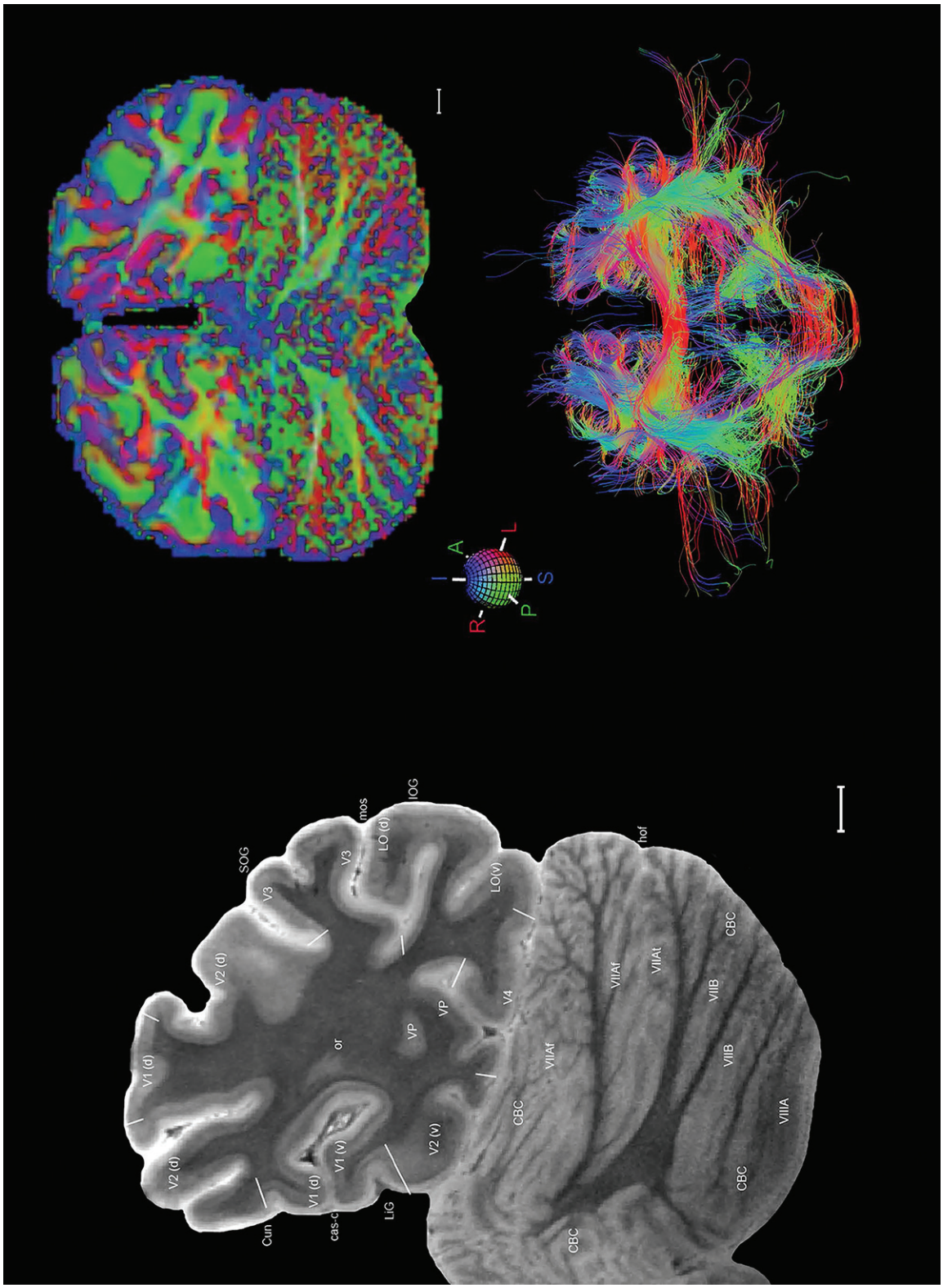

Figure 19. Level 69

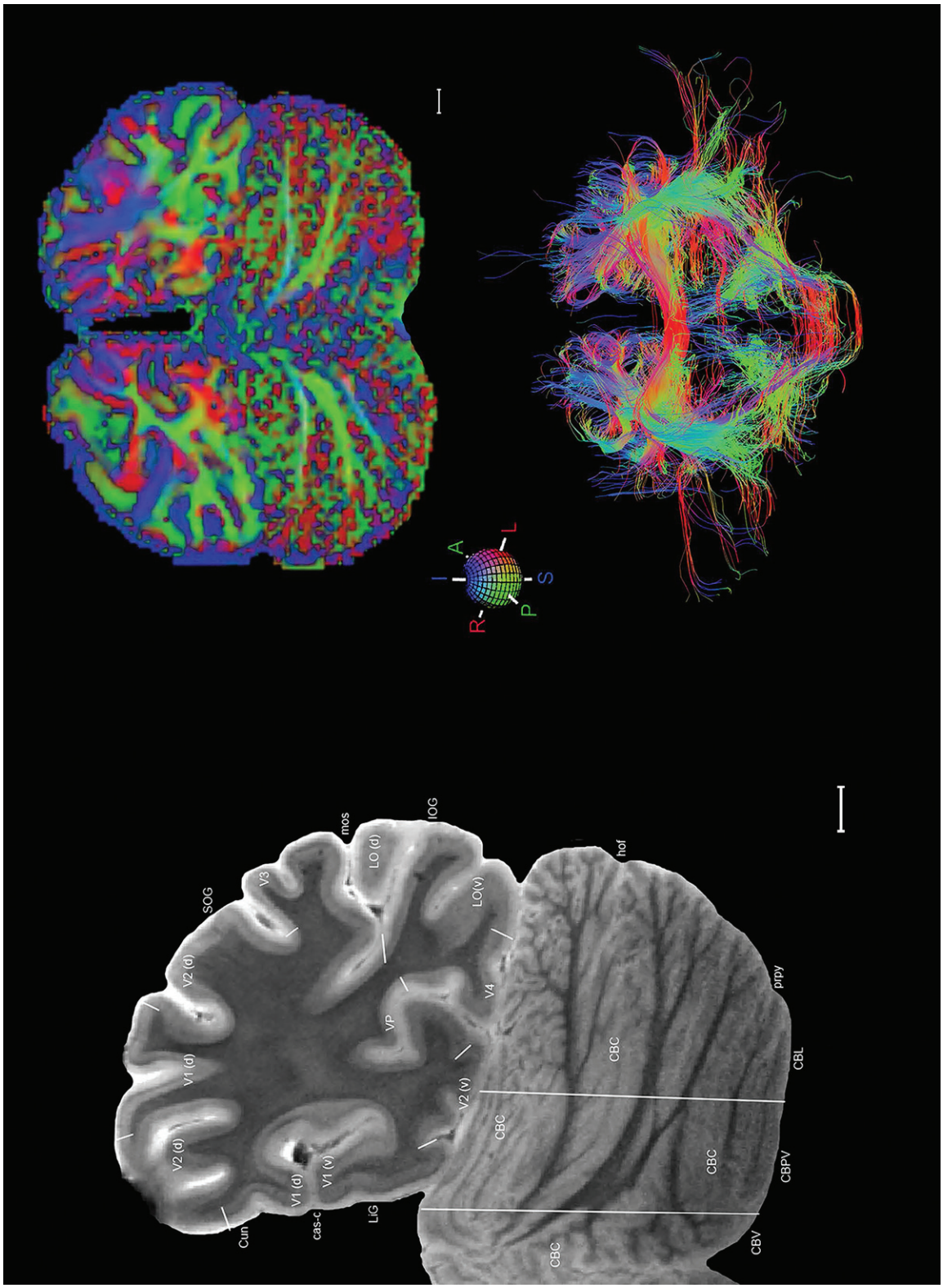

Figure 19. Level 70

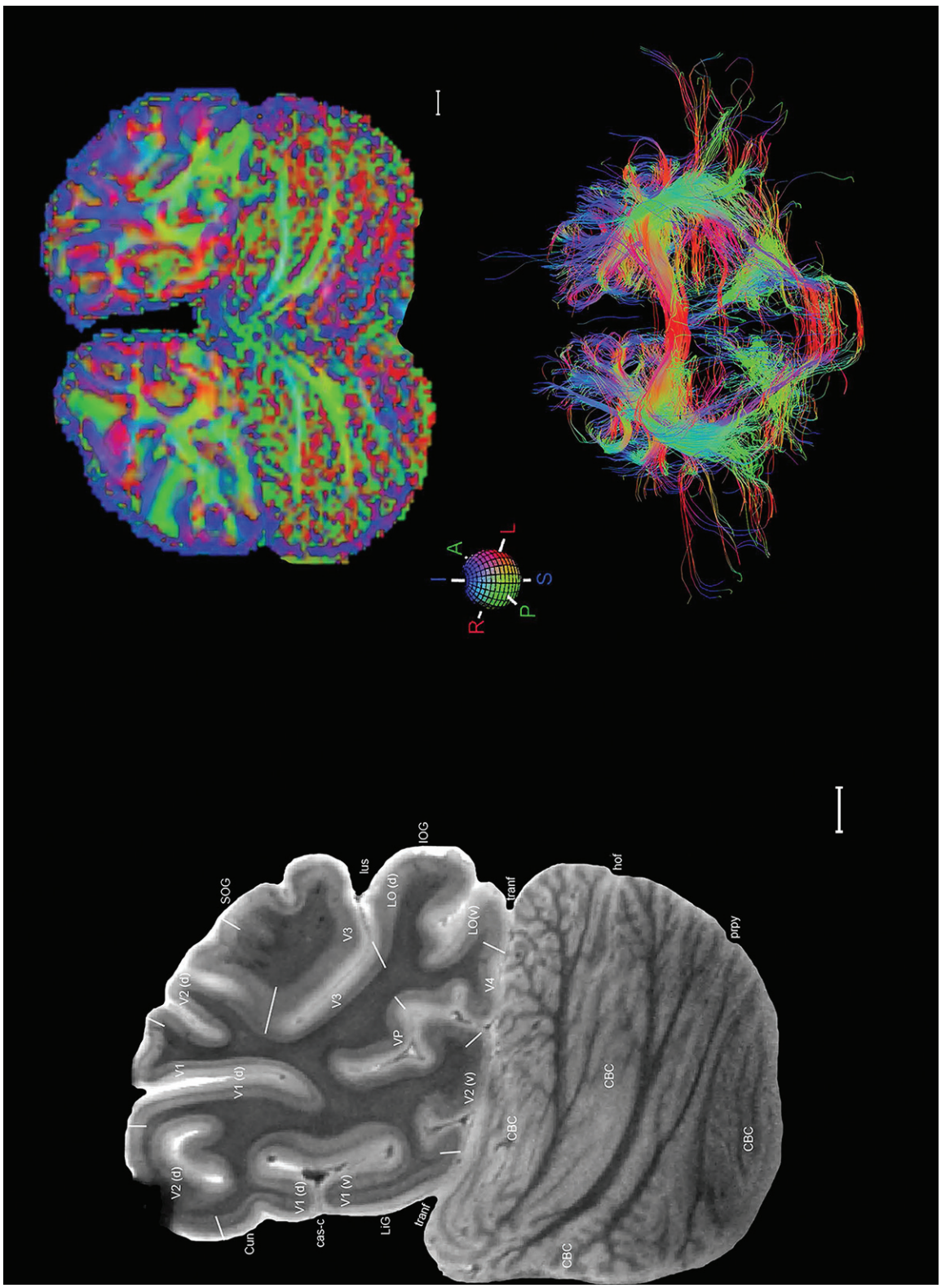

Figure 19. Level 71

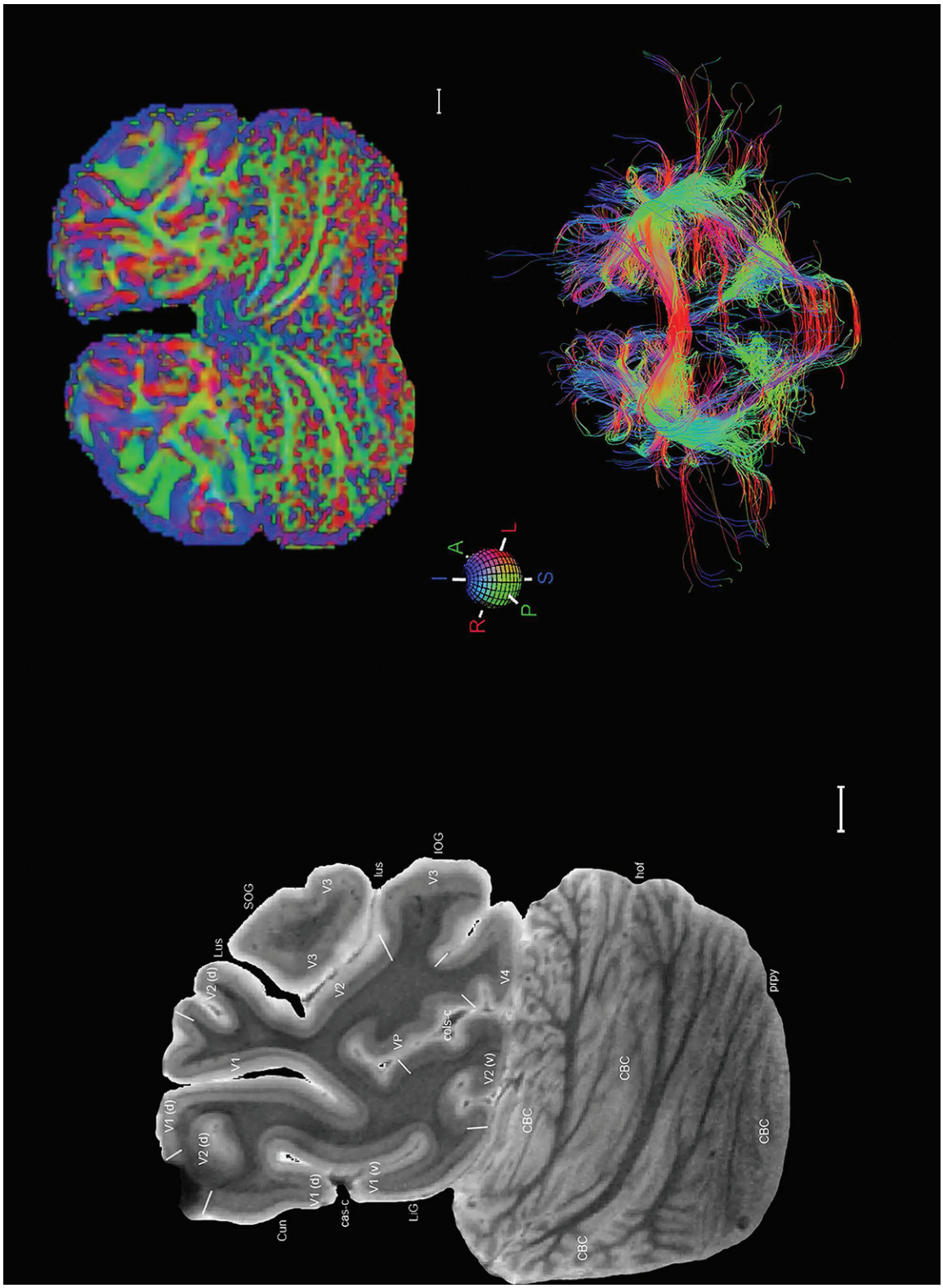

Figure 19. Level 72

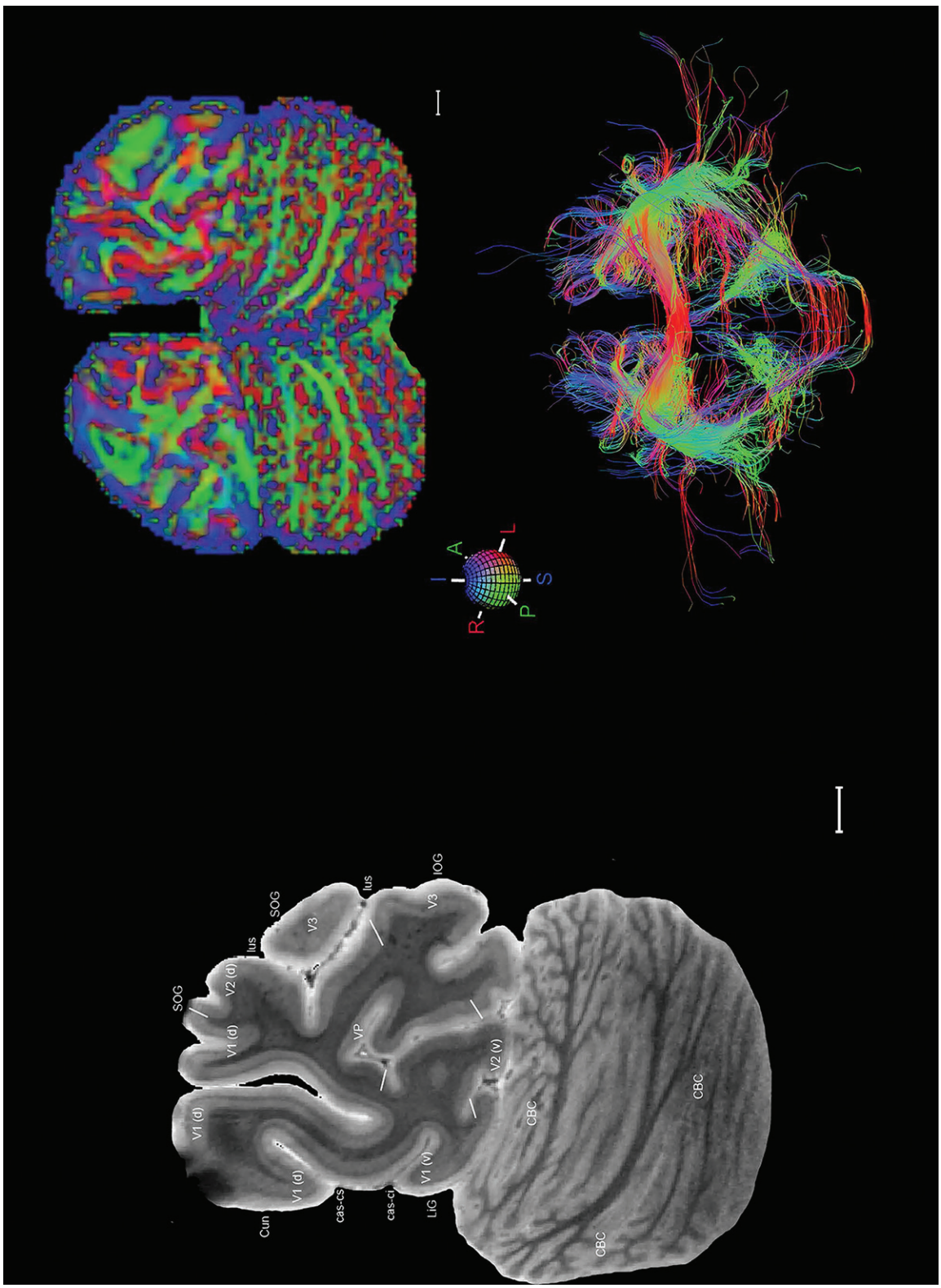

Figure 19. Level 73

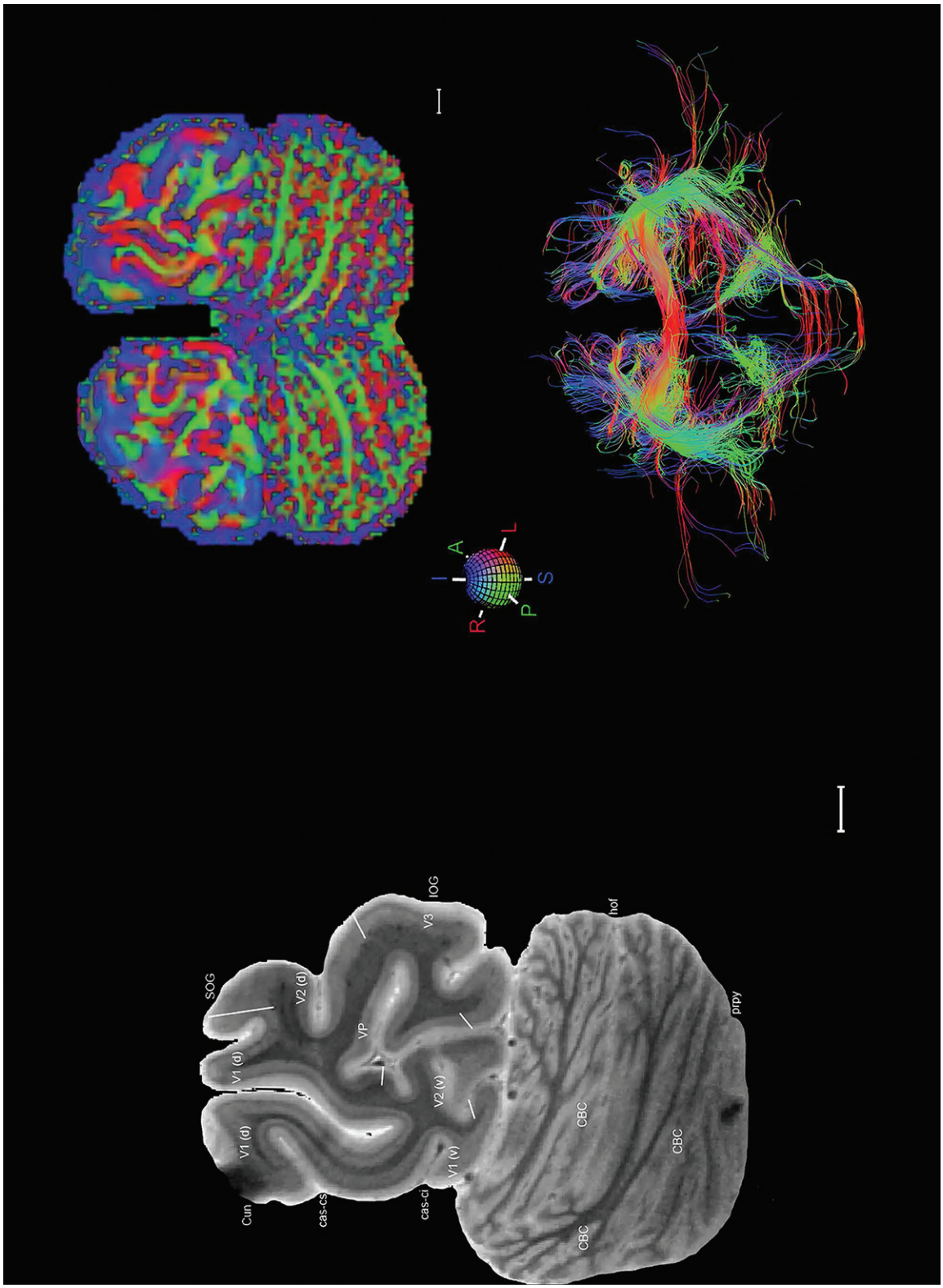

Figure 19. Level 74

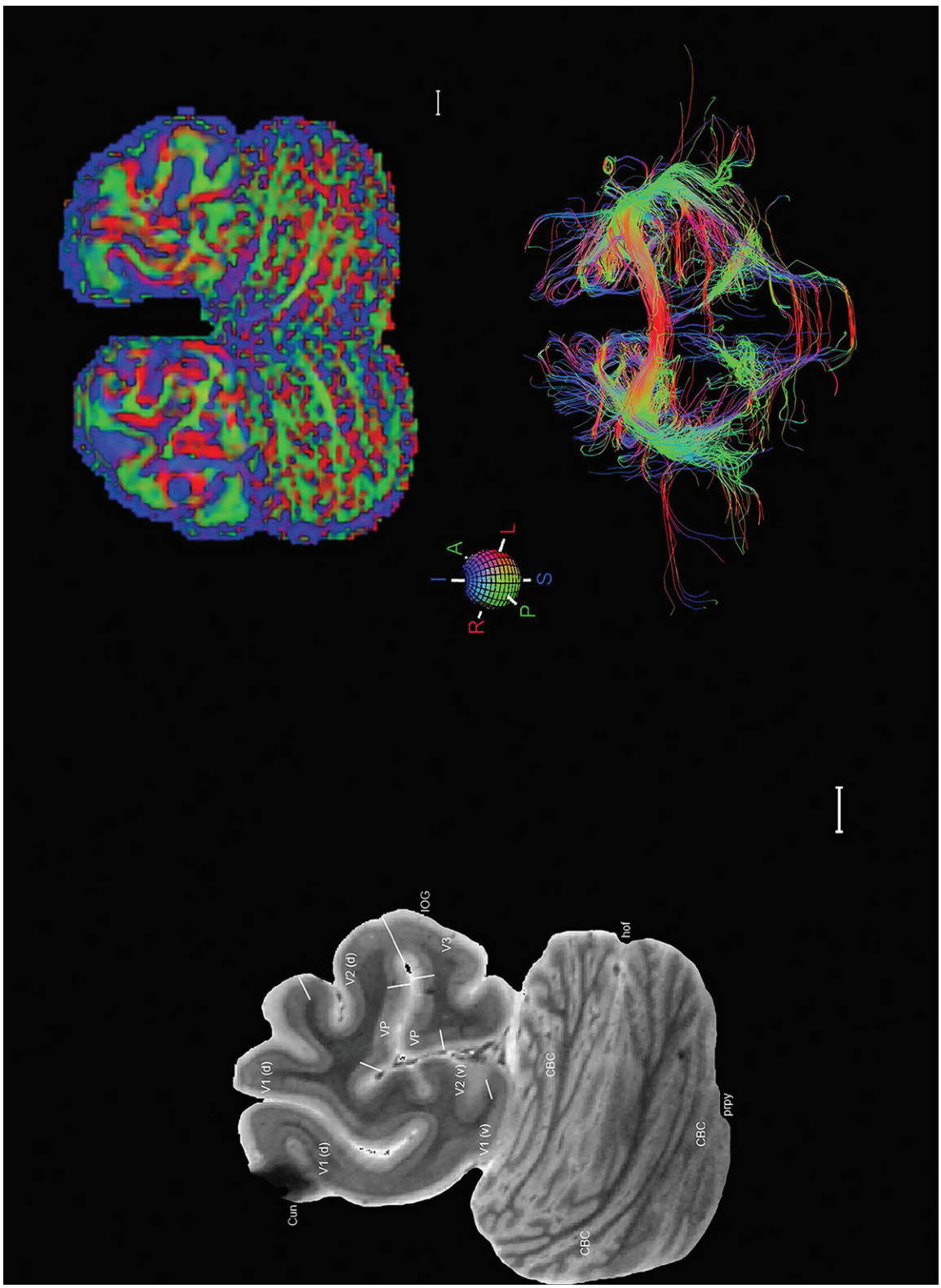

Figure 19. Level 75

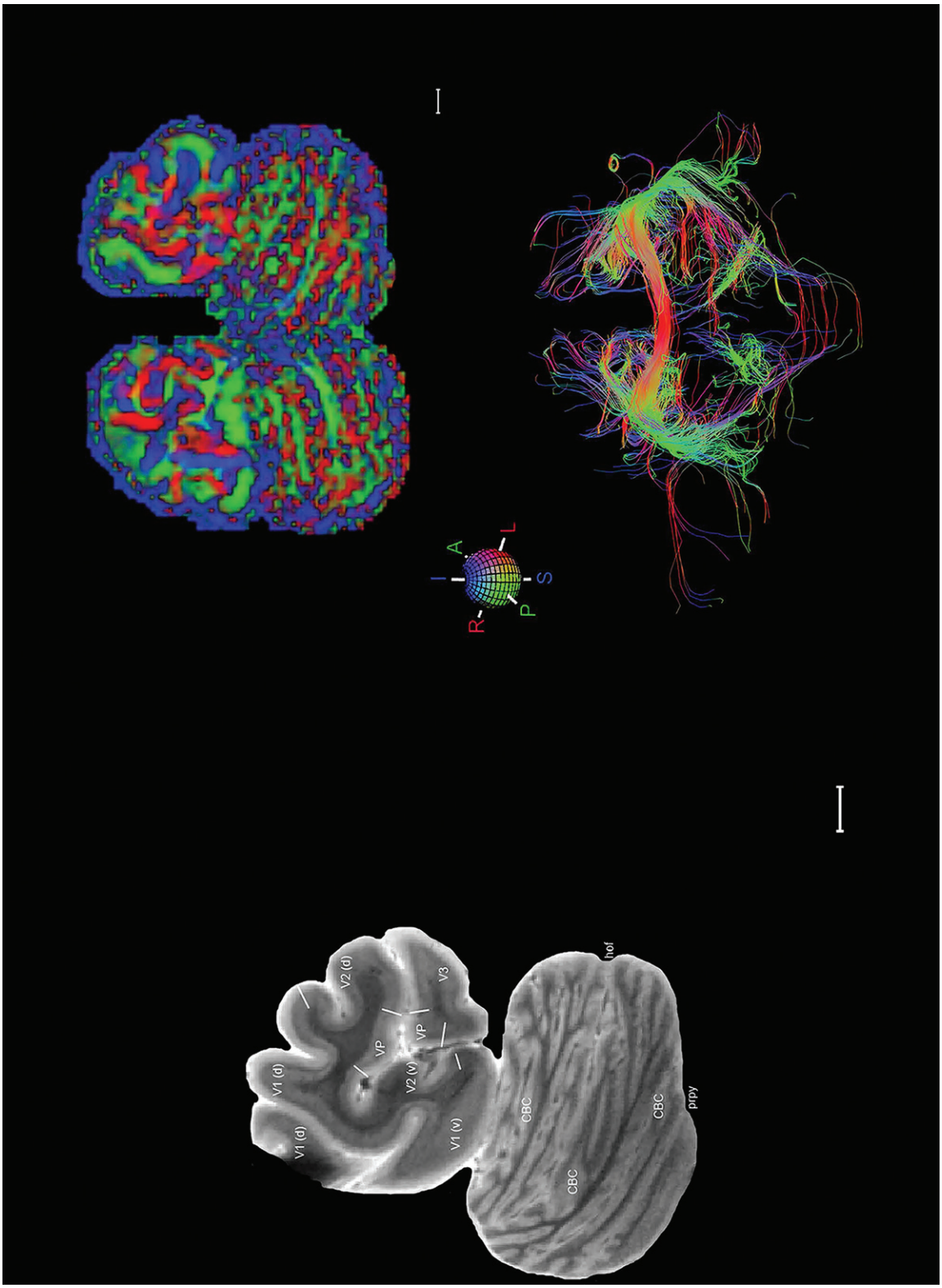

Figure 19. Level 76

WILEY ONLINE LIBRARY

Access this journal and thousands of other essential resources.

Featuring a clean and easy-to-use interface, this online service delivers intuitive navigation, enhanced discoverability, expanded functionalities, and a range of personalization and alerting options.

Sign up for content alerts and RSS feeds, access full-text, learn more about the journal, find related content, export citations, and click through to references.

WILEY ONLINE LIBRARY
wileyonlinelibrary.com